Spectroscopic studies of model biological membranes

Greenhall, Margaret Hope

UNIVERSITY OF DURHAM

A Thesis
entitled

SPECTROSCOPIC STUDIES OF MODEL BIOLOGICAL MEMBRANES

submitted by
MARGARET HOPE GREENHALL B.Sc

A candidate for the degree of Doctor of Philosophy
1993

To Mum, Dad, Margaret and Martin

For all that you have done for me

DECLARATION

The material described in this thesis was carries out by the author in the departments of Chemistry and Applied Physics, University of Durham; and at the centre for research and technology, The Heath, ICI Plc., Runcorn, Cheshire, between October 1989 and October 1992. It has not been submitted for any other higher degree. The work is original, except where acknowledged by reference.

Margaret Greenhall

4th April 1993

ACKNOWLEDGEMENTS

I would like to express my gratitude to Dr. Jack Yarwood and Ron Swart for their guidance and encouragement throughout the project. I would also like to thank Sarah Froggatt, Ruth Brown and Paul Gellert for their assistance. I would also like to thank the technical and non-technical staff at Durham, especially Terry Harrison, for their services. Thank you to all of the friends, both within and outside the department who have made my stay in Durham so enjoyable. Most especially I would like to thank my husband, Martin for his help and encouragement throughout, especially during the production of this thesis.

Thank you to Dr. Mike Petty for access to his Langmuir troughs.The Science and Engineering Research Council and Corporate Colloids, ICI Plc. are thanked for their financial support.

Abstract of a PhD. Thesis entitled :

SPECTROSCOPIC STUDIES OF MODEL BIOLOGICAL MEMBRANES

Margaret Hope Greenhall 1993

Small vesicles of egg lecithin were made by a gel filtration technique. Their size was found to be 24 ± 0.5 nm via photo correlation spectroscopy. The vesicles were proved to be unilamellar by use of phosphorus nuclear magnetic resonance. Fourier transform infrared spectroscopy (FTIR) studies showed that the lipid hydrocarbon chains were fluid (i.e. contained gauche conformations) in all environments studied. The phosphate groups and about half the carbonyl groups were found to be solvated.

Monolayers studies at the air/water interface showed that a mixtures of dipalmitoylphosphatidic acid (DPPA) with dioleoylphosphatidic acid (DOPA) were largely immiscible. There was a slight deviation from complete immiscibility for mixtures of DPPA in DOPA, such that a closer molecular packing occurred compared to monolayers of the pure materials. Mixtures of alamethicin in DPPA were found to be immiscible.

Multilayers of DPPA were deposited via Langmuir-Blodgett (LB) deposition, over water onto both micro attenuated total internal reflection (ATR) silicon crystals and gold coated glass slides. Reflection absorption infra red spectroscopy (RAIRS) and linearly polarised micro ATR studies showed that the alkyl chains of these multilayers were approximately perpendicular to the substrate.

A novel deposition technique was used to make a biological bilayer structures of materials underwater, for examination via FTIR. These were examined in a newly designed micro ATR solution state cell. It was found that for a bilayer of DPPA when the H_2O was exchanged for D_2O that there was H_2O trapped in the bilayer. This took water a long time to become deuterated (about 2-3 hours).

A 30:1 mixture of DPPA:alamethicin was found to deposit in a Z-type manner, via Langmuir-Blodgett dipping. ATR FTIR solution state spectra of a biological bilayer of 16:1 DPPA:gramicidin also retained water, similar to pure DPPA, but the deuteration of the H_2O took approximately half the time.

Abbreviations used in this thesis :

δ	bending vibration
ν	stretching vibration
π-A	surface pressure versus area per molecule
A/W	air/water
APM	area per molecule
as	antisymmetric
ATR	attenuated total internal reflection
CD	circular dichroism
CMC	critical micelle concentration
CPA	close packed area per molecule
DMPA	dimystroylphosphatidic acid
DMPC	dimystroylphosphatidylcholine
DMPE	dimystroylphosphatidylethanolamine
DMPG	dimystroylphosphatidylglycerine
DOPA	dioleoylphosphatidic acid
DPPA	dipalmitoylphosphatidic acid
DPPC	dipalmitoylphosphatidylcholine
DPPE	dipalmitoylphosphatidylethanolamine
DPPS	dipalmitoylphosphatidylserine
EDTA	ethylenediaminetetra-acetic acid
ESR	electron spin resonance
FD	Fourier deconvolution
FT	Fourier transform
FTIR	Fourier transform infrared
FWHH	full width at half height
IPA	iso-propyl alcohol
IR	infrared
LB	Langmuir-Blodgett
LS	Langmuir-Shaeffer
LUV's	large unilamellar vesicles
MLV's	multilamellar vesicles
NMR	nuclear magnetic resonance
PATR	polarised attenuated total internal reflection
PC	phosphatidylcholine
PCS	photo correlation spectroscopy
PTFE	polytetrafluoroethene
RAIRS	reflection-absorption infrared spectroscopy
s	symmetric
S/N	signal to noise
SD	second derivative
SUV's	small unilamellar vesicles
TE	transverse electric
TM	transverse magnetic
TPO	triphenylphosphine
UV's	unilamellar vesicles
ZPD	zero point difference

CONTENTS

CHAPTER 1

BACKGROUND AND INTRODUCTION

1.1 BACKGROUND TO BIOLOGICAL MEMBRANE RESEARCH

Biological membranes are found throughout nature, from protozoa to whales and algae to giant red-woods. Membranes act as barriers, both to separate fluids and to protect organisms from their external environment. However, it is necessary for materials to enter and leave an area surrounded by a biomembrane and this is achieved by selective transport, facilitated by the membrane. Biological membranes form the walls of the basic building blocks of life - cells. Thus, it is of fundamental importance to understand the structure and mechanisms of membranes in order to comprehend fully the biochemistry of any organism.

The work outlined in this thesis was aimed at furthering the understanding of biological membranes at a molecular level. However, any research rests on a foundation of the work of predecessors and is often in parallel with the contemporary research of other scientists using different techniques. Thus, before it is possible to propose new results, and theories based thereon, the history of membrane research should be described.

1.2 : HISTORICAL ACCOUNT OF THE RESEARCH INTO BIOMEMBRANES

(General references 1-12)

1.2.1 Cells and their membranes

The term cell was first used by Hooke in 1665 to describe the box-like compartments that he had observed by examination of cork with a light microscope. Leeuwenhoek improved the resolution of microscopes such that by 1674 he was able to view protozoa and later bacteria.

However, the idea of cells as the basic building units of life forms, in biochemical terms the units of metabolism, was not proposed until 1835 by Schwann. In 1855 Nägeli used the selective absorption of pigments into different regions of the cell to identify specific components of cells. By the end of the 19th century microscopes were approaching the theoretical limit of their resolution (~ 0.2 μm). At this level of resolution the substructures within cells were visible with the aid of staining techniques. The outer walls of the cells could be seen as a line dividing the cell from the rest of the world. This was termed the plasma membrane. Within the cells other dividing membranes could be seen separating small areas with specific functions. In the late 19th century Nägeli and Cramer showed that cells changed volume depending on the osmotic potential of their immediate environment. They suggested that it was the plasma membrane which was responsible for this osmotic activity. Overton continued these studies into the nature of the separating membrane In 1899 he published results of his observations. He found that if a molecule was highly polar its transition across the membrane was very slow, whereas the addition of non-polar groups (*e.g.* alkyl chains) increased the rate of entry. There were some deviations to these observations, suggesting that the membrane performed an active role in transport. Overton concluded, based on his empirical evidence, that the plasma membrane was composed of cholesterol and other lipids.

It was Gorter and Grendal in 1925 who first suggested that the lipids existed as a bilayer. This was based on the studies of lipids at the air/water interface. These showed that lipids extracted from erythrocyte membranes occupied an area approximately double that of the original membrane when spread at the air/water interface. They proposed that the polar groups of the lipids faced outwards towards the aqueous media with the alkyl chains sandwiched in between (figure 1(a)).

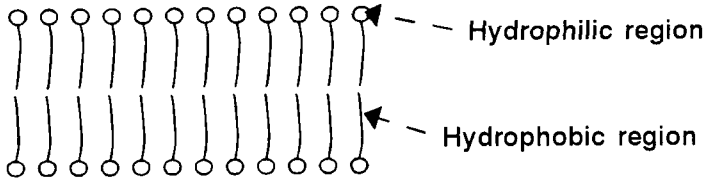

Figure 1(a) The bilayer structure proposed by Gorter and Grendal. The circles represent the hydrophilic region of a lipid and the lines attached are hydrocarbon chains.

Danielli and Davson in 1935 also proposed a bilayer of lipids but now added the idea of the interaction of proteins with the bilayer. They envisioned a lipid bilayer, as described above, sandwiched between layers of proteins (figure 1(b)). This was based on their observations that biological membranes appeared to have very low surface tensions compared to model lipid systems.

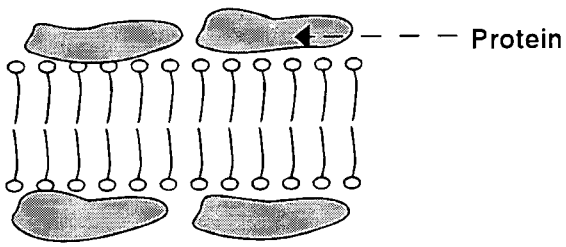

Figure 1(b) A lipid bilayer sandwiched between proteins, as proposed by Davson and Danielli

Destructive studies did give information on the variety of components within the membrane. Studies were hampered by problems of separation of the components once the membranes had been destroyed. The main breakthrough in this problem was by Claude in 1946, followed by de Duve in the 1950's who introduced the quantitative method of differential centrifugation.

Yet still no-one had actually seen the bilayer structure involved. For this a visualisation technique with a much better resolution than optical microscopes was necessary. This was found in the development of the electron microscope. These were first produced in the 1940's and 1950's and have a resolution of ~ 2 nm. By staining the polar groups of lipids the bilayer structure is plainly visible. Robertson in the late 1950's stated that all membranes did indeed follow the structure of Danielli and Davson. This was based on electron microscopy results and supported by X-ray diffraction data giving thickness and periodicity information.

The model proposed by Davson and Danielli and supported by Robertson failed to be consistent with later findings. In 1972 Singer and Nicolsen[13] proposed the 'fluid mosaic' model of a biological membrane. In their model the lipid bilayer is as proposed by Gorter and Grendal but proteins traverse the membrane. Thus a mosaic of proteins and lipids is formed as shown in figure 1(c).

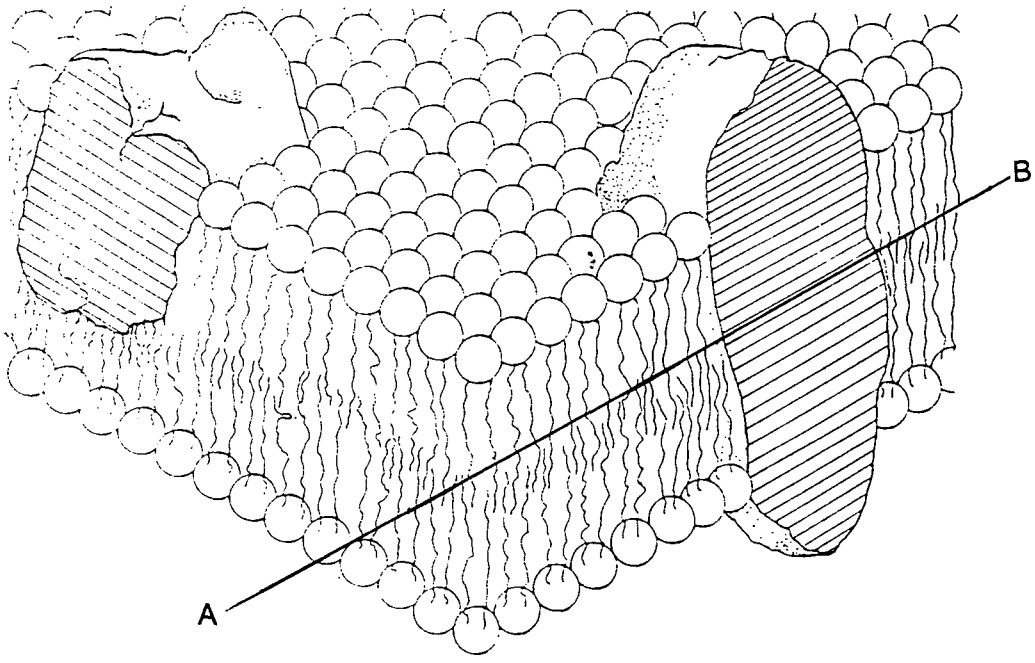

Figure 1(c) : The fluid-mosaic model proposed by Singer and Nicolsen. Reproduced with the kind permission of Blackie & Sons, London (reference 2).

The term fluid is used to suggest that the molecules move quite freely in a lateral direction, as if a liquid. There is limited motion between the two layers of the bilayer. This view of a biomembrane is now widely accepted as the correct structure. Scientists seeking to simulate a biological membrane try to emulate this structure.

Singer and Nicolsen's arguments were based mainly on thermodynamics and the properties of the lipid and protein molecules. Also a strong piece of evidence was electron micrographs of membranes freeze fractured along the dotted line AB shown in figure 1(c). In these the, proteins left in half a bilayer, can be seen as lumps standing proud of the lipids. They proposed that there were two types of membrane proteins. Those which were integral in the membrane (intrinsic) and those which peripheral (extrinsic). The peripheral proteins are not directly contained within the membrane but are associated with it. They can easily be separated by means such as the alteration of the ionic strength or a chelating agent. On the other hand, intrinsic proteins require the destruction of the membrane structure for their release.

1.2.2 Modelling the biomembrane

In the twenty years that have followed Singer and Nicolsen's fluid mosaic model, a variety of techniques have been used to try and understand biological membranes. Natural membranes consist of a large variety of components in different proportions depending on the purpose of the membrane. Some examples of membrane constituents are shown in table 1(i)[5]. It can be seen that biological membranes are complex. Their macroscopic properties are best comprehended by examination of natural systems. However, artificial membranes offer an opportunity to study inter- and intra- molecular interactions in a simpler environment.

As seen in table 1(i) phospholipids make up a large percentage of the constituents of most membranes. Therefore a large part of membrane simulation has concentrated on the production of bilayers for a variety of phospholipids. The effects of the interactions of proteins and cholesterol on these bilayers has been investigated by many research groups[14,30,31].

Lipid class	Plasma membranes	Nuclear membranes	Endoplasmic reticulum membranes Rough	Smooth	Gogli membranes	Lysomal membranes	Mitochon-drial membrane Inner	Outer
Cholesterol	25	10	6.0	8.5	6.7	14	2.5	4.5
Neutral lipids	16	15	10	8.5	34	17	13	12
Phosphatidyl-choline	18	44	55	47	29	24	38	41
Sphingo-myelin	13	3.0	3.0	10	7.3	24	2.0	4.0
Phosphatidyl-ethanolamine	11	17	16	18	11	13	21	19
Phosphatidyl-linositol	3.5	6.5	8.0	6.0	4.9	6.5	5.0	11
Phosphatidyl-serine	8.0	3.2	3.0	0	2.7	0	1.0	1.5
Diphosphatidyl glycerol	0	0	0	0	0	0	15	3.0
Other phospholipids	5.0	1.0	2.0	2.0	5.8	5.0	2.5	3.5

Table 1(i) : Lipid composition (in weight percentage) of sub cellular membranes, averaged from membrane preparations of mammalian cells. Taken from Oraganelles , by M.Caroll [5].

Several methods have been employed to produce a bilayer structure. Many rely on the self assembly of the lipids into ordered structures which depend on the nature of the lipid and the experimental conditions. Phase diagrams are available for the more common phospholipids[14]. The volume occupied by the lipid and its shape dominate the phase behaviour[15]. Not all of the phases are of a bilayer structure *e.g.* micelles, inverted micelles or the hexagonal cylindrical phase. Others have a multi-bilayer structure such as planar bilayers or multi-lamellar vesicles (MLV). Unilamellar vesicles (UV) are spheres formed by a single bilayer of lipids and they probably represent a cell membrane best. Though it could be argued that MLV's and planar bilayers are similar to some internal cell structures[2]. Some techniques for preparing the self assembled structures are described in a review by Bangham[16]. The theory of self assembly is given in the books by Cevc and Marsh[14]; and Israelachivili[17].

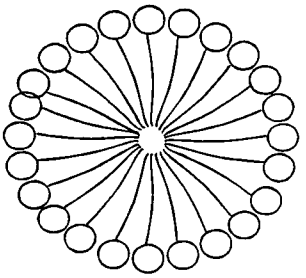

(i) Micelles

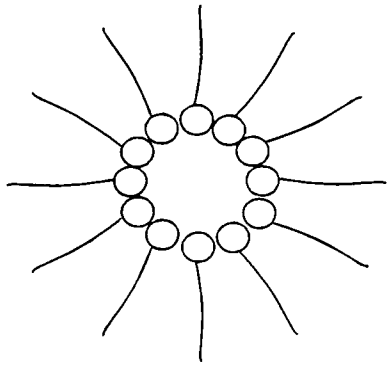

(ii) Inverted micelles

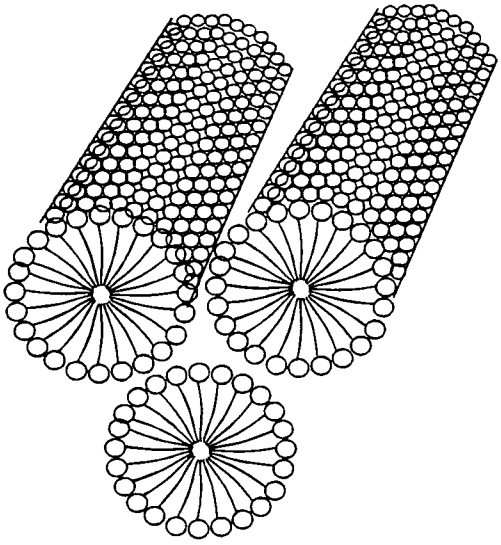

(iii) Hexagonal micelles

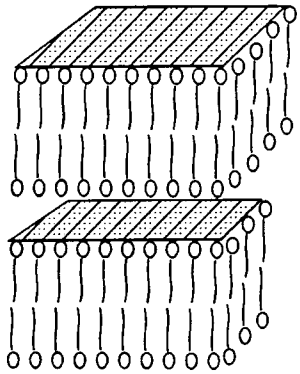

(iv) Planar bilayers

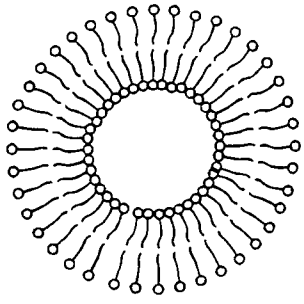

(v) Unilamellar vesicles

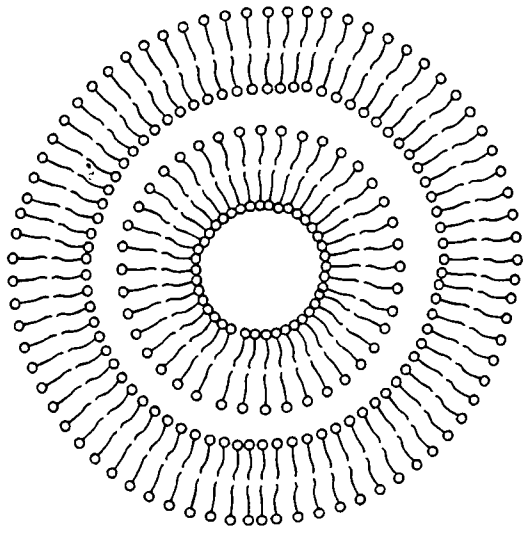

(vi) Multilamellar vesicles

Figure 1(d) : Self assembled phases of lipids.

There are also other techniques which create bilayer structures by imposing order rather than relying on self-assembly. One well established method is known as the black lipid membrane technique[1,7,11]. These artificial membranes are mainly used to perform electrical and transport measurements. A solution of lipid in a non-polar solvent is spread over a very small hole ~1 mm in diameter in thin polytetrafluoroethylene (PTFE) or 'Lucite' sheets under water. As the solvent drains, the membrane thins to a bilayer at the centre in an inverted soap bubble form *i.e.* a biological bilayer. The thinning to a bilayer can be followed by observing the interference colours, due to the thickness of the membrane, change to black.

An alternative method, which avoids the use of solvents[11], is to use a variation of Langmuir techniques. A very thin PTFE sheet with a small hole in it is placed between two chambers of water (figure 1(e-i)). On the surface of the water a layer of lipid is deposited. The sheet is then lowered through the surface of the water and as the holes pass through the monolayers a bilayer is formed. This technique produces bilayers which are stable for several hours.

Frey and Tamm[18] describe a technique which incorporates the imposed order of Langmuir-Blodgett deposition[19] with self-assembly. A monolayer of a phospholipid was deposited, by Langmuir-Blodgett deposition, onto a hydrophilic substrate. Unilamellar vesicles, made by sonication, were then flowed past the deposited monolayer. Some of these spontaneously fused with the monolayer to produce a bilayer (figure 1(e-ii)). A similar method is to covalently link a lipid monolayer to a substrate, by alteration of the head-group, and then deposit a second layer via Langmuir-Blodgett techniques[20], or other methods such as vesicle fusion.

Another technique involving Langmuir-Blodgett films is the patch-clamp method. Whereby a pipette tip is passed down through a monolayer, deposited at the air-water interface (figure 1(e-iii)). On removal there is a monolayer suspended across the mouth of the pipette by surface tension. The tip is then pushed slightly into the monolayer and a bilayer is formed so long as the pipette is kept in place[20].

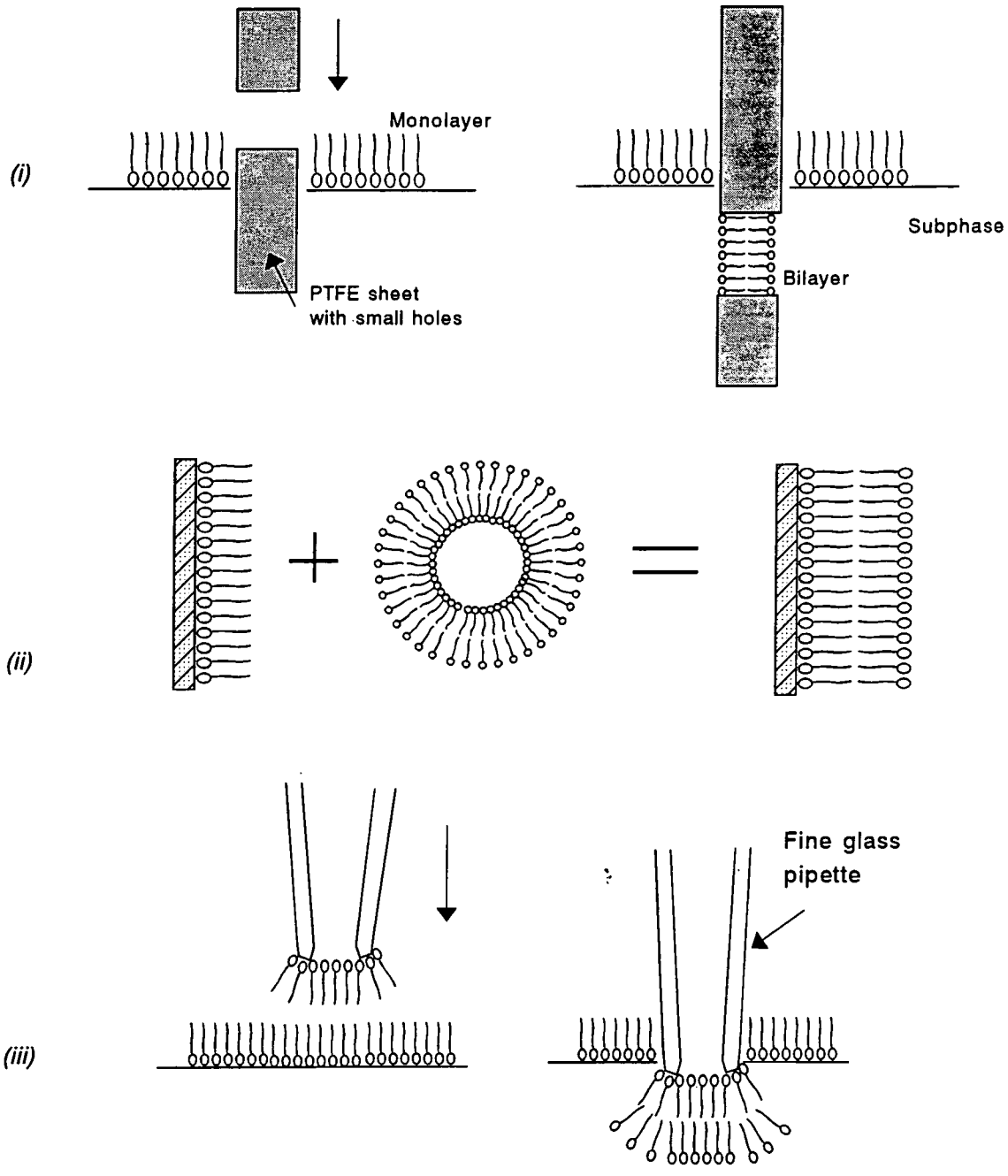

Figure 1(e) : Examples of the different techniques which can be used to fabricate a lipid bilayer.

A monolayer of lipid can be deposited by vertical Langmuir-Blodgett deposition[19] onto a hydrophilic surface. Then a second layer can be deposited via a horizontal deposition technique[22] (Langmuir-Shaeffer deposition) to give a biological bilayer structure (figure 4(1)).

Most of the imposed order techniques can be used to produce bilayers with an asymmetric distribution in the composition of lipids on either side of the bilayer. Thus they can mimic a biomembrane more fully in this respect[23]. However several of them are deposited onto a solid substrate so it is difficult for the bilayer to be completely enclosed in an aqueous environment.

With all of the techniques described it is possible, by alteration of the method, to incorporate peptides, and sometimes proteins into the bilayer structure. One of the most common techniques used is to form the bilayer then to absorb proteins from solution. Sometimes an electrical current is required to cause the protein, or poly-peptide to be inserted across the bilayer, rather than adsorbing at the bilayer-water interface[3]. Another method is to try and ensure that protein is incorporated into the bilayer structure on formation[90].

1.2.3 Techniques for the study of biomembranes

Most analytical techniques impose restrictions on the type of sample they can be used to examine. Therefore, the choice of bilayer preparation is largely dependent on the subsequent proposed experiments. A large variety of analytical techniques are available for the study of bilayers. Each technique gives different information on the nature of the bilayer. Often the biggest problem faced by researchers is collating the information available and comparing different sample preparation and analytical methods to give an overall description of a particular bilayer system.

There are several books which give overviews of techniques used to study biomembranes. A selection of these were used to prepare the following examples of some of the possible methods for biomembrane study (references 1,2,5-7,11,14,15,24-27). Most of the methods are used because they are thought to be non-destructive. Given below is a brief outline of the information which can be derived from a variety of techniques.

Many of the methods can be utilised to monitor the lipid phase transition temperature. The phase transition is from a gel state to a liquid crystalline phase. In the gel state the hydrocarbon chains are constrained in a fully extended trans conformation. As the temperature rises there is a point at which gauche bonds can form in the alkyl chains and contract and this is known as the phase transition temperature. There is also evidence that the bilayers undergo a pre-transition state where only the very ends of the chains can change conformation and the bilayer, if able to, forms a ripple structure[28]. Figure 1(f) illustrates the transition process in a planar bilayer.

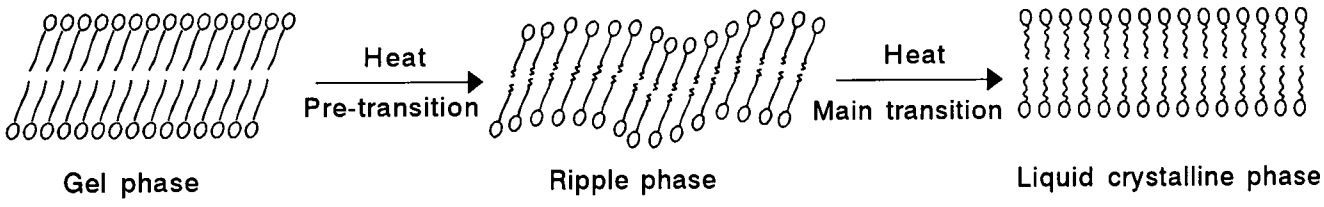

Figure 1(f) : Phase transitions with temperature of a bilayer of lipid in water. (Levin[28])

(A) X-ray diffraction has two main uses in the study of membranes. The first is X-ray crystallography. Some of the molecules which are found in biomembranes can be successfully crystallised and their full three dimensional structure determined. However, very few membrane components can be crystallised, especially the proteins. This is because in a bilayer the protein is able to adopt a conformation such that its non-polar regions are within the hydrocarbon chains of the lipids and the polar regions are in aqueous solution. This variety of environments is not available if the protein is crystallised on its own. Indeed, even if the protein can be crystallised there is some question as to whether the determined structure is indeed the same as in the biomembrane.

The second use of X-ray diffraction for the study of both real and simulated membranes is to elucidate information on the periodicity of the structure. This gives information such as the bilayer thickness and the repeat distance between layers in a multi-lamellar system. This can be used to follow the lipid phase transition because the bilayer contracts when the temperature is raised above that required for the transition.

(B) Neutron and electron diffraction can yield similar information to X-ray diffraction. Neutron diffraction is useful because the neutrons are deflected by nuclei rather than the electron clouds. Deuteration in neutron diffraction studies can give extra data compared to that obtained from X-rays. In particular, the effect of hydrogen atoms can be seen directly rather than inferred from the rest of the data. However it is expensive, so limited studies have been carried out. Electron diffraction can give information concerning very small areas of a sample (~10 nm) but there is always some doubt about the results as the technique requires a very high vacuum. There may be damage to the membrane structure because of the removal of water.

(C) Electron microscopy is a very useful technique for the study of membranes. Particularly when combined with techniques which enhance the contrast such as freeze fracture and fixing particular molecules, or parts thereof, with a dye. Freeze fracturing removes one leaflet of the lipid bilayer but leaves the other layer of lipid with the proteins embedded in it. It can also be used to open up MLV's to reveal the onion like layers within layers.

The use of electron microscopy in deciding the plasma membrane structure has already been mentioned in section 1.2.1. Electron micrographs can be used to find the size and structure of aggregates such as MLV's and UV's produced by self assembly techniques.

When electron microscopy is combined with electron diffraction it is possible to elucidate the three dimensional protein structure as with X-ray crystallography, if the proteins are in two dimensional crystals.

(D) Circular dichroism (CD) can be used to determine the secondary structure of a protein. It relies on the measurement of the difference in absorption between left and right circularly polarised light. It can give the percentage content of α, β and random coil content of a membrane protein. However, the uncertainty in the analysis of the results increases if the protein is embedded in a lipid bilayer. Conformational changes in the protein are detectable so it is possible to compare the secondary structure of proteins when both complexed and uncomplexed. Lipids are difficult to study via circular dichroism so it needs to be used in conjunction with other techniques for the analysis of all the membrane components.

A related technique is optical rotary dispersion. This relies on the measurement of the optical activity of samples by the rotation of linearly polarised light as it passes through . This measures changes in the refractive indices of the sample which is very sensitive to the conformational changes in proteins. However, circular dichroism is preferred by most researchers as the results obtained can be interpreted with more certainty.

(E) Differential scanning calorimetry is particularly useful for the detection of the lipid phase transition. The change is endothermic and highly dependent on the exact mixture of lipids, water, and also the macroscopic phase, *e.g.* planar bilayers or vesicles. A small absorption of heat can be detected at the pre-transition temperature and this can be detected. A natural membrane will have very broad phase transition peaks due to the presence of a complex mixture of lipids and proteins and the presence of metal ions All of these factors mean that there is a variety of different environments even for one type of lipid and with the range of lipids there is also a variety of transition temperatures.

(F) Fluorescence probes can be added to the simulated membranes. These can be used to monitor phase transitions and can give information on the fluidity of the bilayer, *i.e.* how much lateral movement occurs. Most probes give fluorescence due to the presence of lipids but it is possible to use ones which fluoresce due to protein proximity. Indeed, some proteins contain tryptophan residues which are themselves fluorescent. By following the fluorescence intensity conformational changes can be seen but only if the residues environment is altered.

Diffusion coefficients of molecules within the biomembrane can be calculated by the use of fluorescence correlation spectroscopy or fluorescent photo-bleaching recovery. In the first case the intensity changes in fluorescence of a small area can be followed as the number of molecules alters. In the second there is no fluorescence from the bleached area until unbleached molecules diffuse into it.

Another technique is resonance energy transfer which relies on labeling with two different chromophores on the proteins. The transference of energy from one to the other is monitored as the proteins aggregate. Again this is a measure of lateral diffusion.

(G) Nuclear magnetic resonance (NMR) can be used for a variety of nuclei in biological membranes. The most commonly used are ^{1}H and ^{31}P nuclei but studies of enriched molecules have been performed using ^{2}H and ^{13}C nuclei. NMR is useful for elucidating the macroscopic phase of a system. This is due to the fact that NMR spectra are influenced by the freedom of motion available to a molecule. Thus if molecules are constrained in a planar bilayer structure broadening occurs and a change in shape of the signal. Different effects are seen for the variety of self-assembled phases possible. Also the effects of different environments on inner and outer lipids *e.g.* pH or other ion gradients can be observed in closed systems, such as vesicles.

Recently it has been possible to use advanced NMR techniques on small proteins, with substituted nuclei as labels, to determine the three dimensional structure[29].

(H) Electron spin resonance (ESR) requires the presence of a probe with an unpaired electron. Generally nitroxides are used. The rate of exchange of spin influences the widths of the peaks and the hyperfine splitting in the spectra. Levels of spin probe doping are therefore carefully chosen so that in a mixture of lipids if phase separation occurs it can be detected by the partition of the probe into one of the phases. To give the desired effect concentrations of the probe may need to be very high and can disrupt the membrane system.

Lipid lateral diffusion constants can be found using ESR, as they can with fluorescent techniques. ESR can also yield information on the movement of lipids from one side of a bilayer to the other. If the layers of lipid can be selectively exposed to ascorbic acid, which damps the ESR signal, then the study of the movement of the lipids across the bilayer leaflets is possible.

(I) Vibrational spectroscopy can be used for a variety of purposes in the study of biomembranes. The advent of Fourier transform infrared spectroscopy (FTIR) and the use of lasers in Raman spectroscopy have enhanced the uses of vibrational spectroscopy for the study of biological molecules (see Chapman et al[30] for a review). This is due to the greater sensitivity that has been developed in these techniques over the last twenty years. Both FTIR and Raman spectroscopy excite vibrations between the individual atoms within a molecule. Both can give information on the conformation and local environment of molecules. The vibrational frequency and band widths in both techniques are sensitive to the environment of molecules.

By following either the change in frequency or a ratio of band intensities it is possible to use either Raman or FTIR spectroscopy to investigate both the main lipid phase transition and the pre-transition[29]. Recently it has become possible to determine the secondary structure of proteins with both techniques whilst the proteins are still within a lipid bilayer[31]. However FTIR analysis of such systems can be difficult because water has a very strong absorption at the same frequency as one of the most important bands used in the assignment of protein conformation. It is possible to overcome this problem via a variety of methods, one of the most popular is to use D_2O, since the equivalent absorptions to those in H_2O are shifted to a lower wavenumber and thus no longer interferes with the analysis of the protein band. Both FTIR and Raman require fairly high concentrations of proteins compared to most of the other analytical methods mentioned previously (mM rather than μM as in circular dichroism *etc.*).

Vibrational circular dichroism has recently been developed[29]. As for visible light CD, it relies on the difference between right and left polarised radiation but in the infrared region of the spectrum. It can be used to examine minute changes in protein structure.

It is possible to perform vibrational analysis on the nano-second time scale and thus to follow conformational changes in proteins kinetically, but only if artificially slowed by low temperatures.

(J) The transport properties of ions and water across membranes are of paramount importance because this is one of the specialised functions that trans-membrane proteins are thought to perform. Schultz[32] provides a theoretical text on this subject. A multitude of experiments have been used to study the effects of transporting different ions across a variety of membranes, both real and simulated. For transport to occur a carrier ion is often required to travel with the main component being transported.

Some transfer processes do not require the use of energy, this is known as passive transport. Active transport processes require energy before they will happen. This is often provided in the form of a change in electrical potential. In both cases selectivity occurs, *i.e.* some ions pass through the membrane faster than others. Stein[3] provides a description of the role of proteins in transport.

(K) Electrical measurements such as the conductance of biomembranes are important because a potential is developed across membranes during transfer processes. These potentials are maintained by the selective transport of ions by membranes causing an electrical imbalance between the inside and outside of a cell. This ion/charge gradient can act as a potential energy source for a cell. In particular it is used during adenosine triphosphate (ATP) synthesis[4].

Through electrical measurements of artificial membranes Cifu et al have observed the opening of a single ion channel[33].

The electrical properties of biomembranes can be measured either directly by micro-electrodes or by following the ion concentration itself by techniques such as observing the distribution of a dye.

(L) The elastic properties of a bilayer can be measured for model systems. This information can be used to predict how lipid layers oppose applied stress. These measurements can also be used to understand the morphology of membranes. The elastic response of a membrane can be related to the dynamic molecular properties of the constituents such as the moduli of compressibility. The Langmuir technique is often used to monitor the stress response of monolayers (see chapters 4&5).

(M) Theoretical studies of bilayers are beginning to approach the level where they can be compared to the results obtained by experimentalists. It is now possible to take simulation of ~1000 molecules, similar in nature to lipids[20], and follow their interactions via a computer calculation. This type of simulation requires enormous amounts of computing time just to follow it for exceedingly short periods of time (ps). As computational power increases it can be expected that theorists will be able to achieve even more accurate simulations.

1.3. AIMS AND REASONS FOR THE RESEARCH GIVEN IN THIS THESIS

1.3.1 Aims

To simulate a biological bilayer structure and to study the conformations and interactions of phospholipids and peptides, via FTIR.

1.3.2 Spectroscopic techniques

Of the techniques outlined in section 1.2 only a few are able to investigate the structure of the individual molecular components within a membrane. Such fundamental information is necessary in order to understand why molecules self-assemble into biomembrane structures and how they function once there.

Diffraction techniques require crystals of pure material to elucidate the molecular structure. These are very difficult to obtain[35]. More success has been achieved with the determination of the crystal structure of lipids[24]. As crystals of pure materials are required for diffraction techniques the structure of molecules within a bilayer cannot be found using these methods.

CD spectroscopy is widely used to find the secondary structure of proteins[29] but cannot be used to study a whole membrane as the lipids are not easily detectable. Also there is a problem of light scattering from membranes which reduces CD's usefulness. There are also some protein conformations between which it cannot distinguish[30].

The use of NMR spectroscopy to the study of proteins is limited to small proteins with a molecular weight less than 15000 g/mole and requires isotopic substitution of nuclei which is expensive[30]. This technique is difficult to use in the presence of a bilayer due to broadening effects caused by the removal of isotropic motion.

Vibrational spectroscopy has in the past suffered from a poor signal to noise ratio but this has been overcome recently with the advent of Fourier transform (FT) techniques. FTIR is now well established whilst FT Raman is still in its development stage. For conventional Raman instruments there is still a problem with the sensitivity when examining small amounts of material such as single bilayers.

FTIR and Raman spectroscopy can both be used to study both proteins and lipids in a biological bilayer structure. Simulated membranes can be used to study the interactions of proteins and lipids in biomembranes. FTIR has one large drawback in the study of biological systems : the large absorption in regions of spectral interest by water. This is a particular problem for the study of proteins as the amide I band is found at the same frequencies and the H_2O bending mode[30]. However techniques are now available[35-37] for reducing the relative amount of water sampled such as internal reflection sampling methods (for a review see Mirabella[39]) and reduction in the path lengths of cells in transmission[30]. The use of computerised techniques for the spectral subtraction of water has also increased the ability to remove the interference of the water. Another option is to perform the experiments with D_2O as its absorption due to the bending vibration is shifted to lower frequencies. However as proteins are very sensitive to alteration in hydrogen bonding this may affect the structures found.

The papers by Chapman et al[30], Parker[40] and Mendelsohn & Mantsch[31] are recent reviews on the possible uses of FTIR in the study of biological molecules. More current research is contained within reference 29. One of the most useful advantages in the study of proteins via FTIR has been the development of resolution enhancement techniques[41,42].

By comparison with X-ray data for a variety of well characterised proteins several methods have been developed to correlate infrared spectra with protein conformation[35,43-47]. These can then be used to determine the structure of proteins which cannot be crystallised or are within a biological bilayer.

There have been a variety of IR studies on phospholipids these include references 24,28,32,40,48-59. A lot of work has also been done by scientists interested in lipid-protein interaction (references 18,30-32,45,60-70). Many of the findings of these researchers relate to the work carried out in this thesis and were used to aid the analysis of results found.

A literature search was carried out, which was extensive but obviously not exhaustive. It was found that in very few studies of biological molecules had researchers set out to produce a well characterised single bilayer structure and then observe the interactions via FTIR.

The exceptions found were references 18,63,69&70. Mendelsohn et al[63] have studied the lipid phase transitions of large unilamellar vesicles (LUV's) made from dimystroyl-phosphatidylcholine (DMPC). Takenaka et al[69] have made small unilamellar vesicles (SUV's) of egg yolk phosphatidylcholine (PC) which were studied via polarised attenuated total internal reflection (FTIR-PATR) to follow the interaction of egg lecithin vesicles, produced by sonication, with antibodies. Frey and Tamm[18] used the FTIR-PATR technique to study bilayers of lipids made by the combined Langmuir-Blodgett and vesicle fusion technique. The interaction of the lipid with a peptide melittin was studied. Mantsch et al[70] have reported the production unilamellar vesicles from bovine brain phosphatidylserine (PS). These have been used to study the lipid phase transition and the conformation of glycophorin via FTIR.

1.3.3 Brief overview of research to be presented in this thesis

As seen above very few FTIR studies of well defined biological bilayer structures have been undertaken. It was therefore decided to produce well defined phospholipid bilayers, with peptides incorporated into them and study the system via FTIR.

The first method of bilayer preparation used was to try and assemble one by the use of Langmuir-Blodgett (LB) deposition. This technique was chosen because it is possible to use the deposition ratios to verify the fact that a bilayer has indeed been made. Very few FTIR studies of biological molecules prepared by the LB technique have been undertaken. These include Lotta et al[59] and Takenaka & co.[21] who have both studied dipalmitoyl phosphatidylcholine (DPPC) via FTIR-ATR but not in bilayers. Yarwood and Petty et al[34,90] have studied dipalmitoylphosphatidic acid (DPPA) multilayers, again via FTIR-ATR but have not tried to prepare a biological bilayer structure.

The samples prepared by LB methods in this study were then examined by two surface sensitive FTIR techniques - RAIRS (reflection-absorption infrared spectroscopy) and PATR to determine the molecular conformations and orientations. Specialised PATR equipment, designed and constructed in Durham, for the study of very small amounts of sample was utilised. Although it was not possible, generally, to have aqueous media on both sides of a bilayer fabricated via Langmuir-Blodgett deposition, studies on the effect of placing the samples in water were carried out.

Oligopeptides were to be incorporated, as a simple model for proteins. Alamethicin in particular was studied (see chapters 5 & 7), an oligopepide which forms ion channels by aggregation[71]. This is similar in principle to the supposed formation of an ion channel by a single protein which spans a membrane several times[2].

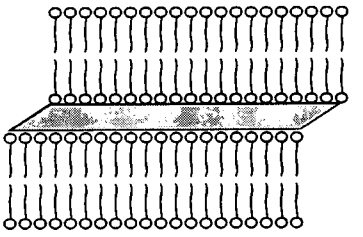

Figure 1(g) : A biological bilayer deposited onto an ATR crystal.

As a comparison a second system was studied, in which the lipid bilayer structure closely resembled a cell plasma membrane. This was large unilamellar vesicles (LUV's) self-assembled in aqueous solution. In this case both sides of the bilayer are surrounded by water. LUV's were chosen as they mimic a cell membrane more fully than SUV's as the curvature of the bilayer in a true membrane is usually very shallow[14]. In SUV's the molecular interactions are possibly influenced by the constraint of the tight curvature.

The vesicles were fabricated in an aqueous environment and small path length, temperature controlled FTIR transmission spectra were recorded. Again oligopeptides were added to study the effects on the phospholipids.

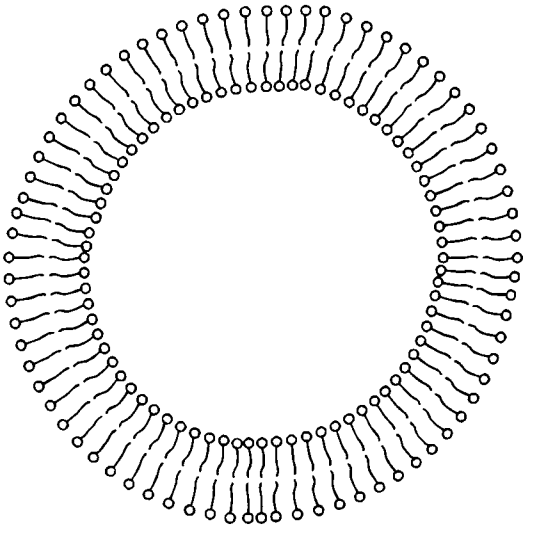

Figure 1(h) : A unilamellar vesicle

CHAPTER 2

BACKGROUND AND DESCRIPTION OF EXPERIMENTS ON VESICLES

2.1 INTRODUCTION TO UNILAMELLAR VESICLE STUDIES

The main objective for this part of the project was to use FTIR to study the interactions of lipids and proteins in large unilamellar vesicles (LUV's), in order to model a cell membrane.

The technique of detergent removal by gel filtration was chosen for their fabrication as a review by Allen et al[72] shows that it is possible to produce LUV's of the order of 100-150 nm, in diameter, with low poly-dispersity. In comparison the paper by Hope et al[73] shows that vesicles produced by probe sonication are usually 25-30 nm in diameter The process of freeze-thaw cycles can increase this to 80 nm but does not always produce LUV's reliably and there is a high dispersity in the sizes made[73]. Recently the technique of obtaining LUV's by extrusion methods has been developed, by Hope et al[23,74] to the stage where it possible to produce LUV's in the range 60-100 nm with relative ease. However there is still a wide diversity in size and specialised equipment is required.

Once aggregates had been made, it was necessary to prove that LUV's had indeed been produced. In order to achieve this two techniques were employed. ^{31}P NMR was used to prove unilamellarity[73] and photo-correlation spectroscopy (PCS) was utilised to measure their size and dispersity. ^{31}P NMR and a dye entrapment experiment were used to investigate the stability of the system with time.

2.2 GEL SEPARATION FOR THE FORMATION OF LUV'S

Sephadex G50 fine polymer beads (these beads capture particles with an average molecular mass less than 10000 g) were hydrated with a pH 7.4 buffer. This gel was placed in a 20 cm X 1.5 cm^2 glass column with coarse sintered glass in the base (figure 2(a)), to allow liquids through. The column of sephadex gel was allowed to settle and then rinsed with 100 ml of buffer solution. The buffer solution used initially was phosphate based (8.7 mM KH_2PO_4 with 30 mM Na_2HPO_4)[75]. However, this was found to interfere with the NMR experiment (section 2.5) so Hepes, a well known biological buffer (figure 2(b)) was used at a concentration of 20 mM. This was made up as a solution and then sodium hydroxide was added to adjust the pH to ~7.4. 150 mM potassium chloride was added, to give the correct electrolyte concentration.

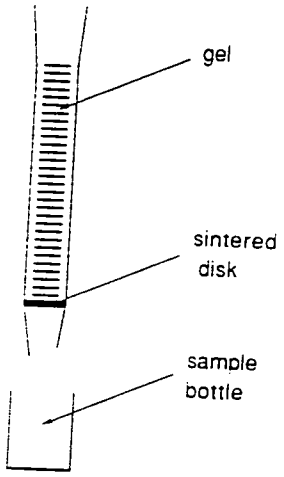

Figure 2(a) : The sephadex column.

It was first necessary to determine the void volume of the column (this is the volume of liquid which is eluted before even the largest particles can pass through). This was found by using a 0.2% by weight solution of the high molecular weight dye, dextran blue. 2 ml were placed at the top of the column and then eluted with water.

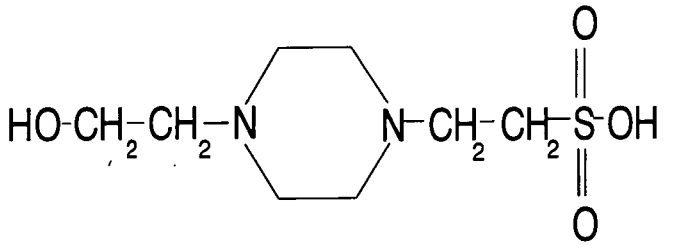

Figure 2(b) : Hepes - a biological buffer.

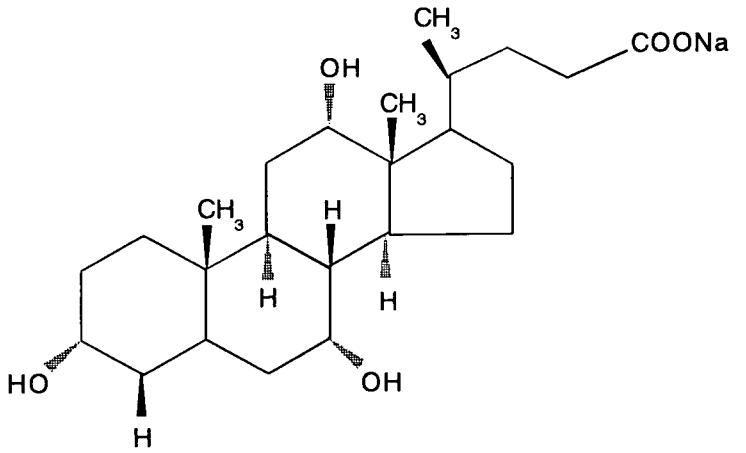

Figure 2(c) : The detergent, sodium cholate.

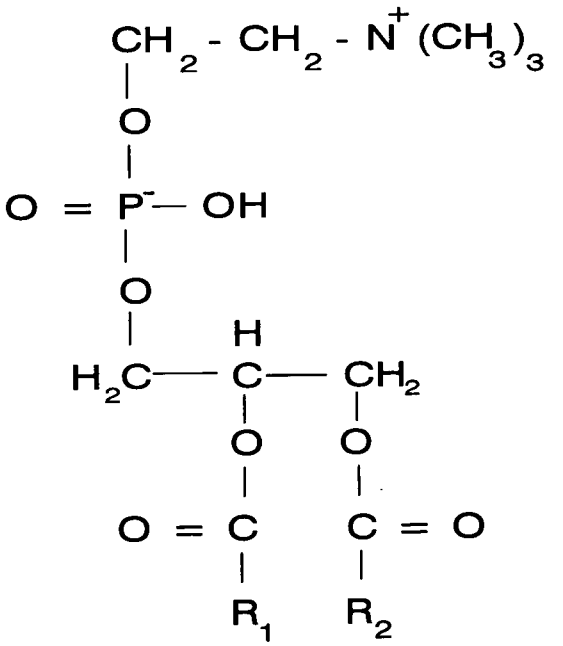

Figure 2(d) : The general structure of a phosphatidylcholine.
For egg lecithin R_1 and R_2 are hydrocarbon chains of different lengths and with a high degree of unsaturation.

30 mg of lipid, dissolved to 1 mg/ml in chloroform were placed in a boiling tube. The lipid used was egg lecithin, a naturally occurring phosphatidylcholine (PC) extracted from egg yolk. Each molecule has two different hydrocarbon chains. There is a high level of unsaturation amongst them. In the experiments in which peptide was added ~3 mg of the particular peptide were dissolved in chloroform and the solution was mixed with the lipid solution. This gives a lipid : peptide weight ratio of ~10:1. The chloroform solution was evacuated whilst being rotated, to give an even layer on the base of the tube. The evacuation was continued for at least three hours, to ensure complete removal of the solvent.

The detergent, sodium cholate, was weighed and dissolved in 2 ml of the same buffer used to prepare the sephadex column. Initially, the amount of detergent used was 22 mg (26 mM) but this was altered to 156 mg (190 mM)(see chapter 3). This was added to the dried lipid to form mixed micelles of lipid and detergent[76]. This process lasted half an hour and was carried out under nitrogen and aided by manual agitation. The lipid/detergent solution was placed at the top of the sephadex column and eluted with buffer. The void volume was collected as a single fraction. Thereafter, the fluid eluted was collected in fractions of ~2 ml. The air above each fraction was replaced with nitrogen. The contents of each fraction were analysed by use of FTIR.

2.3 ENTRAPPED DYE EXPERIMENT

2.3.1 Introduction

If the vesicles are integral, *i.e.* they do not allow the passage of material between the inside and the outside and *vice versa*, it should be possible to develop a pH gradient between the interior and exterior media. If a pH sensitive dye is present then the pH within the vesicles can be monitored visually.

The vesicles can be prepared in the usual fashion at a given pH with dye present. The external fluid is then replaced by a buffer of different pH by elution on a gel filtration column of different bead size. This prevents the disintegration and reformation of the vesicles.

2.3.2 Description of the dye entrapment experiment

A solution of sodium cholate with phenyl red (a pH indicator) was made in Hepes buffer. 1 ml of this was used to hydrate 25 mg of lipid. This was then eluted on a sephadex G50 fine column at pH 6. It was then passed through a sephadex G25 column at pH 8. A small amount was removed and iso-propyl alcohol (IPA) was added. This destroys the integrity of the vesicles. The rest was left over night, in the dark. It was visually examined the next day and then IPA was added to destroy the vesicles.

2.4 PHOTO CORRELATION SPECTROSCOPY (PCS)

2.4.1 Introduction

PCS is a modern technique based on the inelastic scattering of laser light. PCS involves the measurement of the increase in width of the incident light frequency which has been Rayleigh scattered[77]. The scattering of the light is caused by fluctuations in the dielectric constant of the media being measured. The intensity, angular distribution, polarisation and frequency shift of the scattered light are determined by the size, shape and molecular interactions of the scattering centres. A variety of information can be derived using PCS including rotational and translational diffusion coefficients, and the internal motional dynamics of macromolecules.

However, for those with a simpler aim in mind the equipment can also be used to estimate the size and dispersity of colloids in solution. The actual process derives the size distribution from the diffusion coefficients and assumes that the particles are spherical.

2.4.2 PCS Experimental description†

2 ml of the fraction containing the highest concentration of lipid, (determined by FTIR), were placed in a quartz tube ~0.5 cm diameter. This was inserted into the sample compartment of a Malvern 4700 spectrometer. This has an Argon ion laser source set at 488 nm. The sample was centred in the beam. Scattered light was collected at an angle of 90° to the straight through beam. The solvent was assumed to have the same characteristics as pure water, despite the presence of buffer : viscosity = 0.893 g $m^{-1}s^{-1}$, refractive index = 1.33, temperature = 25 °C.

† These experiments were performed by J.Holland in my presence.

2.5 PHOSPHORUS NUCLEAR MAGNETIC RESONANCE (^{31}P NMR)

2.5.1 Background

Each phospholipid molecule has one phosphorus atom which should contribute approximately the same emission intensity as any other in the ^{31}P NMR spectrum. The precise environment will influence the peak shape and chemical shift but at the noise levels present in the original spectra any differences would be difficult to discern (plot 3-5).

If the vesicles are integral then the addition of paramagnetic materials to the solution should only have a major effect on the phosphorus NMR signal of the lipids in the exterior layers (figure 2(e)). Therefore, if a paramagnetic ion, such as Mn^{2+} is added to the solute the ^{31}P NMR signal from these outer groups will broaden but that due to the inner groups will remain unaffected until exchange, either of the lipids or the ions, occurs[73].

If the aggregates are unilamellar and integral then ~50% of the lipid head groups will be in contact with the outer media containing the paramagnetic ions. Whereas, the other 50 % will be shielded from the effect of spectral broadening[74]. If the aggregates are multilamellar a higher proportion of the lipid will be shielded.

Therefore the use ^{31}P NMR should make it possible to tell whether the vesicles are unilamellar. The decay in signal over time can show the rate of exchange of $MnCl_2$ between the internal and external media, surrounding the vesicles.

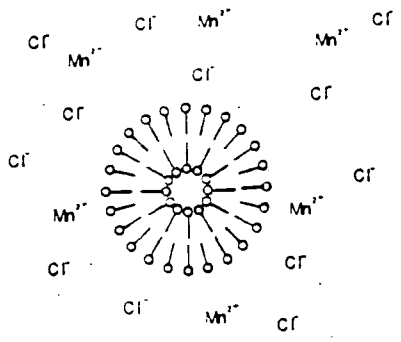

Figure 2(e) : A vesicle in manganese chloride solution.

2.5.2 Experimental description for ^{31}P NMR studies

315 mg of triphenylphosphine oxide (TPO) were dissolved in 10 ml of 2-methylpropan-1-ol. A small amount of this solution was sealed in capillary tube, which was then placed into a 10 mm NMR tube, to act as an external reference.

The two fractions containing the highest concentration of lipid were mixed together and placed in the NMR tube. A Bruker AC250 operating at 101.26 MHz, for phosphorus, was calibrated using phosphoric acid as a reference for the exact chemical shift. The sample was then placed in the NMR machine and spun at 16 revs. s^{-1}. 1024 pulses were applied giving an average free induction decay (FID) which was then Fourier transformed to give a spectrum.

The integration of both the reference and the sample peaks was undertaken and thus the relative areas measured. Three such spectra were taken to obtain an average intensity and an estimate of the precision. The sample was then removed from the spectrometer and 2 mg of manganese dichloride were added (4 mM). The sample was immediately replaced in the NMR machine and a spectrum obtained. Spectra were taken at ~20 minute intervals over a period of several hours and a final reading was generally measured the next day.

For all of the spectra the intensity of signal for the lipid was divided by that for the reference TPO. This ratio was then used as a relative intensity to compare spectra before and after the addition of $MnCl_2$. An external reference is needed to provide a relative measure of the peak integration between different spectra because the absolute intensity in NMR is very dependent on the precise experimental conditions. Even recording spectra consecutively, without removal of the sample can give varying values.

As a control experiment the vesicles were destroyed by addition of IPA and their NMR spectra recorded before and after the addition of $MnCl_2$.

2.6 FOURIER TRANSFORM INFRA-RED SPECTROSCOPY (FTIR)

2.6.1 Introduction

(A) FTIR instruments :

FTIR instruments are based on the Michelson interferometer[78]. Figure 4(f) shows an example of a FTIR spectrometer. Collated radiation from the source (S) passes through a beam splitter (B), usually a half-silvered potassium bromide plate, producing two mutually perpendicular beams. Each of these is reflected off a mirror (M_1 and M_2). If M_1 traverses a distance x away from the beam splitter, then on recombination with the other beam there will be a phase difference and an interference pattern will be formed. Each frequency has its own interference pattern with constructive interference at values of x which are integral multiples of wavelength. These combine, over the frequency spectrum, to form an overall interferogram[79].

In order to record all the information necessary the mirror has to move in steps less than half the shortest wavelength. In most modern FTIR spectrometers, including the Mattson Sirius 100 which shown in the diagram (figure 4(f)), the mirror moves continuously. However, the computer cannot cope with data in an analogue form and needs a reference for digitisation. This is provided by a Helium-Neon laser. The light from this passes through a different part of the interferometer at the same time as the main IR beam. It is separately monitored by a dedicated detector. By using the sine wave interference pattern produced from the monochromatic laser the path difference of the mirrors can be measured in terms of the laser wavelength. By conversion of the sinusoidal laser intensity into a square wave the signal can be used to trigger data acquisition.

The interferogram can be converted back to the frequency domain by use of a mathematical relationship known as a Fourier transform[78]. :

$$F(\bar{\nu}) = \int_{-\infty}^{\infty} f(x)\exp(-2\pi i\bar{\nu}x)\,dx \qquad \textit{Eqn.}\ (2.i)$$

Whereby two dependent variables can be related to one another. Until the advent of widely available high-powered computers the solution of the above was not feasible practically. However now both computers and software to perform fast Fourier transforms are widely available and affordable.

If a sample is now placed between the interferometer and the detector absorptions will take place which will lower the intensity of given frequencies, such that when the interferogram is Fourier transformed an emissivity spectrum is formed with drops in intensity corresponding to the absorptions. When this is ratioed against the background emissivity a normal absorption spectrum is seen.

The main advantages of using FTIR as opposed to a dispersive IR are that all the frequencies are sampled at once, giving a higher through-put and less noise *i.e.* greater sensitivity is achieved. The spectra take ~1 second to gather compared with ~15 minutes for an entire dispersive IR spectrum. These advantages are particularly important for very dilute samples as many spectra can be co-added to improve the signal to noise ratio. This is due to the fact that if a large number of interferograms are co-added random noise will superimpose to give an overall reduction in intensity compared to the signal. However, a dispersive instrument has one advantage, over the FTIR machine used, in that most dispersive instruments have two beams - one for a background and one for the sample. This would alleviate the problem of water vapour in the spectra.

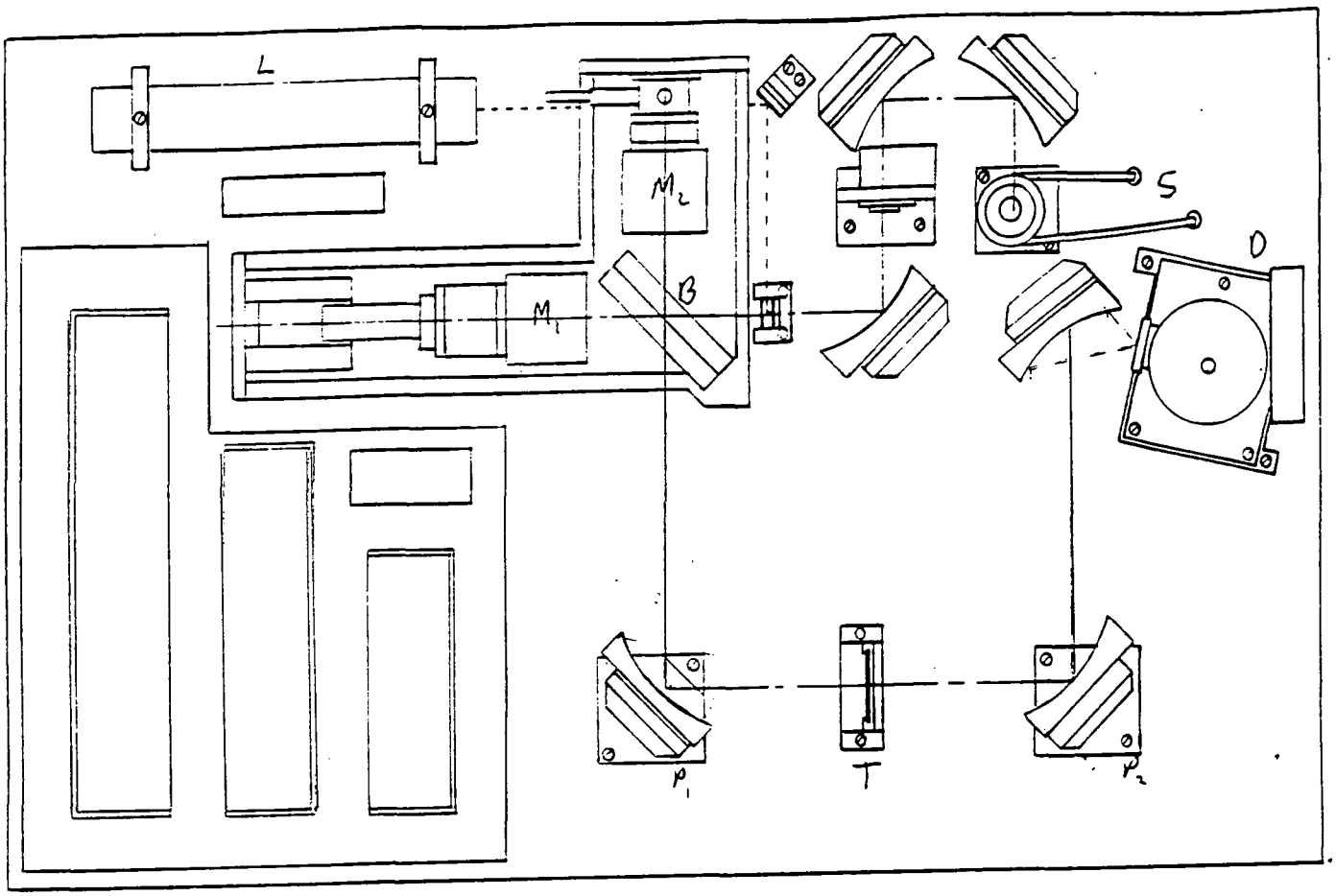

Where : S = source

M_1, M_2 = the mirrors

D = detector

T = sample

B = beam splitter

L = laser

P_1, P_2 = exchangeable mirrors in the sample compartment

Figure 2(f) : A schematic of the Mattson Sirius 100 FTIR spectrometer, drawn by T.D.Harrison.

(B) Absorption ratios

The spectra obtained after Fourier transformation are in the form of emissivity *i.e.* the radiation from the source modified by the absorption of the sample. As the source does not emit evenly over the entire range of frequencies this gives a frequency dependent weighting of spectral intensity. Also as the amount absorbed by the sample may be very small compared to the total output of the source it is very difficult to see the spectrum of the sample. A solution to both of these problems is to ratio two emissivity spectra. One of which contains the sample to be studied the other a similar system but with the sample absent. The following ratios can be used. :

$$\underline{T}\text{ransmittance} = \%\text{ transmitted} = {}^{I}/_{I_o} \times 100 \qquad \textit{Eqn.}\ (2.ii)$$

I = emissivity of the sample
I_o= emissivity of the background

$$\underline{A}\text{bsorbance} = -\log\left({}^{I}/_{I_o}\right) \qquad \textit{Eqn.}\ (2.iii)$$

For the experiments to be described absorption is used as the Beer-Lambert law states that it is proportional to the concentration of the sample[79].

$${}^{I}/_{I_o} = \exp(-\varepsilon c l) \qquad \textit{Eqn.}\ (2.iv)$$

Where c = concentration of the sample
ε = absorption coefficient
l = path length

2.5.2 Description of FTIR experiments

Spectra were obtained on a Mattson Sirius 100 spectrometer (figure 2(f)) with a nitrogen cooled mercury cadmium telluride detector in conjunction with an Opus V computer. 100 interferograms were co-added at a resolution of 4 cm^{-1}, a gain of 1 and the aperture set to 25% of total capability. A fast Fourier transform was then performed to give the emissivity spectrum.

The samples were placed in an aqueous holder consisting of two calcium fluoride plates separated by a very thin tin spacer. A 12 μm cell was used initially, but this was changed to 6 μm for most of the results presented. The cell was maintained at a constant temperature to within $\pm$ 0.2 $^{\circ}C$ for any given experiment by a temperature controlled water jacket around the cell (figure 2(g)). The path length was kept constant for a given set of data by removal of the previous sample via suction with a luer lock syringe. The cell was then rinsed with buffer solution and refilled with the next sample. The emissivity spectra obtained were ratioed versus a spectrum of pure buffer taken under the same conditions. This was then converted to an absorption spectrum.

It was necessary to obtain a set of reference spectra for all the components in the system. In the solution state a 6 μm cell was used with the component dissolved in the appropriate solvent. This was ratioed against the pure solvent. Again, the cell temperature was regulated. Cast film spectra were also obtained. A small drop of the sample in solution was placed onto a single CaF_2 plate. The solvent was allowed to evaporate, aided by evacuation in a desiccator. The emissivity spectrum of this plate was recorded and ratioed against that of a clean CaF_2 plate. A similar technique was followed to obtain RAIRS spectra, this technique is explained in detail in section 4.4. A spectrum of water vapour (figure 2(h)) was recorded by ratioing the emissivity spectrum for the empty spectrometer with that of the spectrometer with a beaker of warm water present.

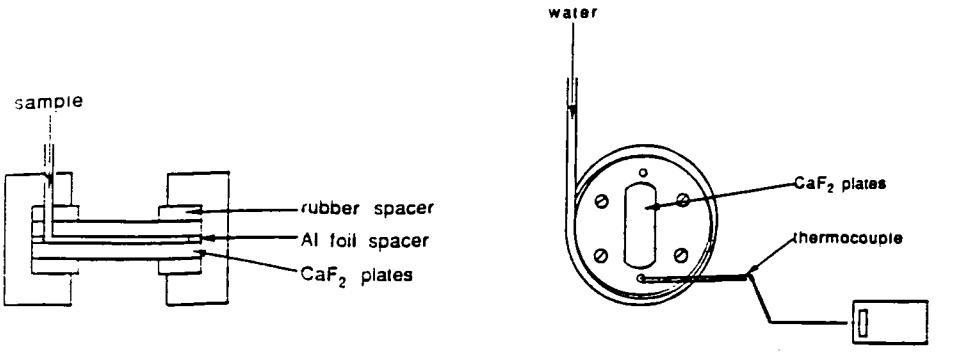

Figure 2(g) : The heated transmission cell.

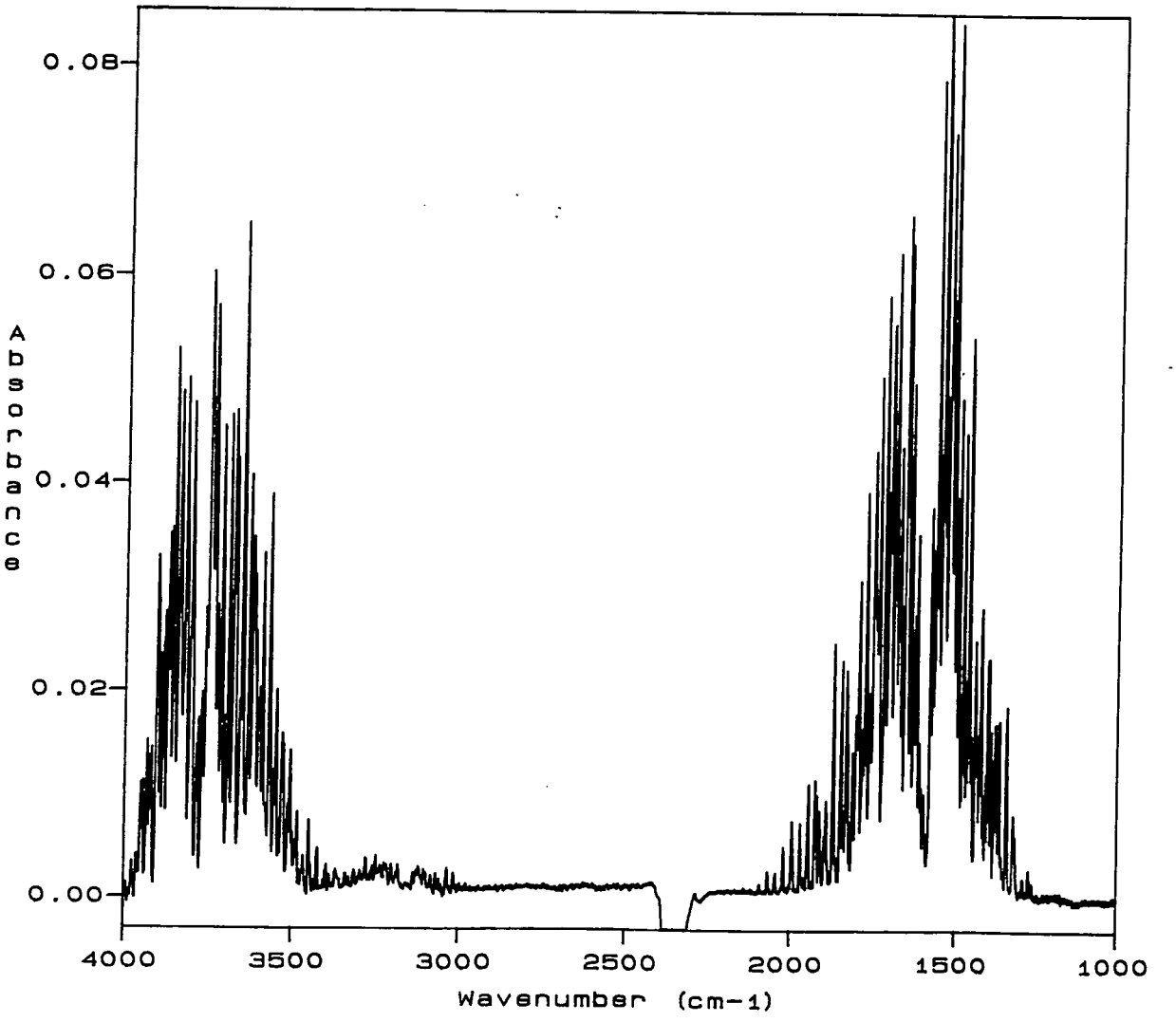

Figure 2(h) : FTIR spectrum of water vapour.

CHAPTER 3

RESULTS AND DISCUSSION OF THE STUDIES ON VESICLES

3.1 CHARACTERISATION OF THE VESICLES

3.1.1 Fractionation of vesicles by gel filtration

(A) Results

The void volume of the sephadex G-50 column was found to be 8 ml, by use of Dextran blue, a high molecular weight dye (see section 2.2). After the initial dye was first eluted the following 8 ml were found to be coloured by the dye. This indicated that elution on the column had caused dilution of a factor of four from the original 2 ml of dye.

Thus the first 8 ml eluted in each experiment were collected as a single fraction. Thereafter fractions were ~2 ml. For each fraction the FTIR spectrum was obtained. Usually 14 such fractions were collected. It was generally found that the lipid content increased from fraction number 2-4/5 then decreased towards fractions 7/8 . Plot 3-2 shows the FTIR spectra of the most intense peaks in the egg lecithin spectrum (plot 3-13). The plot shows the increase and subsequent decrease in the intensity of the bands on elution from the sephadex column. The numbers given are the fraction numbers with F2 being the first fraction collected after the 8 ml of the void volume.

As stated in 2.6.1.B the absorption is proportional to the concentration of a species. Therefore, plot 3-2 indicates the increase and decrease in lipid concentration when the fractions are consecutively collected from the bottom of the sephadex column.

Thereafter, buffer only was eluted until fractions 10-12 which contained detergent. This can be clearly seen in the FTIR spectra. Plot 3-1 is the FTIR spectra for fractions 10-13. It shows a region of the infrared spectrum where the detergent has peaks (plot 3-20) but the lipid does not (plot 3-13). The growth in intensity of these peaks shows the elution of the detergent.

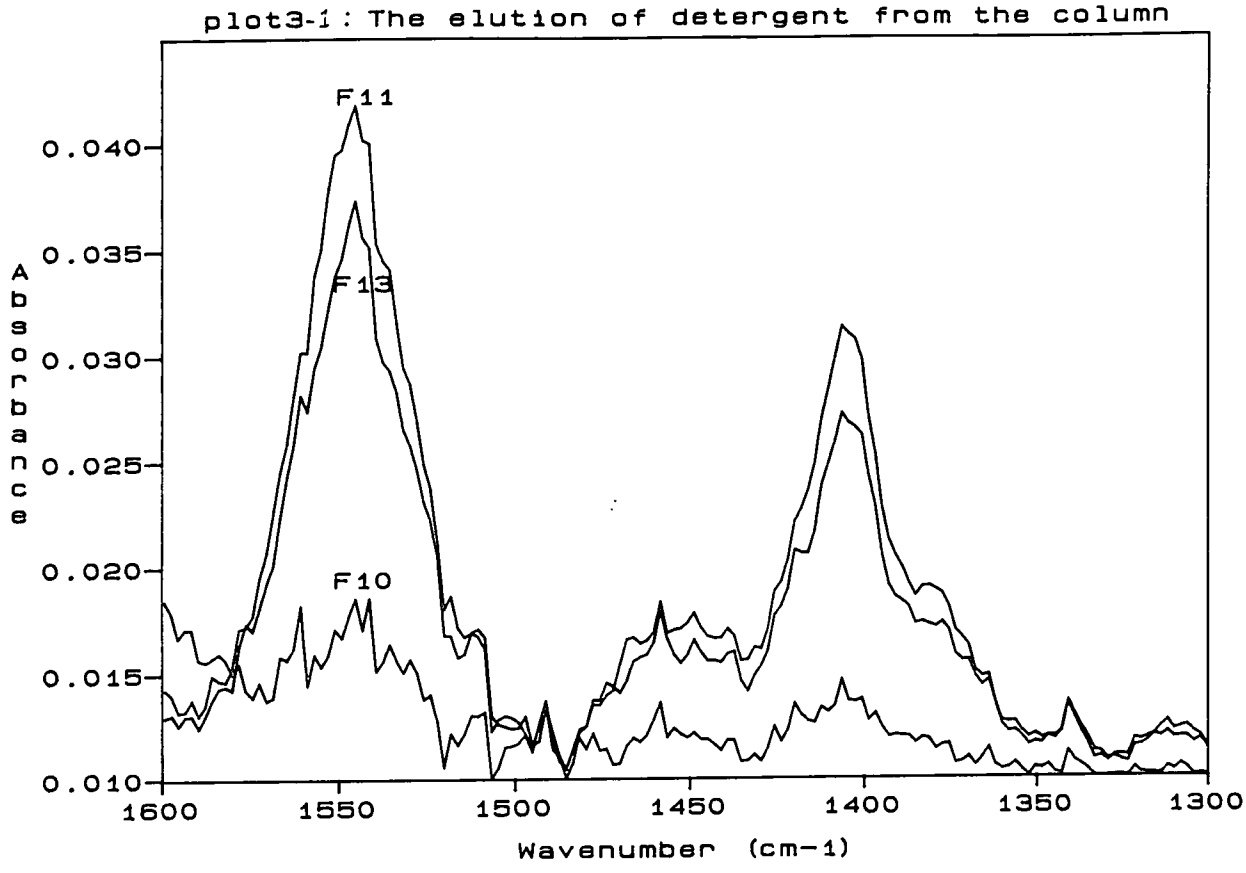

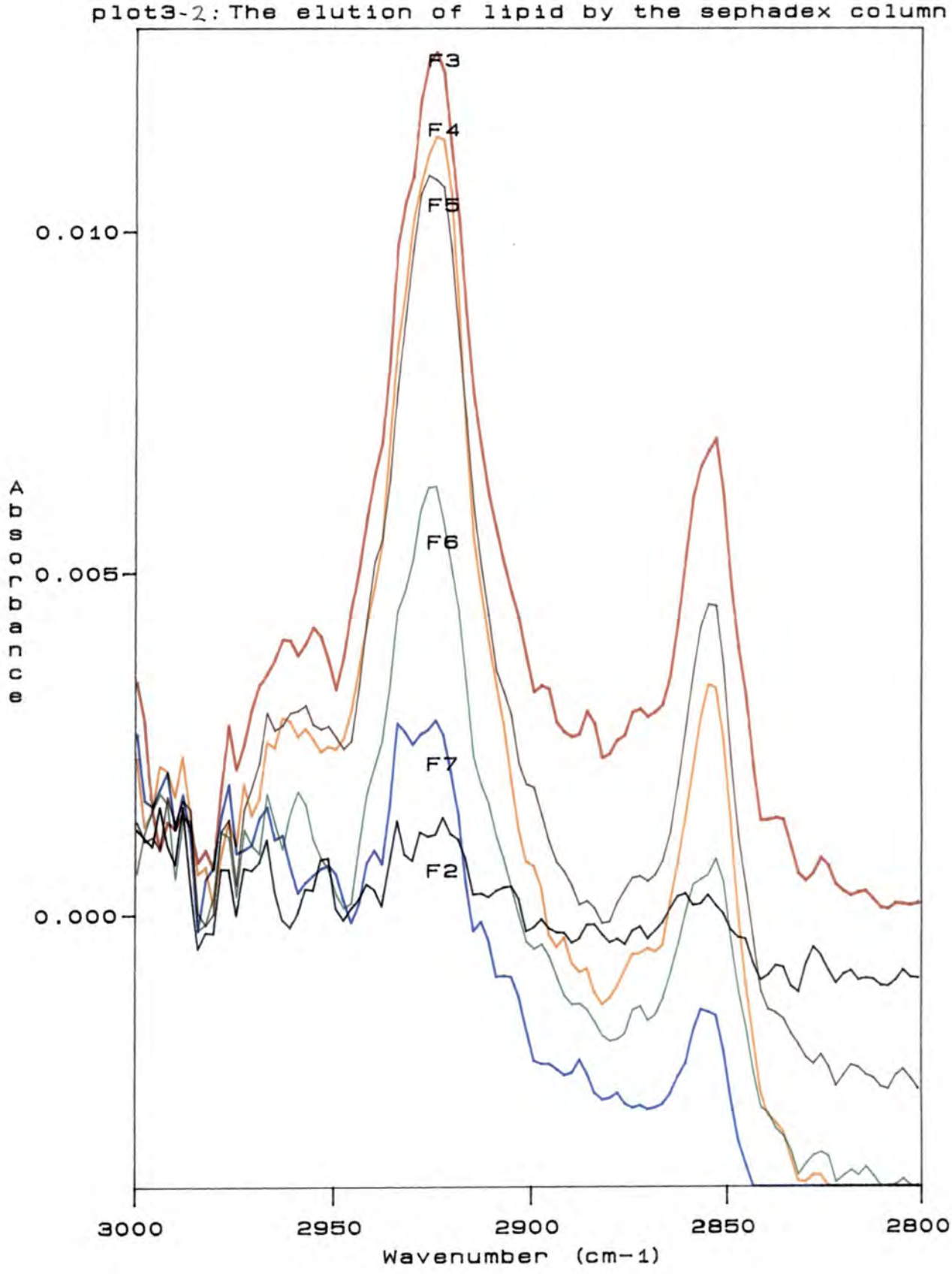
plot3-2: The elution of lipid by the sephadex column
F3
F4
F5
F6
F7
F2
0.010
0.005
0.000
Absorbance
3000
2950
2900
2850
2800
Wavenumber (cm-1)

(B) Discussion of gel separation

The lipid is solubilised by the formation of mixed micelles with the detergent. The critical micelle concentration (CMC) of sodium cholate in 0.15 M NaCl is 50 μM[80]. Thus the operating conditions of mM are well above the CMC of the detergent. Small, Penkett and Chapman[76] found that the mixed micelles formed are cylindrical rather than spherical. The bile salt (detergent), sodium cholate, can be considered as possessing a hydrophilic face and a hydrophobic one (figure 3(a)). A micelle is formed with a bilayer of lipid surrounded by a cage of detergent molecules (figure 3(b)) such that the hydrophobic regions of both lipid and detergent are separated from the aqueous media. The surrounding solution contains monomers of detergent.

As the micelles and monomers traverse the column the concentration of monomers of detergent decreases by entrapment in the sephadex beads[81]. As the concentration of the monomers falls the equilibrium between the micelles and monomers is disrupted and the mixed micelles start to be depleted of detergent. The ratio of detergent to lipid in the micelles decreases until eventually only aggregates of lipid remain.

As the micelles are depleted of detergent they begin to fuse, so that the remaining detergent molecules can still protect the hydrophobic regions of the lipids. These sheets begin to curve as their size increases. Eventually the detergent depletion reaches a level whereby the micelles can no longer remain stable and the lipid bilayers fold over to form a sphere, and unilamellar vesicles are made.

Previous work (16,72,73 & 81) shows that complete removal of the detergent is extremely difficult - even after dialysis for several days Allen et al[72] found that there are still seven detergent molecules per 1000 lipids. However if gel filtration is used then 1% detergent:lipid is retained. The FTIR spectra show no sign of detergent in the lipid containing fractions, but at this concentration (0.03 mg/ml) detection would be problematical.

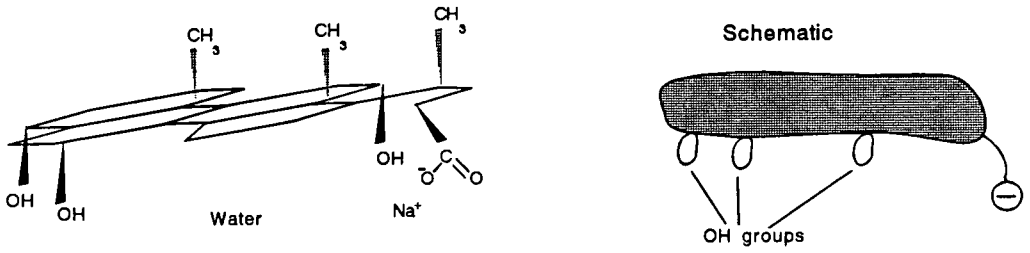

Figure 3(a) : Illustrating the hydrophilic and hydrophobic nature of the 'two sides' of sodium cholate. (Drawn from information given by Small et al[76])

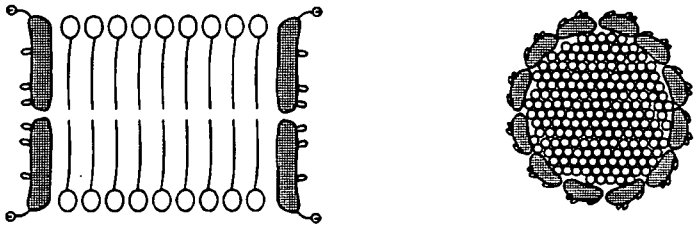

Figure 3(b) : Illustrating the construction of cylindrical micelles. (Drawn from Small et al[76])

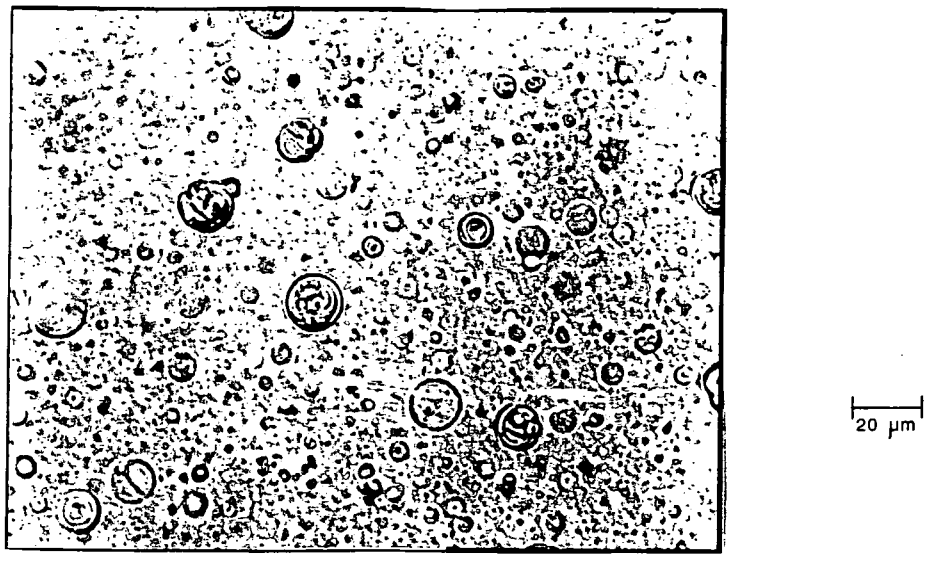

Figure 3(c) : Micrograph of the aggregates produced from an initial detergent to lipid ratio of 15:1.

An experiment was performed on the Durham FTIR spectrometer where the concentration of detergent, in water, in a 6 μm CaF_2 cell was gradually increased. This continued until the spectrum of sodium cholate could be clearly discerned. It was found that the concentration required was quite high ~ 1 mg/ml. Assuming that all of the lipid was eluted in one fraction the level of detection of detergent would be at a level of one molecule of detergent for twenty lipid molecules. As the actual concentration of lipid is lower, due to dilution from passing through the column, the fraction of lipid to retained detergent molecules could be even higher and still not detectable using FTIR spectroscopy.

Therefore, it must be assumed that there are still detergent molecules present in the final liposomes even though the technique was not sensitive enough to detect them. Allen and co-workers[72] have radioactively labeled detergents and have shown the quoted percentage retention. It must be assumed that the experimental technique used has removed no more than this. Thus, interpretation of the results must take this factor into account.

3.1.2 Size and Dispersity

(A) Results

At first the initial detergent : lipid ratio was 3:1, but in order to reduce the final detergent content this was altered to 1.5:1. This is still within the region for the formation of mixed micelles[76,82]. Most of the references quote 3-5 :1 as the optimum ratio (72,80 & 81). It was found that the ratio of 1.5:1 was too low and the aggregates formed were depleted of detergent too quickly and thus large liposomes were formed. These could be viewed via an optical microscope (figure 3(c)). Some were 14 μm in size and could be seen to comprise of layers within layers. It was therefore decided to alter the detergent : lipid ratio. On examination of the literature a ratio of 15:1 was chosen as Allen et al[72] found that a higher proportion of the aggregates (~90%) will be LUV's.

On increasing the concentration of detergent, to a 15:1 ratio compared to the lipid the aggregates could no longer be seen by optical microscopy. The lipid containing fractions were almost clear, compared to the cloudy appearance seen with a 2:1 ratio. However a small change in optical density could be seen with a discerning naked eye, possibly due to a few larger aggregates still being made. The size of the new aggregates was obtained by use of PCS. A good fit to the data was found for each PCS run - normally with a merit factor of 85% certainty.

If the size of the aggregates was found on the same day as they were made then the average size was 24.1 ± 11 nm. This was very reproducible with an error of ± 0.5 nm in the average size and ± 3 nm in the standard deviation. If the size of the aggregates was measured on the subsequent day to formation then the size was 33.4 ± 22 nm with reproducibility errors of ± 2 nm in the average size and ±3 nm in the standard deviation. It was observed that if the samples were left at room temperature for a period of several days that the lipids had aggregated into a white mass at the bottom of the sample tube.

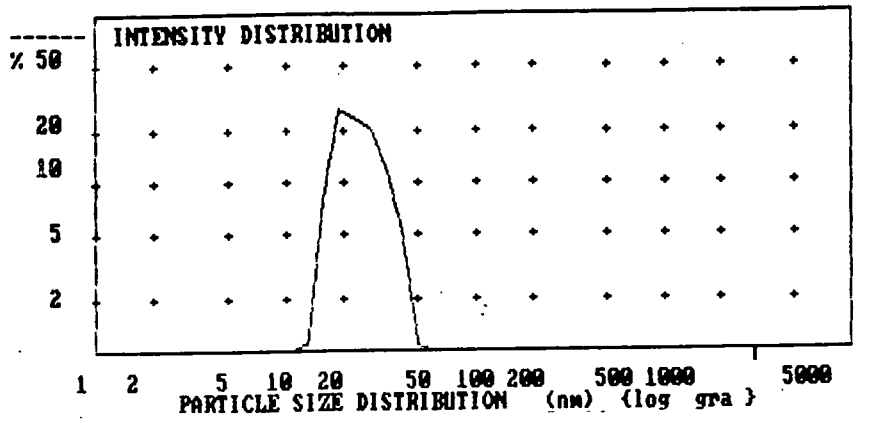

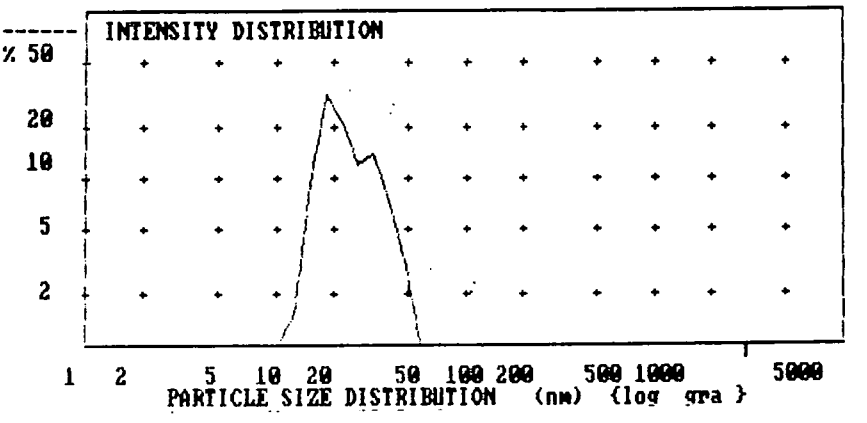

Plot 3-3 a&b : The PCS data showing the spread in size of two samples of vesicles taken within an hour of formation.

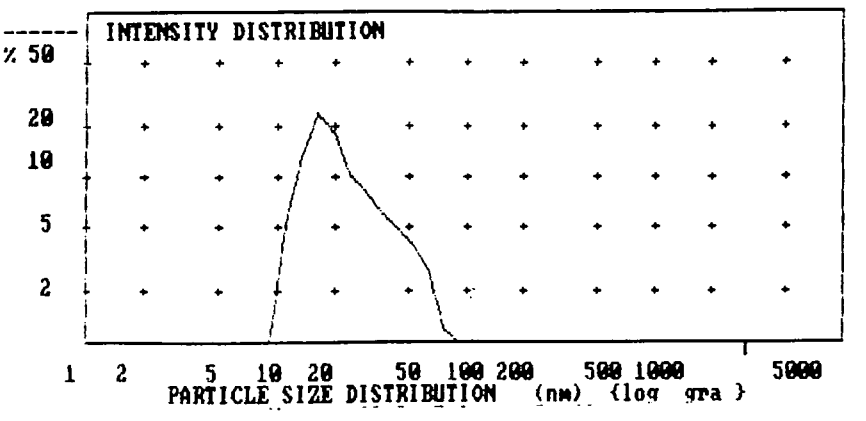

Plot 3-4 :The spread in size for a sample of vesicles whose PCS spectrum was taken the day following formation.

(B) Discussion of the size of the aggregates produced

Initially the aggregates formed with the 2:1 detergent to lipid ratio were not LUV's. So the detergent to lipid ratio was changed to 15:1. This produced aggregates of average size 24.1 ± 0.5 nm with a fairly small spread in diversity 67 % were within 14-35 nm in size. This contradicts the early expectation of 100-150 nm vesicles. A recent paper by Rotenberg and Lichtenberg[80] surveys a number of different detergent removal procedures and the results thereof. This gives a size for vesicles produced by the same method of 30.3 ± 1.2 nm. This indicates that the experimental procedures used at Durham differ in some manner from the original workers, who obtained 100 nm vesicles, but are similar to more recent work. The most probable change is that the lipid traversed the column faster and thus there was less time for the micelles to grow before they fused to make the vesicles.

As the detergent is removed Lasic[84] hypothesises that the bilayer micelles fuse and form larger disc like micelles. These eventually grow so large that the net hydrophobic interactions increase until the discs fold back on themselves to form vesicles. The slower the detergent removal, the longer the time the micelles can enlarge by fusion and thereafter form bigger UV's. Although the work of Vinson et al[85] indicates that the vesicles may be formed via a transition through a cylindrical micellar state rather than flat discs, the principle of growth by fusion would be the same.

3.1.3 Proof of unilamellarity of the vesicles produced by gel separation

(A) Introduction

As described in section 2.5 it is possible to use ^{31}P NMR to investigate the layer structure of the aggregates. If only the exterior lipids of the aggregates are affected by the presence of Mn^{2+} there will be a drop in the intensity of the ^{31}P NMR signal related to the ratio of the exterior to interior lipids.

From section 3.1.2 the average diameter of the aggregates is 24 nm with a standard deviation of 11 nm. From the X-ray data of Parsegian et al[86] the width across a bilayer of egg PC is 3.5 nm. If we assume that the aggregates formed are unilamellar vesicles and that the area occupied, by each lipid, is the same in both the inner and outer spheres then, given that the surface area of a sphere is $4\pi r^2$, the intensity of the ^{31}P NMR signal should drop by a factor of :

$$\frac{4\pi r_2^2}{4\pi(r_1^2 + r_2^2)} \qquad \textit{Eqn. 3(i)}$$

$$= \frac{\text{area of interior of sphere}}{\text{area of interior + exterior}}$$

$$\alpha \frac{\text{NMR intensity from the internal lipids (I)}}{\text{total NMR intensity from all of the lipids } (I_o)}$$

$$= I/I_o \qquad \textit{Eqn. 3(ii)}$$

radius of the outer sphere = 12 nm = r_1

radius of the inner sphere = 8.5 nm = r_2

Thus the fraction is $(8.5)^2/((8.5)^2+(12)^2) = 0.33$

Therefore if all the assumptions are correct the NMR intensity should fall to exactly a third of the original on addition of the Mn^{2+} with a standard deviation, in the fraction, of 0.05 (calculated from the average standard deviation of the PCS data).

(B) Results of ^{31}P NMR experiments

The fractional fall in relative intensity between the initial peaks, due to phospholipid, and the peaks after addition of $MnCl_2$ was calculated for each spectrum. A graph was plotted for the intensity ratio, followed with respect to time. The fraction was extrapolated back to the point of addition of the salt. It was assumed that the broadening effect would occur as soon as Mn^{2+} had been added. Plot 3-8 is a typical response from vesicles made from an original lipid:detergent ratio of 15:1.

The ^{31}P NMR signal fell to a fraction of 0.84 of the original intensity for the 1.5:1 detergent to lipid ratio. These results confirmed the microscopy results that unilamellar vesicles had not been formed. The data indicates that the aggregates formed are multilamellar as the decrease is very small implying that only ~16 % of the lipids are on the external surfaces of the aggregates. The decay of the ratio over a period of several hours is shown in plot 3-7.

Seven results were recorded for the 15:1 detergent/lipid ratio. The initial intensity ratios were as follows 0.31, 0.29, 0.41, 0.28, 0.18, 0.50 and 0.245. The average value for the fraction of the original ^{31}P NMR signal after the addition of Mn^{2+} was therefore 0.32 ± 0.10.

Before $MnCl_2$ was added three spectra of each sample were recorded to gauge the reproducibility of the relative intensity between the phospholipid peak and the external reference. These proved that there was quite a large error in making a measurement. Over all of the sets of three readings, the standard deviation was 14 % of the recorded value. Propagating this through the eqn. 3(ii) using the equation below :

$$\sigma_z^2 = \sigma_x^2 \left(\frac{\delta f}{\delta x}\right)_y^2 + \sigma_y^2 \left(\frac{\delta f}{\delta y}\right)_x^2 \qquad \textit{Eqn. 3(iii)}$$

σ = standard deviation
x,y = the variables in a function z = f(x,y)

The differentials are calculated at the average recorded value for x and y. The standard deviation of the ratio would be 0.07 given the mean of 0.32. Thus the recorded deviation of 0.1 is quite a bit larger than the value expected purely on instrumental error.

(C) Discussion of the type of vesicle made

The recorded value of 0.32 ± 0.1 is within the error of the expected value of 0.33 ± 0.05. Thus it can be concluded that there is a strong possibility that the aggregates are unilamellar vesicles. However, the standard deviation in the results obtained is higher than would be expected from purely experimental error in the measurement of the relative NMR intensities. It is possible that samples prepared on different days had varying ranges in the sizes of the aggregates. This was seen, to some extent in the PCS experiments. Although the average size was fairly constant the spread around that mean varied substantially (plots 3-3 a&b) for different samples. This would affect the average intensity ratio because the theoretical ratio is not a simple linear relationship with the diameter, as shown in plot 3-6. If the distribution of sizes around the mean is broad then the average intensity ratio will be lower than a narrow spread as the theoretical curve begins flatten and at very large vesicle diameters will asymptote to a value of 0.5.

Another possibility is that some of the aggregates on a given day are MLV's and others easily penetrated by the manganese, either of these would increase the error in measurement. The first would give ratios higher than predicted, the second lower than expected.

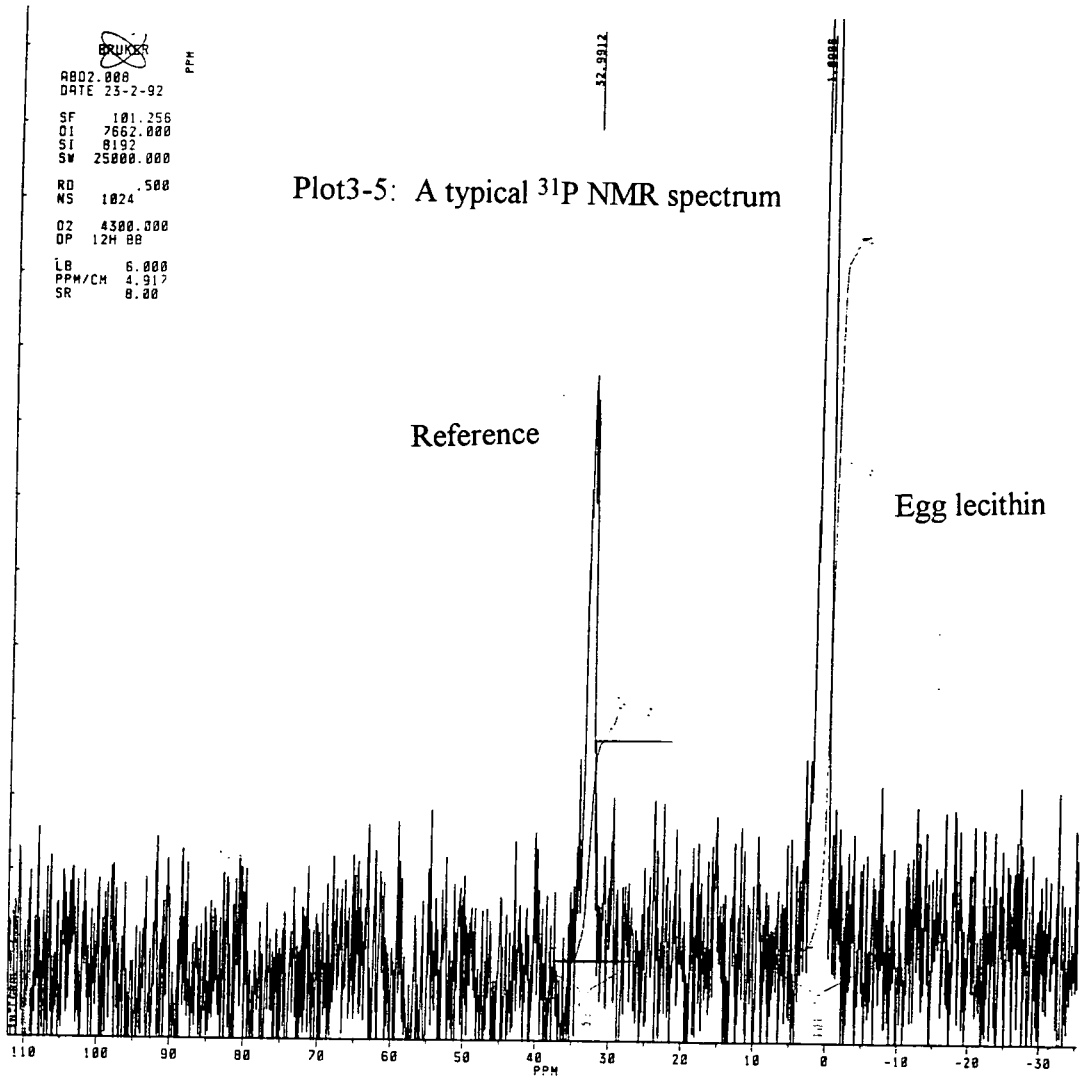

Plot3-5: A typical ^{31}P NMR spectrum

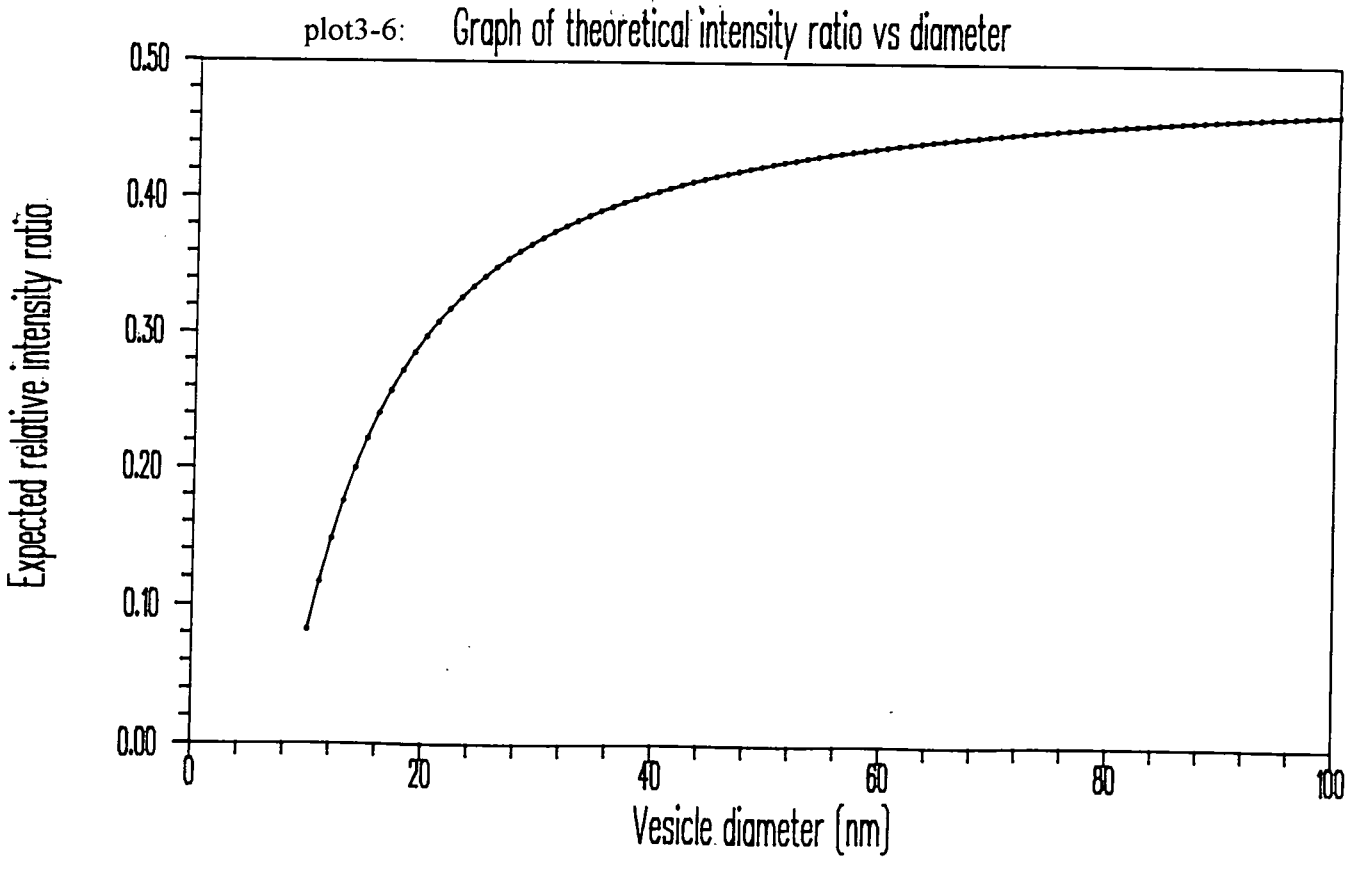

plot3-6: Graph of theoretical intensity ratio vs diameter

Plot3-7 : Graph of intensity ratio vs time for the 1.5:1 detergent\lipid mole ratio

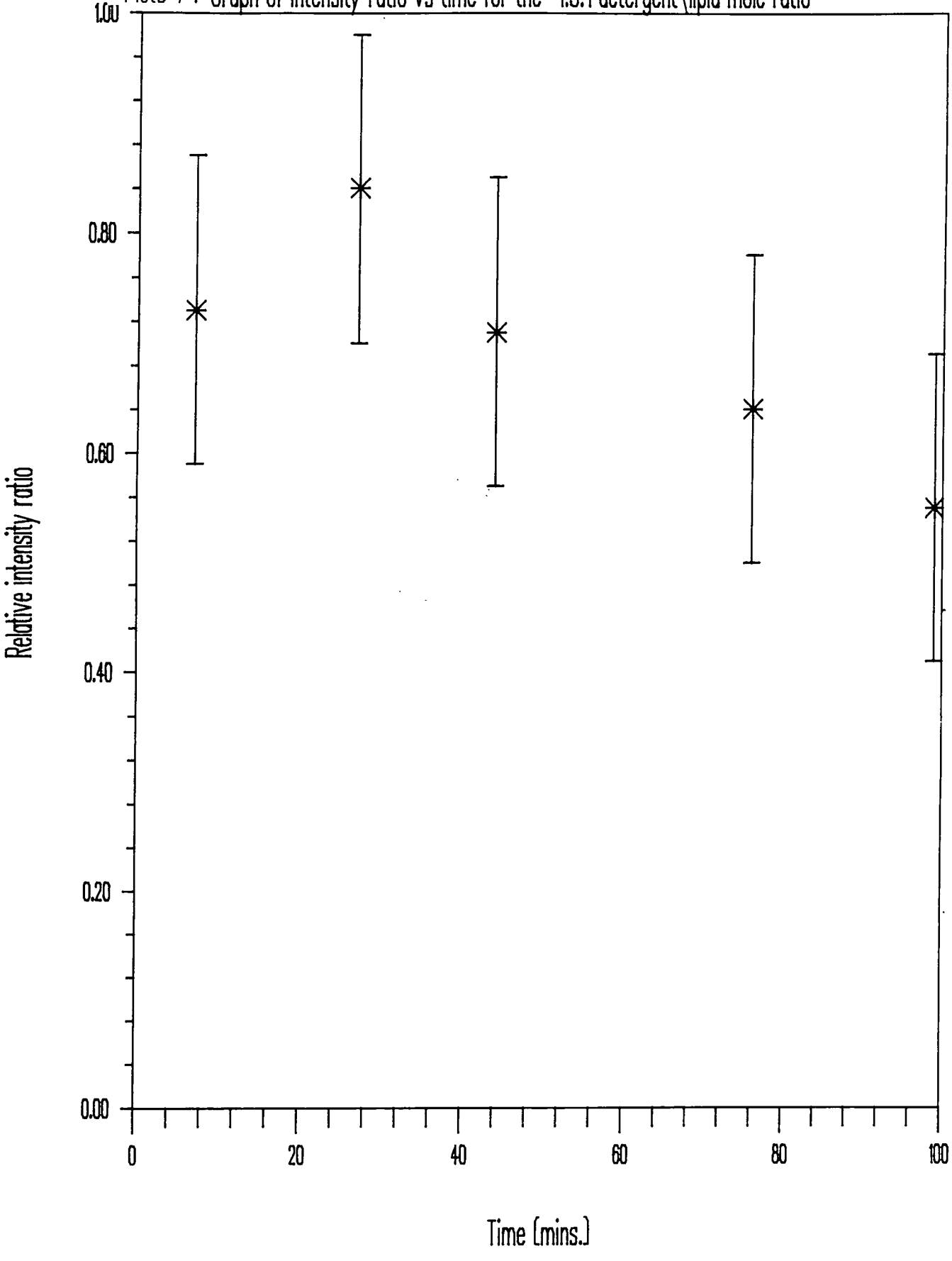

plot3-8:

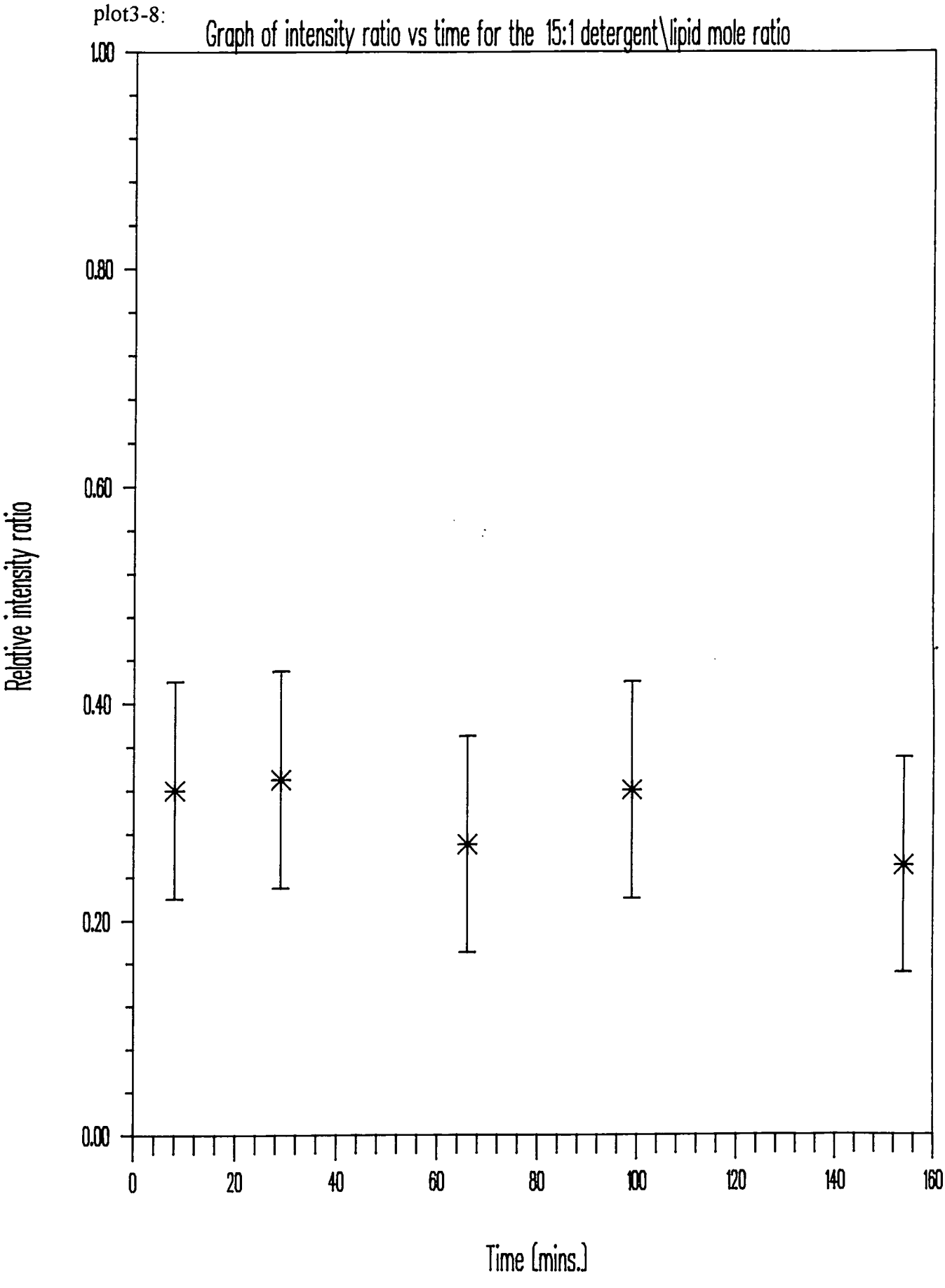
Graph of intensity ratio vs time for the 15:1 detergent\lipid mole ratio
Relative intensity ratio
1.00
0.80
0.60
0.40
0.20
0.00
0
20
40
60
80
100
120
140
160
Time (mins.)

3.1.4 Stability of the vesicles

(A) Dye entrapment results

Phenyl red, the indicator is yellow at pH6 and purple at pH8. The vesicles were originally made at pH6 then eluted on a sephadex G50 column at pH8. The solution was yellow before the second elution but became purple afterwards. This indicated that the vesicles had reformed on the column with pH8 buffer inside. A second experiment was tried with a different capture volume for the column. The vesicles were again formed on a sephadex G-50 column at pH6 but the second elution took place on a much shorter sephadex G-25 column. The solution eluted was yellow indicating that the buffer trapped within the vesicles was at pH 6 whereas that of the surrounding medium was pH 8. On addition of IPA the vesicles were destroyed and the contents disgorged giving a purple colour. On leaving the vesicles whole overnight the yellow colour was still present but appeared paler. On addition of IPA the solution again became pinkish.

The disintegration of the vesicles, when the second elution was performed on a sephadex G-50 column could be due to the presence of detergent molecules within the solution. These would again become depleted further causing any detergent molecules in the vesicles to be removed and thus releasing the dye.

(B) NMR results

There is a very gradual decay in the intensity ratio over a period of 3 hours (plot 3-8). However the next morning, 12 hours after the addition of the manganese, the ratio had fallen to 0.18 for the sample shown. This decay overnight was a reproducible trend.

(C) Discussion of the stability of the vesicles

The vesicles appear to begin degrading almost as soon as made. However, this process is quite slow and there is still a high percentage of the vesicles which remain stable overnight.

The PCS data shows a larger size and dispersity the day after formation. It was also observed that although samples were clear at the time of elution, on being left to stand they gradually became more opaque. Eventually, about a week later a mass of white material could be seen at the bottom of the sample tube.

All of the data described suggest that as time passes the vesicles coalesce to form larger aggregates and finally join together as one mass. This is due to the fact that whilst it is possible to form vesicles they are none the less thermodynamically unstable. They only exist for any length of time due to the slow kinetics for conversion to other phases[83]. The vesicles produced seemed less stable than those made by extrusion techniques. Hope and co-authors[74] reported that their vesicles remained integral for periods of days. Whereas the apparent time scale found for the stability of the vesicles made in the experiments described here suggests that the are not stable for more than a few hours.

3.2 : CONFORMATIONAL ANALYSIS USING FTIR

3.2.1 Introduction

Each of the various chemical groups of a lipid molecule have vibrational modes which are active in the infrared. From each small piece of information understanding of the molecular conformation and interactions is possible.

The table overleaf shows a general outline of infrared assignments for molecular groups which are commonly found in biological systems. The results found will first be discussed in terms of the information which can be gained from the consideration of the whole spectra. Secondly each spectral region of interest will be studied in depth. Then all of the information will be drawn together to give an overview.

Plots 3- 12-23 are FTIR spectra of egg lecithin in a variety of environments. They show the whole of the spectral region of interest for the lipid in an aqueous medium. At wavenumbers above 3200 cm^{-1} and below 1000 cm^{-1} water absorbs so strongly that the detector receives an extremely low signal. Even using very small path lengths spectral information, for low concentrations of molecules within water, is lost beyond the wavenumbers mentioned.

If more than one spectrum is shown on a plot then, in most cases a normalisation factor has been used to enable the spectra to be seen on the same scale. The absorbance scale in each case is for the main spectrum on that plot. This is shown as a solid line. The exceptions to this are plots 3- 19,29-32&34 in which the absorbance scale relates to all of the spectra displayed.

Wavenumbers (cm^{-1})	Description of assignment	Reference
3490	ν_{as} (H_2O)	95
3280	ν_s "	"
3300	Amide A } Fermi resonance between N-H and	88
3100	Amide B } excited state of amide II	"
3020-3030	ν_{as} (CH_3) in N-(CH_3)$_3$	"
3010	ν (CH) in alkenes	95
2960	ν_{as} (CH_3)	31
2919-2930	ν_{as} (CH_2)	"
2875	ν_s (CH_3)	"
2850-2854	ν_s (CH_2)	"
2125	H_2O association band	95
1700-1740	ν (C=O)	"
1650	Amide I : in plane mode mainly C=O mixed with N-H	88
1645	δ (H_2O)	95
1550	Amide II : in plane mode	88
1470-1490	δ_{as} (CH) in N(CH_3)$_3$	88
1463-1470	δ (CH_2) scissoring	31
1410-1420	δ (CH_2) scissoring attached to CO or PO	151
1375-1388	δ_s (CH_3) (umbrella mode)	95
1300	Amide III : (weak) in plane mode	88
1230-1250	ν_{as} (PO_2^-)	"
1350-1250	ν (P=O)	"
1188	ν_{as} (COC)	"
1088	ν_s (PO_2^-)	"
1064	ν_s (COC)	"
1050-970	ν (POC)	"
1040-910	ν (PO) in POH	151
970	ν_{as} (N-(CH_3)$_3$)	88

Key :

ν = stretching vibration
δ = bending vibration
s = symmetric
as = antisymmetric
amide = one of the bands found in proteins

Table 3(i) : General assignments of interest in the infrared spectra of biological molecules.

3.2.2 Background to FTIR studies

(A) Estimation of the position of a peak

Atoms are bound together by electrons to form bonds. These bonds are elastic and act as anharmonic oscillators. Consider a diatomic molecule. Figure 3(d) shows the empirical shape of the energy curve. This has been fitted to an equation by Morse[79]. The vibrational energies only occur at quantised steps within the energy well. These are given by :

$$\varepsilon_v = (v + 1/2)\bar{\omega}_e - (v + 1/3)^2 \bar{\omega}_e x_e \quad (cm^{-1}) \qquad Eqn.\ 3(iv)$$

Where :- ε_v = vibrational energy level v

$\bar{\omega}_e$ = equilibrium oscillation wavenumber (for infinitely small vibrations about the equilibrium length)

x_e = the anharmonicity constant

v = vibrational quantum number

The selection rule for anharmonic oscillators is :

$$\Delta v = \pm 1, \pm 2, \pm 3, \ldots \qquad Eqn.\ 3(v)$$

At room temperature Boltzmann's distribution may be used to calculate the population of the unexcited states, 99 % of the population is in the energy level v = 0. Thus the most prominent absorption (the fundamental) arises from a transition v = 0 to v = 1 and $\Delta\varepsilon = \bar{\omega}_e(1 - 2x_e)$ cm^{-1} The first overtone arises from the transition v = 0 to v = 2 and usually has a small intensity. From empirical measurements of the absorption frequencies these equations can be used to find $\bar{\omega}_e$ and x_e. Once these are determined it is possible to use the classical equation for the oscillation frequency to determine the force constant of the bond :

$$\bar{\omega}_e = (2\pi c)^{-1} \sqrt{k/\mu} \qquad \textit{Eqn. 3(vi)}$$

Where c = velocity of light in cm s^{-1}

k = force constant

μ = reduced mass of the system e.g. $m_1 m_2/(m_1 + m_2)$

Polyatomic molecular vibrations stem from similar potentials but instead of one fundamental vibration there are now several. These can be determined by normal mode analysis. If there are N atoms in a molecule each of them can be described by a set of there coordinates; x,y and z. Thus the molecule has 3N degrees of freedom. The molecule can translate as an entity through space and thus 3 of these degrees of freedom are used. The rotation of the molecule can be described using another 3 degrees of freedom, thus leaving 3N - 6 degrees of freedom to describe the molecular vibrations. If the molecule is however linear then 2 dimensions are sufficient to describe the rotational motion leaving 3N - 5 vibrations. These vibrational modes are known as normal modes of vibration because, in general, all the atoms move in phase and with the same frequency. For both linear and non-linear (acyclic) molecules there are N - 1 bonds between the atoms thus N - 1 of the fundamental vibrations are stretching modes and the rest are bending modes.

The modes of vibration are further split into symmetric and antisymmetric. The former if the molecule undergoing the vibration is unchanged on rotation about the symmetry axes of the functional group and the latter if the image is different.

In order for any of these vibrations to be detected via infrared spectroscopy there must be a change in the dipole moment during the vibration. If the molecule is large then there are liable to be a lot of normal modes from the 3N - 6 which are infra-red active. Some of these may involve the whole molecule and are known as skeletal modes whereas others are approximately concentrated in particular regions of the molecule and are known as characteristic group frequencies. These frequencies involving small groups of atoms can be treated as arising solely from that group (although there will be a small effect on the rest of the molecule) and normal mode analysis may be undertaken for these groups as if they were separate small molecules. The characteristic frequencies of these vibrations will fall in similar regions of the infrared spectrum from molecule to molecule and may be used to assign molecular structure to unknown compounds.

If environmental factors alter the electronic distribution within the bond then the fundamental resonant frequency is shifted, because the force constant is changed. Therefore if the molecular conformation alters this often leads to a small change in the frequency of the corresponding characteristic peak in the IR. This is due to the immediate environment of the atoms and their bonds being changed. A large effect on the bond strength or the vibrating masses, such as hydrogen bonding or isotopic exchange is easily discernible.

The resolution of the spectra reported here is 4 cm^{-1}. This means that the instrument should be set up so that peaks which are ≥ 4 cm^{-1} apart should be resolved. The digitisation of the spectra with the set parameters is every two wavenumbers. Therefore if the computer software is used the error in the measurement at a given point in the spectrum is ± 1 cm^{-1}. However, if the peak picking facility is used the actual difference between the manual and computer measured wavenumbers of a peak could higher than 1 cm^{-1}. This is because the software gives the wavenumber of the highest point in the recorded peak. This can be up to 1.5 cm^{-1} away from the most accurate measurement possible from the given data.

Figure 3(e) illustrates the problem. The graph shows a simulation of peaks made up from point separated by 2 cm^{-1}. In (i) the computer would give a value of either 6 or 8 units but it is plain to the eye that the centre of the peak is at 7 units. (ii) illustrates a second peak of the same shape but shifted by one unit with respect to the sampling points. This time the computer would chose the highest point which is 6 units. By visual estimation the peak position would be 6.5 units. Therefore if the bandwidth is much greater than the resolution , as in the examples shown, it is possible to estimate the peak position more accurately than the resolution of 4 cm^{-1} implies. It is possible to find the wavenumber from a 4 cm^{-1} resolution plot to at least the nearest 0.5 cm^{-1}, if plotted on a scale such that 1 mm $\cong$ 1 cm^{-1}. Reported data are therefore given to half wavenumbers.

The reproducibility of the spectrometer repeating the same measurement for a sample, even on different days should be more accurate than it is possible to measure the peak position. This is because its limitation relies on the frequency of the laser used as the digitisation reference, not on the resolution chosen. This should give an accuracy to of $\pm$ 0.1 cm^{-1}.

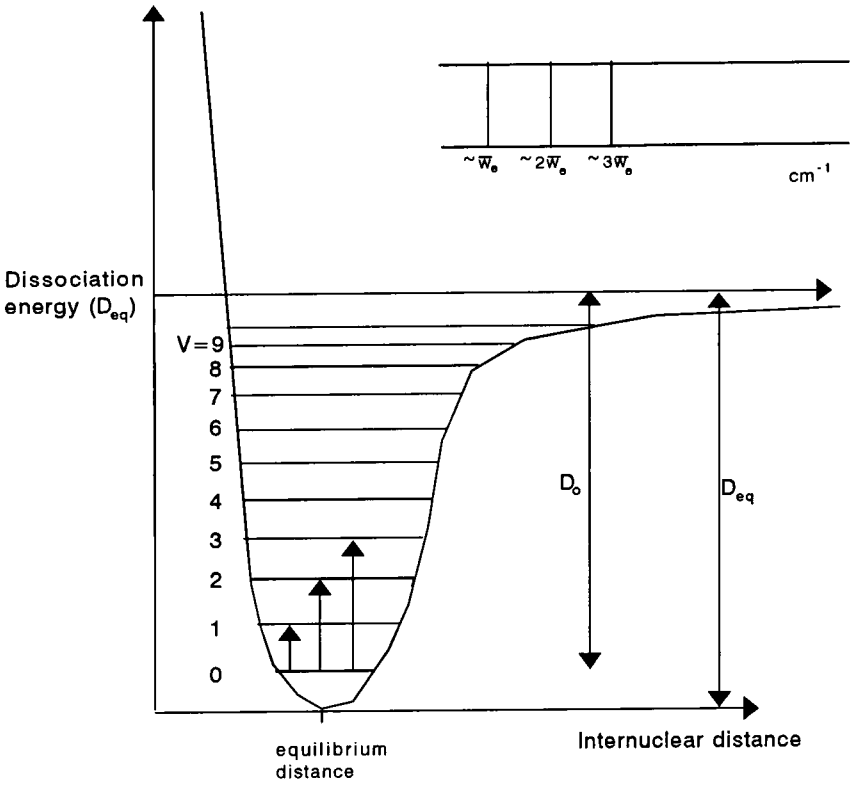

Figure 3(d) : The Morse potential, showing allowed vibrational energies and some transitions between them for a diatomic molecule undergoing anharmonic oscillation. (Redrawn from the Fundamentals of Molecular Spectroscopy by Banwell[79])

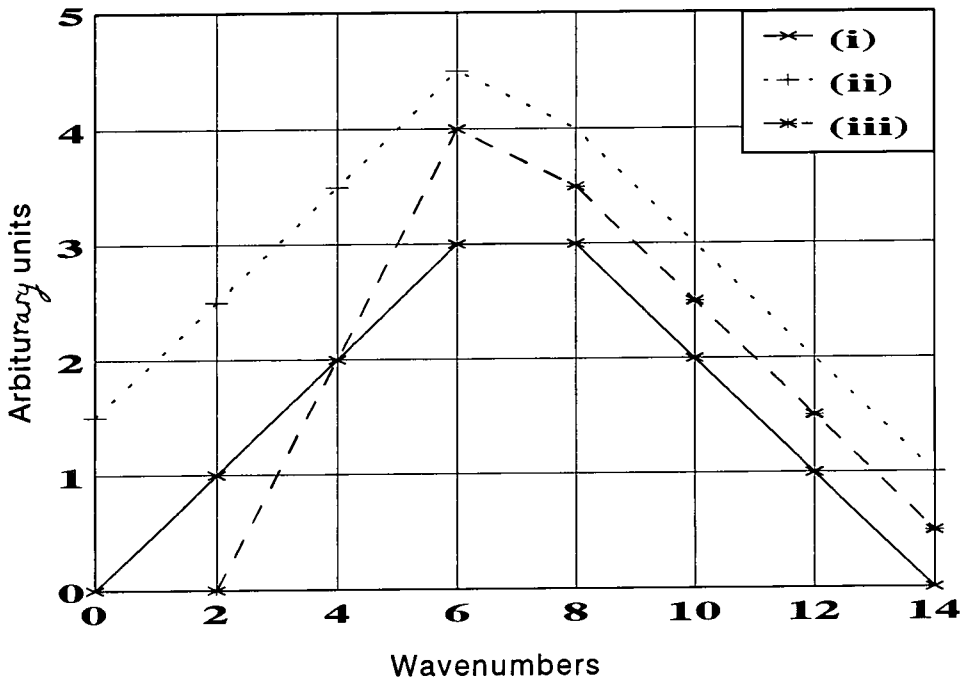

Figure 3(e) : Illustration of peak position problem.

(B) Measurement of the width of a band.

The shape of an IR band is dependent on the environment in which a molecule is situated. It is not generally as sensitive as the band position to conformational changes but can be affected by a variety of external factors. For any IR absorption the peak will not be a single line at one frequency. There will be a distribution in frequency about a central value, this is dependent on a number of factors.

Even for an isolated molecule the absorption will have a certain width due to the Heisenberg uncertainty principle[79]. In liquids and gases there are two other broadening effects. In liquids collision broadening is dominant, where molecules collide and this interferes with molecular vibrations. In gases broadening due to the Doppler effect is more pronounced[79].

For a given vibration there will not only be the effects described above but also the number of different environments in which the atoms of the molecules are found will give a distribution for the fundamental frequency.

An estimate of line width in an IR peak can be found by measuring the width, in wavenumbers, at half the peak height (FWHH). One of the most difficult problems in making this measurement is that in order to find the height an estimation of the baseline position of the peak is necessary. Manual measurement again gives an advantage, because if there is a slope in the baseline it can be taken into account. However, care must be taken to ensure that the baseline chosen is valid. Overlapping peaks may mean that the the absorbance does not fall to the baseline value. It is best to consider a region of the spectrum with no peaks present to gain an idea of both the position of the baseline and whether there is any general slope to the baseline of the whole spectrum. A sloping baseline can occur due to different reasons. The most commonly encountered reason with the Durham instrument was a drift in the detection of the zero point difference (ZPD) in the interferogram of the reference laser.

(C) Spectral enhancement

If more than one peak is present in a spectrum then the peaks will superimpose to give a resultant absorption. If the separation in frequency between the peaks is of the same order, or less, than the band width then it will not be possible to measure the intensities of the individual peaks. This is due to the fact that the other peaks in the superimposed band will contribute a significant amounts to the peak to be measured.

In a spectrum where the instrumental resolution is greater than the band separation then the peaks will not be resolved. In this case increasing the spectrometer resolution may separate the peaks. An example of this is the spectrum of gaseous carbon monoxide. The rotational fine structure peaks in vibrational spectrum of CO are separated by less than 4 cm^{-1} and have a band width around 1 cm^{-1}. Thus at an instrumental resolution of 4 cm^{-1} most of the information on this fine structure is lost but at a resolution of 0.5 cm^{-1} each peak is clearly seen[79].

If the band widths, of peaks in close proximity, are much larger than the smallest possible spectral resolution available then it will not be possible to separate the peaks satisfactorily by altering the experimental conditions. To separate peaks which are closer than their band widths it is necessary to use one of several computational techniques which are now available.

Fourier deconvolution (FD), of spectra, artificially narrows the superimposed peaks so that they can be separated. FD has been applied to a variety of spectral techniques[87] and specific software relating to each particular type of spectroscopy is becoming more common. A Fourier transform is performed on the data. Whilst in the Fourier domain a function is used which on the return FT has the effect on narrowing the peaks. Two parameters are needed to perform the most common type of FD in IR, as developed by Kauppinen et al [96,97]. An estimate of the real band width (w) and the length of the apodisation function to be used (k). The signal to noise of the original spectrum needs to be very good and the band widths of the

component peaks should be similar as they are assumed to be the same in the FD technique. The information obtained is the number of superimposed peaks in a particular band, their positions and their relative intensities. If two peaks are very close together FD may not be able to resolve them.

The second derivative (SD) of a spectrum will give information on the position and number of peaks in a band. The first derivative of a turning point is zero and the SD is zero for a point of infection, negative for a maximum and positive for a minimum. At the frequency of a peak a negative spike is seen in the SD spectrum. All data on the relative intensities is lost.

Another technique for the assessment of underlying peaks is to fit theoretical curves so that when superimposed the shape is the same as the experimental data. There are a number of variables in such a process.

The number of component peaks to generate is the first variable to be decided. Visual examination of the spectra is one of the best starting points to determine both the number of peaks and their relative intensities. FD and second derivative techniques can also aid this decision. The positions of the components should be the next piece of information to be determined. FD and derivative techniques can also aid this problem as outlined above. FD can yield information about the relative intensities of the components. The next variable is the widths of the peaks. Information on an initial estimate can come from the consideration of the total width of the original band. The last variable is perhaps the hardest to chose; this is the percentage composition of the theoretical band shapes. There is generally a choice of two theoretical band shapes - Gaussian Lorentzian. As the shape of a real IR peak may not be either of these theoretical possibilities it may be necessary to mix them. In general IR peaks are more Lorentzian in nature[98]. So once a starting point has been chosen for all of the variables mentioned it is necessary to optimise them so the the theoretical curve is as close to the real one as possible.

Many software packages are available for curve fitting for a variety of different spectral techniques. The one used for the fitted data shown in plots 3-29 & 30 *etc.* was in the FTIR software provided by Mattson plc. (called FIRST). However, the optimisation algorithms provided were not satisfactory. The fits shown were made by finding the wavenumber of the peak maxima and number of peaks by eye, FD and derivative methods. Then a estimate of the band-width was made. The generated shape chosen was that which fitted the curves to the baseline best. The values for all the variables were then optimised by manual iteration until the simulated curve was a close as possible to the experimental data. The final curves fitted probably are not a unique solution but they are a good manual fit based on the available data. The last step with curve fitting is to check whether the final result makes chemical sense.

(D) Water subtraction

The absorption of certain IR frequencies by water is so large that it can cause such a very low signal to reach the detector that on ratioing an aqueous sample against a background information about the sample is lost. Unless the temperature and the path length of the aqueous cell were kept constant the strong absorption of water swamped the sample. The magnitude and shape of the water absorbances are very sensitive to changes in temperature.

Initially the spacing between the two calcium fluoride plates was 12 μm to compromise between the absorption of the water and the dilute samples. However, it was found that even at this thin spacing the water absorption was so strong that the the sample spectrum was difficult to separate from the water spectrum. Eventually it was decided to use 6 μm spacers but this then meant that the signal level from the lipid was smaller due to reduced amounts of samples.

Despite all of these precautions there was still a net negative absorption due to water in the spectra because the vesicles replace a volume of water that was present in the background. There are several methods to deal with the problem. The first method is to ignore it and look at a different region of the spectra but this is not feasible if peptide conformation is to be studied. Furthermore, the strong negative absorption affects one of the most interesting bands in the lipid spectrum - the carbonyl band. The next method is to use a variable path length cell and to try and balance the volumes of water. The third technique is to try the tedious and difficult method of adding a water spectrum to the sample spectrum. The fourth possibility is to use D_2O as the solvent and thus shift the absorption to a different region of the spectrum. This may change the peptide interactions as they are highly dependent on hydrogen bonding[30].

In general the third option was chosen for the research described herein. The first technique was not practical given the aims of the project, the second was not used because the path lengths in the variable spacing cell were quite large (>20 μm) and thus the detector would receive no signal in the regions

of strong spectral absorption by water. The fourth method was used twice but due to the expense it was not possible to perform all of the experiments in D_2O. The extent to which the addition procedure was successful is illustrated in plot 3-9c.

The main problem encountered with spectral addition was that the water band in the ratioed vesicle spectrum was narrower than that in the pure water spectrum (~60 cm^{-1} compared to ~80 cm^{-1}). This could be due to the presence of hydrogen bonded water in the vesicle sample. Also the superimposition of sharp peaks, caused by the absorption of water vapour, on the main water bending mode gave problems as they were not always exactly the same relative intensities (plots 3-9 a&b). A variety of techniques were used to obtain a reference water spectrum, including ratioing spectra recorded in different path length cells such as 6 μm versus 12 μm, 12 μm versus 24 μm and ratioing cells full of water against an empty spectrometer. None seemed to give an adequate reference for spectral addition. One of the best attempts is shown in plot 3-9c.

plot3-9a: Negative spectrum of water

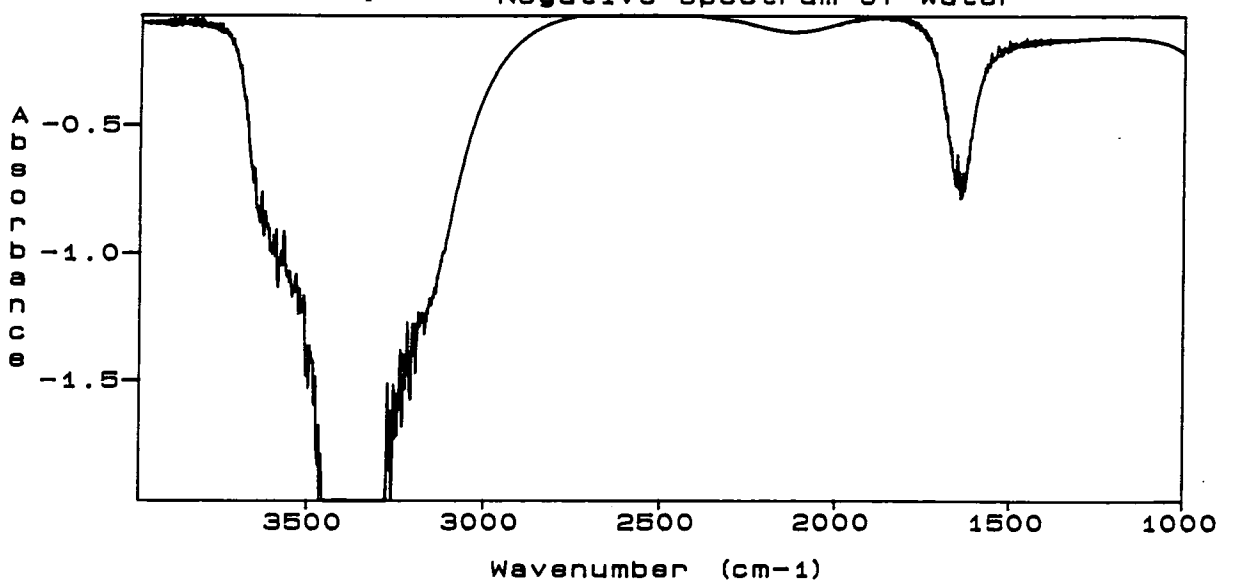

plot3-9b: Vesicles with negative water spectrum

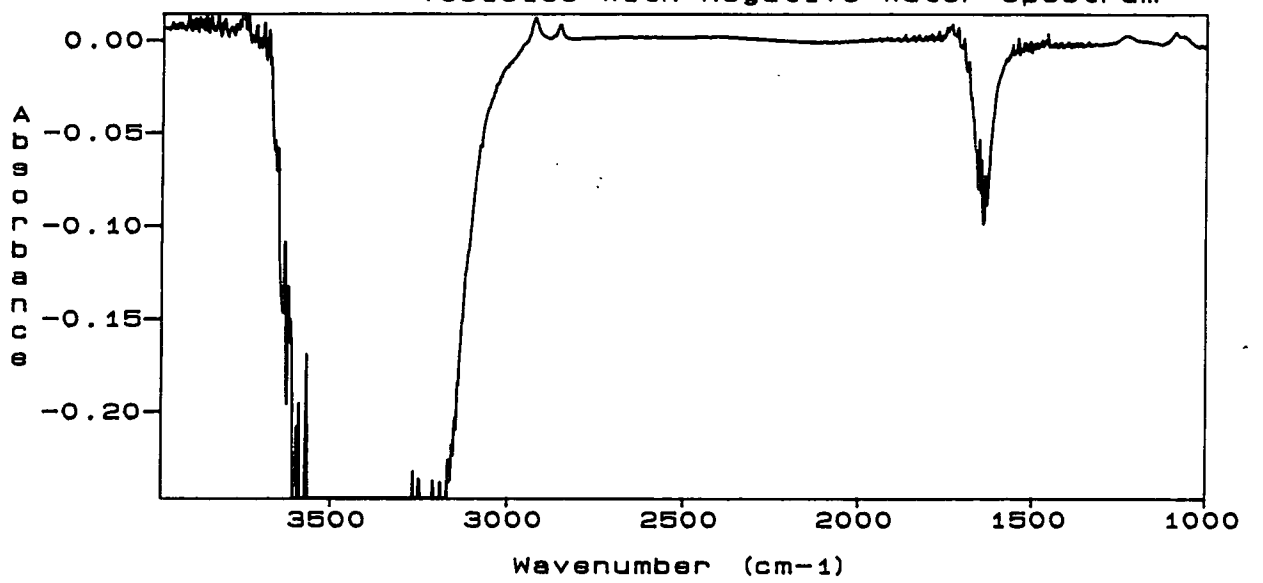

plot3-9c: : Vesicle spectrum after water subtraction

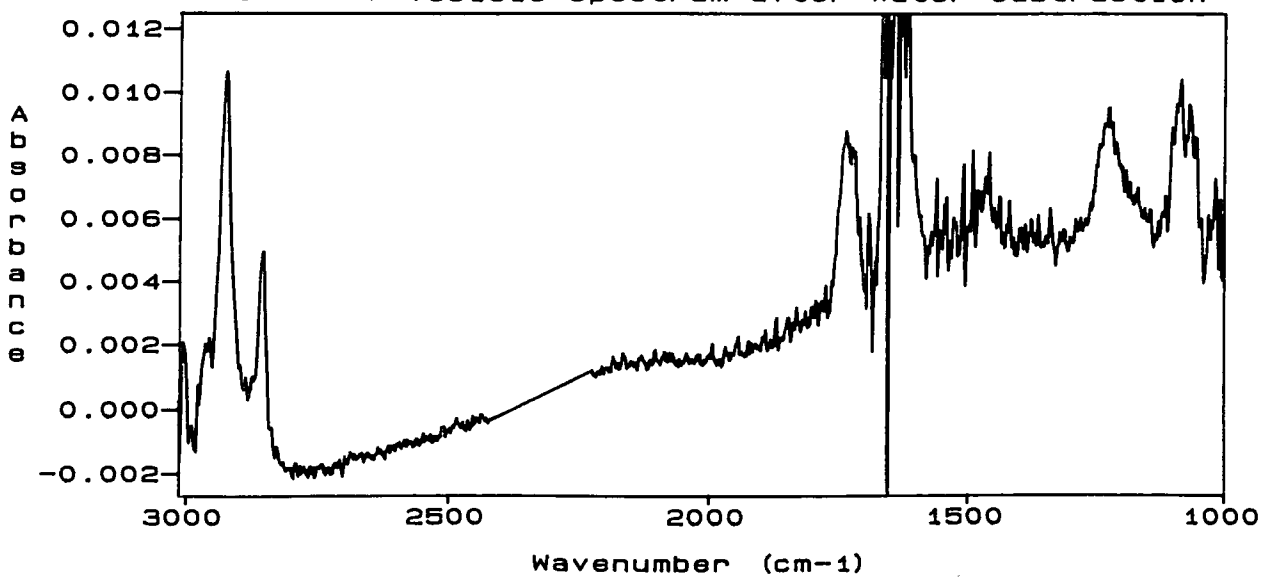

3.2.3 FTIR results

(A) Egg lecithin in solvents and as cast films

The spectra of ~1 mg/ml egg lecithin in three different solvents are displayed in plots 3-10,11&12. The sample emissivity spectra were ratioed against those of the pure solvents. Both sample and background were acquired at ~37 °C, within 0.1 °C of each other. The three solvents chosen were chloroform, carbon tetrachloride and methanol. Carbon tetrachloride was chosen because it is apolar. Methanol was used because a hydrogen bonding solvent was helpful in assigning the carbonyl peaks (see section 3.2.4.B). The spectrum in chloroform is shown because this is the solvent that the egg lecithin is dissolved in when supplied by Sigma.

Most of the differences between the spectra are due to the absorptions of the solvents. These are most noticeable in the methanol spectrum. The interpretation of the CH stretching region (3010-2800 cm^{-1}) of the spectrum (plot 3-12) is impossible due to the strong absorption of CH stretching vibration in methanol. The peak at 1661 cm^{-1} in plot 3-12 is due to the bending vibration of the OH group of methanol which is hydrogen bonded to the lipid. The strong absorption below 1000 cm^{-1} is also due to the OH bond absorbing of the IR energy. In the spectrum obtained in chloroform a negative peak due to C-H bending of chloroform is seen at 1220 cm^{-1}. The spectrum of carbon tetrachloride has not interfered with the recording of the lipid spectrum (plot 3-11). The strongest IR absorption of carbon tetrachloride in the region shown is at 1550 cm^{-1}. Evidently the amount of solvent in both sample and background must be the same as this peak has been ratioed out.

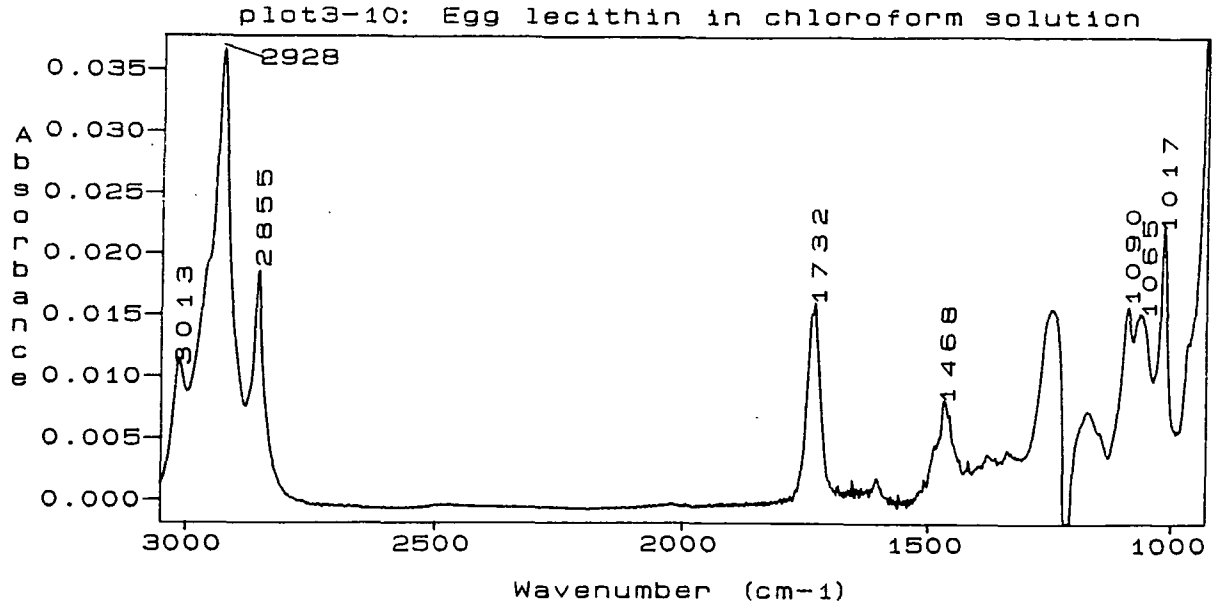
plot3-10: Egg lecithin in chloroform solution
Absorbance
0.035
0.030
0.025
0.020
0.015
0.010
0.005
0.000
2928
3013
2855
1732
1468
1090
1065
1017
3000
2500
2000
1500
1000
Wavenumber (cm-1)

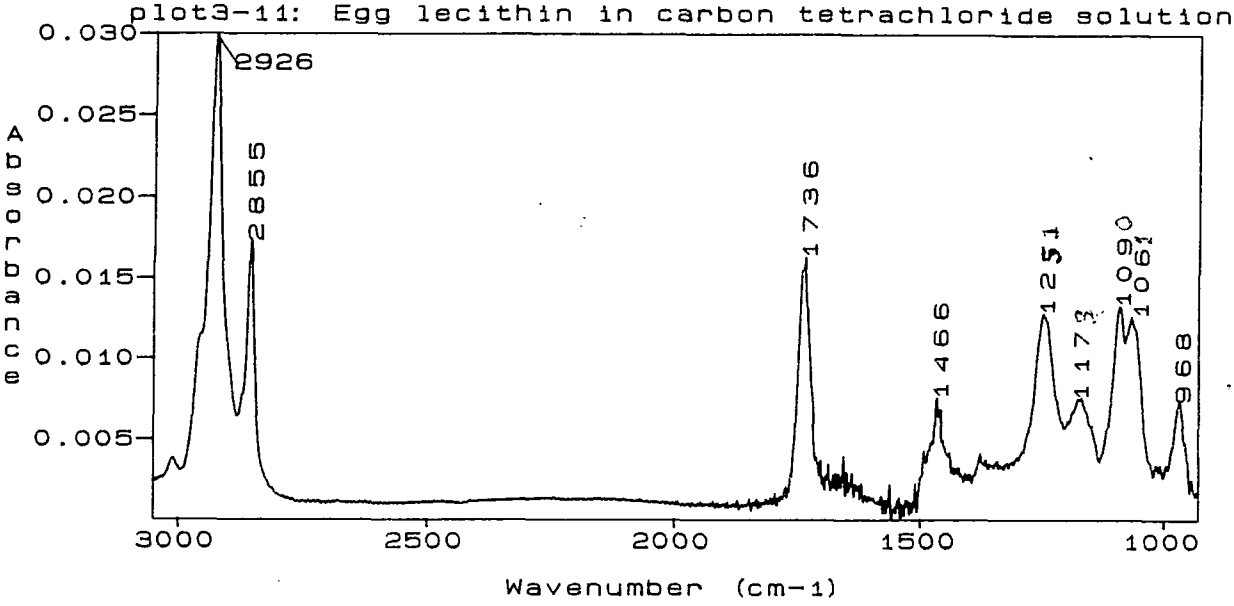
plot3-11: Egg lecithin in carbon tetrachloride solution
Absorbance
0.030
0.025
0.020
0.015
0.010
0.005
2926
2855
1736
1466
1251
1173
1090
1061
968
3000
2500
2000
1500
1000
Wavenumber (cm-1)

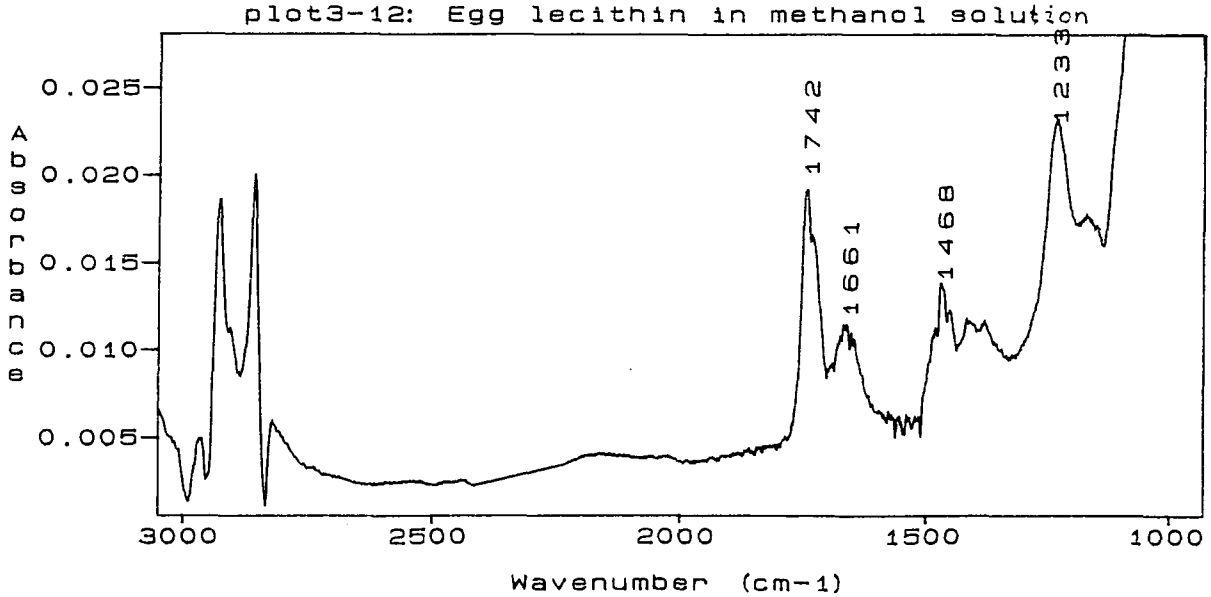
plot3-12: Egg lecithin in methanol solution
Absorbance
0.025
0.020
0.015
0.010
0.005
1742
1661
1468
1233
3000
2500
2000
1500
1000
Wavenumber (cm-1)

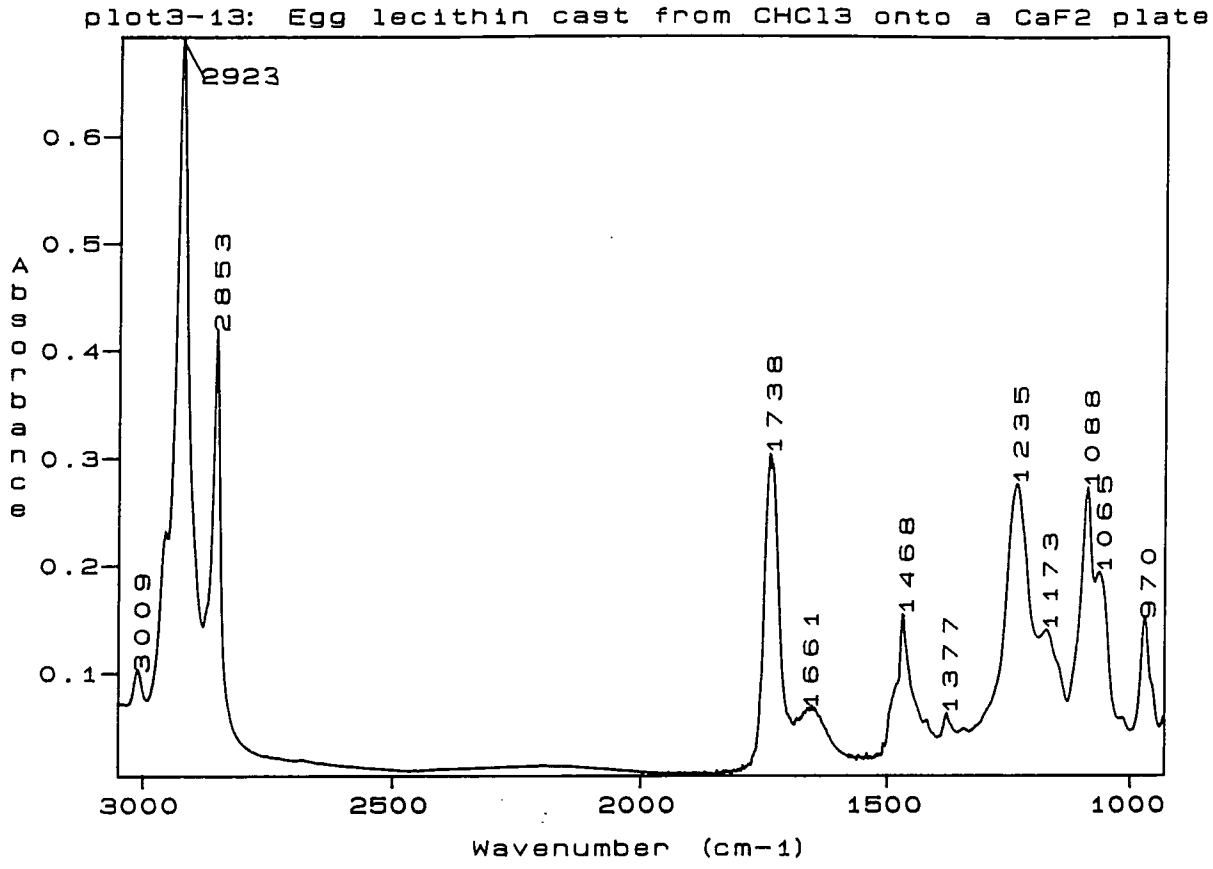
plot3-13: Egg lecithin cast from CHCl3 onto a CaF2 plate
Absorbance
0.6
0.5
0.4
0.3
0.2
0.1
2923
2853
3009
1738
1661
1468
1377
1235
1173
1088
1065
970
3000
2500
2000
1500
1000
Wavenumber (cm-1)

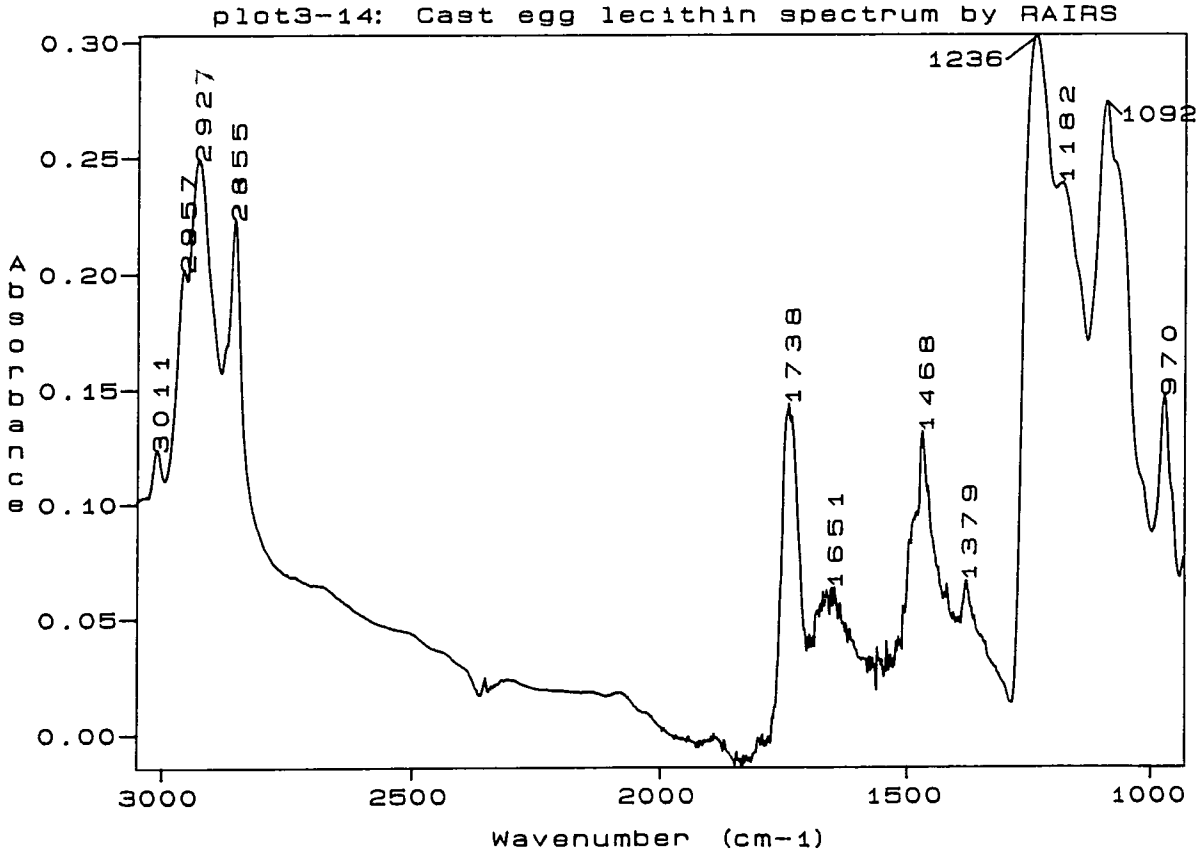
plot3-14: Cast egg lecithin spectrum by RAIRS
Absorbance
0.30
0.25
0.20
0.15
0.10
0.05
0.00
3011
2957
2927
2855
1738
1651
1468
1379
1236
1182
1092
970
3000
2500
2000
1500
1000
Wavenumber (cm-1)

One of the most notable differences between the phospholipid spectra, in different solvents, is the positions of the peaks due to the antisymmetric phosphate stretch. In methanol it is 1232 cm^{-1}; in chloroform it is at ~1241 cm^{-1} (the shape of the band is distorted by the negative absorption of the solvent) and in carbon tetrachloride it is 1251 cm^{-1}. These wavenumbers correspond to the those of hydrated and dry films of DMPC (respectively) obtained by Takenaka et al[51] via ATR. They recorded a value of 1231 cm^{-1} for the $\nu_{as}(PO_2^-)$ band of a hydrated film of DMPC and 1254 cm^{-1} for the same vibration in a dry film. The same trend is seen for egg lecithin itself. Fringeli and Grünthard[88] found that egg lecithin has a $\nu_{as}(PO_2^-)$ wavenumber of 1220 $cm^{-1}$for a hydrated film and 1252-1262 cm^{-1} for a dry film, with an intermediate value of 1225 cm^{-1} at 60 % humidity. Showing that the change in position must be due to hydrogen bonding between the solvent and the phosphate group.

Plot 3-13 shows a film of egg lecithin cast from a solution of chloroform onto a calcium fluoride plate. It is ratioed against a clean calcium fluoride plate. The peak at 1661 cm^{-1} has been assigned as the bending mode of water. This was still present after evacuation overnight, indicating that it was strongly bound to the lipid. The position of the $\nu_{as}(PO_2^-)$ peak also confirms the fact that the phospholipid is hydrated. Linearly polarised spectra were obtained, both s and p polarisations, and it was found that there was no significant difference between them.

Plot 3-14 is the RAIRS spectrum of a film of egg lecithin cast from chloroform. This technique is described in section 4.4.1.A. Only vibrations which involve a change in the perpendicularly (with respect to the substrate) resolved component of the vibrational dipole moment are coupled in RAIRS. The PO and COC stretching vibrations appear to be coupled much more strongly in the RAIRS spectrum compared to the other vibrations in the lipid. This indicates that although the cast film would be presumed to be disordered there is ordering of the molecules with respect to the substrate. The peaks due to methyl stretching vibrations (2957 and ~2871 cm^{-1}) are more intense relative to those of the methylene stretching vibrations than in the transmission spectrum (plot 3-13) again indicating ordering. It would appear that there is a preferred orientation of the vibrational dipole moments of the groups forming the hydrophilic region of egg lecithin which is largely perpendicular to the substrate. The alkyl chains chains are probably orientated at many different angles to the surface. This statement arises from the fact that both peaks from vibrations with dipole moments which are perpendicular to the axis of the chains (e.g. $\delta(CH_2)$) and with components parallel to the chain axis (e.g. $\delta_s(CH_3)$) show strong adsorptions in the RAIRS spectrum . The orientation of the headgroups may be facilitated by the presence of water, which could cause formation of planar bilayers.

(B) Vesicles

Plots 3-15&16 show the spectra of the fractions from the sephadex column with the highest concentration of lipid. In both cases the spectra were obtained in a 12 μm cell at 30 ± 0.2 °C. The background spectra were obtained using the same cell filled with buffer solution at the same temperature. Plot 3-15 is for a fraction produced from a starting solution with a 1.5:1 ratio of detergent to lipid. Plot 3-16 shows a fraction where the original detergent to lipid ratio was 15:1. In both cases the subtraction of water spectrum has been attempted. With more success in the case of the 1.5:1 ratio.

Both spectra have a very low signal to noise (S/N) ratio, particularly in the spectral region 2000-1500 cm^{-1}. Plot 3-15 has a S/N ratio of 180 in the CH stretching region (300-2800 cm^{-1}) but this falls to 30 in the carbonyl region (2000-1500 cm^{-1}) and the S/N ratio of the band due to the absorption by the carbonyl group (~1730 cm^{-1}) to the noise from the liquid water subtraction (~1700-1600 cm^{-1}) is only 5. The respective figures for plot 3-16 are 60, 14 and 3. This high level of noise is due to a number of factors. The spectral subtraction of liquid water bands even if complete distorts the spectra, as it was not possible to obtain a water spectrum for subtraction which exactly matched the water in the sample spectrum. Water vapour also absorbs strongly in this region and may have to be subtracted from the spectrum. Even if two spectra are recorded one after the other there is usually a small difference in the level of water vapour. If the span of time is half an hour and the lid of the sample compartment has been opened to change the solution then this difference can be quite large (0.03 absorbance units) compared to the sample spectrum. It is usually possible to subtract a reference water vapour spectrum from the sample spectrum. This does add to the general noise level of the spectrum and in particular increases the noise in the region where the water vapour absorbs. However, the main cause of the low signal to noise ratio is the low concentration of the samples. This means that the background noise level due to the instrumental factors is high compared to the sample spectrum.

This will affect all regions of the spectrum. An indication of the background noise is seen in regions of the spectra where there are no sample peaks, such as 2800-1900 cm^{-1}. The straight lines seen in the middle of this region are due to the carbon dioxide spectrum being removed via 'lining out' rather than subtraction.

The two spectra (plots 3-15 & 16) are representative of several experiments. There is little difference between the spectra obtained from repeating an experiment. Indeed, even in the spectra with the best signal to noise ratios no reproducible differences between the spectra obtained from the two different detergent/lipid ratios could be found. Nor was there any change on the addition of Mn^{2+} to the samples.

Plot 3-19 is the spectrum of the mixed detergent and lipid (15:1) micelles before being eluted on the column. The dotted line is the original spectrum - it can be seen that its form appears the same as plot 3-20. This is due to the large number of detergent molecules compared to lipid. The solid line on plot 3-19 is the same spectrum but with the sodium cholate spectrum subtracted. The peaks at 1404 and 1547 cm^{-1} in the detergent spectrum were used to determine the subtraction factor at which all of the detergent spectrum had been removed. Revealed beneath the detergent spectrum is that of the lipid which is also present. This spectrum will be considered in detail in section 3.2.4.

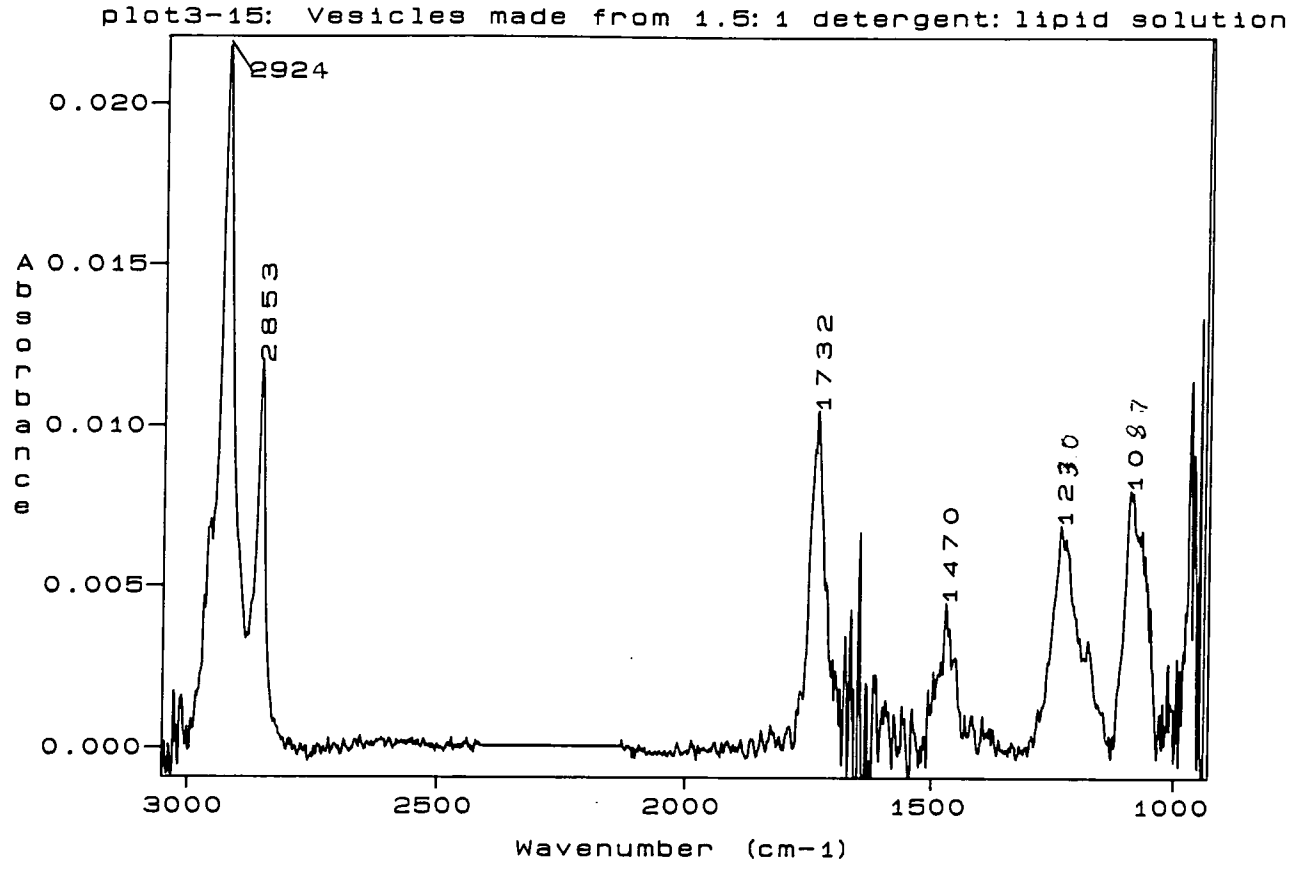
plot3-15: Vesicles made from 1.5: 1 detergent: lipid solution
Absorbance
0.020
0.015
0.010
0.005
0.000
2924
2853
1732
1470
1230
1087
3000
2500
2000
1500
1000
Wavenumber (cm-1)

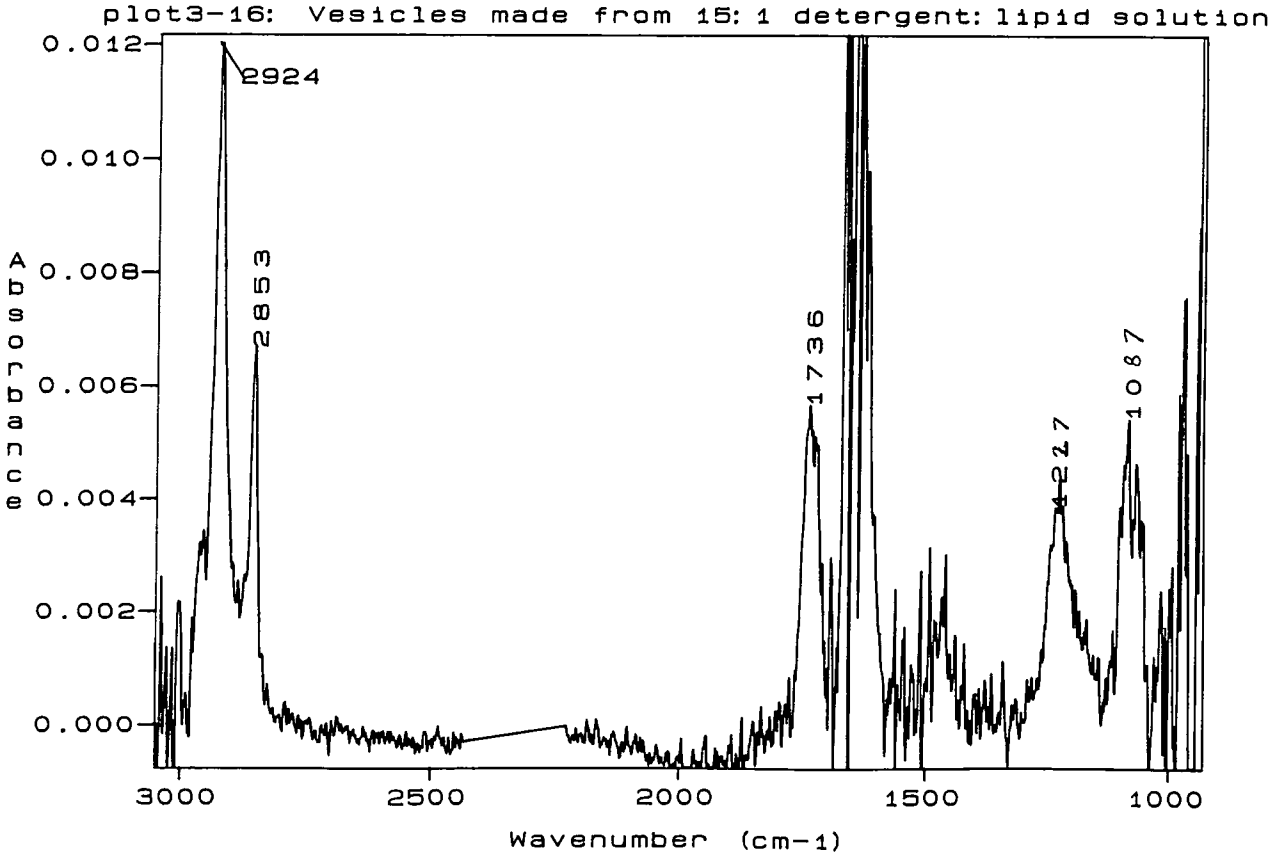
plot3-16: Vesicles made from 15: 1 detergent: lipid solution
Absorbance
0.012
0.010
0.008
0.006
0.004
0.002
0.000
2924
2853
1736
1217
1087
3000
2500
2000
1500
1000
Wavenumber (cm-1)

Plot 3-23 shows the spectrum of vesicles made from the 15:1 detergent:lipid ratio but in D_2O to act as a reference spectrum for subsequent experiments involving peptides. Unfortunately, the detergent appears not to have been removed from the sample by the column. This can be seen by the presence of peaks at ~1550 and ~1400 cm^{-1}. However, these could be due to another contaminant as there is a peak at 2982 cm^{-1} where neither lipid, buffer nor detergent spectra showed any peak. These peaks in the sample spectrum were only seen on the one particular day of these experiments. Apart from the buffer being phosphate based rather than hepes (see section 2.2) which was slightly unusual but had been used several times before, and the solvent being D_2O there were no other major deviations in experimental procedure. The only difference which may have had some effect was the fact that the sephadex column was not rinsed as thoroughly as usual. Normally ~100 ml of buffer were used to rinse the column but in this case, due to the expense, only 20 ml of buffer were used for rinsing. It was a new column of sephadex so the contaminant was not detergent left on the column from a previous experiment. Therefore either the detergent was not fully separated or there was a contaminant.

(C) Cast films from vesicle solutions

Plots 3- 17&18 show the spectra obtained when a solution of the vesicles was cast as a film and dried. Plot 3-17 is the spectrum via transmission. PLot 3-18 is a spectrum taken using the RAIRS technique. These spectra were recorded to see whether the lipids retained any of the ordered bilayer structure on the removal of the water. As the vesicles were in buffer solution on casting the film the spectrum of hepes could be seen with the lipid spectrum. Spectral subtraction of a cast film of pure buffer solution was therefore performed. The resultant spectra are those shown. All of the transmission spectra were recorded at 37 $^{\circ}$C but there was no temperature control for the RAIRS equipment so experiments were carried out at room temperature, ~19 $^{\circ}$C.

Linear polarisation of the transmission sample showed no dichroism indicating that there was no difference in the ordering in the x or y directions. In the RAIRS spectrum the region below 1300 cm^{-1}, containing peaks relating to the C-O-C and O-P=O groups was very intense compared to the rest of the spectrum. The bands in the CH stretching region were of the lowest intensity. This would seem to indicate that the lipids were ordered with respect to the surface such that the phosphate groups are largely perpendicular to the surface but the alkyl chains are randomly orientated. As seen in the cast film, plot3-14.

There appear to be some major changes in the transmission spectrum of the cast vesicles compared to the film cast from chloroform, and from the vesicle experiment. These were reproducible. Plots 3-25a&b show the solution state and cast films respectively of the buffer, hepes. It can be seen that the two spectra have very different shapes for bands positioned below 1300cm^{-1}. Although subtraction of cast film of buffer solution was undertaken for the cast vesicles it would seem that the difference in the lipid spectrum, compared with any of the other lipid spectra obtained may because buffer peaks are narrower than in solution. Bands below 1300 cm^{-1} which are the most intense in the aqueous buffer also occur in the cast film spectra of the buffer but are much narrower than when cast with the vesicles. This is possibly due to the water retention by the cast vesicles.

plot3-17: Cast film of the vesicles by transmission

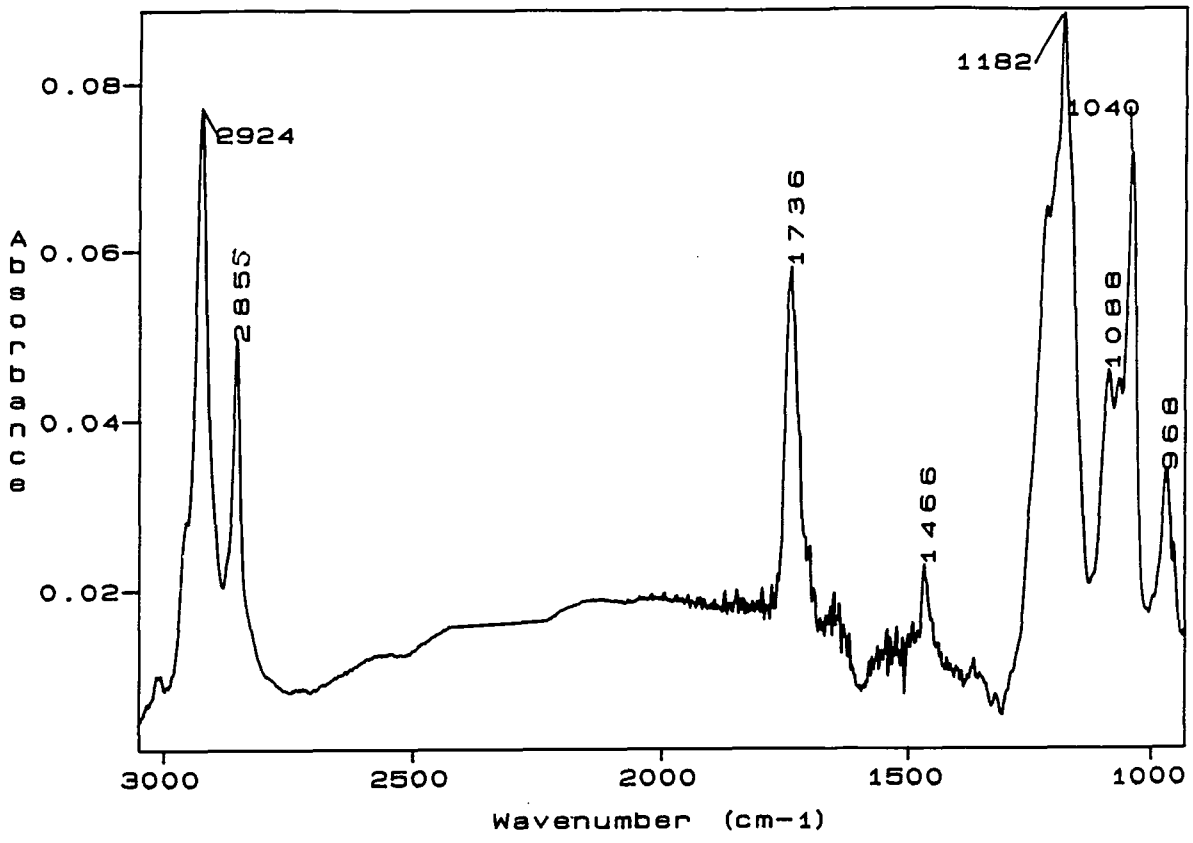

plot3-18: Cast film of the vesicles by RAIRS

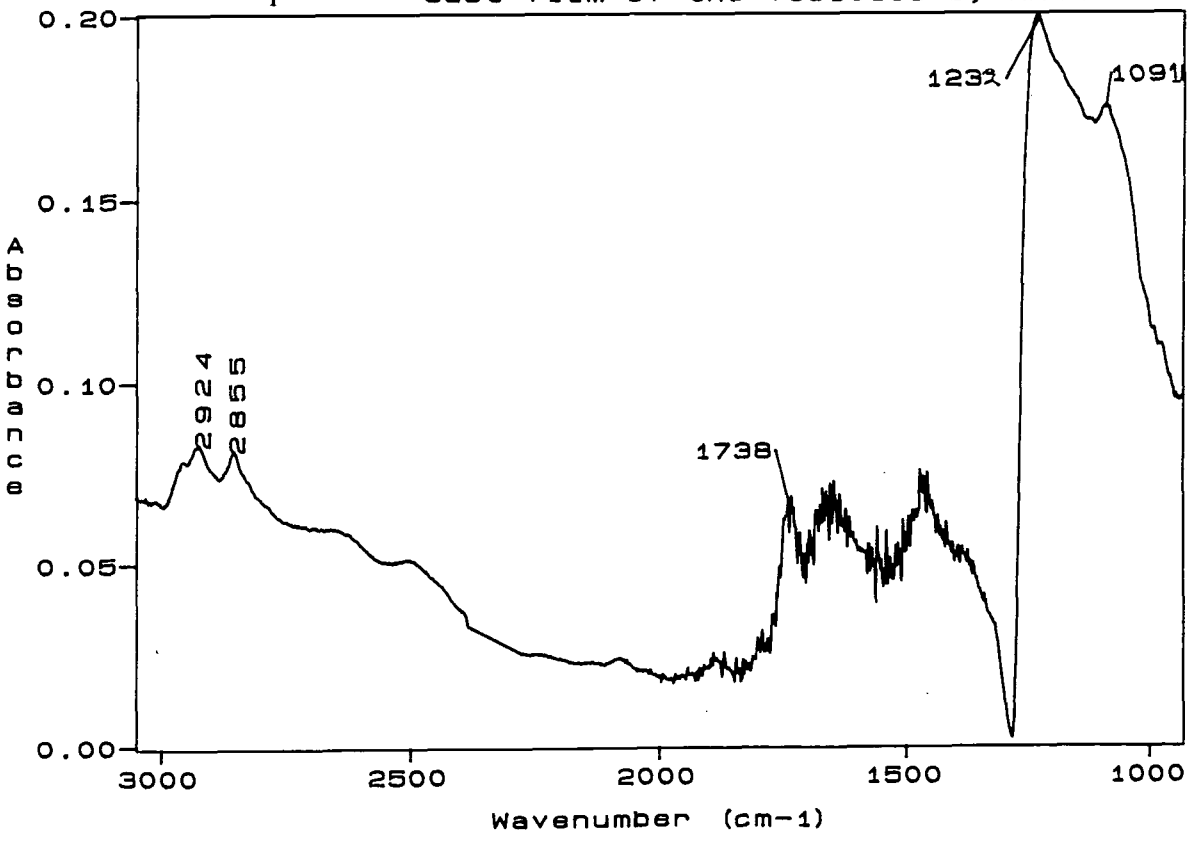

plot3-19: Pre-column solution, 15: 1 ratio

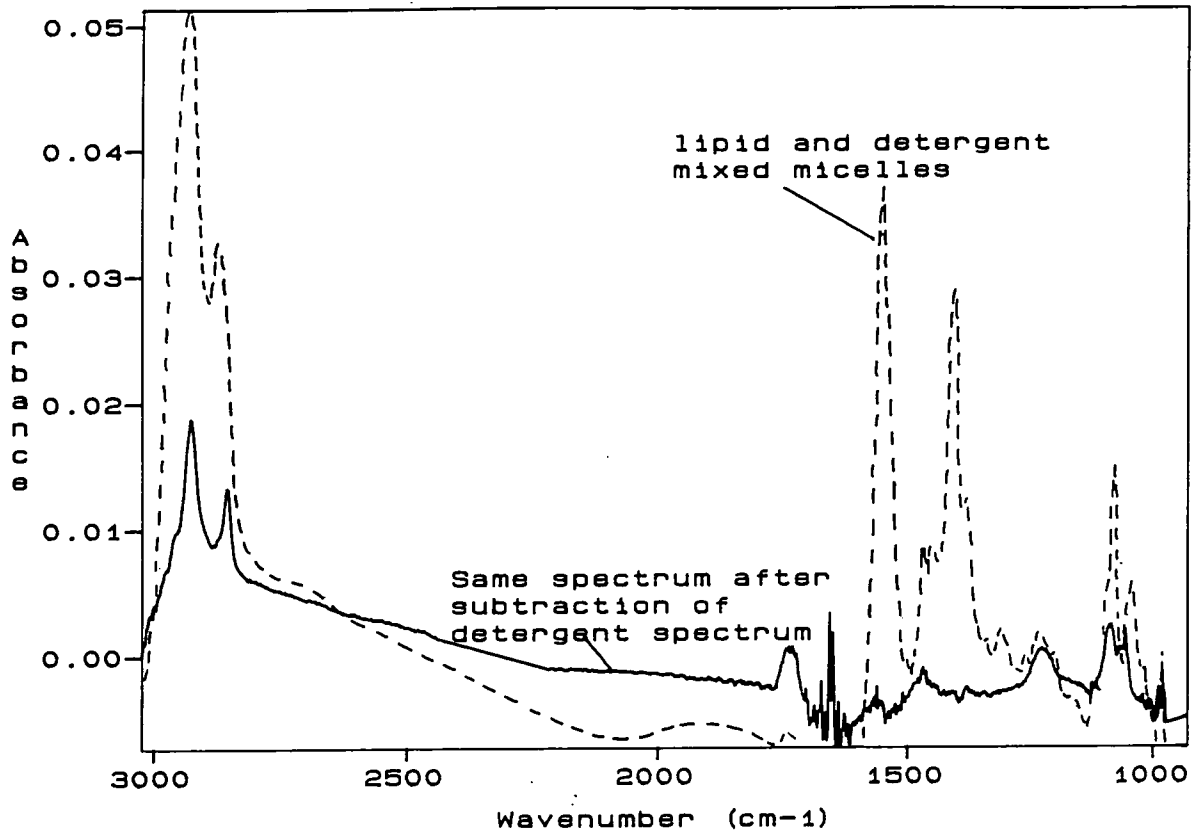

plot3-20: Sodium cholate (detergent) in water

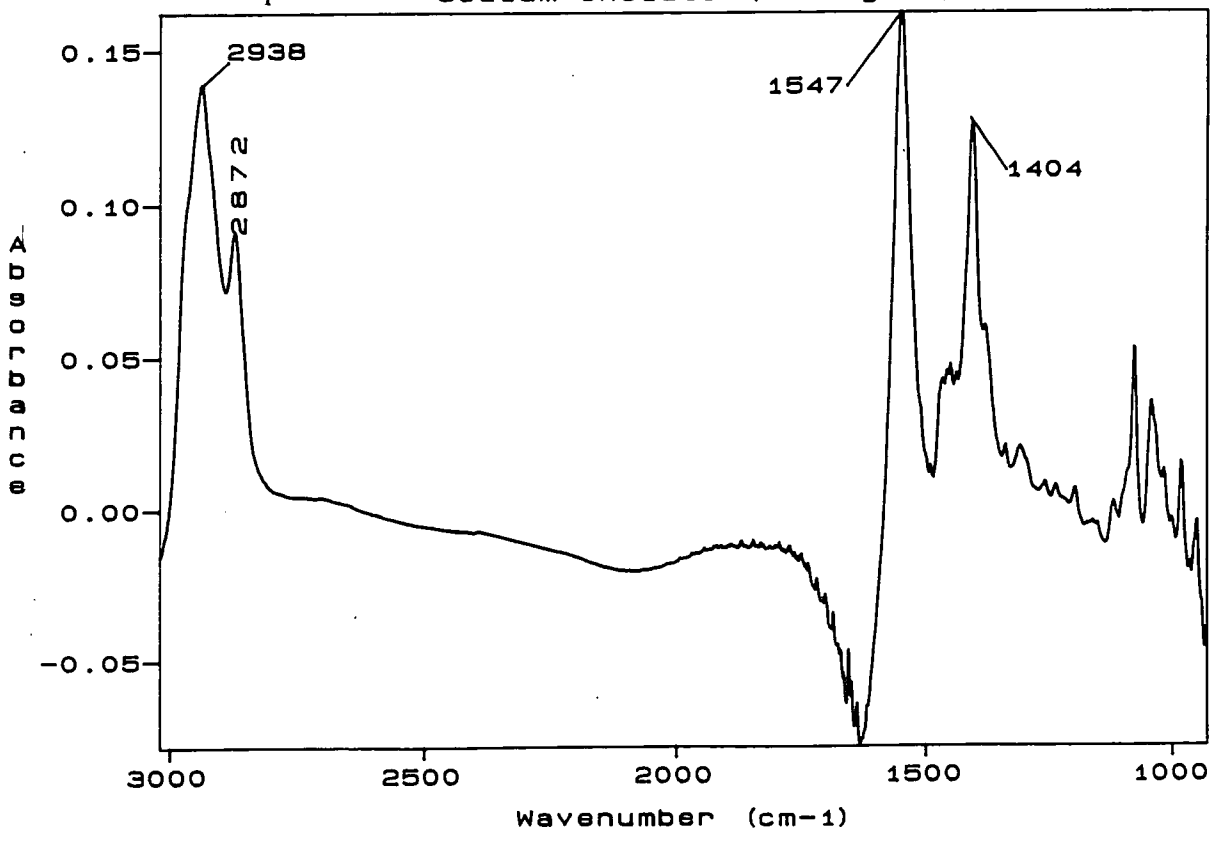

plot3-21a: Hepes buffer as a film cast from water onto CaF2

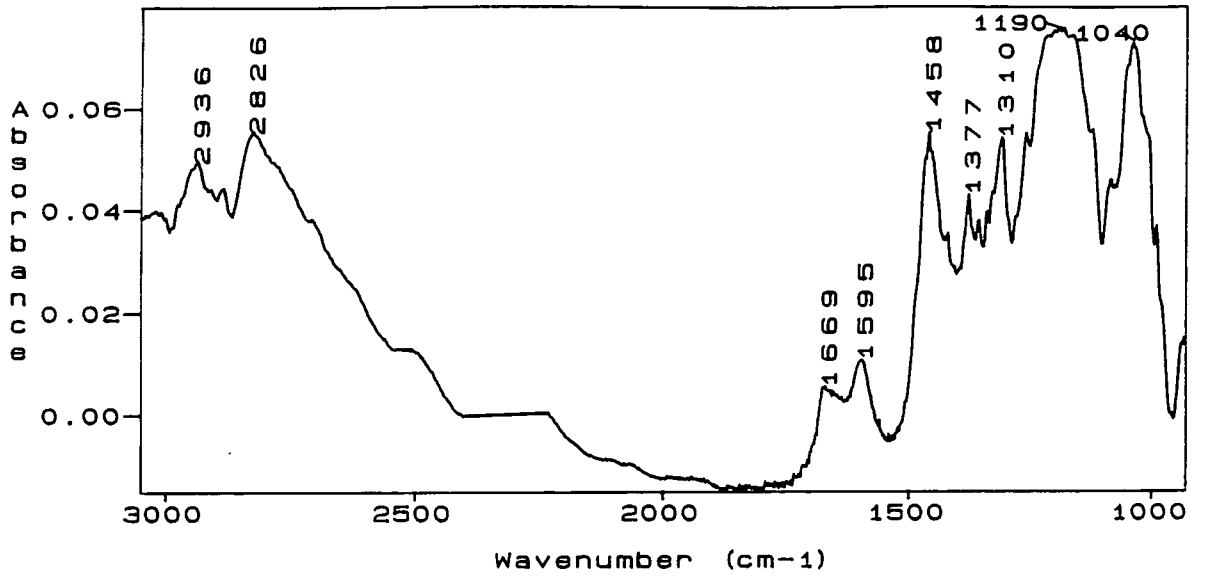

plot3-21: Hepes buffer in water

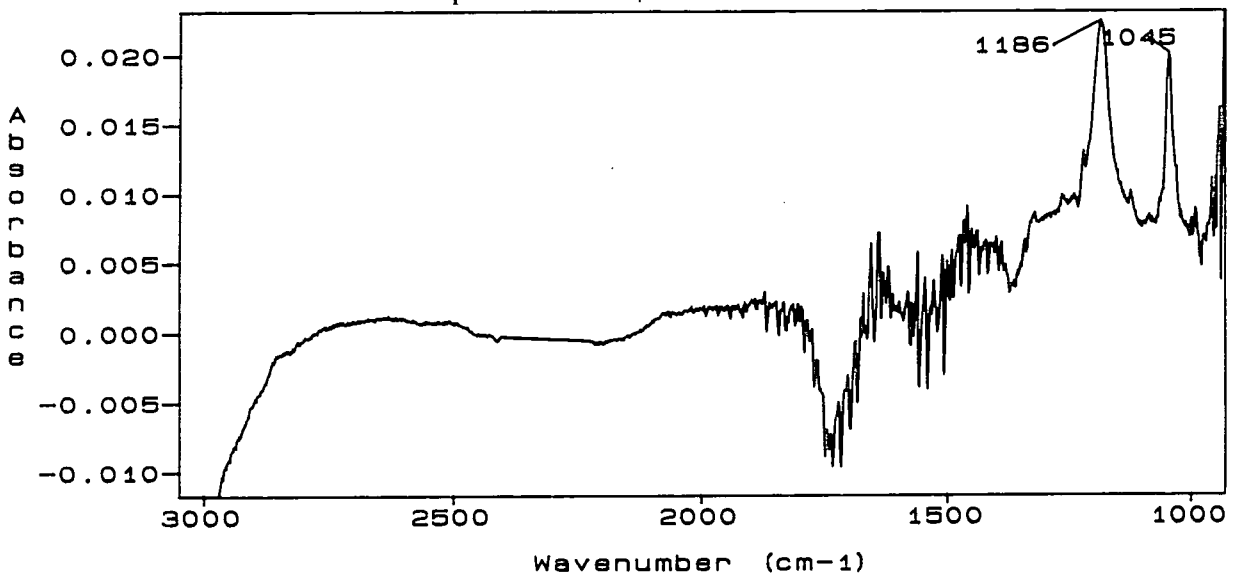

plot3-22: Phosphate buffer in deuterium oxide

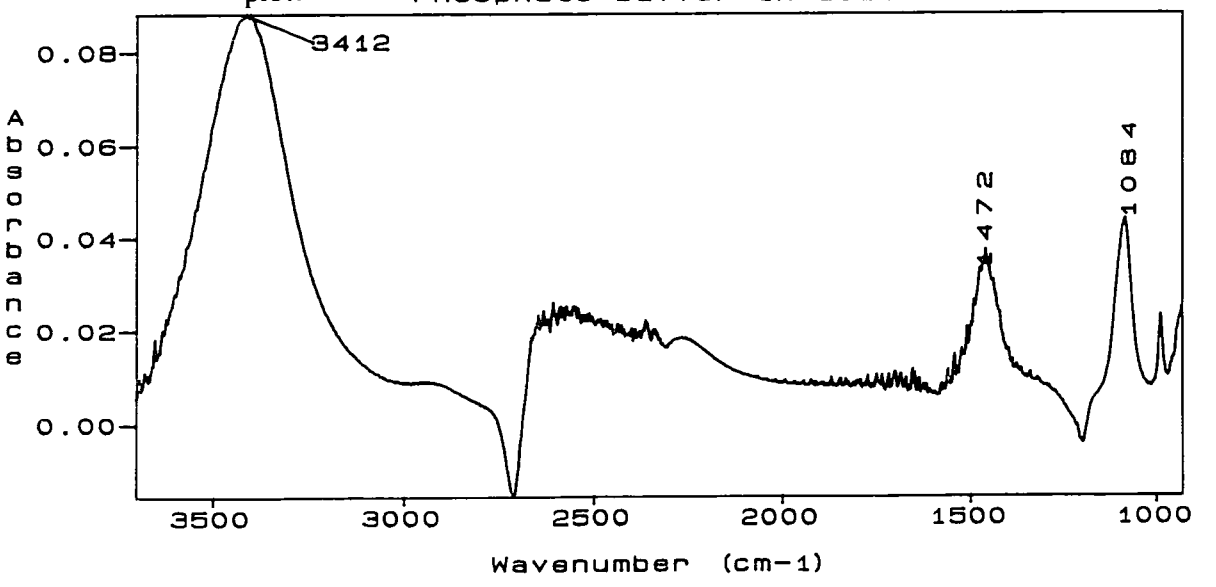

(D) The addition of peptides

Plots 3-24,25&26 are spectra of the attempts to incorporate peptides into the vesicles. Plot 3-24 was carried out in water, but the experiments for plots3-25&26 were done in deuterium oxide. In all cases the buffer was phosphate. The last two were carried out on the same day as the experiment whose results are shown in plot 3-23 and discussed in section 3.2.3.B.

Plot 3-24 is the spectrum from an experiment where polybenzylglutamate (figure 3(f)), a polypeptide with only one type of monomer unit, was added as a chloroform solution to the lipid chloroform solution. Its average relative molecular weight is 21000. It was chosen because it is thought to span a bilayer membrane[91].

This experiment appears to have been successful in so far as the peptide has traversed the column and been eluted in the same fraction as the lipid (plot 3-24). This can be seen by comparison with the reference spectrum of cast peptide. The peak at ~1650 cm^{-1} has changed position from the cast film to the eluted solution. However, it must be remembered that this is the spectral region where water absorbs strongly and may weight the spectrum (see section 3.2.4.C). Unfortunately, there is no positive proof that the peptide has been incorporated into the vesicles and not just eluted with them in the same fractions. The weight of the peptide is such that it is greater than the exclusion limits of the polymer beads and would elute in the fraction immediately following the void volume whether incorporated or not.

It is difficult to tell whether the presence of the peptide has altered the lipid structure. This is mainly due to the fact that the peptide absorbs strongly in both the ν(C=O) region and ν(COC) region. The peptide absorbs weakly in the CH stretching region and no change in this region of the spectra was detected compared to vesicles prepared solely with lipid. There is one major difference in the lipid spectrum - the peak due to the antisymmetric PO_2^- stretching vibration has moved to 1223 cm^{-1} compared to 1227 cm^{-1} in lipid vesicles. This indicates a higher degree of hydration. This could be caused by a number of factors:

the phosphate peak could be superimposing with the peaks in the peptide spectrum to give an apparent shift in the wavenumber; the peptide may have altered the method of formation of the vesicles on the sephadex column; or the peptide may be interacting with the vesicles, either on the outside of the bilayer and possibly trapping water between it the the lipid or the peptide may be incorporated across the bilayer and the lipid structure changing to accommodate it. Without further information it is impossible to choose one of these as the best explanation.

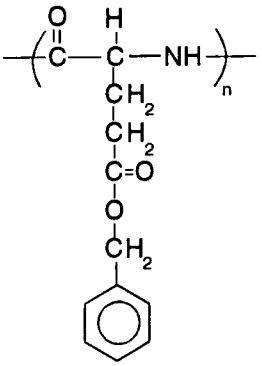

Figure 3(f) : The structure of polybenzylglutamate.

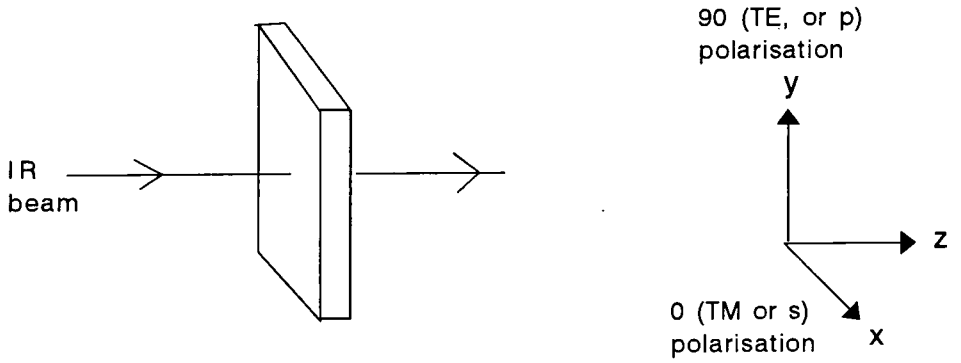

Figure 3(g) : Definition of directions of polarisation and axes.

Plots 3-25&26 are spectra of attempts to incorporate alamethicin and gramicidin D respectively. Details of these oligopeptides may be found in chapter 7. At this point suffice to say that both of them are known to incorporate across a biological bilayer in aggregates[3,38]. Although there is some controversy as to whether alamethicin will traverse a bilayer without the presence of an external electric field[89].

In the case of the plot 3-25, where alamethicin was used, no evidence for the presence of the peptide is seen in the spectrum of the lipid containing fractions. Thus it must be concluded that either concentrations of alamethicin were too low to detect or that it had not incorporated into the vesicles.

Plot 3-26 shows the same experiment but with gramicidin D as the peptide. At first glance it might appear that the gramicidin has indeed been transferred down the column with the lipid. However the dashed line is the spectrum of a film, cast from chloroform, of the mixed solution of lipid and gramicidin. It shows that the most intense peak in the gramicidin spectrum is at ~1650 cm^{-1} (the amide I band) but in the spectrum of the fraction eluted from the column the most intense peak which could come from the gramicidin alone is at ~1550 cm^{-1}. Incorporation of gramicidin D into the bilayer should not cause such a large change in the relative absorption coefficients[90] as would be necessary to cause such a reversal in the peak intensities. The experiment was performed on the same day and on the same sephadex column as the experiment connected with plot 3-23 where it was concluded that there was either detergent or a contaminant present in the fraction. It must be concluded that there is a strong possibility that this is the case once again. The only peculiarity with the possible contaminant is that the experiment with alamethicin was undertaken on the same day and same sephadex column. It was done between the pure lipid experiment and the one with gramicidin D so it is surprising that there is no large contribution from a peak at 1550 cm^{-1} in the spectrum shown in plot 3-25.

plot3-23: Vesicles made in D2O from 15: 1 detergent: lipid

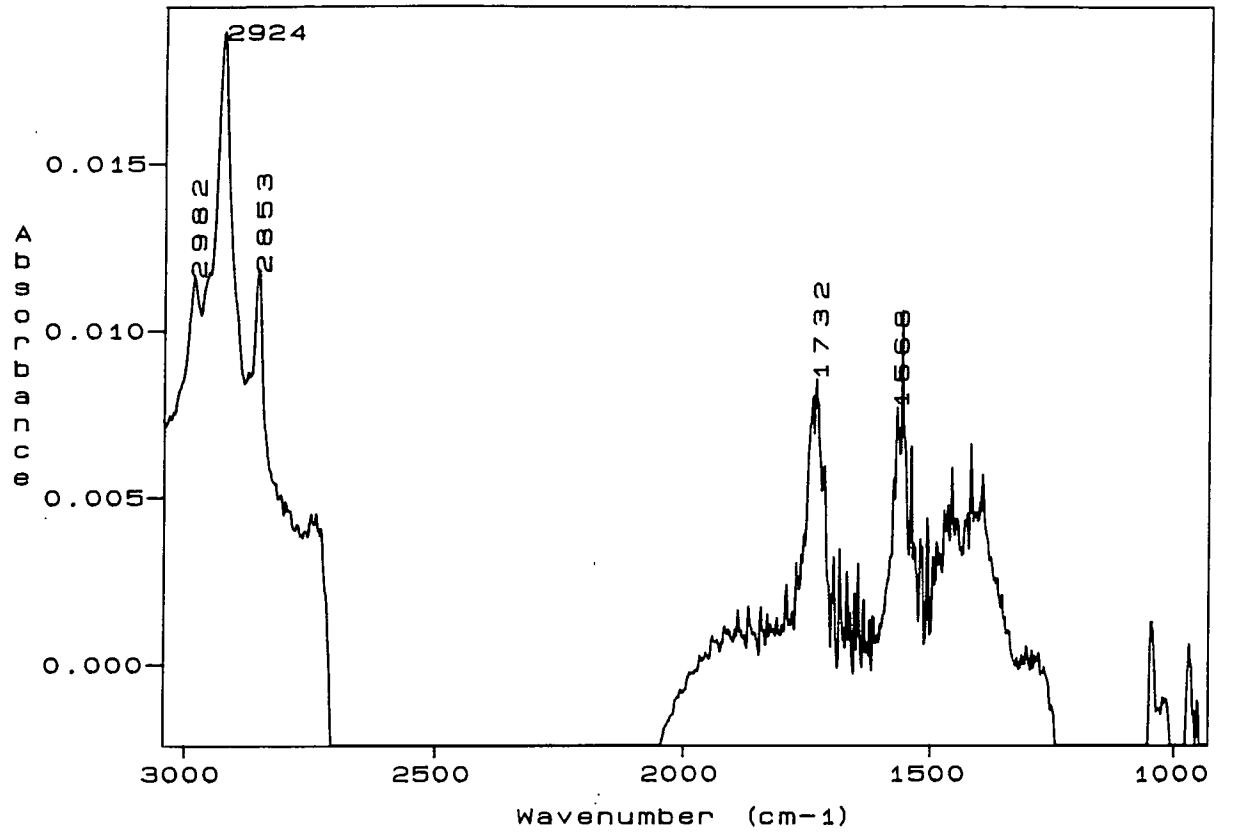

plot3-24: Aggregates with polybenzyl-glutamate

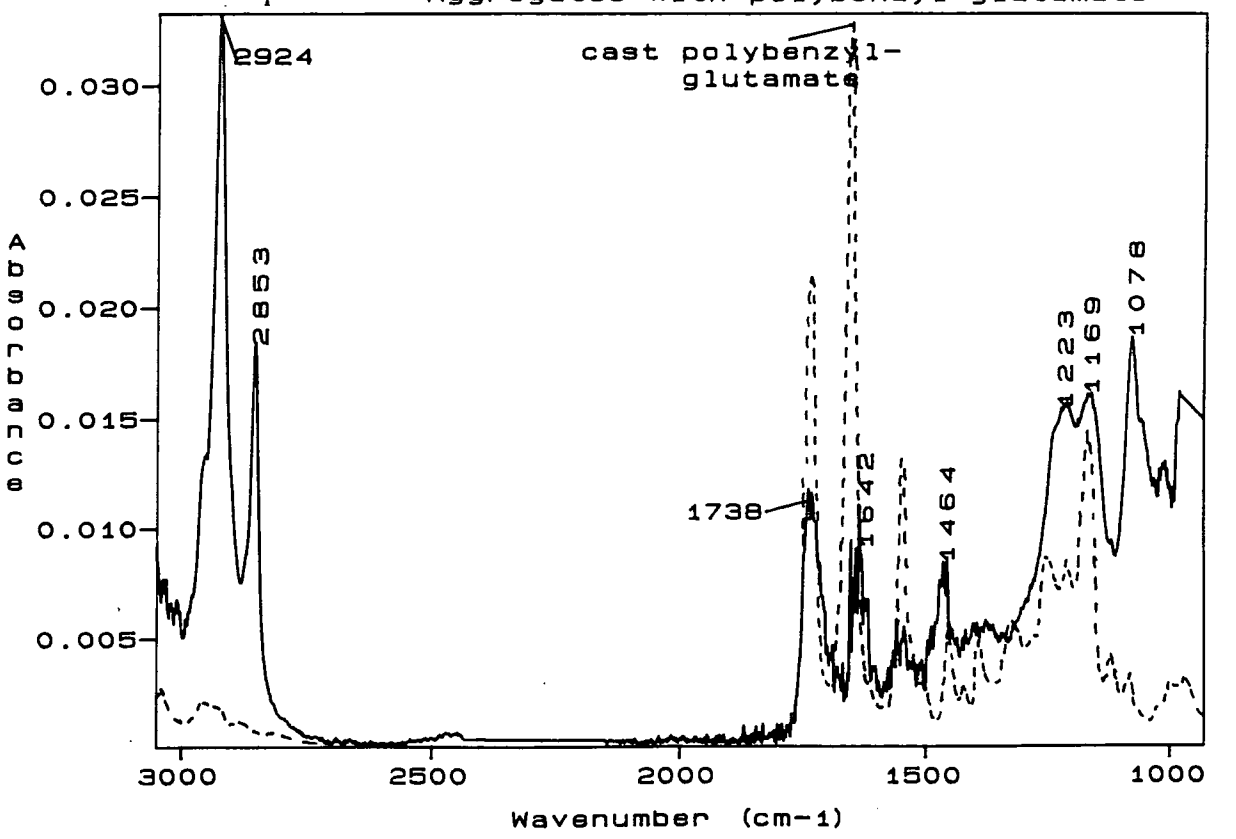

plot3-25: Vesicles made in D2O with alamethicin

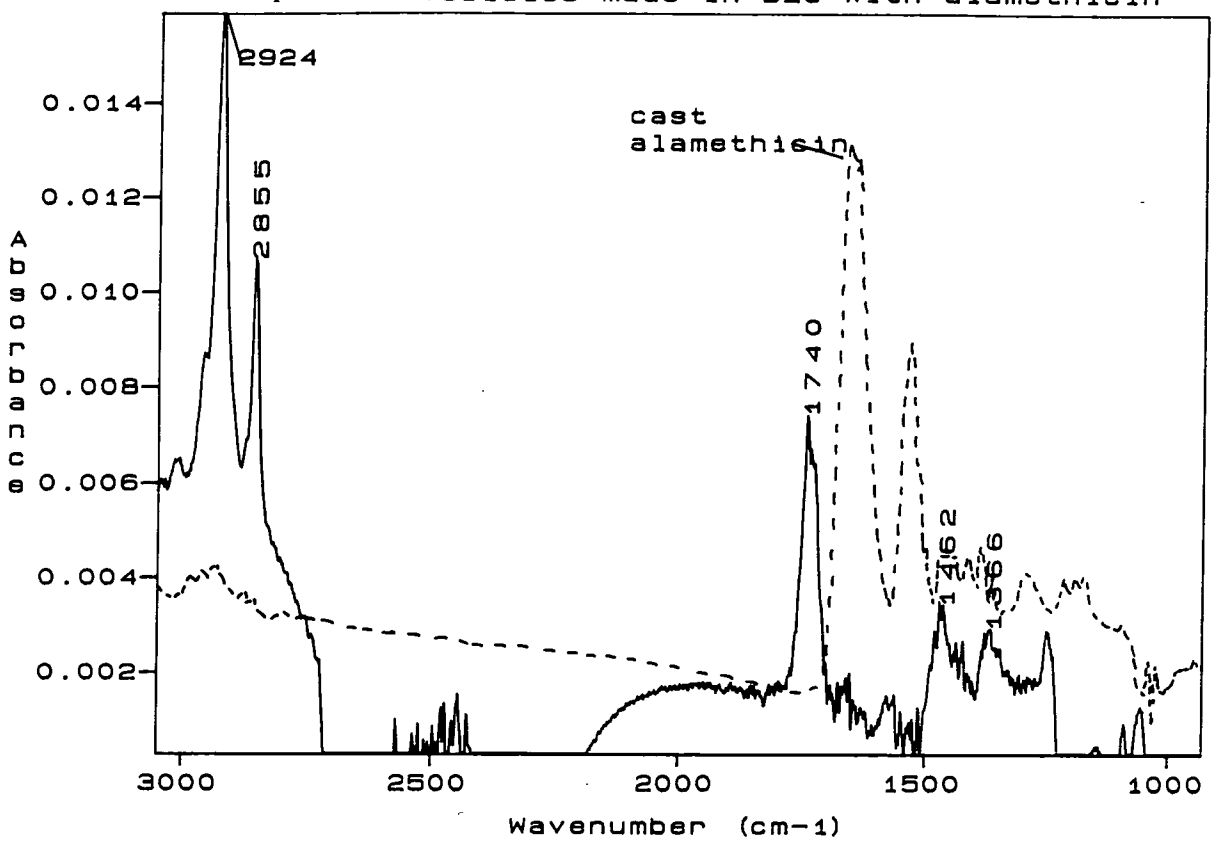

plot3-26: Vesicles made in D2O with gramicidin D

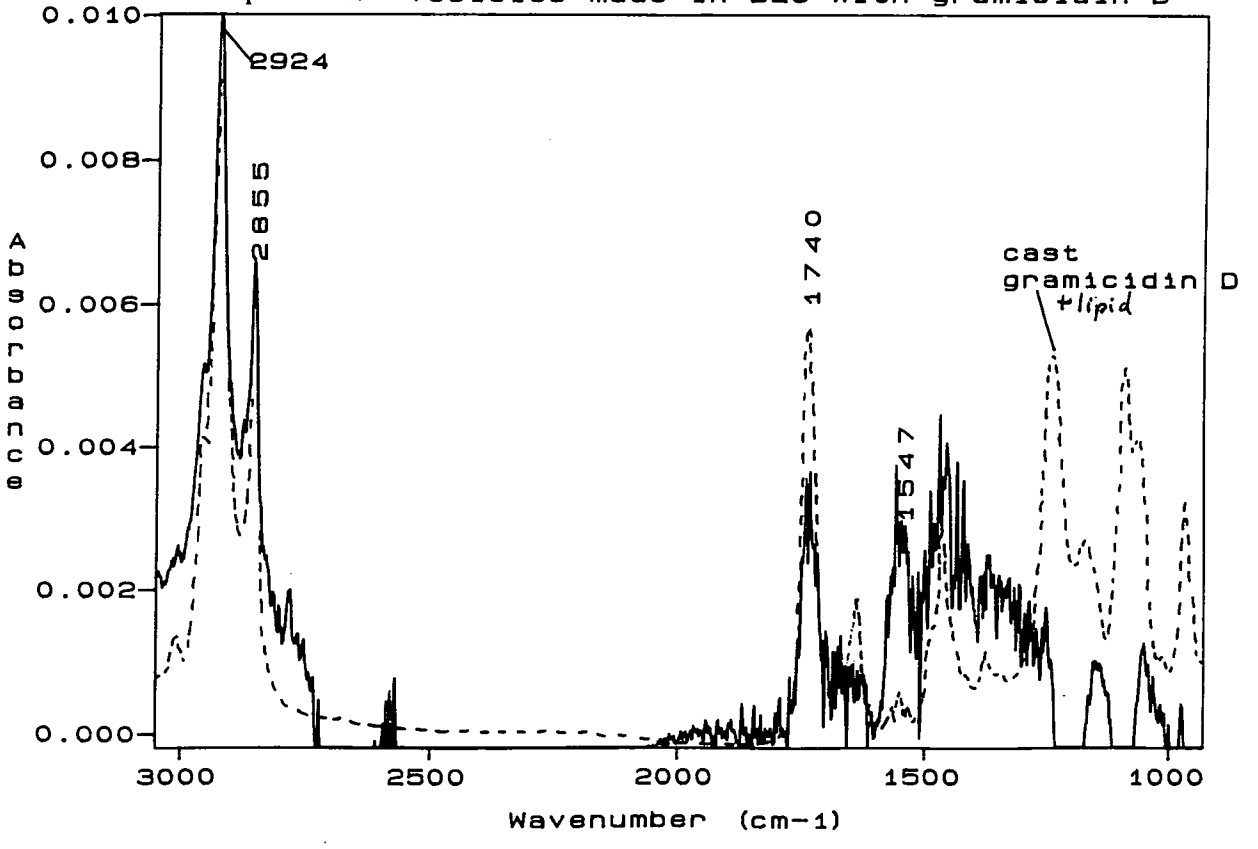

3.2.4 In depth analysis of spectral regions

(A) 3050-2800 cm^{-1} - CH stretching vibrations :

Description of sample	ν (CH) in alkenes	$\nu_{as}(CH_3)$	$\nu_{as}(CH_2)$	$\nu_s(CH_3)$	$\nu_s(CH_2)$
in chloroform	3014.0 0.019 23.5	2958.5 0.023	2929.0 0.038 44.5	2873.5 sh.→	2855.0 0.018 22.0
in carbon tetrachloride	3009.5 0.0013	2954.5 0.0095	2926.5 0.028 29.5	2872.0 sh.→	2854.5 0.016 18.5
in methanol	3011.0 0.004	-----	2927.0 0.018 31.0	sh.→	2857.0 0.016 22.0
film cast from chloroform	3010.0 0.038	2955.5 0.174	2923.0 0.634 27.0	2872.2 sh.→	2853.0 0.370 17.5
RAIRS of film cast from chloroform	3010.0 0.025 22.0	2957.5 0.105	2927.0 0.155 66.5	2873.5 0.080	2855 0.135 28.5
mixed detergent and lipid micelles	3009 (noisy)	2955.5 0.0028	2925.0 0.012 29.0	2873.5 sh.→	2854.5 0.0069 19.5
multilamellar vesicles (from 1.5:1 ratio)	noisy	2956.0 0.067	2925.0 0.022 27.0	2871.5 sh.→	2853.0 0.012 18.5
unilamellar vesicles (from 15:1 ratio)	noisy	2957 0.007	2924.5 0.018 33.0	2871.5 sh.→	2853.5 0.011 22.0
" + $MnCl_2$	"	sh.→	2924.0 0.0086 26.0	2873.5 sh.→	2853.5 0.0045 16.0
cast film of unilamellar vesicles	3007.5 0.006	2953.1 0.045	2924.5 0.127 30.5	2873.4 0.08	2855 0.135 28.5
RAIRS of cast film of UV vesicles	3011	2958.0 0.024	2929.5,2924.5 0.033	2872.1 sh.→	2855 0.029

Key : Each of the boxes has the data laid out in the following manner :

Peak position	cm^{-1}
Intensity (absorption)	
Full width at half height	cm^{-1}

sh.→ this notation means that the stated band is a shoulder of the next peak.

Table 3(ii) Measurements on peaks in the CH stretching region 3050-2800 cm^{-1} for FTIR spectra of egg lecithin in a variety of environments.

Plot 3-27 shows the spectra of egg lecithin in three very different environments : in chloroform solution (dots); as a film cast from chloroform (dashes); and in an aqueous environment in the form of vesicles (solid line). There is clearly a shift in the wavenumber of the peak due to the $\nu_{as}(CH_2)$ stretching mode to a higher value as the lipid environment changes state, in the order: cast film; to aqueous media; to non-polar solvent (chloroform). This is confirmed by the measured values given in table 3(ii) where the position of the $\nu_{as}(CH_2)$ peak ranges from 2923 to 2929 cm^{-1} for the respective environments.

The positions of both the CH_2 stretching vibrations are dependent on the fluidity of the chains[28]. Gauche bonds interrupt the interactions between CH_2 groups and thus the wavenumber increases as the number of gauche conformations rises. The highest wavenumbers are found for the most fluid chains. Fluidity in this respect refers to the number of possible conformations an alkyl chain may adopt. If no gauche bonds can be formed, as is the case below the phase transition temperature[28] then the alkyl chains have only one possible conformation, which is all trans. At the pre-transition temperature a few more conformations are possible as gauche bonds may be formed at the methyl end of the chains[28]. Above the transition state the number of possible states is much higher as many gauche conformations can be formed at different points along the chains. However, the actual movement of the chain between different conformations may be limited by environmental factors.

The range of peak positions found is from 2919 to 2925 cm^{-1} for the antisymmetric CH_2 vibrations and 2850 to 2854 cm^{-1} for the symmetric CH_2 vibrations[92]. The lower values correspond to the all trans chain and the higher wavenumbers to fluid chains where the temperature is above that required for the lipid phase transition. There are many papers in which the sensitivity of the peaks due to the methylene stretching vibration have been used to follow the phase transition of lipids (refs. 28,30,50,63,69,70,87). A sharp rise in the wavenumber of ~4 cm^{-1}, in either of the peaks due to CH_2 stretching modes, is seen as the lipid passes through the phase transition temperature. The band widths also increase and can be used as alternative measurements.

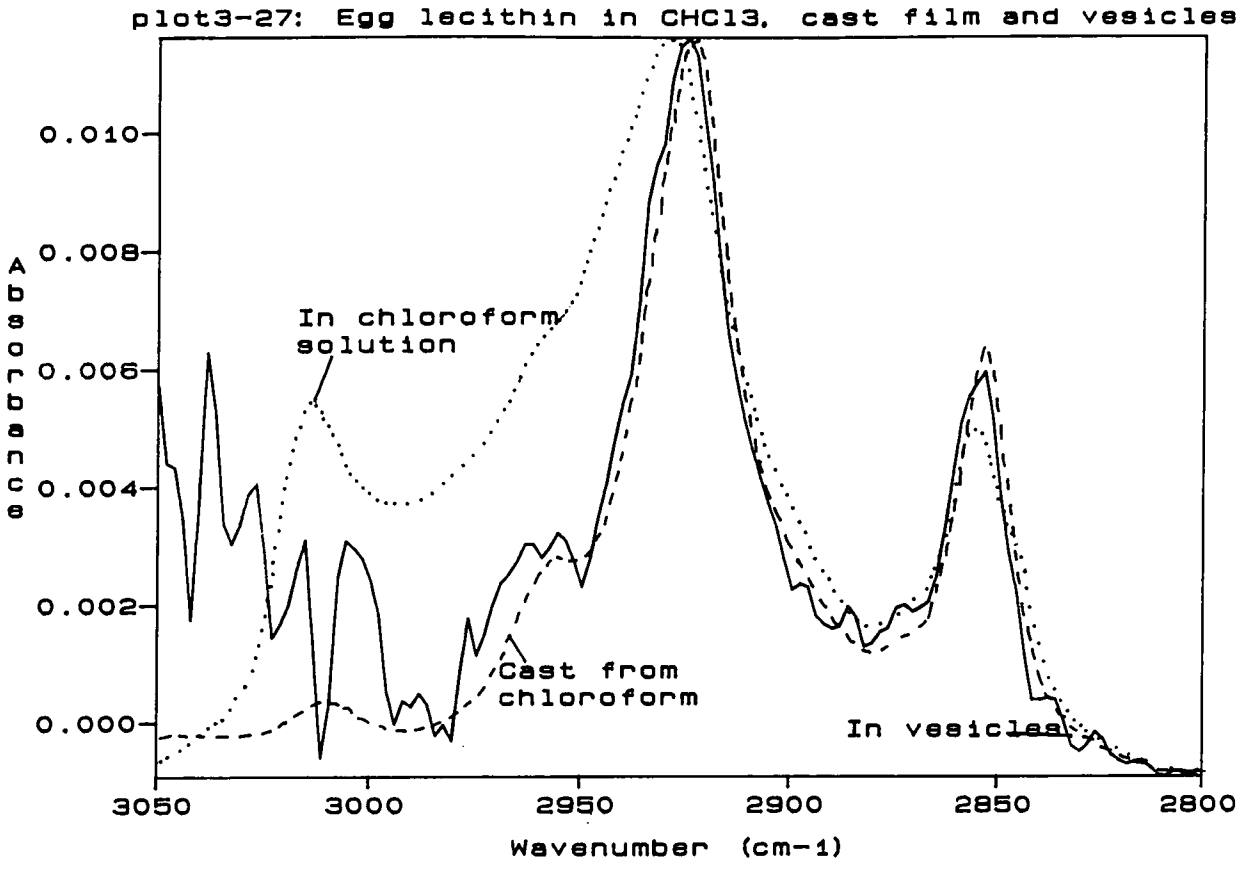
plot3-27: Egg lecithin in CHCl3, cast film and vesicles
Absorbance
0.010
0.008
0.006
0.004
0.002
0.000
In chloroform solution
Cast from chloroform
In vesicles
3050
3000
2950
2900
2850
2800
Wavenumber (cm-1)

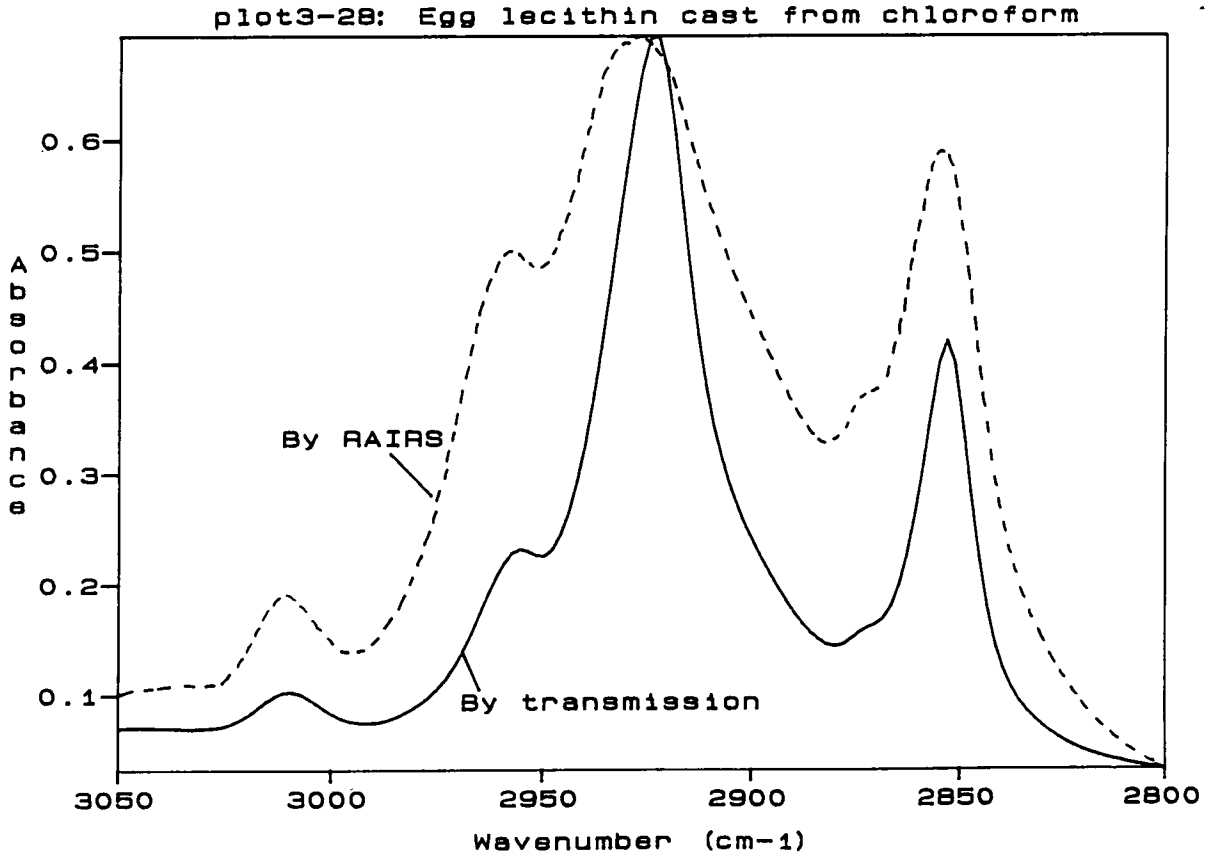
plot3-28: Egg lecithin cast from chloroform
Absorbance
0.6
0.5
0.4
0.3
0.2
0.1
By RAIRS
By transmission
3050
3000
2950
2900
2850
2800
Wavenumber (cm-1)

The peak positions found for egg PC in all of the different environments confirm that its chains are very fluid (*i.e.* have a high proportion of gauche conformers) at temperatures above 30 °C. This is to be expected since egg PC was chosen because its phase transition temperature is below zero °C [93]. Many of the studies which were carried out on the phase transition of phospholipids, were undertaken with lipids whose chains are saturated[73]. Therefore the higher value of 2929 cm^{-1} recorded for egg PC in chloroform is probably connected with the fact that most of the chains are alkenes not alkanes. The double bonds may be at different positions on either of the two chains thus increasing the total number of different conformations and therefore the fluidity.

The increase in the wavenumber, of the $\nu_{as}(CH_2)$ peak, from 2923 to 2924 cm^{-1} from a film cast from chloroform to the vesicles is contrary to what might be expected. The macroscopic ordering of egg lecithin in vesicles should be greater than that of the cast film, thus decreasing the number of possible conformations. However, the evidence suggests that the hydrocarbon chains are more fluid in the vesicles than in the cast film. As mentioned previously plots3-13&14 show the presence of water in the films cast from chloroform. It is possible that in the ordered structure of the vesicles, water is largely excluded from the hydrocarbon chains. In the cast films there is evidence for some macroscopic ordering of the phospholipid (section 3.2.3.A). However, it is possible that the water is not completely excluded from the region of the hydrocarbon chains and therefore acts as a constraining factor on the fluidity of the lipid chins. In the cast films of the vesicles the position of the $\nu_{as}(CH_2)$ peak is 2924.5 cm^{-1} implying that the fluidity of the hydrocarbon chains is maintained, possibly by the maintenance of the original bilayer structure.

In the mixed detergent and lipid micelles (assuming complete subtraction of the detergent spectrum) the lipid chains exhibit a higher value than the vesicles for the $\nu_{as}(CH_2)$ peak position - 2925 cm^{-1}. This adds weight to the argument that it may be the water which is constraining the number of different conformations of the lipids. The lipid head groups and detergent molecules would be even more effective in preventing the entry of water into the hydrocarbon chains. The configuration of the detergents and head groups of the lipids (figure 3(b)) is similar to the Roman foot soldiers technique for protection from attack of joining all their shields together to form an impenetrable barrier.

The wavenumbers of the CH stretching vibrations are much higher in the RAIRS spectrum of the cast film than in the transmission spectrum (plot 3-28). This does not necessarily have a bearing on the fluidity of the chains because the optical effects in this method are completely different from either transmission or ATR and such wavenumber differences are normally seen[94]. For most of the spectra of egg PC obtained the full width at half height is between 27 and 30 cm^{-1}. There appears to be no significant width changes from the cast films to the vesicles[1†]. The band widths are much larger in chloroform, although it is difficult to estimate the numerical values of the band widths due to the presence of shoulders on the main peaks. The increase in width is probably due to a rise in the number of different environments of chains. It is possible that the extra peaks seen in chloroform are due to the two chains in each lipid being in completely different environments. One of them may be folded over the head group to shield it from the hydrophobic solvent.

[1†]This is contrary to the proceedings of ESCOMB 1991[29]. In those a diagram was shown where the width of the CH stretches of the cast film was much larger than that of the vesicles. This proved to be completely irreproducible. The latter findings of no width change on vesiculation were reported in the poster at the conference.

(B) 1800-1500 cm^{-1} - The carbonyl stretching and OH bending region.

RESULTS :

Table 3(iii) contains the data obtained from the fitting of synthesised peaks to the recorded spectra for the carbonyl and adjacent peaks in the spectra of egg lecithin. Examples of these are shown in plots3- 29 to 32.

Description of sample	No. of fitted peaks	Position (cm^{-1})	FWHH (cm^{-1})	absorbance intensity	percentage Lorenzian	integrated intensity (I) (cm^{-1})	$\frac{I_{1741}}{I_{1726}}$
in chloroform	1	1733	31	0.0165	40	0.567	--
in carbon tetrachloride	1	1738	29	0.0148	20	0.490	--
in methanol	3	1744 1724.5 1661	21 25 69	0.0123 0.0089 0.0072	50 " 100	0.294 0.254 0.144	1.16
film cast from chloroform	3	1741 1726 1653	22 26 95	0.203 0.166 0.063	50 " 100	5.26 4.99 8.23	1.06
RAIRS of film cast from chloroform	3	1744 1726 1653	22 26 95	0.105 0.098 0.074	50 " 100	2.75 2.99 8.90	0.92
mixed detergent and lipid micelles	2	1742 1725	22 20	0.0030 0.0028	50 "	0.0776 0.0612	1.16
multilamellar vesicles (from 1.5:1 ratio)	2	1743 1726	22 26	0.0062 0.0073	50 "	0.156 0.216	0.72
unilamellar vesicles (from 15:1 ratio)	2	1741 1726	35 "	0.0029 0.0037	50 "	0.121 0.156	0.78
" + $MnCl_2$	2	1741 1726	22 26	0.0061 0.0075	50 "	0.0061 0.0075	0.69
cast film of unilamellar vesicles	2	1743.5 1728	22 26	0.092 0.076	50 "	2.42 2.46	0.99

Table 3(iii) Measurements on fitted peaks in the carbonyl stretching region 1800-1600 cm^{-1} for FTIR spectra of egg lecithin in a variety of environments.

Plot 3-29 shows an enlargement of the region 1800-1550 of the film of egg lecithin cast from chloroform. The line with illustrated with small dashes is the original spectrum. To aid the fitting of synthetic curves to this spectrum both second derivative and Fourier deconvolution were utilised. The second derivative of the sample spectrum is displayed as a solid line at the bottom of the plot. This clearly shows the presence of two peaks within the main carbonyl band which can also be discerned by visual examination. However, the third band at ~1650 cm^{-1} is not seen in the second derivative plot, either because of its width or the decrease in the S/N ratio in this region. Unfortunately, for most other spectra, of egg lecithin, recorded the S/N ratio was too low for the second derivative of the spectrum to be of use. The inset at the top of plot 3-29 is the Fourier deconvoluted spectrum of the region shown in the main plot. Again a splitting of the carbonyl band is seen. The broader peak at ~1650 cm^{-1} can be seen but not as clearly as the other two. Again this could be due to noise in the original spectrum. However, it is much broader than the two carbonyl peaks and therefore the parameters used in the deconvolution are not appropriate for it. Thus, both second derivative and FD show the presence of two peaks in the carbonyl band - one at ~1740 cm^{-1} and the other at ~1728 cm^{-1}. Visual inspection of the spectrum supports this analysis but also indicates the presence of a much broader peak at ~1650 cm^{-1}.

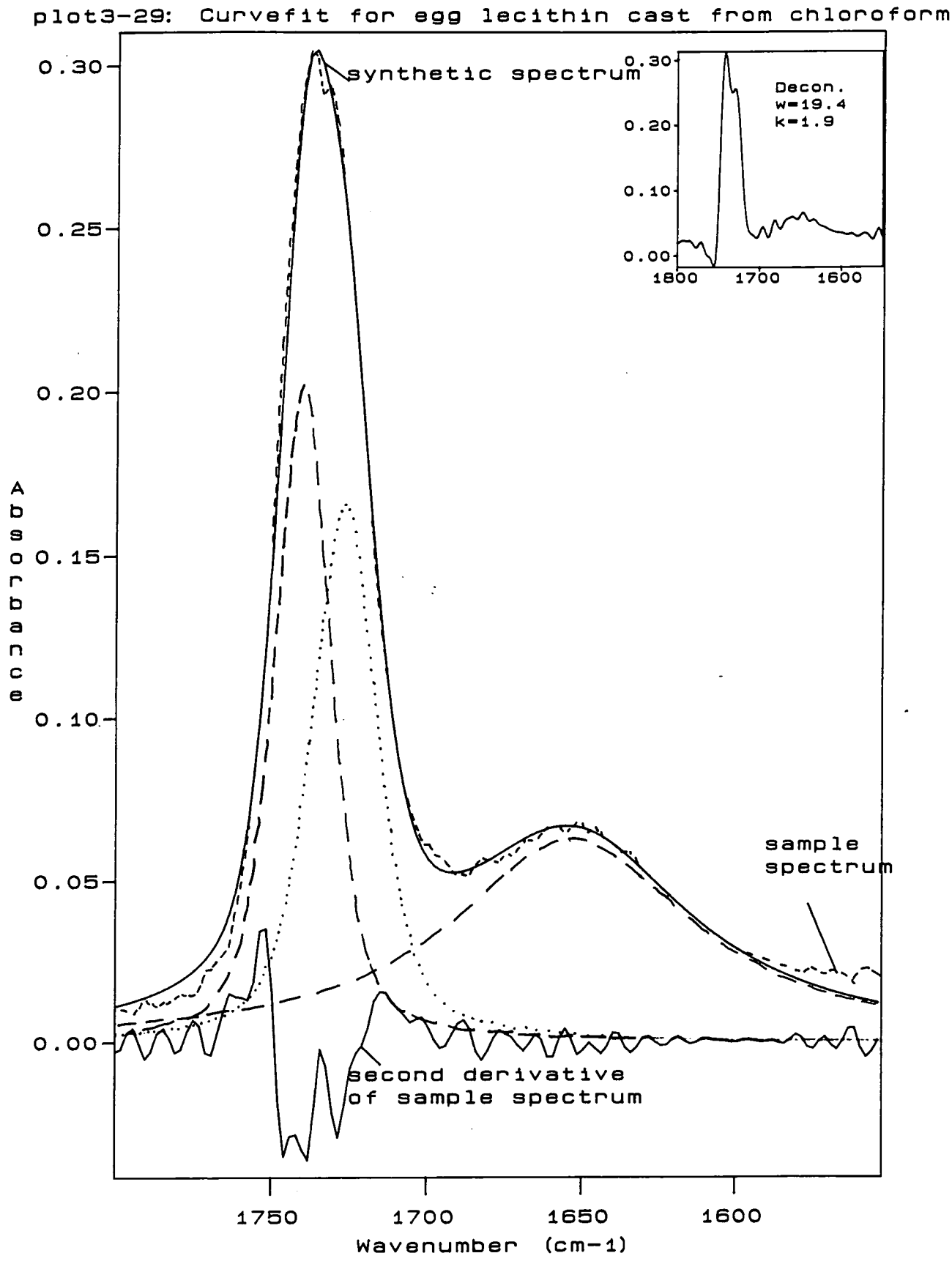
plot3-29: Curvefit for egg lecithin cast from chloroform
synthetic spectrum
Decon.
w=19.4
k=1.9
0.30
0.20
0.10
0.00
1800
1700
1600
0.30
0.25
0.20
0.15
0.10
0.05
0.00
Absorbance
sample
spectrum
second derivative
of sample spectrum
1750
1700
1650
1600
Wavenumber (cm-1)

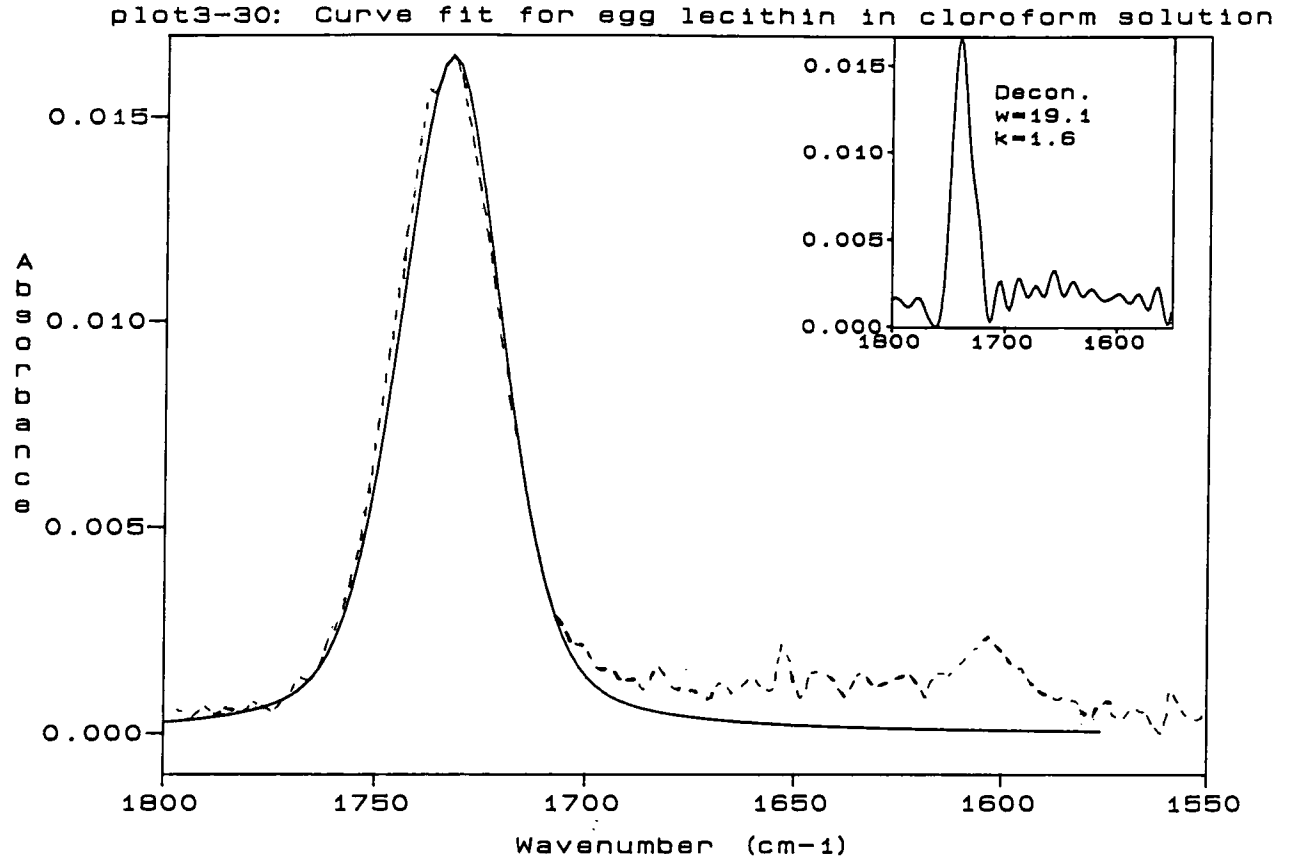
plot3-30: Curve fit for egg lecithin in cloroform solution
Absorbance
0.015
0.010
0.005
0.000
1800
1750
1700
1650
1600
1550
Wavenumber (cm-1)
Decon.
w=19.1
k=1.6
0.015
0.010
0.005
0.000
1800
1700
1600

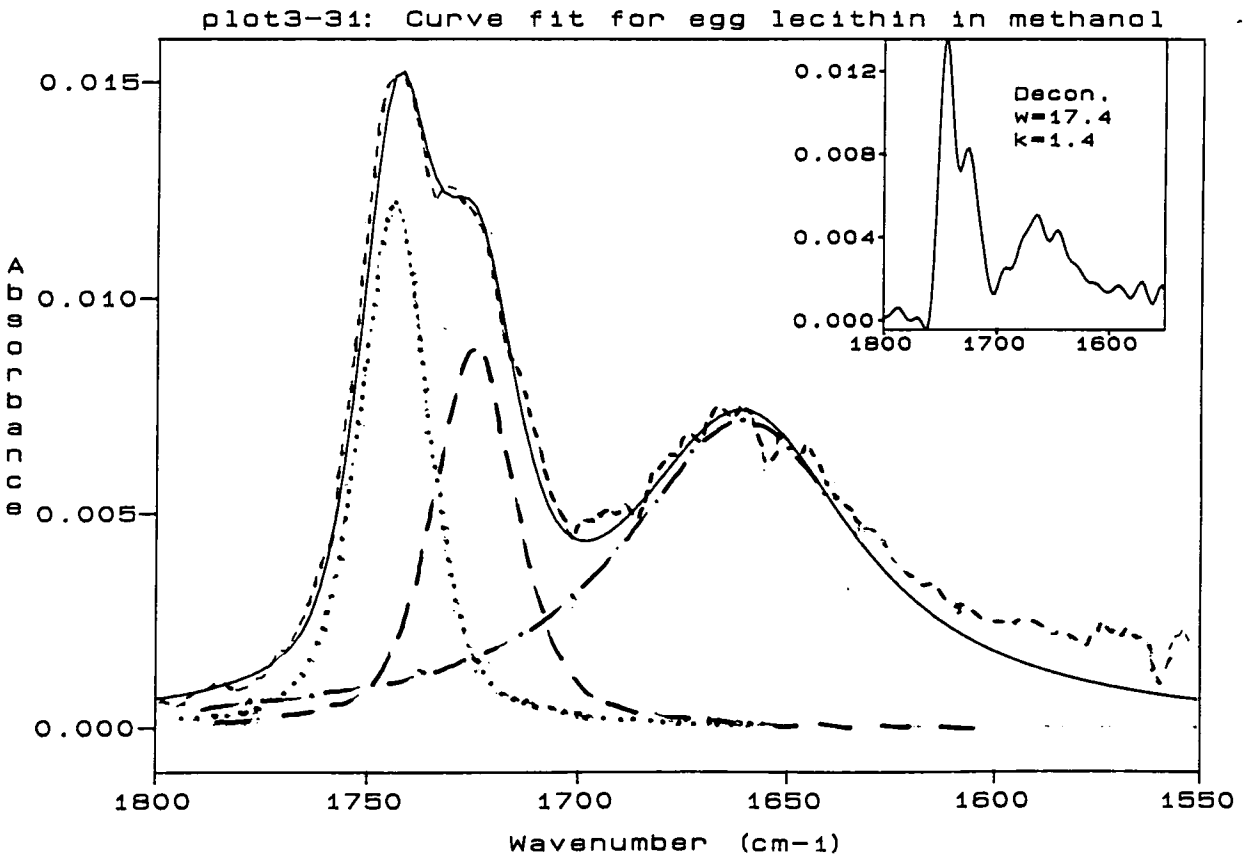
plot3-31: Curve fit for egg lecithin in methanol
Absorbance
0.015
0.010
0.005
0.000
1800
1750
1700
1650
1600
1550
Wavenumber (cm-1)
Decon.
w=17.4
k=1.4
0.012
0.008
0.004
0.000
1800
1700
1600

plot3-32: Curvefit for vesicle spectrum

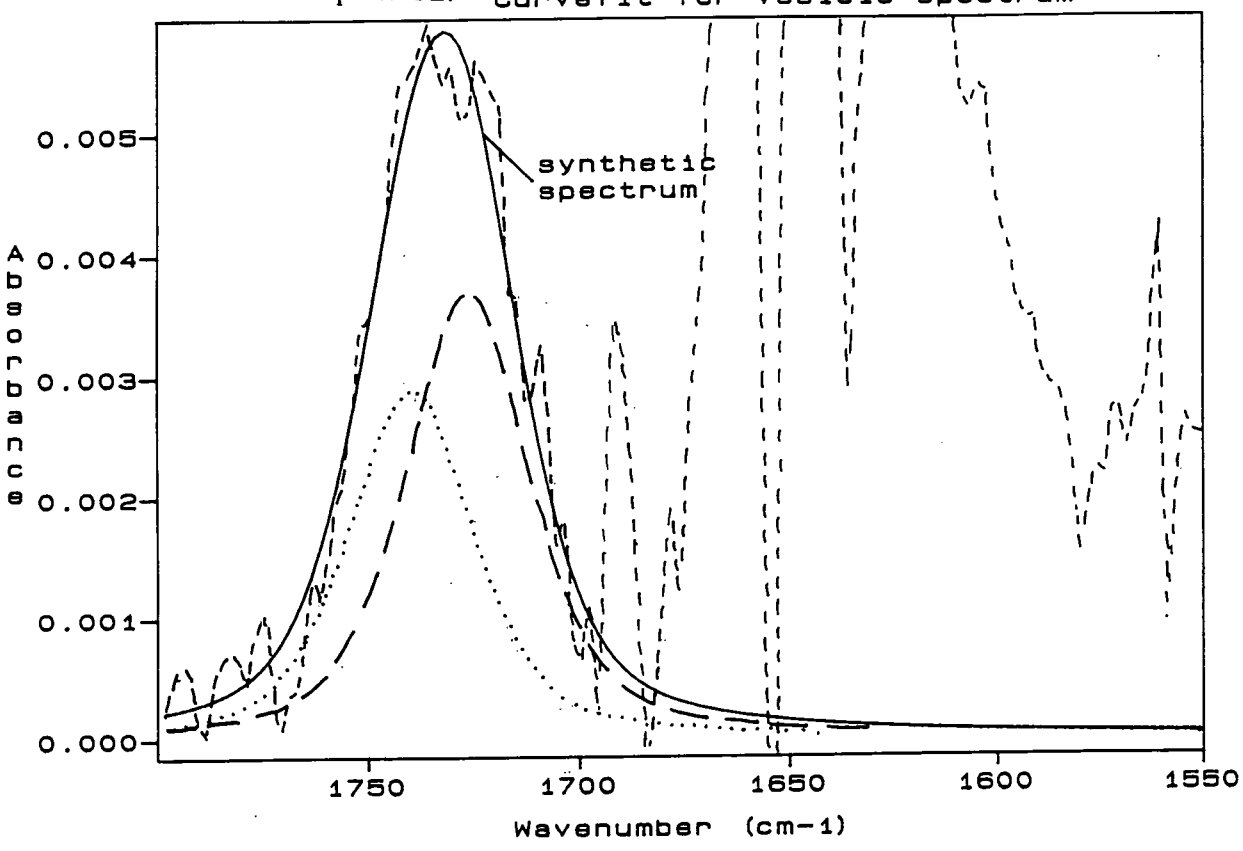

From the data obtained by FD, second derivative and visual inspection three peaks were fitted (as in section 3.2.3.C.) to the experimental data. These can be seen on plot 3-29. The solid line is the summation of the three theoretical curves.

A similar process to that described above was undertaken for all data given in table 3(iii). In the case of the vesicle spectra (plots3-15,16&32) the data obtained must be treated with scepticism given the low S/N ratios. To minimise the number of parameters to be fitted an assumption was made that some of them should be fixed, in the vesicle spectra, at the same values as the cast film. This was considered to be a valid assumption given the fact that the cast film appeared to be hydrated and the general shape and position of all the peaks in the vesicle and cast film spectra were very similar, indicating a similar environment for the lipid molecules. In general the parameters which were held constant were the number of peaks, the wavenumber and band shape. The main variables altered were the peak intensities and occasionally the band widths. In the case of the example shown in plot 3-32 an investigation was carried out into the effects of altering each of the variables in turn whilst keeping the rest of them constant and the same as in the cast film. It was found that, although the fitting gave rise to different individual parameters, the ratio of the integrated intensity of the ~1740 cm^{-1} and ~1726 cm^{-1} peaks remained fairly stable. For a fit where the absorption was the variable this ratio was 0.71, for any of the other variables the ratio was 0.77.

The results for the vesicles must also be considered with caution because of the incomplete spectral subtraction of water may be distorting the spectra of the lipid.

Despite the problem with the S/N ratio there does seem to be a significant difference in the ratio of the two fitted peaks at 1740 and 1726 cm^{-1} between the different environments. In cast films and the mixed micelles the ratio, of the ~1740 cm^{-1} to 1726 cm^{-1} integrated intensities, is about one or slightly larger, showing that there is an equal contribution to the carbonyl band from both peaks. Whereas in vesicles the ratio of the two peaks falls to ~0.7 as the contribution from the two peaks is weighted in favour of the peak at 1726 cm^{-1}.

DISCUSSION :

The bands at ~ 1650 cm^{-1} arise from the bending mode of OH in the solvents. They have been fitted because their proximity to the carbonyl band means that they contribute to the overall intensity in this region. The assignments of the two peaks, seen within most of the carbonyl bands, are not so easily achieved.

There are two conflicting assignments for the carbonyl peaks made in the literature. The first, made by Levin et al[99,100,101], arises from the comparison of glycerides, with one to three chains, whose conformation is known from X-ray data. The assignments are made for each of the two chains : sn1 chain 1727-1744 cm^{-1} and the sn2 chain 1716-1728 cm^{-1}. The large shift in the wavenumber of the two chains is thought to arise from a difference in the conformation at the C-O-C region (figure 3(i)). The sn1 chain is proposed to be in a trans conformation, whilst the sn2 chain is in a gauche conformation. The lower wavenumber of the sn2 carbonyl (gauche) group is thought to be due to the fact that the group has a higher degree of hydration. If the chains have the same chemical formula then the existence of a gauche bond in one of the ester groups will cause that chain to be shorter than the other, as in DMPC and DPPC studied by Levin[99,100,101] (figure 3(j)). This could aid the interleaving of the two sides of a phospholipid bilayer. In egg PC the chains are different and therefore it may not be advantageous for packing for there to be an equal distribution between the two chains of the conformations.

The second set of possible assignments have been proposed by Blume, Hübner et al[54,55]. In their study ^{13}C has been substituted for the carbonyl carbon on one of the acyl chains of the lipids DMPC, DMPE, DMPG and DMPA. With this isotopic labelling the positions of the peaks due to the carbonyl stretching vibrations of the two chains are separated by ~40 cm^{-1}. Two peaks were observed for DMPC in chloroform, one at 1732 cm^{-1} and the other at 1690.5 cm^{-1}. This splitting is caused solely by the isotopic substitution. If the lipid is in an aqueous environment each of these bands becomes a doublet with peak

positions of 1741, 1727, 1696, and 1685 cm^{-1}. Blume et al then reversed the labelling of the carbonyl groups e.g. if the ^{13}C was on the sn1 chain and the ^{12}C on the sn2 then these were swapped. They found that the positions of the either the two or the four peaks changed only by 1-2 cm^{-1} thus showing that Levin's assignment of the two peaks seen in the unlabeled case to be incorrect. The assignment made by Blume et al of the two peaks seen in each of the two isotopic bands was that the lower wavenumber was caused by hydrogen bonding and they ruled out any conformational change.

The two approaches to assignment seem irreconcilable. Indeed Blume dismisses Levin's work and Levin just appears to ignore that of Blume et al. However, there is really only one barrier to reconciliation and that is the assignment of the two different conformations to specific chains. Now we could have some sn1 ester groups which are gauche and some trans and the same for the sn2 chain. This would then fit the X-ray data of Levin[99]. The wavenumber range 1727-1744 cm^{-1} would now apply to a trans conformation about the C-O-C group and the range 1716-1728 $cm^{-1}$to a gauche conformation but neither specifically on one chain. There are now two options - either the splitting seen in non-labelled samples is due to hydrogen bonding with the solvent or only one peak is seen in non-polar solvents because all of the chains are in one conformation. The latter appears unlikely given the fluidity of the hydrocarbon chains in non-polar solvents it would seem a reasonable supposition that there is also rotation around the ester group. The former hypothesis fits all the data found including NMR work[54,55] and the fact that hydrated cast films show splitting of the carbonyl peak whilst dehydrated do not[54].

Therefore, a new assignment is suggested for the carbonyl groups of phospholipids. The two different conformations of the ester group exist, on either chain, but the peaks are only split when the gauche group becomes hydrated. *I.e.* peaks in the region 1744-1727 cm^{-1} are due to a trans conformation about the ester group and peaks in the region 1728-1716 cm^{-1} arise from a gauche conformation at the ester group which is possibly solvated.

Having assigned the two peaks to solvated and non-solvated C=O groups it should be possible to make a correlation between the spectra recorded and the percentage of H-bonded carbonyl groups. However, life is never that simple. Blume et al[54] discovered, by comparison between NMR and IR data that the extinction coefficients of the IR peaks due to hydrogen bonded carbonyls were different to those of 'free' carbonyl groups. They estimated that in order to compare the number of chains which were hydrogen bonded to not, in bilayer forming phospholipids, it was necessary to reduce the integrated intensity of the carbonyl peak due to hydrogen bonding by a factor of ~40 %.

Now considering the results obtained for egg lecithin - In chloroform and carbon tetrachloride there is clearly only one major peak in the carbonyl band at 1733 and 1738 cm^{-1} respectively (plot 3-30). Although there is a small amount of asymmetry associated with the FD spectrum. This could be due to a small amount of water being present. In methanol, however there are two peaks in the carbonyl band. Evidently methanol hydrogen bonds to the carbonyl group of egg PC in a similar fashion to water. In the spectra where water is present the carbonyl band is always split into two components. This data fits with the hypothesis the hydrogen bonding is responsible for the splitting of the carbonyl peak but provides no evidence as to whether the wavenumber difference is due to the hydration of different conformations.

If the correction for the extinction coefficient derived by Blume et al[54] is appropriate then approximately a third (~32-36%) of the carbonyl groups of egg PC in the cast films, mixed micelles and methanol are solvated. Though, in the RAIRS spectrum the extinction coefficients of the two peaks may be different from transmission. In the vesicle spectra a larger percentage of the carbonyl groups are hydrated ~42-46 %. It would be expected that if all of the acyl chains were in the same conformation that if water could reach half of them it could reach all. As only ~half of the carbonyl groups are hydrated in the vesicles it would suggest that there is indeed a difference in the position of the hydrated carbonyl groups relative to the water

interface compared to the non-hydrated groups. Thus Levin et al's[99-102] assignment of the two wavenumbers to different conformations would make sense. With the gauche conformation bringing the carbonyl group closer to the hydrophilic region of the lipid and therefore more accessible to water.

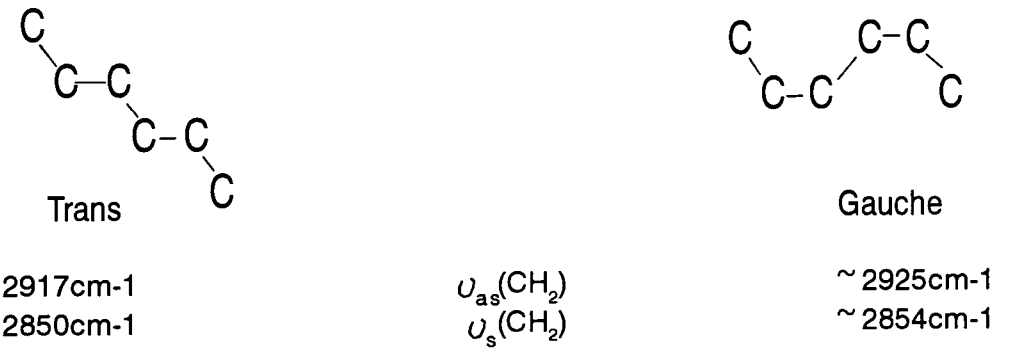

Figure 3(h) : The configuration of the carbons in trans and gauche conformers on the hydrocarbon chain (Levin[28]).

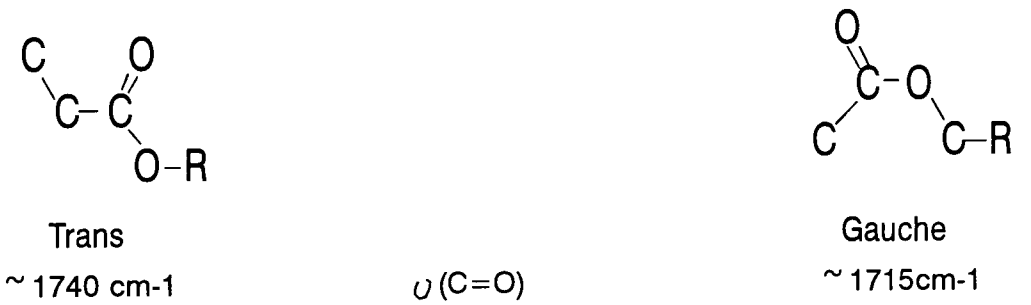

Figure 3(i) : The configuration of the carbons and oxygens in trans and gauche conformers at the ester linkage (Levin et al [99-102])

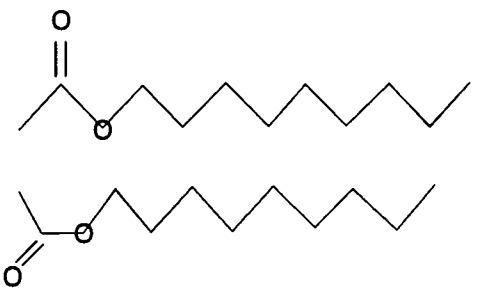

Figure 3(j) : The effect of a gauche conformer at the ester linkage on the chain lengths.

(C) 1690-1600 - The Amide I region

As mentioned in section 3.2.3.D experiments to incorporate a peptide into the bilayer structure of the vesicles were attempted. In only one case - polybenzylglutamate was the peptide eluted in the same fraction as the lipid. Now there is no way of proving, from the data obtained, whether the peptide is even loosely associated with the vesicles, let alone incorporated across the bilayer. However, it is still of interest to examine the amide I region of both the cast film of polybenzylglutamate and the eluted fraction.

RESULTS :

Plot 3-33 is an enlargement of the region containing the amide I band of the spectra shown in plot 3-24. It shows the spectrum of a cast film of polybenzylglutamate on its own (dashed line) and the composite spectrum obtained after passing a solution of detergent, lipid and peptide down a sephadex G-50 column. Plot 3-34 is a further enlargement, to show the amide I band alone. In this case the dashed line is the experimental data for the cast film of the peptide and the solid line is the Fourier deconvoluted spectrum.

Description	Positions of components of amide I band (cm^{-1})	Absorbance intensity
Film of polybenzylglutamate cast from chloroform	1664.5	0.15
	1658.5	0.82
	1650.0	0.86
	1640.0	0.24
Eluted with fraction which contained vesicles	1650	0.0074
	1642	0.0073
	1633	0.0091
	1620	0.0047

Table 3(iv) : Positions of the components of the amide I band for polybenzylglutamate.

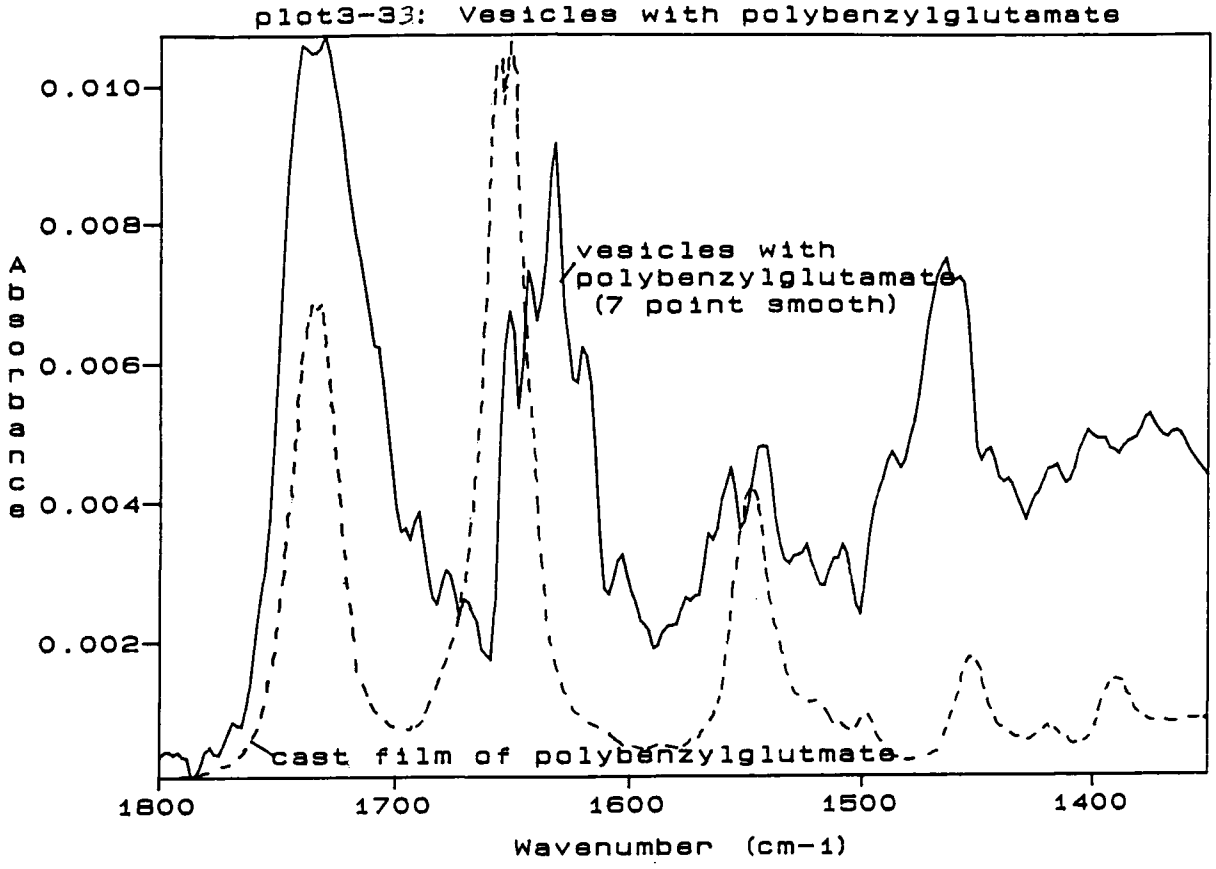
plot3-33: Vesicles with polybenzylglutamate
0.010
0.008
0.006
0.004
0.002
Absorbance
vesicles with
polybenzylglutamate
(7 point smooth)
cast film of polybenzylglutmate
1800
1700
1600
1500
1400
Wavenumber (cm-1)

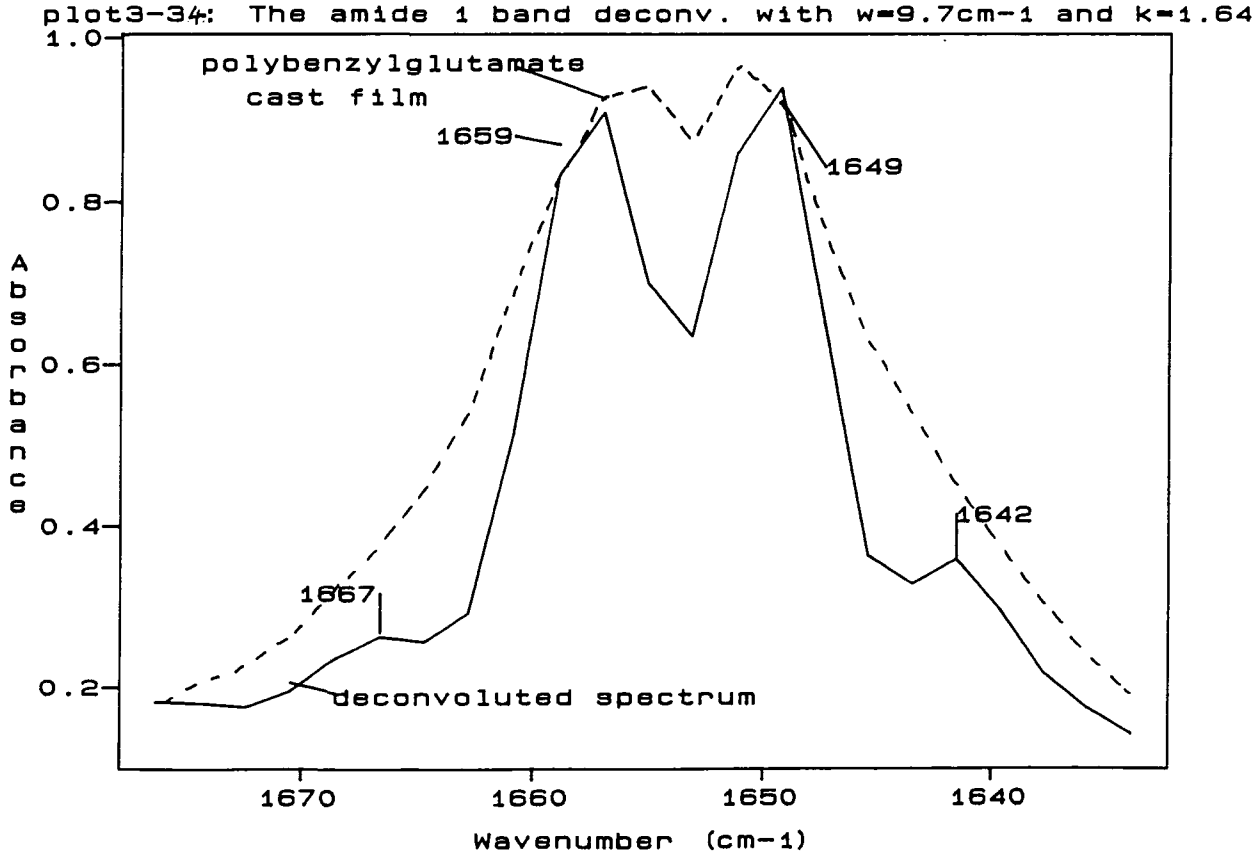
plot3-34: The amide 1 band deconv. with w=9.7cm-1 and k=1.64
1.0
0.8
0.6
0.4
0.2
Absorbance
polybenzylglutamate
cast film
1659
1649
1642
1667
deconvoluted spectrum
1670
1660
1650
1640
Wavenumber (cm-1)

DISCUSSION

Several studies of the relationship between the positions of the components of the amide I band to the secondary structure of protein have been undertaken. For reviews see Chapman et al[30,180]; Parker[40]; and Mendelsohn & Mantsch[31]. There is still a lot of discussion as to which combination of peaks corresponds to a given structure. Table 3(v) shows three different sets of assignments. One of the biggest factors leading to the controversy is that the assignments generally arise from proteins whose X-ray structure is known and it is assumed that their structure in water is largely unaltered. Therefore, the precise history of the protein sample is necessary to be able to determine whether the protein structure recorded in the aqueous IR spectra is the same as that in the X-ray sample.

Presuming that a polypeptide such as polybenzyl-glutamate would exhibit the same peak positions for the same structure as a protein, then it would appear that in a cast film the structure of polybenzylglutamate is predominantly α-helical. This is confirmed by the amide II peak at 1548.5 cm^{-1}. After passing through the column the analysis becomes hampered by the presence of water and a low S/N ratio. The amide I band has certainly shifted (plot 3-33). The peak positions suggest that the structure is now mixed α and β helixes. This change in structure could be caused by the change to an aqueous environment or the association of the peptide with the lipid. Studies have shown[30] that the wavenumbers of the components of the amide I peak of mono-polypeptides are different to those of proteins. Peaks at 1650-1660 cm^{-1} are generally associated with α-helical structures. In conclusion - from the data obtained it is not possible to tell, with certainty, the secondary conformation of polybenzylglutamate

Secondary structure assignment	Positions (cm^{-1})	Reference
α helix	1650-55	Chapman et al ref. 30
β helix	1630-40 1680-90	
3_{10} turns	1644	
random coils		
α helix	1655, 1550	Mendelsohn & Manstch ref. 31
β helix	1630	
β pleated	1685, 1530	
random coils	1660, 1540	
α helix	1656 ± 2	Jakobsen & Wasacz ref. 35
β helix	1637 ±2	
β and lowα helix	1636 ± 2	
α and low β helix	1652 ± 2	
α and β helix	1644 ± 2	

Table 3(v) : Literature assignments for the correlation between protein IR spectra and their secondary structure

Description of sample	$\nu_{as}(PO_2^-)$	ν_{as}(COC)	$\nu_s(PO_2^-)$	ν_s(COC)	ν_{as} (N-$(CH_3)_3$	Any other peaks
in chloroform	1248.0 0.0117	1172.0 0.0042	1090.5 0.0109	1064.0 0.0101	965 0.008	1017 0.0169
in carbon tetrachloride	1251.0 0.0094	1173.0 0.0044	1090.0 0.0107	1061.0 0.0096	967.5 0.0053	
in methanol	1232.0	← sh.	1086			
film cast from chloroform	1234.0 0.235	1172.5 0.102	1088.0 0.232	1064.0 0.0154	969.5 0.112	
RAIRS of film cast from chloroform	1236.5 0.283	1181.0 0.215	1092.0 0.240	1071.5 0.209	971.5 0.102	
mixed detergent and lipid micelles	1230.0 0.0035	← sh. 0.0012	1091.5 0.0057	1066.0 0.0039		spike at 1056.0 0.0054
multilamellar vesicles (from 1.5:1 ratio)	1229.5 0.0073	1185.0 0.0050	1086.5 0.0082	1067.0 0.0070		
unilamellar vesicles (from 15:1 ratio)	1227.5 0.0053	1176.0 0.0023	1087.0 0.0073	1067.0 0.0053		
cast film of unilamellar vesicles	1218.0 0.056	1182.0 0.077	1087.0 0.032	1066.5 0.029	969 0.016	1039.5 0.055
RAIRS of cast film of UV vesicles	1232.0 0.188	← sh.	1090.5 0.131	← sh.		

Key : Each of the boxes has the data laid out in the following manner :

Peak position Intensity (absorption)	cm^{-1}

← sh. this notation means that the stated band is a shoulder of the previous peak.

Table 3(vi) : Measurements on peaks in the region 1300-900 cm^{-1} for FTIR spectra of egg lecithin in a variety of environments.

(D) 1300-900 - The head group vibrations

The band which shows the most significant positional changes with environment in this region is that which arises from the antisymmetric phosphate stretching mode. As stated in section 3.2.3.A, the position of this peak is very sensitive to the presence of water. A shift of 30 cm^{-1} is seen in the wavenumber of this peak between hydrated and non hydrated molecules[51,88]. The position of the $\nu_{as}(PO_2^-)$ peak for egg lecithin changes from ~1250 in non-polar solvents to ~1230 cm^{-1} in polar solvents (table 3(vi). Such a large shift is due to hydrogen bonding between the phosphate group and the solvent. Whether this wavenumber shift is accompanied by a conformational change is not apparent from the literature[56].

The widths and relative intensities of the peaks in this region appear to be largely unaffected by environment (plots3- 10 to 16 & 35). The main exception to this appears to be the spectrum of the cast vesicles (plots3- 17&35)† . However, it seems likely that these changes are due to the presence of buffer within the cast film (section 3.2.3.C) and not a major change in the lipid structure. It would seem likely that the lipid spectrum is hidden beneath that of the buffer. The shoulder seen on the left of the peak at 1217 cm^{-1} (plot 3-36) is probably the $\nu_{as}(PO_2^-)$ peak and the band discernible at 1088 cm^{-1} the $\nu_s(PO_2^-)$ peak. The spike at 1056 cm^{-1} in the mixed micelle spectrum (plot 3-26) is probably noise. However, the spike seen in the spectrum in chloroform at 1017 cm^{-1} is definitely reproducible. Its origin is problematical as chloroform has no peaks in this region.

The $\nu_{as}(N-(CH_3)_3$ peak would possibly give interesting information, unfortunately in aqueous solution the signal is too small to detect on top of the strong water absorption.

† The spectra of vesicles shown in plots 3-35&36 are different from that shown in plot 3-16 because the S/N ratio in the spectrum shown in plot 3-35 was extremely low in the carbonyl region but very high in the region 1300-1000 cm^{-1}.

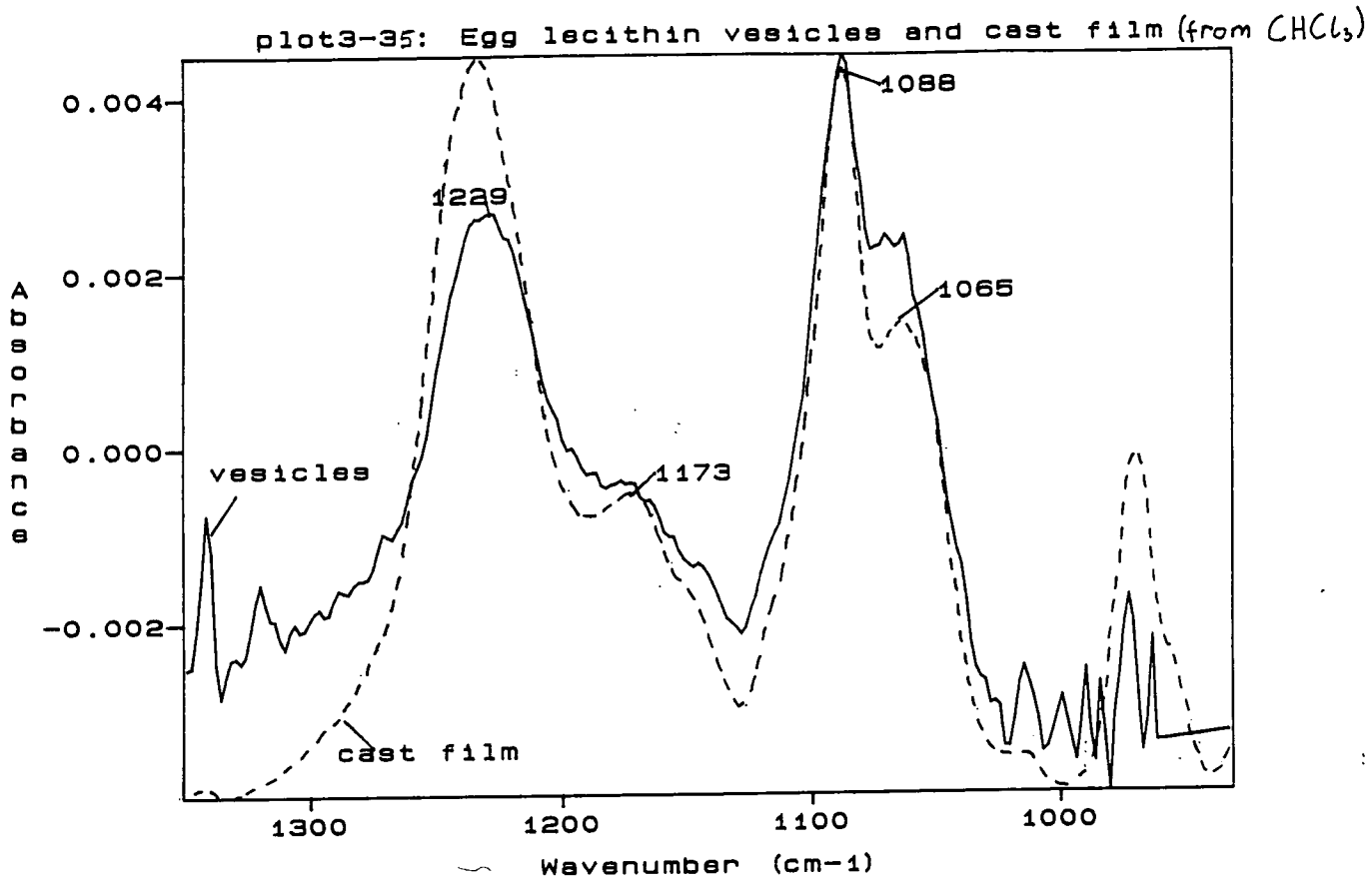
plot3-35: Egg lecithin vesicles and cast film (from $CHCl_3$)
0.004
0.002
0.000
-0.002
Absorbance
1229
1088
1065
1173
vesicles
cast film
1300
1200
1100
1000
Wavenumber (cm-1)

plot3-36: Egg lecithin vesicles in solution and cast

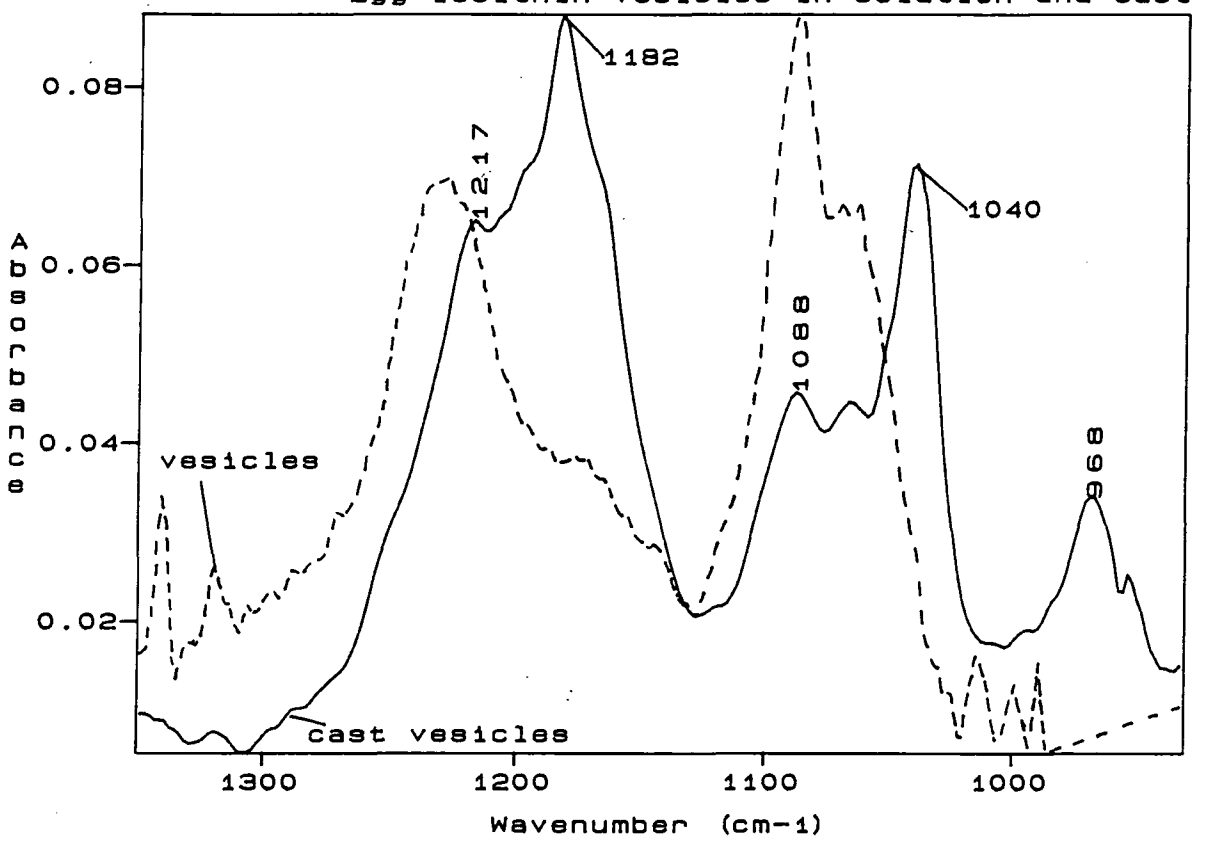

plot3-37: lipid and detergent mixture before elution

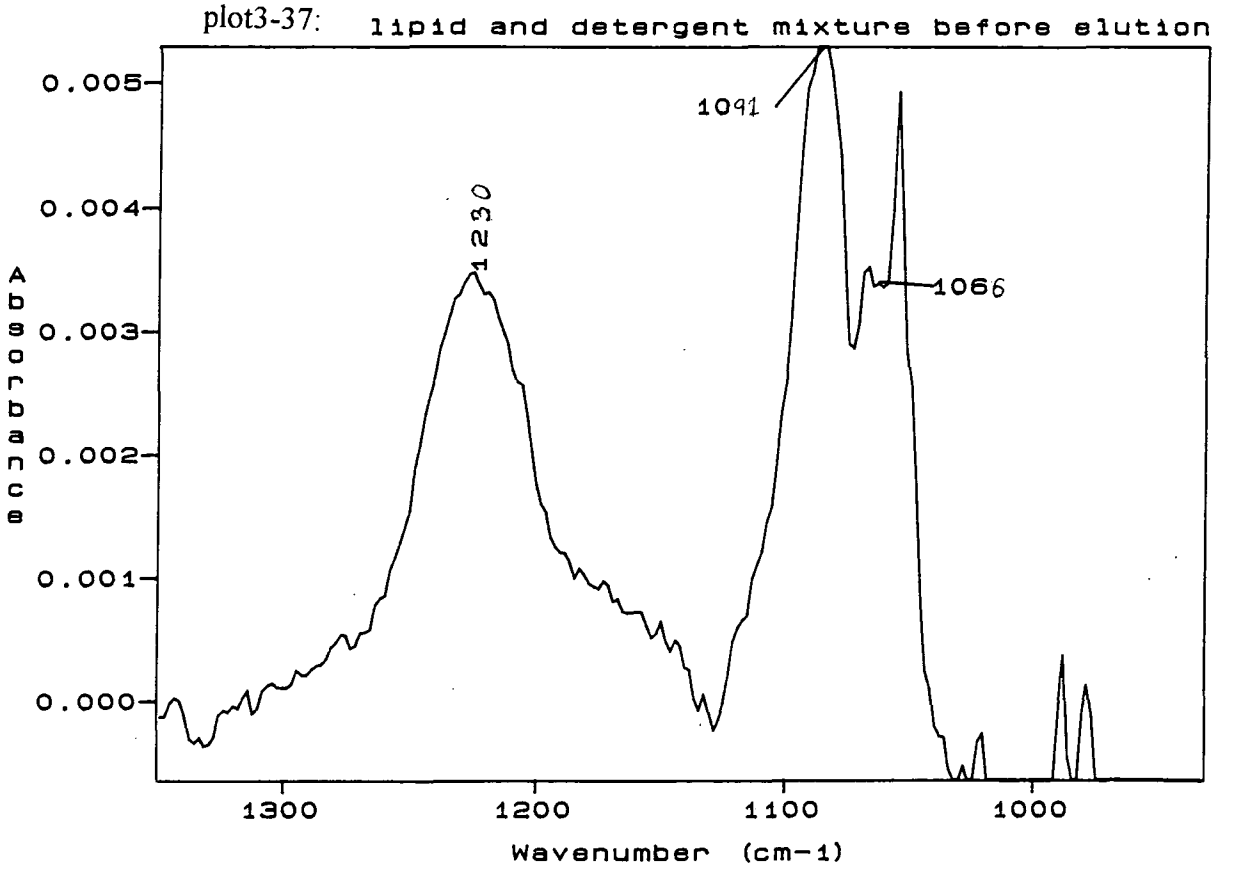

3.3 : SUMMARY

Unilamellar vesicles were made via the detergent removal by gel filtration. However, they were not large (~100nm) as hoped but small (~24 nm). This means that the method of ultra-sonication[73] would have made vesicles of a similar size without the problem of remnant detergent and at a much higher concentration in solution.

The FTIR analysis was hampered by the presence of water and low concentrations of sample. The sonication method would again have solved these problems. As sonication requires only 1-2 ml of water per experiment there would have been no problem with the use of D_2O apart from the effect of altering the hydrogen bonding in proteins. Sonication yields lipid concentrations of ~50 mg per ml and thus low signal levels would have been avoided.

At the S/N ratios achieved there appeared to be no major differences between the multilamellar vesicles (plot 3-15) and the unilamellar vesicles (plot 3-16). This would imply that there is no change in the lipid structure between the outer layer of a MLV and the inner layers.

It was found that the hydrocarbon chains are fluid in all of the environments tested even when a macroscopic order occurred such as in vesicles. Both the phosphate and carbonyl groups undergo hydrogen bonding in the presence of either water or methanol. However only ~half of the carbonyl groups were hydrogen bonded indicating that there was a conformational difference at the ester linkage. Water probably does not penetrate further into the bilayer than the first layer of carbonyl groups.

The cast films which were presumed initially to be disordered did appear to have macroscopic ordering of some form as seen from the RAIRS data.

There was no evidence in the studies undertaken of peptide incorporation into the vesicles.

CHAPTER 4

BACKGROUND AND DESCRIPTION OF EXPERIMENTS FOR STUDIES OF MONOLAYERS AT THE AIR/WATER INTERFACE, DEPOSITION ONTO SUBSTRATES AND THE FTIR OF THIN FILMS

4.1 ISOTHERMS :

4.1.1 Background to isotherm studies

Materials which are insoluble in water can sometimes be deposited onto the water surface to form monolayers. To construct a stable monolayer, in general, there has to be an attractive force with the water to induce spreading and a repulsive force which causes the molecules to be insoluble. Thus an ideal molecule is one which is amphiphilic. Examples of such molecules are phospholipids. These have hydrophilic phosphate head groups and hydrophobic hydrocarbon chains separated by an ester region which is of intermediate nature with respect to water (see figures 2(d),5(a)&5(b)). These monolayers may then be transferred from the water surface onto a substrate.

Before proceeding to transfer the monolayer onto a solid substrate it is first necessary to characterise the material on the surface of the aqueous subphase. The best method is to record a π-A isotherm[19], where surface pressure is measured as a function of surface area, at constant temperature. Such isotherms can also yield information on molecular packing and interactions in their own right (see chapter 5).

4.1.2 Theory

(A) Surface pressure

The surface pressure (π) of a material is defined as the difference in surface tension between the clean subphase and the subphase with material deposited onto it[19].

$$\pi = \gamma_o - \gamma \qquad \textit{Eqn.}\ 4(i)$$

Where γ_o = surface tension of subphase
γ = surface tension with monolayer

It is a 2 dimensional analogy with 3-dimensional pressure. Surface pressure is usually measured by the use of a Whilhelmy plate and a micro balance[103]. A Wilhelmy plate is generally a piece of filter paper (1 cm wide for ease of calculation of the surface tension) attached to a microbalance. Surface tension is defined as the force per unit length. This is balanced by a weight on the microbalance.

$$\gamma = {}^{F}/_{l_1} = {}^{mg}/_{2l} \qquad \textit{Eqn.}\ 4(ii)$$

Where m = mass used to balance the force at the surface
g = gravitational constant
l = length of Wilhelmy plate
F = force at the surface
l_1 = total length along which the tension is measured

(B) Mixtures

If we have two components A and B on the surface, then if the mixture is either ideally miscible or completely immiscible the system will follow equation 4 (iii)[103], at a given pressure. *I.e.* either the interaction A-B is the same as the interactions A-A and B-B or there is no interaction between A and B. Deviations from this equation suggest non-ideal mixing *i.e.* that the components A & B are miscible to some extent.

$$A_{AB} = N_A A_A + N_B A_B \qquad \textit{Eqn.}\ 4(iii)$$

Where : A = area per molecule
N = mole fraction

If two compounds are immiscible then[134] the π-A isotherm will exhibit the following behaviour. The components will be present separately and as the surface pressure reaches a value equivalent to the lowest collapse pressure of the component molecules then that component will enter a collapse state and be ejected from the monolayer. The second component will then be compressed to its collapse pressure where it will no longer be a monolayer. If two components are miscible then a single collapse pressure is usually seen at a different value from either of the pure components and varies with the molar compositions[19].

The measurement of the collapse pressure is not under equilibrium conditions. The equilibrium spreading pressure would be a measurement under stable conditions. This involves placing a crystal of the material on the water surface and allowing an equilibrium pressure to be achieved. The equilibrium spreading pressures of the pure components can then be compared to those of the mixture to determine whether the mixture is immiscible, by using an equivalent equation to 4(iii). However, practically it is easier to measure the collapse pressure.

(C) Close packed area (CPA)

A typical isotherm is shown below. In the simplistic approach one considers that the monolayer goes though phase changes analogous to those seen in three dimensions. If the gradient of the solid region is used to extrapolate back to a state of zero pressure then the area found is that which would be expected for the hypothetical state of an uncompressed close packed layer[19]. This is known as the close packed area (CPA) of the molecules.

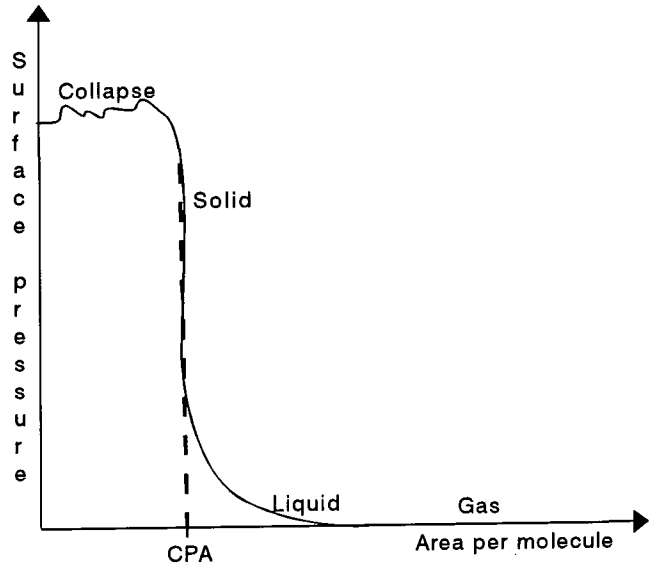

Figure 4(a) : An example of a π-A isotherm.

4.1.3 Experimental description for recording isotherms

Two types of Langmuir-Blodgett troughs have been used in this work. Joyce-Loebl (figure 4(b)) style troughs have been used for the majority of the measurements but some have been performed on a Fromherz trough (figure 4(c)). In the former case the monolayer was enclosed within a continuous PTFE coated glass fibre band and in the latter case the monolayer sits proud of trough due to the hydrophobic nature of PTFE, and is confined by a PTFE barrier. Both troughs were filled with water purified by passing it through a reverse osmosis unit then through a Milli-Q water polishing unit (Millipore Corp.) giving a resistivity greater than 18 MΩ cm.

Before depositing the monolayer the surface of the subphase was aspirated. The cleanliness was checked using the criterion that on compression the pressure change was less than 0.1 mN m^{-1}. 1 mg/ml solutions of the materials were made in Aristar chloroform. The materials were purchased from Sigma UK at 99+% purity and used without further purification. Mixtures were made from 1 mg/ml stock solutions of the components in the correct proportions. Known volumes of these solutions were deposited onto the cleaned surface of the subphase with a micrometer syringe, within the area confined by the fully expanded barriers. The two subphases studied were the pure H_2O described above, and 2.5 X 10^{-4} M calcium acetate in the purified H_2O. Their respective pHs were 5.5 and 6.3 (±0.3). The temperature was either held constant by a heating coil at 26 ^{0}C or the experiments were performed at ambient temperature, normally around 20 ^{0}C in the trough. The chloroform was allowed to evaporate for at least five minutes before compression. The π-A isotherm was then recorded, on a calibrated X-Y plotter, by gradual reduction of the area available to the monolayer. The rate of compression was 1.8 cm^2 s^{-1} for the Joyce-Loebl trough and 0.5 cm^2 s^{-1} for the Fromherz trough.

As the initial area of the troughs and the number of moles deposited are known, calculation of the area occupied per molecule (APM) was possible. This is used as the abscissa scale of the isotherms.

In some cases instead of compressing the monolayer beyond the point of collapse, into multilayers, hysteresis tests were performed. The material was compressed to a certain pressure then the barriers were re-expanded and the monolayer allowed to relax for five minutes before re-compression. These tests were carried out to investigate the stability of the monolayers and ensure that material was not being absorbed into the subphase.

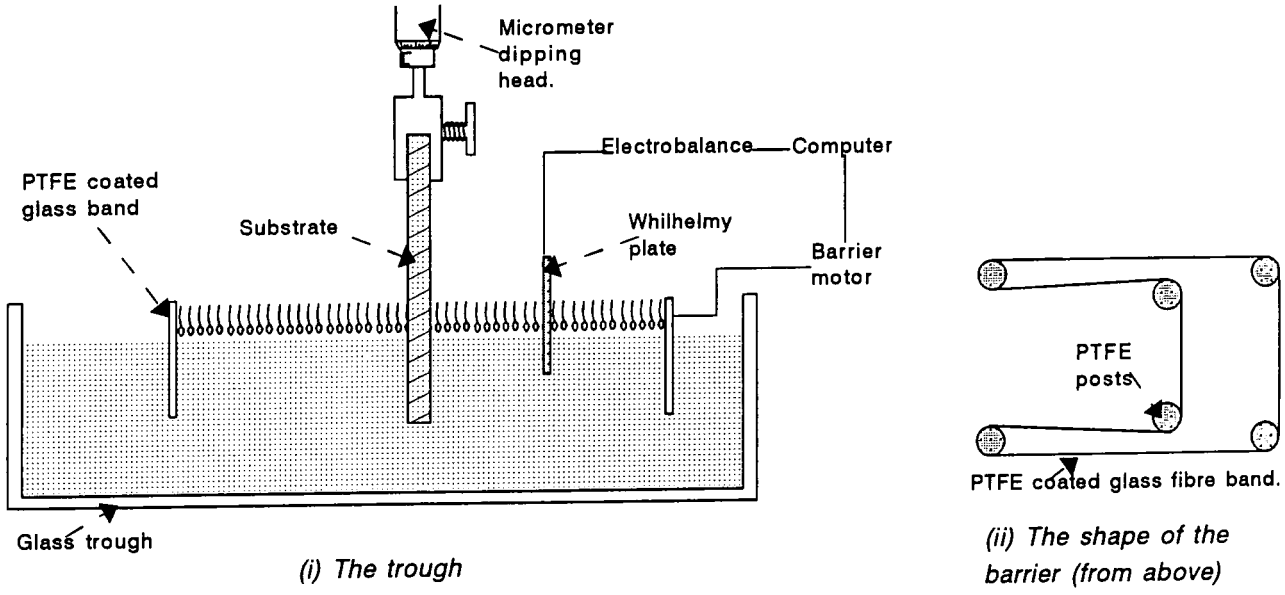

(i) The trough

(ii) The shape of the barrier (from above)

Figure 4(b) : Joyce-Loebl style of trough.

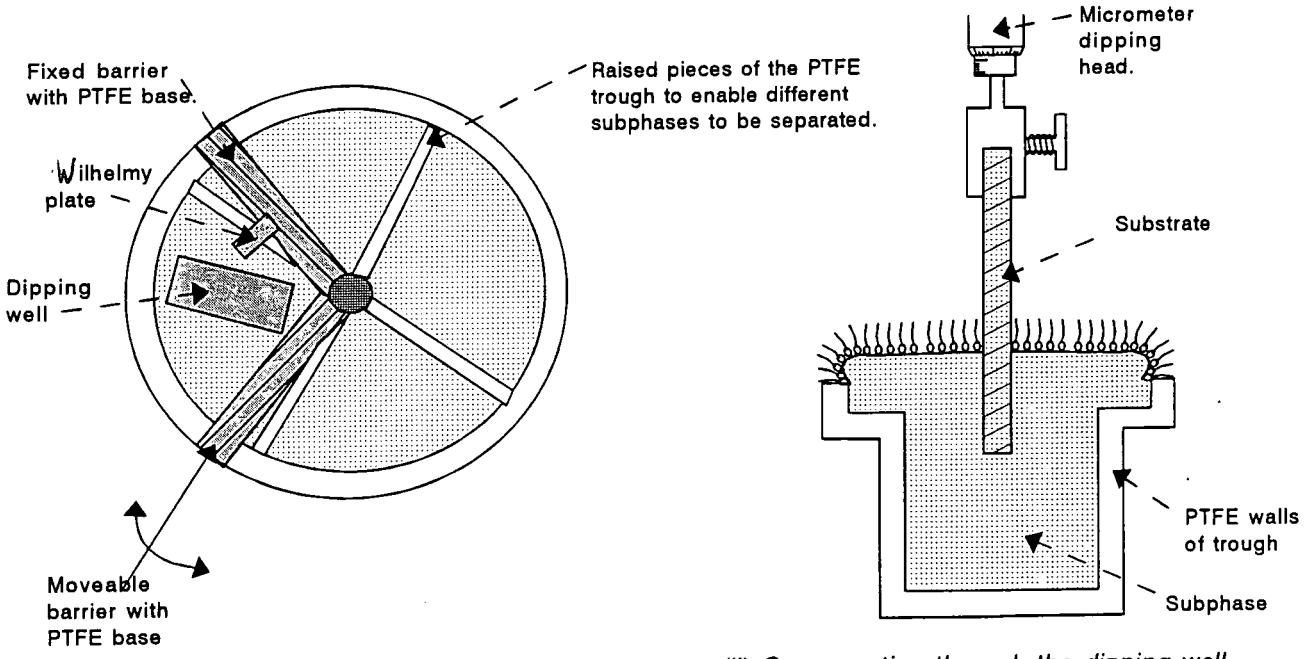

(i) Birds eye view of trough.

(ii) Cross section through the dipping well.

Figure 4(c) : Sections through a Fromherz trough.

4.2 SURFACE POTENTIALS

4.2.1 Background and Theory

The addition of a material to the surface of the subphase will alter the electrostatic potential. This change is known as surface potential. Gaines[103] gives an overview of this subject.

The surface potential, at a given pressure, should follow equation 4(iv)[103] for either ideally miscible or immiscible mixtures. This is of a similar form to equation 4(iii).

$$\Delta V_{AB} = N_A \Delta V_A + N_B \Delta V_B \qquad \textit{Eqn. } 4(\text{iv})$$

Where ΔV = surface potential
N = mole fraction

The change in surface potential will be related to the increase in concentration of the molecules on the surface. Compensation for this is necessary when considering the results. A method of compensating for the concentration of the molecules is to consider $\Delta V/n = \Delta VA$, where n is the number of molecules per cm^2 of the monolayer and A is the area per molecule in the monolayer[103].

The usual method of relating the measured surface potential with a molecular property is to consider the monolayer as a parallel plate capacitor. The Helmholtz model[104] treats an uncharged monolayer as a uniform assembly of molecular dipoles each of which contributes directly to a polarisation across the monolayer. The perpendicular component of this polarisation (P_n) gives rise to the potential difference. Equating this system with a parallel plate capacitor leads to the equations below :

$$P_n = \varepsilon_r \varepsilon_o \Delta V/d = \mu_n/Ad \qquad \textit{Eqn. } 4(v)$$

Where : ε_r = the relative permittivity of the monolayer.
ε_o = the permittivity of free space.
μ_n = the perpendicular component of the molecular dipole.
A = the average area occupied by each molecule in the monolayer.
d = separation between imaginary plates.

Equation 4(v) leads to the Helmholtz equation for an unionised monolayer (equation 4(vi)).

$$\Delta V = \mu_n/\varepsilon_o A \qquad \textit{Eqn. 4(vi)}$$

Where it is assumed that the relative permittivity of the monolayer is unity. This assumption may not be correct and ε_r has been suggested to lie between 5 and 10 by Adam et al[105]. The dipole moments of the molecules in the monolayer may cause polarisation of the water at the interface. If the monolayer is charged then a double layer of ions will be formed close to the water/monolayer interface (figure 4(d))[103]. This has its own associated potential (ψ_o). Equation 4(vi) now becomes :

$$\Delta V = \mu_n/\varepsilon_o A + \psi_o \qquad \textit{Eqn. 4(vii)}$$

If the water surface is considered as a uniformly charged homogeneous plane with a charge density E per cm^2, and the double layer ions are considered to be single point charges, the Guoy model[103] leads to equation 4(viii) :

$$\psi_o = 2kT/e \sinh^{-1}(E/(2nDkT/\pi)^{1/2}) \qquad \textit{Eqn. 4(viii)}$$

Where : n = the number of ions per cm^3 in the bulk solution
D = dielectric constant of the medium (= 80 for water)
T = temperature in K
k = Boltzmann's constant
e = the charge on an electron

If the charge density is taken[103] as the number of monolayer ions per cm^2 *i.e.* 10^{16}/A then at 26 °C equation 4(viii) becomes :

$$\psi_0 \text{ (mV)} = 51.5\sinh^{-1}(133/A.c^{1/2}) \qquad \textit{Eqn. 4(ix)}$$

Where c = the molar concentration of ions

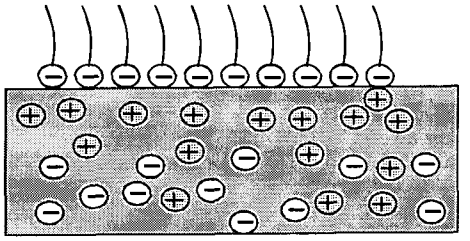

Figure 4(d) : The double layer of ions at the air/water interface with a charged monolayer.

A refinement of the Helmholtz model was made by Davies and Rideal[106]. They proposed a three layer capacitor, as shown in figure 4(e) . In this model the measured effective dipole moment is considered to be made up of three components : μ_1 from the subphase water; μ_2 from the hydrophilic head-group region; and μ_3 from the hydrophobic tail region of the molecules. Demchak and Fort[107] further refined this model by assigning local relative permittivities to each of the three regions.

$$\Delta V = (\mu_1/\varepsilon_1 + \mu_2/\varepsilon_2 + \mu_3/\varepsilon_3)/A\varepsilon_0 \qquad \textit{Eqn. 4(x)}$$

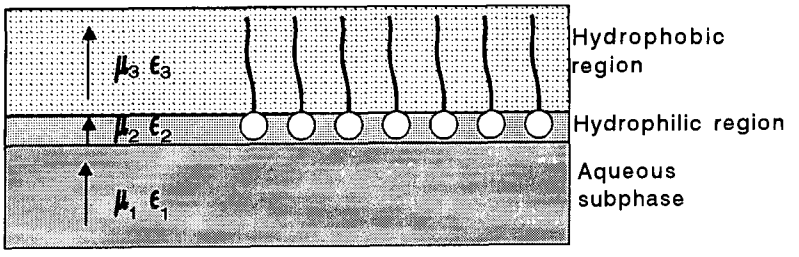

Figure 4(e) : The three layered capacitor model of a monolayer at the air/water interface.

4.2.2 Experimental determination of surface potentials

An Americium 241 100 μC α-source was suspended ~0.8 mm above the surface of the water, within the area surrounded by the PTFE band (on a Joyce-Loebl trough). A silver/silver chloride electrode was placed in the opposite end of the trough (figure 4(f)). The source ionises the air in the space between it and the surface. Any change in the potential of the surface will alter the potential difference between the source and the electrode which is measured by an electrometer.

The surface of the trough was cleaned as described in section 4.1.3, and the system was allowed to stabilise, with the band fully expanded, for an hour. The output was monitored using an x-t plotter registering the potential. The steady state value for the pure water was recorded. A layer of material was spread (as in section 4.1.3) and the chloroform allowed to evaporate for five minutes. The monolayer was then compressed. The surface potential was continuously monitored on the x-t plotter. A π-A isotherm was recorded simultaneously. The surface potential of the monolayer is the difference between that of the material and the water[103].

$$\Delta V_A = V_A - V_W \quad (mV) \qquad \textit{Eqn.}\ 4(xi)$$

Where ΔV_A = surface potential of A
V_A = potential recorded for the monolayer
V_W = potential measured for pure water

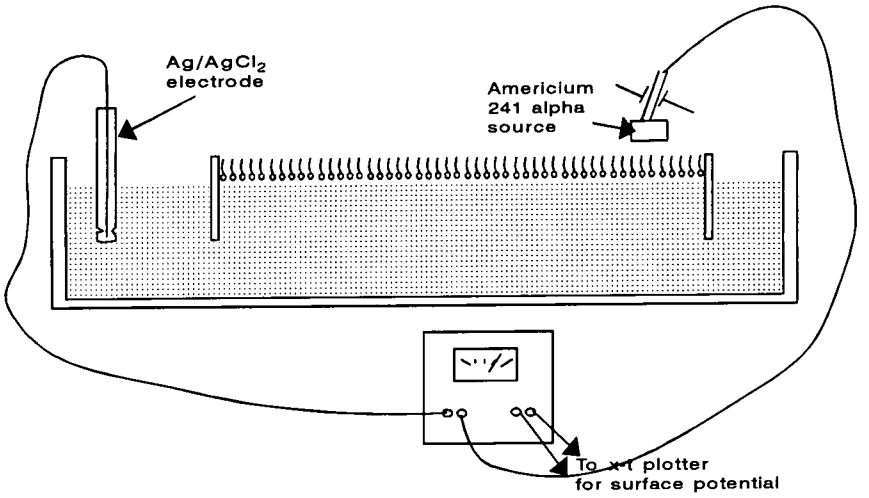

Figure 4(f) : Diagram of the apparatus for surface potential measurements.

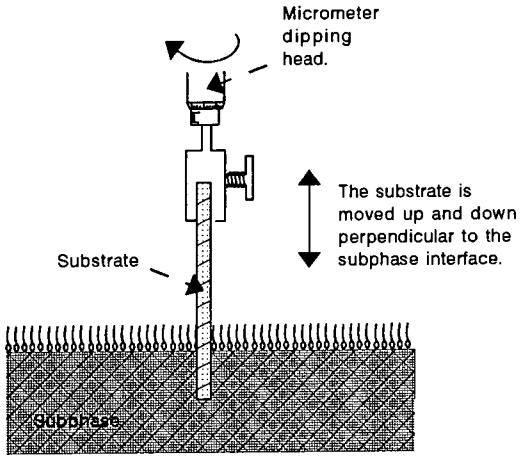

Figure 4(g) : Vertical Langmuir-Blodgett deposition.

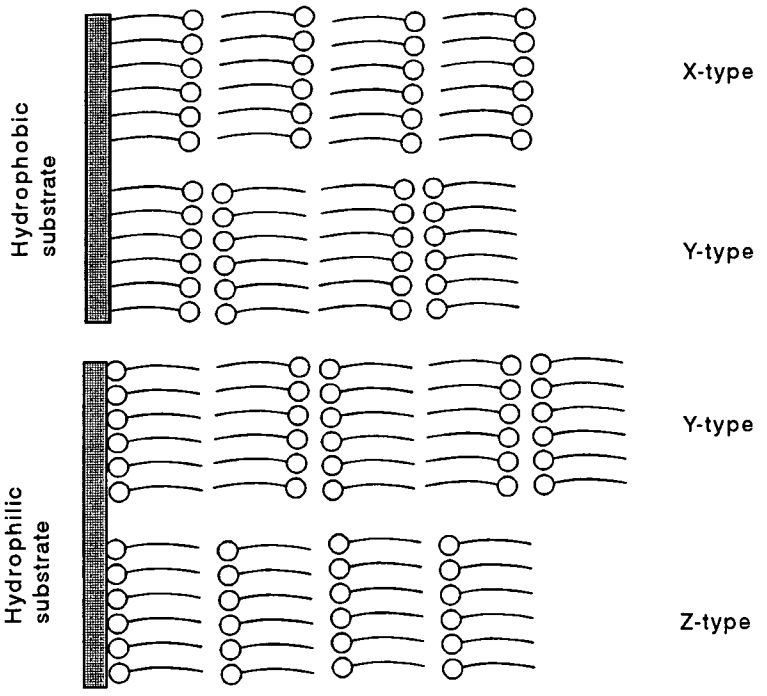

Figure 4(h) : X,Y and Z type Langmuir-Blodgett deposition.

4.3 DEPOSITION ONTO A SUBSTRATE

4.3.1 Background to Langmuir-Blodgett deposition

It is possible to transfer part of a monolayer from the surface of the trough onto a substrate. By repeating this process layered structures can be fabricated which are built up a monolayer at a time. The most common method used for this is vertical dipping (figure 4(g)) where a substrate perpendicular to the surface is moved slowly through it. This is known as Langmuir-Blodgett deposition. With this technique three different types of deposition are found, or can be engineered : X, Y, and Z type[19] (figure 4(h)). In X type deposition a monolayer is deposited onto the substrate only on entry into the subphase. In Y type deposition a monolayer is deposited on both the down and up strokes of a cycle. In Z type deposition monolayers are deposited only when the substrate is removed from the subphase.

During deposition the monolayer is maintained at a constant surface pressure by the use of a feedback circuit. To keep the pressure steady, as material is removed from the surface, the barriers move inwards to reduce the area available. The magnitude of this pressure is chosen empirically, generally in the region of solid like behaviour. However, any pressure from the π-A isotherm at which the monolayer can be stabilised may be used.

If Y-type deposition only is considered then if the substrate is hydrophobic the material should deposit as it is first passed from the air into the water and a second layer will be deposited on leaving the water. If the substrate is then cycled through the monolayer again, two further layers are deposited. However, a monolayer will not deposit onto a hydrophilic substrate during initial entry as the interactions are not attractive. On withdrawal the interactions will allow a layer to be deposited and thereafter further bilayers should be added with each cycle.

Thus with Y-type dipping on a hydrophobic substrate only even numbers of layers can be deposited with a hydrophobic group attached to the substrate. On a hydrophilic material only odd numbers of layers can be produced, with a hydrophilic group towards the substrate (figure 4(h)).

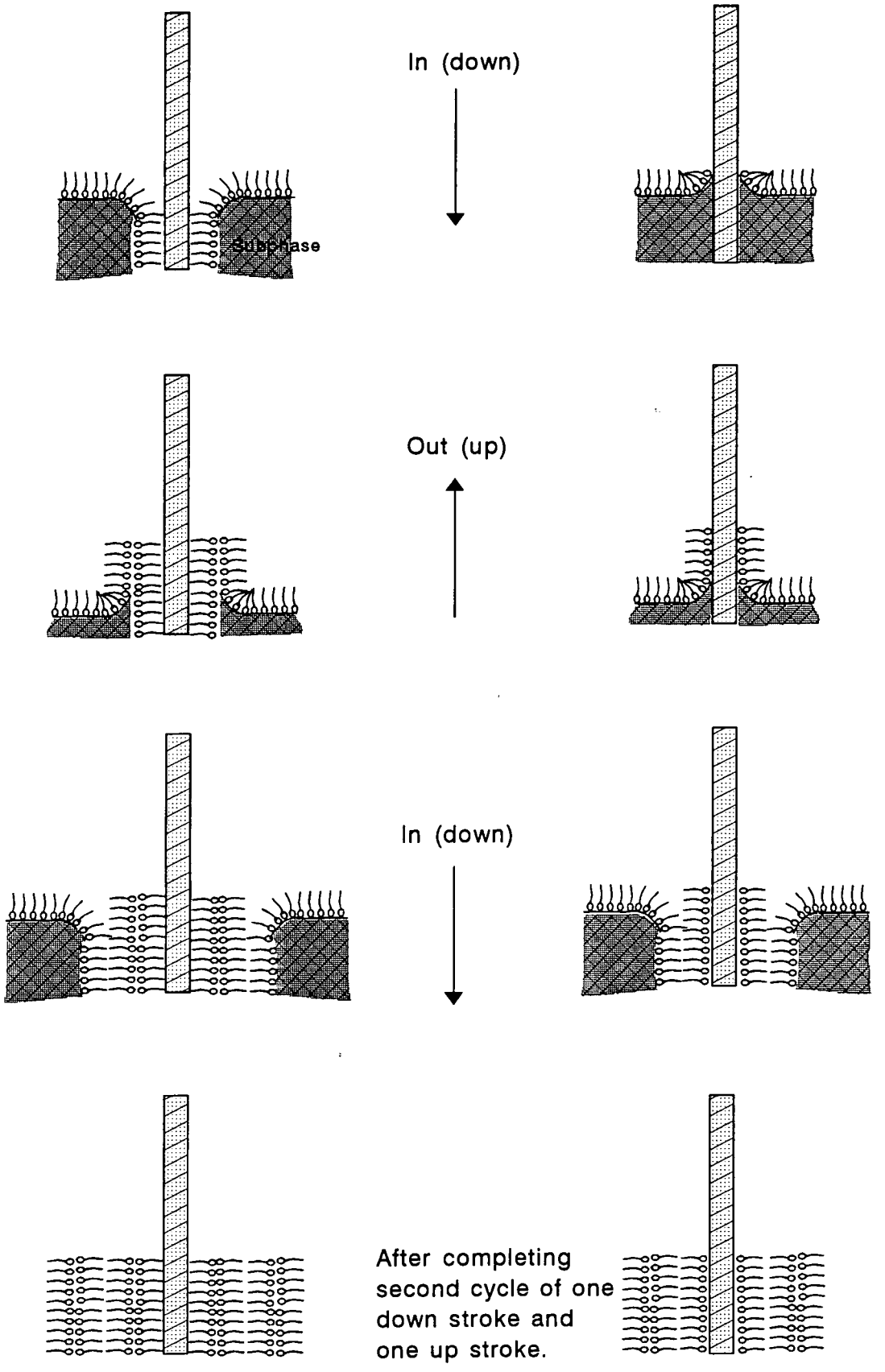

(i) Hydrophobic substrate - only even numbers of layers may be deposited.

(ii) Hydrophilic substrate - only odd numbers of layers may be deposited.

Figure 4(i) : Deposition onto substrates by Y-type Langmuir-Blodgett dipping.

4.3.2. Experimental conditions for LB deposition

(A) General :

Monolayers were formed on the surface of the trough as described in section 4.1.3 and were compressed to the chosen pressure. The L-B trough was set up so that this pressure would be maintained, via the feedback circuitry.

In some cases pre-conditioning took place to enhance deposition. This involved compressing the monolayer to ~half the final dipping pressure then expanding the barriers for 15 minutes and re-compressing to the deposition pressure.

The compressed monolayer was then allowed to stabilise for at least one and a quarter hours before deposition.

Changes in area during stabilisation and deposition were monitored via an x-t plotter. This records the response of the system in mV. By calibration this can be converted into a change in surface area of the trough. This information can be used to monitor how stable the monolayer is at a given pressure by following the drift in area of the trough. It can also be used to calculate the percentage coverage of the substrate by a monolayer.

$$\% \text{ coverage} = \frac{\text{area change of trough during deposition } (cm^2)}{\text{area of the substrate } (cm^2)} \times 100$$

Eqn. 4(vi)

Presuming there is no change in molecular packing a deposition value of 100 % should show that the substrate is completely covered by a layer one molecule thick. In this thesis deposition ratios will be used. These are the above ratio but without the multiplier of 100. Thus, a deposition ratio of 1 indicates monolayer coverage of the substrate.

(B) Preparation of substrates for LB deposition

The substrates used were gold and aluminium coated glass slides or silicon ATR crystals, cut from wafers. All of these are hydrophilic in nature when prepared as outlined below.

Glass slides were sonicated in the purified water then refluxed in iso-propyl alcohol (IPA) for two hours. The slides were coated with metal, either gold or aluminium, by evaporation. For a good mirror either a very thick layer is required or a thin preparatory layer of a metal which will bind well to the glass. Aluminium was deposited to a depth of 2000 Å. 15 Å of chromium were deposited before 1000 Å of gold. The slides were used only once as it was not possible to clean them without the removal of the metal.

New silicon ATR crystals were refluxed in IPA for two hours. On re-use, however, the procedure for cleaning was as given below. The crystals were cleaned manually with a straw coated in cotton wool, (commonly known as Q-tips) initially with acetone as a solvent, and then with chloroform. They were then sonicated for ten minutes, in batches of five in a PTFE holder, with aristar solvents in the order given :- acetone, EDTA solution, water, chloroform and acetone. They were then refluxed in IPA for two hours. Their cleanliness was verified by FTIR, to show that there was no material present on the surface, in comparison with the empty spectrometer.

(C) Vertical (Langmuir-Blodgett) deposition

Samples were held in a small clamp attached to a motor driven micrometer. The lower 4 cm of the metal coated glass slide was cycled back and forth through the monolayer to deposit the required number of layers. The top part was left blank to use as a reference in FTIR. Material was deposited onto ~1.2 cm of the silicon crystals which are only 1.7 cm in length. Care was taken to ensure that they were dipped in the correct orientation or no FTIR spectrum could be obtained due to the asymmetry of the crystal (see figure 4(q)).

The rate of deposition varied. Initially, most of the experiments were performed at a micrometer speed of 5 mm/min but deposition took place at 1.5 mm/min for later samples.

(D) Sub-aqueous sample preparation

With normal Langmuir-Blodgett deposition techniques it is not possible to deposit a structure which is a bilayer with the hydrophilic groups outermost. Using Y-type deposition onto either a hydrophilic or hydrophobic substrate the outer monolayer is always hydrophobic in nature *i.e.* the alkyl chains of the lipid are outermost not the hydrophilic group as desired. It was therefore decided to use Y-type dipping, in a novel manner, to form a bilayer on a silicon ATR crystal by depositing one layer in the first cycle then to deposit a second layer but keep the crystal under water (figure 4(j)). This procedure avoids the deposition of a third layer on passing back through the monolayer. If the monolayer is removed from the air/water (A/W) interface then rearrangement of the already deposited layers takes place[108]. This technique prevents the above from occurring. The samples were kept under water throughout their usage, including the filling of the FTIR cell.

The device used to allow the same monolayer to prepare 4 crystals is shown in figure 4(k). Material was deposited from a monolayer at the A/W onto a micro-ATR crystal. The clamp holding the crystal was then released and the crystal was allowed to drop gently into one of the tubes in the collecting device (figure 4(k)). The beaker was then turned, using the holding rod, so that an empty tube was below the next crystal to be used. The monolayer was allowed to re-stabilise, then LB deposition of material onto the second crystal took place. In this manner the same monolayer at the A/W interface could be used to produce four samples in one day.

The beaker and four tubes were then removed with the water in them from the trough into a bucket full of purified water. The crystals could then be removed from the tubes and placed in the micro ATR solution state accessory (figure 4(v)). This was completed under the surface of the water and care was taken to ensure that the crystal did not pass through the A/W interface. The cell was then removed from the bucket and put in the FTIR spectrometer where spectra were obtained (section 4.4.2.B).

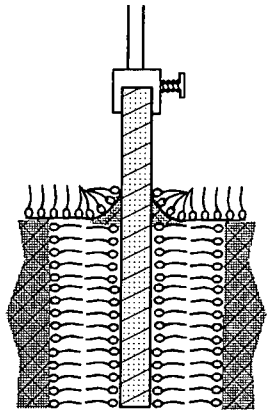

Figure 4(j) : A biological bilayer onto a hydrophilic substrate after two entries into the subphase with Y-type deposition.

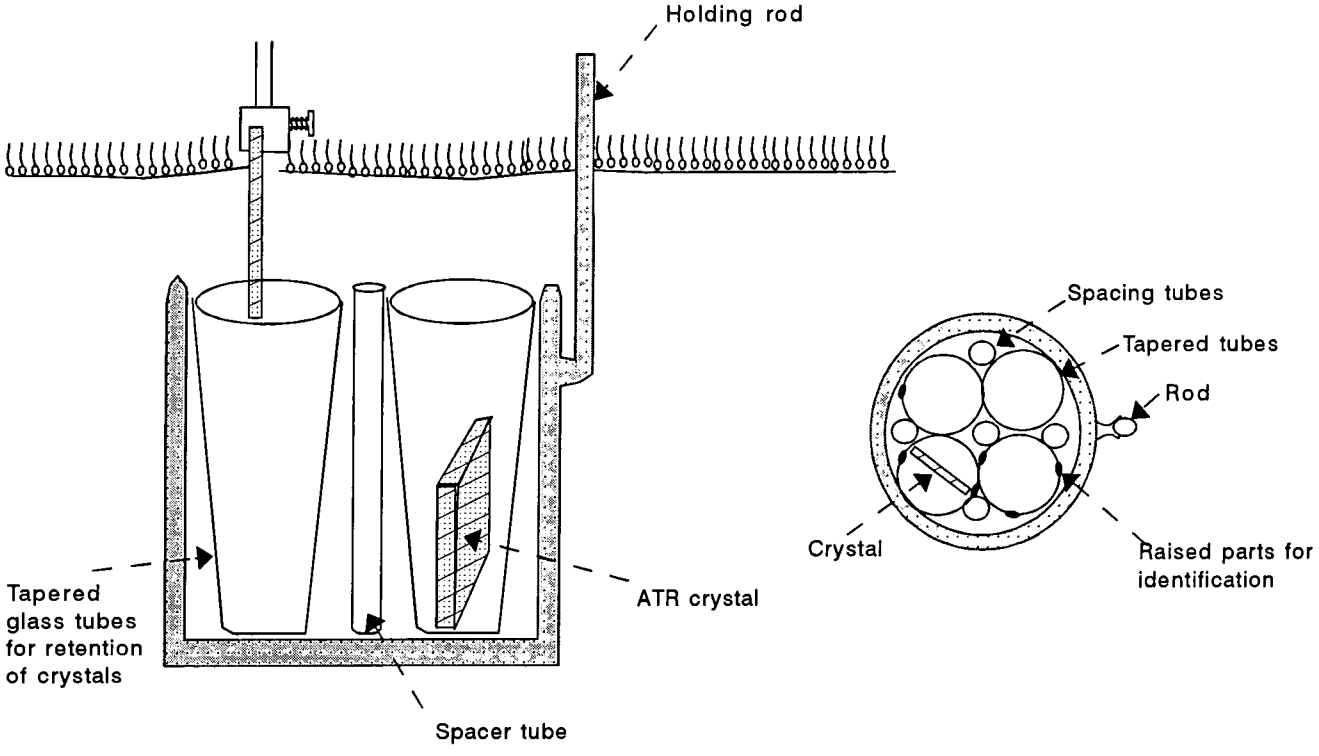

(i) Cross section *(ii) Birds-eye view*

Figure 4(k) : Underwater holder for the collection of four crystals to be deposited using the same monolayer on the water surface.

(E) Horizontal (Langmuir-Shaeffer) deposition

A more unusual method of deposition than Langmuir-Blodgett dipping is to hold the substrate parallel to the surface of the monolayer. The sample is brought down onto the monolayer then pulled away (figure 4(l))[109]. This is known as the Langmuir-Schaeffer (LS) technique[22] and has been used recently by von Tscharner and McConnell[110] and also by Virtanen et al[111]. The substrate was held horizontal by a suction pump on the reverse side. Glass coated slides were broken in half to avoid the FTIR reference portion collecting material from the surface.

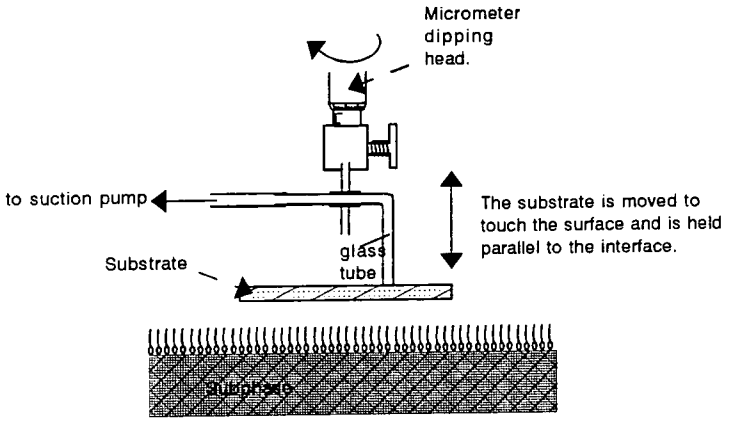

Figure 4(l) : Horizontal Langmuir-Shaeffer deposition.

Three different techniques were utilised for controlling the monolayer's behaviour. The first, used for larger samples, was to keep the feedback mechanism on during the cycle. The second was to bring the sample onto the surface with the feedback mechanism on but to switch it off before withdrawal, allowing the monolayer to relax. In the third method, the sample was brought down onto the surface and the barriers were then expanded before removing the sample. This was used for smaller samples (~2 cm^2). The variation in technique was needed because of the fact that, for smaller samples, more than one monolayer was deposited if the monolayer at the air/water interface was unable to relax. In the first two techniques information regarding the percentage deposition was retained but in the third method it was lost.

In order to get the spectrum of the equivalent of a biological membrane two main strategies utilising LS deposition were pursued : The first was to deposit x layers vertically and then one horizontally, then to subtract the spectrum of a sample with x-2 layers dipped vertically and one horizontal (figure 4(m)). This was mainly used for the glass slides because the FTIR RAIRS equipment (see section 4.4) was only useful for 6 or more monolayers. The second method was to deposit one layer using the vertical technique and one with the horizontal onto a silicon crystal. The spectrum of a biological bilayer could thus be examined directly.

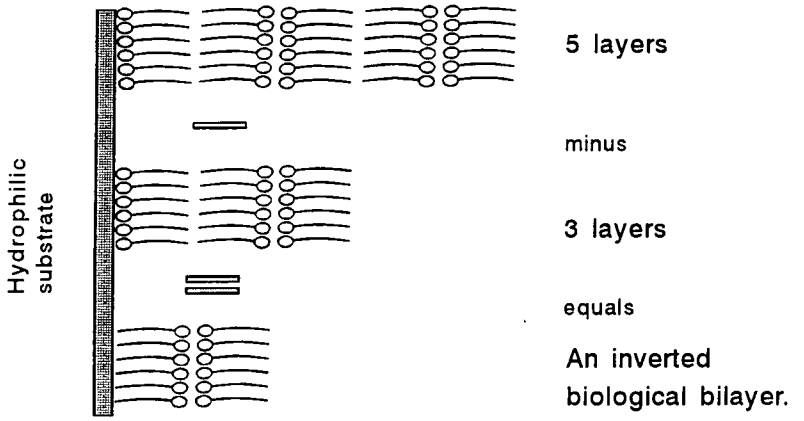

(i) Just using the spectra of samples prepared by vertical deposition.

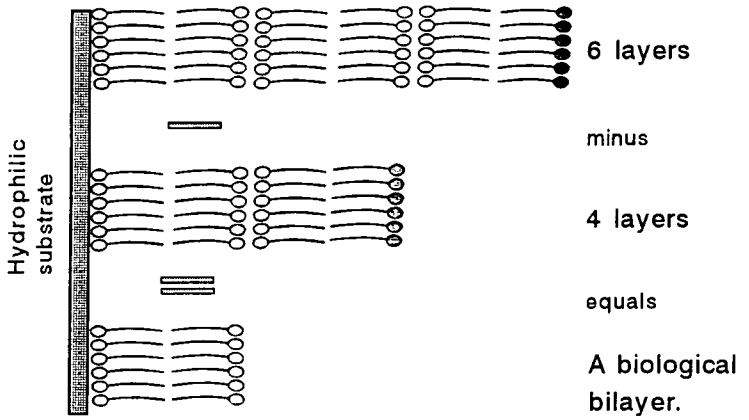

(ii) Using the spectra of samples prepared by vertical dipping with a final layer added to the samples by horizontal deposition.

Figure 4(m) : The FTIR spectrum of a biological bilayer can be obtained by the subtraction of multilayer LB structures.

4.4 FTIR of THIN FILMS :

4.4.1 Background

There are three main methods used to obtain FTIR of ultra-thin films: transmission; external reflection and internal reflection. The first is useful for relatively thick layers (of the order of microns) but poor signal to noise ratio is achieved with low numbers of monolayers. The second requires at least 5-6 layers for a good spectrum, using the equipment available in Durham, but is extremely useful for studying orientational effects. With the third technique it is possible to record the spectrum of less than one monolayer[39].

The external reflection technique used is known as reflection-absorption infra-red spectroscopy (RAIRS or IR-RAS). It is particularly useful if performed at a high angle of incidence from a metal surface[112], described overleaf, which gives a selection rule such that only transition dipole moments for vibrations which are perpendicular to the surface will be coupled, and thus observed in the IR spectrum.

For internal reflection equipment the number of reflections is mainly dependent on the shape and size of the crystal. Depending on the optics of the equipment, in multiple attenuated total internal reflection (ATR) an IR beam may sample the film from 8 to 50 times, thus greatly enhancing the signal compared to the noise. Whilst there is no surface selection rule for ATR it is possible to linearly polarise the radiation entering the crystal and thus observe orientational effects.

The increased sensitivity of FTIR instruments (compared to a dispersive IR instruments) is necessary to perform experiments on mono/bi-layers. The speed for each scan is also an important factor as it allows the co-addition of large numbers of interferograms to give an increase in the signal to noise ratio.

(A) Reflection / absorption IR spectroscopy (RAIRS)

If light is reflected,at a high angle of incidence (~85°) from a metal surface then the electric vectors,of the reflected beam, undergo phase shifts due to the conducting nature of the surface[112]. The light polarised perpendicular to the plane of incidence (s polarised) undergoes a 180° phase change at the surface (figure 4(n)). Therefore, a node in the wave function is formed at the surface. As there is no intensity at the surface there can be no absorption of the beam by any material present[113]. The light polarised parallel to the plane of incidence (P polarised) has a phase shift of 90° on reflection. Thus when the incoming and outgoing beams are superimposed there is a net amplitude at the surface.

If a very thin sample (<100 nm) is placed on the surface the phase shifts are not affected to any great extent but any part of the beam which has an amplitude at the surface will interact with the sample and be absorbed at the resonant vibrational frequencies. Thus only p polarised light will interact and produce a spectrum. This is parallel to the plane of incidence which is perpendicular to the substrate (see figure 4(n)). However, as only one reflection occurs it is necessary (for the commercial equipment used in this work) to have 5-6 monolayers before a good signal to noise can be achieved.

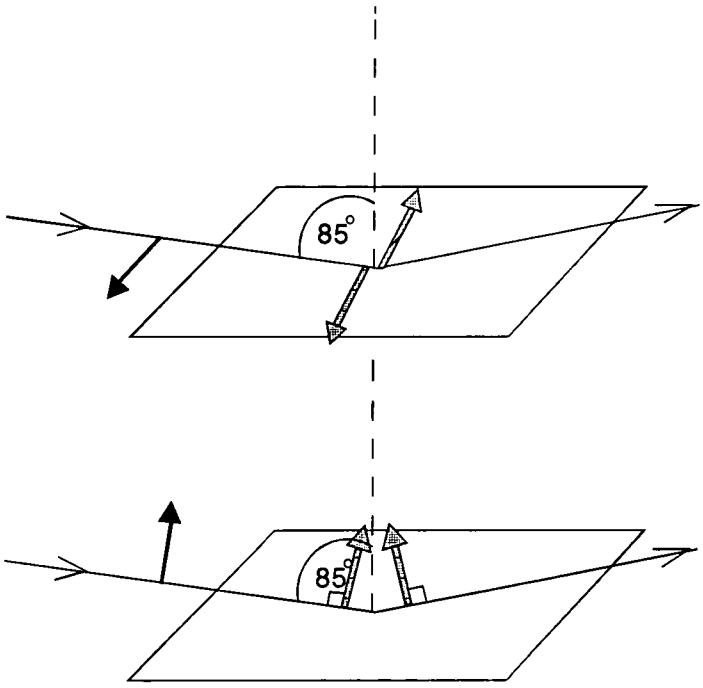

(i) 180° phase shift of s polarised light (polarised parallel to the substrate).

(ii) 90° phase shift of p polarised light (polarised perpendicular to the substrate).

Figure 4(n) : The phase changes of polarised light on reflection from a conducting surface at a high angle of incidence. Redrawn from Ferraro and Basile.[112]

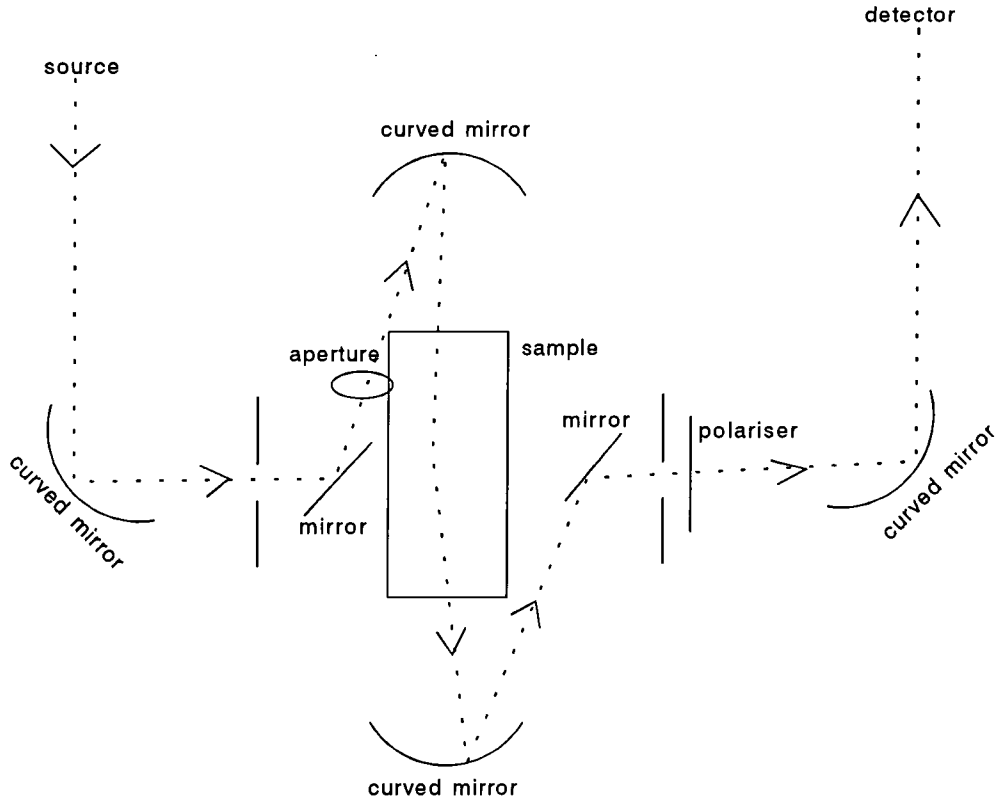

Figure 4(o) : A schematic for the optics of the RAIRS instrumentation.

(B) Attenuated total internal reflection (ATR)

If a crystal with a high IR refractive index is cut to a specified shape, usually a parallelepiped, and the initial beam reaches the interface between the inside of the crystal and the external medium at an angle greater than the critical angle, then total internal reflection (TIR) will occur. If the optics are chosen such that the TIR beam is incident at the opposing interface again at an angle greater than the critical angle and this is repeated along the crystal then the beam can emerge at the other end of the crystal having been reflected off the sides several times. The loss of reflected light at the initial interface can be reduced by arranging the equipment such that the incident beam is normal to the entry face.

Most ATR crystals are cut with 45° edges as shown. However, for depth profiling the angle of the crystal faces and incident beam can be changed, in most equipment.

Although the reflection is called total internal reflection the electric field of the beam does penetrate into the rarer media in the form of an evanescent wave. If a sample is on the exterior of the crystal then the attenuated beam will interact with it. If the refractive index of the sample changes, as in the region of an absorption band, then a change in the amount of energy reflected will occur. The resultant spectrum may, for unpolarised light, approximate a normal transmission spectrum. However, only a very small amount of energy is absorbed in a single reflection, many are needed to ensure a good spectrum[24]. This is especially important for thin films where there is very little sample.

The evanescent wave decays within the sample and this is generally given by[39].

$$E = E_o \exp\left(^{-z}/d_p\right)$$

z = the distance from the surface of the crystal
E_o = the initial electric field
E = the electric field at z

$$d_p = \frac{\lambda_1}{2\pi\left(\sin^2\theta_i - n_{21}^2\right)^{-}} \qquad \textit{Eqn. } 4(xii)$$

d_p = penetration depth for the field to decay to $E_o * \exp^{-1}$
λ_1 = wavelength of the radiation
θ_i = the angle of incidence
n_{21} = n_2/n_1=refractive index ratio of sample and crystal

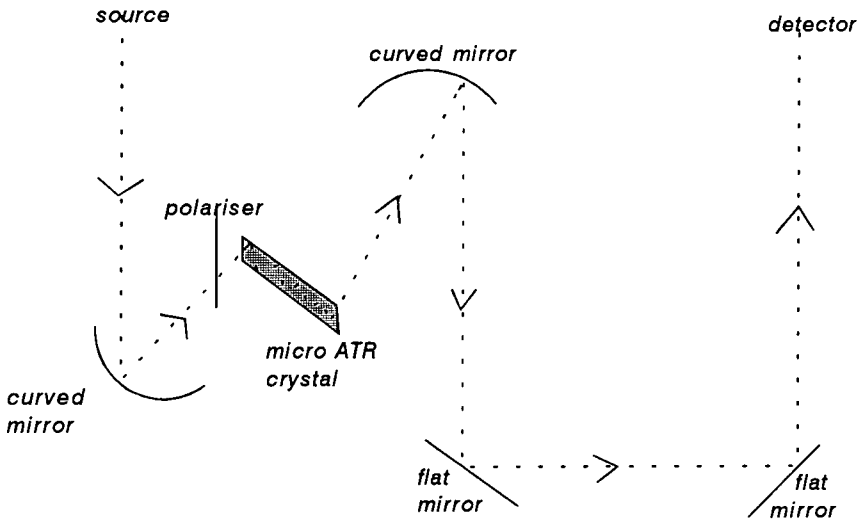

Figure 4(p) : A schematic of the micro ATR optics.

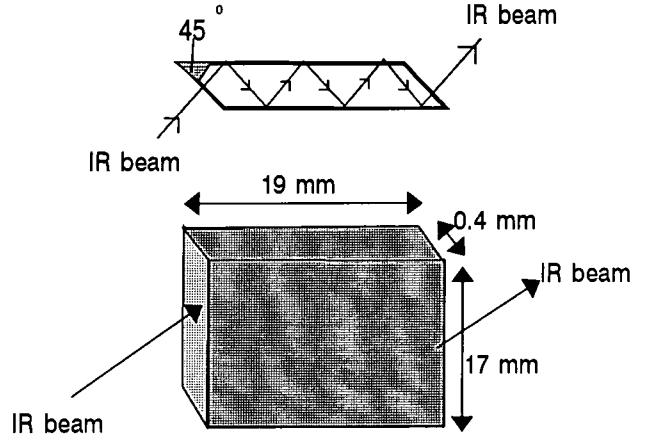

Figure 4(q) : The micro ATR silicon crystal.

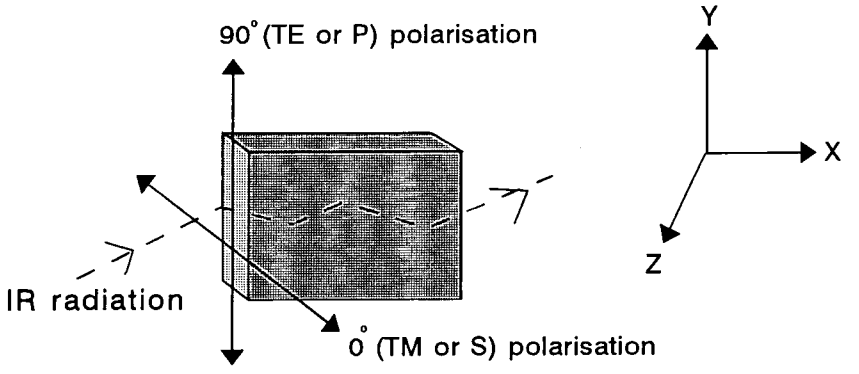

Figure 4(r) : The linear polarisation directions in ATR

4.4.2 Description of the FTIR experiments for thin films

(A) RAIRS

Reflection spectra were gathered with a Mattson Sirius 100 spectrometer as out-lined in section 2.6. The gain was set to 2, with a 98% iris , and a resolution of 4 cm^{-1}. 1024 interferograms were accumulated and Fourier transformed to give a reflectivity spectrum (equivalent to an emissivity spectrum).

The samples were either aluminium or gold coated glass slides, prepared as in section 4.3.2.B, with Langmuir-Blodgett layers deposited on them. These were placed onto the platform of a 'Graseby Specac' standard RAIRS accessory and the infra-red beam was reflected at an incident angle of $85^{\circ} \pm 2^{\circ}$. The optics are shown in figure 4(o). A polariser was attached to the arm of the exit mirror. This was set to 90° as Song et al[114] have shown that not only does the addition of a polariser reduce noise it also enhances the relative signal intensity. The background spectra were obtained, in a similar manner, from the clean half of the metallised slide.

(B) ATR

The spectra were gathered with a Mattson Sirius 100 spectrometer. The gain was set to 4, with an iris of 98 % and a resolution of 4 cm^{-1}. 1024 interferograms were co-added to be Fourier transformed into a spectrum. They were ratioed against a similar but clean crystal, whose spectrum had been obtained the same day.

The equipment used has been developed at Durham[34,90,115,116]. The ATR crystal is a very small piece of silicon with 45° angled edges and dimensions of 19 X 17 X 0.4mm, cut from a silicon wafer. The advantage of this system is that a high number of reflections can be obtained, ~48 compared to 10 for a standard ATR crystal. Thus, for the study of small amounts of material (*i.e.* bilayers) this represents considerable advantage. However there is a problem as silicon has a fairly small infra-red spectral window and reliable data is difficult to obtain below 1000 cm^{-1}.

Polarised spectra were obtained by placing a linear polariser between the focusing mirror and the crystal at either 90°or 0° linear polarisation (figure 4(r)).

For solution state spectra the cell was as described in section 4.4.3.B. For bilayer work the crystal was placed into the holder within a container full of water thus avoiding contact with air. As water (H_2O) is a strong absorber in the IR spectral regions of biological interest, (table 3(i)) it was necessary to replace it with D_2O. This was achieved by use of a syringe and D_2O slowly replaced H_2O without emptying the cell.

Cast film spectra of samples, for comparative purposes, were prepared by deposition from solvent onto either a CaF_2 plate, metal coated glass slides or silicon ATR plates depending on what type of spectrum was required. The solvent was evaporated and the spectra recorded as for the Langmuir-Blodgett films.

4.4.3 Development of new equipment

(A) Cell holder

Initially the ATR holder was a metal jaw supported on a column. This system had many degrees of freedom for movement but none were reproducibly controllable. Indeed it was difficult and frustrating to align this system in the infra-red beam and exact re-positioning of a crystal or a similar one was impossible (figure 4(s)). Another problem was that precise positioning of the crystals involved manually moving them in the jaw. This often resulted in breaking the crystals, as the thin silicon is brittle. It was therefore decided to re-design the holder.

The main criteria were: (a) that the crystal could be placed in a holder, then components of the holder moved until the crystal was aligned; (b) that there be some method of measuring the position of the crystal; and (c) that the entire unit should fit into the space available. It was decided that a 3-way translational stage would fit these criteria (figure 4(t)). A three stage x,y,z positioner was purchased from Micro-Controle. Each translation stage is moved with a micrometer with a range of 13 mm and the scale on these can be read to hundredths of a millimeter. A small piece of one of the mirror stands had to be removed in order to fit the x,y,z positioner in the small space available in the spectrometer. A holder for the crystal was fabricated by the university workshop and attached to the positioner. This still allowed the crystal to be placed at a variable position in the holder so Dr P.Lukes designed a new one with a slight nick to push the crystal against.

Thus it is now possible to place a crystal in the holder and use the x,y and z translational stages to move the 45° face of the crystal into the optimum focal point of the beam and thus a higher through-put is seen. This increases the signal to noise ratio as the beam is able to interact with a larger area of sample. Finding the focal point has also been aided by the purchase of a card, from Sunstone Inc., which converts an infra-red beam into visible light. The greatest advantages are that the sample and background crystals can now be placed accurately in the same position, and it now takes 10 minutes to align the sample as compared to several hours on the old unit.

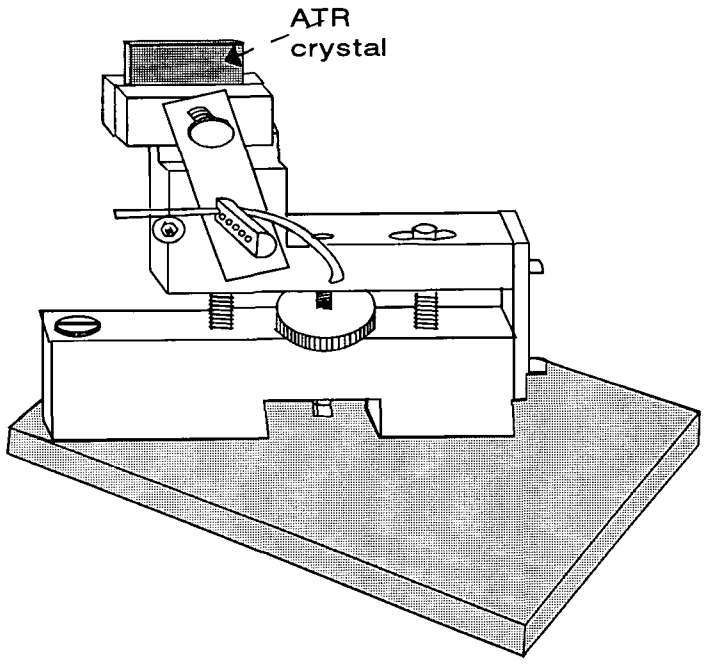

Figure 4(s) : The Old crystal holder.

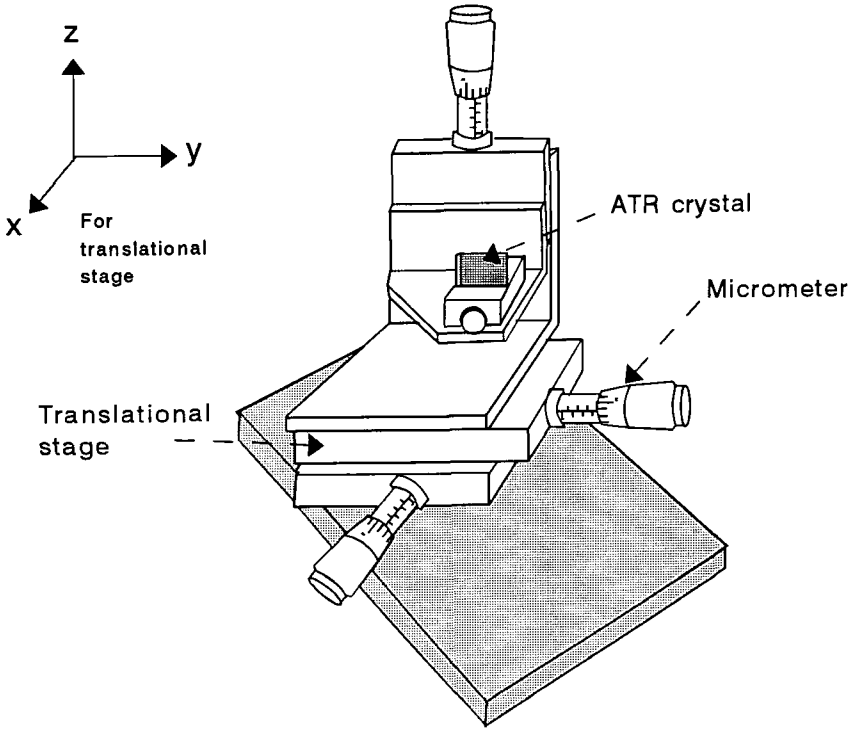

Figure 4(t) : The new ATR crystal holder.

(B) Solution state cell

Early in the project it was decided that solution state spectra from the micro ATR unit would be highly desirable, particularly for the study of the effect of an aqueous environment on the Langmuir-Blodgett layers. Thus it was a high priority to design and build a suitable unit.

The first two designs were inadequate. The first was a steel U-shape with a free piece of metal in the centre which was held against one of the U faces with a screw (figure 4(u)-A). The crystal was inserted between the U-face and the metal plate, sealing was performed by PTFE rings. Solutions could enter cavities cut into the metal pieces through lure lock filling tubes. There were two main problems with this cell. The first was that the recesses for containing fluid were fairly deep and thus the volume contained was quite large (~1 ml) for the very expensive peptides that we planned to use. The second, and major, problem was that the unit was virtually impossible to seal. Even in air the crystal and seals kept moving out of position. The situation was impossible under water where slight eddies would cause the crystal to fall out of the cell. The second design consisted of an L-shaped piece of steel with a solid piece which fitted into it (figure 4(u)-B) The spacers and the crystal were placed between the pieces of steel and the whole unit was held together with a clamp. It had the same intrinsic problems, as the first, as it too had separate spacers, but its major flaw was poorly fitting parts. Again it was difficult to handle under water as both hands were required to seal it.

Finally, it was possible to achieve better design and construction in the current cell (figure 4(v) & 4(u)-C). The main design advantages are the recessed O-rings (made from viton) and the spring which allows the closure of the cell with one hand - perfect for underwater closure. Both of the last two cells had smaller liquid volumes (~0.3 ml) and had two filling tubes into both sides with one of the tubes reaching to the bottom of the sample chamber and the other at the top. This was to stop gravitational effects causing air bubbles on filling. Most of the results presented were obtained with the current cell.

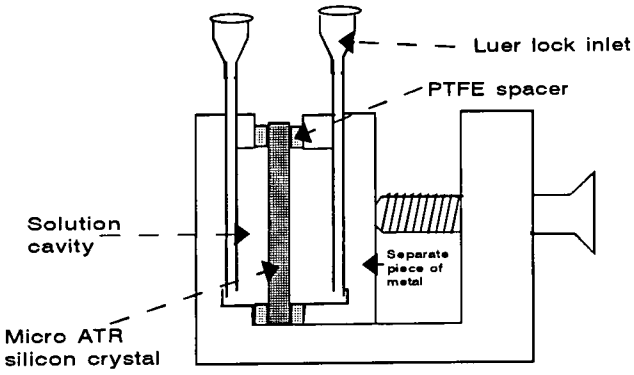

(A) First cell

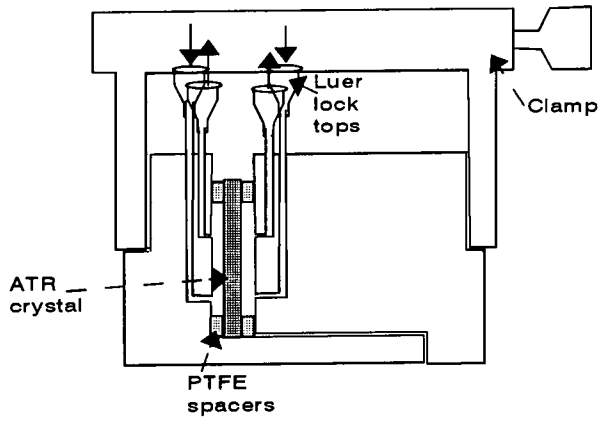

(B) Second cell

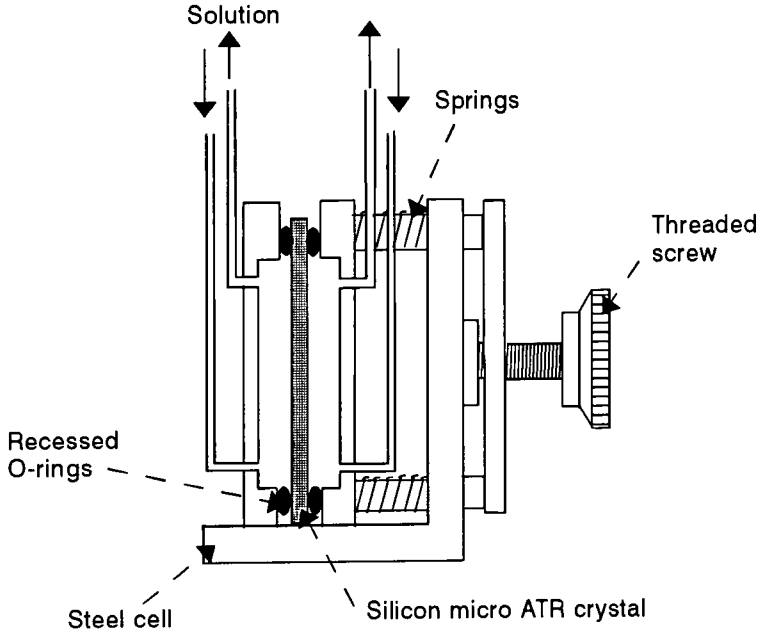

(C) Third cell

Figure 4(u) : The three micro ATR solution state cells.

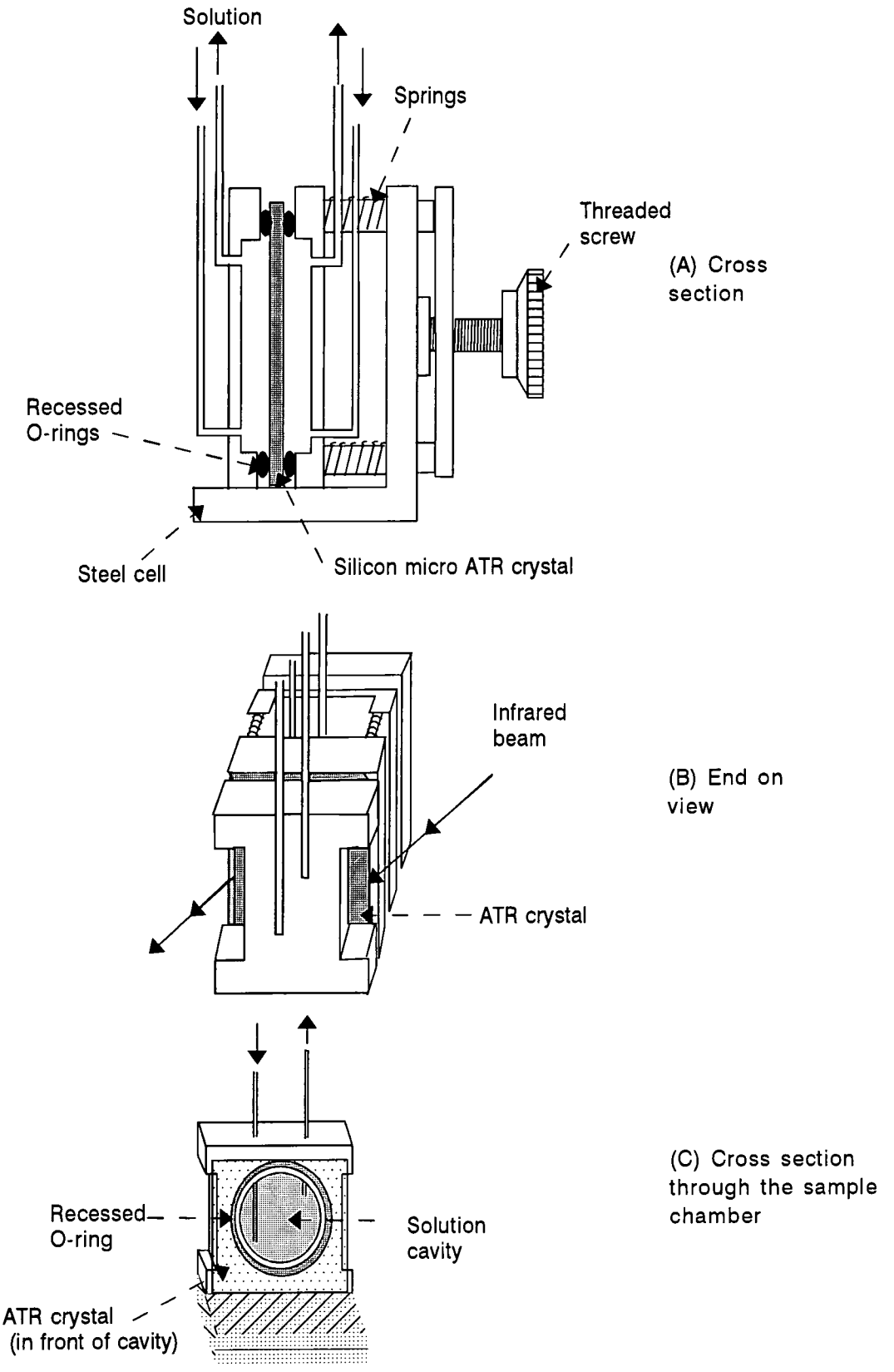

Figure 4(v) : The current micro ATR solution state cell

CHAPTER 5

RESULTS AND DISCUSSION OF MONOLAYER STUDIES AT THE A/W INTERFACE

5.1 INTRODUCTION TO MONOLAYER MEASUREMENTS :

The results for studies of monolayers at the air/water interface will be presented in sections, which will relate to either a single compound or particular mixtures of different compounds.

The choice of material for monolayer studies was determined by one of the primary aims of the project, which was to deposit a biological bilayer of phospholipid. The main phospholipid which was investigated was 1,2,-dipalmitoyl-sn-glycero-3-phosphatidic acid (DPPA[†1] - see figure 5(a)). This was primarily chosen because Hasmonay[117], Petty[34], Matuoka[118], Swart[119] and their respective co-authors have achieved success in depositing DPPA onto substrates by the Langmuir-Blodgett techniques. Apart from the last, all of these scientists used calcium in the subphase to aid deposition by producing a monolayer with a higher degree of rigidity and crystallinity. However, in order to aid interpretation of FTIR results it was hoped that it would be possible to deposit DPPA over a pure water substrate. Unpublished work by Swart and Froggatt[119] led to the conclusion that this might be possible. Other phospholipids have been successfully deposited as multilayers by the Langmuir-Blodgett

[1]†Where DPPA is referred to in this thesis without a prefix it is the mixture of D and L enantiomers.

technique but only in the presence of metal ions. Examples of these include the deposition of dipalmitoylphosphatidylcholine (DPPC) by Prakash et al [120], over uranyl acetate; DPPC over water but only z-type by Lotta et al[59]; and dipalmitoylphosphatidyl-ethanolamine (DPPE) over water by Taylor & Mahboubian-Jones[143] (but only to three layers). However, no reports of Y-type deposition of high numbers of multilayers of a phospholipid, over pure water, were to be found until Lukes et al[90] reported the successful y-type deposition of DPPA over pure water. That work was performed in close collaboration with the author of this thesis.

As one of the main objectives of this project was to incorporate a polypeptide into the bilayer structure monolayer studies of the interactions of DPPA with alamethicin (figure 5(f)) were undertaken. Due to problems encountered with the deposition of alamethicin/DPPA mixtures (see chapter 7) it was decided that a mixture of lipids at the air/water interface might aid deposition by the formation of a more fluid monolayer. The lipid chosen was 1,2-dioleoyl-sn-3-phosphatidic acid (DOPA), figure 5(b). The head group of DOPA is the same as DPPA therefore it was thought that it would not affect the interactions of the lipid with water to a great extent. The hydrocarbon chains of DOPA contain a cis double bond half way along the chains. DOPA is above its phase transition temperature at room temperature (see section 6.9) and the monolayers formed should be more fluid in nature. The monolayer studies of DPPA, DOPA, alamethicin and mixtures thereof are presented in the following sections.

The π-A isotherms (section 4.1) are presented in the common manner of the area available (on the subphase surface) to each molecule, in $Å^2$, versus the surface pressure. The tables given are to show reproducibility. It is possible to read the results of the isotherms to ± 0.2 $Å^2$ per molecule and ± 0.1 mN m^{-1}. Thus the greatest source of error is in the reproducibility of the isotherms. This can be affected by a number of factors: including the concentration of the solution used; whether the calculated amount of lipid solution was deposited onto the water surface or passed through into the bulk water; the temperature of both the subphase and the deposited solution; and the length of time allowed for the solvent to evaporate. The following factors would give rise to high values of APM being recorded: the depositing solution being more concentrated than planned; the solution being colder than room temperature; incomplete evaporation of the solvent. The opposite of the preceding would give results with areas per molecule (APMs) lower than they should be, as would the loss of deposited material through the subphase surface.

The average percentage standard deviation for the reproducibility of the isotherms recorded was 3%. This represents an error of ± 1.2 $Å^2$ per molecule on a value of 40 $Å^2$ per molecule. The error on recording the surface pressure should be low. This is due to the fact that the zero value is reset at the start of an experiment. Factors which could affect the surface pressure are the presence of impurities both in the subphase and on its surface. Those on the surface would tend to increase the recorded pressure, whilst those in the subphase may have a variety of effects. One major error could arise from different compression speeds. This is because the conditions under which π-A isotherms are recorded, as given in section 4.1, are non-equilibrium and the monolayer may respond differently under different time constraints[103].

The isotherm numbers are those of the actual experiments performed and therefore relate to the chronology of the data rather than the order in which they are presented in this thesis. The starting area per molecule (APM) is the initial calculated area of the trough (in $Å^2$) divided by the number of molecules deposited on the surface. The pressure at which the change in slope of the isotherm due to the liquid to solid phase transition is given for isotherms for which it could be measured. The initial pick-up is the APM at which a detectable surface pressure is first recorded on the isotherm. The close packed APM (CPA) is the extrapolation of the gradient in the solid region to zero pressure. The APM is also given at three different pressures, where possible. These were chosen to give a 'snapshot' of the π-A response, primarily for use in investigating the relationship of the data with the theoretical model given in 4.1.2.B. These values were found by dropping a vertical line from the isotherm, at the pressure stated, to the APM axis. Three pressures 10, 25 and 50 mN m^{-1} were chosen. 10 mN m^{-1} is below the liquid/solid phase transition of DPPA; 25 mN m^{-1} is in the solid phase region of DPPA; and 50 mN m^{-1} is below the collapse pressure of DPPA but above both those of DOPA and alamethicin (see results to follow).

The results for the stability tests are given in units which can be used to directly compare the rate of condensation of different materials ($Å^2$ per molecule per hour). The recorded change in area of the given trough is also quoted in brackets (cm^2 per minute).

The surface potential (see section 4.2) results are presented with the x-axis as time rather than area per molecule because this displays the hysteresis experiments adequately. All of the surface potential data was recorded on a Joyce-Loebl style trough. The top plot in each case shows the change in area per molecule as a dotted line (*i.e.* it reflects the change in the area enclosed by the ribbon on the Joyce-Loebl trough). The upper plots also show the surface pressure of the monolayer vs time, which is an equivalent plot to a π-A isotherm as the APM is directly proportional to the time. The lower plots are of the measured surface potential difference (ΔV), with the surface potential of the water subtracted. The dotted lines on the bottom plots show the relative contribution of each molecule to the surface potential ($\varepsilon_o \Delta V * A * 2.65X10^{-2}$), this is equivalent to the perpendicular dipole moment per molecule measured in milliDebyes per molecule. The constant $2.65X10^{-2}$ is to convert the values from mV $Å^2$ F m^{-1} to mD (1 D = $1/(3.33*10^{-30})$ C.m)

For all of the surface potential measurements the barriers were fully compressed, expanded then re-compressed. This was in order to investigate the hysteresis of the surface potential of the monolayer.

5.2.1 : Results for L-α-DPPA

Three isotherms of L-α-DPPA were recorded on the Fromherz trough. Unfortunately isotherms were not recorded for this enantiomer on the Joyce-Loebl trough.

		Pressure mNm^{-1}		Area per molecule Å^2				
Isotherm number	Starting apm	Liquid change	Collapse pressure	Initial pick-up	Close packed	at 10 mNm^{-1}	at 25 mNm^{-1}	at 50 mNm^{-1}
40	80	15	46	50	42.6	42.6	38.7	28.5
41	"	"	"	49	39.3	39.0	37.0	27.2
42	"	"	"	"	40.9	40.9	38.2	30.4
Average					**40.8** ±1.8	**40.8** ±1.8	**38.0** ±0.9	**28.7** ±1.6

Table 5(i) Results for L-α-DPPA on a Fromherz trough

Stability : A monolayer of L-α-DPPA was maintained, via the feed back circuitry on the Fromherz trough, at a constant pressure of 30 mN m^{-1}. Initially (in the first 15 minutes after compression) in order to maintain the surface pressure at 30 mN m^{-1} the feedback mechanism had to decrease the trough area at an average rate of 2.5 Å^2 per molecule per hour (0.65 cm^2/min.). The monolayer stabilised after this period and the rate of contraction reduced to 0.65 Å^2 per molecule per hour (0.17 cm^2/min).

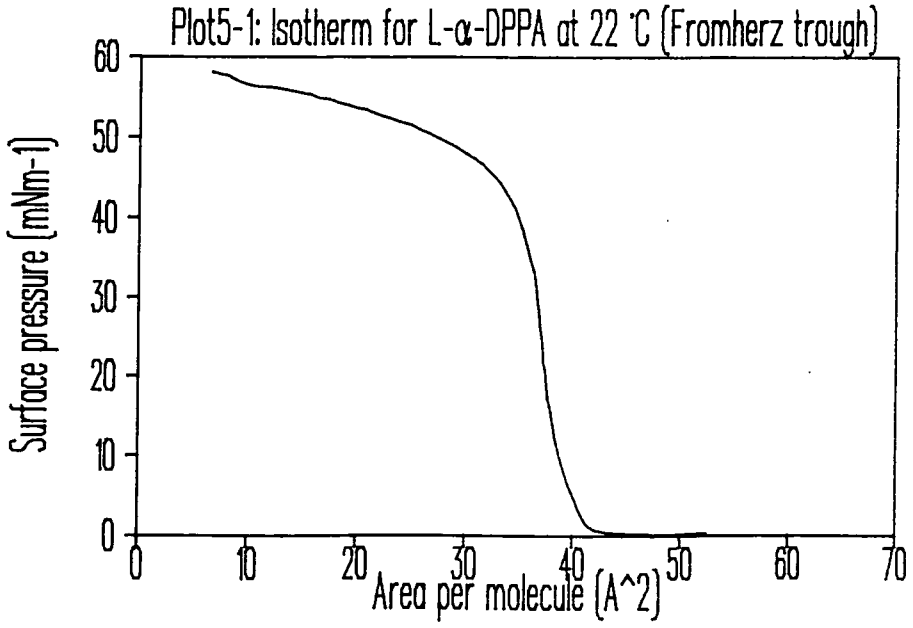

5.2.2 :Results for DL-α-DPPA

		Pressure	mNm^{-1}		Area per	molecule	$Å^2$	
Isotherm number	Starting apm	Liquid change	Collapse pressure	Initial pick-up	Close packed	at 10 mNm^{-1}	at 25 mNm^{-1}	at 50 mNm^{-1}
3	120	16	53.0	58	43.0	43.7	41.0	37.7
4	"	"	54.5	"	42.2	43.0	40.6	37.9
62	"	14	53.0	62.5	44.6	43.0	38.4	33.6
63	"	15	56.0	"	43.4	43.2	39.8	36.5
64	"	"	53.0	"	44.6	44.2	41.3	38.4
Average					**43.6** ±1.0	**43.2** ±0.8	**40.2** ±1.2	**36.8** ±1.9

Table 5(ii) Results for D-L-α-DPPA on a Joyce-Loebl trough

Hysteresis : The collapse pressure was exceeded, using a Joyce-Loebl trough, then the barriers were expanded. The pressure dropped suddenly from the collapse pressure with a gradient similar to that during compression in the solid phase. A change to a shallower gradient was seen at 15 mN m^{-1}. The layer was allowed to relax at full expansion for 5 minutes then re-compressed. The new curve followed the shape of the original but the area, at the same pressure, was 0.5 $Å^2$ less than the original compression.

Stability : A monolayer of DL-α-DPPA was maintained, via the feed back circuitry on the Joyce-Loebl trough, at a constant pressure of 30 mN m^{-1}. Initially (in the first 15 minutes after compression) in order to maintain the surface pressure at 30 mN m^{-1} the feedback mechanism had to decrease the trough area at an average rate of 3.0 $Å^2$ per molecule per hour (0.78 cm^2/min.). The monolayer stabilised after this period and the rate of contraction reduced to 0.93 $Å^2$ per molecule per hour (0.24 cm^2/min). The overall rate of contraction was 1.8 $Å^2$ per molecule per hour (0.46 cm^2/min).

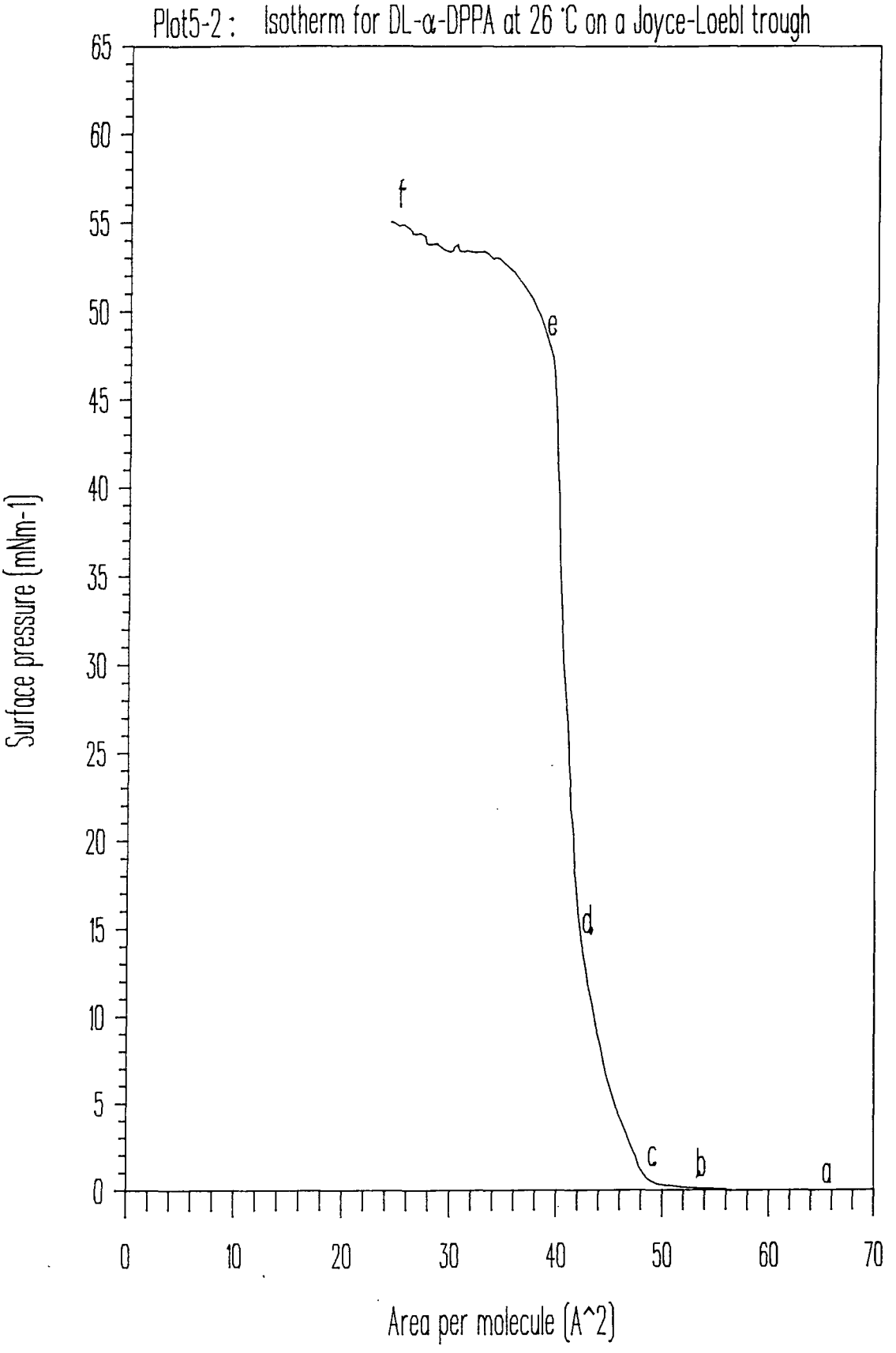
Plot5-2 : Isotherm for DL-α-DPPA at 26 °C on a Joyce-Loebl trough
Surface pressure (mNm-1)
Area per molecule (A^2)
0
5
10
15
20
25
30
35
40
45
50
55
60
65
0
10
20
30
40
50
60
70
a
b
c
d
e
f

Surface potential : Plot 5-3 shows the variation in pressure, surface potential, and perpendicular dipole moment for DL-α-DPPA with respect to time. The experiment was repeated three times up until the collapse pressure. Only in the plot shown was hysteresis investigated. The average maximum surface potential was 228 ± 11 mV. In the experiment shown in plot 5-3 the barriers were contracted then expanded, and left expanded until the surface potential reached a steady value. This surface potential (20 mV) was higher than the original value on spreading the monolayer (-15 mV). The monolayer was then compressed to 30 mN m^{-1} where the feedback mechanism was switched on and the surface pressure maintained at 30 mN m^{-1}. On re-compression the magnitude of the recorded surface potential was higher (270 mV) than that recorded for the initial compression.

Monolayer studies over a subphase containing calcium acetate:

		Pressure mNm^{-1}		Area per molecule Å^2				
Isotherm number	Starting apm	Liquid change	Collapse pressure	Initial pick-up	Close packed	at 10 mNm^{-1}	at 25 mNm^{-1}	at 50 mNm^{-1}
17	120	17.5	58	89	55.7	55.7	53.3	50.9
18	"	"	57	82	58.1	58.1	55.7	53.3
Average					**56.9** ±1.7	**56.9** ±1.7	**54.5** ±1.7	**52.1** ±1.7

Table 5(iii) Results for D-L-α-DPPA over calcium acetate on a Joyce-Loebl trough

There is an inflection on both curves at 53.5 mN m^{-1}, at the same point as the collapse pressure without calcium. At 58 mN m^{-1} the monolayer began to respond in a linear manner, to the change in area. This was at an APM of 34 Å^2. This part of the isotherm had a gradient shallower than either the liquid or solid phases.

Stability : A monolayer of DPPA over the calcium acetate solution was maintained, via the feed back circuitry on the Joyce-Loebl trough, at a constant pressure of 30 mN m^{-1}. In order to maintain the surface pressure at 30 mN m^{-1} the feedback mechanism had to decrease the trough area at an average rate of 3.1 Å^2 per molecule per hour (0.67 cm^2/min.).

Plot 5-3A : Surface pressure and area vs. time for DPPA

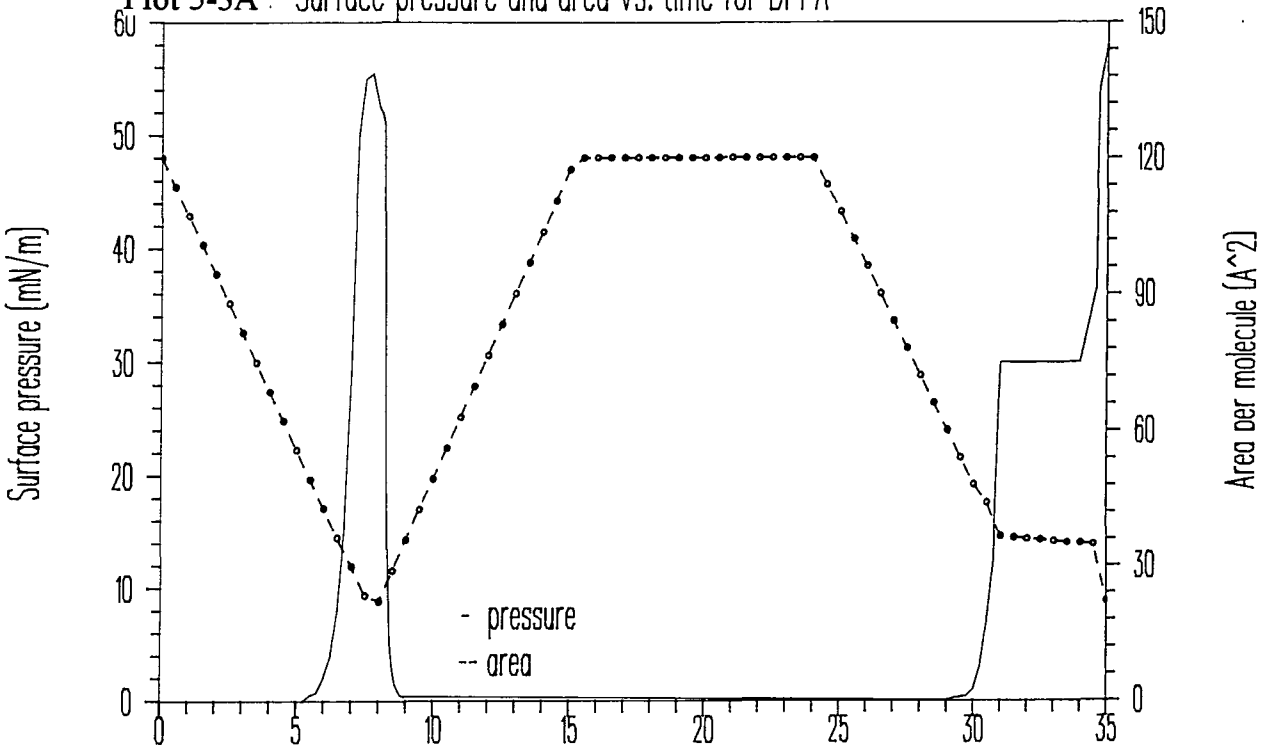

Plot 5-3B Perpendicular dipole moment and surface potential vs time

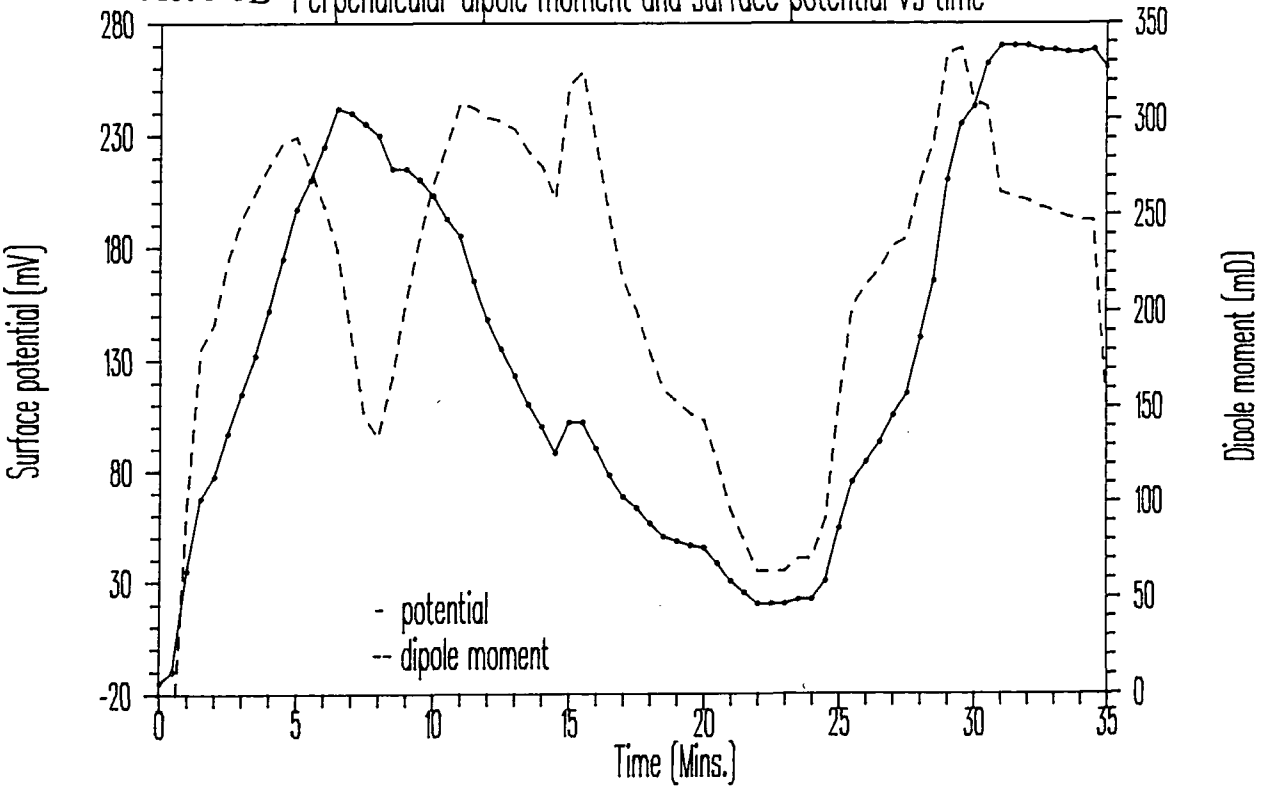

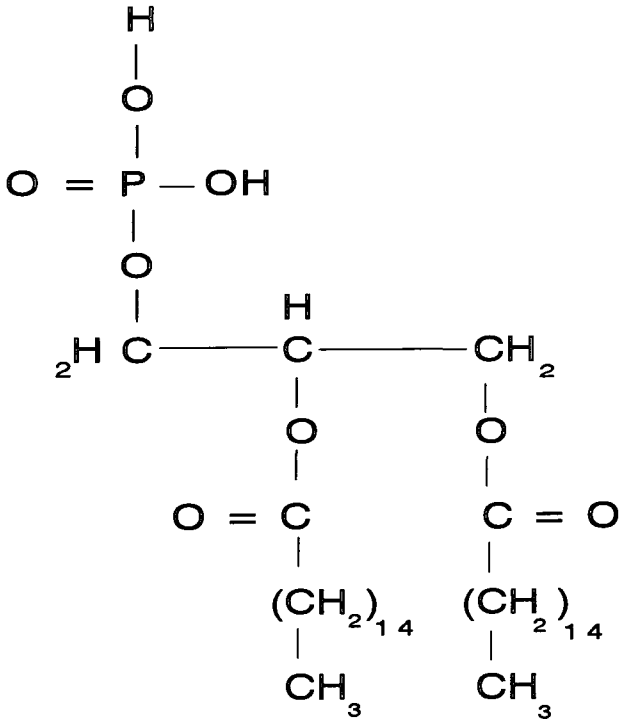

Figure 5(a) : The structure of dipalmitoylphosphatic acid.

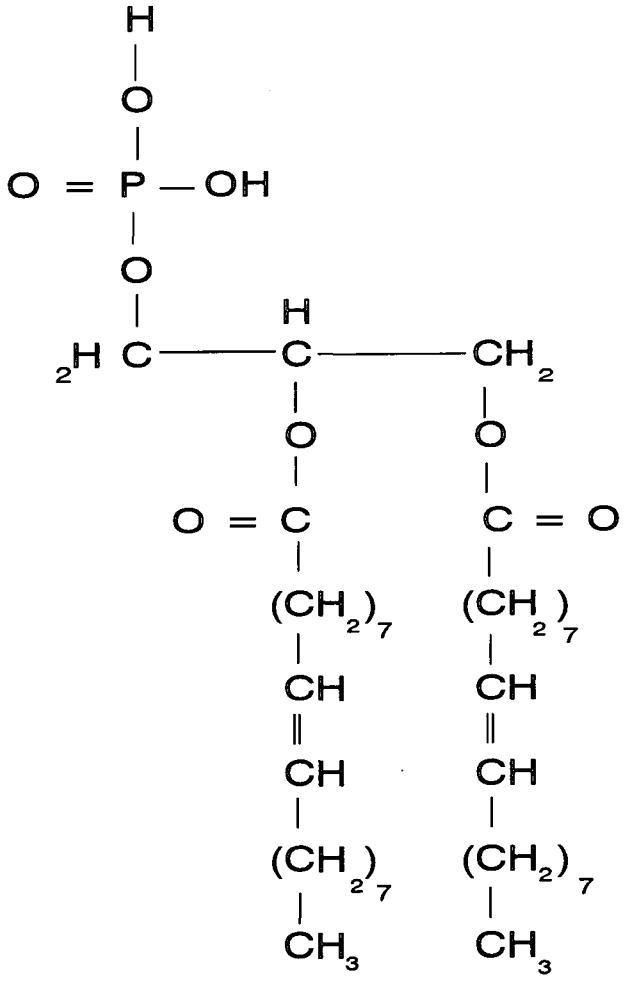

Figure 5(b) : The structure of dioleoylphosphatic acid.

5.2.3 Analysis and discussion of the monolayer studies of DPPA

(A) Isotherms

The average result for the CPA of L-α-DPPA (table 5(i)) is 3.5 $Å^2$ lower than that for DL-α-DPPA (table 5(ii)). These results were acquired on two different styles of Langmuir troughs. Tables 5(vii) & 5(v) and 5(viii) & 5(ix) indicate that the Fromherz trough, on which the results for L-α-DPPA were obtained, would be expected to give larger APM's at a given pressure rather than lower values. Thus, it may be concluded that not only is the difference real it may be greater if the measurements had taken place on the same style of trough. This would lead to the supposition that if only one enantiomer is present the molecules can form a closer packed crystal structure. Probably a more regular crystal structure is possible with one enantiomer rather than two. This is an important observation, because in nature there is a predominance of enantiomeric specificity, namely for the L configuration. It would be of interest to pursue this matter further, but it was not possible in this study, due to the lack of time.

Results for DL-α-DPPA have been published previously by other researchers. The data obtained is consistent with their findings. Taylor[145] and Lukes[90] and their co-authors both found the CPA for DL-α-DPPA to be 42 $Å^2$. This compares favourably with the value of 43.6 ± 1.0 $Å^2$ recorded. At a pressure of 48 mN m^{-1} Wood[123] and Taylor et al[104] recorded values for the APM of DL-α-DPPA to be 35 and 36.8 $Å^2$ respectively. The results reported here give a value of 36.8 ± 2.0 $Å^2$ at a surface pressure of 50 mN m^{-1}, again a good agreement with literature.

The CPA for a single alkane chain in a monolayer[124] is ~20 Å^2. The area of a phosphatidic acid group[123] is only 24 Å^2. The CPA of DPPA was found to be 42 Å^2. The molecular packing arrangement for DPPA must therefore be dominated by the interactions of the alkyl chains. This contrasts with molecules such as DPPC, the CPA of which was determined by Lösche et al[124] to be ~60 Å^2, where the choline group must contribute a large effect to the nature of intermolecular interactions.

It can be seen in plot 5-2 that there are five regions in the DL-α-DPPA isotherm. From a → b there is no surface pressure recorded. Thus the molecules must be in a state analogous to the gaseous phase in three dimensions. The molecules are not constrained and can freely respond to the movement of the barrier. Gaines[103] suggests that at this point the hydrocarbon chains may be lying flat on the water surface. From b → c the molecules begin to interact with one another and resist the movement of the barrier. This is the region referred to as the liquid expanded state[129]. The liquid condensed region of the isotherm is from c → d. The monolayer is becoming less compressible and its response to the applied force is now almost linear, similar to that of a three dimensional liquid. In the region d → e the monolayer is considered to be in a solid like phase. Again a linear response to the reduction in area is found but with a steeper gradient than in the liquid condensed phase.

Eventually the monolayer can no longer be compressed and collapses. The curve at e is no longer linear but the response is smooth similar to the region of slip in a three dimensional structure. This may indicate that the monolayer of DPPA is crystalline in nature, and that the different domains are slipping against one another in the monolayer plane. After this point the curve becomes uneven and the layer is very compressible. This suggests that in the region e → f the monolayer has folded up on itself and become a multilayered structure. The monolayer could collapse in a disordered manner or in a ordered fashion to become a bilayer[19] (figure 5(c)). Whatever the condition of the collapsed state it is reversible back to a monolayer when the barriers are expanded, as seen by the lack of hysteresis on re-compression. This observation is relevant to biomembrane

structures because it shows that the bilayer/multilayer structure are probably not formed due to the attraction of the lipid chains but rather the attraction of the head groups for water and the repulsion of the alkyl chains by the aqueous environment.

Although results for DPPA isotherms have been reported previously[90,104,122,123] only Wood[123] attempts to understand the shape of the isotherm. Studies have, however, been carried out for similar molecules. Most notably by Möhwald et al[109,125-127] who have studied DMPA mainly by fluorescence; and by von Tscharner and McConnell[129] who have studied DPPC, by fluorescence; Mitchell and Dluhy[92] followed the phase changes of DPPC, DMPC and DSPC by FTIR at the air/water interface. These studies have shown that for phospholipids the phase changes are not as distinct as the isotherms would imply. In particular that the phase change from liquid expanded to liquid condensed[129] phases is not distinct as a mixture of the two phases seen. Möhwald[126] has shown that DMPA forms domains of the two different phases, in the progression from liquid expanded to liquid condensed phases.

DPPA is very stable when held at a surface pressure of 30 mN m^{-1}, with very little movement of the monolayer. The small amount of adjustment made to maintain the pressure could be due to the coalescence of crystalline domains. This was chosen as a pressure suitable for the deposition of DPPA onto substrates.

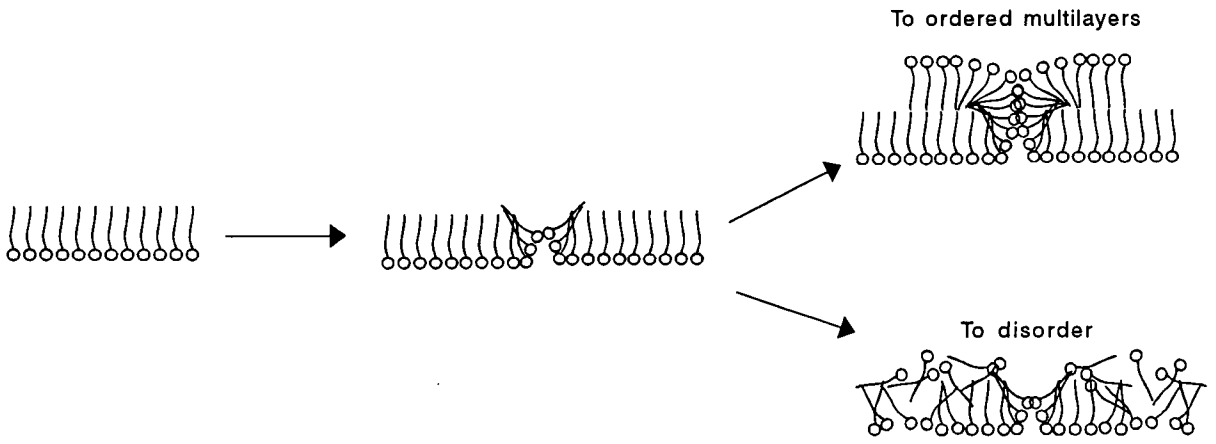

Figure 5(c) : The collapse of a monolayer at the air water interface.

(B) Surface Potential

The maximum value of 228 ± 11 mV for the surface potential (ΔV) during the initial compression corresponds closely to results of other researchers. Taylor et al[104] obtained a value of 242 ± 20 mV for ΔV of DPPA in the condensed phase, and Wood[123] recorded a maximum value of 220 mV.

Papahadjopoulos[130] found that the first pK_a of PA is below pH 3.5 and the second is above pH 6.5. Therefore, at pH 5.6 DPPA has a charge of minus one. The consideration of the surface potential data therefore should, according to the literature - Davies and Rideal[140], Gaines[103] and Oliveira et al[104,141], take the double layer potential into account. This would imply the application of equations 4(vii) and 4(ix). Plot 5-4 shows the variation of the double layer potential with time as calculated from the area per molecule (shown in plot 5-3). It can be seen that the area and ψ_o follow a similar pattern. I.e. as the area per molecule increases the double layer potential increases. The effect of such a potential on the perpendicular dipole moment is shown in plot 5-5 (dotted line).

However, it must be suggested that equation 4(ix) is not suitable for the measurement made. This equation calculates the excess charge at liquid interface given that it is touching an evenly charged surface which is impenetrable[140]. It is also assumed that the counter ions behave as point charges. Given that the counter ions are hydrogen ions the latter is a fair assumption. However, the monolayer consists of charges associated with each headgroup therefore the charge exists as point sources rather than an even distribution. Also, there is a strong probability that the hydrogen ions do penetrate into the headgroup region of the molecule. Möhwald[124] has shown by X-ray reflectivity that phospholipid monolayer headgroups are within the water. Therefore a small counter ion such as hydrogen will definitely penetrate the charged layer. Therefore, the first two assumptions in Gouy's calculation do not apply to a lipid monolayer. However, there is a greater disparity which must be pointed out. Gouy's equation calculates the double layer potential due to a surface excess of ions already present in the

subphase. It does not cover a situation where each charge in the monolayer has its own counter ion. Thus, although there is nothing intrinsically wrong with Gouy's equation, its application[103,104,140] to a charged monolayer would seem to be suspect as almost none of Gouy's assumptions apply.

Now consider the nature of the experiment which was undertaken (section 4.2.2). The potential difference was measured between two electrodes, one above the surface of the trough and the other a large distance away (~70cm horizontally) and ~10 cm below the water surface. Even if a double layer potential, as proposed by Gouy, does exist for a charged monolayer it would not be measured as part of the potential difference because of the depth and nature of the silver / silver chloride electrode. This arises from the fact that there may be an excess of ions due to the subphase, at the interface, but this will be counteracted by a layer of oppositely charged particles and so on until the effect of the charged monolayer is dissipated. As the subphase must be electrically neutral (neglecting the effect of the counter ions of the lipid) then at the distance of the second electrode there will be no ion imbalance and thus no potential difference due a double layer will be detected. Therefore what is measured in the surface potential experiment is the change in potential from pure water due only to the lipid and its counter ion. The only way to make a measurement which would include a contribution from a double layer potential would be for the second electrode to be a flat plate placed within nanometers of the interface before the effect due to the monolayer could dissipate.

The fact that a double layer potential is not measured is reflected in plot 5-5 where the dipole moment closely follows the shape of the APM. This is due to the magnification of the incorrect application of equation 4(ix) by multiplication by the APM. This is even more evident when a correction for ψ_o is applied to the dipole moment of DOPA and the mixtures of DPPA with DOPA and alamethicin (not shown). Almost all recorded structure of the dipole moment curves is lost due to the correction for a potential which has not been measured.

The above considerations do not explain the difference in measured surface potential between monolayers formed

from lipids with uncharged, charged, and zwitterionic headgroups. Surface potential data for phospholipids is recorded by Oliveira et al[104]. They found values for surface potentials for DPPA of 440 and 242 ± 10 mV at pH's of 2 and 5.6 respectively and for DPPC of 544 ± 20mV at pH 5.6. They attributed the difference between charged and uncharged DPPA to the presence of a double layer potential but following the arguments used before this could not have been measured. Again the nature of the measurements must be considered. ΔV is the difference in electrical potential energy between the subphase and the subphase with the monolayer. Thus effectively the potential difference between the bottom of the charge due to the monolayer and the top is measured (figure 5(d)). Even though the methyl group only carries a fraction of a charge its weighting in the measurement of ΔV is large because of the disparity in the dielectric constant between the hydrocarbon chain (2-5)[104,140] and water (~80)[103]. If the monolayer carries no charge then the potential will be measured from the headgroup to the end of the tail. However, if the monolayer if negatively charged then the starting point for measuring the potential will be the positive charge of the counter ion. Therefore, the potential difference will be between that charge and the charge associated with the tail of the lipid. The effect of this on the measured potential is shown in figure 5(d)-(ii). Now a zwitterion could be aligned so that the measured potential starts from a negative value, positive or zero (figure 5(d)-(iii)). The crystal structure of DMPC crystals[14] would suggest a molecular shape as seen in figure 5(d)-(iii)-(2), but the structure of the molecules will differ on the surface of water. X-ray and neutron reflectivity measurements on DPPC at the air water interface have been undertaken by Vaknin et al[124]. They concluded that the headgroup was not parallel to the interface but went deeper in the subphase. Their data did not show an orientation of the group which could still be in any of the three possibilities shown. There is therefore no supporting evidence for the following but it could be suggested that if DPPC were orientated such that either patterns (1) or (3) were followed then the large increase in ΔV compared to a charged monolayer could be explained.

Plot 5-4 : The double layer potential (Ψ_o) for a fully ionised monolayer of DPPA.

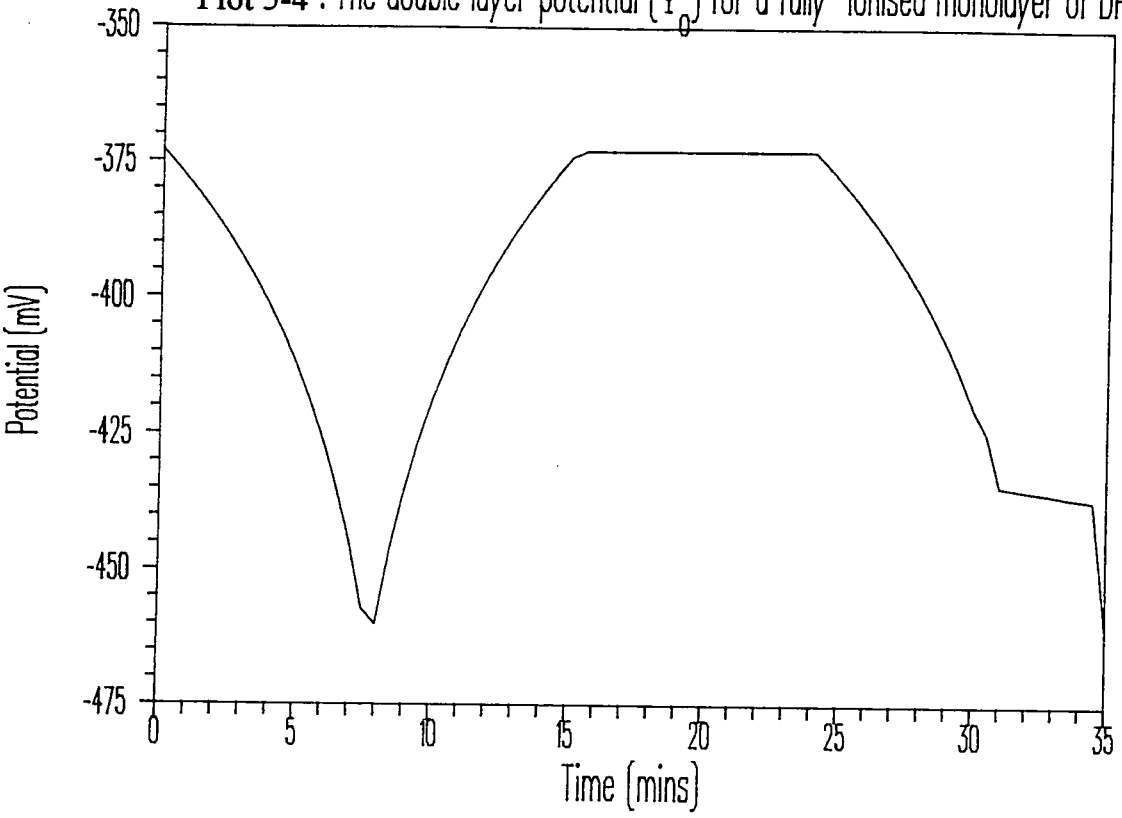

Plot 5-5 : The potential and dipole moment for DPPA with the correction for the double layer potential.

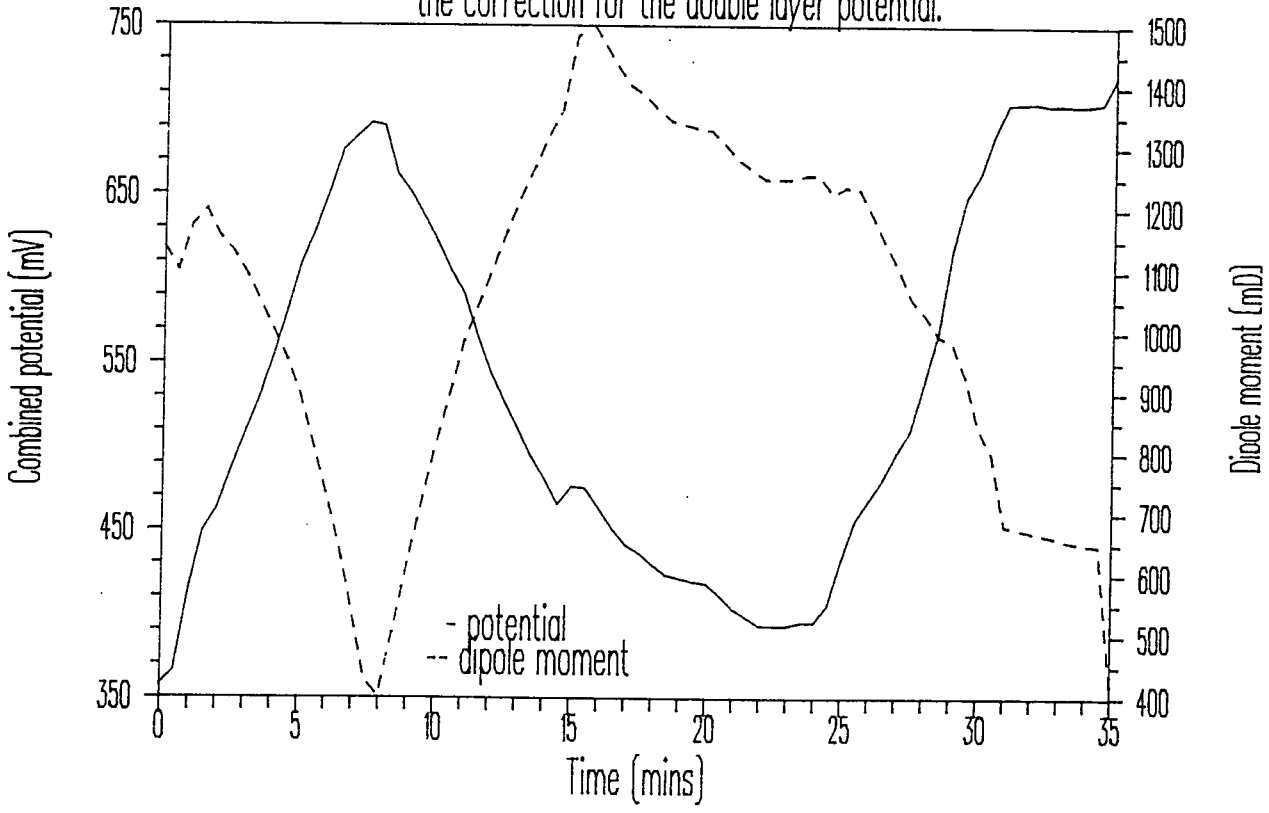

For an analysis of the surface potential data the original plot 5-3 must be utilised. The quantitative values are probably not the actual dipole moments associated with each molecule because the relative permittivity of the monolayer will almost certainly not be equal to one[105], as assumed in section 4.2. However, the qualitative nature of the the surface potential plots may be discussed in terms of relative changes of the potential and the dipole moments.

The dotted line in the lower half of plot 5-3 (dipole moment) rises steeply as soon as the barriers of the trough begin to move. This is probably due to the alkyl chains straightening gradually and therefore increasing the distance between the charges of the dipole. As to why the increase in dipole moment occurs as soon as the barriers move but well before the detected rise in surface pressure it is only possible to speculate. It is possible that what is being detected is the the alignment of the alkyl chains only when in contact with other DPPA molecules. Thus, instead of measuring the slow increase in angle of the chains from the subphase for all the molecules (figure 5(e)-(i)), what may be being measured is the aggregation of the DPPA molecules (figure 5(e)-(ii)). This would explain why the dipole moment begins to rise as soon as the barriers move because the movement is causing the molecules to meet and cluster. It is also consistent with Möhwald at al's[125-127] research where crystallites of different phases of DMPA were found. It is difficult to conceive that the lifting of individual molecules would occur as soon as the barriers moved and so long before there is a pressure response.

As soon a surface pressure is detected the dipole moment begins to fall. There are three possible reasons for the fall: (a) There could be a loss of material from the surface; (b) The distance between the charges of the dipole could decrease; (c) The magnitude of the charges could fall. In the case of DPPA the first of these possibilities can be discounted as any loss of material would be detected by the surface pressure measurement. It seems unlikely that at the onset of pressure the dipole length should begin to shrink as the only methods for such a change would be the formation of gauche bonds or a tilting of the molecule

towards the water or a decrease in the distance between the counter ion and the headgroup. The first would not occur because DPPA is above its phase transition temperature and it has been shown by Mitchell and Dluhy[92] by the use of FTIR at the air-water interface that phospholipids above their transition temperature retain the all trans alkyl chain structure throughout a compression. The second possibility, that the chains are tilting does not occur as in this case the APM would increase as the pressure rose and not decrease as found in the π-A isotherm (plot 5-2). The third suggestion that the counter ion moves closer to the DPPA molecule is a possible explanation of a change in dipole length. This could come about through a re-orientation of the phosphatidic acid group or because the increase in charge density of the monolayer is drawing the hydrogen ions closer. However the third method of decrease the dipole moment (c) still has not been considered. This could be caused by one of two factors. Either the induced dipole in the end of the alkyl chain decreases or the number of ionised molecules of DPPA decreases. The former could occur in order to decrease the repulsion between the dipole moments on different alkyl chains which are now being pushed together. The latter could occur if the local concentration of hydrogen ions at the surface of the subphase decreased the pH to below that of dissociation for DPPA. However, this would actually increase the measured dipole moment as shown by Oliveira et al[104].

At the end of this discussion two possibilities for the decrease in the dipole moment of DPPA as the pressure increases. These are that either the counter ion is closer to the headgroup or the enforced close proximity of other alkyl groups is decreasing the size of the induced charge of the end of the chain. From the data it is not possible to state which of these is occurring, or whether some other factor is involve. Indeed there may be several processes involved in the decrease. Whatever the reason for the decrease in the dipole moment it is definitely dependent on the pressure and reversible. As soon as the area increases the dipole moment increases. The increase of the dipole moment continues beyond the point of pressure detection (at 9 minutes). It is possible that the monolayer has broken up into small pieces which are still tightly packed and slowly these

aggregates relax. The decline in the dipole moment is much slower than the rise. Again this could be due to a slow break-up of small aggregates. There is a jump in the dipole moment at ~15 minutes. This coincides with the barriers of the trough stopping. It is possible that this caused a wave in the trough which could have interfered with either the dispersion of the aggregates or the measurement of the surface potential.

After eight minutes at the full expansion of the barriers the dipole moment becomes steady. However, the value is still higher that the original recorded. This could be because the molecules simply have not had enough time to relax to the original state or that the process is not completely reversible. This would explain why pre-conditioning (section 4.3.2) may increase the crystallinity of the monolayer because the starting point for the orientation of the molecules on a second compression is different from the original one. Indeed the dipole moment for the molecules for the re-compression, at the point of detection of pressure, is higher than on the initial compression. This was re-producible. It is could be due to the alkyl chains being aligned at a higher angle to the subphase than on the previous compression or to the number of molecules per aggregate being larger earlier on the original compression.

When the pressure of the monolayer was held at 30 $mN\ m^{-1}$ (31 minutes) the surface potential remained constant but the dipole moment decreased slightly as the molecules packed closer together.

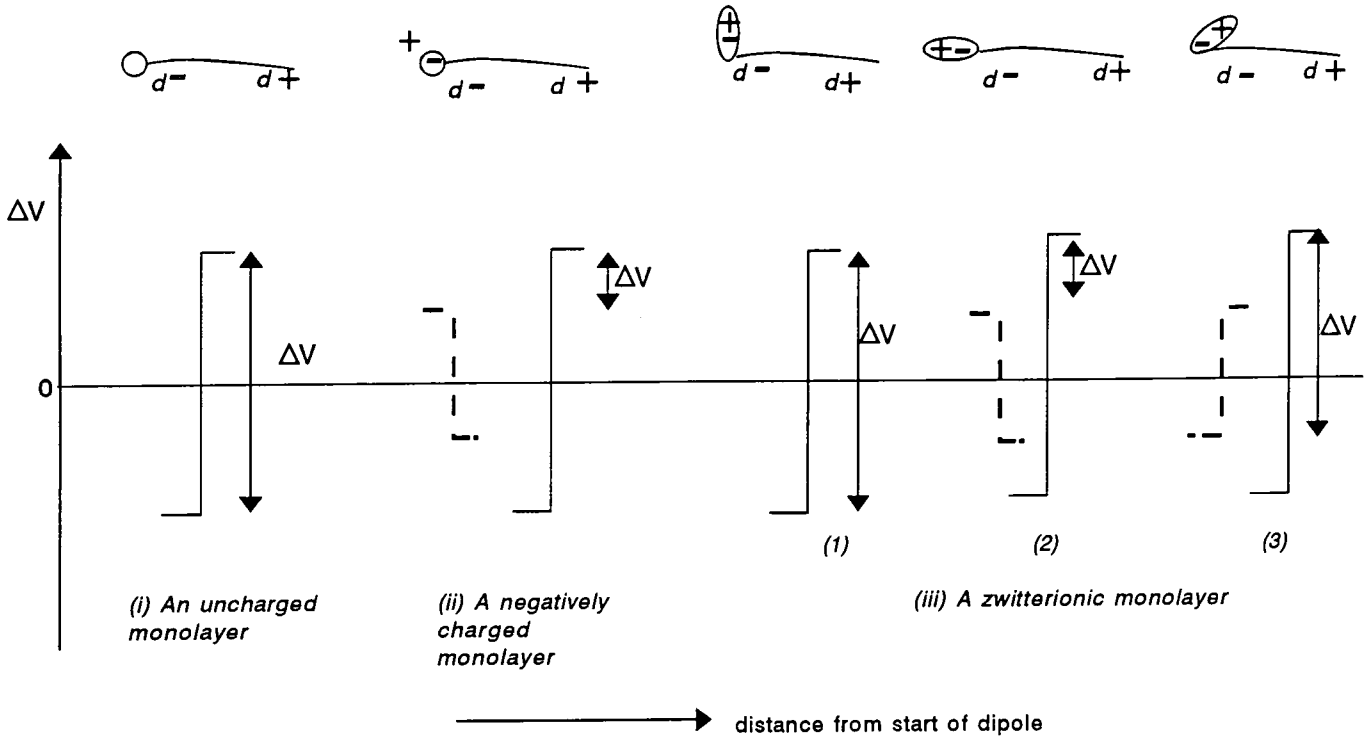

Figure 5(d) : The effect of different arrangements of charge, at the headgroup, on the magnitude of the surface potential. The dotted lines represent potential difference due to the headgroup and the solid lines the effective potential difference due to the hydrocarbon chains.

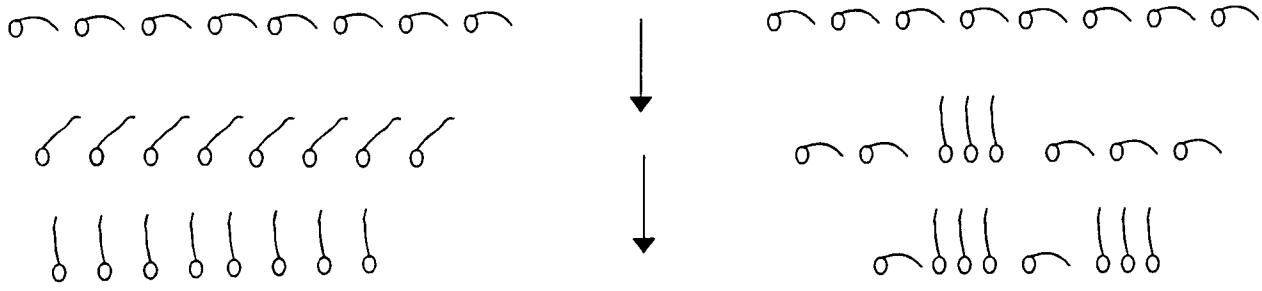

(i) By a general re-orientation of all the alkyl chains.

(ii) By re-orientation of the alkyl chains by aggregation.

Figure 5(e) : Two possible methods for a gradual increase in the dipole moment before the detection of surface pressure.

(C) The effect of addition of Calcium to the subphase

When calcium is added to the subphase there appears, from the data found (table 5(iii)), to be an expansion of the monolayer compared to DPPA over water (table 5(ii)). However, this conflicts with the data recorded by other researchers. Howarth et al[34] found a value of 43 $Å^2$ per molecule for the CPA of DPPA over calcium acetate; Hasmonay et al[131] recorded a value of 38 $Å^2$ per molecule over calcium chloride; Swart and Froggatt[119] have also found that there is very little change in the areas per molecule for DPPA over a calcium containing substrate. These findings concur with those of Gorwyn and Barnes[132] who report the contraction of monolayers of DPPC and DMPE in the expanded liquid phase in the presence of UO_2^{2+}. Möwald and Lösche[133]see the condensation of DMPA on addition of calcium and Papahadjopoulos[130] also cites a condensation of negatively charged phospholipids with calcium containing sub-phases.

With all of this evidence from the literature it is certain that the areas values recorded in table 5(iii) are in error. The most probable reason for this was that the concentration of the solution was greater than 1 mg/ml. On consultation of records it appears that it is possible that the DPPA solution may have been used to prepare monolayers for deposition prior to recording the isotherms. Although stored below 0 °C and sealed to prevent evaporation it is possible that, during the process of removing solution to deposit the monolayers, some of the chloroform evaporated. As the main purpose of the isotherms was to determine a suitable pressure for deposition the experiments were not repeated.

5.3:MONOLAYER STUDIES OF DOPA AT THE AIR/WATER INTERFACE

5.3.1 Results of monolayer studies of L-α-DOPA (sodium salt)

(A) Fromherz trough

		mNm^{-1}		Area per molecule $Å^2$		
Isotherm number	Starting apm	Collapse pressure	Initial pick-up	Close packed	at 10 mNm^{-1}	at 25 mNm^{-1}
46	120	42	100	77.8	70.8	51.1
47	"	"	"	87.8	77.8	56.6
48	"	43	"	87.4	78.7	58.1
Average				**84** ± 6	**76** ± 4	**55** ± 4

Table 5(iv) Results for L-α-DOPA on a Fromherz trough

Hysteresis : The monolayer was compressed to pressures of 10, 25, and 40 mN m^{-1} consecutively. After each compression the barrier was re-expanded and the monolayer allowed to relax. The results can be seen in plot 5-6.

Stability : A monolayer of DOPA was maintained, via the feed back circuitry on the Fromherz trough, at a constant pressure of 25 mN m^{-1}. In order to maintain the surface pressure at 25 mN m^{-1} the feedback mechanism had to decrease the trough area at an average rate of 230 $Å^2$ per molecule per hour (11 cm^2/min.). A different monolayer was held at a surface pressure of 27 mN m^{-1}. The rate of contraction was 218 $Å^2$ per molecule per hour (9.5 cm^2/min). In both cases the area of the trough had to be rapidly decreased by the feedback mechanism in order to maintain the chosen surface pressure. This continued steadily, at the rates given, until the trough area reached its minimum possible value.

Plot 5-6 : Hysteresis for L-α-DOPA at 22 C (Fromherz trough)

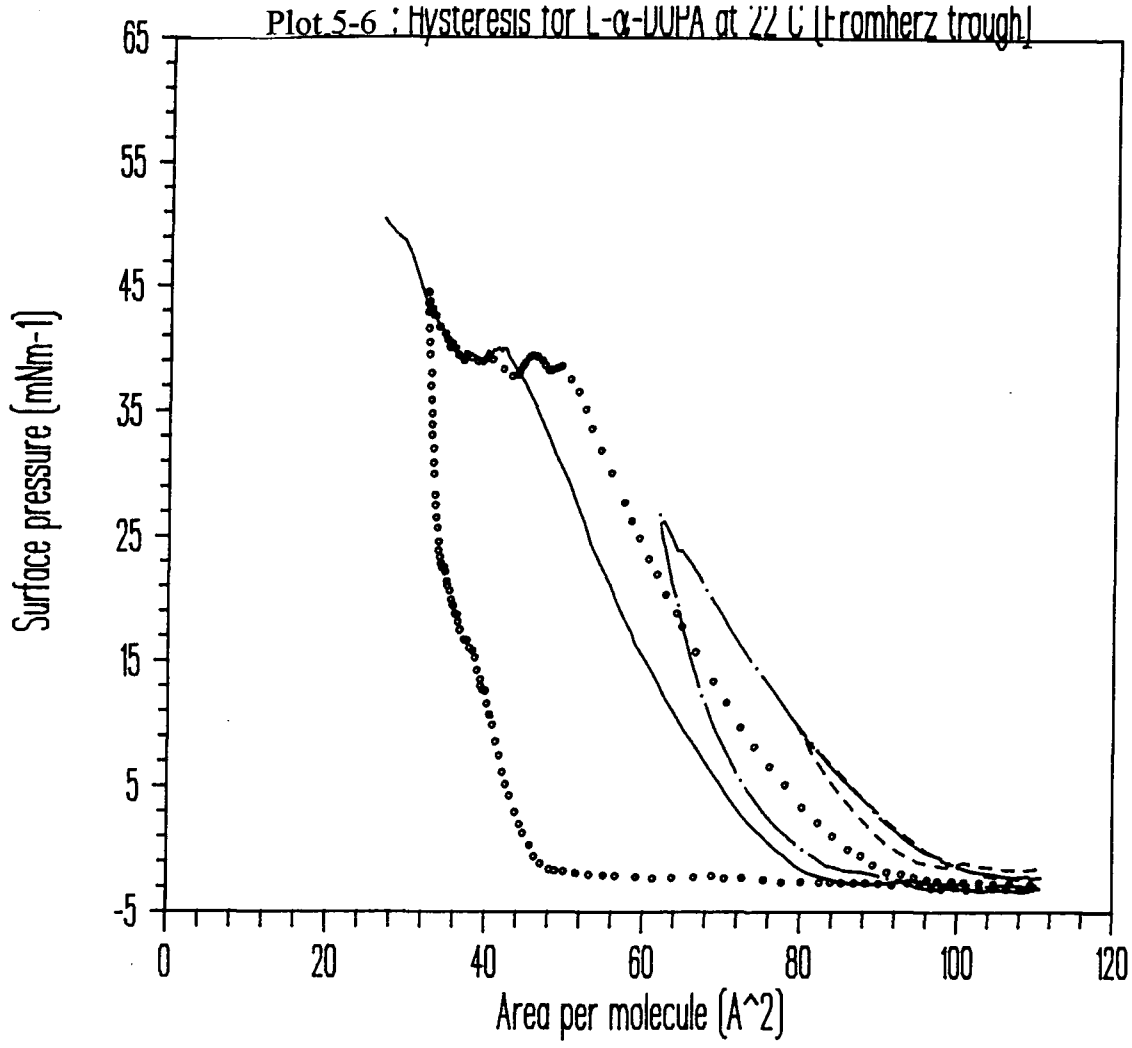

Plot 5-7 : L-α-DOPA on Fromherz and Joyce-Loebl troughs

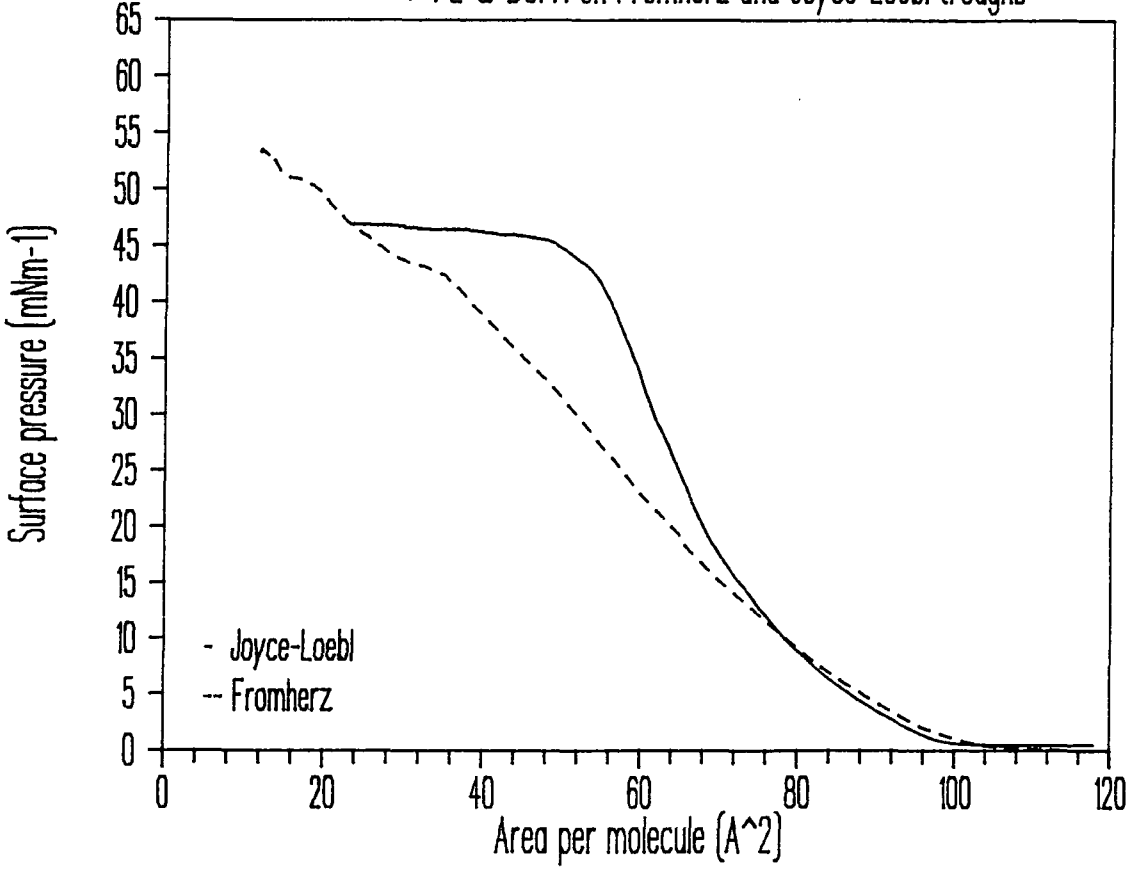

(B) Joyce-Loebl trough :

		mNm^{-1}		Area per	molecule	$Å^2$
Isotherm number	Starting apm	Collapse pressure	Initial pick-up	Close packed	at 10 mNm^{-1}	at 25 mNm^{-1}
67	120	45	100	79.7	77.8	64.3
68	"	"	"	"	"	64.8
69	"	"	"	78.7	"	64.6
90	"	"	"	79.2	76.3	60.5
Average				**79.3** ±0.5	**77.4** ±0.8	**63.6** ± 2

Table 5(v) Results for L-α-DOPA on a Joyce Loebl trough

Hysteresis : Compression of the monolayer took place to an APM of 18 $Å^2$ (beyond the collapse pressure). The barriers were then expanded and re-compression took place. On expansion the shape of the isotherm largely followed that of compression but the values for the APM were ~8 $Å^2$ less, for a given pressure than on compression. On re-compression there was a decrease in the APM at a given pressure, from the original compression, of 10 $Å^2$.This gradually decreased to 5.5 $Å^2$ at higher pressures (~35 mN m^{-1}). There was therefore a difference in gradient between the π-A isotherms of the two compressions.

Surface potential : Plot 5-8 shows the surface potential data for DOPA. In the first compression the surface potential reached a maximum of 228 mV then on expansion fell to a lower value than on deposition (60 mV *c.f.* 78 mV). On re-compression the maximum surface potential reached was 280 mV.

Plot 5-8A Surface pressure and area vs. time for DOPA

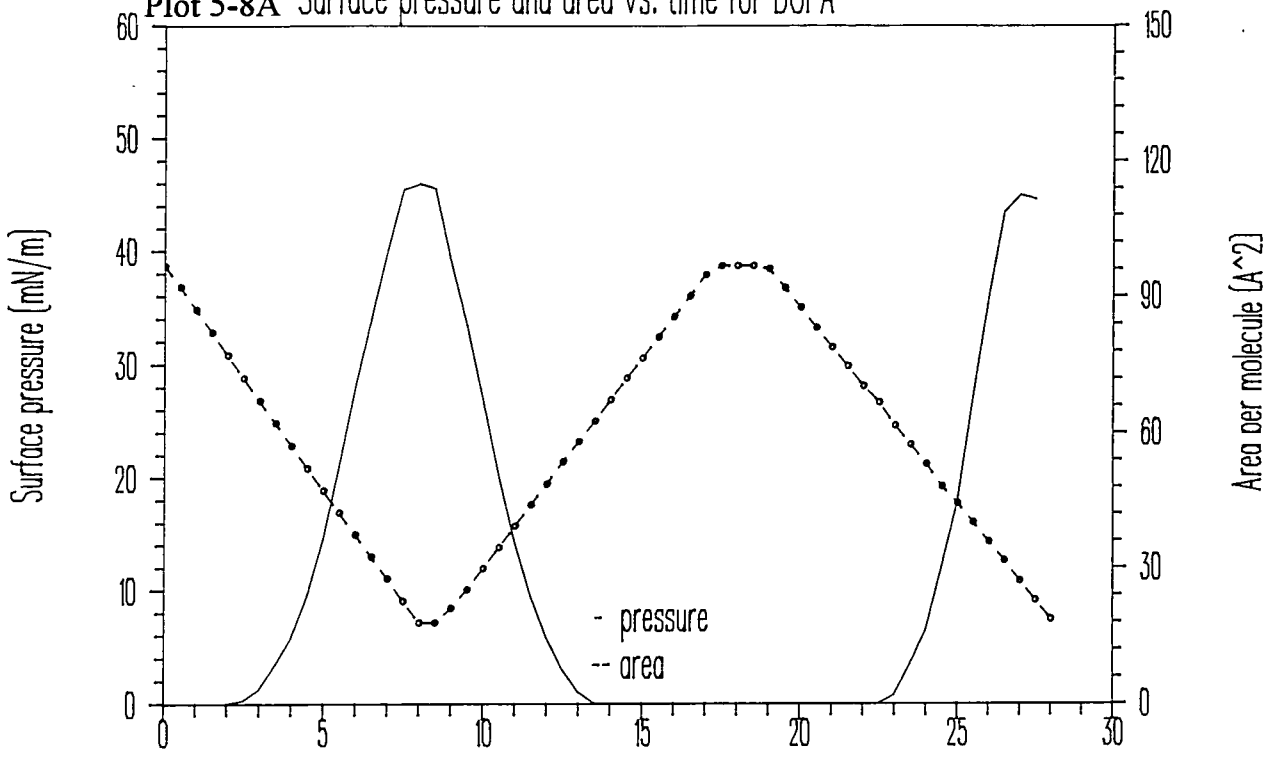

Plot 5-8B Perpendicular dipole moment and surface potential vs time

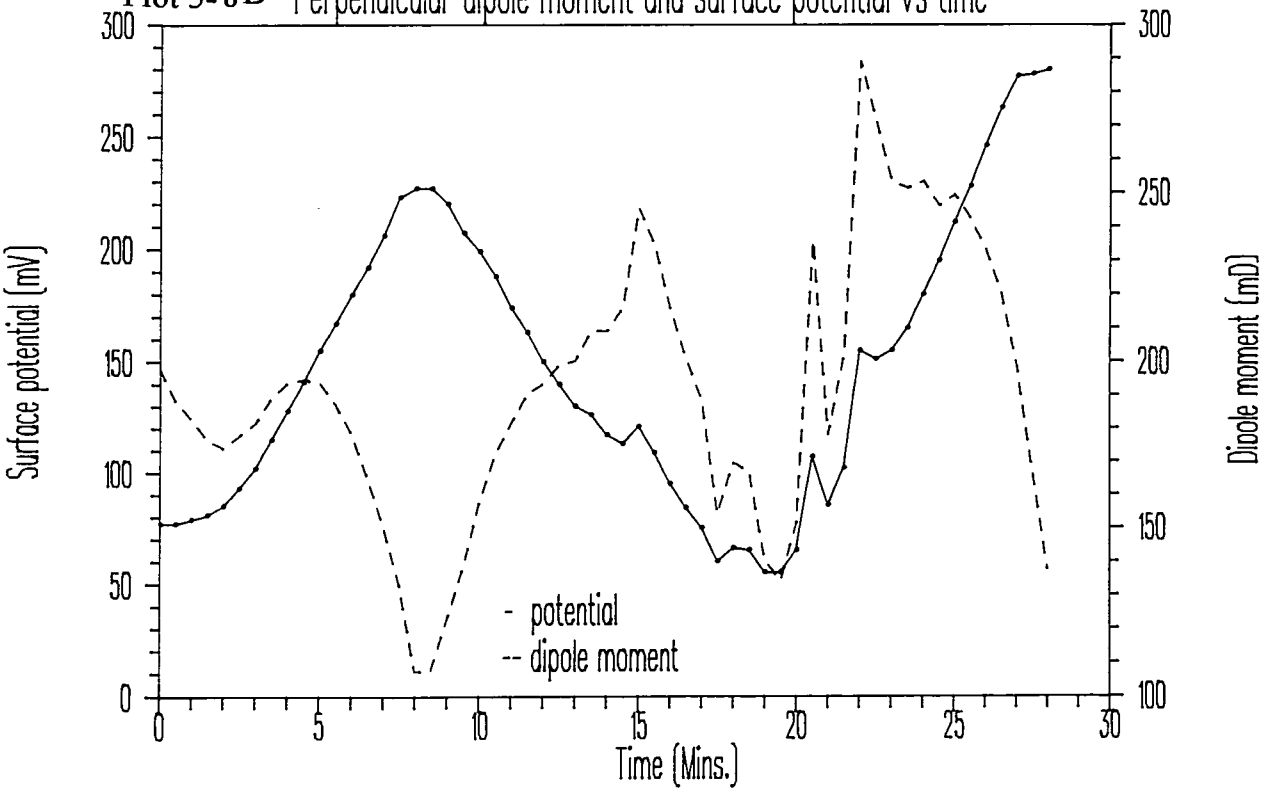

5.3.2 Analysis and discussion of monolayer studies of DOPA

(A) π-A isotherms :

For both styles of trough L-α-DOPA has a CPA which is approximately twice that of DPPA (~80 compared to ~43 $Å^2$ per molecule) As the phosphatidic acid group is the same for both molecules, this can only be due to the difference in the hydrocarbon chains. Both chains in DPPA are saturated, whereas the chains are both unsaturated in DOPA. The alkene group is half-way along the length of the DOPA chains and is cis in configuration. The only other difference between the chains of DPPA and DOPA is that those of DOPA have a greater number of carbons (17 *cf.* 15). Möhwald et al[125] have studied the isotherms of DMPA (with a chain length of 13 carbons), and found its CPA to be ~45 $Å^2$. Thus the chain length would appear not to affect the packing of the molecules to a large extent. It must therefore be the presence of the alkene group which is affecting the monolayer characteristics of DOPA.

There is a difference between the CPA's measured on the two different types of trough. The CPA measured on the Fromherz trough is 5 $Å^2$ larger than that found on the Joyce-Loebl trough, however the error in the measurements taken on the Fromherz trough is ± 6 $Å^2$ so this difference may not be significant. The biggest difference between the two troughs is the shape of the isotherms (plot 5-7). The isotherm measured on the Joyce-Loebl trough has a steeper gradient and at 45 mN m^{-1} the compressibility of the monolayer increases greatly, indicating a collapse of the monolayer. The isotherms recorded on the Fromherz trough exhibit a point of inflection at ~42 mN m^{-1} and then the original gradient is recovered. There are probably several factors influencing these differences. The first of which is the large variation in the rate of compression between the two troughs - 1.8 cm^2 s^{-1} for the Joyce-Loebl trough and 0.5 cm^2 s^{-1} for the Fromherz trough. The slower compression rate would allow more time for the monolayer to respond to the external pressure, perhaps causing the shallower gradient on the isotherms recorded on the Fromherz trough. The second factor is that the dissimilar

shapes of the enclosed areas during compression exert different stresses on the monolayer. This affects the manner in which the monolayer flows and possibly the packing of the molecules. The third factor contributing to the differing isotherms, is the surface area available for the monolayer. On the Joyce-Loebl trough this is controlled solely by the movement of the barriers. For the Fromherz trough (figure 4(c)) the meniscus sits above the trough, and as the monolayer is compressed, the radius of the meniscus curvature at the water/PTFE interface can increase. In the case of DPPA this increase was visible to the naked eye. On one occasion the curvature of the meniscus increased beyond the point of stability, for one of the mixtures of DPPA/DOPA, such that the water overflowed, table 5(vii). Thus, although intensive studies of the differences between the two trough types were not undertaken it should be noted that not only were there numerical differences in the isotherms but the behaviour of the monolayer itself depends on the manner in which the isotherm was collected. The differences in the shapes of isotherms recorded on various types of Langmuir trough is largely due to the fact that isotherms are recorded in non ideal conditions.

For both types of trough the isotherms of DOPA show a slow rise in surface pressure and distinct phase changes are not seen. *I.e.* the monolayer remains in a fluid state throughout the compression. DOPA is above its lipid phase transition temperature (see Chapter 3) at 19 °C. The evidence for this is contained in section 6.9 of this thesis. There appears to be no data on for DOPA previously published to verify this but there is data, mainly from differential scanning calorimetry, for the phase transition temperatures of a variety of other phospholipids[1,2]. Some of the available data is given in table 5 (vi).

It can be seen from table 5(vi) that the unsaturated molecules have a much lower phase transition temperature than the saturated lipids. There appears to be ~70 °C difference between similar phospholipids with unsaturated and saturated chains of comparable length. The result for DPPA is 67 °C thus the lipid phase transition for DOPA would be expected at ~ 0 °C. This extrapolation and the FTIR data (Plot 6-30) show that DOPA is above its phase transition temperature.

Therefore, not only are the cis double bonds in each chain preventing the alkene chains from forming orderly crystalline solid phases but also the chains will have gauche conformers at different positions along the chain, increasing the molecules fluidity but decreasing the possibility of regular crystalline structures. Indeed, this fluid like behaviour of DOPA was why it was chosen to be mixed with DPPA to try and produce a monolayer which would allow the mixing of alamethicin with the lipids and aid the deposition of alamethicin mixtures (chapter 7).

Monolayers of DOPA exhibit large hysteresis, on re-compression, on both styles of Langmuir trough (plot 5-6). There are two main possible contributing factors. The first is the loss of material from the surface layer into either the bulk phase or by the formation of a multilayer system. The second is that compression and expansion anneal the monolayer and allow closer packing of the molecules on re-compression. From the isotherm data alone it is not possible to distinguish between these two possibilities. The stability tests carried out (section 5.3.1) support the first case, of absorption of DOPA into the bulk medium. If all of the material is still on the surface as a monolayer, at the smallest possible area of the Fromherz trough, each molecule would have an APM of 8 $Å^2$. Which given the size of space filling models of single alkane chains[124] (~20 $Å^2$) would seem to be impossible. Thus, there must be fewer molecules on the surface than calculated. These disappearing molecules have two directions in to go - either on top of the DOPA which is at the water interface; or into the bulk water. So having eliminated the possibility that annealing is primarily responsible for the hysteresis, the most likely explanation, for the instability, is the the loss of material from the surface of the water.

Lipid	Lipid phase transition temperature (°C)	Chain configuration sn1/sn2	Reference
DSPC	55	18:0/18:0	2
DMPC	24	14:0/14:0	2
DPPC	41	16:0/16:0	2
DPPE	63	"	1
DPPS	55	"	1
DPPG	41	"	1
DPPA	67	"	1
DOPC	-20	$18{:}1c\Delta^9/18{:}1c\Delta^9$	2
dipalmitoleic PC	-36	$16{:}1c\Delta^9/16{:}1c\Delta^9$	2
Egg PC	< 0	unsaturated	93

Table 5(vi) Phase transition temperatures of different phospholipids. The chain configuration is given such that the first number is the number of carbons in the acyl chains, Δ denotes the position of any double bonds.

(B) Surface potential data for DOPA

Unlike DPPA (plot 5-3) there is no increase in dipole moment until the pressure begins to rise. Indeed initially there is a fall in the dipole moment. When a pressure rise is detected the dipole moment begins to increase, probably due to the angle of the alkyl chains to the subphase increasing. This rise is soon counteracted by a similar process to those discussed in section 5.2.3.B and the total dipole moment begins to fall.

The discussion of the re-compression of the monolayer is complicated by the fact that the hysteresis of DOPA clearly shows that material has been lost from the monolayer. Thus, the APM used to calculate the dipole moment is too low. There do appear to be several spikes in both the potential and the dipole moment curves. As this is the only data recorded for DOPA it is impossible to say if these are re-producible. They could be due to patches of DOPA passing under the electrode which are thicker than a monolayer.

Even though there is very little data and not qualitative, it is clear that the behaviour of DOPA molecules is very different to those of DPPA.

5.4 : MONOLAYER STUDIES OF MIXTURES OF DPPA AND DOPA

5.4.1 : Results for mixtures of DL-α-DPPA and DOPA

(A) Fromherz trough :

				mNm^{-1}	Area per molecule Å^2			
Mole ratio	Mole fraction	Isotherm number	Starting apm	Collapse pressure	Close packed	at 10 mNm^{-1}	at 25 mNm^{-1}	at 50 mNm^{-1}
3:1	0.75	57	120	60	47.0	47.0	40.8	34.3
		58	"	62	46.1	46.6	40.1	33.8
		Average			**46.6** ±0.6	**46.8** ±0.3	**40.5** ±0.5	**34.1** ±0.3
4:1	0.80	55	120	52	44.6	44.2	38.8	33.1
		56	"	56	45.6	45.4	39.8	33.6
		Average			**45.1** ±0.7	**44.8** ±0.8	**39.4** ±0.6	**33.4** ±0.4
5:1	0.83	53	120	55	46.8	45.8	40.8	34.8
		54	"	42.5*	45.6	44.6	39.4	--*
		Average			**46.2** ±0.8	**45.2** ±0.8	**40.1** ±1.0	**34.8**
9:1	0.90	51	120	55	44.4	43.9	38.9	33.4
		52	"	57	46.8	45.9	40.6	34.1
		Average			**45.6** ±1.7	**44.9** ±1.4	**39.8** ±1.2	**33.8** ±0.5

Table 5(vii) Results for mixtures of DPPA and DOPA on a Fromherz trough
mole ratios are for DPPA:DOPA and mole fractions for DPPA

* The monolayer was so rigid that the meniscus broke and the monolayer escaped from the trough.

All of the ratios which follow, in this section, 5.4, are mole ratios of DPPA:DOPA. None of the above isotherms exhibited a point of inflection except the 3:1 ratio where it occurred at 52 mN m^{-1}. The distinct phase changes seen for DPPA were more gradual. There was a continuous change in the gradient until ~15 mN m^{-1} where the isotherms showed a constant gradient in the solid region.

Hysteresis : A hysteresis test on the 4:1 mixture was undertaken. No change occurred on compression and expansion to 10 mN m^{-1}. On re-compression to 25 mN m^{-1} the original curve was followed. On expansion the pressure dropped faster than before, returning to zero at 52 $Å^2$ compared with the initial value of 56 $Å^2$. However on re-compression to 40 mN m^{-1} the original isotherm was traced. On relaxation a faster descent was again found. On the final compression the original curve was again followed.

Stability : A monolayer of 4:1 DPPA:DOPA was maintained, via the feed back circuitry on the Fromherz trough, at a constant pressure of 30 mN m^{-1}. In order to maintain the surface pressure at 30 mN m^{-1} the feedback mechanism had to decrease the trough area at an average rate of 2.7 $Å^2$ per molecule per hour (0.17 cm^2/min.). A different monolayer was held at a surface pressure of 35 mN m^{-1}. The rate of contraction was 2.4 $Å^2$ per molecule per hour (0.23 cm^2/min).

Plot 5-9 : Isotherms for D-L-α-DPPA and L-α-DOPA mixtures

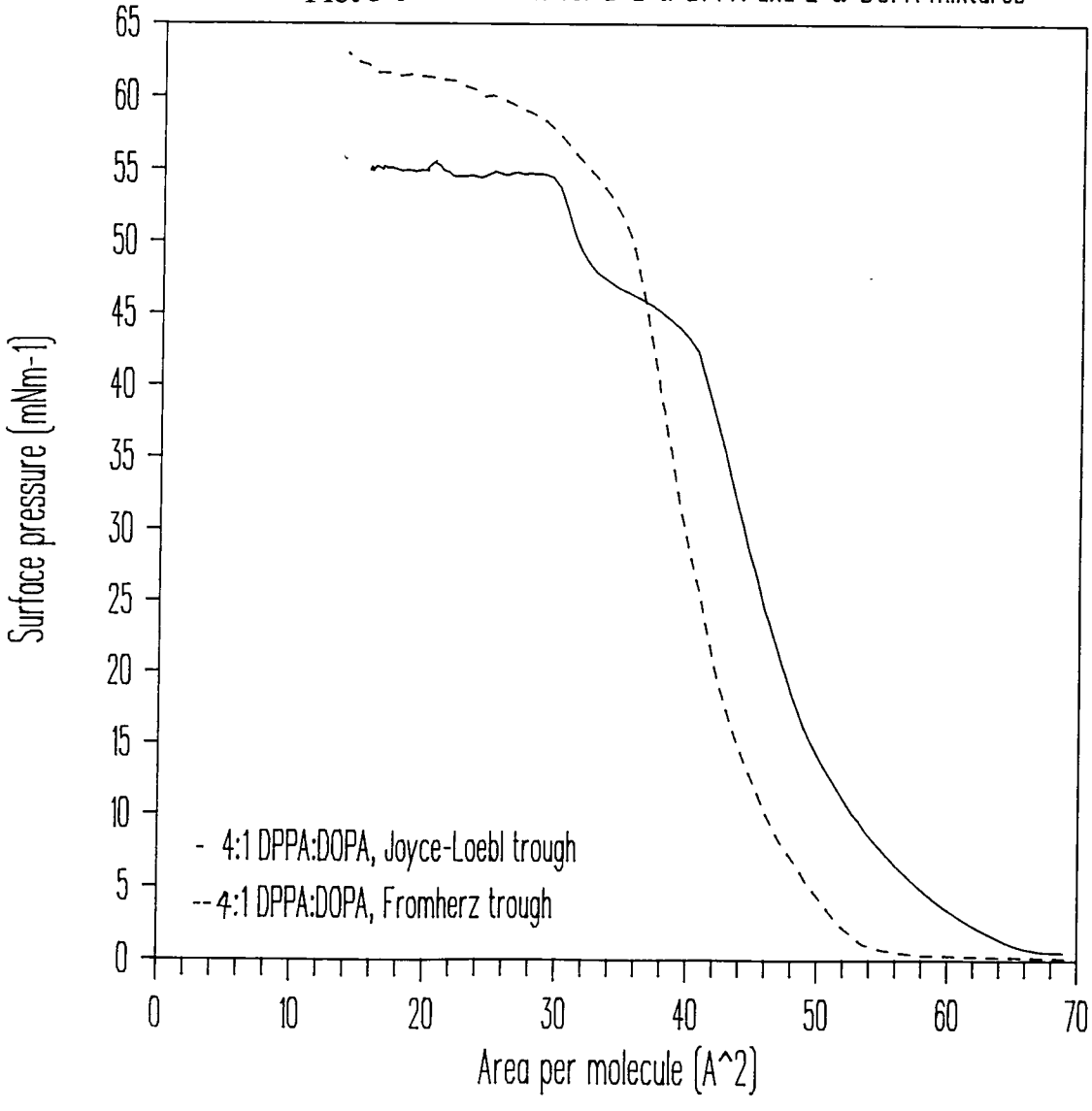

(B) Joyce-Loebl trough :

For mole fractions of DPPA above 0.5 a point of inflection was seen at ~45 mN m^{-1} with the main collapse pressure at ~55 mN m^{-1}. For mole fractions below 0.5 there was only the collapse pressure at ~43 mN m^{-1}.

				mNm^{-1}	Area per	molecule	$Å^2$
Mole ratio	Mole fraction	Isotherm number	Starting apm	Collapse pressure	Close packed	at 10 mNm^{-1}	at 25 mNm^{-1}
1:3	0.24	93	120	44	72.5	73.0	51.4
		94	"	45	71.5	71.5	51.8
		Average			**72.0** ±0.7	**72.3** ±1.1	**51.6** ±0.3
1:5	0.167	95	120	44	73.9	73.4	58.1
		96	"	45	"	73.9	58.1
		Average			**73.9** ±0.0	**73.7** ±0.4	**58.1** ±0.0
1:9	0.10	89	120	41	81.1	77.2	61.0
		92	"	43	78.2	75.9	59.5
		91	"	41	74.9	71.0	55.4
		Average			**78.1** ±3.1	**74.7** ±3.3	**58.6** ±2.9
1:15	0.063	97	120	43.5	79.4	77.8	63.4
		98	"	41.5	81.4	79.2	62.4
		Average			**80.4** ±1.4	**78.5** ±1.0	**62.9** ±0.7
1:20	0.048	99	120	44	78.2	77.3	62.6
		100	"	43	83.0	81.6	64.8
		Average			**80.6** ±3.4	**79.5** ±3.0	**63.7** ±1.6

Table 5(viii) Results for mixtures of DPPA in DOPA on a Joyce-Loebl trough mole ratios are for DPPA:DOPA and mole fractions for DPPA

				Pressure mNm^{-1}		Area per molecule $Å^2$			
Mole ratio	Mole frac	Iso. No.	Start apm	Inflect. point	Final collapse	Close packed	at 10 mNm^{-1}	at 25 mNm^{-1}	at 50 mNm^{-1}
1:1	0.5	70	120	44	--	65.8	63.4	53.3	---
		71	100	"	55	67.6	67.2	56.4	19.2
		72	"	42	58	68.4	66.8	56.2	18.6
		Ave.				**67.3** ±1.3	**65.8** ±2.1	**55.3** ±1.7	**18.9** ±0.4
4:1	0.8	101	80	40	50	55.0	53.4	45.6	26.9
		102	"	44	54	53.1	52.2	45.4	31.0
		Ave.				**54.1** ±1.3	**52.8** ±0.8	**45.5** ±0.1	**29** ±3
6:1	0.86	73	100	47	56	48.0	48.0	42.6	31.0
		74	80	"	55	50.4	50.4	45.3	33.6
		75	"	46	54.5	49.9	49.9	44.8	32.6
		Ave.				**49.4** ±1.3	**49.4** ±1.3	**44.2** ±1.4	**32.4** ±1.3
10:1	0.91	76	80	46	54	47.5	47.0	42.9	34.2
		77	"	48	57	49.0	49.3	45.0	37.4
		84	"	45	"	44.2	43.8	40.3	32.6
		Ave.				**46.9** ±2.5	**46.7** ±2.8	**42.7** ±2.4	**34.7** ±2.4
15:1	0.94	81	80	46	54	47.7	47.5	43.8	37.2
		82	"	45	"	49.0	49.3	45.6	38.7
		83	120	46	55.5	50.3	50.1	46.7	40.7
		Ave.				**49.0** ±1.3	**49.0** ±1.3	**45.4** ±1.5	**38.9** ±1.8
20:1	0.95	78	80	49	57	47.7	47.7	44.2	38.9
		79	"	45	55	48.0	48.0	44.6	39.2
		Ave.				**47.9** ±0.2	**47.9** ±0.2	**44.4** ±0.3	**39.1** ±0.2

Table 5(ix) Results for mixtures of DOPA in DPPA on a Joyce-Loebl trough
mole ratios are for DPPA:DOPA and mole fractions for DPPA

Hysteresis : Hysteresis tests were carried out on the 10:1 and 4:1 mole ratios. The monolayer of a 4:1 ratio was taken over the final (~53 mN m^{-1}) collapse pressure to an APM of 30 $Å^2$ the barriers were then expanded and the monolayer was re-compressed. On expansion the pressure dropped very rapidly at first, then at 35 mN m^{-1} the gradient mimicked the original compression but with APMs 12 $Å^2$ less than the original isotherm. A distinct gradient change was seen at 15 mN m^{-1}. On re-compression initially the APM was 11 Å less than the original curve, for equivalent pressures, but the gradient of the new isotherm was steeper. Just before the point of inflection, at ~45 mN m^{-1}, the area difference between the two isotherms had fallen to 3 $Å^2$. After this the curves became even closer, the difference fell to 0.5 $Å^2$ per molecule. The point of inflection itself was shallower than that of the original isotherm. The final collapse pressure was 57 mN m^{-1} compared to 55.5 mN m^{-1} on the initial compression. The 10:1 mixture was compressed to 15, 35 and 51 mN m^{-1} consecutively and was expanded after each compression. The first two pressures were beneath the pressure of the point of inflection, whereas the third was between the point of inflection and the final collapse pressure. No hysteresis was seen for compression of the first two cycles. However, on re-compression, after the compression to 51 mN m^{-1} (over the point of inflection, there was a difference of 2 $Å^2$ between the isotherm and the original. After the point of inflection there was no discernible difference between the two curves. For all of the expansions the pressure dropped faster than it had risen, particularly after the compression to 51 mN m^{-1}.

Surface potential : Plot 5-11 shows the surface potential characteristic for a 4:1 mixture of DPPA:DOPA. The initial surface potential was 33 mV this rose to a maximum of 285 mV on compression. On expansion the surface potential fell to -5 mV. On re-compression a new maximum of 330 mV was reached.

Plot 5-10: Isotherms for DL-α-DPPA and L-α-DOPA mixtures on a Joyce-Loebl trough

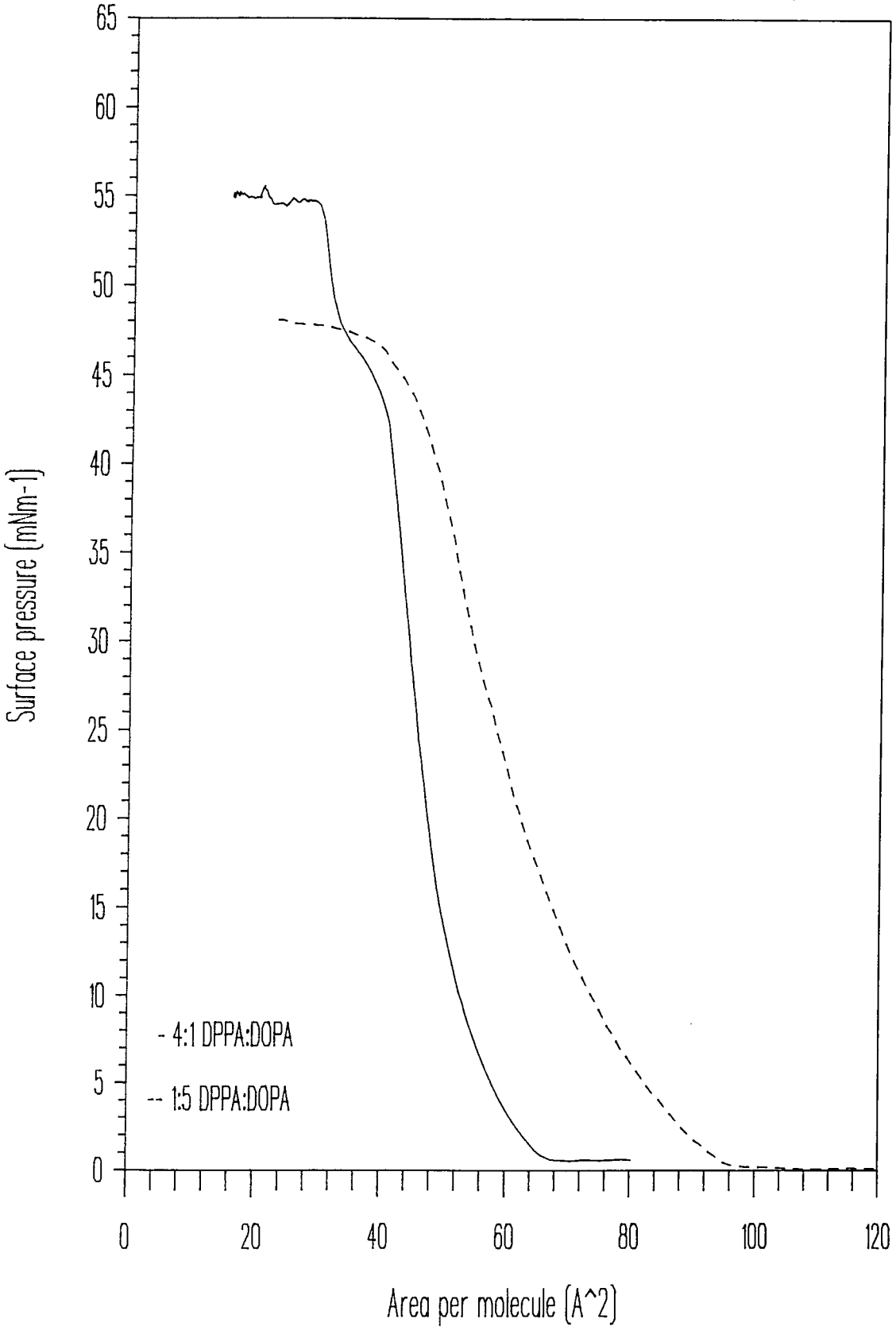

Plot 5-11A Surface pressure and area vs. time for 4:1 DPPA:DOPA

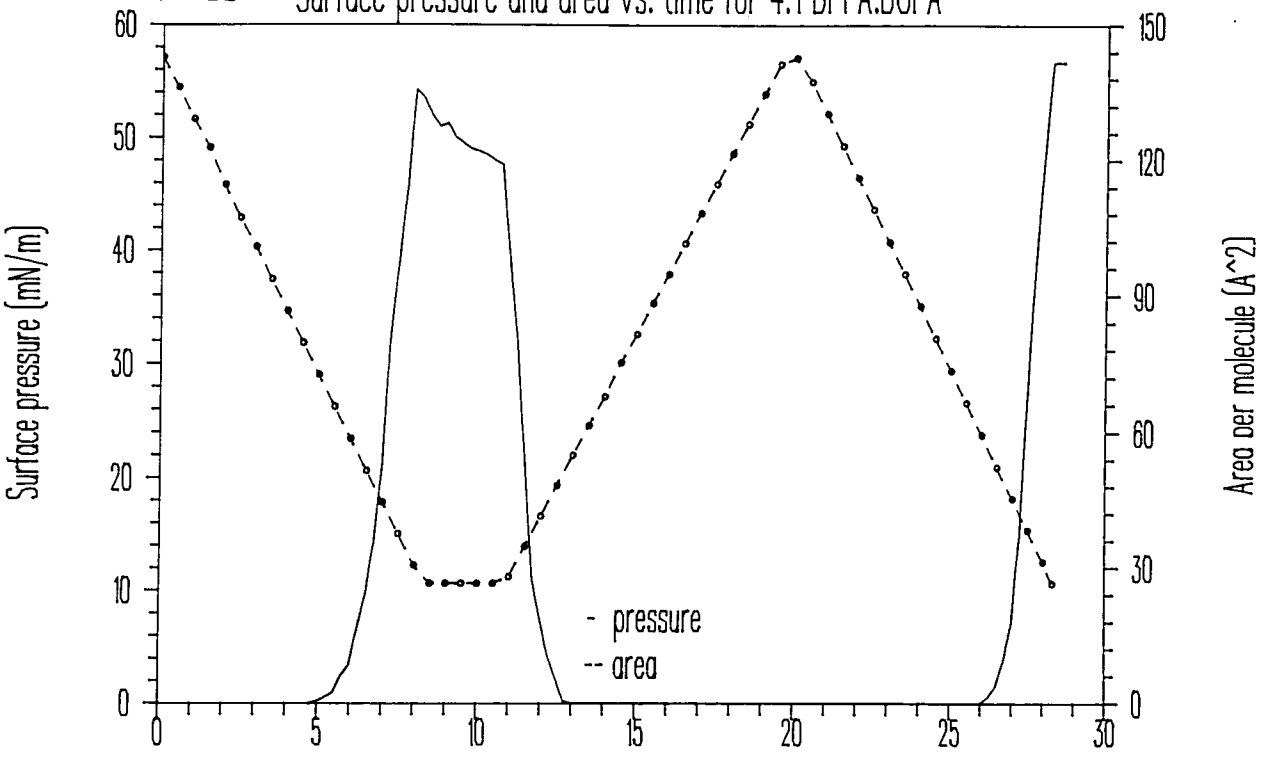

Plot 5-11B Perpendicular dipole moment and surface potential vs time

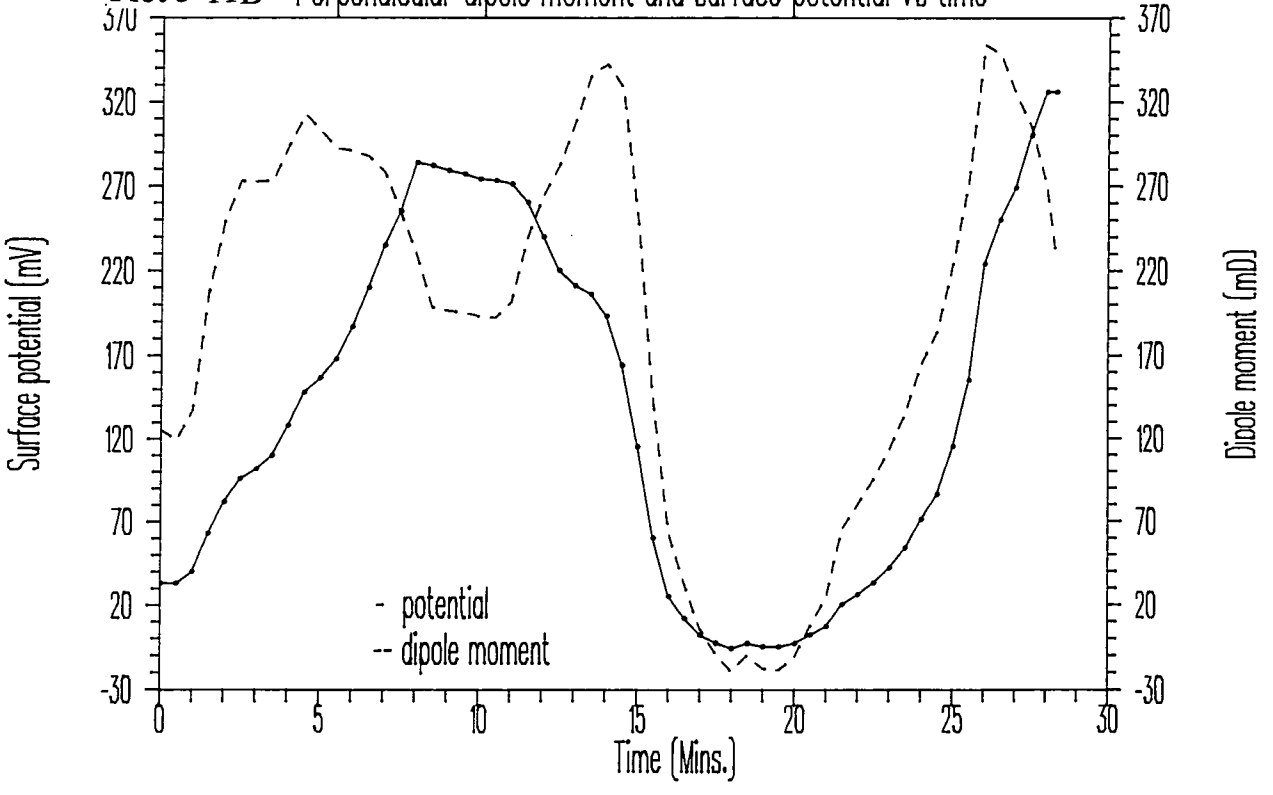

5.4.2 Analysis and discussion of monolayer studies of mixtures of DL-α-DPPA and L-α-DOPA :

(A) Discussion of isotherm data

There are again large differences not only in the APMs recorded (tables 5(vii) & 5(viii)) but also in the shape of isotherms observed on Fromherz and Joyce-Loebl troughs. Plot 5-9 shows the isotherms of a 4:1 mixture of DPPA:DOPA recorded on both troughs. The differences found are typical of those for other similar mixtures. The APMs measured on the Fromherz trough are all lower than those measured on the Joyce-Loebl trough. This is probably due to the extra area available to the monolayer on the curving meniscus of the Fromherz trough, or to leakage of the material. For the study of mixtures the shape difference is more disconcerting as the two isotherms in plot 5-9 lead to completely different conclusions concerning the miscibility of DPPA and L-α-DOPA (see section 4.1.2.B). On the Fromherz trough there is only one collapse pressure at ~60 mN m^{-1}, thus characteristic of a miscible mixture. On the Joyce-Loebl trough there are clearly two inflection points one at ~44 mN m^{-1} and the other at ~54 mN m^{-1}, the same pressures as the collapse pressures of DOPA (table 5(v)) and DPPA (table 5(ii)) respectively. *I.e.* the monolayer is exhibiting two collapses, each characteristic of the isolated separate components. Given the possibility that the meniscus on the Fromherz trough may change shape and the monolayer flow due to compression is more even (apart from in the side arms) on a Joyce-Loebl style trough. There is also a higher possibility for the leakage of the monolayer due to the raised barrier on the Fromherz trough[145]. Therefore, the data from the Joyce-Loebl trough appears more trustworthy. Plot 5-12 shows the measured APM at 25 mN m^{-1} for a variety of mole fractions of DPPA (on a Joyce-Loebl trough). The solid line is the theoretical value calculated using equation 4(iii) (section 4.1.2.B). This is calculated from the experimental values for the APMs of pure DPPA

and DOPA at 25 mN m^{-1}. Linear fits to the data have been made and are illustrated. However, it was decided that it would be appropriate to consider the plot in two sections: DPPA in DOPA; and DOPA in DPPA. Whilst there is a need for further confirming data, there does appear to be a difference in the mixing between mole fractions of DPPA above and below 0.5.

Where DOPA is mixed into DPPA there appears to be a slight positive deviation from the expected values. This is probably due to a small amount of mixing occurring between the DPPA and DOPA such that the DOPA disrupts the crystalline structure of DPPA. However, given the shape of the isotherms (plot 5-10 : the solid line) the mixtures appears to be largely immiscible. It is possible that it may be islands of DOPA which are disrupting the overall packing of the DPPA molecules.

At mole fractions of DPPA below 0.5 there is a negative deviation from ideal mixing, indicating a contraction of the monolayer compared to the expected values for the APM. This would again indicate some miscibility between the molecules but now the addition of DPPA to DOPA aids the formation of a more closely packed structure. Plot 5-10 (dotted line) shows the typical isotherm of such a mixture. The lack of a second collapse is not significant due to the fact that all of the isotherms were recorded such that the initial APM was 120 $Å^2$. Thus, on maximum compression the APM for DPPA alone never reaches the close packed structure, let alone the collapse point. *E.g.* for the 1:3 mixture the final APM, at full compression, for all of the molecules is ~20 $Å^2$. If the area available is just filled by the DPPA present this would give an APM of ~80 $Å^2$ comparing this to the APM at collapse for DPPA (~37 $Å^2$) it is obvious that the collapse pressure for DPPA will not be reached under the experimental conditions. In order to see the two collapse pressures much less material would have to be deposited on the surface. Unfortunately such an experiment was not performed. The fact that the collapse pressures (table 5(viii)) found are very close to that of pure DOPA (table 5(v)) would indicate immiscibility.

Plot 5-12 : Area per molecule at 25 mNm^{-1} vs. mole fraction DPPA for various mixtures of DPPA and DOPA

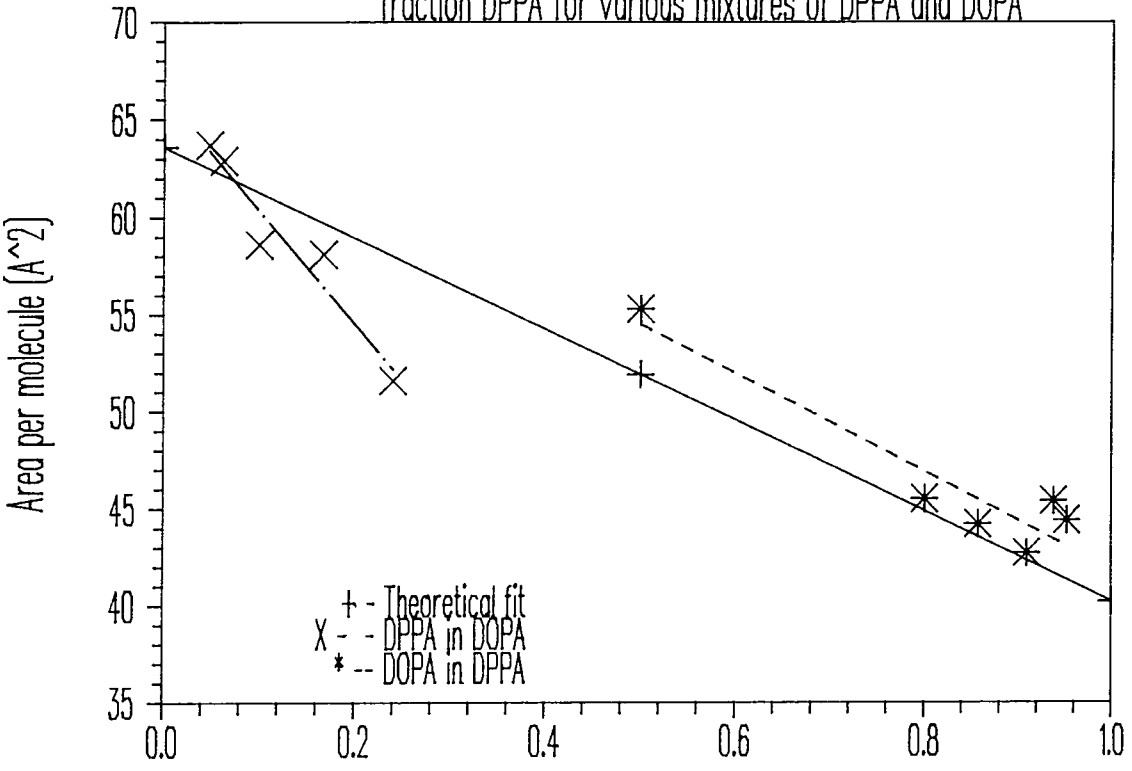

Plot 5-13 : Area per molecule at 50 mNm^{-1} vs mole fraction DPPA for various mixtures of DOPA and DPPA

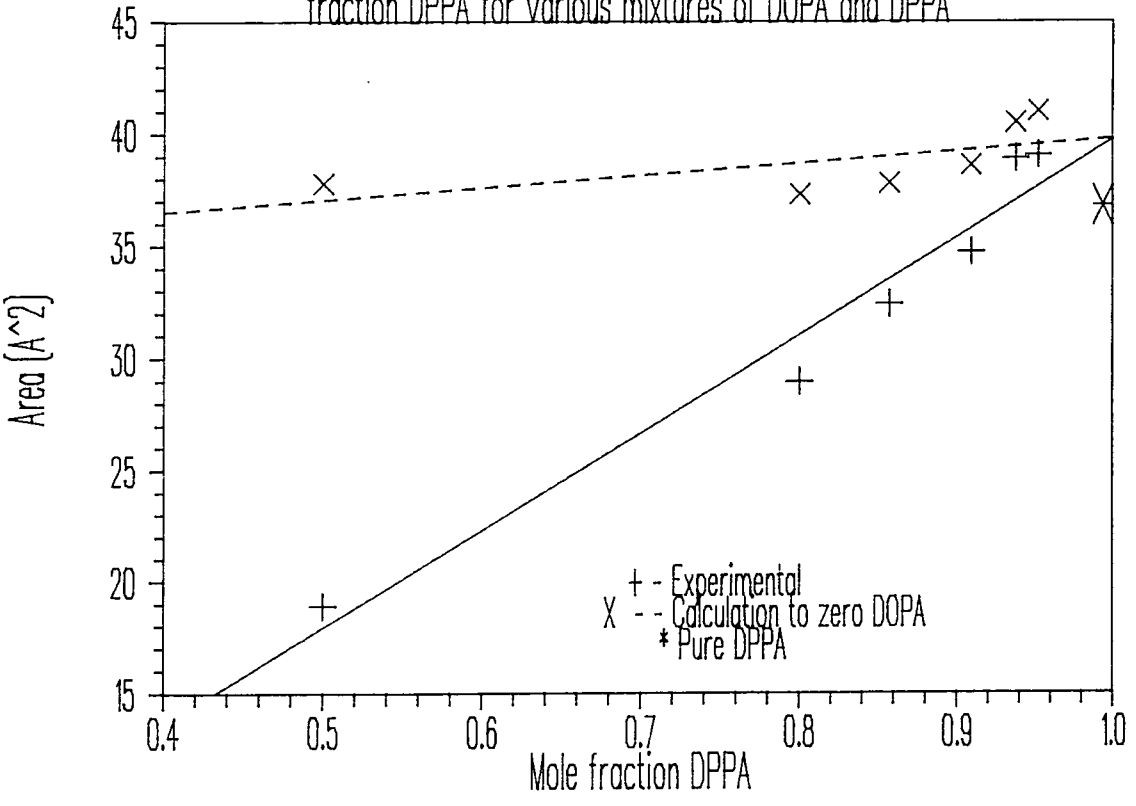

Plot 5-13 shows the APM at 50 mN m^{-1} for the same isotherms. This pressure is above the point of inflection but below the final collapse pressure. No data was available for mole fractions of DPPA below 0.5 as the pressure does not reach 50 mN m^{-1}. Similarly it is not possible to calculate the expected APM because the surface pressure of DOPA does not reach 50 mN m^{-1}. The solid line in plot 5-13 is a linear fit to the experimental data. The first point to note is that its slope is in the opposite direction to the expected. As the mole fraction of the component with the largest APM (DOPA), at lower pressures, is decreased the total APM is increasing. The shape of the isotherms suggests that DOPA and DPPA are largely immiscible and that the DOPA islands had collapsed. Therefore, a calculation was made to see whether the pressure response being detected, at 50 mN m^{-1} was from a monolayer composed solely of DPPA.

The amount of DPPA in the original layer deposited was found. Then the area of the trough was divided by the number of DPPA molecules to give an APM that related solely to DPPA. The results of these calculations are shown in plot 5-13 as a X's. The dotted line is a linear fit to the calculated data. The equation for the fit is $Y = 5.5X + 34.3$ and the average value is 39 ± 2 $A^{\circ 2}$. Pure DPPA at 50 mN m^{-1} has an APM of 37 ± 2 $Å^2$ per molecule (table 5(ii)). Thus, the calculated APM, for DPPA being the only component on the surface at 50 mN m^{-1}, is slightly higher than the APM for pure DPPA at this pressure. However, the fit is fairly close. The slight increase in the calculated APM could be due to a number of factors: all of the DOPA might not have been ejected from the monolayer; the ejected DOPA may be affecting the behaviour of the DPPA monolayer; or the presence of DOPA in the monolayer below 44 mN m^{-1} may have caused the formation of irregularities in the crystalline structure of DPPA. The last of these factors is quite a strong possibility as Möhwald[126] has found, by fluorescence, that in the liquid state there is a strong variation in the pattern of crystal growth between different lipids. Although he has yet to publish data on mixtures it would be a fair assumption that mixtures exhibit further differences in crystal structure during the growth stage. Thus, the final close packed structure would also differ.

The hysteresis characteristics of the mixtures seem follow those of the pure monolayers. There is very little hysteresis below the collapse pressure of DOPA. However, if the monolayer is compressed beyond this point hysteresis is seen for pressures below the point of inflection but largely disappears after this point. The magnitude of the APM difference between isotherms before and after compression increases with the amount of DOPA. Therefore the monolayers of mixed DPPA and DOPA seem to have characteristics which are similar to the pure monolayers but combined into one isotherm. Thus it must be concluded that the mixtures are largely immiscible with separate domains of DPPA and DOPA.

(B) Discussion of surface potential data

It was hoped that equation 4(iv) could be applied to the surface potential data of the mixture. However, as both DPPA and DOPA have the same maximum value this would seem to be an irrelevant calculation. It is very difficult to even estimate whether the dipole moments of the mixture are the result of adding the individual components because DPPA and DOPA have such a different characteristics dependent on the pressure rather than the APM. An initial rise of 200 mD for the dipole moment is seen for the mixture. This is compared to 245 mD seen in pure DPPA. This compares very favourably with the fact that only 4 parts in 5 of the molecules in the monolayer are DPPA. After 5 minutes the pressure starts to rise so there will be a competing influence of the increase in dipole moment of the DOPA and the fall of DPPA so qualitative comparison becomes difficult. The dipole moment seems to be a mixture of the pure components rather than a miscible mixture.

5.5 : MONOLAYER STUDIES OF ALAMETHICIN

5.5.1 Results of monolayer studies of alamethicin

		mNm^{-1}	Area per	molecule	$Å^2$
Isotherm number	Starting apm	Collapse pressure	Close packed	at 10 mNm^{-1}	at 25 mNm^{-1}
6	500	32	329	320	308
7	"	29	346	334	316
11	"	31.5	348	334	316
Average			**341** ±10	**329** ±8	**313** ±5

Table 5(x) Results for Alamethicin on a Joyce Loebl trough

With an APM of 500 $Å^2$ at the start there was an initial surface pressure present of ~ 0.5 mN m^{-1}. Once the pressure began to rise there were no further changes in the gradient until ~31 mN m^{-1} where the curve turned but the gradient was constant not uneven as in a normal collapse. This can be seen in plot 5-14.

Hysteresis : Two tests were performed. In the first the monolayer was compressed to 10 mN m^{-1} , expanded, re-compressed to 32.5 mN m^{-1}, re-expanded then re-compressed. On expansion in both cases the pressure dropped faster than it had risen but after the initial drop followed the gradient of the first curve. On re-compression to 32.5 mN m^{-1} the gradient was as for the original curve but the APM was 4 $Å^2$ greater for equivalent pressures. On re-compression for the third time the original curve was followed. The results of the second test are shown in plot 5-14.

Stability : A monolayer of alamethicin was maintained, via the feed back circuitry on the Fromherz trough, at a constant pressure of 23 mN m^{-1}. In order to maintain the surface pressure at 23 mN m^{-1} the feedback mechanism had to decrease the trough area at an average rate of 50 $Å^2$ per molecule per hour (0.6 cm^2/min.).

Plot 5-14 : Hysteresis of Alamethicin on a Joyce-Loebl trough, 26°C

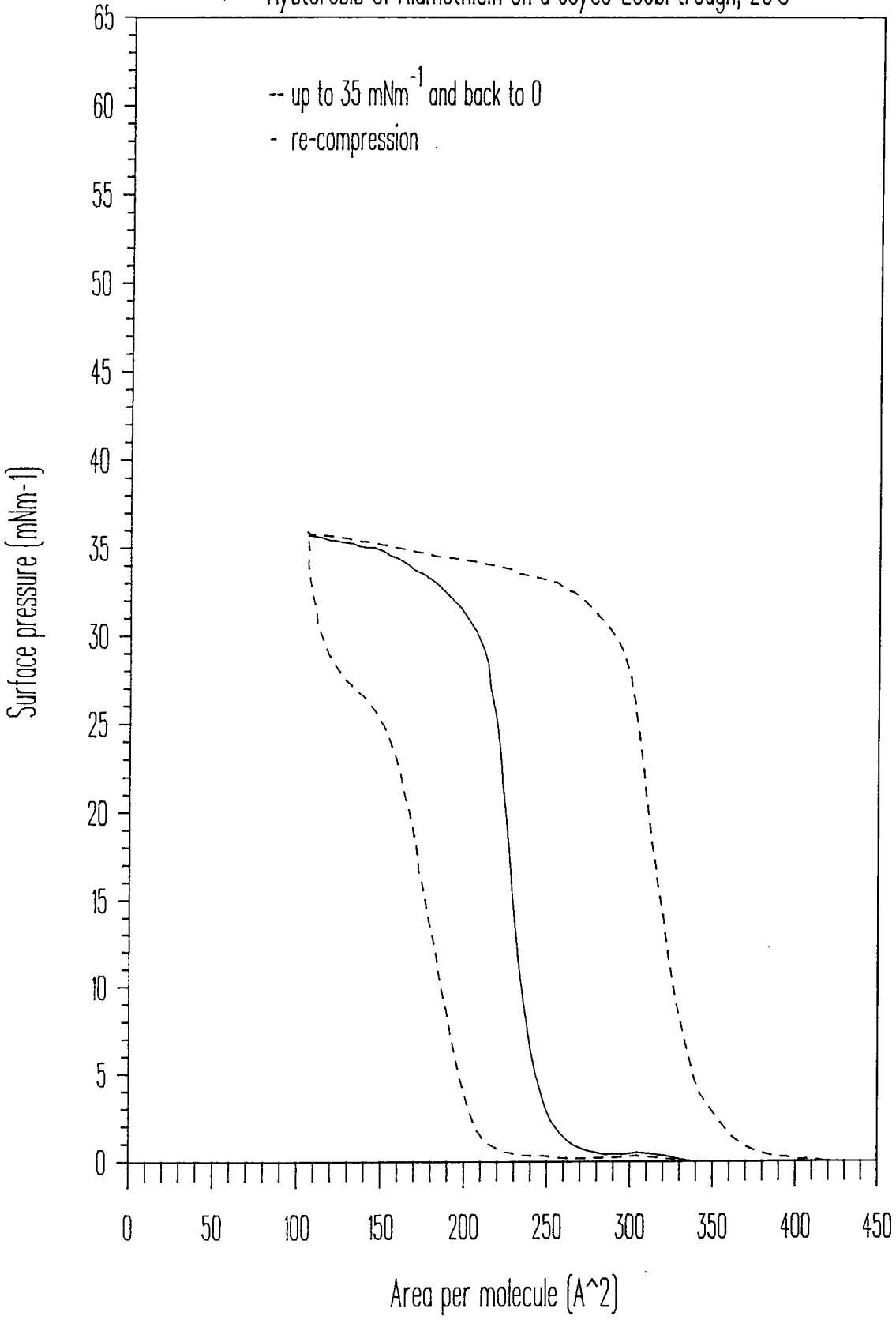

Surface potential : On spreading the alamethicin a surface potential of 330 mV was recorded (plot 5-15). On compression the potential reached 510 mV. On expansion the surface potential fell to 250 mV, lower than the original value. On re-compression the potential rose to 545 mV.

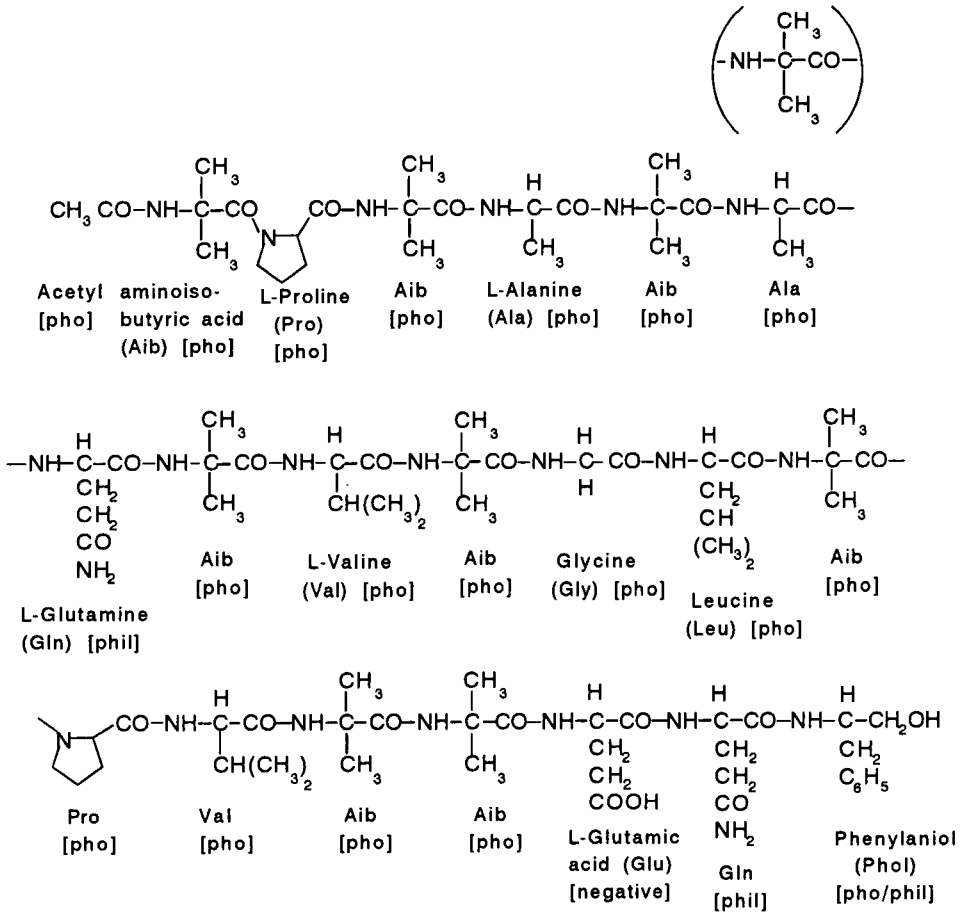

Figure 5(f) : The primary structure of the major and minor components of alamethicin.[139] The square brackets note the general hydrophobic [pho] and hydrophilic [phil] nature of the amino acid groups.[134]

Plot 5-15A: Surface pressure and area vs. time for Alamethicin

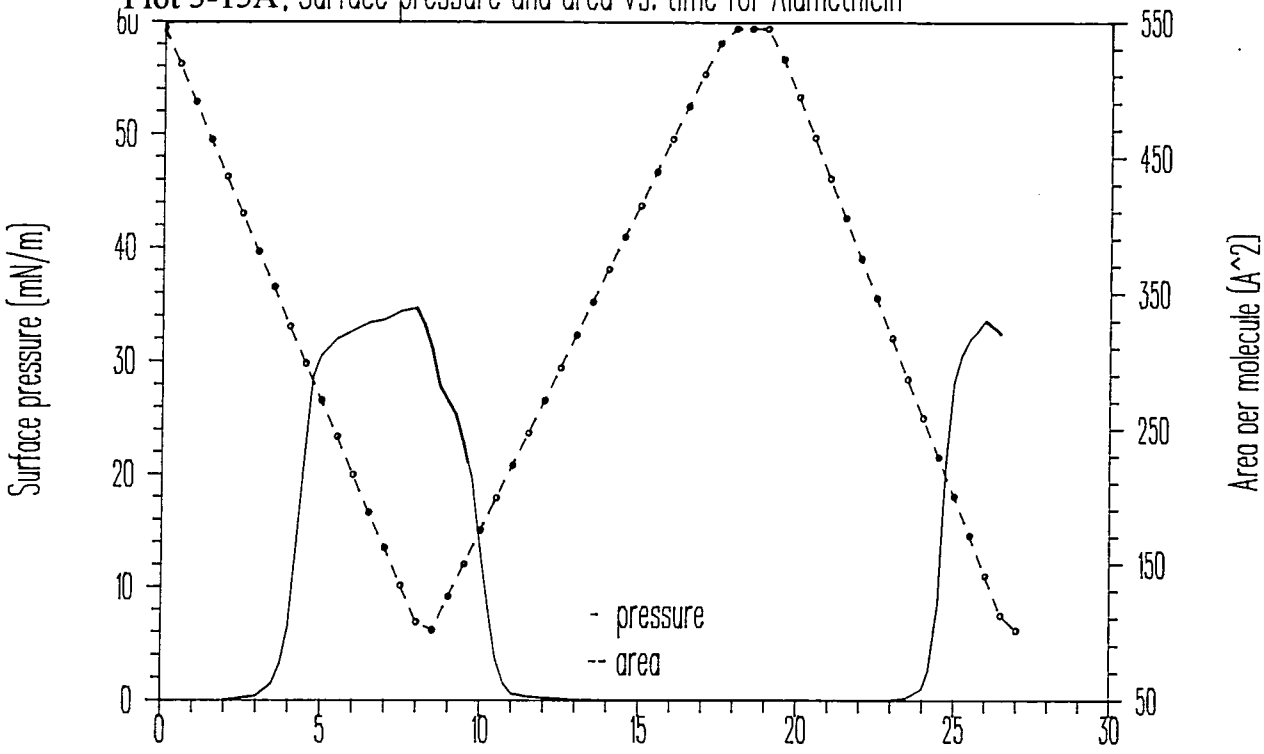

Plot 5-15B Perpendicular dipole moment and surface potential vs time

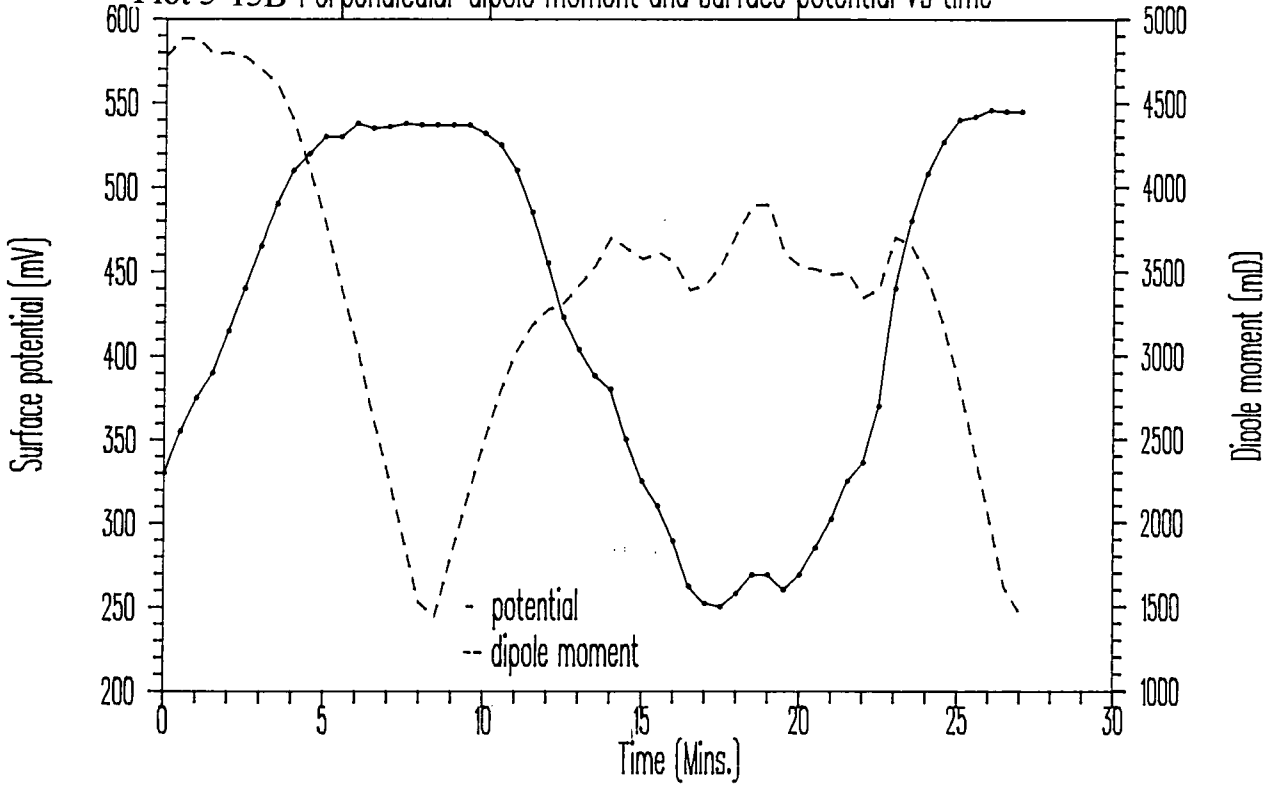

5.5.2 Results and discussion for alamethicin

(A) Surface Pressure measurements

The value of 341 ± 10 $Å^2$ per molecule for the CPA of Alamethicin is in agreement with the value of 330 $Å^2$ per molecule found by Gordon and Haydon[128]. This large size indicates that either alamethicin is denatured on the water interface or is lying such that the helixes are parallel to the interface. The first possibility is unlikely as it is easy to achieve reproducibility in re-recording the isotherms and the data recorded in this study agrees closely with other studies. If the peptide were denatured large fluctuations in results would be expected.

The recorded area per molecule corresponds closely to dimensions found by X-ray crystallography. Fox and Richards[137] report that crystals of alamethicin were formed with space group $P2_1$, a = 33.33, b = 29.62 c = 23.20 Å, $\beta = 120.4^\circ$, with three alamethicin molecules per asymmetric unit. This gives an average individual molecular dimension of 33.3 X 9.87 X 23.20 Å. With the dimension of 33.33 Å as the length of the helix. The helixes were found to be predominantly α-helical, apart from the C-terminus where the last couple of residues were 3_{10} turns[4]. Assuming that alamethicin retains this conformation at the air-water interface then if the molecules were orientated with their helical axis perpendicular to the interface the CPA would only be 229 $Å^2$ per molecule (figure 5(g)-(ii)). If however the helixes are parallel to the interface with the smaller cross-sectional length touching the surface then this would give a CPA of 330 $Å^2$ per molecule, corresponding closely with the areas found. According to the crystal structure the hydrophilic groups of alamethicin all point in the same direction off the central helical core and this would tally with the results found on the trough.

Figure 5(f) shows the primary structure of alamethicin. The residues are marked as to whether they are considered to be hydrophilic, hydrophobic or charged in general nature. Despite the predominance of hydrophobic residues Gordon and Haydon concluded, from their studies of alamethicin at the air/water interface and the interface between glycerol monoleate in n-decane / sodium chloride solution (where they found an APM of 530 $Å^2$), that the dominant interaction of alamethicin at the interfaces was hydrophilic. This again fits with the molecule being the same, or a very similar conformation to that determined by X-ray crystallography[137]. Hall et al[138] cite that alamethicin is also found in a predominantly α-helical form in non-polar solvents. It would therefore be logical to assume that it had adopted a predominantly α-helical conformation, as found in the X-ray work, in the chloroform and remained so at the air-water interface.

The monolayer of alamethicin exhibited little hysteresis below the collapse pressure. However, once the pressure had exceeded the collapse pressure a large hysteresis was seen (>90$Å^2$ per molecule) There are the afore mentioned possible reasons of loss of material into the subphase or incomplete separation from a multilayer structure back to a monolayer to explain the hysteresis. However, two other possibilities must also now be considered, the peptides could either have adopted a different conformation or it may now be orientated such that the helixes are perpendicular to the interface. The large hysteresis found is possibly connected with the fact that in order to maintain the monolayer at 23 mN m^{-1} the contraction of the trough was large (50 $Å^2$ per molecule per hour). *I.e.* the monolayer of alamethicin was not very stable at 23 mN m^{-1}.

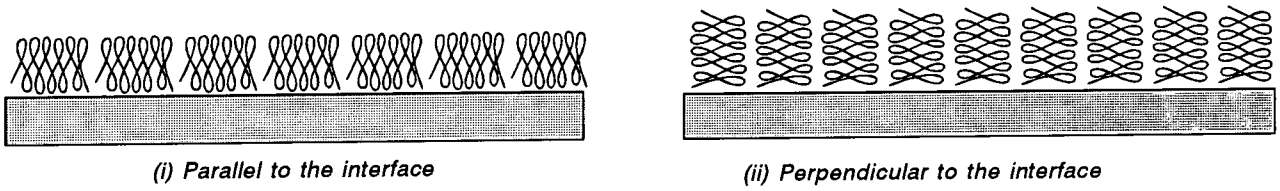

(i) Parallel to the interface *(ii) Perpendicular to the interface*

Figure 5(g) : Two possible orientations of the helixes of alamethicin on water.

(B) Surface potential data

One of the main reasons for undertaking the surface potential measurements was to determine whether the change in gradient at 30 mN m^{-1}, for alamethicin, was due to a collapse of the monolayer or to changes in either conformation or orientation of the helixes to the air water interface.

Initially, before a pressure rise is seen the dipole moment of alamethicin is constant but an order of magnitude greater than for the lipids. A fall in the dipole moment is recorded as the surface pressure begins to rise. This could again be due to the reduction of induced dipoles in the molecules. The fall in apparent dipole moment continues until the barriers are expanded. At the point where the surface pressure fell back to zero the dipole moment evened out with only a ripple where the barriers stopped and started again. However the new value for the maximum dipole moment was apparently 3600 mD compared to 4900 mD found before compression began. Now assuming that the alamethicin remains in the same conformation then the explanation for the fall in dipole moment could be that the helixes are now perpendicular to the interface so that alamethicin occupies a much smaller area on the trough. The area per molecule that this new orientation would have, based on the work by Fox and Richards[137], would be of the order of 230 $Å^2$. Therefore the minimum area shown in plot 5-14 of 100 $Å^2$ would not fit with the hypothesis that the alamethicin is re-orientating with its helixes perpendicular to the interface. Nor would it seem reasonable that a re-orientation would change the dipole moment but not the shape of the π-A isotherm.

The best hypothesis which fits all of the data is that some of the alamethicin is ejected from the monolayer into the subphase and that this is a continuous process above 30 mN m^{-1}.Also that some of the alamethicin never re-enters the monolayer but is lost to the bulk phase. This would explain the smooth nature of the π-A isotherm above 30 mN m^{-1} and the hysteresis of the isotherm (as the APM scale is no longer relevant). The sharp decrease in the dipole moment, as the pressure rises, would now not be a real effect but an error due to the APM not decreasing but remaining fairly constant. The decrease in the dipole moment at full expansion of the barriers, compared to the original value, would also be due to the fact that the actual APM is probably ~80 $Å^2$ higher (taken from the hysteresis graph) than that used to calculate the dipole moment.

Now above it was assumed that the alamethicin did not change it's conformation. From this assumption it was possible to find a hypothesis which fitted all of the data. The only evidence to support the assumption is that the shape of the isotherm does not change on re-compression but the APM has. A conformational change would affect the intermolecular interactions of alamethicin and therefore the shape of the isotherm. If there was a conformational change caused by pressure it would be very unlikely that the peptide could relax back to its original conformation and if it did this would not explain the hysteresis seen in the π-A isotherm. Therefore it is fair to accept, as a working hypothesis, that the monolayer collapses in a usual manner with the permanent loss of some material into the subphase.

5.6 : MONOLAYER STUDIES OF MIXTURES OF DPPA AND ALAMETHICIN

5.6.1 Results for DL-α DPPA and alamethicin mixtures

All of the ratios mentioned in this section (5.6) are for DPPA:alamethicin mole ratios. All of the mixtures examined showed a point of inflection at ~32 mN m^{-1}. For the higher concentration of alamethicin this became a plateau, with a further rise in pressure at a smaller APM. This APM was 25 $Å^2$ for the 1:1 mixture and around 45 $Å^2$ for most other mixtures. This is shown in plot 5-16. For the lower concentrations of alamethicin the distinct gradient change at 15 mN m^{-1} was seen but for higher concentration a more gradual gradient change was observed.

Hysteresis : Five different hysteresis tests were carried out on the following mole ratios (DPPA : alamethicin) 5:1, 10:1, 20:1, 27:1, 50:1. If compression took place to an pressure less than the point of inflection then on re-compression no hysteresis occurred. If the point of inflection was passed then on re-compression the APM, for a given pressure, was less than the original until the point of inflection was reached where the curves coincided again (see plot 5-16). When the collapse pressure was exceeded, before expansion, then on re-compression the alteration in the area was initially larger than if the point of inflection only has been surpassed, (see table 5(xi)) but again above the point of inflection the curves coincided.

			initial compression	Difference in area $Å^2$	on re-compression
Isotherm number	Mole ratio	Starting apm	pressure mNm^{-1}	below 32 mNm^{-1}	above 32 mNm^{-1}
105	5:1	120	20	0	--
		"	45	4.2	0
32	10:1	"	7.5	0.6	--
		"	20	0.3	--
109	20:1	"	51.5*	3.6	0.4
124	27:1	"	57*	6.1	0.4
116	50:1	"	25	0.5	--
			45	1.6	0.3
		"	52.5*	2.0	0.3

Table 5(xi) Results for hysteresis of DPPA/Alamethicin mixtures.
*Above the collapse pressure

Plot 5-16 : Hysteresis of 30:1 DPPA : Alamethicin, Joyce-Loebl trough

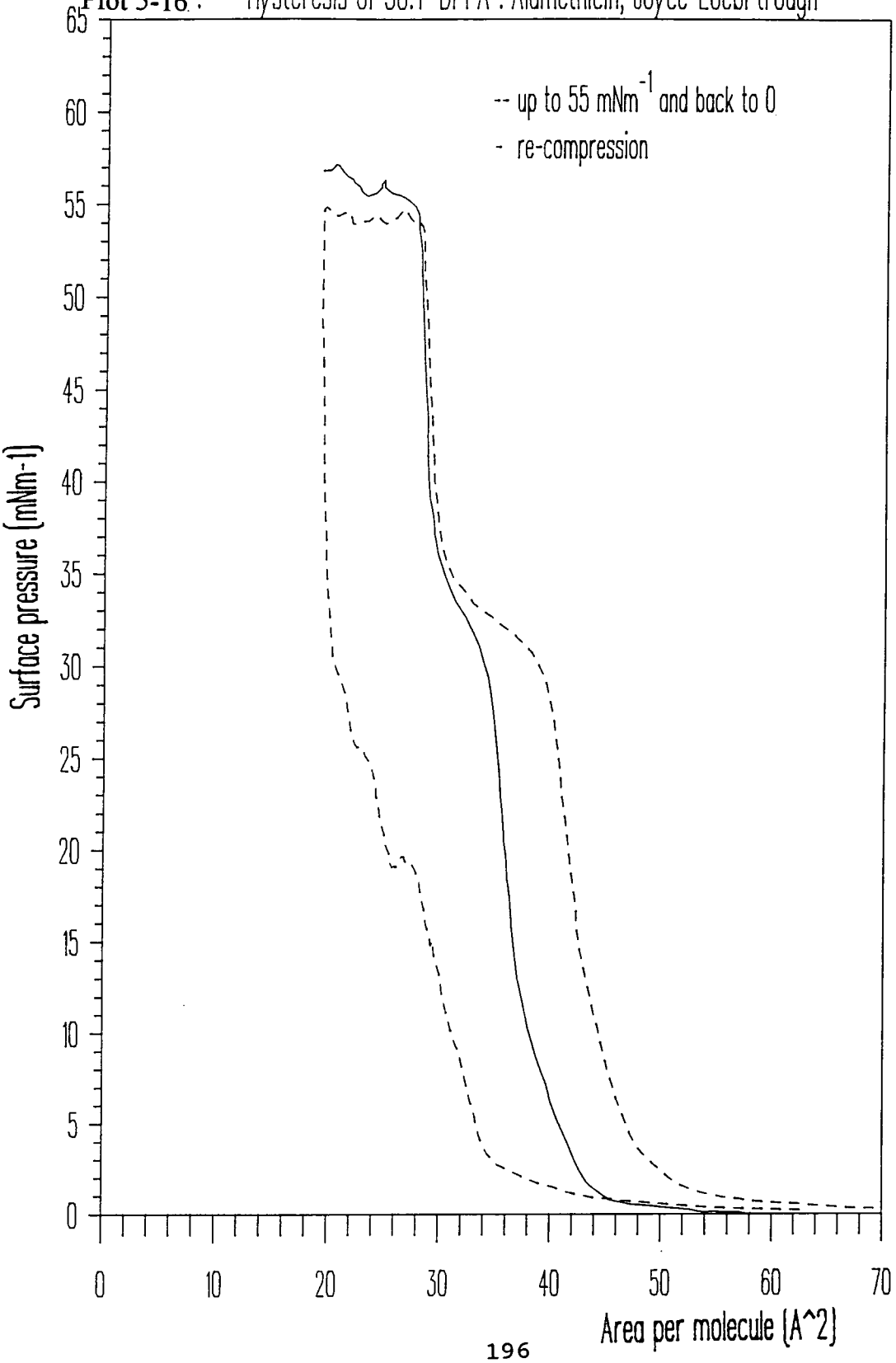

				Pressure	mNm^{-1}	Area per	molecule	$Å^2$	
Mole ratio	Mole frac	Iso. No.	Start apm	Inflect. point	Final collapse	Close packed	at 10 mNm^{-1}	at 25 mNm^{-1}	at 50 mNm^{-1}
1:1	0.5	33	320	--	34	147.0	144.5	138.1	--
		34	200	--	27	146.2	142.2	134.1	--
		35	"	--	"	149.8	145.0	136.3	--
		Ave.				**148** ± 2	**144** ± 2	**136** ± 2	
5:1	0.83	37	152	27.5	49.5	89.8	87.7	83.2	--
		38	"	30.5	53.0	90.1	88.0	83.7	37.0
		Ave.				**90.0** ±0.2	**87.9** ±0.2	**83.5** ±0.4	
5:1	0.83	104	150	34.0	56.5	69.6	67.8	64.2	38.4
		105	"	33.5	57.5	70.2	67.8	64.2	38.7
		Ave.				**69.9** ±0.4	**67.8**	**64.2**	**38.6** ±0.2
10:1	0.91	30	161	31.0	50.0	79.2	75.6	68.9	--
		31	"	30.0	53.0	81.1	77.9	70.8	41.8
		32	"	33.0	--	79.2	75.9	69.8	--
		Ave.				**79.8** ± 1	**76.5** ± 1	**69.8** ± 1	
15:1	0.94	106	120	33.0	55.5	51.4	50.4	48.1	37.0
		107	"	31.0	53.0	54.7	54.2	51.4	40.3
		119	"	33.0	56.0	57.1	56.6	53.8	42.7
		120	"	32.0	53.0	51.4	50.4	48.1	37.0
		Ave.				**54** ± 3	**53** ± 3	**50** ± 3	**39** ± 3
20:1	0.95	108	100	32.5	54.5	52.2	51.2	48.6	40.0
		116	"	"	"	52.4	51.4	48.8	39.2
		109	"	30.0	50.0	54.8	54.0	50.8	40.4
		Ave.				**53.1** ± 1	**52.2** ± 1	**49.4** ± 1	**39.9** ± 1
24:1	0.96	24	106	33.0	54.0	52.7	51.8	49.1	37.9
		26	"	36.0	55.0	51.3	49.9	47.4	36.4
		29	"	33.5	52.0	52.9	52.7	50.3	38.3
		28	"	35.0	55.0	52.5	52.0	49.5	37.2
		Ave.				**52.1** ± 1	**51.6** ± 1	**49.5** ± 1	**37.0** ± 2
27:1	0.965	13	179	35.0	55.0	73.0	71.6	68.7	57.3
		14	107	34.0	54.0	65.5	64.6	61.8	49.2
		15	"	33.0	"	66.3	65.3	62.5	44.1
		Ave.				**68** ± 4	**67** ± 4	**64** ± 4	**50** ± 7
29:1	0.966	21	108	32.5	53	50.3	48.6	44.4	36.1
		22	"	"	53	57.2	54.3	50.7	44.9
		23	"	30	48	56.3	52.7	49.9	--
		Ave.				**55** ± 4	**52** ± 3	**48** ± 3	**41** ± 6
50:1	0.980	110	80	32.5	53.5	45.4	45.1	42.4	37.1
		111	"	"	54	49.0	49.0	46.2	43.8
		116	"	31	53	44.2	44.2	41.3	36.8
		Ave.				**46** ± 3	**46** ± 3	**43** ± 3	**39** ± 4
100 :1	0.990	112	80	30	50	48.3	48.2	45.8	41.0
		113	"	"	49	45.6	53.4	42.6	--
		118	"	"	50	45.8	"	42.9	38.7
		Ave.				**47** ± 2	**52** ± 3	**48** ± 2	**40** ± 2
200 :1	0.995	114	80	30	52.5	47.5	47.4	44.6	41.3
		115	"	"	50.5	48.0	47.9	45.2	"
		Ave.				**47.8** ±0.4	**47.7** ±0.4	**44.9** ±0.4	**41.3** ±0

Table 5(xii) Results for mixtures of Alamethicin in DPPA on a Joyce-Loebl trough mole ratios are for DPPA:Alamethicin and mole fractions for DPPA.

Stability : A monolayer of 27:1 DPPA:alamethicin was maintained, via the feed back circuitry on the Joyce-Loebl trough, at a constant pressure of 23 mN m^{-1}. In order to maintain the surface pressure at 23 mN m^{-1} the feedback mechanism had to decrease the trough area at an average rate of 1.1 $Å^2$ per molecule per hour (0.22 cm^2/min.).

Surface potential : Plot 5-17 shows the surface potential for a 30:1 mixture of DPPA:alamethicin. The initial potential on depositing the monolayer was 40 mV. On compression this rose to 290 mV. This began to decline as the monolayer surface pressure reached the point of inflection. The potential then fell to 245 mV at the point of the second collapse pressure. On expansion the surface potential returned to the original value of 40 mV. As the monolayer was re-compressed the surface potential rose to 300 mV at the point of inflection in the pressure curve. This then fell to 280 mV at the point of the second collapse pressure.

Plot 5-17A: Surface pressure and area vs. time for 30:1 DPPA:Alamethicin

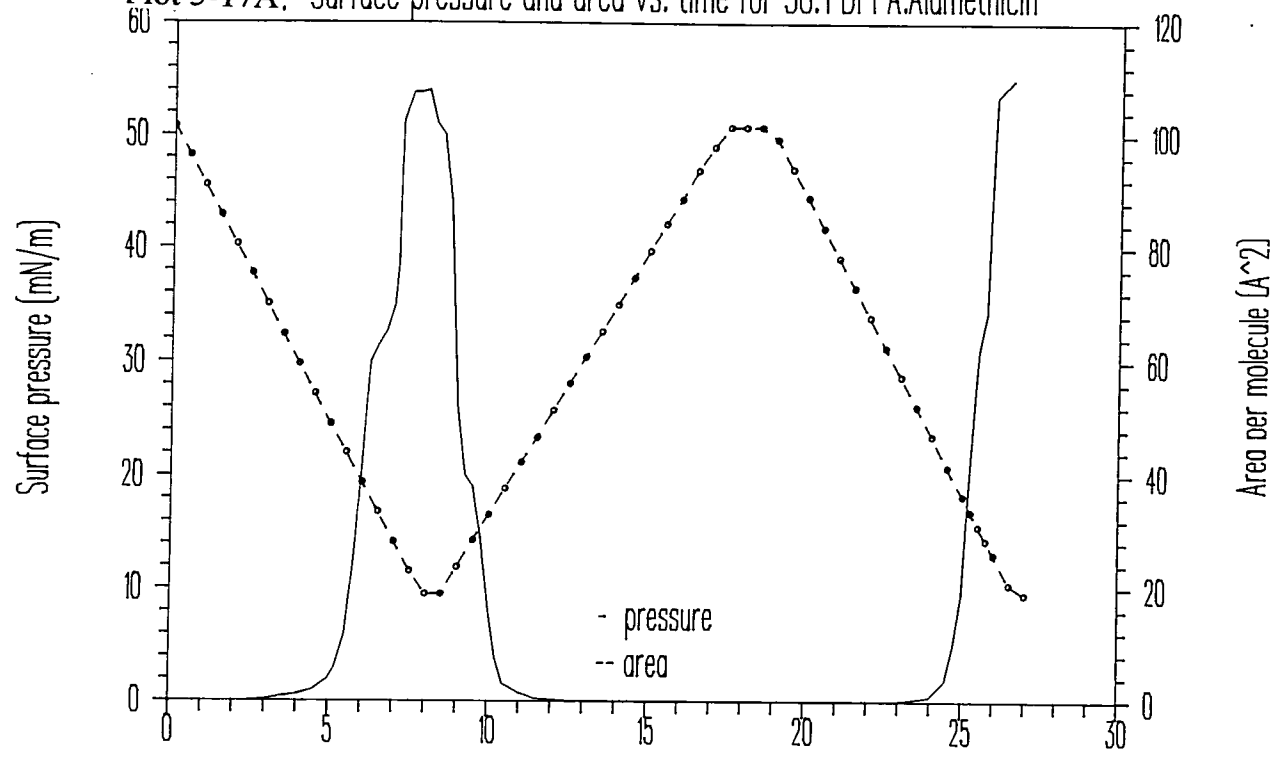

Plot 5-17B Perpendicular dipole moment and surface potential vs time

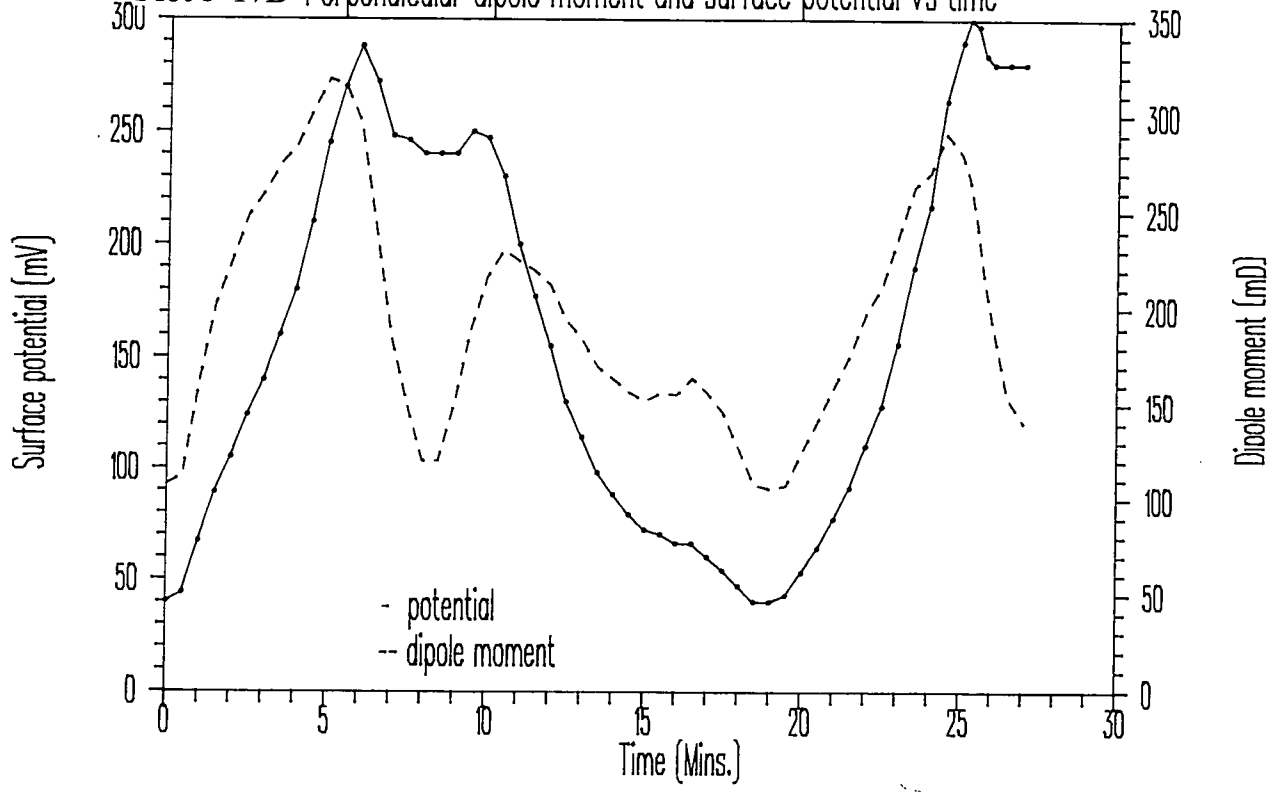

5.6.2 Analysis and discussion for monolayer studies of mixtures of DPPA and Alamethicin

The isotherms for mixtures of alamethicin in DPPA show characteristics of an immiscible mixture. There is an initial collapse pressure at 30-33 mN m^{-1} and a final collapse pressure at 50-55 mN m^{-1} for all of the mixtures studied except the 1:1 ratio. As not enough DPPA was present for the collapse pressure to be reached at the minimum area of the trough for a 1:1 ratio. The two collapse pressures are representative of the presence of two components which are immiscible[134].

Plot 5-18 shows the experimental data for the APM of different mole fractions of DPPA at 25 mN m^{-1}. The solid line shows the expected values, calculated from equation 4(iii), for either a completely miscible or completely immiscible mixture. To a large extent the experimental data lies on the calculated line. There is one point which may lie off the line due to incorrect solution making (at mole fraction 0.83), especially since there was a repeat experiment performed which lay on the line. The point at 0.5 mole fraction may or may not be correct as it is the only one recorded at a mole fraction lower than 0.8.

Plot 5-19 shows the experimental data for the APM's at 50 mN m^{-1}. As for plot 5-13, the slope of a line fitted to the data increases as the amount of the component with the largest area decreases. Again a calculation for the APM for DPPA as the only component in the monolayer was performed (plot 5-20). It can be seen that to a large extent these calculated values are very close to that of pure DPPA.

By combination of plots 5-16&18 it can be seen that at mole fractions of DPPA greater than 0.8 the mixtures are largely immiscible. At the collapse pressure of alamethicin it is ejected from the monolayer, as shown in plot 5-20.

The data also indicates that alamethicin is being lost into the subphase, if its collapse pressure is exceeded. No hysteresis is seen for re-compression after reaching a pressure below 30 mN m^{-1}. As soon as this is exceeded (plot 5-16) a large hysteresis is seen below the collapse pressure of alamethicin but none above it.

The loss of alamethicin is also seen in the surface potential data (plot 5-17) as there is a sudden fall in the potential at exactly the same point in time as the collapse pressure of alamethicin is reached. The loss of alamethicin is also seen by the decrease in this fall on the second compression. The dipole moment data is really of no use in the assessment of miscibility, due to the unreliability of the APM as material is ejected from the monolayer.

Plot 5-18. Area per molecule at 25 mN m^{-1} vs. mole fraction DPPA for various mixtures of Alamethicin and DPPA

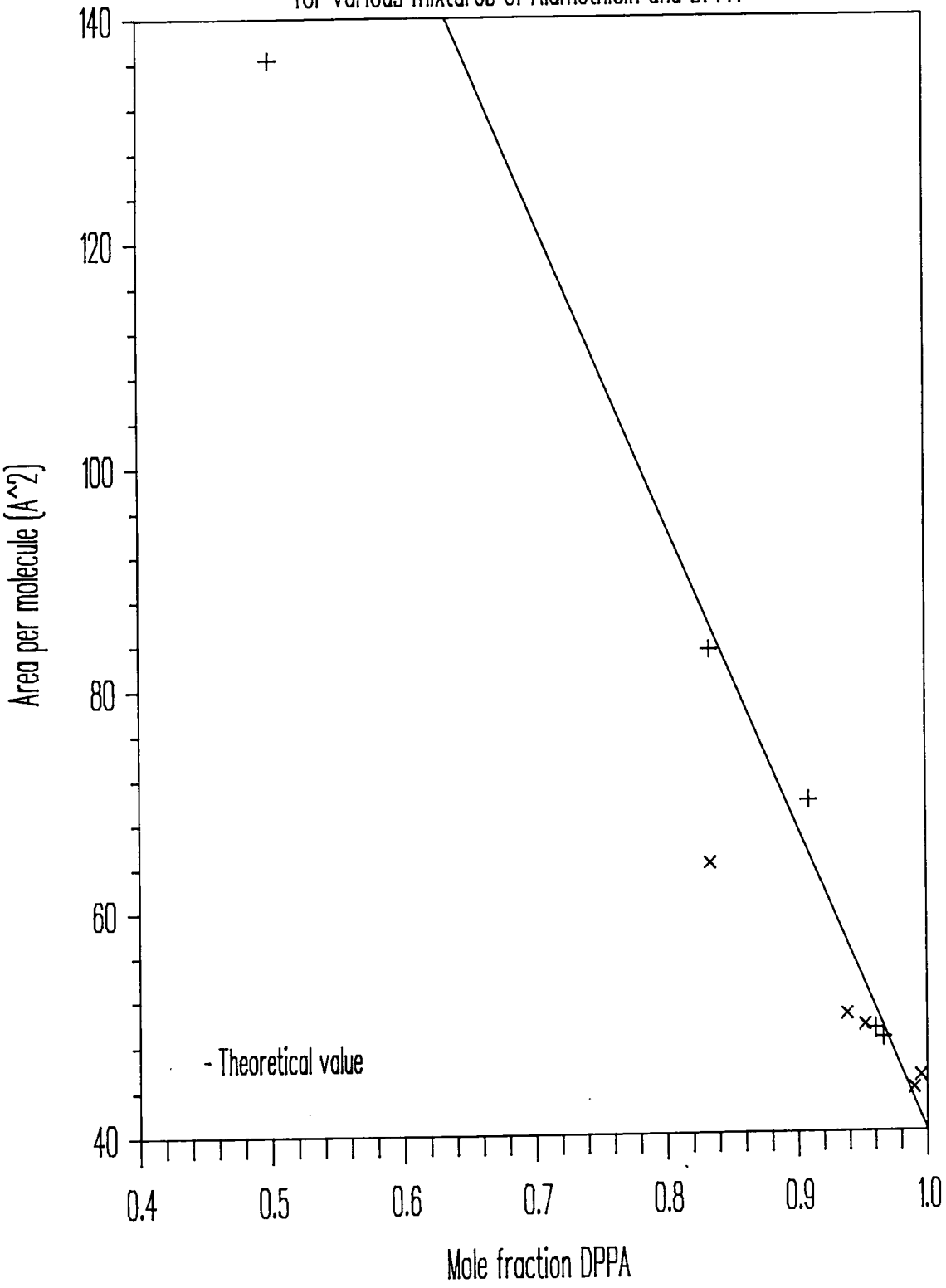

Plot 5-19: Area per molecule at 50 mNm^{-1} vs. mole fraction DPPA for various mixtures of DPPA and Alamethicin.

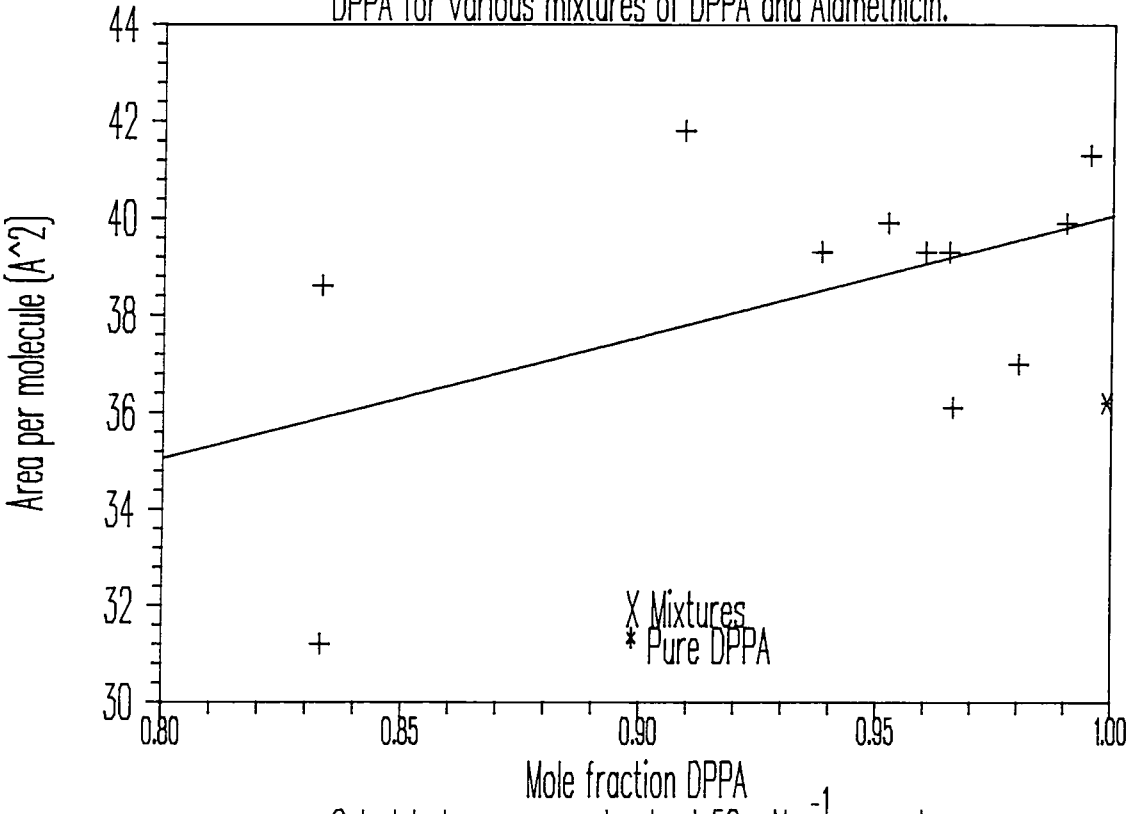

Plot 5-20: Calculated area per molecule at 50 mNm^{-1} vs. mole fraction DPPA for various mixtures of DPPA and Alamethicin.

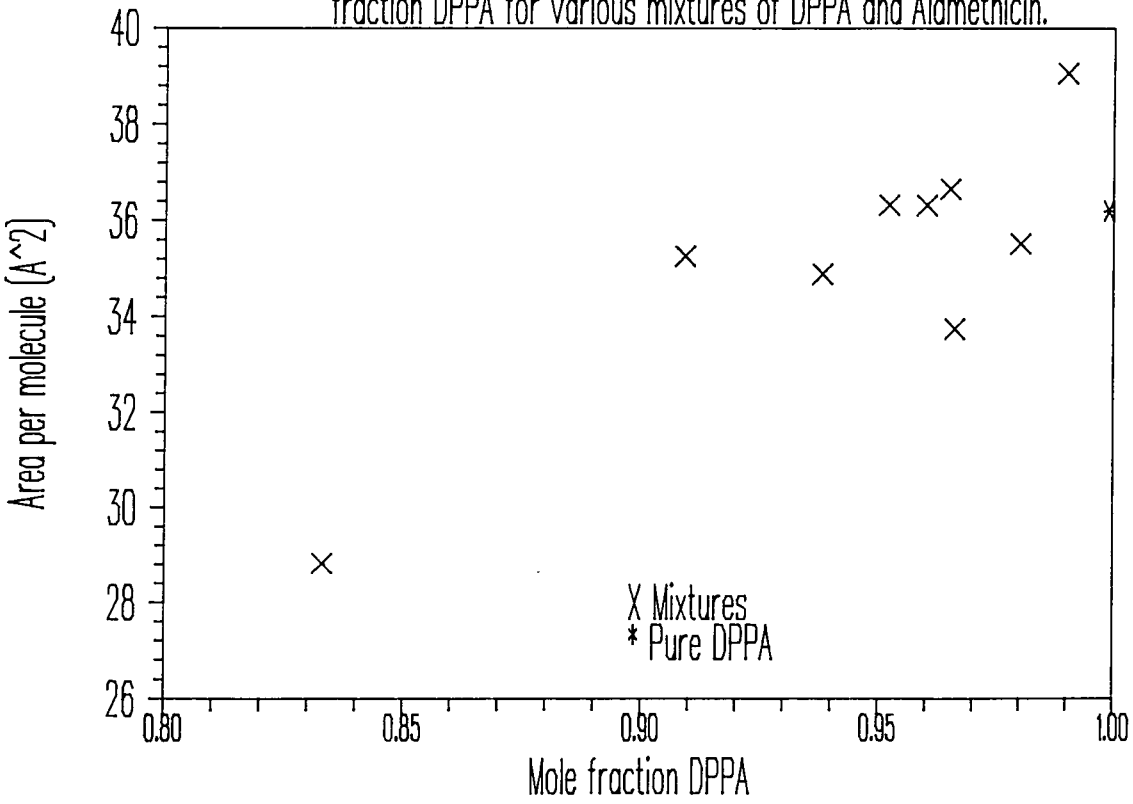

5.6.3 A mixture of DL-α-DPPA/DOPA/Alamethicin

Only one isotherm was run on this combination in a ratio of 24:6:1 DPPA:DOPA:Alamethicin on a Fromherz trough. The area was stable at 28 mN m^{-1} with a drift of ~1 $Å^2$ per molecule per hour (0.11 cm^2 per min).

There is little which can be said of one isotherm taken on the Fromherz trough for a single mixture of a complex system. It is only really of use for choosing a suitable deposition pressure. It did seem to be a very stable mixture and suitable for deposition at a surface pressure of 30 mN m^{-1}.

		Pressure mNm^{-1}		Area per molecule Å^2				
Isotherm number	Starting apm	Inflect. point	Collapse pressure	Initial pick-up	Close packed	at 10 mNm^{-1}	at 25 mNm^{-1}	at 50 mNm^{-1}
61	150	33	41.5	60	38.2	37.8	33.3	18.6

Table 5(xiii) Results for 24:6:1 DPPA:DOPA:Alamethicin on a Fromherz trough

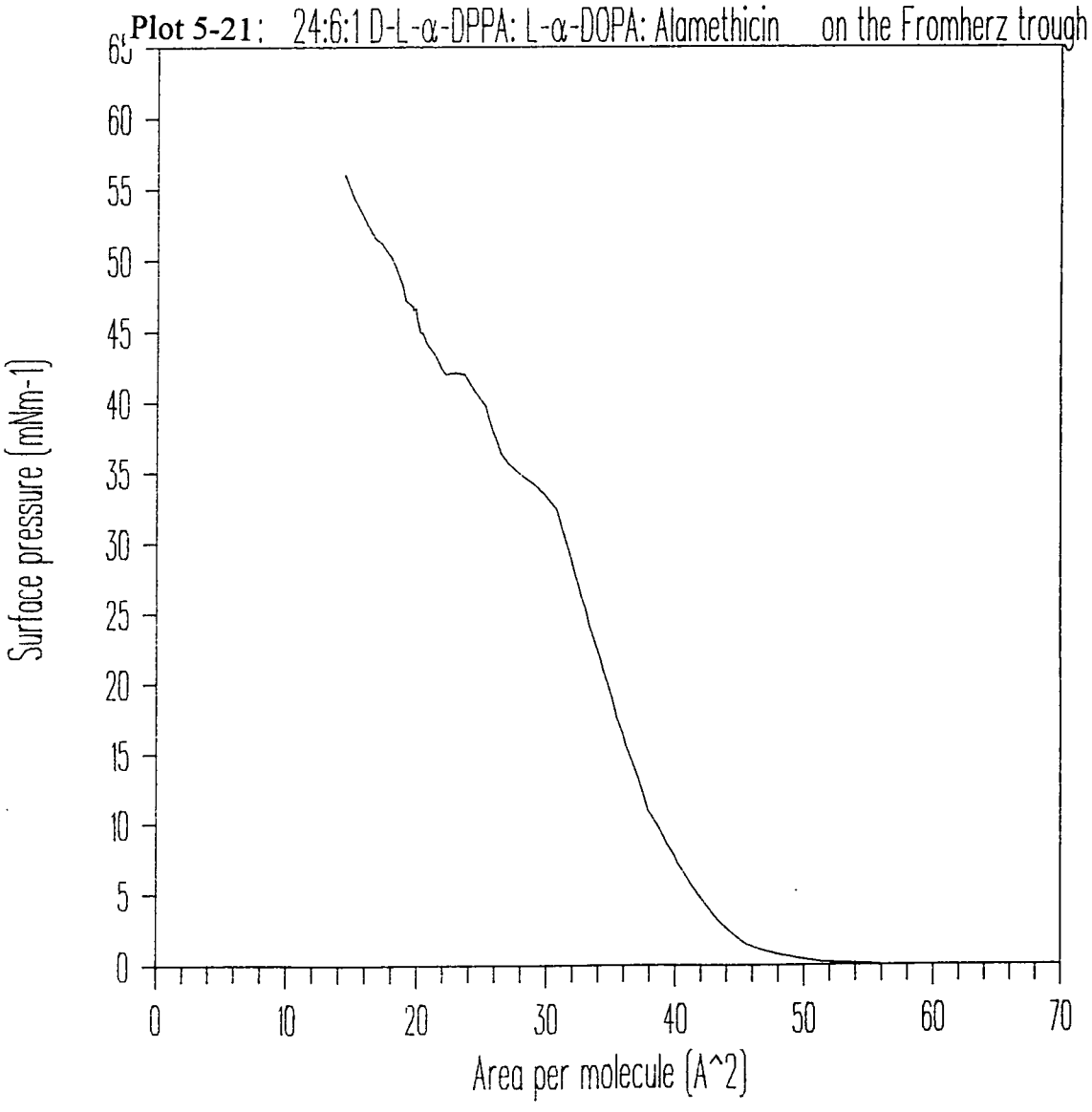

5.7 SUMMARY OF MONOLAYER STUDIES

DPPA isotherms were re-producible and the data correlated well with literature values. DPPA has well defined regions in the π-A isotherm which correspond to the equivalent phases in a three dimensional system. When held at a surface pressure of 30 mN m^{-1} it is stable. There is a strong possibility that it is crystalline in the solid phase of its response to pressure.

The surface potential data suggests that DPPA responds to the movement of the barriers in a detectable manner, probably due the alignment of the alkyl chains at a high angle to the interface. This effect is not completely dissipated on allowing the monolayer to relax and may form the basis of evidence that the use of pre-conditioning does anneal the monolayer.

The isotherms of DOPA monolayers do not exhibit distinct phase changes. The monolayer remain in a state which is analogous to a fluid in three dimensions. It is not stable when held at surface pressures of either 25 or 27 mN m^{-1}.

Mixtures of DPPA in DOPA exhibit a negative deviation from ideal mixing. This indicates that DPPA is miscible in DOPA to some extent but not ideally so,and aids the formation of closer packed structures. However, mixtures of DOPA in DPPA show only a small positive deviation from ideality. The isotherms of such mixtures show two collapse pressures, one at that found for pure DOPA and the other at that of DPPA. DOPA appears to be ejected from the monolayer at its collapse pressure. The conclusion reached is that DOPA is immiscible in DPPA. At a surface pressure of 30 mN m^{-1} a 4:1 mixture of DPPA:DOPA was found to be stable enough for deposition.

Alamethicin is probably in the same conformation on the LB trough (pre-dominantly α-helical) as in solution and in crystal form. If it is in this conformation then it rests on the surface of the water with the axis of its helixes parallel to the interface. It was concluded, from the isotherm and surface potential data, that if its collapse pressure is exceeded then some of the material is lost from the monolayer into the bulk medium. An alamethicin monolayer held at 23 mN m^{-1} was not completely stable but would allow deposition to proceed if required.

From isotherm data it was concluded that mixtures of alamethicin in DPPA are immiscible. Both hysteresis of the π-A isotherm and the surface potential showed that at the collapse pressure of alamethicin it is ejected from the mixed monolayer and some of it is permanently lost into the bulk medium. At a surface pressure of 23mN m^{-1} a 27:1 mixture of DPPA:alamethicin is very stable.

CHAPTER 6

RESULTS AND DISCUSSION OF DEPOSITION AND FTIR OF LIPIDS

6.1 : INTRODUCTION TO THE DEPOSITION AND FTIR OF DPPA

Before examining the FTIR spectra of DL-α-DPPA (DPPA) as Langmuir-Blodgett films it is useful to consider the spectra of DPPA in solution and as films cast from solution. These will give a range of background spectra for the lipid for each of the FTIR techniques to be employed after LB deposition.

It would have been preferable if these background spectra could have arisen by deposition from different solvents, to see whether the solvent affected the orientation and conformation of the molecules. Apart from chloroform DPPA was found to have a low solubility in the solvents tested. These included acetone, carbon tetrachloride and iso-propyl alcohol.

There are a variety of FTIR techniques involved in the recording of the spectra for this chapter (see chapter 4 for details on the acquisition of the spectra and the techniques) and many different samples. Therefore, the data will be presented in sections which correspond to the sample preparation rather than the regions of the spectra which were used in chapter 3. Within each section the both the FTIR spectra and the LB deposition results and analysis will be presented.

6.2 : FTIR TRANSMISSION SPECTRA OF A VARIETY OF NON-LB DPPA SAMPLES

6.2.1 Results

Plots 6-1 & 6-2 are both FTIR transmission spectra of DPPA deposited from chloroform onto calcium fluoride plates. The spectra were obtained as described in section 2.5.2. Plots 6-1A & 6-2A are enlargements of the carbonyl regions of the spectra. The convention is as for similar spectra shown in chapter 3. The solid lines are the composites of the peaks fitted to the experimental data. The original spectra are shown as short dotted lines and the other peaks shown are the component peaks used to produce the fitted curve. In the right hand corner of each plot is a deconvoluted spectrum of the region using the procedures given in section 3.2.2.C. Table 6(i) gives the wavenumbers and widths of the peaks fitted to each of the carbonyl bands in this section.

Plots 6-3 A&B show the change in the FTIR spectrum of a film of DPPA cast from chloroform as the temperature changes. Plots 6-3 C&D show the same spectra but in more detail. The solid line in each of these plots is the spectrum of the sample obtained at 20 $^{\circ}$C, the dashed line is the spectrum taken at 69 $^{\circ}$C and the dotted line is the spectrum of the same sample at 32 $^{\circ}$C after the temperature rise to 69 $^{\circ}$C

A powder FTIR spectrum of DPPA was obtained (plot 6-5). The sample was prepared by compressing DPPA crystals, as obtained from Sigma UK, between two calcium fluoride plates and then removing one of the plates to avoid interference fringes being recorded in the spectrum.

Plot 6-1 cast film of DPPA on a CaF2 plate

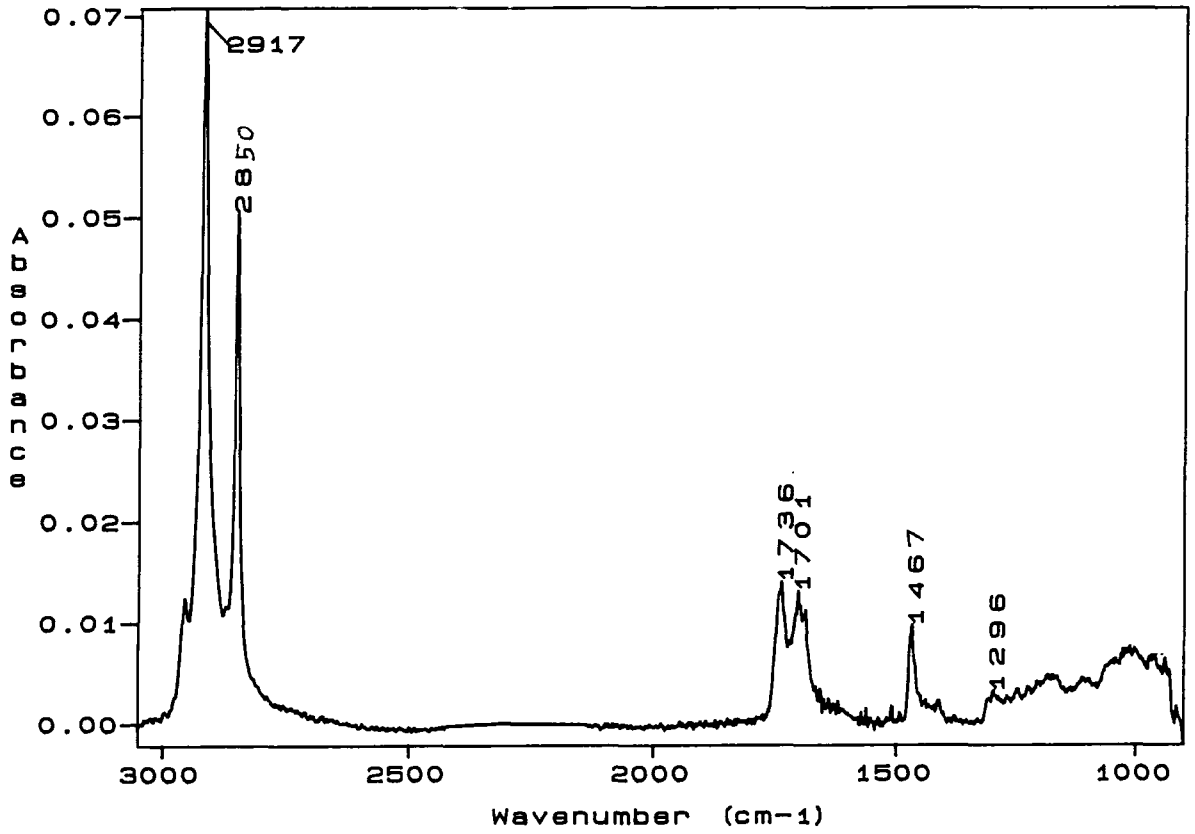

Plot 6-2 cast film of DPPA on a CaF2 plate

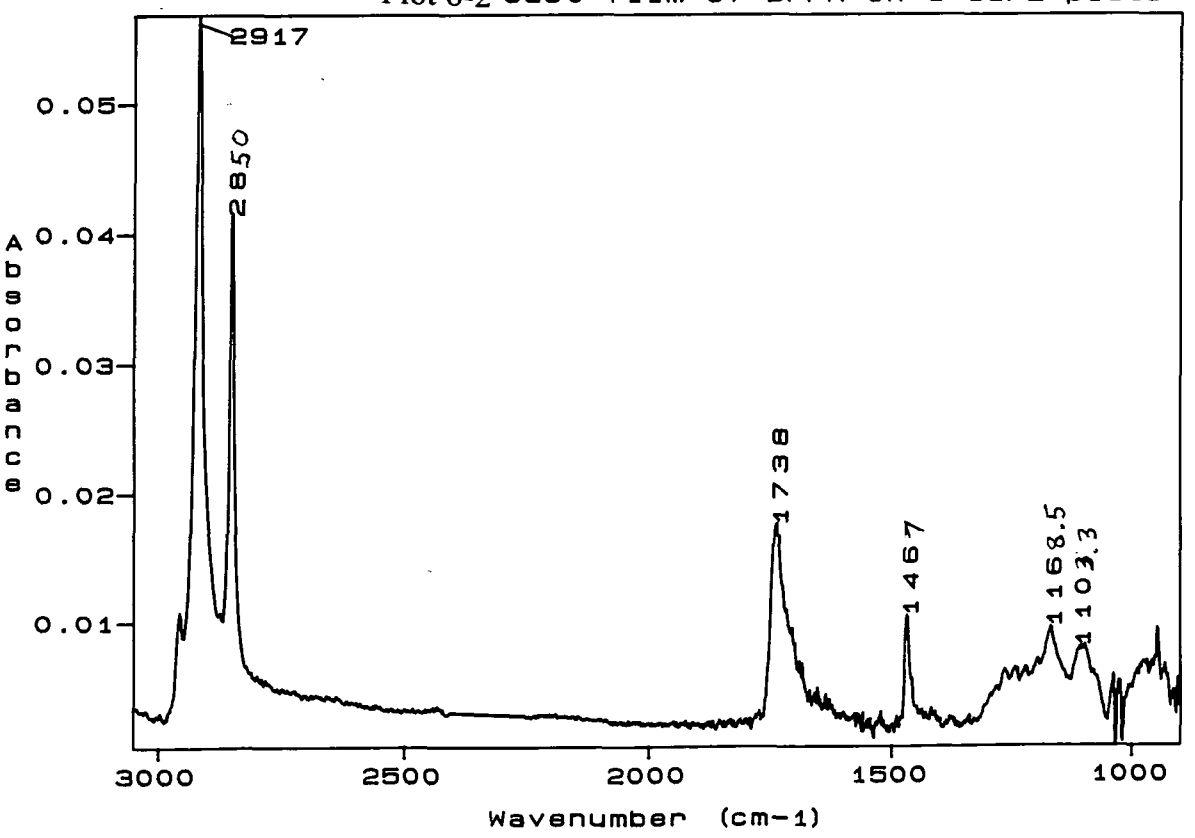

Plot 6-1A: Curve fit for carbonyl region of plot6-1

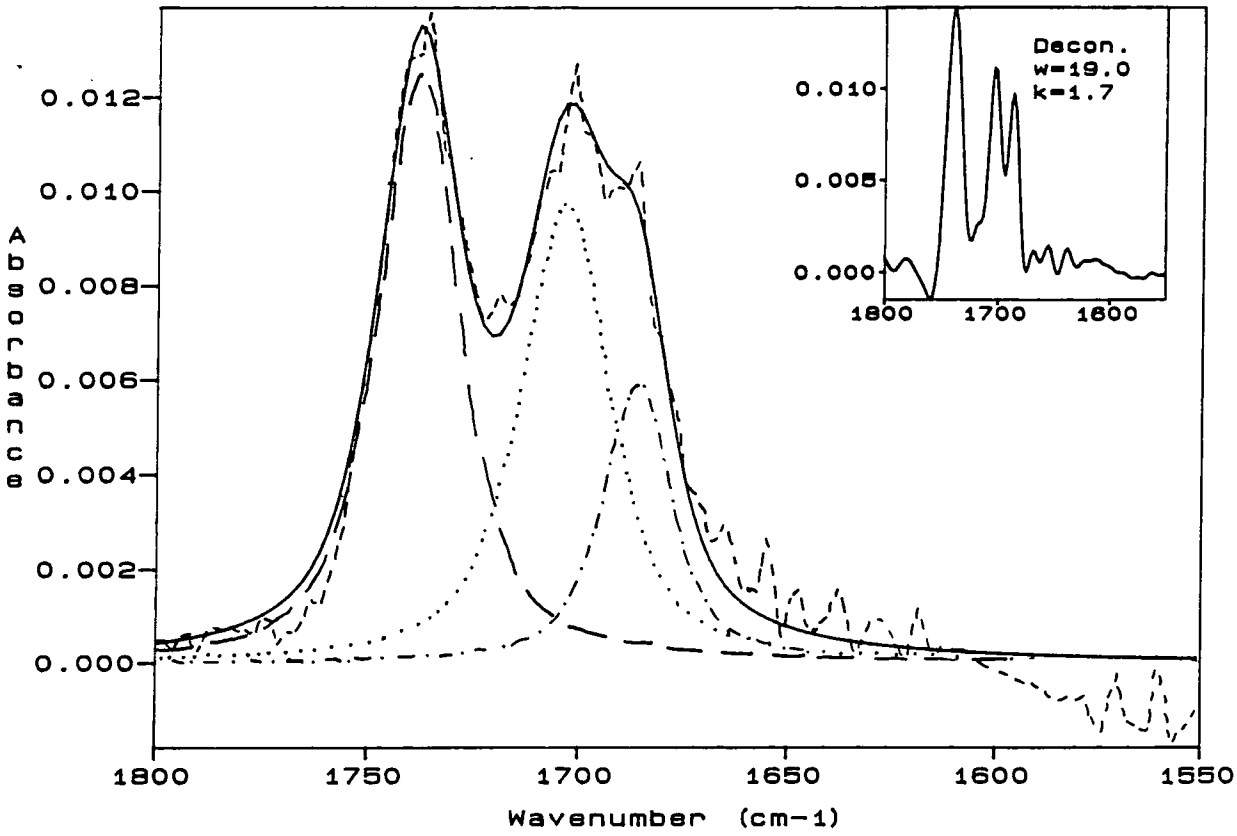

Plot 6-2A: Curve fit for carbonyl region of plot6-2

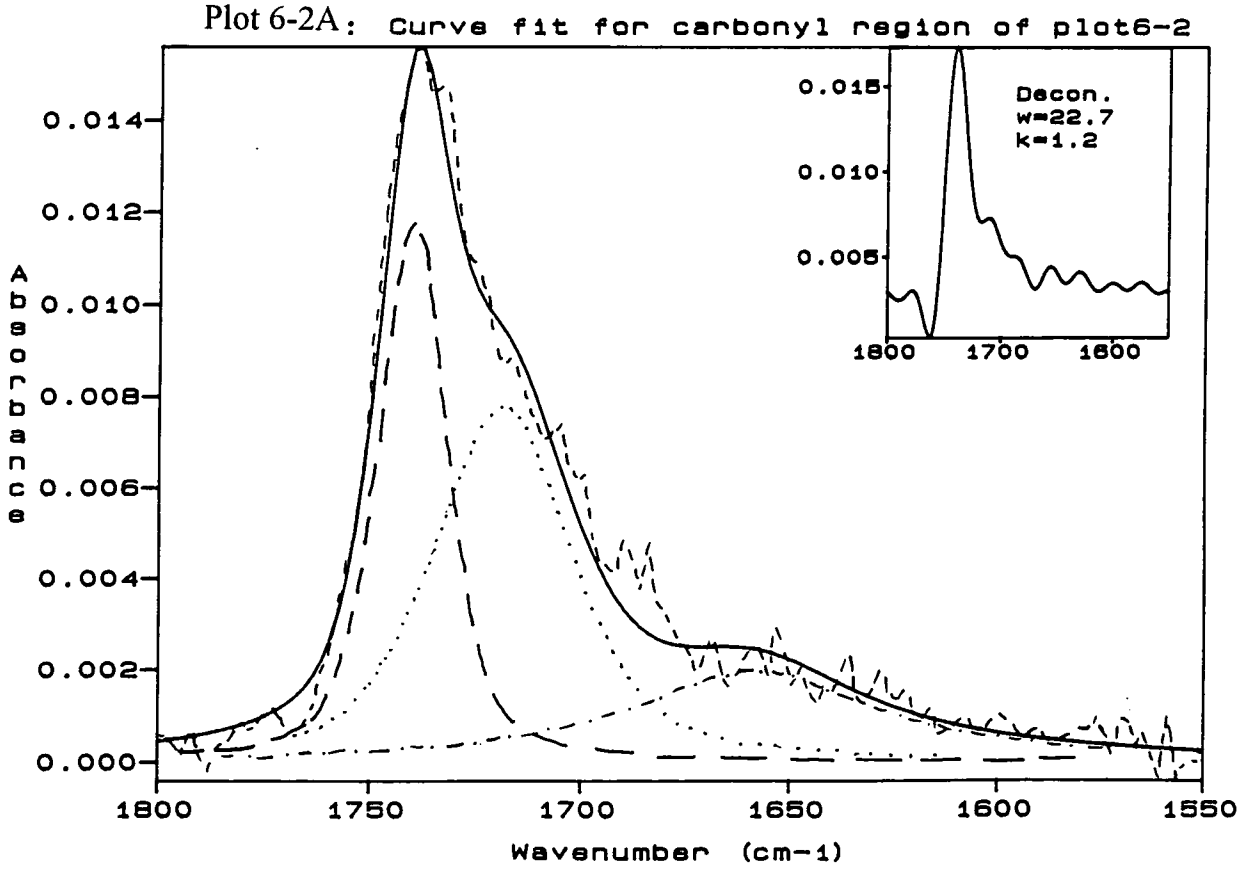

Plot 6-3A: Cast film of DPPA on CaF2 : Temp. = 20 °C

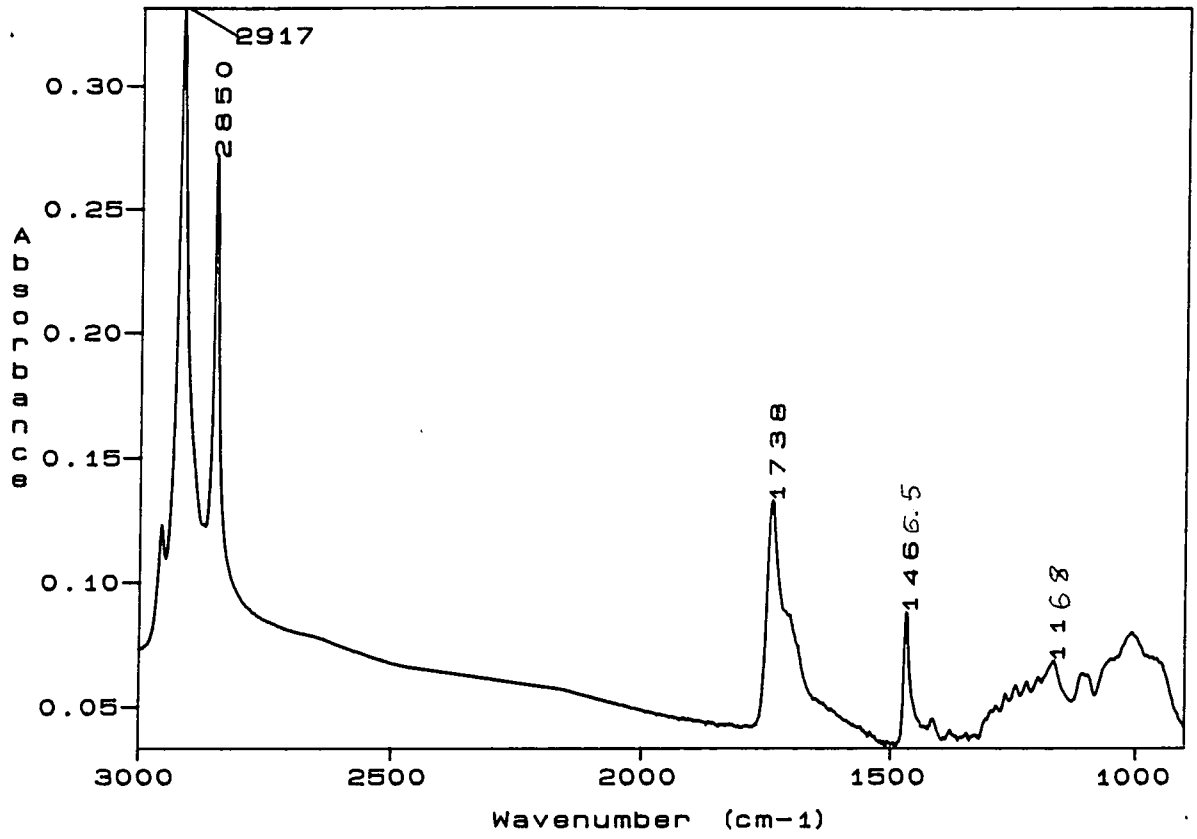

Plot 6-3B: Same sample of cast DPPA : Temp. = 69 °C

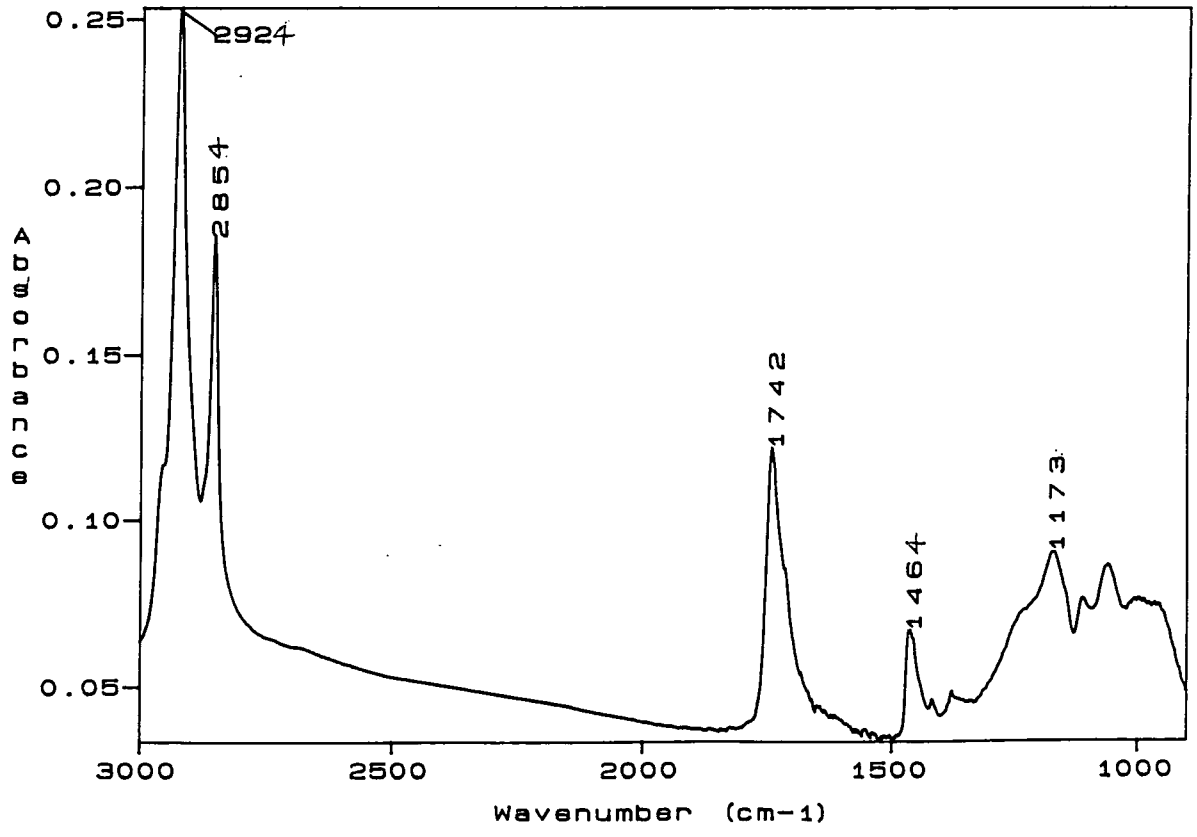

Plot 6-3C: DPPA cast from chloroform followed with temperature

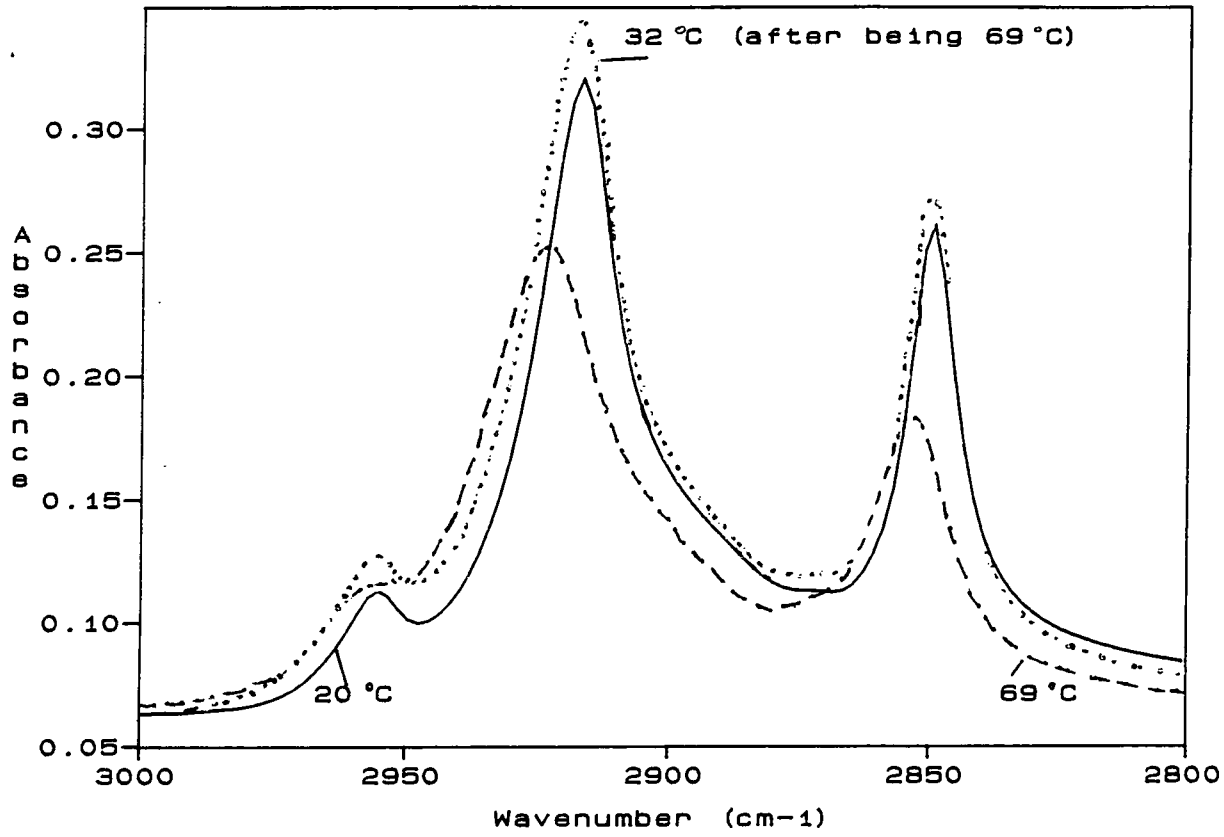

Plot 6-3D: DPPA cast from chloroform followed with temperature

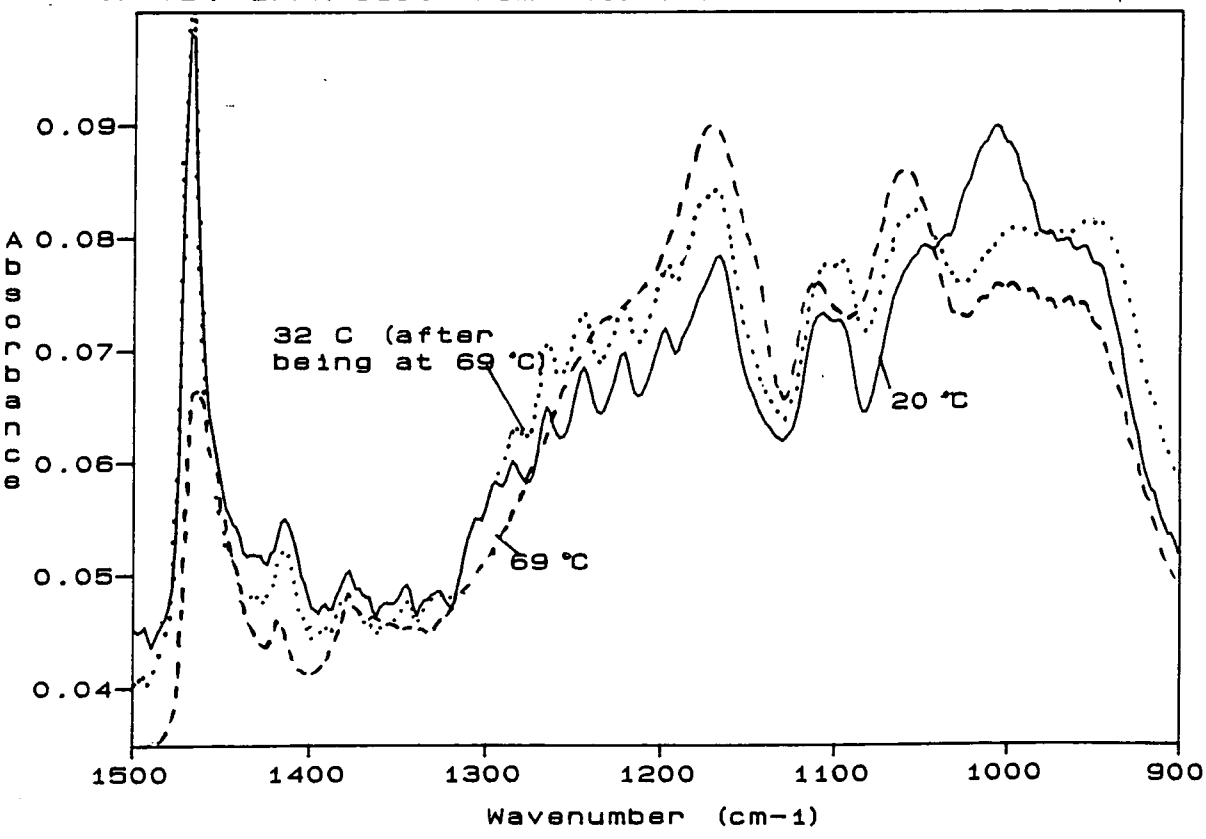

Plot6-4 : The position of the CH2 anstisymmetric peak for DPPA vs temperature

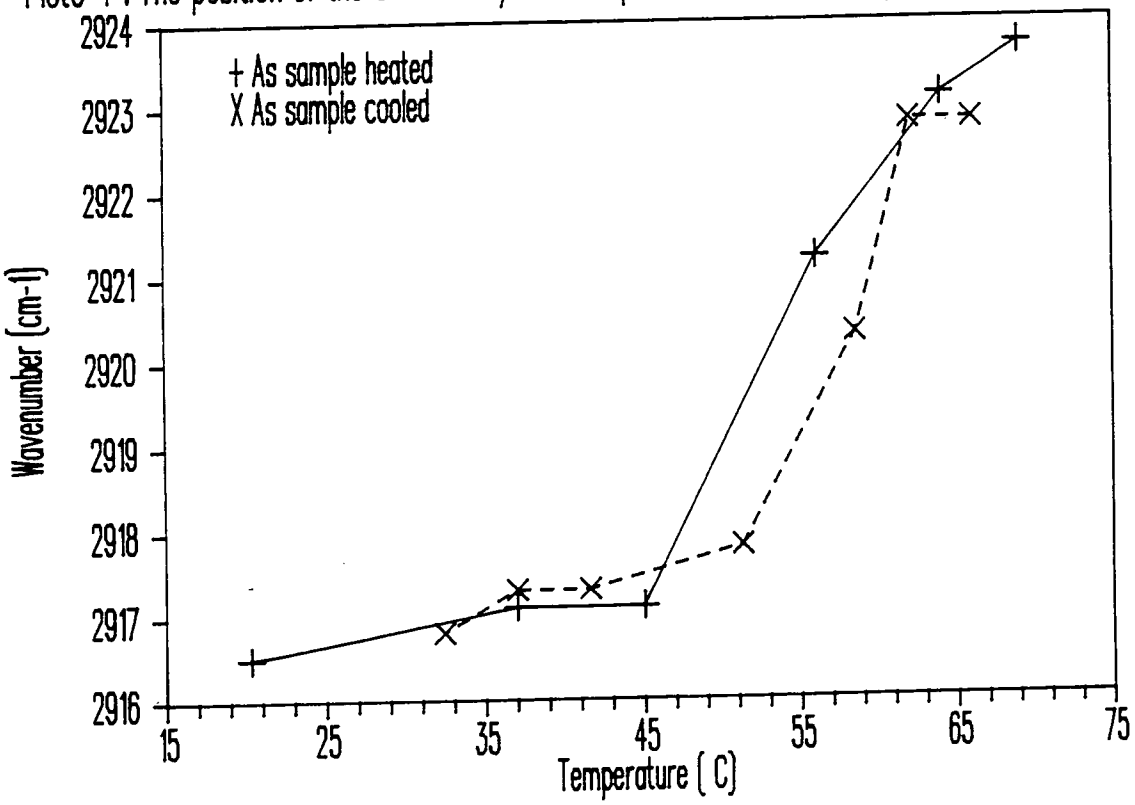

Plot 6-5: Powder spectrum of DPPA by transmission

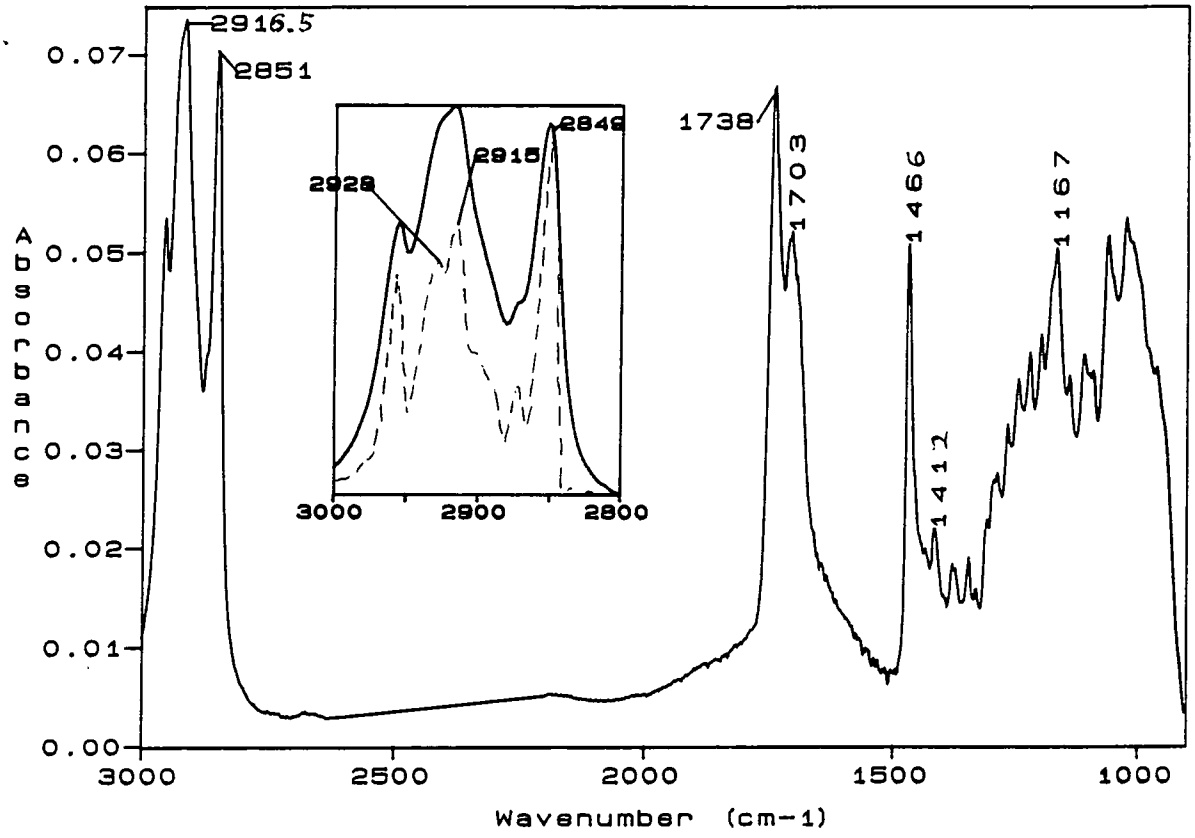

Plot 6-6: DPPA in chloroform solution

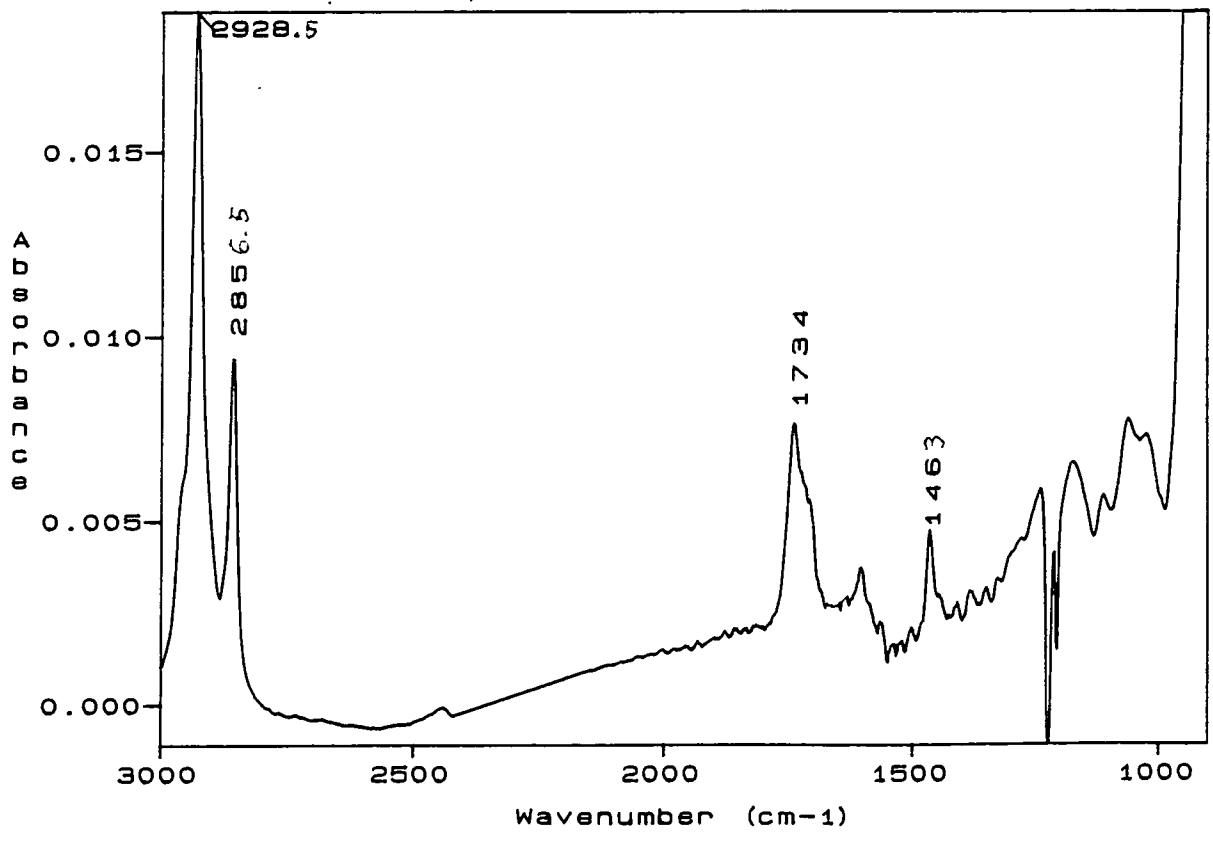

Plot 6-5A: Curve fit for carbonyl of DPPA powder spectrum

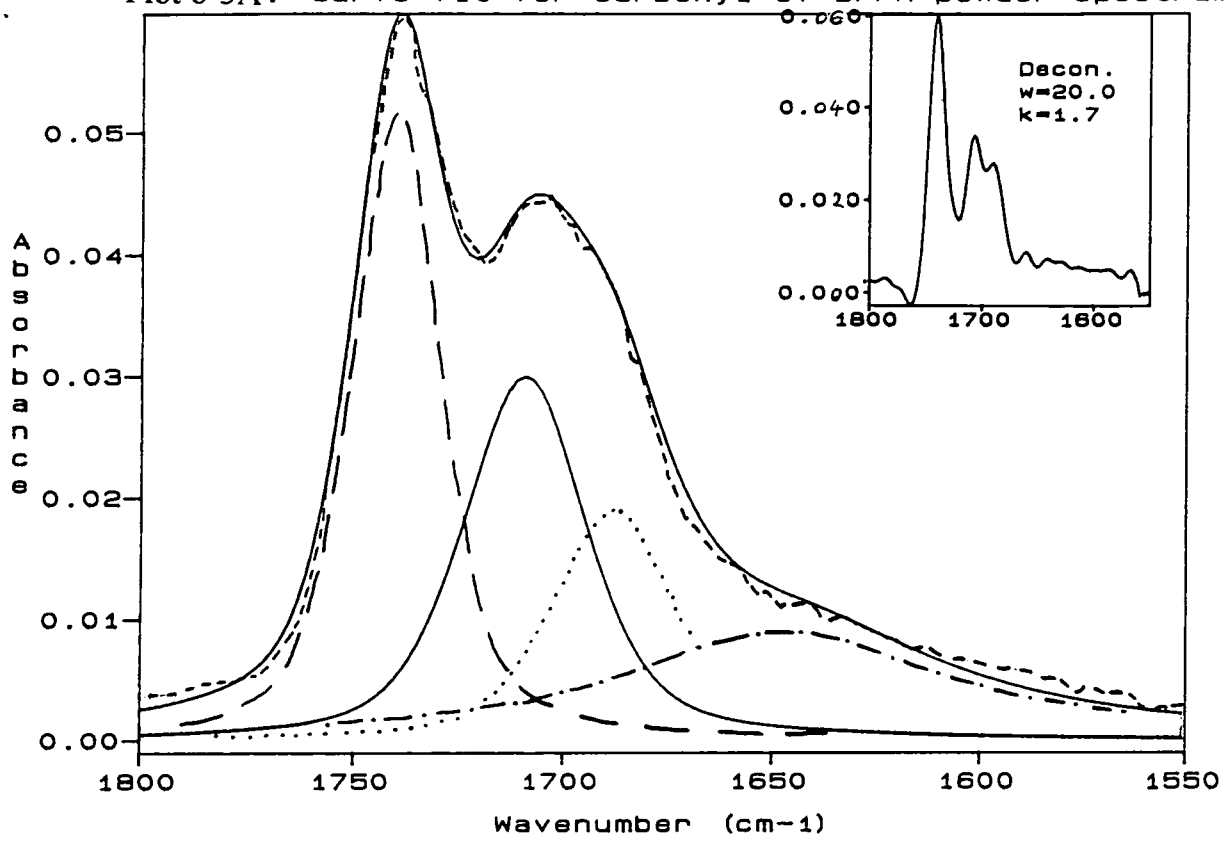

Plot 6-6A: Curve fit for carbonyl for DPPA in chloroform

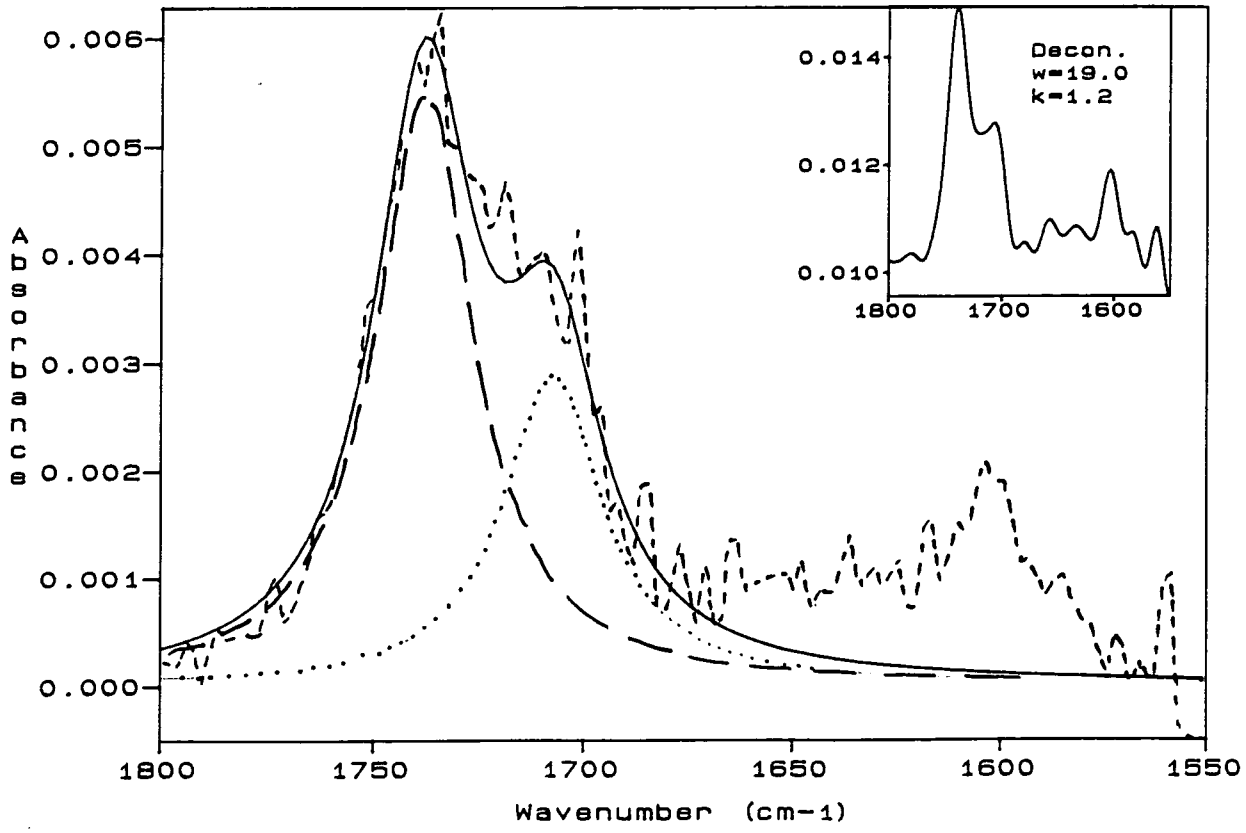

6.2.2 Analysis and discussion of results obtained via FTIR transmission spectroscopy (plots 6- 1 to 6).

(A) 3000 - 2800 cm^{-1} : The CH stretching vibrations.

The wavenumbers of the CH_2 stretching vibrations (2917 and 2850 cm^{-1} for the antisymmetric and symmetric stretching vibrations respectively) for both the cast films at ambient temperatures, and the powder spectra (plots 6-1,2,3 &5) indicate that DPPA is below its phase transition temperature (see section 3.2.4). This is consistent with the value of 67 °C reported by Liao and Prestegrad[146] for the phase transition temperature of DPPA vesicles at pH 6.5. Since DPPA is well below its phase transition temperature at room temperature then the alkyl chains must be in an all trans configuration.

In chloroform the wavenumbers of the two peaks increase to 2928.5 and 2856.5 cm^{-1} respectively. An experiment was tried to see if increasing the temperature led to n increase in these wavenumbers. Unfortunately the chloroform evaporated at about 40 °C and the spectrum was unchanged.

Plots 6-3&4 show the effect of raising the temperature, of a film cast from chloroform, above the phase transition. Above the phase transition temperature (plots 6-3 B&C) the wavenumbers of the two CH_2 stretching modes increase to 2924 and 2854 cm^{-1}. The full width at half height (FWHH) also increases at higher temperatures. E.g. for $\nu_{as}(CH_2)$ the FWHH increases from 22 cm^{-1} at 20 °C to 32.5 cm^{-1} at 69 °C. Whereas the height of the same peaks decreases from 0.25 to 0.19 absorption units. Either the increase in wavenumber or width of the peaks can be used to follow the phase transition.

Plot 6-4 shows the variation of the wavenumber of the $\nu_{as}(CH_2)$ peak with temperature for the film of DPPA cast from chloroform. The plot shows the characteristic rise for a lipid[92] of 4 cm^{-1} at the phase transition temperature, this change is reversible. However, this occurs between 55 and 60 °C which is below the phase transition temperature given for DPPA vesicles[146]. This discrepancy could be due to the difference in nature of the two samples. It is possible that when molecules of DPPA are constrained as vesicles that more energy is required for the formation of gauche conformers. Another explanation may be that the temperature measured, in the results given here, does not correspond to the temperature of the DPPA which is within the beam. Figure 2(g) shows the equipment arrangement for this experiment. The IR beam passes through the centre of the cell shown but the temperature is measured at the outside of the cell. As the temperature of the phase transition was much higher than room temperature, it is possible that there was a temperature gradient between the probe and the part of the cell where the IR beam passed through. As the objective of this experiment was to observe the FTIR spectrum of DPPA above its phase transition it was felt that it was not necessary to redesign the equipment to ensure that the measured and sample temperatures were identical.

In plot 6-5 the peak due to the antisymmetric stretching mode of the methylene groups is asymmetric (inset plot 6-5, dashed line is the F.D. with w=13.8 and k=1.8). There is definitely a large peak present, centred at ~2927 cm^{-1} and possibly a second peak which is seen as a shoulder on the lower wavenumber side of the $\nu_{as}(CH_2)$ peak. These peaks may be present in the cast film spectra (plot 6-3c) but are not as intense. The large peak at 2927 cm^{-1} arises from a Fermi resonance between the $\nu_s(CH_3)$ vibration and the first overtone of the $\delta(CH_3)$ mode (Swalen et al[147]). The direction of this transition moment is parallel to the C-CH_3 bond. The shoulder on the $\nu_{as}(CH_2)$ peak is due to another Fermi resonance. This is an interaction between the $\nu_s(CH_2)$ mode and the first overtone of the CH_2 scissoring mode. The direction of this transition moment is parallel to the H-C-H plane.

Description	Plot no.	No peaks fitted	wavenumber (cm^{-1})	FWHH (cm^{-1})	absorption amplitude	integrated intensity (cm^{-1})	% Lorentzian
cast from chloroform	6-1a	3	1738 1703 1685	25 27 20	0.0126 0.0098 0.0060	0.381 0.324 0.159	70 70 70
cast from chloroform	6-2a	3	1740 1719 1659	20 40 70	0.0118 0.0078 0.0020	0.283 0.358 0.190	50 50 100
" at 20 °C	6-3a	3	1738 1710 1636	25 62 100	0.070 0.040 0.009	1.97 2.66 0.67	50 50 100
" at 69 °C	6-3b	3	1743 1715 1636	27 45 100	0.070 0.040 0.004	2.10 2.10 0.53	50 50 100
as a powder	6-5a	4	1741 1710 1689 1647	27 35 35 95	0.052 0.030 0.019 0.009	1.63 1.29 0.78 1.15	50 50 50 100
chloroform solution	6-6a	2	1738 1715	30 30	0.0055 0.0029	0.223 0.118	100 100

Table 6(i) : Data for the peaks fitted to the band arising from the carbonyl stretching mode for FTIR spectra of DPPA

Band position in wavenumbers (cm^{-1})				
Cast film plot6-1	Cast film plot6-2	Cast film at 69 °C (6-3b)	As a powder plot6-5	In chloroform solution (6-6)
1467.0	1466.5	1464.0	1466.0	1463.0
1410.4	1414.0	1417.5	1412.0	1408.0
	1377.5	1378.5	1375.5	1384.5
	1345.5		1344.5	1350.5
	1326.5		1329.5	1328.5
	~1305		1308.5	1301.0
1296.0	1285.5		1290.0	1280.5
1267.5	1266.0		1267.0	
1246.0	1244.5	sh ~ 1240	1245.0	
1223.0	1222.0		1223.0	
1205.5	1199.0		1198.5	
1170.5	1168.0	1173.0	1167.5	
			1140.5	
1102.0		1113.0	1111.5	1112.5
			1092.0	
		1061.0	1063.5	1061.5
			1023.0	1025.0

Table 6(ii) : Peak positions for transmission spectra of DPPA in the region 1500-900 cm^{-1}

(B) 1800 - 1600 cm^{-1} : The carbonyl stretching modes

Plots 6-1&2 are both transmission spectra of films of DPPA which have been cast from chloroform. Whilst the spectra in the region discussed above (3000-2800 cm^{-1}) are indistinguishable there are plainly differences in the structure of the band due to the carbonyl stretching vibration. The structure of this band as seen in plot 6-1 was the obtained for almost all of the films cast (see plots 6- 13&8). Indeed spectra for cast films which were similar to plot 6-2 were recorded only twice - in the example shown and also on the day of the temperature study (plots 6-3). No difference between the preparation of the samples could be discerned.

The spectrum of the crystalline DPPA (plot 6-5) shows a structure which is closest to that of cast film 6-1. Whereas, in the spectrum of DPPA recorded in chloroform solution the band due to the carbonyl stretching vibration is closer in form to that seen in plots 6-2&3.

The fitting of a simulated curves to the experimental data was undertaken to aid interpretation. For most of the spectra it was necessary to add a small peak into the simulations at ~1650 cm^{-1}, this is due to the bending mode of OH in water. Even after evacuation it was not possible to remove all of the water. The only spectra where small corrections for water were not required were the first cast film (plot 6-1A) and the chloroform solution (plot 6-6A). The fact that there was very little water in the cast film 6-1 is probably not relevant to the carbonyl band structure as other cast films with similar shaped carbonyl bands (plots 6- 8A&13A) did have water present. The noise on plot 6-1A is possibly obscuring a small peak due to the bending mode of OH in water.

Three synthetic peaks were required to obtained a satisfactory fit to both the carbonyl bands of the cast film 6-1 and the powder spectra. Two peaks are enough for the simulation of the carbonyl bands of the cast films 6-2&3 and the solution of DPPA in chloroform (plot 6-6A).

The two peak structure seen for the carbonyl stretching vibration for DPPA in cast films 6-2&3 and in chloroform can be correlated with the analysis in chapter 3 (section 3.2.4.B). The peaks at ~1740 and ~1717 cm^{-1} correspond to those found at ~1740 cm^{-1} and ~1728 cm^{-1} for egg lecithin in chapter 3. The assignment given in chapter 3 was that the higher wavenumber (1744-1727 cm^{-1}) peak was due to a trans conformation of the ester group. The peak with the lower wavenumber (1728-1716 cm^{-1}) was assigned to a gauche conformation about the ester group (see figure 3(j)) which is possibly solvated.

The three peak structure seen in the carbonyl band for DPPA as a crystalline powder and most commonly found in films cast from chloroform is not so easily explained. The closest to this pattern of peaks for a phospholipid is found in the literature is in a paper by Mushayakarara et al[148]. They examined the Raman spectrum of DPPC dihydrate, the crystal structure of which has been determined by Pearson and Pascher[149]. A bilayer packing arrangement was found with two DPPC molecules per asymmetric unit (A & B) in the crystal structure. Mushayakarara et al[148] reported that three peaks were present in the region 1800-1650 cm^{-1} in the afore mentioned spectrum. The wavenumber displacement of these were 1743, 1730 & 1716 cm^{-1}. The assignment they made was that the peak a 1743 cm^{-1} was due to the carbonyl stretching vibration on the sn-1 chain of molecule A. This ester group is in a trans conformation and is deepest into the hydrophobic region of the bilayer of all the four possible carbonyls on molecules A&B. The peak at 1716 cm^{-1} was assigned as arising from the stretching vibration of the carbonyl situated on the sn-2 chain of molecule B. This is the carbonyl which is closest to the phosphate groups in the crystal structure. The ester group associated with this carbonyl is in a gauche configuration. The peak at 1730 cm^{-1} was assigned as an overlap of peaks arising from the stretching modes of the carbonyls situated on the sn-1 chain of molecule B (trans at the ester group) and the sn-2 chain of molecule A (gauche at the ester group). The environment of both these two carbonyls, due to the proximity of the hydrocarbon chains and the phophatidyl choline

group, was similar and intermediate between the other two carbonyls. This assignment was made because the peak at 1730 cm^{-1} was broader than the other two and of intermediate wavenumber displacement. In a paper Mushayakarara and Levin[99] published later that year they had examined a range of lipids and found that only crystalline 1,3-dipalmitoylglycerol (DPG) gave rise to a broad peak at less than 1720 cm^{-1}. They assigned this peak (at 1708 cm^{-1}) as the stretching vibration of a carbonyl which was hydrogen bonded to a hydroxyl group.

From the above discussion it is likely that the structure of the carbonyl stretching vibration band seen in plots 6- 1A,5A, 8A&13A arises from the inequivalence of carbonyl groups within a crystalline structure. The low value for the wavenumber of the smallest peak (1689-1674 cm^{-1}) for all of these is highly indicative of strong hydrogen bonding. This could either be to water or to the P-OH groups of another molecule. If it were to the POH groups then a change in the spectrum in the region 1040 - 910 cm^{-1} of the spectra (where there should be strong absorption due to the PO stretching vibration in POH - see table 3(i)) would be expected. There appears to be no significant changes in this region between the spectrum of powdered DPPA (plot 6-5) and DPPA in chloroform (plot 6-6). For the two cast films (plots 6-1&2) the region around 1000 cm^{-1} has a low signal to noise ratio and it really is not possible to draw any conclusions from these spectra. The crystal structures which are known for phospholipids (e.g. DPPC and DMPE) have bilayer structures[14] with clearly defined positions for the headgroups and the acyl chains which would not allow hydrogen bonding between them. From the above considerations it is likely that the peak at ~1685 cm^{-1} is due to a stretching vibration of a hydrogen bonded carbonyl, probably to water.

Without the crystal structure of DPPA it is very difficult to make further assignments. It really is only possible to speculate on the nature of the environment of the peaks. Based on the findings of Blume et al[54&55] and Levin et al[99-101&148] it would seem likely that the peak at 1743-1738 cm^{-1} is due to the vibration of a carbonyl attached to an ester group in the trans

conformation and therefore closer to the alkyl chain of the neighbouring chains. The peaks found at 1719 - 1710 cm^{-1} would arise from the vibration of a carbonyl attached to an ester in the gauche conformation. The extremely low value for the wavenumber of this peak compared to literature values[99] (see above) for other phospholipids is probably due to the increased electronegativity of the phosphatidic acid group compared to phosphatidylcholine and phosphatidylethanolamine. The peak at ~1685 cm^{-1} could also be due to a gauche conformation at the ester group but one which is hydrogen bonded.

There is an increase of 5 cm^{-1} in the position of each of the two carbonyl peaks found for sample 6-3 on raising the temperature from 20 to 69 °C. This is due to the internal environment of the carbonyl changing[150]. There is one further possibility which should be considered for the assignment of the peak centred at 1685 cm^{-1}. This is that it arises from a vibration of the POH group. Colthup[151] reports that in phosphinic acids (with one OH group) a broad band appears at 1700-1630 cm^{-1}. However, he states that this band is not generally present in phosphonic acids where there are two OH groups. Daasch and Smith[156] report the IR spectra of a variety of phosphinic acids. The peak at 1700-1630 cm^{-1} has a FWHH of at least 100 cm^{-1}. It therefore seems unlikely that the peak centred at 1685 cm^{-1} is due to a POH vibration.

(C) The spectral region 1500 - 900 cm^{-1}

The first peak in this region is centred at ~1467 cm^{-1} (table 6(ii)) for the cast films and powder spectra of DPPA. This arises from the scissoring mode of the CH_2 groups. Assignments have been made[31] for the relationship between the position of this peak and the packing of phospholipids in aqueous assemblies. The wavenumber found is indicative of a hexagonal crystal structure reported by Fookson and Wallach[152]. This is confirmed by the position of the peak due to the CH_2 rocking mode which is at 721 cm^{-1} (not shown). The crystal structure is definitely not orthorhombic as this would produce a double peak at 1472 and 1463 cm^{-1} for the CH_2 scissoring mode[31]. This is due to the fact that in an orthorhombic crystal structure the hydrocarbon chains of two adjacent molecules are at 90° to each other[24].

There are no detectable differences in the peaks due to the CH_2 scissoring vibration between the two cast film samples 6-1 and 6-2 or the powder spectrum. Therefore, it is likely that if the differences in the band due to the stretching vibration of the carbonyl group are due to a different crystal structure that the environment of the hydrocarbon chains remains constant.

The asymmetric structure of the band centred at 1467 cm^{-1} is largely due to the presence of a smaller peak at ~1450 cm^{-1}. This arises from the antisymmetric bending mode of the methyl groups.

The peak which is centred at ~1412 cm^{-1} for DPPA has been assigned as the scissoring mode of CH_2 which is attached to an oxygen atom. There are three such groups in a molecule of DPPA, two attached to the ester linkages and the other attached to the phosphatidic acid. The intensity per group of this peak is enhanced, relative to the CH_2 scissoring peak for the alkyl chains, by the proximity of the CO and PO groups[151].

The peak seen in the spectra at 1375 - 1384 cm^{-1} arises from the symmetric bending vibration of the methyl groups (known as the umbrella mode). Whilst no further analysis of this peak will take place its assignment is important for identifying the starting point of the progression bands from 1350 - 1180 cm^{-1}. The assignment for this group of peaks is that they are due to wagging modes of CH_2 on alkyl chains in the all trans configuration. The relative intensity of these peaks in hydrocarbon spectra is enhanced by the presence of electro-negative groups such as esters[31,95]. Meiklejohn et al[153] studied a series of fatty acids with chain lengths varying from 3 to 36 carbons. They found that the number of peaks in the progression was half the number of carbons in the chain. If the hydrocarbon chains had an odd number of carbons then the number of peaks in the progression series was equal to half of (the number of carbons in the chain plus one). There was no change in the positions or numbers of peaks in the progression series on going from the fatty acid to a soap, except that they were easier to identify since a peak due to the COH group (1307 cm^{-1}) was no longer present. Different soaps of the same acid produced a progression series with the same number of peaks in the same positions. For a soap with a palmitic chain (C_{15}) there were found to be eight peaks in the progression series. The positions of these peaks were[153] 1348, 1330, 1308, 1283, 1257, 1233, 1210, and 1186 cm^{-1}.

The assignment of the peaks to a progression series in the spectra of DPPA is complicated by the presence of bands due to the stretching modes of the P=O and C-O-C groups. As the progression series is only detected in the FTIR spectra of DPPA below its transition temperature plot 6-3D can be used to aid the process of assignment. From the spectrum at 69 $^{\circ}C$ (above the phase transition temperature) it can be clearly seen that there are two peaks which are not due to the progression series but are in the same region. There is a peak at 1173 cm^{-1} due to the antisymmetric stretching vibration of the C-O-C group[31] and a large shoulder to this peak at ~1240 cm^{-1} which arises from a P=O stretching mode of the phosphate (Thomas and Chittenden[154]). The position of this shoulder is consistent with the the relationship

derived by Tannenbaum et al[155] for the shift in wavelength, due to the electronegativity of the substituent groups, of the peak due to the phosphoryl stretching mode.

$$\lambda(\mu) = \frac{39.96 - \Sigma x}{3.995} \qquad \text{Eqn. 6(i)}$$

Where : $\lambda(\mu)$ = wavelength in μm of phosphoryl absorption
Σx = the sum of the phosphoryl absorption shift constants of the substituents.

The shift constants for OH and OR are 2.3 and 3.0 respectively. On substituting these values into equation 6(i) the wavelength of the P=O absorption is 8.10 μm (1235 cm^{-1} in wavenumbers).

Now the positions of the bands, due to P=O and COC absorptions, in the spectra taken at ambient temperature would be expected to be ~4 cm^{-1} lower than those found in the heated sample. Whilst the same shape and relative intensities of these peaks may differ at lower temperatures, it would seem appropriate to assume that the sharp peak seen at 1168 cm^{-1} in plots 6-1,2&5 is also due to the COC stretching vibration and is not part of the progression series as assumed by Lukes et al[90]. Now it is likely that the peak arising from the ν(P=O) mode at ~1240 is narrower below the phase transition temperature than above it. Thus it is possible that the peak seen at ~1245 cm^{-1} in the powder and cast film spectra is due to this vibration. However, initially it will be assumed that the peak due to P=O absorption remains a shoulder on the peak centred at 1168 cm^{-1}. If the spectrum of DPPA powder is considered, there are eight peaks between those at 1376 cm^{-1} and 1167 cm^{-1}. This fits with the expected number from Meiklejohn et al's findings[153]. The positions of the peaks are not identical but his experiments were based on soaps and fatty acids not phospholipids. The assignment of the peak at 1168 cm^{-1} to a COC stretching vibration explains the discrepancy reported by Lukes at al[90] where nine peaks were assigned to the progression series. The gradual rise in peak height of the progression series from 0.012to 0.035 is due to the P=O absorption at ~1245 cm^{-1} which is probably broad as assumed.

It is not possible to observe all of the peaks in the progression series for the cast film spectra. Although the signal levels in plots 6 - 1,2,&5 are similar, the signal to noise ratio in the spectral region 1350 - 1280 cm^{-1} is much lower for the spectra of the cast films. This is probably due to the use of a tired and worn out detector on the FTIR instrument for the recording of the spectra in plots 6- 1&2 which had been replaced by the time plot 6-5 was recorded.

At least the last five of the CH_2 wagging progression series are clearly visible in the spectrum of the film of DPPA cast from chloroform shown in plot 6-3A. When the sample is heated to beyond the phase transition temperature of DPPA the progression series is no longer present (plots 6-3B&D). This is to be expected as the progression series is only seen for alkyl chains in the all trans configuration. As the temperature falls back below the phase transition temperature the progression series re-appears in the spectrum. It is perhaps surprising that on cooling the all trans configuration is regained. A possible explanation for this is the re-crystallisation of the DPPA at lower temperatures. This occurs in lipid dispersions over a longer period of time (days). However, Cevc and Marsh[14] note that a reduction in the water content of a sample increases the rate of re-organisation of the lipids. At 10 % water they cite that diauroylphosphatidylethanolamine re-crystallises in minutes. Thus the recovery of the all trans configuration on cooling of the DPPA sample with a very small amount of water is not so surprising.

The signal to noise ratio seen in the spectrum of DPPA in chloroform is poor in the region in question. However there may also be the start of the progression series (table 6(ii)) before the strong absorption by the solvent obscures the sample spectrum.

Peaks in the spectral region below 1150 cm^{-1} are extremely difficult to assign[152]. The band found at ~1112 $cm^{-1}$is probably due to a symmetric stretch of the POH and P=O bonds in the headgroup. The strong band seen at ~1062 cm^{-1} must be due to the symmetric stretch of the COC linkage[31]. The band at ~1023 cm^{-1} is likely to arise from predominantly a stretching vibration

of the POC linkage[156]. However, there may be a contribution from the stretching mode of PO in POH[151].

In the study of the effect of temperature on the FTIR spectrum of a film of DPPA cast from chloroform most of the peaks in the spectrum largely regain their original shape and position when the sample is cooled (plots 6-3C&D). The exception to this is the band centred at 1023 cm^{-1}. This is either less intense or broader after the sample has been heated. It is difficult to understand this behaviour especially as there is probably more than one vibrational mode contributing to the band.

6.3 : LANGMUIR-BLODGETT DEPOSITION OF DPPA OVER WATER

6.3.1 Results

It has been reported by Hasmonay et al[131], Matuoka et al[118] and Petty et al[34] that it is possible to deposit high numbers of monolayers DPPA (80 layers) via Y-type LB deposition over a subphase containing calcium salts. However, due to effects to be reported in section 6.7 of this thesis attempts were made to deposit DPPA with a subphase of pure water.

A surface pressure of 30 mN m^{-1} was chosen for the deposition. This was based on the unpublished findings of Swart and Froggatt[119] who had previously made attempts to deposit DPPA with some success (to 5 layers).

The Langmuir-Blodgett deposition was found to be Y-type over water. All of the substrates, as prepared in section 4.3.2.B, were hydrophilic. It was found that there were large problems associated with the deposition of DPPA onto the metallised glass slides to thicknesses beyond 4 monolayers and onto the silicon micro ATR crystals to more than 2 layers.

For the metallised glass slides out of 25 samples deposited only 7 had deposition ratios greater than 0.9 for all cycles through the monolayer at the air-water (a/w) interface. The inward strokes of each cycle tended to give deposition ratios of ~1. However, on the upward stroke deposition ratios varied from 1 down to -0.9. A negative deposition ratio means that material was transferred from the substrate to the monolayer at the air water interface. Of the 7 samples with deposition ratios greater than 0.9 for all cycles 3 had 9 layers in total, 3 had 7, the last had 55 layers. The sample whose spectrum is given in plot 6-9 arose from 28 cycles through a a monolayer of DPPA at the a/w interface. In order to do this the monolayer had to be replenished several times with extra DPPA and then allowed to stabilise again before deposition proceeded. The technique for deposition had been modified in order to get this sample. The speed of deposition was slowed from 5 mm/min to 1.5 mm/min.

For deposition onto the micro ATR silicon a similar problem was encountered but there was a tendency for the incomplete transfer of the monolayer to occur after the first monolayer was deposited. I.e. as the crystal was passed down through the a/w interface for the second time either a fraction of a monolayer of DPPA was transferred onto it or occasionally material was transferred from the crystal to the a/w interface. Out of 22 samples only 9 had deposition ratios of 1 ± 0.5 for more than two layers. The number of monolayers deposited onto these nine samples were 3 (four of), 5 (two of), 9, 19, 25. The last two were fabricated using the slower deposition speed.

6.3.2 Discussion of the results for deposition of DPPA

Slowing the speed, of deposition, drastically increased the number of layers which could be deposited. However this was not a fail safe technique. It merely increased the chances of success from 1 in 3 to 4 to 1 in 2 of achieving samples with deposition ratios close to 1 for all layers. In fact, the three samples with high numbers of layers (55 on the glass slide and 19&25 on the micro ATR crystal) were all deposited within days of one another. It does seem possible based on the lack of success most of the time that either there was a contamination of the trough by ions which aided deposition or the DPPA used formed monolayers at the a/w interface which were easier to deposit. Lukes et al[90] have also succeeded in the deposition of DPPA over pure water. As stated previously we have been working together and one of the spectra presented in this paper was recorded by the author of this thesis. As both the work recorded in this thesis and in reference 90 was carried out using the same LB trough the possibility of contamination can not be ruled out. If there is contamination then it does not have strong mid-IR active modes as nothing obvious is seen in the spectra recorded. Hasmonay et al[131] state that if EDTA (which complexes calcium) is added to the subphase that it was impossible to transfer layers. Thus it is a strong possibility that the good depositions are aided by ions in the subphase. The second possibility that the monolayers of DPPA at the a/w interface were simply better suited to deposition could be due to a different packing structure of the lipid. It is possible that DPPA deposits better over calcium salts because a different crystal structure is produced at the a/w interface.

The slower deposition speed probably aided deposition by allowing all of the water to drain from the sample before re-entry into the sub-phase. It was observed that if the experimenter was impatient and tried to start the next cycle before the slide was completely dry (or only dry visually) then poor deposition resulted. In general at least half an hour was required for the sample to drain.

6.4 : FTIR RAIRS SPECTRA OF DPPA SAMPLES PREPARED BY CASTING AND LANGMUIR-BLODGETT DEPOSITION.

6.4.1 Results of FTIR RAIRS measurements on DPPA

Plot 6-7 is a graph of the peak height of the peak due to the $\nu_{as}(CH_2)$ vibration versus the number of layers deposited onto RAIRS slides by Langmuir-Blodgett dipping. The lower points are not all at 7 or 9 layers because some of the samples had extra layers added by Langmuir-Shaeffer (LS) deposition. The results for these are reported in section 6.6&7.

Plot 6-8 is the RAIRS spectrum of a film of DPPA cast from chloroform onto a gold coated glass slide. Plot 6-9 is the RAIRS spectrum of 55 monolayers of DPPA deposited by Y-type LB deposition. This plot is representative of all of the RAIRS spectra of DPPA samples prepared by LB and LS deposition. The signal to noise ratio for this spectrum is 150:1 for most of the spectrum compared to ~15:1 for 10 monolayers of DPPA (plot 6-19A), which is why only the spectrum in plot 6-9 will be examined in this section.

Plots 6-8A&9A are enlargements of the spectral region 1800 - 1550 cm^{-1} for the cast film and LB sample respectively. The bands seen in this region have had synthetic peaks fitted to them. The numerical values for the parameters of the fitted peaks are in table 6(iii).

Plots 6-10A&B are enlargements of other spectral regions of the spectra in plots 6-8&9. The wavenumber scale is correct for both spectra, but absorption scales are only valid for the spectrum of the LB sample. The absorptions of all points in the spectrum of the cast film have been multiplied by a factor (different for the two plots). So that the maximum and minimum absorptions for the cast film spectrum, in each plot, are the same as those of the spectrum of the sample with 55 layers deposited by LB dipping.

Plot 6-7

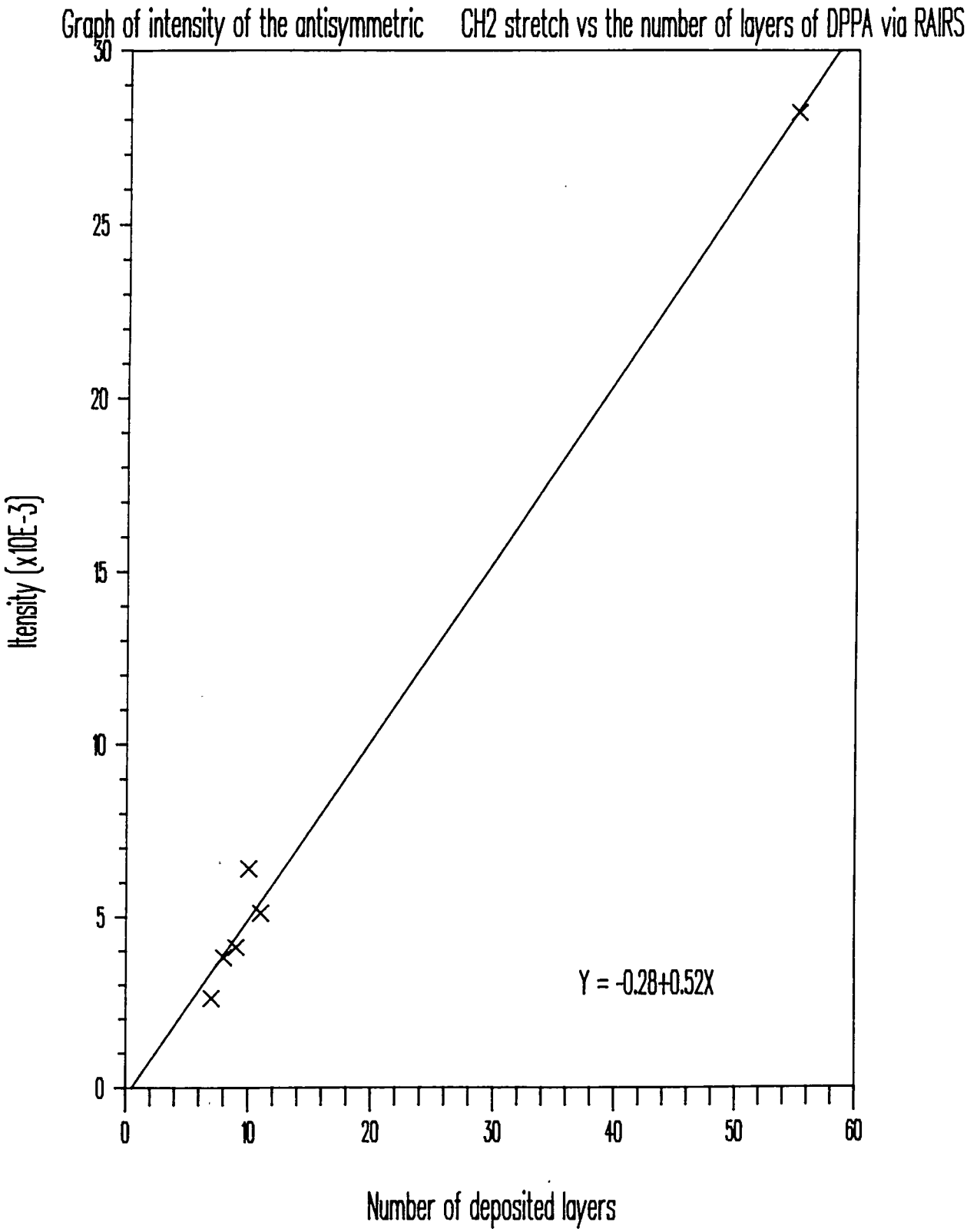
Graph of intensity of the antisymmetric CH2 stretch vs the number of layers of DPPA via RAIRS
Itensity (x10E-3)
Number of deposited layers
Y = -0.28+0.52X
0
5
10
15
20
25
30
0
10
20
30
40
50
60

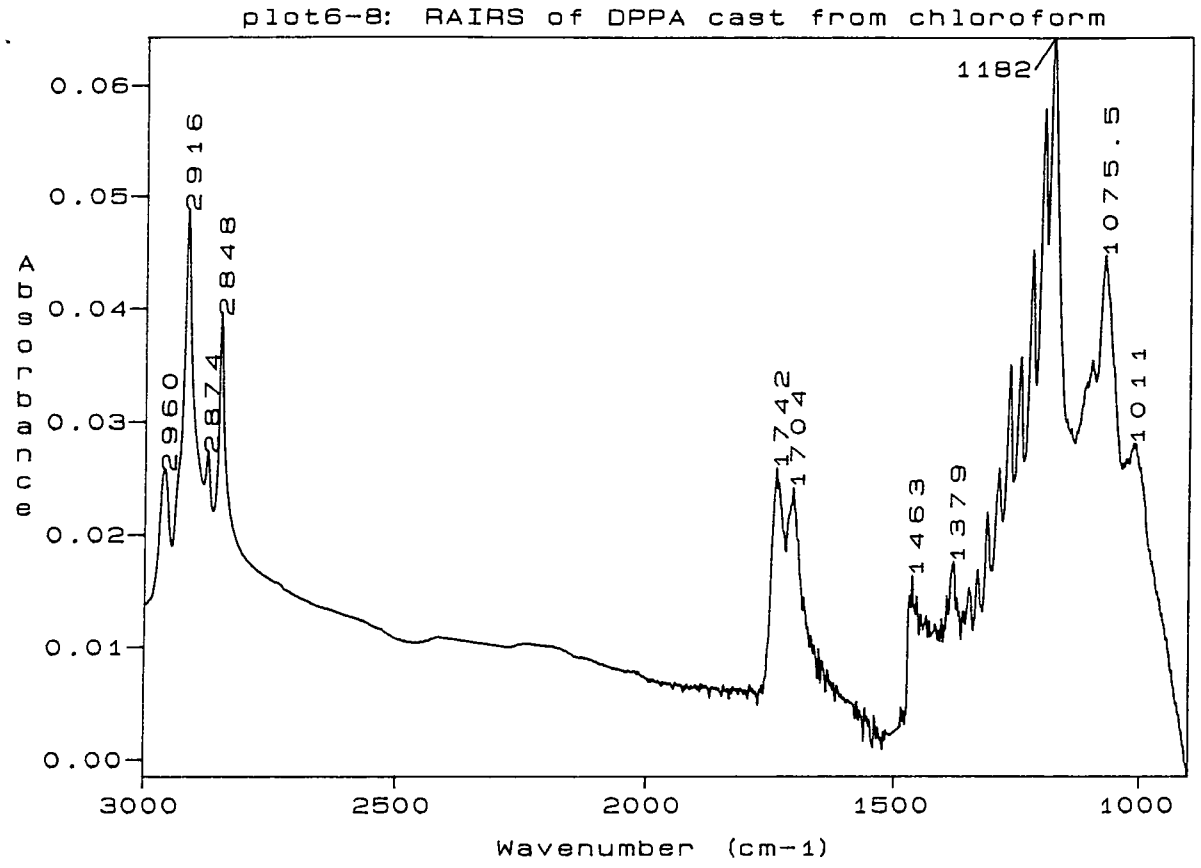
plot6-8: RAIRS of DPPA cast from chloroform
Absorbance
0.06
0.05
0.04
0.03
0.02
0.01
0.00
2960
2916
2874
2848
1742
1704
1463
1379
1182
1075.5
1011
3000
2500
2000
1500
1000
Wavenumber (cm-1)

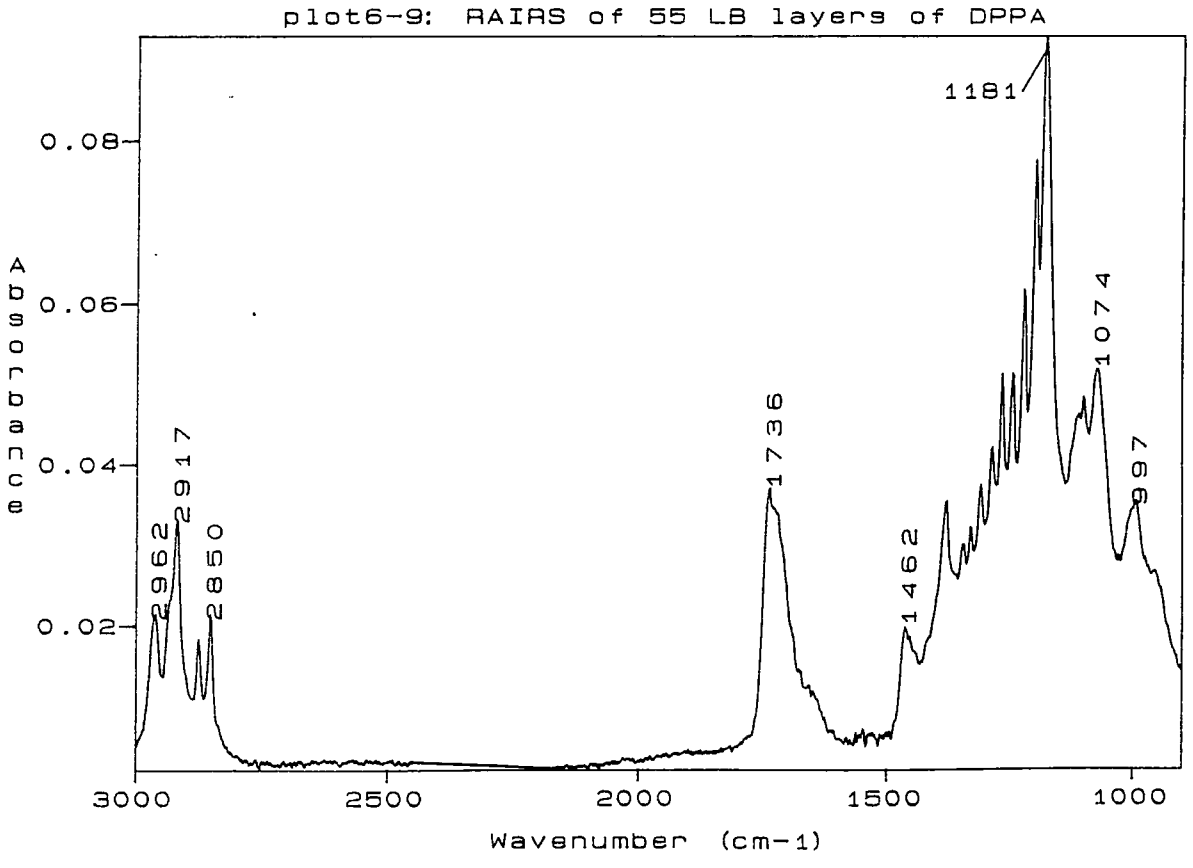
plot6-9: RAIRS of 55 LB layers of DPPA
Absorbance
0.08
0.06
0.04
0.02
2962
2917
2850
1736
1462
1181
1074
997
3000
2500
2000
1500
1000
Wavenumber (cm-1)

Plot 6-8A: Curve fit for carbonyl band of cast DPPA by RAIRS

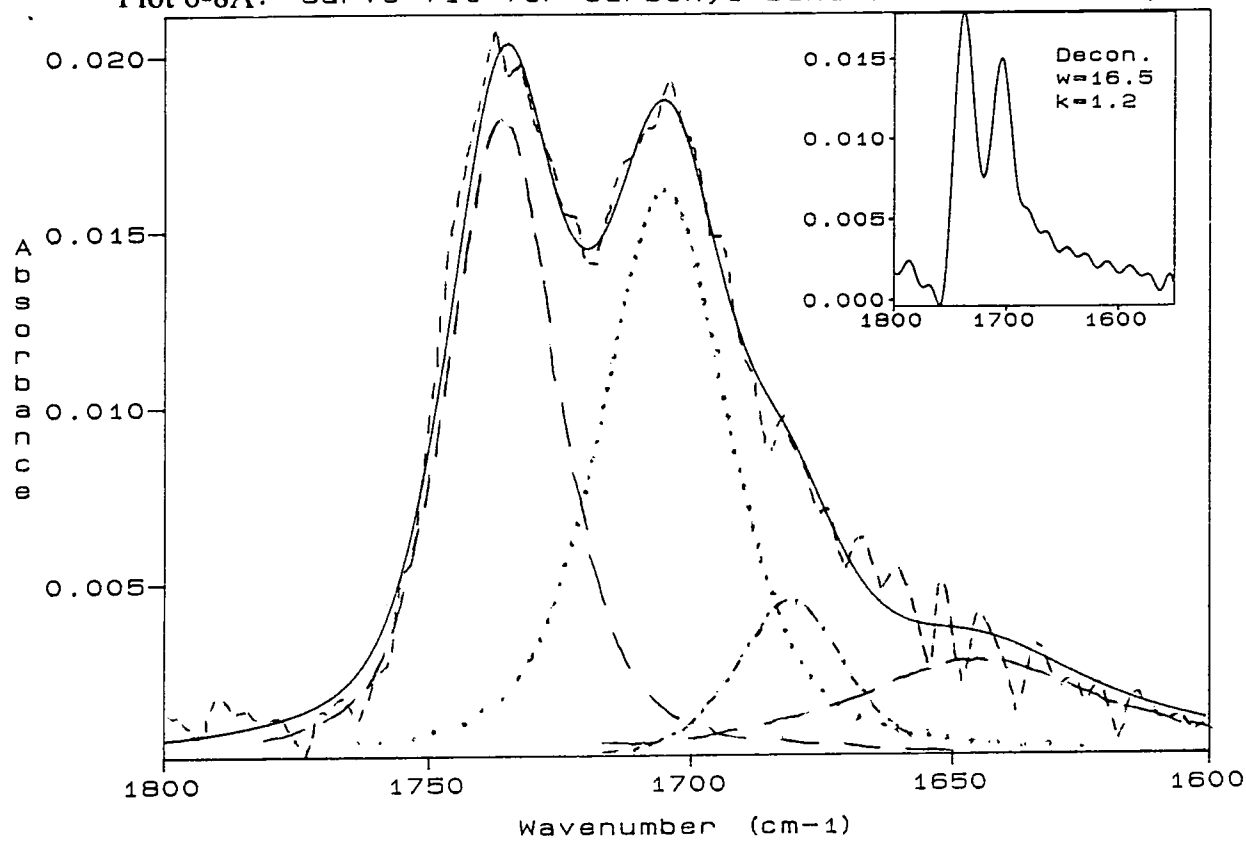

Plot 6-9A Curve fit for carbonyl of 55 LB layers (RAIRS)

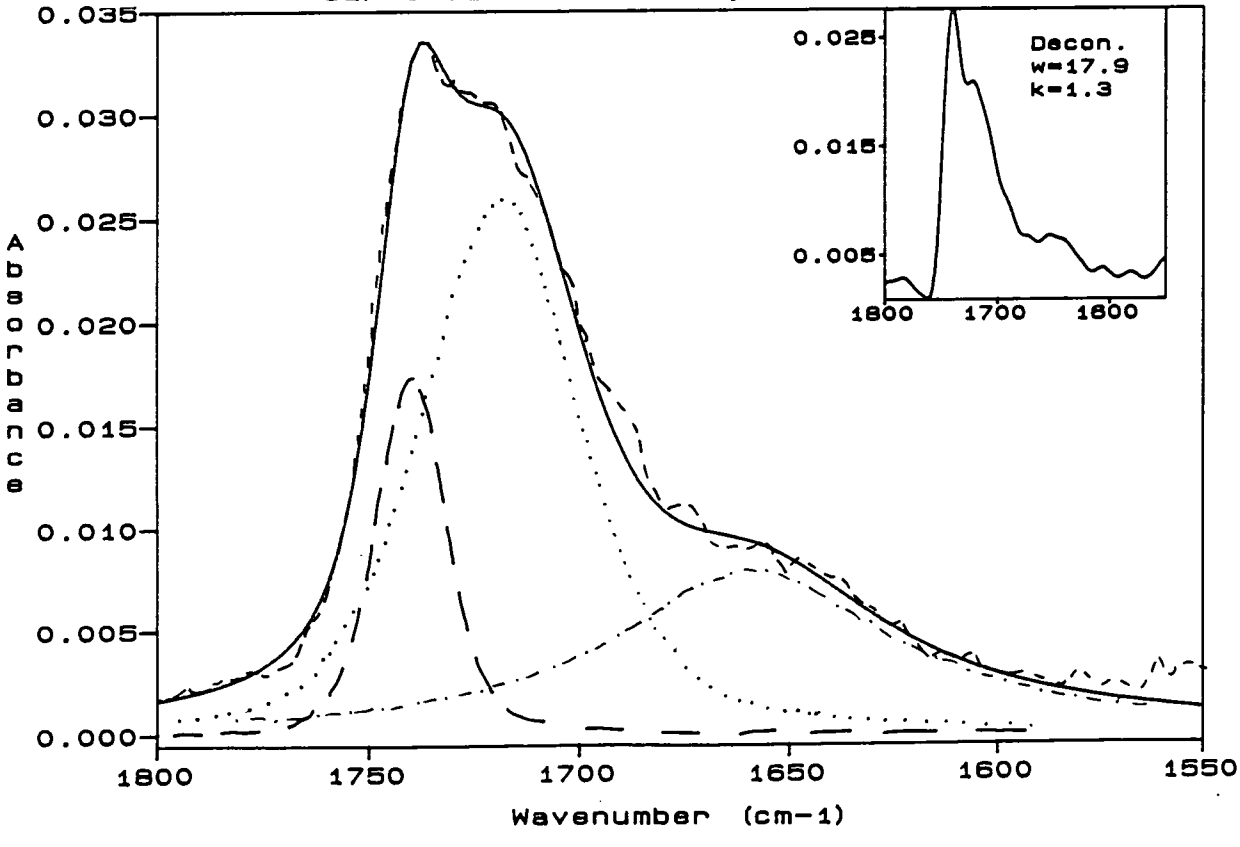

Plot 6-10A : CH stretching region for RAIRS (normalised)

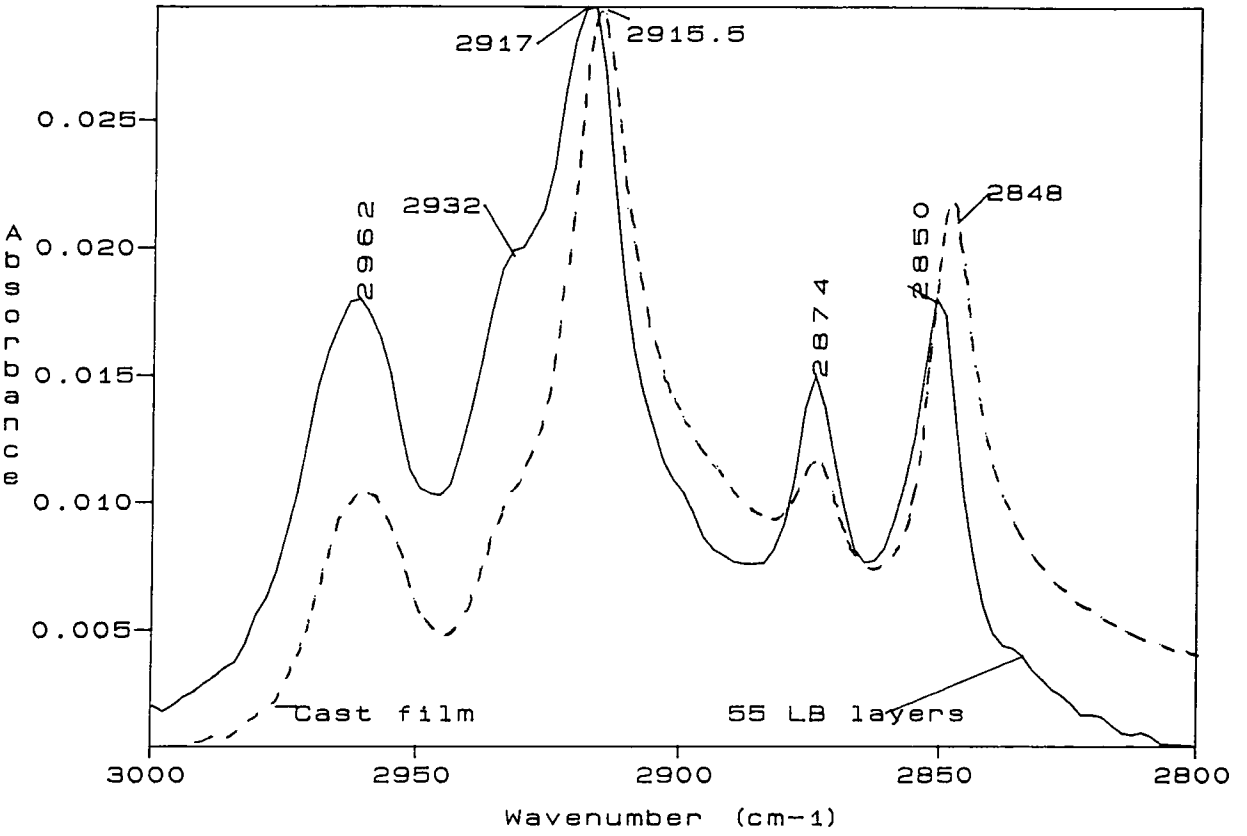

Plot 6-10B : RAIRS in the region 1500-900 cm-1 (normalised)

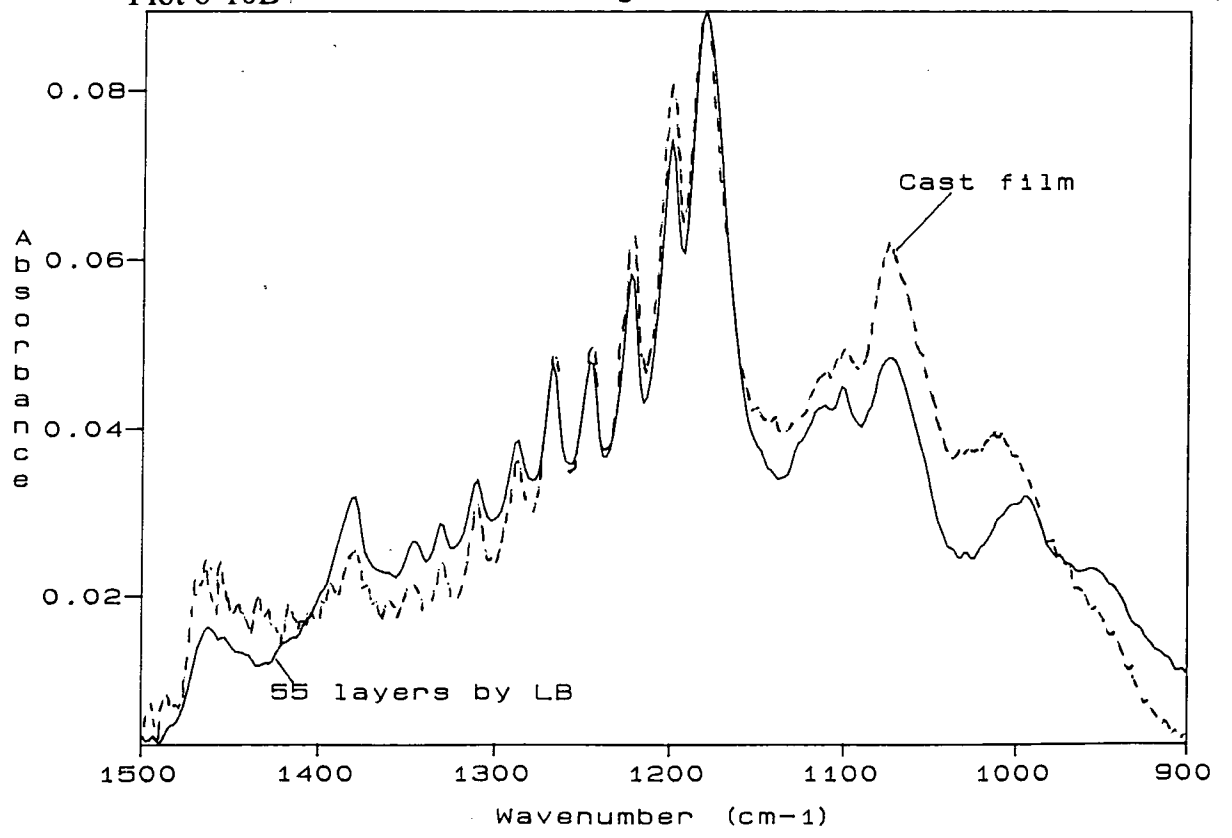

Plot 6-11 RAIRS : unpolarised and 90° polarisation

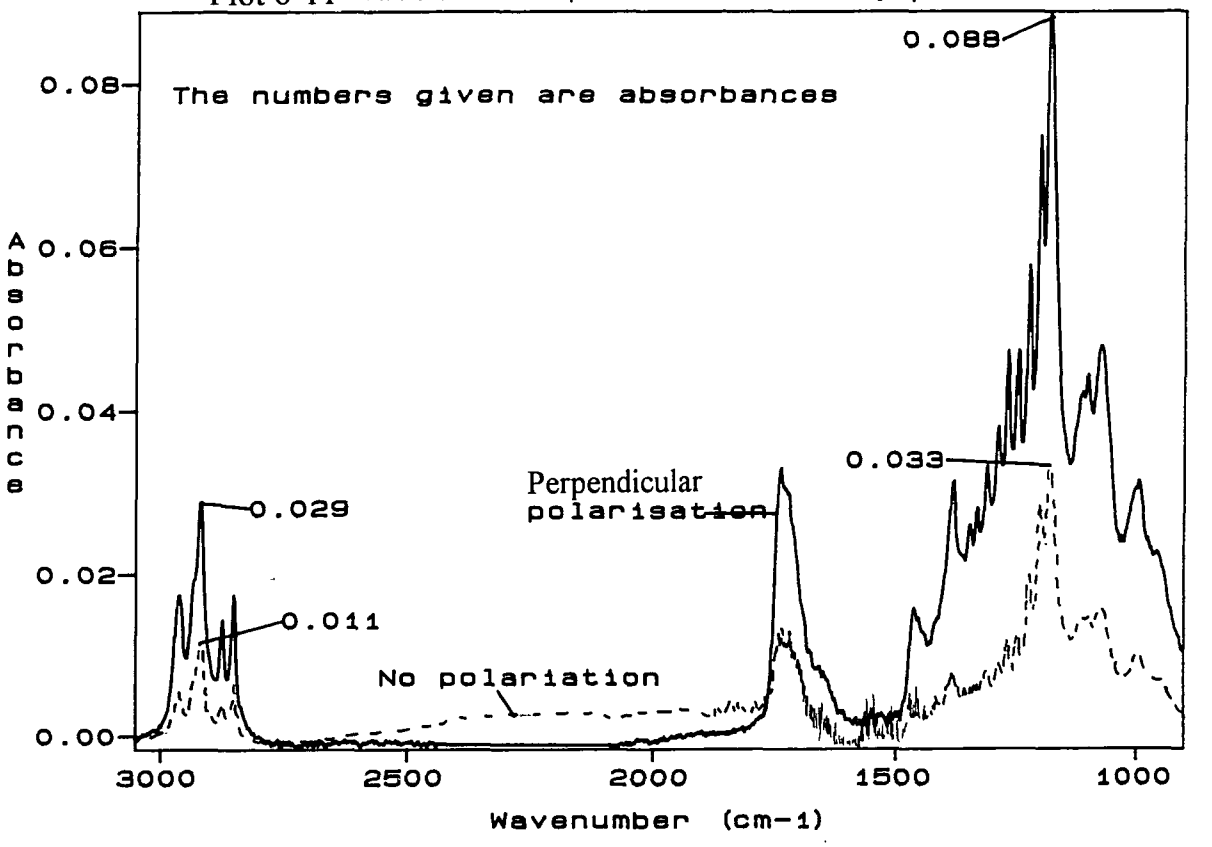

6.4.2 Analysis and discussion of RAIRS results.

Plot 6-7 shows a good correlation of the height of the $\nu_{as}(CH_2)$ peak and the deposition ratios. Within experimental error the fitted line passes through the origin.

(A) 3000-2800 cm^{-1}

Plot 6-10A shows the spectrum of this region for both the cast film and LB sample with 55 monolayers. The spectrum of the LB film in this region is very similar to that seen for the powder spectrum in plot 6-5. The Fermi resonances discussed in section 6.2.2.A are also prominent in the RAIRS spectrum.

The positions of the peaks due to the CH_2 stretching vibrations (see plot 6-10A) are indicative of alkyl chains which are below their phase transition temperature.

The four main peaks due to CH stretching vibrations in the RAIRS spectra have different relative intensities compared to transmission spectra of a cast films (plots 6-1&2). For both samples (plot 6-10A) the peaks at 2691 and 2874 cm^{-1}, due to the antisymmetric and symmetric methyl stretching vibrations respectively, are much more intense in the RAIRS spectrum compared to the peaks arising from stretching modes of the CH_2 groups. The ratio of the peak height of the $\nu_s(CH_3)$ peak to the $\nu_s(CH_2)$ peak has been calculated. This ratio is 0.15 for the transmission spectra of the cast films (plots 6-1&2); 0.51 for the spectrum of crystalline DPPA (plot 6-5); 0.50 for the RAIRS spectrum of a cast film (plot 6-10A); and 0.81 for the RAIRS spectrum of the LB film of DPPA (plot 6-10A).

It is possible that the difference in the $\nu_s(CH_3)$ to $\nu_s(CH_2)$ peak height ratio (PHR) between the cast film via transmission and via the RAIRS technique is solely due to different relative absorption / reflectivity coefficients of the two vibrations in the two techniques. However, the further increase in this ratio for the RAIRS spectrum of the LB film is due to the alkyl chains being aligned with their axis close to the perpendicular to the substrate. This arises from the fact that RAIRS will only couple transition dipoles which are perpendicular to the surface. Figure 6(a) illustrates the direction of the IR vibrational dipoles for the symmetric stretches of the methylene and methyl groups[95]. As shown (above and below) the hydrocarbon chains of DPPA are in an all trans configuration. The transition dipole moment of the methyl symmetric stretching vibration at an angle of ~35° to the axis of the alkyl chains, whereas the transition dipole due to the methylene symmetric stretching mode is perpendicular to the axis of the chains (figure 6(a)). Therefore, in a RAIRS spectrum where the alkyl chains were all completely perpendicular to the substrate the peak due to the $\nu_s(CH_2)$ vibration would be have an extremely low intensity as the transition dipole moment of the vibration would be parallel to the substrate. The $\nu_s(CH_3)$ vibration would however, be strongly coupled in such a situation. Thus, although the peak due to $\nu_s(CH_3)$ is relatively much stronger in the RAIRS spectrum of the LB film compared to the cast film the chains are not completely perpendicular to the substrate because the $\nu_s(CH_2)$ vibration is still being coupled.

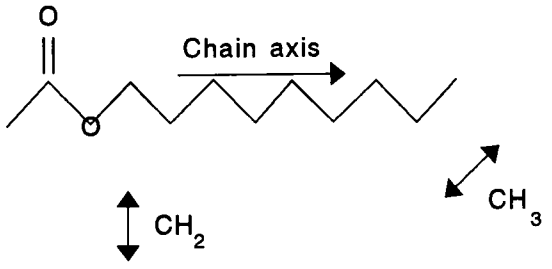

Figure 6(a) : Showing approximate vibrational dipole moment directions for the symmetric stretches of the methyl and methylene groups.

(B) 1800 -1600 cm^{-1}

As observed in section 6.2 the cast film spectrum (plot 6-8A) has a similar structure for the band due to the carbonyl stretching vibration to the transmission spectrum of cast film 6-1. The RAIRS spectrum for this region, for the sample with 55 monolayers of DPPA deposition by LB dipping (plot 6-9A), has a similar structure to that observed for the transmission spectra of cast films 6-2 and 6-3. The general shape of the carbonyl band was the same as that seen in plot 6-8a for all RAIRS spectra of LB samples. Unfortunately the S/N ratio (see plot 6-19A) for the rest of the samples was to low to fit a synthetic peak. The intensities of the synthetic peaks fitted to the cast film RAIRS spectrum (plot 8A) are very similar to those of the cast film via transmission (plot 6-1A) For the LB film the intensity ratios of the fitted peaks differ from those seen for the transmission spectra of the cast films. For the LB sample (plot 6-9A) the peak fitted at a position of 1718.5 cm^{-1} is very broad and may consist of two peaks. Unfortunately there really is not enough data to know how to split the peak up. Attempts were made to find a fit where four peaks were used to find a good synthetic spectrum for this sample (plot 6-9A) but the shape was always unsuitable on comparison with the experimental data.

The increase in intensity, relative to the peak at 1735 cm^{-1}, of the bands at 1701 and 1719 cm^{-1} (plots 6-8A and 6-9A) is an indication that the acyl chains are largely perpendicular to the substrate. The transition dipole moment of the C=O stretching mode is parallel to the the C=O bond. Figure 3(i) shows that a trans conformation about the ester linkage will result in a C=O group which is perpendicular to the chain axis. A gauche conformation about the ester linkage leads to a carbonyl group which is at an angle to the chains such that if the transition dipole moment of its stretching vibration were to be resolved with respect to the axis of the hydrocarbon chains there would be both parallel and perpendicular components. Therefore if a RAIRS spectrum was taken of a sample whose chains were

Description	Plot no.	No peaks fitted	wavenumber (cm^{-1})	FWHH (cm^{-1})	absorption amplitude	integrated intensity (cm^{-1})	% Lorentzian
cast from chloroform	6-8a	4	1736	26	0.0183	0.567	50
			1705	29	0.0164	0.572	50
			1681	25	0.0045	0.135	50
			1645	60	0.0028	0.238	100
cast from chloroform	not shown	4	1735	20	0.0090	0.207	50
			1701	26.5	0.0127	0.382	50
			1674	27	0.0040	0.147	50
			1645	97	0.0030	0.367	100
55 LB layers	6-9a	3	1740	21	0.0175	0.403	50
			1718.5	45	0.0260	1.364	50
			1660	80	0.0079	0.119	100

Table 6(iii) : Data for the peaks fitted to the band arising from the carbonyl stretching mode for RAIRS spectra of DPPA

wavenumbers (cm^{-1})	
Cast film plot6-8	55 LB layers plot6-9
1461	1462.0
	sh.↓ 1419
1378	1380.5
1347.0	1346.0
1330.5	1330.5
1310.0	1313.5
1288.0	1288.0
1266.0	1267.5
1246.0	1246.0
1222.0	1224.5
1201.5	1200.0
1182.0	1181.0
	1113.5
1100	1101.5
1075.5	1074.5
1010	997.5

Table 6(iv) : Peak positions for RAIRS spectra of DPPA in the region 1500-900 cm^{-1}

completely perpendicular to the substrate the peak arising from the trans conformation would have negligible intensity whereas that arising from the gauche conformer would give rise to a peak due to the component of the C=O vibrational transition dipole moment which is resolved perpendicular to the substrate i.e. parallel to the chains. However what is observed is an increase in the relative intensity of the peaks due to the gauche conformer. Again indicating that the chains are orientated close to the perpendicular to the surface but not exactly so.

(C) 1500-900 cm^{-1}

The peak arising from the methyl umbrella mode (~1380 cm^{-1}) is relatively more intense in the RAIRS spectrum of the LB film compared to either the transmission spectra or the RAIRS spectrum of cast films. The transition dipole moment of this mode is parallel to the C-C bond. Thus as it was a strong band in the RAIRS spectrum it again points to the fact that the alkyl chains are aligned close to the vertical of the substrate.

For both the cast film and the LB sample the RAIRS spectra show very intense CH_2 wagging progression peaks. There are clearly eight peaks from 1346 - 1200 cm^{-1} which can be attributed to the CH_2 wagging progression series. This series of peaks and the peak due to the COC antisymmetric vibration have the greatest peak heights in both the RAIRS spectra. The analysis of this groups of peaks is complicated by the underlying peaks due to the COC and P=O vibrations. The direction of the transition dipole moment in the of the CH_2 wagging mode is parallel to the chains[88] so this could be the sole cause of the increase in relative intensity. However, the transition dipole due to the symmetric COC stretching vibration has a transition dipole moment ~ perpendicular to the C=O bond. Thus, for either gauche or trans conformations at the ester linkage (figure 3(i)) there will be a

component of the COC stretching vibration parallel to the hydrocarbon chain axis. This would again lead to a strong peak in the RAIRS spectra for chains which are almost perpendicular to the interface.

The peak at 997 cm^{-1} which is probably due to an stretching vibration of the PO bond in the POC linkage[151] seems to be enhanced in the RAIRS spectrum of the LB film compared to that of the cast film (plot 6-10B). Now the transition dipole associated with this vibration is likely to be close in direction the the PO(-C) bond. Therefore it seems likely that this linkage is orientated in the LB film with its transition dipole largely perpendicular to the substrate, i.e. the POC linkage is probably largely perpendicular to the substrate for the LB film.

(D) Polarisation of the IR radiation

Plot 6-11 supports the findings of Song et al[114]. It shows that not only is there an increase in the S/N ratio on the attachment of a polariser to the RAIRS equipment but also an increase in the intensity of all of the sample peaks within the spectrum.

6.4.3 Summary of the findings for the RAIRS spectra

It is apparent that in the LB film the alkyl chains are orientated such that on average their axes are largely perpendicular to the substrate but not at exactly 90° to it. There is probably also information in the spectra concerning the orientation of the headgroup. Unfortunately this is largely obscured by the progression series resulting from CH_2 wagging modes. As in plot 6-3D heating the sample might have been a useful technique. The dichroism of the RAIRS spectrum of a cast film compared to the transmission spectra indicates that the molecules in the cast film are not completely randomly orientated.

6.5 : FTIR MICRO-ATR SPECTRA OF DPPA SAMPLES PREPARED BY CASTING AND LANGMUIR-BLODGETT DEPOSITION

6.5.1 ATR results for DPPA

Plot 6-12 shows the peak heights of both the $\nu_{as}(CH_2)$ and $\nu_s(CH_2)$ peaks in micro ATR spectra versus the number of layers deposited via the LB technique. The sample with 25 LB layers is not shown as it was deposited on a longer ATR crystal (& therefore more reflections would result).

Plot 6-13 is the micro ATR spectrum of a film cast from chloroform onto one side of a micro ATR crystal. The negative peak at ~1100 cm^{-1} is due to an absorption by the silicon crystal. Plot 6-13A shows the synthetic peaks fitted to the experimental data for the spectral region 1800-1600 cm^{-1}. Plots 6-15A&B are linearly polarised spectra of the same sample. A diagram showing definitions of the polarisation directions can be found in chapter 4 (figure 4(r)).

Plot 6-14 is the micro ATR spectrum of 19 monolayers deposited via LB deposition. Plot 6-14A is the spectral region 1800-1600 cm^{-1} showing the synthetic band fitted to the data. Plots 6-16A&B are linearly polarised spectra for the same sample.

Plot 6-12

Graph of CH_2 stretch intensity versus the number of layers for DPPA on a micro ATR crystal

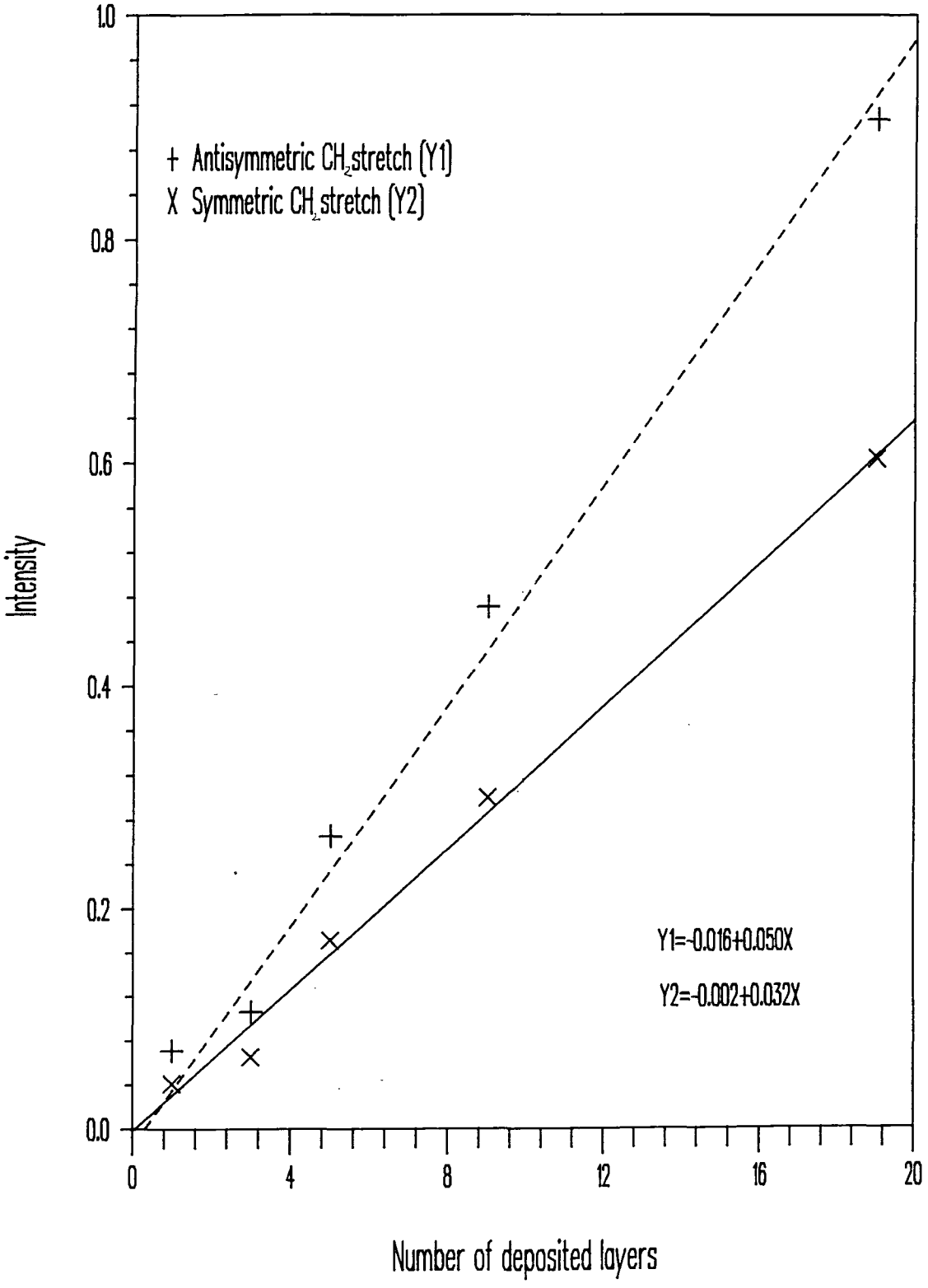

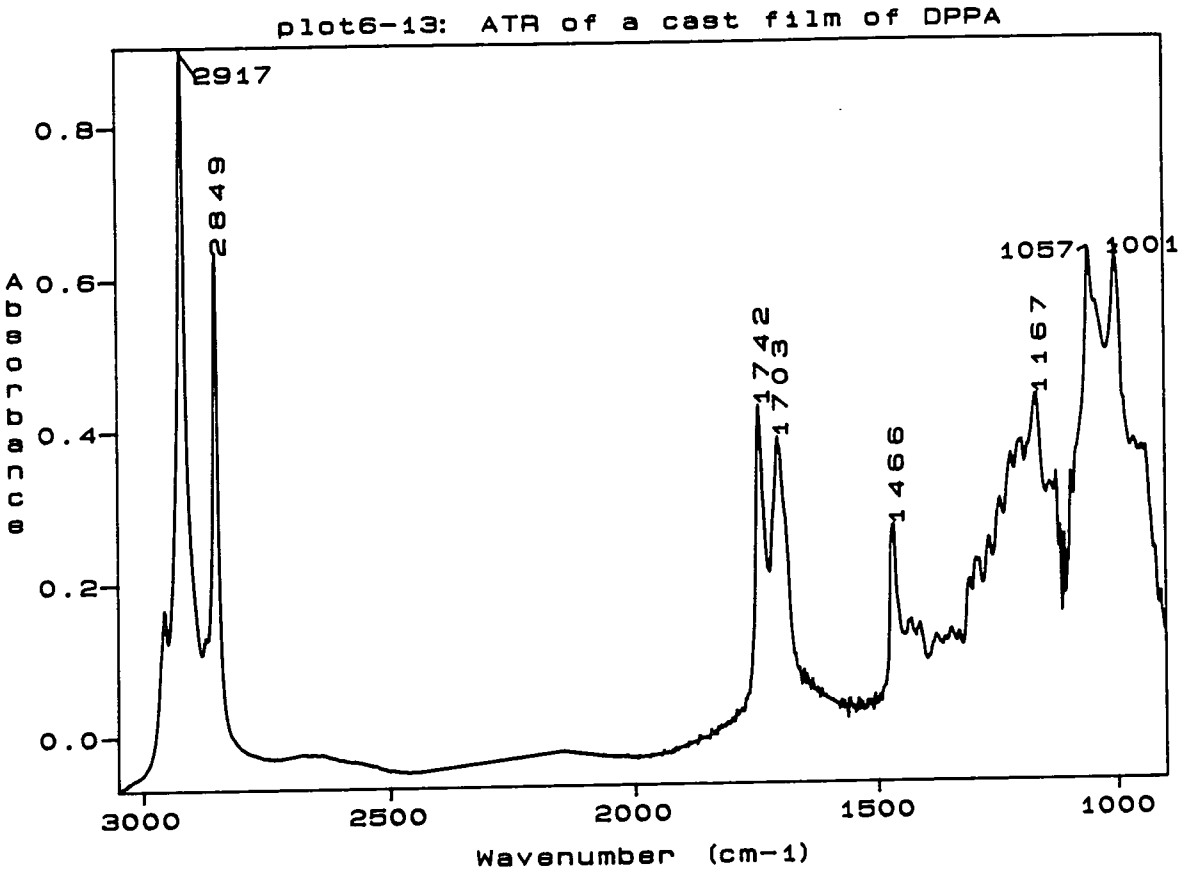
plot6-13: ATR of a cast film of DPPA
2917
2849
1742
1703
1466
1167
1057
1001
Absorbance
0.8
0.6
0.4
0.2
0.0
3000
2500
2000
1500
1000
Wavenumber (cm-1)

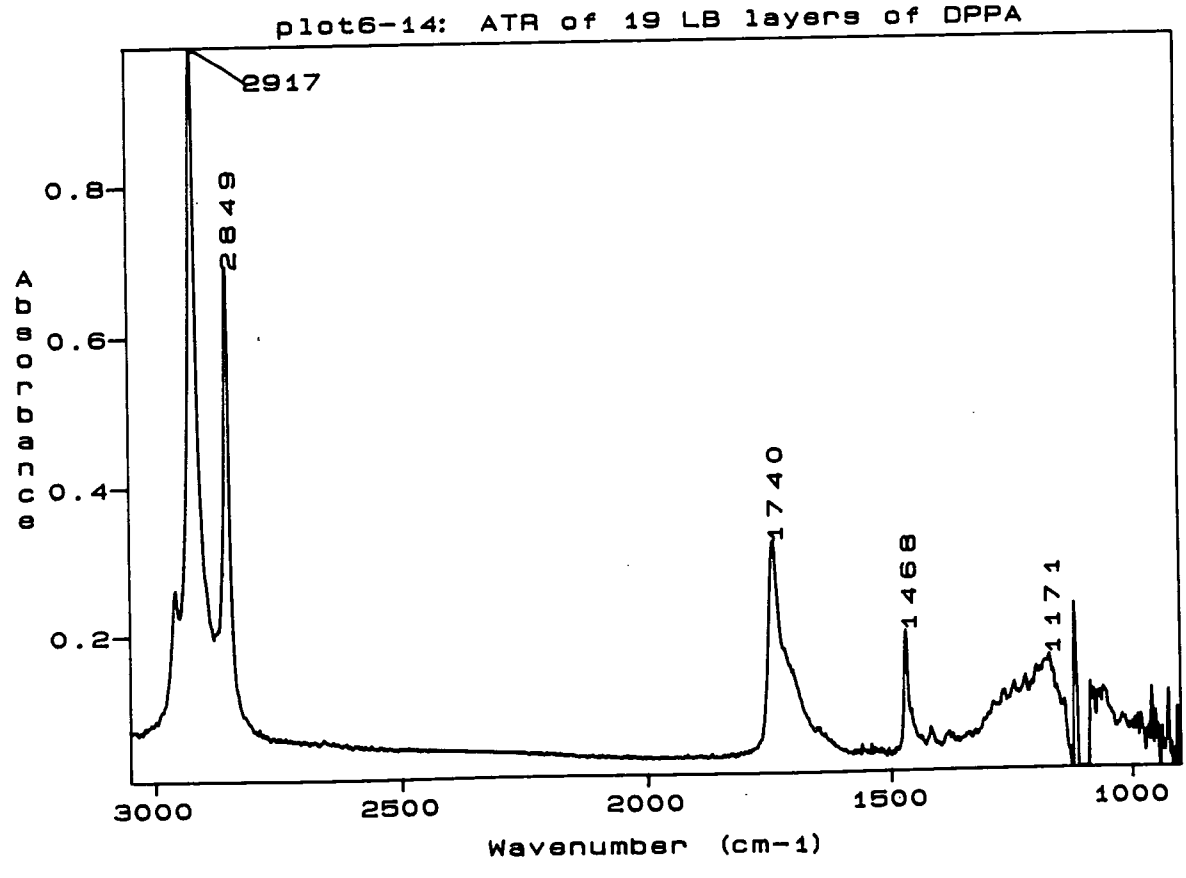
plot6-14: ATR of 19 LB layers of DPPA
2917
2849
1740
1468
1171
Absorbance
0.8
0.6
0.4
0.2
3000
2500
2000
1500
1000
Wavenumber (cm-1)

Plot 6-13A Curve fit for carbonyl on plot6-13 (cast ATR)

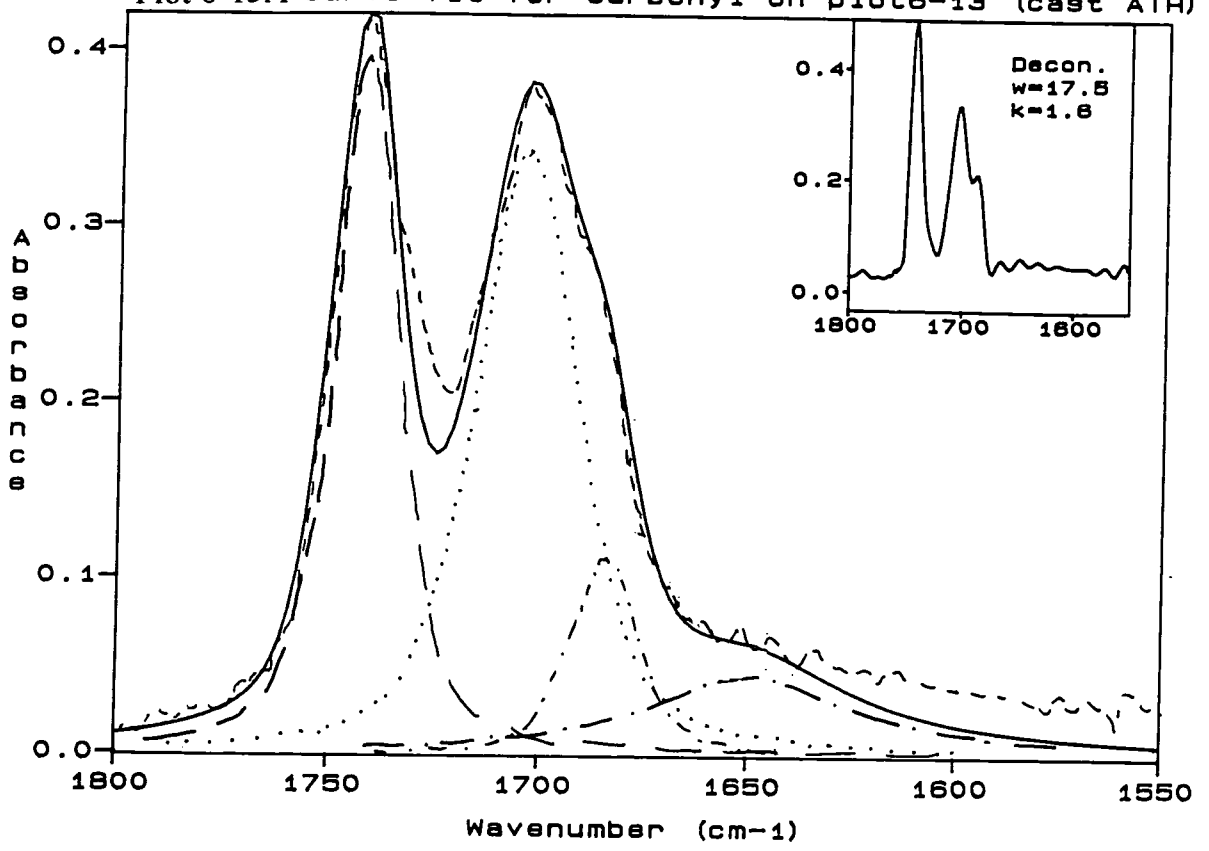

Plot 6-14A: Curve fit for carbonyl for 19 LB by ATR

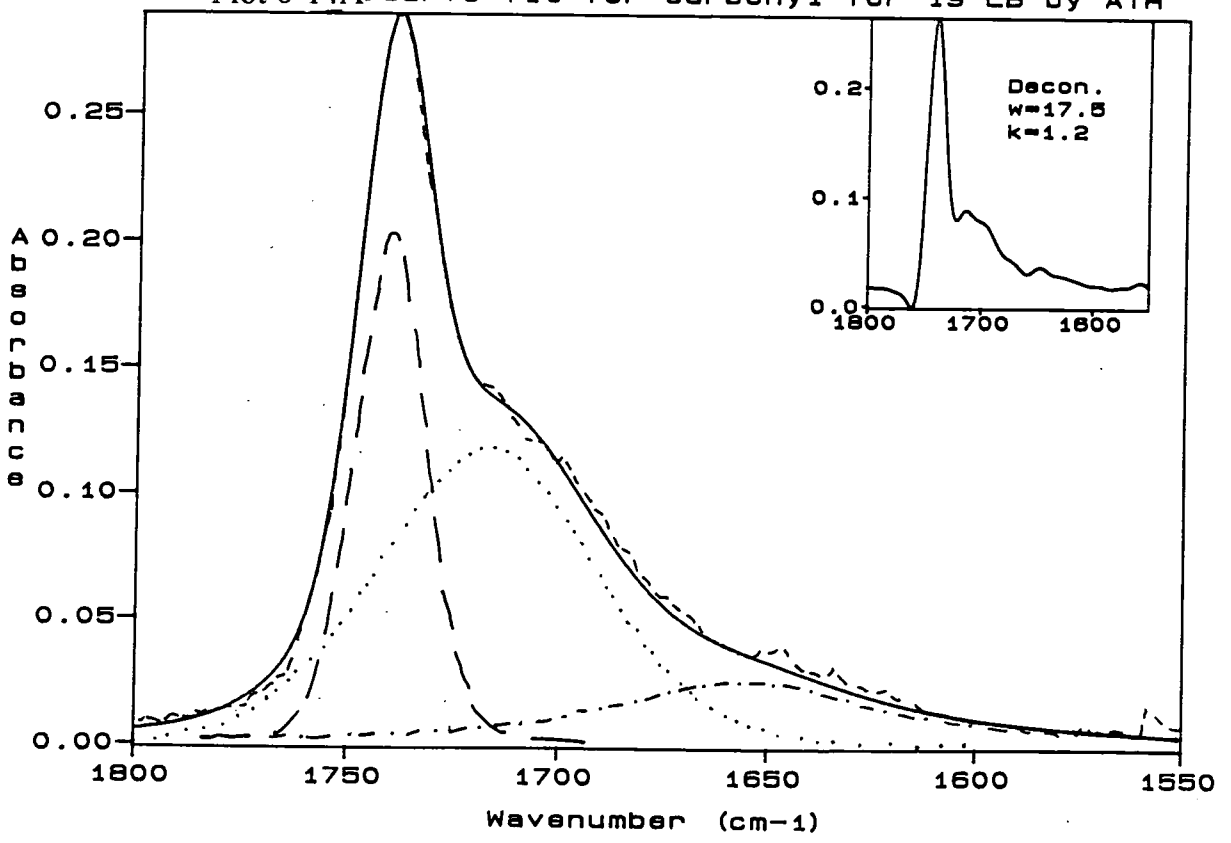

Plot 6-15A : Polarisation of the cast film

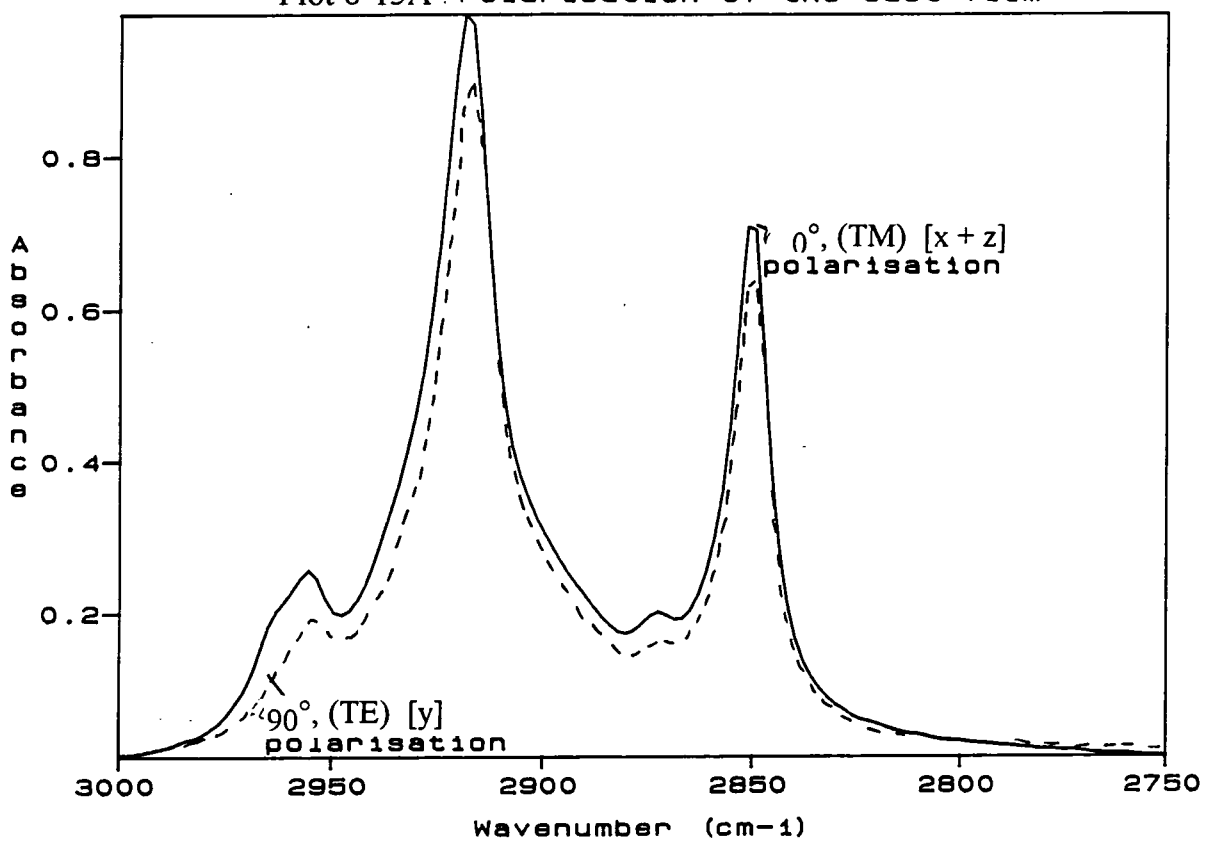

Plot 6-15B : Polarisation of the cast film

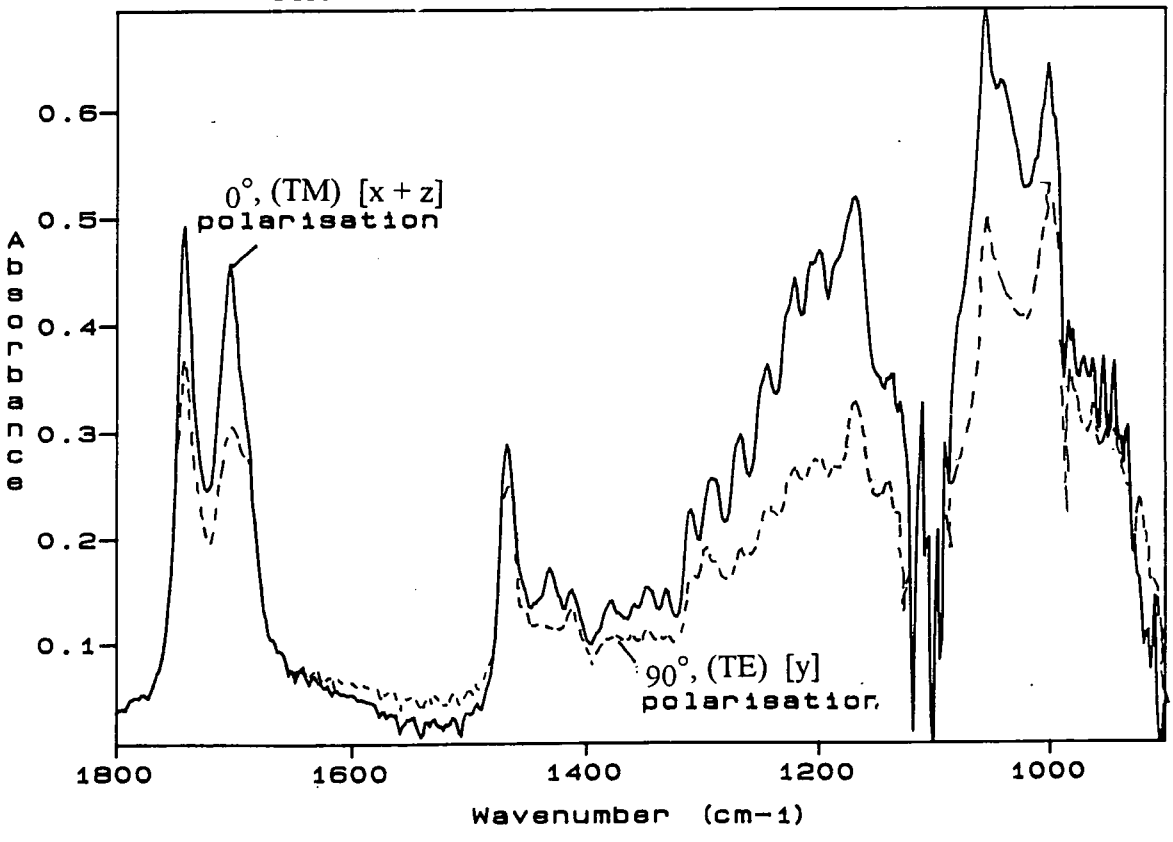

Plot 6-16A: Polarisation of 19 LB layers of DPPA

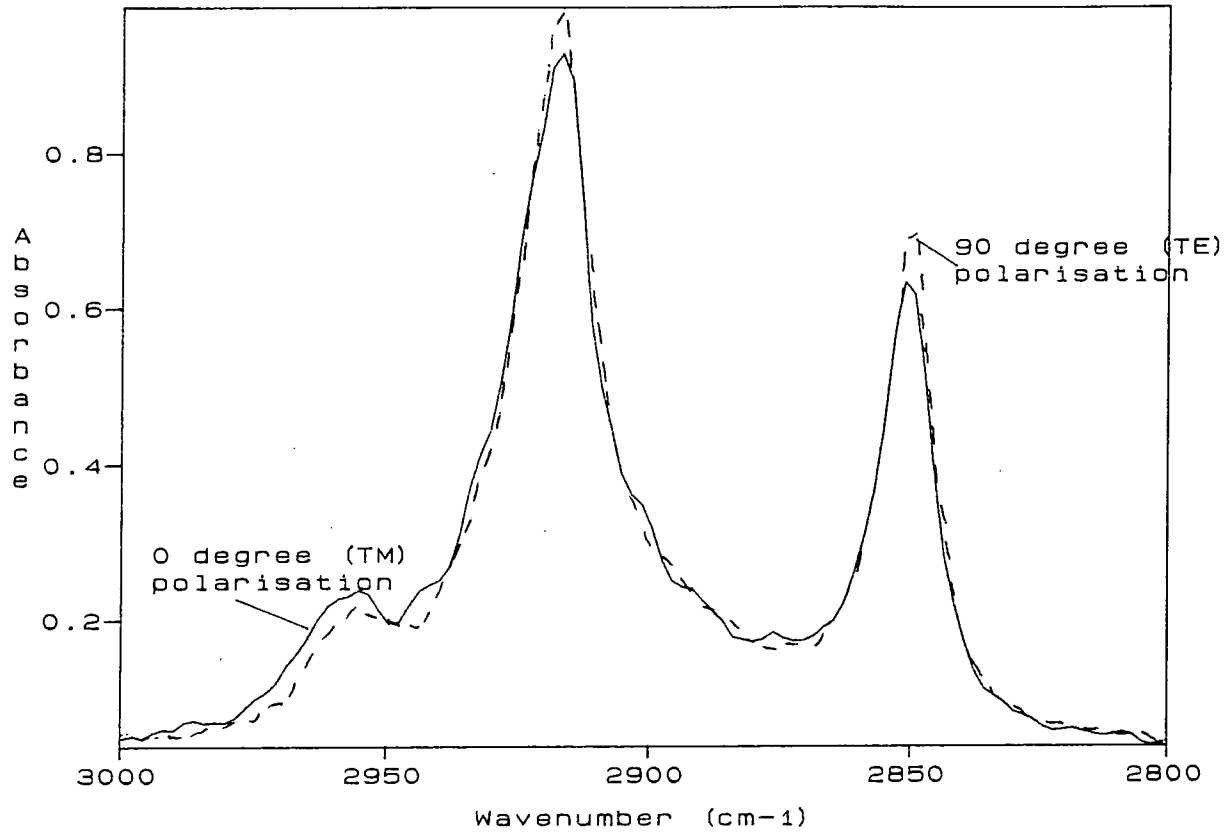

Plot 6-16B: Polarisation of 19 LB layers of DPPA

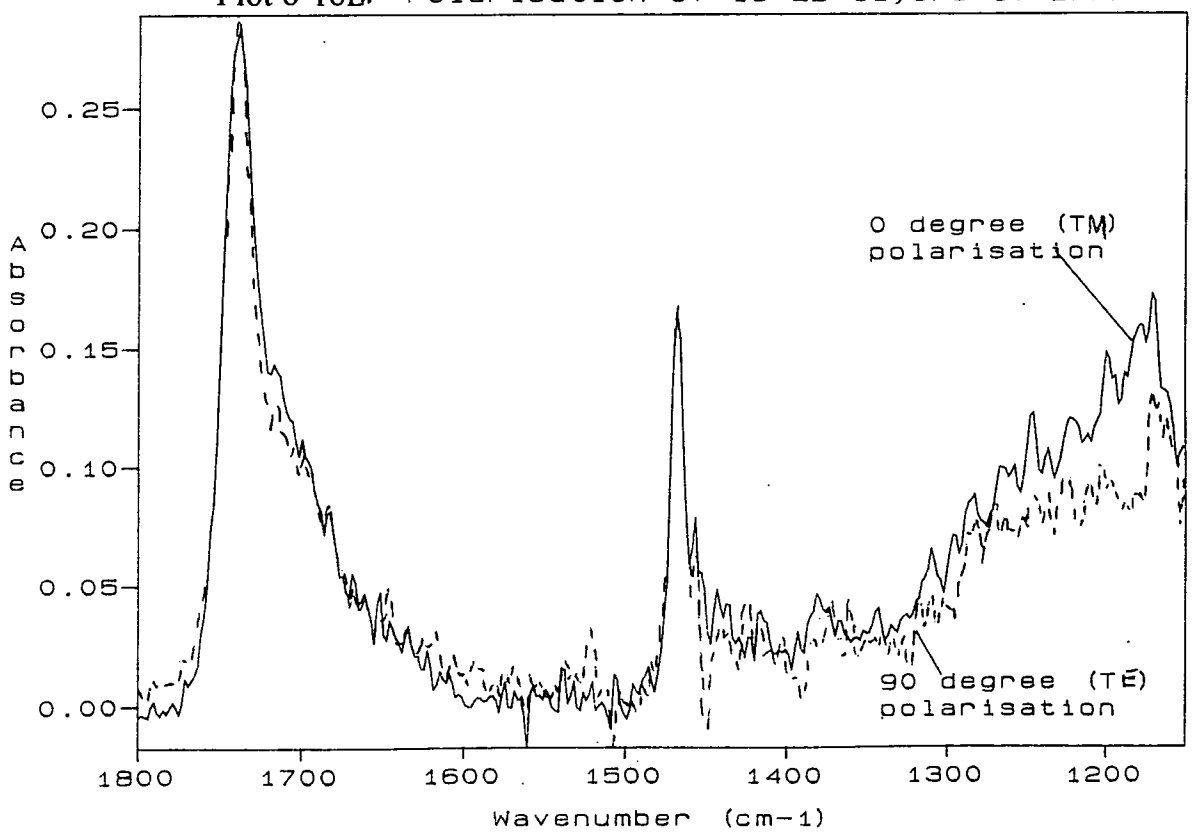

6.5.2 Analysis and discussion of ATR results

There is a linear relationship between the peak heights of the bands due to CH_2 stretching modes (plot6-12). The points due to one, three and five layers are average values. The error on these is shown in plot 6-20.

The ATR spectrum of the cast film (plot 6-13) is similar to the transmission spectrum seen in plot 6-1. Please refer to section 6.2.2 for a detailed analysis of the spectrum. The shape of the carbonyl peaks are very similar for the ATR and transmission spectra of the cast films (plot 6-1A & plot 6-13A). The main difference is that the peaks in the region 1350 - 1000 cm^{-1} seem to enhanced compared to the same peaks in the transmission spectrum. A similar effect is seen in the transmission spectrum of DPPA crystals (plot 6-5). The reasons for this enhancement are not known but it may be possible that it is due to coupling between the P=O stretching vibrations of two molecules in close proximity, because of a particular crystal structure.

The shape and relative intensities of all of the peaks in the ATR spectrum of DPPA deposited via LB dipping (plot 6-14) are virtually identical to that seen in the transmission spectrum of the cast films 6-2 & 6-3.

The evidence suggests that the structure of DPPA molecules an LB film is similar to that of the type of film cast from chloroform which was the least frequently found for the technique of deposition used. At present it is difficult to propose the structure of the molecules in either of the types of cast films observed. X-ray diffraction measurements on at least the crystalline sample would aid this analysis.

Table 6(v) shows that there is a narrowing of some of the bands due to CH vibrations as the number of deposited monolayer is increased (reported in reference 115). The narrowing (smaller FWHH) of the peaks due to CH_2 stretching vibrations is real. The numbers quoted are taken from single spectra but spectra

have been overlaid on the computer screen and it has been observed that $\nu(CH_2)$ peaks in spectra of multilayers are always narrower than those of monolayers. However, the difference is very small (of the order of 0.5 - 1 cm^{-1}) and about the order of the error in measuring the peak width. More significant, perhaps is the decrease in the width of the band arising from the CH_2 scissoring mode, as the number of layers is increased. This indicates that the number of different environments for the hydrocarbon chains decreases as the number of monolayers increases. It is possible that the initial monolayer, attached to the silicon has a different packing arrangement to the subsequent monolayers. Or that the alkyl chains of monolayers within the LB structure have less freedom of motion than the outer monolayer. Obviously all of the samples have an outer monolayer but its relative contribution to the IR spectra deceases as the number of monolayers increases.

Vibration	$\upsilon_{as}(CH_2)$	(cm^{-1})	$\upsilon_{s}(CH_2)$	(cm^{-1})	$\delta_{s}(CH_3)$	(cm^{-1})
	position	FWHH	position	FWHH	position	FWHH
Cast film	2918.0	19.6	2850.2	12.5	1467.5	16.4
1 LB layer	2918.7	20.2	2850.7	12.8	1468.2	20.3
5 LB layers	2917.7	18.7	2850.5	12.3	1466.9	13.5
19 LB layers	2917.9	19.1	2850.2	12.5	1468.2	11.0

Table 6(v) : Peak positions and widths for selected CH vibrations

Description	Plot no.	No peaks fitted	wavenumber (cm^{-1})	FWHH (cm^{-1})	absorption amplitude	integrated intensity (cm^{-1})	% Lorentzian
cast from chloroform	6-13a	4	1743	21	0.400	9.30	50
			1703	30	0.345	11.80	50
			1685	20	0.113	2.51	50
			1649	62	0.045	2.75	100
19 LB layers	6-14a	3	1740	21	0.205	4.55	50
			1717	60	0.119	8.08	50
			1655	80	0.026	2.90	100

Table 6(vi) : Data for the peaks fitted to the band arising from the carbonyl stretching mode for ATR spectra of DPPA

wavenumbers	(cm^{-1})
Cast film plot6-8	19 LB layers plot6-9
1467.5	1468.0
1431.5	
1412.0	1417.5
1378.0	1377.5
1347.5	1340.0
1330.0	1328.5
1311.0	noisy
1292.0	1288.0
1268.0	1266.5
1244.5	1244.5
1222.5	1222.0
1200.0	1198.5
1170.0	1172.0

Table 6(vii) : Peak positions for ATR spectra of DPPA in the region 1500-900 cm^{-1}

6.5.3 Polarised microATR of DPPA films

(A) Background

Figure 4(r) illustrates the relationship between the linear polarisations used and the micro ATR crystal and a set of orthogonal axes. Mirabella[39] and Harrick[157] have written reviews covering the background and uses of polarised ATR. In reference 115 we used an order parameter (Takenaka et al[21]), this did not yield any useful results.

The approach used now utilises the computer program designed and written by Dr.Y.P Song to calculate the electric field density in each of the three directions x,y&z for a thin film. The calculations for this program are derived from Maxwell's equations[158]. Plots 6-17A&B show the results of this program for thicknesses of 1 monolayer and 19 monolayers DPPA at 2917 cm^{-1}.

Table 6(viii) shows the integrated intensities of the electric field over the whole film thickness for one reflection, using the afore mentioned program. The thicknesses of the film are from recent unpublished work by Lukes et al[159] where low angle X-ray measurements have been made on LB films of DPPA. A d-spacing of 51.2 ± 0.3 Å was found for an LB film of DPPA on silicon[159]. This is the repeat unit which in Y-type deposition will be a bilayer of lipid. The thickness of the cast film was based on the fact that approximately the same absorption intensity was observed in the spectra of 19 LB layers and the cast film. Thus, if the absorption by the film is proportional to the amount of material in both cases then the cast film must be twice as thick as the 19 layers (as the 19 LB layers are on both sides of the crystal but the cast film is only on one side of the micro ATR crystal. As this was only an estimate of the film thickness the electric field calculation was also performed for a film twice as thick again. The complex part of the refractive index (k) was taken as zero. The validity of this approximation for a thin film is discussed in Mirabella[39]. For the calculation on the thickest

film k=0.1 was tried as an alternative (table 6(viii)). It can be seen that this changes the electric field densities only slightly and the ratios to be considered below are very close to the those used when k was taken to be zero. The refractive indexes of the materials used as given in Sagiv and Mooz[160] - 3.42 for the silicon substrate, 1.5 for the DPPA films, 1 for air.

Consider the definition of the orthogonal axes in figure 4(r). If polarised light is used the perpendicular (90° or TE)) polarisation radiation will couple with transition dipoles aligned in the y direction and the parallel (0° or TE) polarisation will couple transition dipoles in both the x and z directions[39]. Now Haller and Rice[161] proposed that if a vibration is considered whose transition dipole orientation with respect to the rest of the molecule is known then it is possible to use polarised ATR to obtain a qualitative notion of the average orientation of the molecules with respect to the substrate. If the alkyl chains of the molecules were orientated perpendicular to the substrate then the transition dipole moment of the symmetric CH_2 stretching vibration would be parallel to the substrate. In this case the z component of the parallel (0°) polarised light would not couple with the transition dipole, and the dichroic ratio of the peak intensities should be equal to that of the electric field densities in the y and x directions. If the molecules were randomly distributed with respect to the substrate then the dichroic ratio would be the same as that of the y component of the electric field density with both the x and z components.

Perfect orientation : $$\frac{A_\perp}{A_\parallel} = \frac{E_y^2}{E_x^2}$$ Eqn 6(ii)

Random orientation : $$\frac{A_\perp}{A_\parallel} = \frac{E_y^2}{E_x^2 + E_z^2}$$ Eqn 6(iii)

Where : $A_\perp$ = absorption by sample, perpendicular (TE) polarisation

$A_\parallel$ = " parallel (TM) polarisation

E_d^2 = electric field in the sample in direction d

(B) Results and analysis of polarised micro ATR studies

Table 6(viii) contains the calculated dichroic ratios for the both random and parallel orientation of the $\nu_s(CH_2)$ stretching transition dipoles. The final column in the table is the experimental ratio of the $\nu_s(CH_2)$ (centred at 2850 cm^{-1}) from spectra of the same sample polarised in the two directions shown in figure 4(p). Therefore if this ratio is close to that arising from equation 6(iii) then the molecules have a random orientation with respect to the substrate. If the experimental ratio is equal to the value obtained from equation 6(ii) then the DPPA molecules are orientated with the $\nu_s(CH_2)$ vibrational transition dipole moment parallel to the substrate. I.e. with the alkyl chains perpendicular to the substrate. All the LB films show a dichroic ratio for the peak at 2850 cm^{-1} which is very close to the value expected from perfect parallel orientation of the transition dipoles with respect to the substrate. The cast film on the other hand gives a value for the dichroic ratio which is indicative of neither random nor perfect alignment of the transition dipoles.

Plots 6-15B&16B show the polarised micro ATR spectra of the LB and cast films. Of most interest perhaps is the dichroism of the carbonyl peaks. Table 6(ix) gives the calculated ratios for the electric field density at 1740 cm^{-1} for the cast film and the 19 layered LB film. The experimental ratios are also given for the peaks at ~1740 & 1710 cm^{-1}. The dichroic ratio for the peak at 1740 cm^{-1} for the LB film is very close to that expected for a transition dipole orientated parallel to the substrate. This peak has been assigned as being due to the stretching mode from a carbonyl which is attached to an ester linkage in the trans conformation (see above). Thus,if the alkyl chains are perpendicular to the surface as proposed above the transition dipole moment of this vibration will be parallel to the substrate. This confirms the data from the $\nu_s(CH_2)$ peak. The dichroic ratio at 1720 cm^{-1} is between the values for a random orientation and parallel alignment of the transition dipole moment of the vibration. This is to be expected because this peak has been assigned to the vibration of a carbonyl group attached to an

ester linkage in the gauche conformation. Therefore the transition dipole moment of this vibration has components in direction both perpendicular to the alkyl chains and parallel to them and will therefore be coupled by both the x and z components of the 0° polarised light. The dichroic ratios of the cast film peaks are close to those expected for random orientation of the transition dipole moments involved in the vibration being coupled. The ratio for the peak at 1740 is greater than that at 1710 cm^{-1}. Over this short change in wavenumbers the calculated electric field ratio will not have changed much. Thus it is possible that there is some alignment of this transition dipole.

In the region of the CH_2 wagging progression (1350-1180 cm^{-1}) the dichroism of the cast film and LB film are similar (plots 6-15B&16B). It is very difficult to quantify the ratios due to a low S/N ratio for the LB film in this region. However, the transition dipole moment of the CH_2 wagging progression is largely parallel to the alkyl chains, i.e perpendicular to the substrate if the chains are perpendicular to the substrate. Now in this case the x component of the 0° polarised light will not couple strongly with the transition dipole moment nor will the y component of the 90° radiation. Once again the presence of the peaks due to P=O and COC vibrations complicates the analysis, but the spectrum of the wagging progression for the LB film (plot 6-16B) is at the noise ratio of the 90° polarised light spectrum and is weakly seen in the 0° polarised spectrum. Again this points to the alkyl chains being orientated largely perpendicular to the substrate

Thus the polarised IR dichroic ratios support the RAIRS findings that the alkyl chains of DPPA in an LB film are orientated largely perpendicular to the substrate. The dichroic ratio for the cast film also agrees with the conclusion made from the RAIRS spectra that the orientation of the molecules is not random.

Plot 6-17A : The calculated electric field for a 0.00256 μm film on silicon.

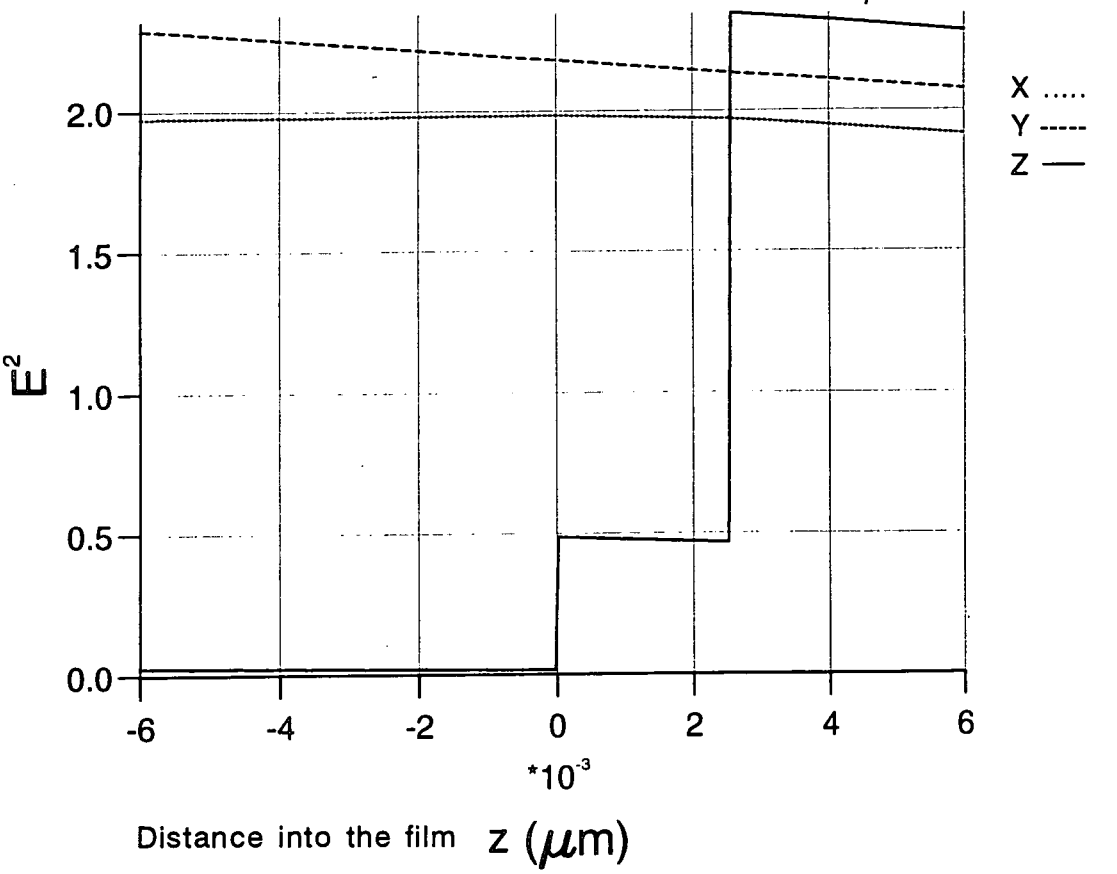

Plot 6-17B : The calculated electric field for a 0.0486 μm film on silicon.

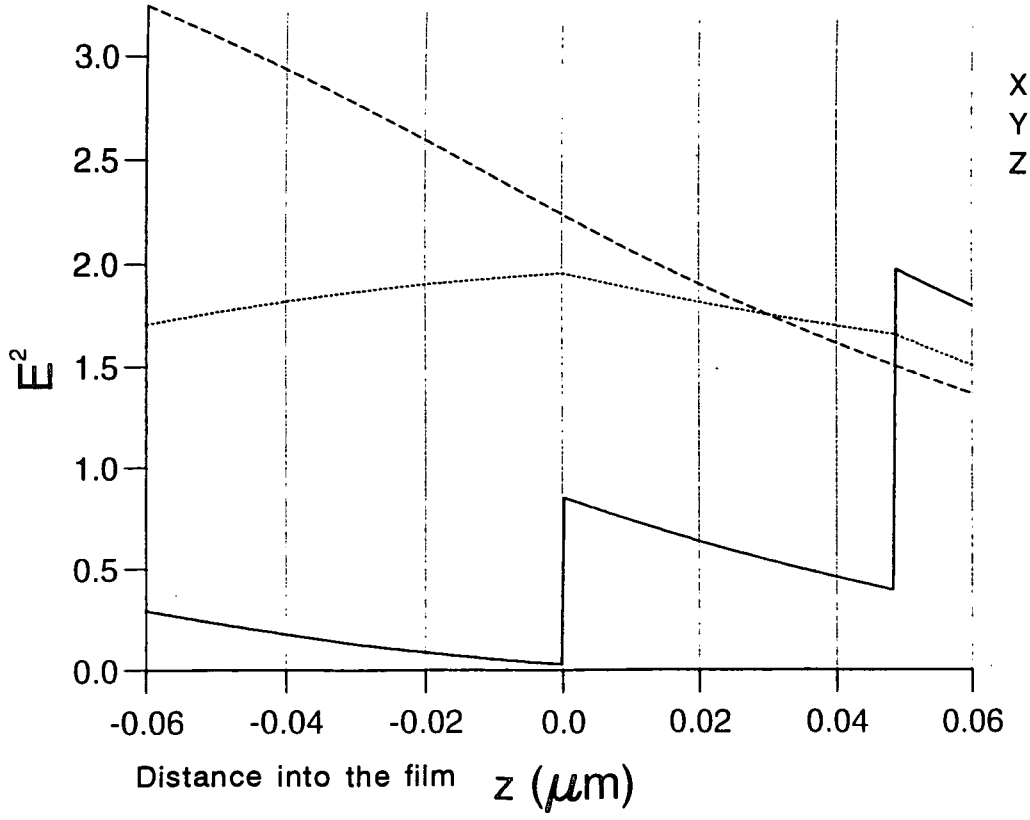

		integrated electric field density					
No. layers	Thickness (μm)	E_x^2	E_y^2	E_z^2	$E_y^2/(E_x^2+E_z^2)$	E_y^2/E_x^2	Expt. ratio
1	0.00256	0.005035	0.005532	0.001245	0.88	1.10	1.06
5	0.0128	0.02494	0.02698	0.006601	0.86	1.08	1.01
19	0.0486	0.08852	0.09200	0.02973	0.78	1.04	1.09
cast	0.1	0.1626	0.1640	0.07340	0.69	1.01	0.90
"	0.2	0.2484	0.2532	0.1735	0.60	1.02	
" k=0.1	0.2	0.2373	0.2458	0.1615	0.61	1.04	

Table 6(viii) : The calculated electric fields and ratios thereof for thin films at 2850 cm^{-1} with experimental ratios for polarised spectra.

			integrated electric field density					
No. layers	wave-number	Thickness (μm)	E_x^2	E_y^2	E_z^2	$E_y^2/(E_x^2+E_z^2)$	E_y^2/E_x^2	Expt. ratio
19	1740	0.0486	0.09146	0.09620	0.02724	0.82	1.02	1.0
19	1710							0.84
cast	1740	0.1	0.1771	0.1809	0.06471	0.77	1.03	0.73
cast	1710							0.63

Table 6(ix) : The calculated electric fields and ratios thereof for thin films at 1740 cm^{-1} with experimental ratios for polarised spectra.

6.6 : HORIZONTAL (LANGMUIR-SHAEFFER) DEPOSITION OF DPPA ONTO SLIDES AND MICROATR CRYSTALS

6.6.1 Results

The process of LS deposition is described in section 4.3.2.E. It was found that if the surface pressure feedback mechanism was active during the whole of a horizontal cycle that material equivalent to two monolayers of DPPA was transferred onto the sample. This was true whether the surface of the substrate was hydrophilic or was hydrophobic due to the presence of vertically deposited monolayers. The samples were extremely wet on removal, after the horizontal deposition, and took a long time to dry, indicating a hydrophilic surface.

A variation in the technique was tried in order to transfer a single monolayer. This was to use the feedback circuit until the sample touched the water and then to switch it off whilst the sample was withdrawn. The control mechanism was switched back on after the sample had been removed and thus the deposition ratio could be found. This method achieved deposition ratios varying from 0.5 to 1.0 for the larger samples (the RAIRS slides ~8 cm^2). However, for the smaller samples (the micro ATR crystal ~3 cm^2) it was found that this still led to a deposition ratio of 2.

A third variation in the technique was tried for the smaller samples, the micro ATR crystals. This involved bringing the sample into contact with the monolayer whilst the surface pressure control mechanism was switched on. The trough barriers were then fully expanded, allowing the monolayer to relax. The substrate was then withdrawn from the surface of the water. Using this technique all information on the deposition ratio was lost, because it was found that on recompression the area occupied by the monolayer had increased by orders of magnitude more than the size of the crystal. This is because a compressed monolayer was only used for deposition after stabilisation for 1.5 hours and expanding the barriers disturbed the close packing thus achieved.

Plot 6-18

Graph of CH_2 antisym. stretch intensity versus the number of layers for DPPA on a micro ATR crystal

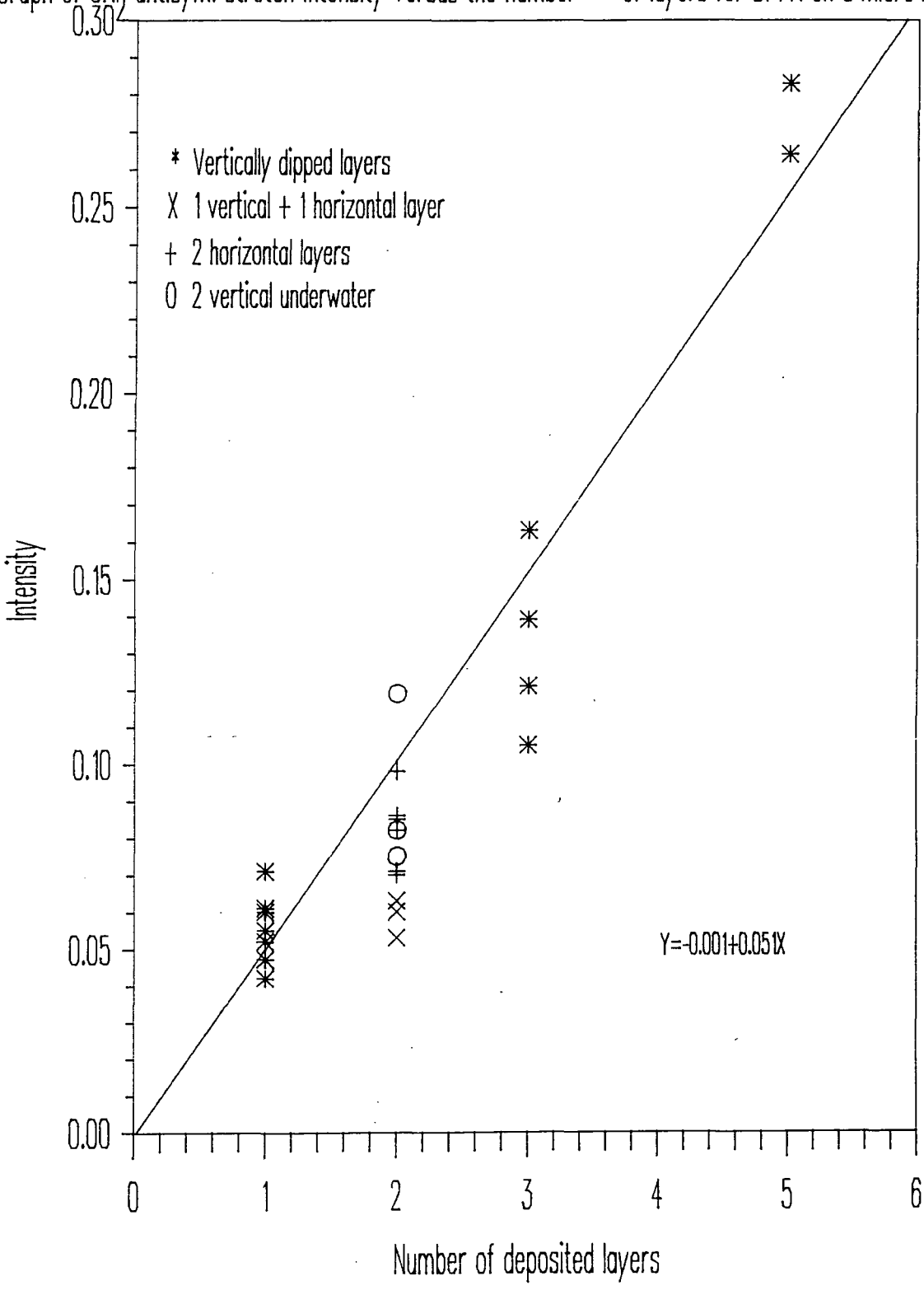

6.6.2 Discussion of the LS deposition results

The LS deposition of two layers during one cycle was recently reported by Virtanen et al[111] for stearic acid onto a hydrophobic substrate. They found that the incremental thickness for each cycle was equal to the thickness of a bilayer by LB deposition. They were able to build up bilayers of material in a similar fashion to the more usual LB deposition. Therefore it is probable that bilayers of DPPA were deposited onto the hydrophobic surface. Now for the hydrophilic surface of the clean crystal material equivalent to two monolayers was also deposited. The crystals are known to be hydrophilic from their LB deposition characteristics, so it seems likely that the DPPA will orientate such that its headgroup is against this surface. The observation that the crystal appeared wet after the deposition indicates that the surface was still hydrophilic. Therefore the most likely structure for the DPPA is as a biological bilayer. A possible mechanism for the formation of such is shown in figure 6(b). Whether the structure of the layers remained as a biological bilayer after the evaporation of the water is open to debate. It is known that monolayers deposited via one type of LB deposition can rearrange with time to give different layered structures[19]. Also that monolayers can rearrange on passing through the air water interface[108]. So it is possible that although the LS deposition deposited DPPA as a biological bilayer that by the time the FTIR spectrum was recorded this structure was no longer intact.

Plot 6-18 shows the ATR peak heights of the $\nu_{as}(CH_2)$ vibration versus the number of deposited layers for a variety of vertically and horizontally deposited layers. This confirms that for a hydrophilic substrate with two LS layers deposited in one cycle the deposition ratio of ~2 layers was correct.

Plot 6-18 seems to show that when the third method of horizontal deposition was used onto a micro ATR crystal with one LB monolayer that the amount of material on the sample was equivalent to one monolayer not two as hoped. This does not

completely exclude the possibility that a bilayer was produced because the error can be seen to be quite large on the peak heights of the $\nu_{as}(CH_2)$ for vertically deposited samples with the same number of layers (E.g. the large number of samples with only one monolayer show a variation of 0.04 to 0.07 absorption units). However, the FTIR spectra of three samples with one LB layer and one LS layer were recorded. All of these gave the same peak height intensity as a monolayer and were in the range 0.055 ± 0.01 whereas the fitted line gives a value of 0.1 for the peak height of the $\nu_{as}(CH_2)$ arising from a bilayer. Another possibility may also be considered. This is that the reflectivity coefficients of LS deposited layers differ from those of LB layers. As no deposition ratios could be recorded the more probable conclusion is that there is only one monolayer of material and not two.

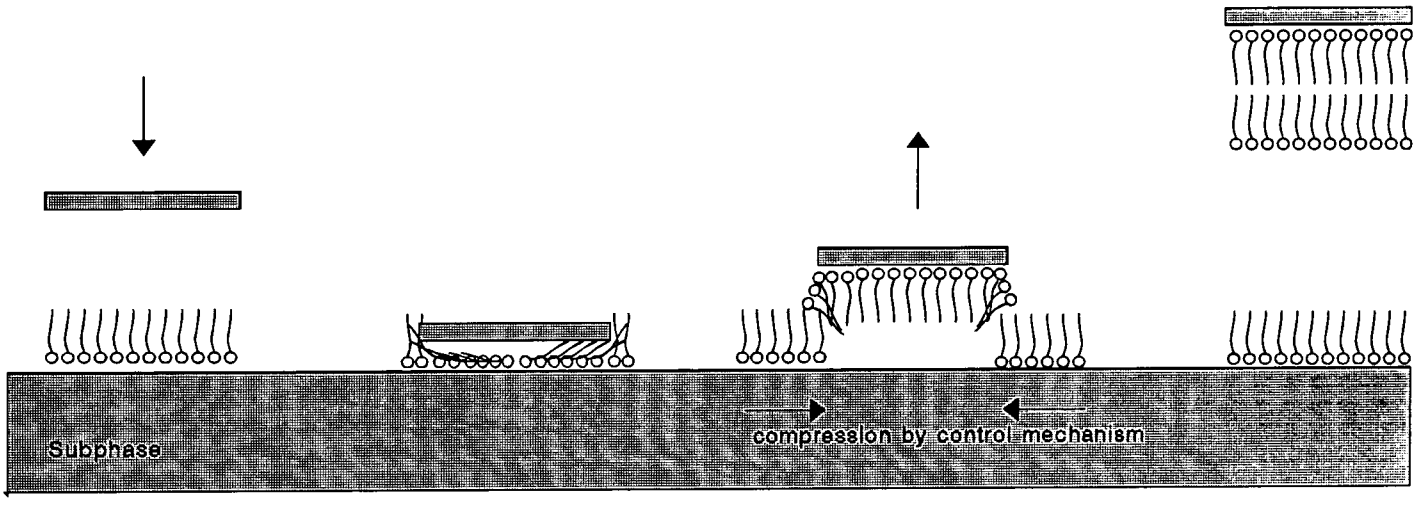

Figure 6(b) : A mechanism for the deposition of a biological bilayer via horizontal dipping.

6.7 : FTIR SPECTRA OF BIOLOGICAL BILAYERS OF DPPA

6.7.1 Via spectral subtraction

The technique of spectral subtraction to obtain the spectrum of a biological bilayer is described in section 4.3.2.E and is illustrated in figure 4(m).

The technique was not very successful, mainly due to the problems encountered with vertical deposition described in section 6.3. However, the one success is shown in plots 6-19&20. Plot 6-19 shows the smoothed RAIRS spectra of two samples. The spectra illustrated as a solid line is of a sample with 9 LB layers and then one LS layer. The deposition ratio of the LS layer was 1.1. The dashed line in, plot 6-19, shows the RAIRS spectrum of a sample with 7 LB layers and one LS layer (deposition ratio 0.85). The real spectra, unsmoothed are shown in plot 6-19A. There is an extremely low S/N ratio (~2) for the sample with 10 layers in the spectral region where the bending mode of OH in water vapour occurs. This looks like a differentiation of the water vapour spectrum and is impossible to remove by spectral subtraction. This is caused by an unknown optical effect in the RAIRS equipment. The S/N ratio of the sample with 8 layers is much better over the whole spectrum.

Plot 6-20 is the smoothed spectrum which results from the subtraction of the spectrum of the sample with 8 layers from that of the sample with 10 layers. This should be the spectrum of a biological bilayer (figure 4(m)). Whilst this may seem to give a valid spectrum the unsmoothed version (plot 6-20A) shows that the S/N ratio is so low that it is difficult to draw many positive conclusions from this technique. The CH_2 wagging mode progression is apparent. The relative intensities of all the peaks appear to be the same as the original spectra.

There was also a doubt as to whether the spectrum arising from the subtraction was indeed a biological bilayer. It could be argued that the part of the spectrum arising form the first and last layers cancel in the subtraction. Then the rest of

the spectra arise from pairs of inverted bilayers. Thus the spectrum which results from the subtraction of a spectrum of 8 layers from 10 results in an inverted bilayer (figure 6(c)).

The technique of spectral subtraction was also used for micro ATR spectra of 5 and 3 layers. Again a low S/N ratio of the resultant spectra indicated that this technique was not very useful.

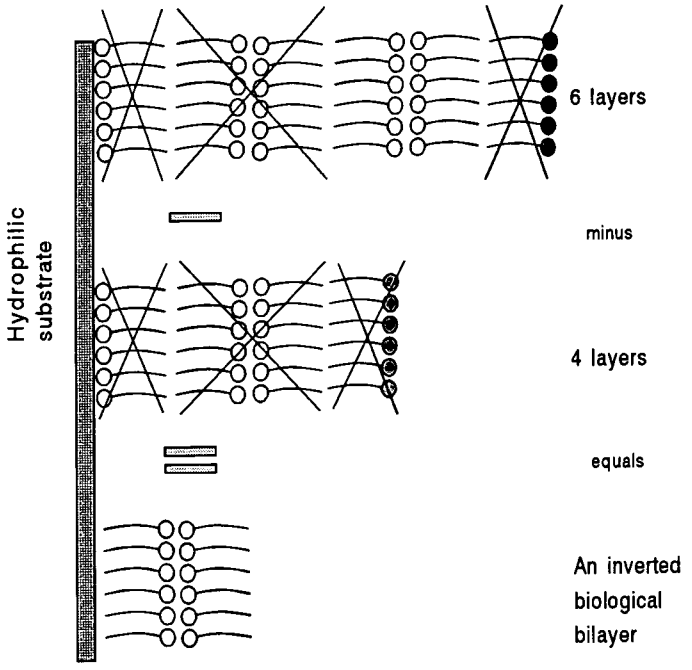

Figure 6(c) : The possibility that the subtraction strategy in fact gives the spectrum of an inverted biological bilayer. Crosses indicate the layers which cancel on subtraction.

Plot 6-19: 10 and 8 LB layers by RAIRS (9 point smooth)

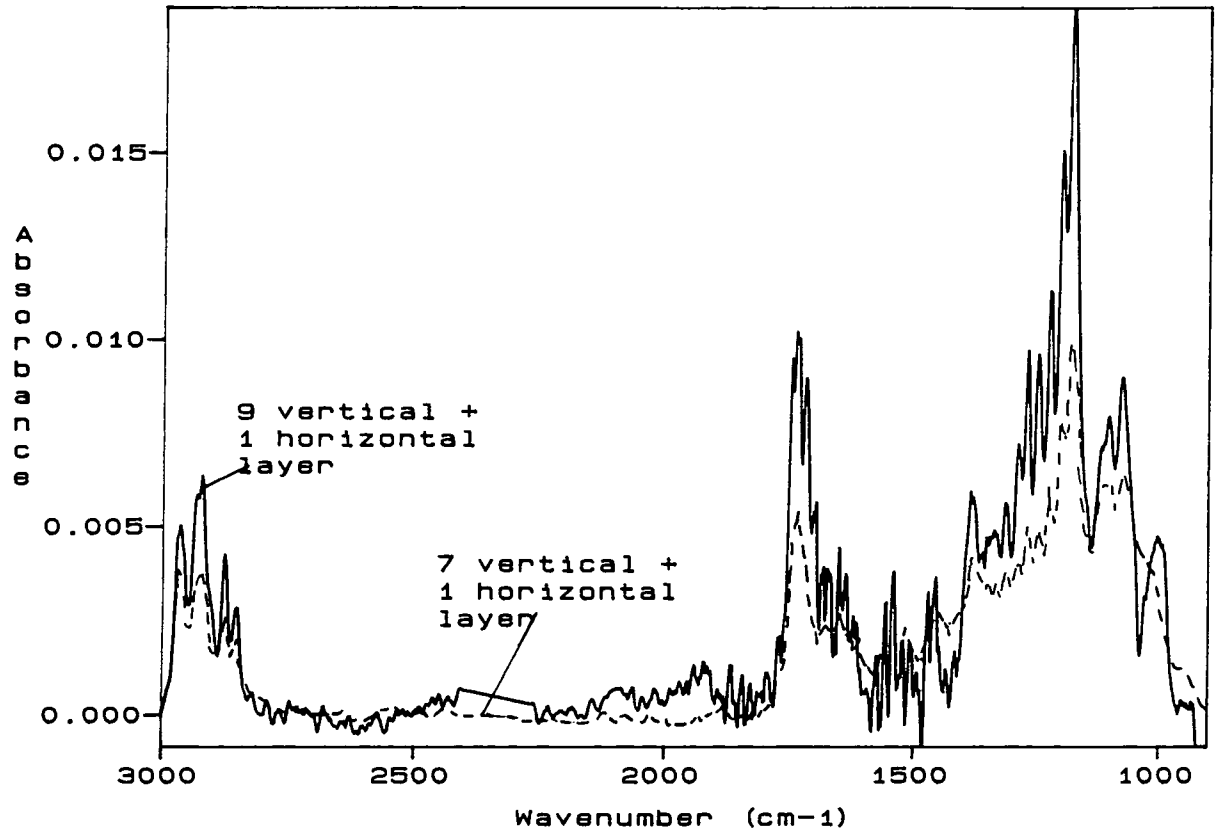

Plot 6-20: Bilayer RAIRS spectrum by subtraction 11 point smooth

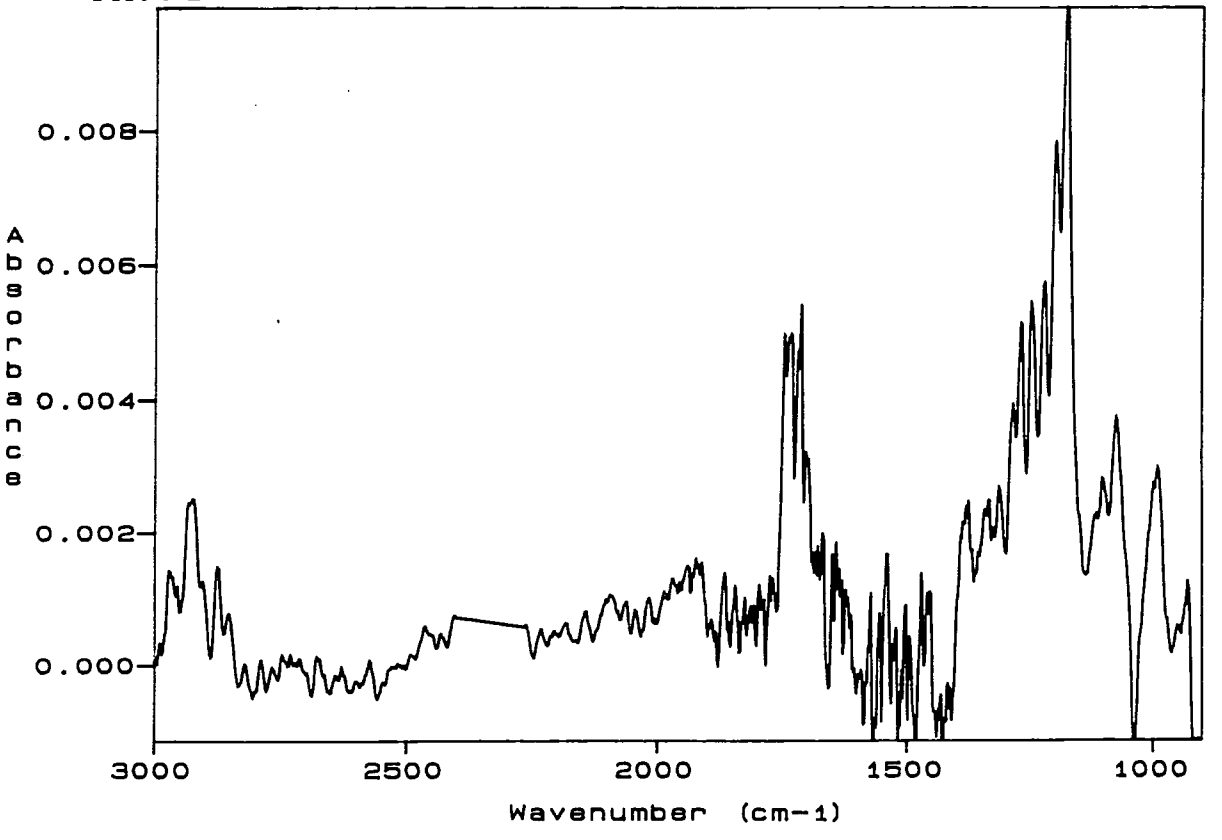

Plot 6-19A: Unsmoothed version of plot6-21

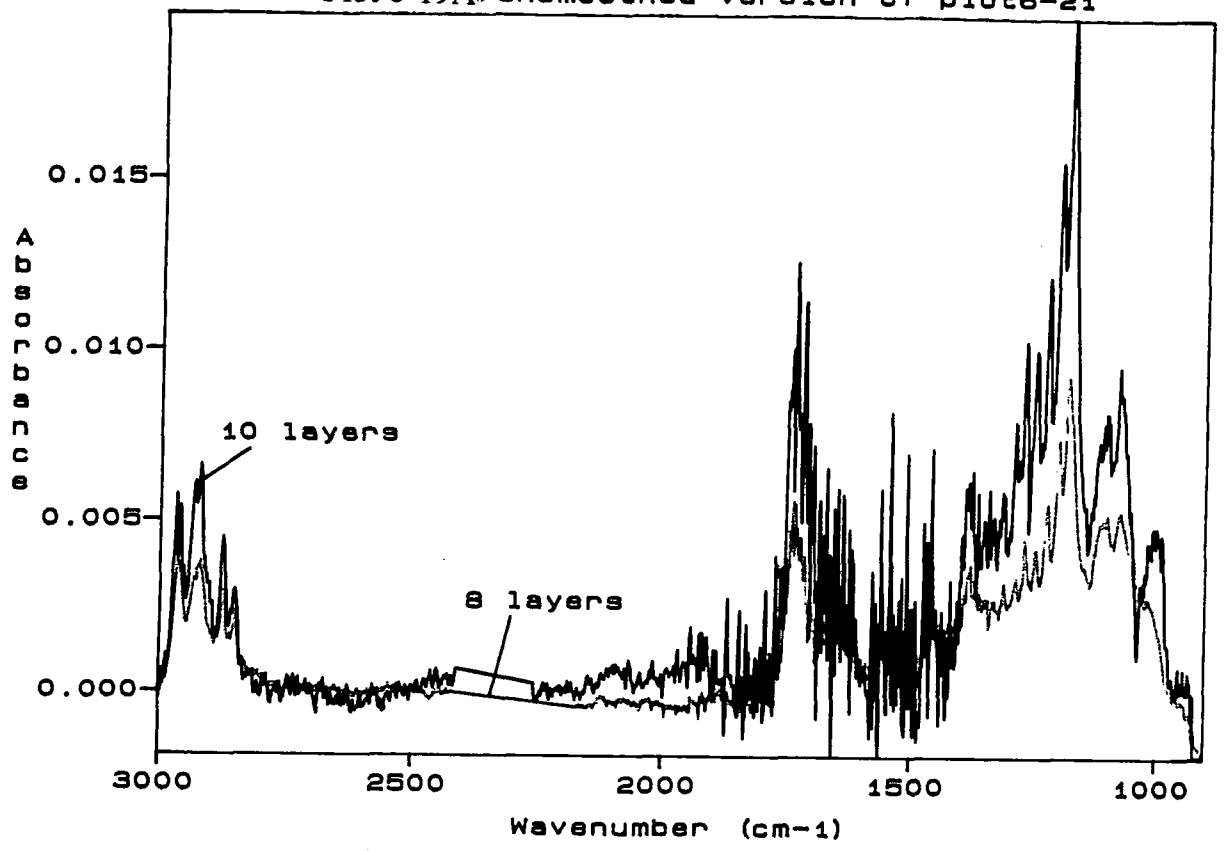

Plot6-20A: Unsmoothed version of plot6-22

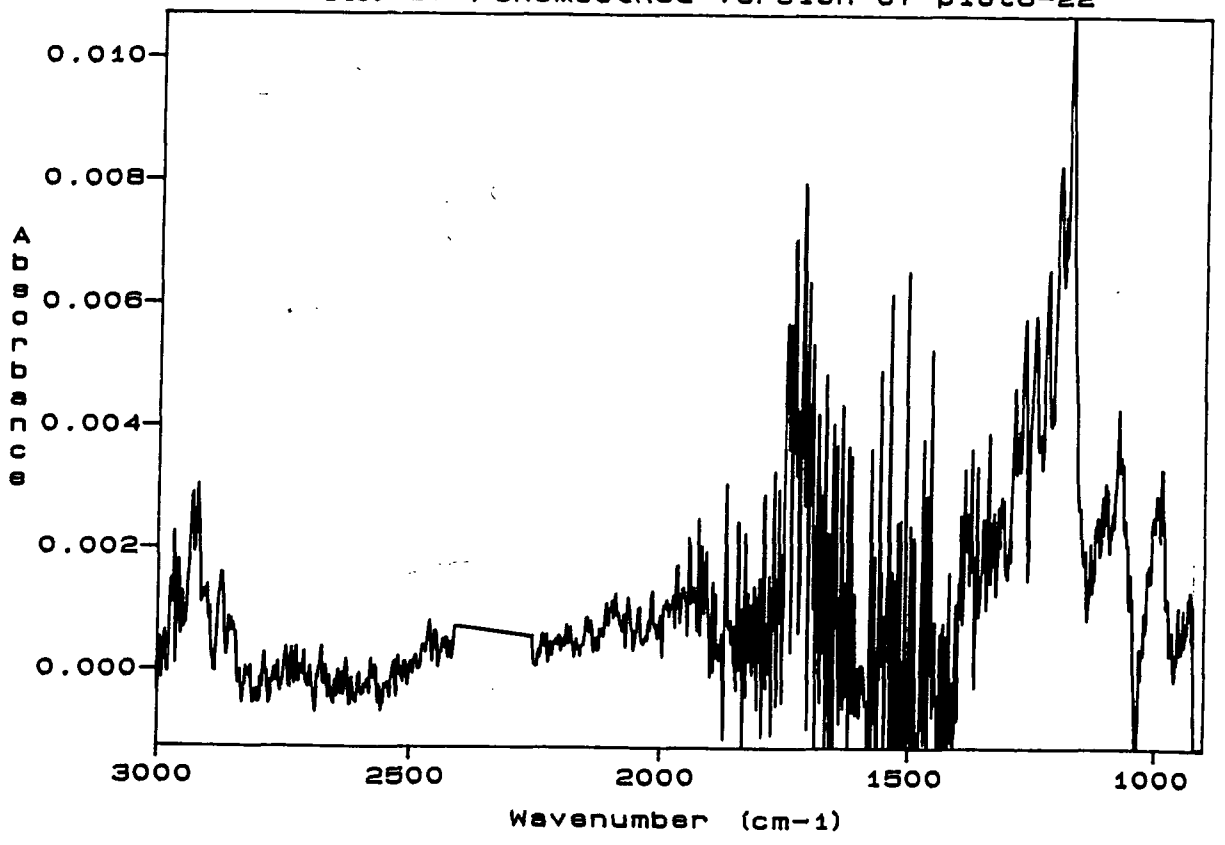

6.7.2 The ATR spectra of a biological bilayers obtained by the use of horizontal deposition techniques

Plot 6-21 shows the micro ATR FTIR spectrum of a monolayer of DPPA deposited by LB dipping. It seems to be similar to the spectrum of 19 LB layers (plot 6-14). The band due to the symmetric bending mode of the CH_3 groups is very broad, this has been discussed in section 6.5.2. There is no evidence of the peaks due to the wagging mode of the CH_2 chains. Whether this is because the chains are no longer all trans or the peaks are too low in intensity to be detected difficult to tell. However, the position of the peaks due to the CH_2 stretching modes indicate that the molecules are below their phase transition temperature, thus the chains should be all trans in conformation.

Plot 6-22 shows the spectrum obtained from a sample which had one monolayer deposited via LB dipping and the other via the third technique of LS deposition. As discussed in section 6.6 the intensities of the peaks are low relative to those in the monolayer spectrum (plots 6-18&6-21). The positions of the peaks due to the ν (CH_2) vibrations again indicate an all trans chain. The most interesting point about the spectrum is that the band due to the carbonyl stretching mode is similar to those seen for cast films (plots 6-1,6-8 & 6-13). This same structure is also seen in the spectrum of a sample where the second LS technique was utilised to produce the sample (deposition ratio 2.2) (plot 6-23). Therefore, the technique of horizontal deposition must be produce films with a structure closer to the films cast from chloroform and the crystalline powder rather than those prepared by LB deposition.

Plot 6-21 : A monolayer of DPPA by ATR (verical deposition)

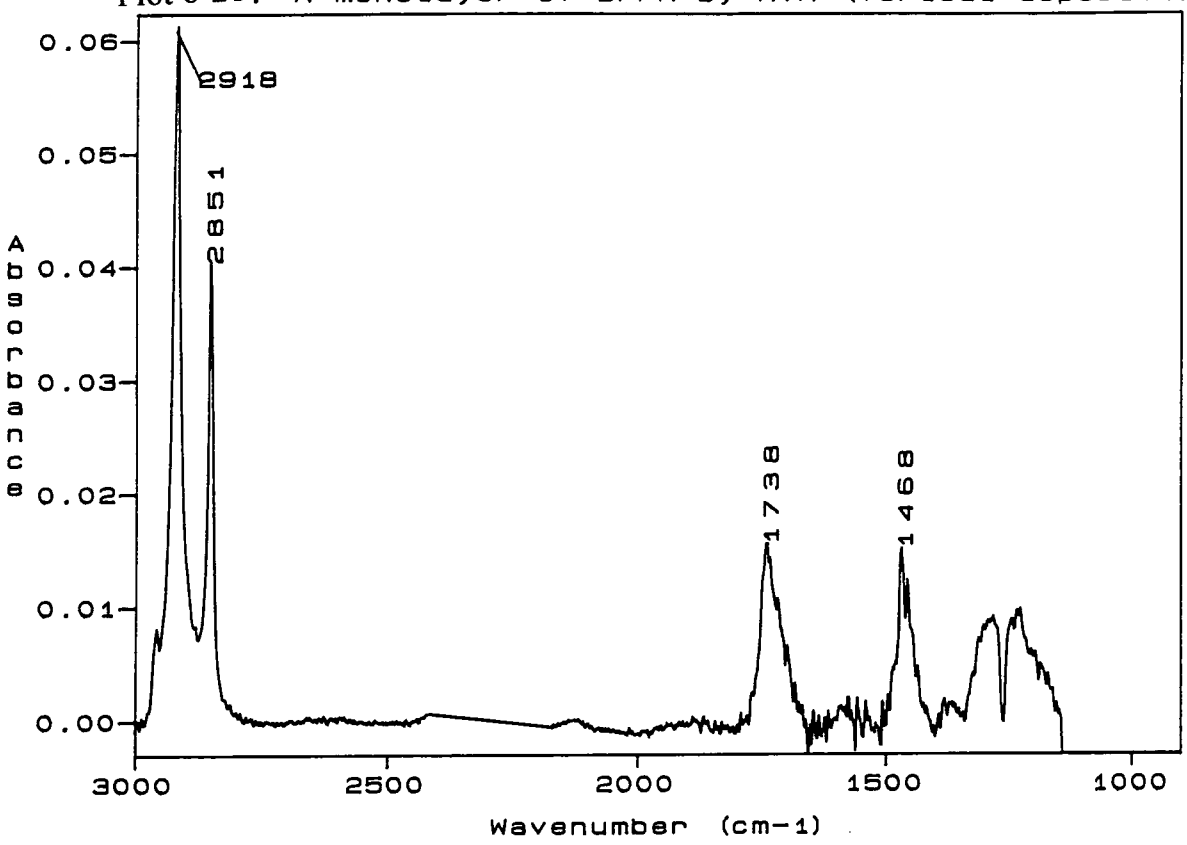

Plot 6-22 : Bilayer of DPPA : One vertical and one horizontal layer

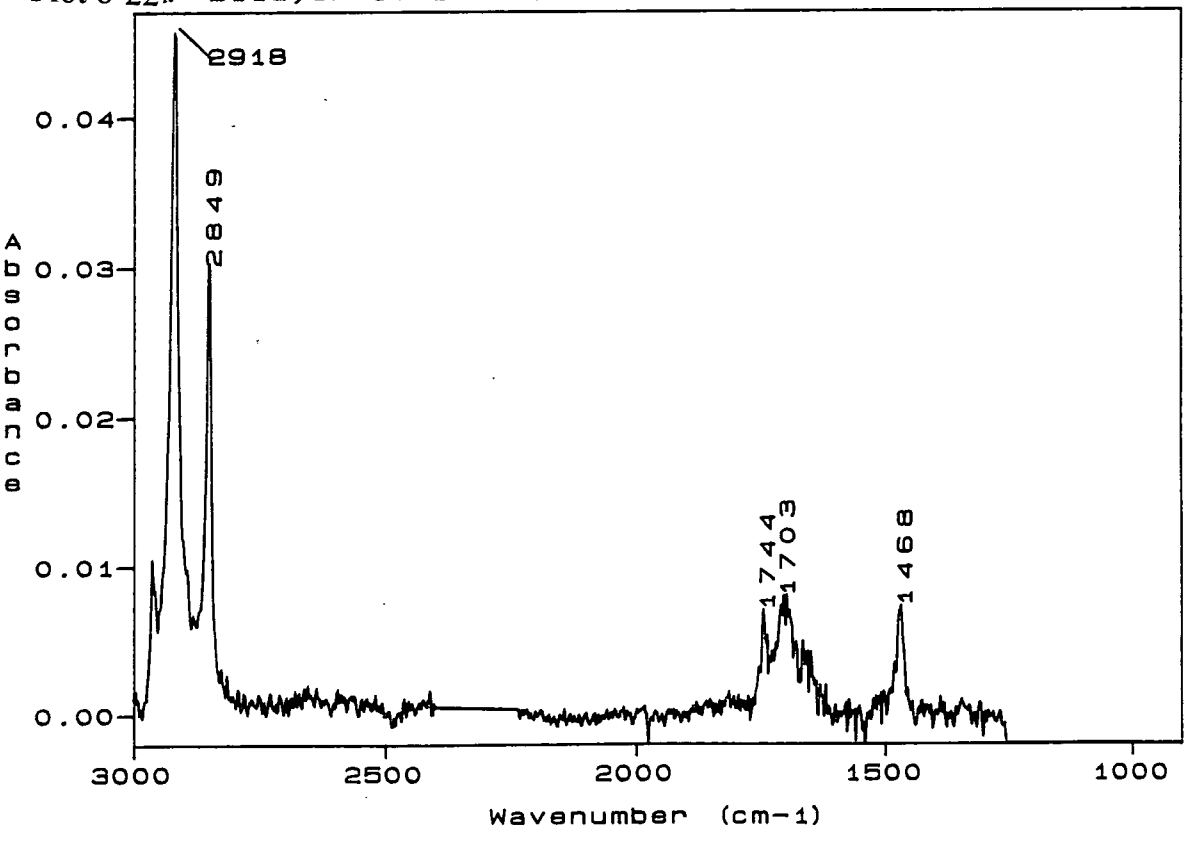

Plot 6-23: Bilayer of DPPA : Two horizontally deposited layers

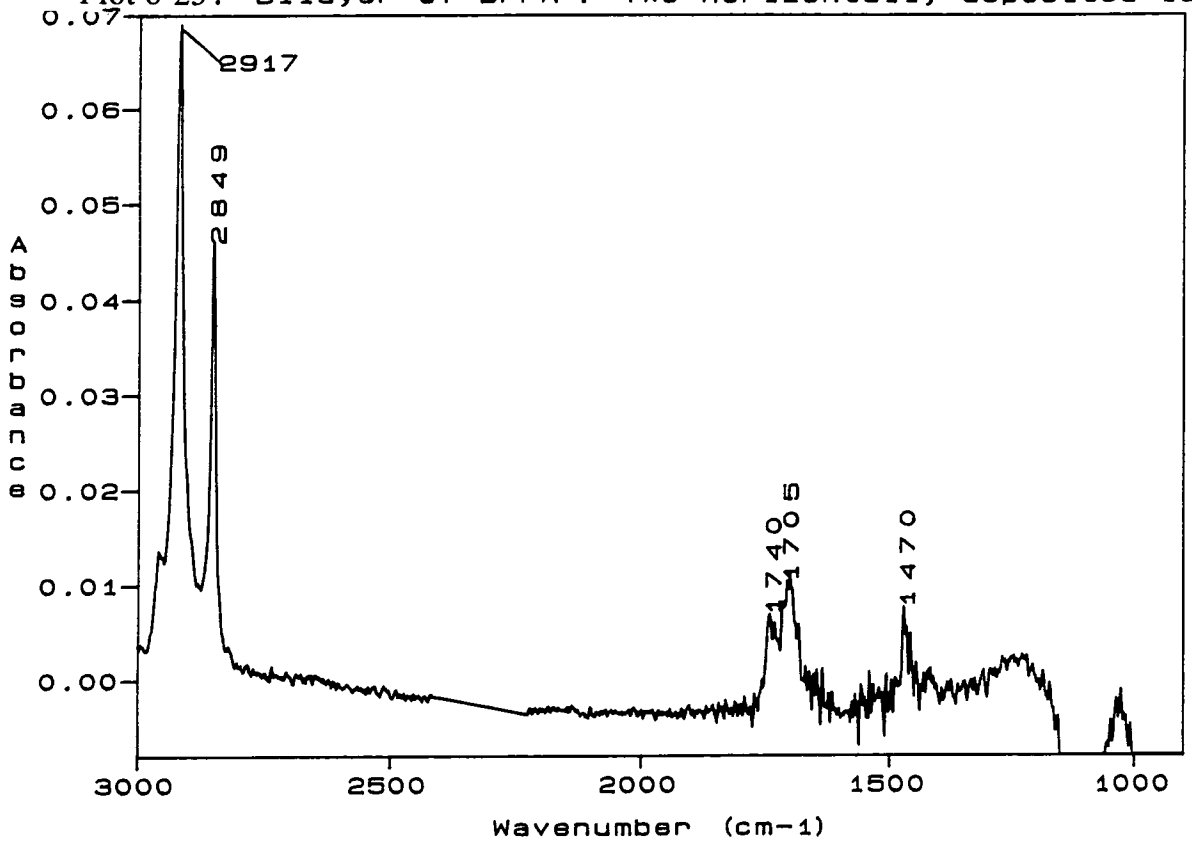

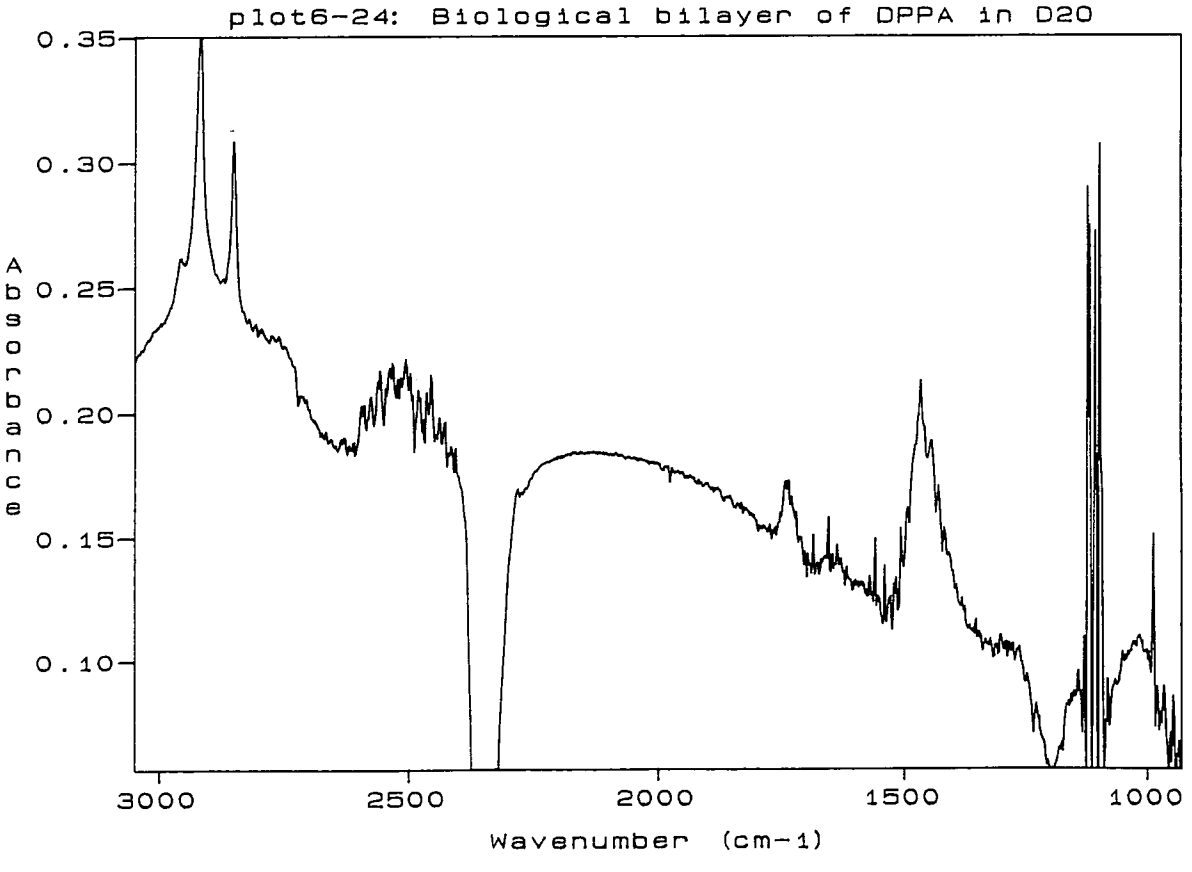

6.7.3 The preparation of a biological bilayer by LB deposition onto a micro ATR crystal, keeping the crystal underwater

This technique for preparing a biological bilayer of DPPA is outlined in section 4.3.2.D. A typical micro ATR spectrum of such a bilayer, where the H_2O has been replaced by D_2O, is shown in plot 6-24. The H_2O was replaced by D_2O, partly to examine the peak at ~1740 cm^{-1} but mainly as a background experiment for later ones in which peptides were utilised. The change of solution was achieved without exposing the sample to air by slowly injecting D_2O through the cell (shown in figure 4(v)). The spectrum (plot 6-24) is similar to that of the monolayer, i.e. typical of films deposited by the LB technique.

Plot 6-25 shows the spectral region 1800-1300 cm^{-1} for this sample. The small peak at 1740 cm^{-1} in the black spectrum is due to the lipid. There will also be a small peaks at ~ 1470 and 1375 cm^{-1} from the lipid, the first about half the intensity of the peak at 1740 cm^{-1} and the second much smaller still. The two large peaks seen in the spectra at ~1650 and ~1380 cm^{-1} have been assigned as bending modes in the molecules H_2O and HOD respectively[31]. The numbers on the spectra correspond to time in minutes since the H_2O was exchanged for D_2O. A control experiment was performed where both crystals with a monolayer and the sample with 19 monolayers, prepared by usual LB techniques, were placed in the aqueous cell with water which was then replaced with D_2O. In neither case, nor for the same experiment with clean micro ATR crystals, was there any peak due to H_2O or HOD, after the exchange, only those of D_2O. Therefore it was concluded that the H_2O present in the biological bilayer must be trapped by the lipid, probably between the headgroups and the silicon crystal.

Plot 6-26 shows the decay in the peak height of the band due to the bending mode in H_2O for two different experiments. There appears to be more water in the one sample than in the other. There is a gradual decrease in the intensity of the 1650 cm^{-1} peak with time. This has been interpreted as the loss of H_2O from the sample. Plot 6-27 shows the peak heights of the band arising from the bending mode of HOD. These increase to a maximum then decrease.

Plot 6-25: The exchange of H20 for D20 in a bilayer of DPPA

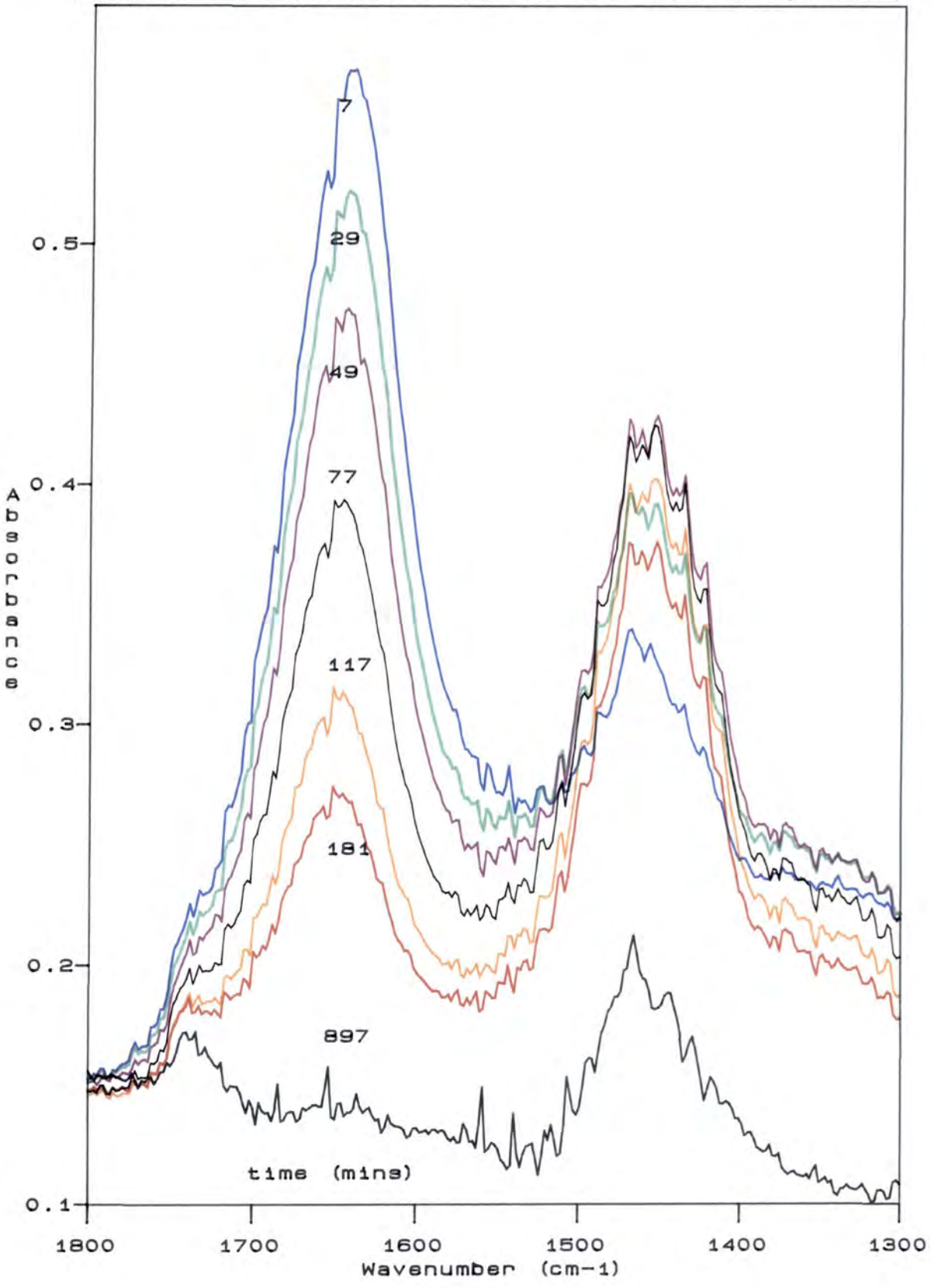

Plot 6-26 Graph of intensity of the H2O bending mode vs the time since exchange of H2O for D2O

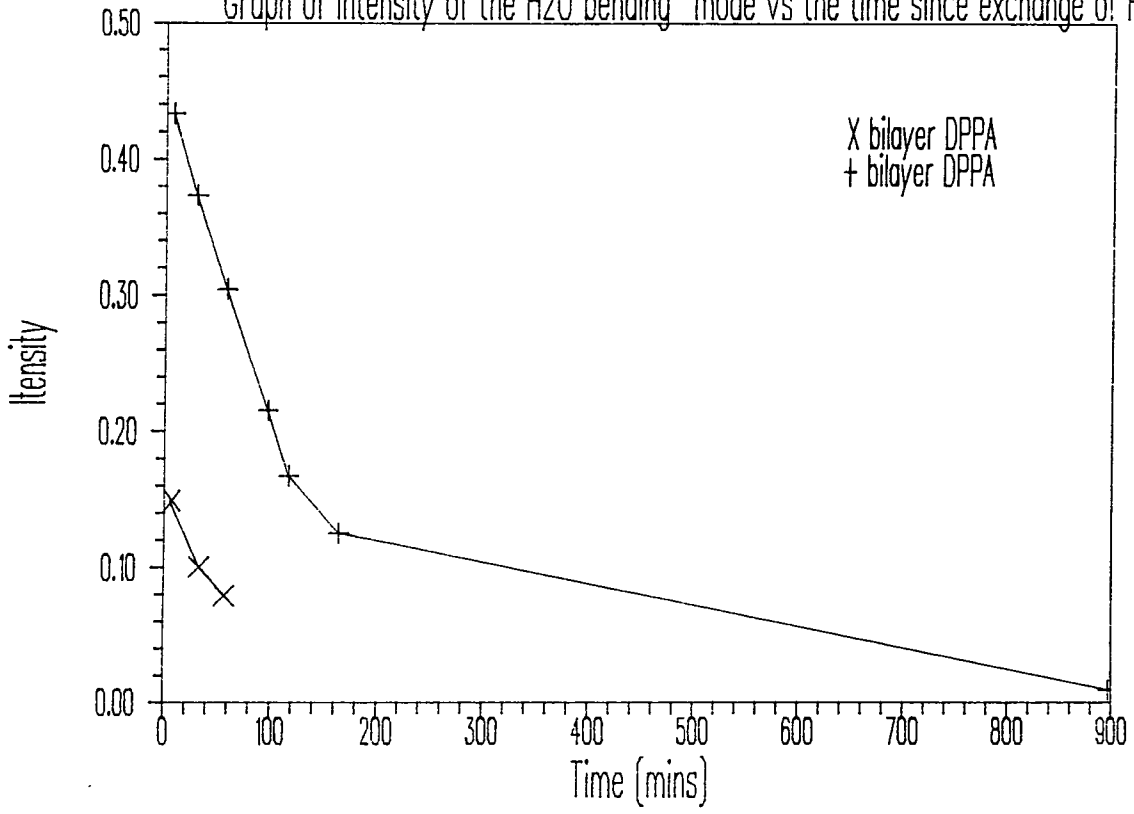

Plot 6-27 Graph of intensity of the HOD bending mode vs the time since exchange of H2O for D2O for biological bilayers of DPPA

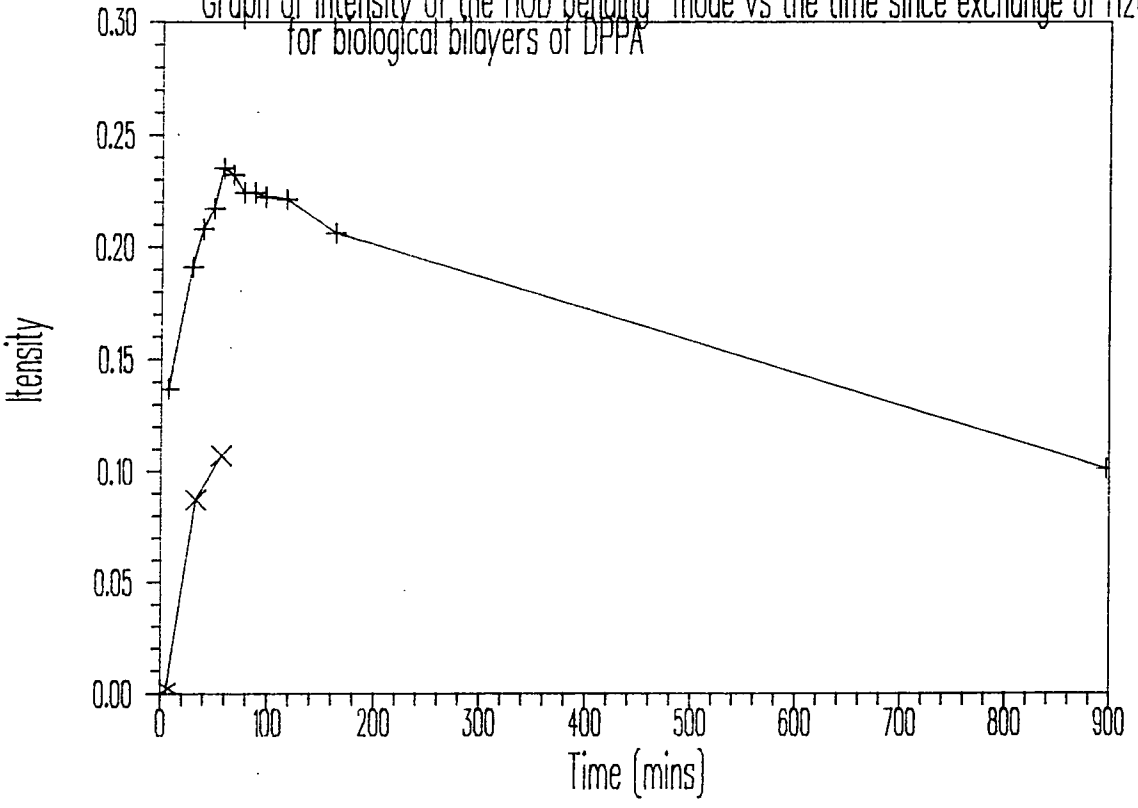

Now obviously more experiments need to be performed for confirmation of the results (in chapter 7 another similar experiment is described where the oligo-peptide gramicidin has been incorporated). However, some explanation of the results obtained must be made. It is proposed that there was H_2O bound tightly to the lipid. When the H_2O was replaced with D_2O this was not displaced with the rest of the H_2O. As time progressed the D_2O diffused through the bilayer where the deuterium exchanged for the hydrogen on the bound water. This produced the increase in the concentration of HOD. However, the intensity due to the HOD bending mode started to fall after one hour. The HOD must have been diffusing through the bilayer into the bulk. The recorded intensity falls because the HOD is moved into the bulk D_2O where the electric field density will decrease[39]. Thus, the kinetic processes occurring are (figure 6(d)) several fold. There is diffusion of D_2O, HOD and probably H_2O both ways through the bilayer, then there is the deuteration process. Now deuteration of H_2O occurs on a very short time scale (~μs). Therefore the rate limiting step should be the diffusion of the D_2O to where the H_2O is. The rates of diffusion for all the isotopic forms of water should be about the same.

The equations for a first order rate equations (Atkins[163]) were applied to the data shown as +'s in plot 6-26. The last point was not used as it was not certain at what time in the night the intensity had fallen to this ratio. A straight line was seen for the plot of $\ln(A_t/A_o)$ vs time (plot 6-26A). Where A_t = absorbance (α the concentration) at a time t (minutes) and A_o is the absorbance at t=0. The rate constant was found to be 0.0082 min^{-1}. This gives a half life of 85 minutes.

The FWHH for the band due to the bending mode of H_2O at ~1645 cm^{-1} is ~85 cm^{-1}. This is greater than the width normally found for bulk water[162], which is 75 cm^{-1}.

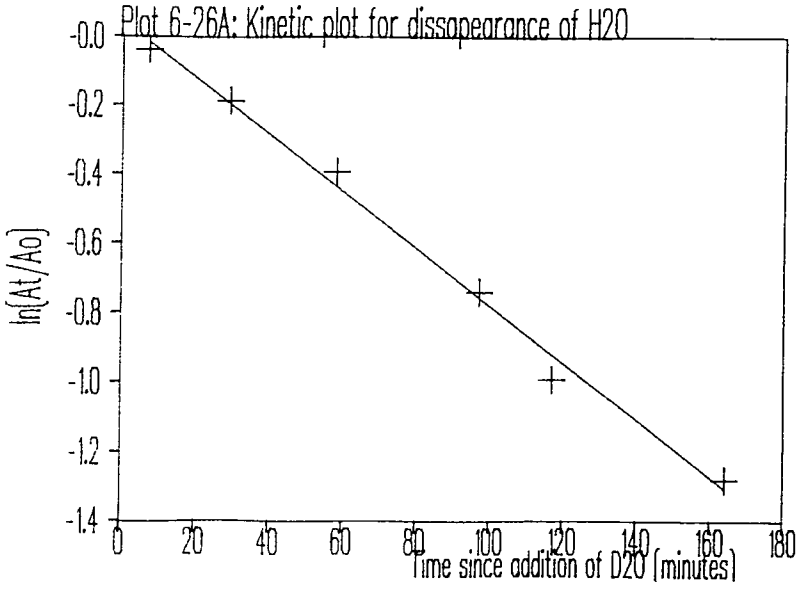

At this stage it is very difficult to draw conclusions on the results presented above. It is certain that whatever the processes occurring that they are not equivalent to the diffusion of water from bulk liquid to bulk liquid through a lipid bilayer. This arises from the data of other researchers. Stein[3] reports that the diffusive permeability of water through an artificial lipid bilayer is between 1 and 11 X 10^4 cm s^{-1}. There is an equation which relates the permeability to a half life for the diffusion of the material through a membrane. This is the time taken for the concentration to reach half its equilibrium value. This is given in Stein[3] as :

$$t_{1/2} = 0.693*V/(PA) \qquad \text{Eqn 6(iv)}$$

Where $t_{1/2}$ = the half life for the passage of a material through a membrane

P = the diffusive permeability

A = the area of the membrane

V = the volume of the cell into which the material into which permeation is occurring

Now the area of the membrane in the experiment described in this thesis is ~1 cm^2. Therefore, taking the minimum permeability, to estimate the maximum half life, the half life for the diffusion of water would be $V*10^{-4}$ $cm^{-3}s$. In the the case of a thin film of water trapped between a lipid and the surface, with an area of 1 cm^2, the volume is obviously going to be very small, possibly of the order of 10^{-7} cm^3. Therefore it would be expected from this that the large amounts of D_2O would diffuse through the bilayer in a fraction of a second. Therefore, either the H_2O is so tightly bound that exchange does not occur, or more likely the diffusion of D_2O (and other water analogues) is very slow through the bilayer. Thus indicating that the bilayer formed is not completely analogous to a bilayer surrounded by aqueous media on both sides.

The data obtained in these two experiments is very new and exciting but further studies will have to be undertaken in order to understand the processes occurring.

6.8 : DEPOSITION OF DPPA OVER CALCIUM ACETATE

Plot 6-28 shows the ATR spectra of a monolayer (scaled by a factor of 9) and 9 LB layers of DPPA, both samples were deposited over a subphase containing calcium acetate. The spectra are in general similar to that of the 19 LB layers deposited over pure water (plot 6-14). Plot 6-28A shows the spectral region 3000-2800 cm^{-1} for both the sample of 9 layers deposited over calcium and the 19 layers over water (normalised spectra shown). It can be seen that the peak shapes and positions are in close agreement. Thus once again the DPPA is below its phase transition temperature.

The $\nu_{as}(CH_2)$ wagging series of peaks is very weak in the spectrum of the 9 layers deposited over calcium acetate (plot 6-28). On close examination of the region 1350-1180 cm^{-1} it is possible to see the first six peaks in this series.

Plot 6-28B shows the synthetic peaks fitted to bands in the region 1800-1500 cm^{-1}. The parameters for the synthetic peaks are given in table 6(x). There is an extra peak at ~1550 cm^{-1}, compared to plot 6-14A. This was reported in reference 115. At the time that paper was written it was hypothesised that this peak could be due to a bending mode of perturbed water. However this now seems unlikely, because such a large shift in the position of the bending mode of water has not been recorded before[162].

Description	Plot no.	No peaks fitted	wavenumber (cm^{-1})	FWHH (cm^{-1})	absorption amplitude	integrated intensity (cm^{-1})	% Lorentzian
9 layers deposited over Ca acetate	6-28B	4	1739	25	0.103	1.94	50
			1710	34	0.037	2.93	50
			1655	80	0.034	3.80	50
			1558	50	0.029	1.70	100

Table 6(x) : The peaks fitted to the band arising from the carbonyl stretching mode of the ATR FTIR spectrum of DPPA deposited over calcium acetate

The peak is however at the same position as an intense band in the spectrum of calcium acetate solution (plot 6-29) (the rest of the spectrum is not shown as the only other major peaks all arise from the spectrum of water). The peak at 1550 cm^{-1} is not seen in the spectrum of calcium chloride solution, nor in the spectrum of a DPPA mull with calcium chloride. Therefore, it seems likely that the peak at 1550 cm^{-1} in plots 6-28&28B arises from acetate ions which are incorporated into the LB film on deposition. There is one problem with this analysis. That is, that there should also be a higher relative intensity of the peak centre at 1412 cm^{-1} in the lipid spectrum due to a contribution from a peak at a similar wavenumber in calcium acetate. This does not seem to have occurred.

To conclude, the ATR spectrum of DPPA deposited over calcium acetate is similar in form to that obtained from DPPA deposited over water. The exception is the occasional presence of a peak centred at 1550 cm^{-1}. This was observed in the spectra of several samples, deposited on different days. However, it does not occur on every occasion that DPPA is deposited over a subphase containing calcium acetate (Petty et al[34]). There are three main possibilities for the assignment of this peak: (a) it is due to a stretching mode in the carboxylate of the acetate anion; (b) it is due to the presence of an impurity in the film; (c) it is due to a vibration involving the lipid. Without further studies it is difficult to positively assign this peak at 1550 cm^{-1}.

Plot 6-28: 9 layers DPPA dipped over calcium acetate (ATR)

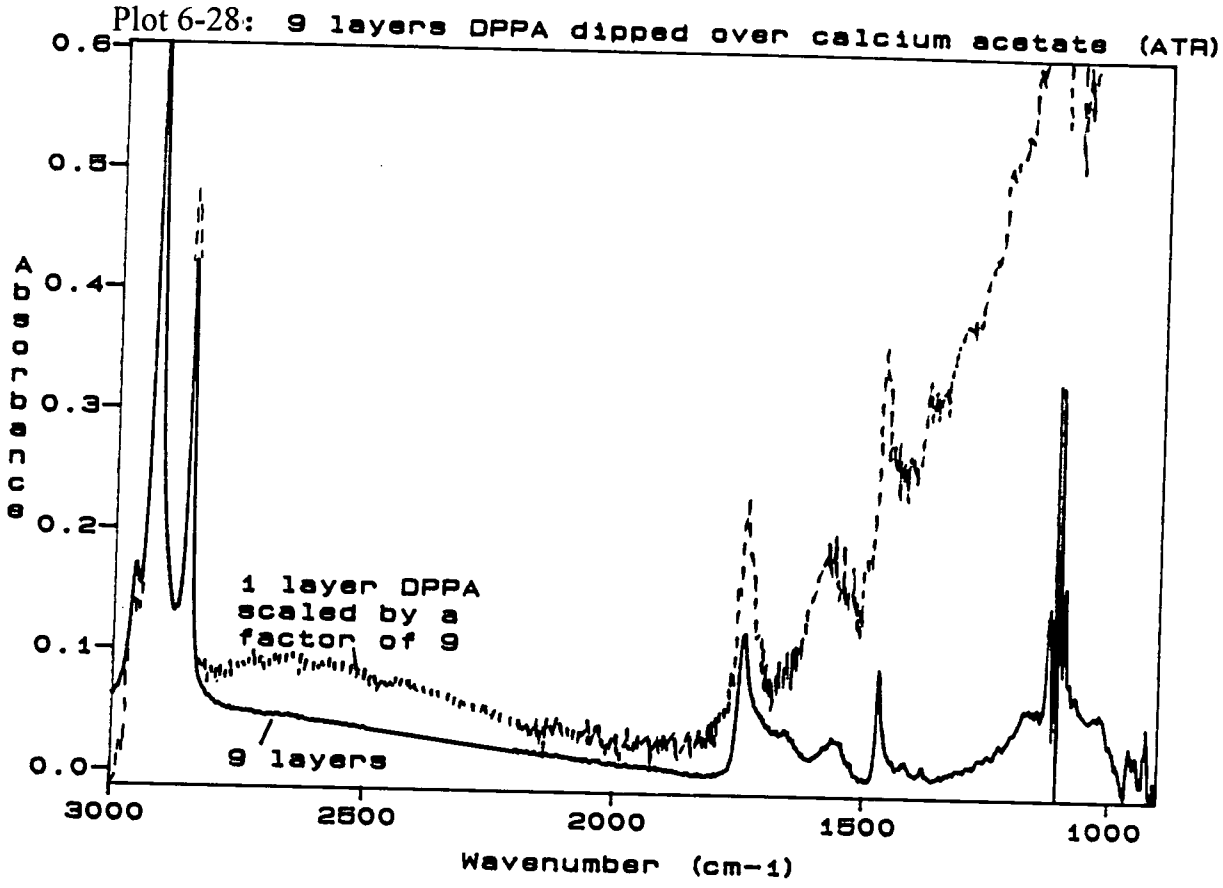

Plot 6-28A: DPPA over water and calcium by ATR (normalised)

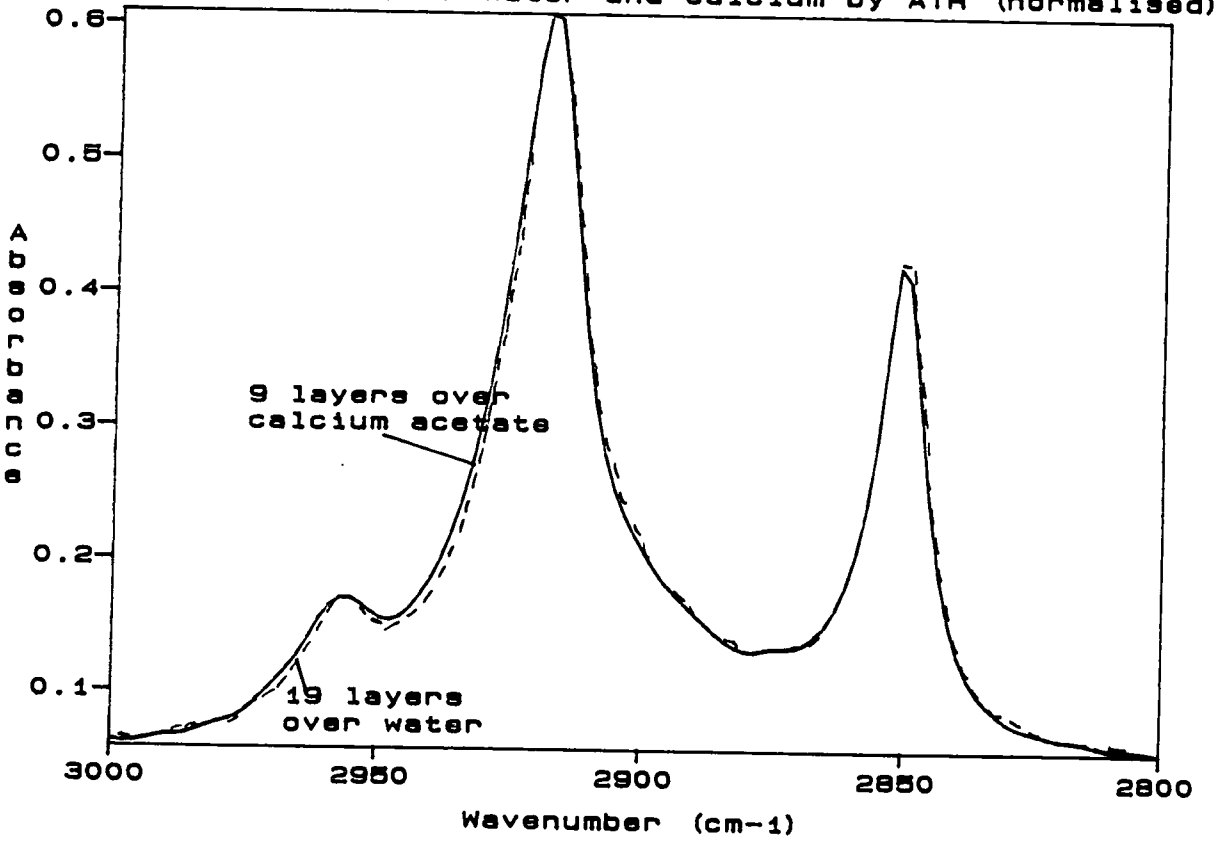

Plot 6-28B: 9 layers DPPA dipped over calcium acetate (ATR)

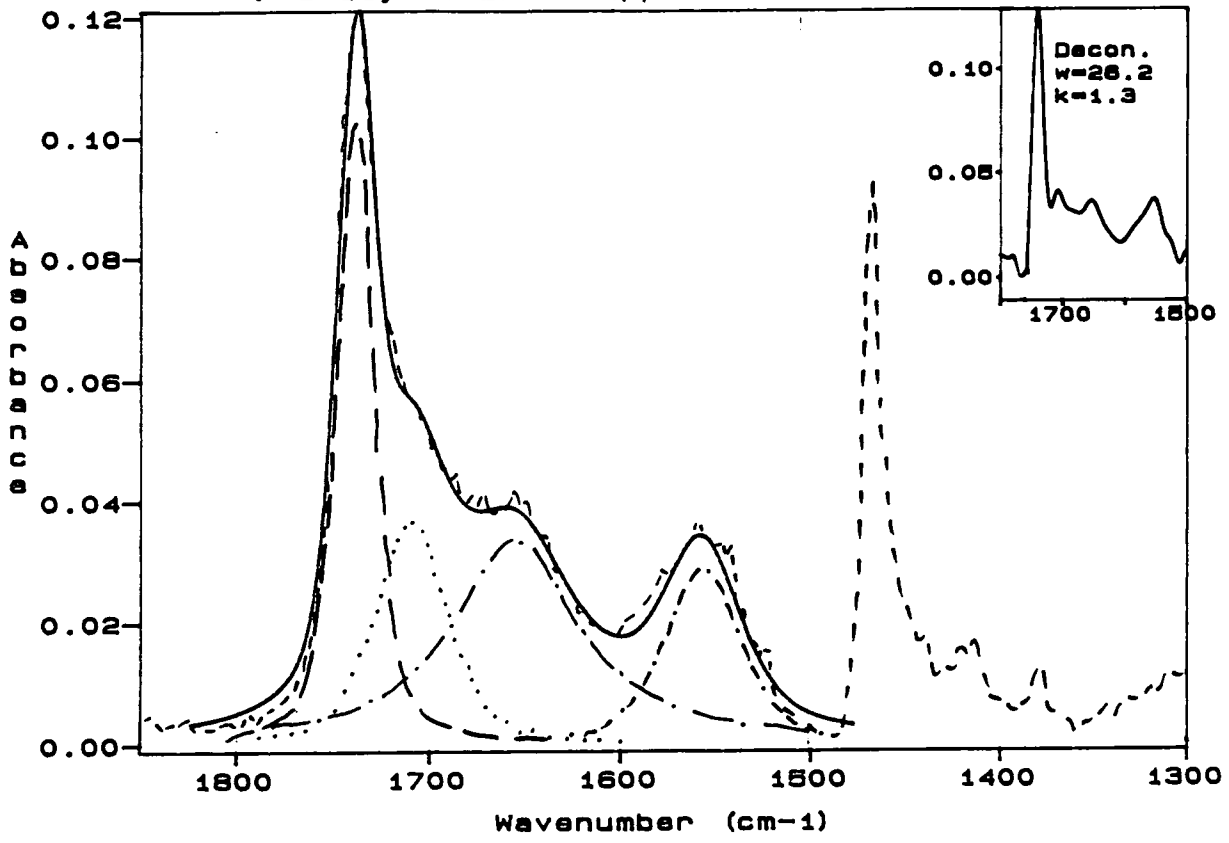

Plot 6-29: Calcium salts in water by transmission

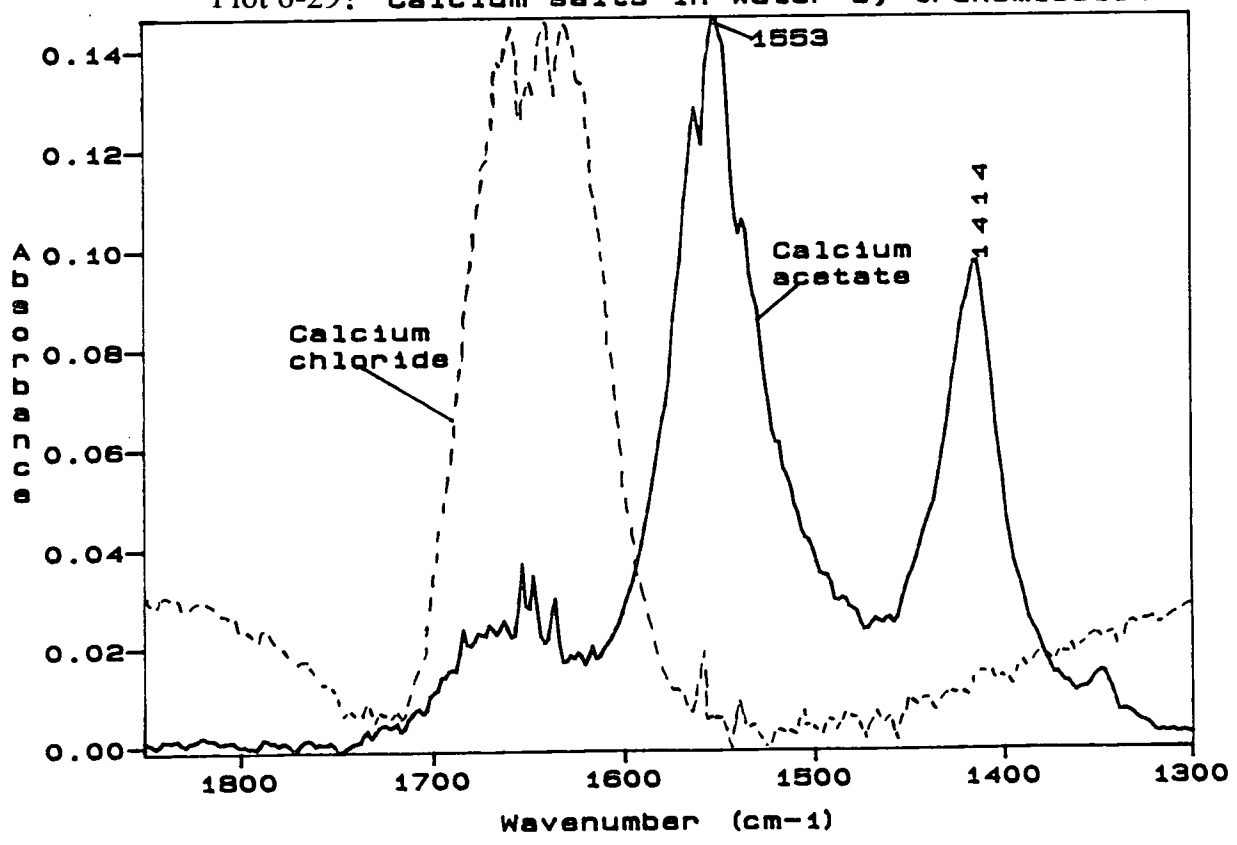

6.9 : DOPA AND THE DEPOSITION OF A 4:1 DPPA:DOPA MIXTURE

As monolayers of DOPA, at the A/W interface, were not stable at a constant pressure (section 5.3.2) it was not possible to use LB deposition for pure DOPA. A 4:1 mixture of DPPA: DOPA was stable enough at at a surface pressure of 30 mN m^{-1} for LB deposition to be attempted. Only 9 samples were made. The deposition was Y-type in general. For the glass slides the deposition ratio was 1 for the first three layers (first 2 cycles) but the deposition ratio for the inward stroke of the third cycle showed loss of material from the substrate onto the A/W interface. Similarly for the micro ATR crystals the deposition ratio was ~1 for the first upward stroke but on re-entry into the water there was either no further deposition or part of the first monolayer was lost. The FTIR spectra of ATR samples were very noisy but resembled those of LB films of DPPA.

Plot 6-30 shows the spectrum of a cast film of DOPA by transmission. It can be seen that at 19 $^{\circ}C$ DOPA is above its phase transition temperature. The evidence for this is the positions of the peaks due to the CH_2 stretching vibrations at 2924 and 2853 cm^{-1}. As stated before these values are indicative of a lipid above its phase transition temperature[28]. It can also be seen that there are no peaks due to the CH_2 wagging modes between 1350-1180 cm^{-1}. Only the peaks due to stretching vibrations of the phosphatidic acid and the COC groups (1242 and 1181 cm^{-1} respectively) are present in this region, as in the heated sample of DPPA (plot 6-3). The peak at 3005 cm^{-1} which is not present in the spectra of DPPA arises from the stretching vibration of CH groups attached to the double bonds.

Plot 6-30 Spectrum of DOPA as a film cast from chloroform (by transmission)

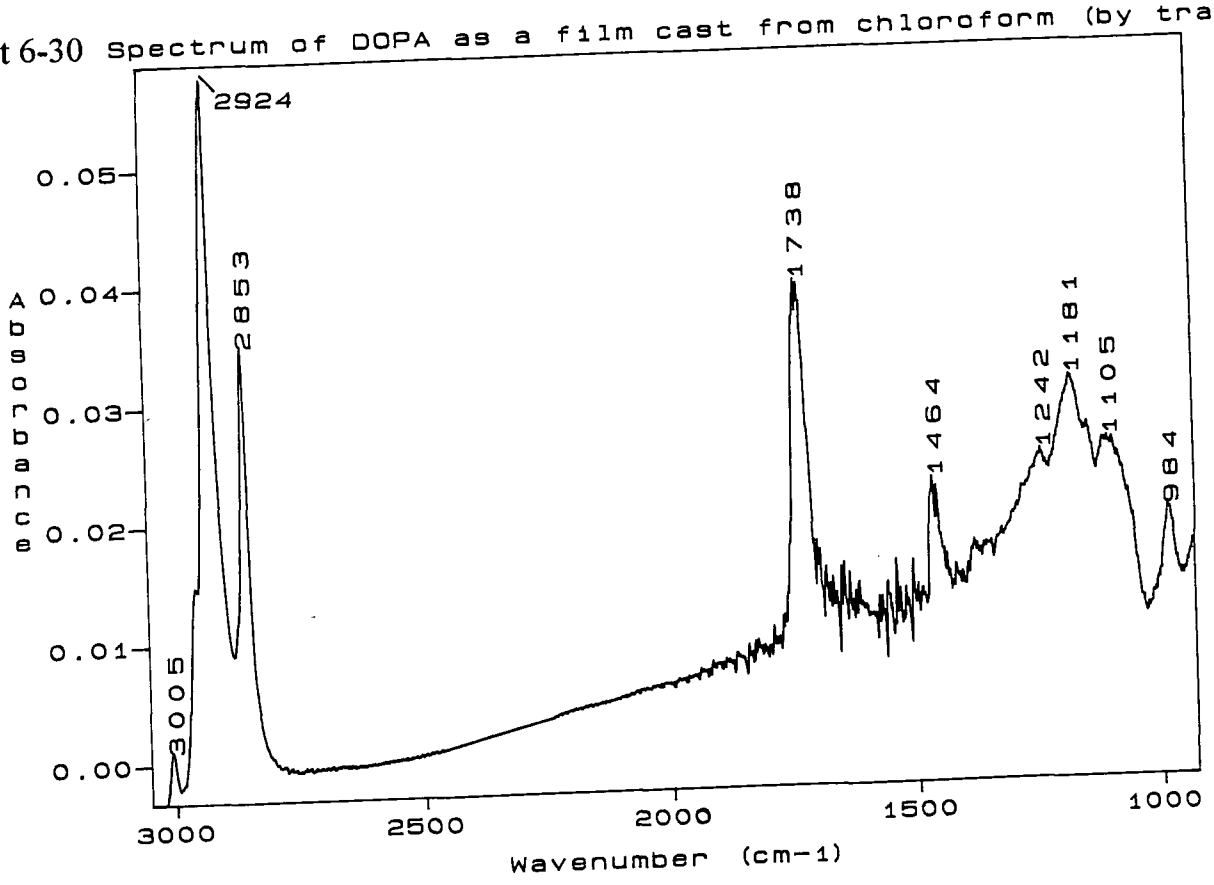

6.10 SUMMARY OF THE DEPOSITION AND FTIR OF DPPA (& DOPA)

At room temperature DPPA, as both a film cast from chloroform and deposition via LB dipping is below its phase transition temperature. The evidence arises form both the positions of the peaks due to CH_2 stretching modes and the presence of a series of eight peaks between 1350-1170 cm^{-1} which arise from the wagging mode of CH_2 in alkyl chains which are in an all trans conformation.

At 69 °C a cast film of DPPA was above its lipid phase transition temperature. The progression series due to the CH_2 wagging vibrations was not observed at this temperature. The A shift in the positions of the peaks due to $\nu_{as}(CH_2)$ and $\nu_s(CH_2)$ vibrations of ~5 cm^{-1} was observed at ~55 °C. This may be the phase transition temperature of DPPA as a cast film but experimental problems raise doubts about this. The phase transition was reversible. As the sample was cooled to below 50 °C the positions of the peaks due to the CH_2 stretches fell by 5 cm^{-1}. The peaks due to the wagging modes of the CH_2 chains also returned.

There were two different types of spectra seen for the cast films. The difference was in the shape of the band at 1740-1680 cm^{-1}. One form was seen for the spectra of most of the cast films and a crystalline sample (type 1, e.g. plot 6-1A). The other was seen only rarely as a cast film (type 2, e.g. plot 6-2A) and in chloroform solution. The conclusion is that the different types of spectra relate to different crystal structures in the films. X-ray data is needed for positive confirmation of this.

Interestingly films of DPPA deposited by Langmuir-Blodgett dipping always gave spectra similar to type 2 cast film. Whereas horizontal deposition (LS) gave rise to spectra similar to that of type 1 cast films. It is possible that the differences in the spectra are due to hydrogen bonding to the carbonyl groups of the molecules in samples which gave rise to type 1 spectra.

Both RAIRS and polarised ATR spectra of LB films of DPPA showed that the alkyl chains are orientated with their axes close to the vertical of to the substrate. There is also an indication that the cast films of DPPA may not have a random orientation of the molecules, i.e. there is a natural alignment process occurring between the molecules.

An interesting point on the preparation of LB films is that the FTIR spectra showed that water is always present in the films of DPPA, even when made by LB deposition and allowed to drain. This water could not be removed by evacuation and must therefore be tightly bound to the samples.

A novel technique for the preparation of an LB sample for the study of the micro ATR FTIR of biological bilayers has been shown to work (section 6.7.3). Water trapped between the bilayer and the silicon crystal, took several hours to diffuse into the bulk liquid.

When LB deposition occurred over calcium acetate there was possibly a transfer of acetate ions from the subphase into the lipid monolayers and probably calcium ions as well.

DOPA was shown to be above its phase transition temperature at 19 $^{\circ}$C.

CHAPTER 7

RESULTS AND ANALYSIS OF THE DEPOSITION AND FTIR OF PEPTIDES AND MIXTURES OF PEPTIDES AND LIPIDS

7.1 : INTRODUCTION TO LB AND FTIR STUDIES OF ALAMETHICIN

The primary structure of alamethicin is given in figure 5(f), as determined by Rinehart et al[139]. The crystal structure of this peptide was reported by Fox and Richards[137]. The crystal structure was found to contain three alamethicin molecules per asymmetric unit, all in a pre-dominantly α-helical conformation with a short (one or two residues) region of 3_{10} helical conformation at the carbon terminal. Alamethicin has been reported to have a similar structure in methanol solution, as determined by NMR spectroscopy by Esposito et al[164]. It is a natural peptide produced by the fungus *trichoderma viride*[165].

Alamethicin has been widely used as a model peptide for the investigation of ion transport by voltage gating (*e.g.* Boheim & Kolb[71]; Fox & Richards[137]; Brumfeld & Miller[166]; Cafiso et al[167]; Taylor & de Levie[168] and Stankowski et al[169]). It is known that the molecules of alamethicin aggregate in a lipid bilayer to form an ion channel,[71,137] when there is an applied potential. However, the mechanism of the pore formation and the interaction between the alamethicin and the lipid bilayer, particularly in the state where there is no applied potential, has been the subject of several studies and is still being debated.[38,89,136,138,170-179] For a recent review see Wooley and Wallace.[181]

Huang and Wu[89] propose that there are four likely states for the position of alamethicin molecules before a voltage is applied, for a system where there is a bilayer of lipid surrounded by an aqueous solution. These are that the alamethicin could be dispersed in the solution, bound to the surface of the bilayer, fully or partially absorbed in the bilayer. They found by use of CD that a phase diagram could be drawn. At high relative humidity (> 92%) and high concentration of alamethicin (lipid : alamethicin ratio < 100 :1) the alamethicin was incorporated into the bilayer. At lower humidities and concentration of alamethicin the peptide was found to lie on the surface of the lipid bilayer. They also reported that alamethicin could move between these two states as the conditions changed. This would explain the controversy as to whether alamethicin affects the polar headgroups[172,178], the hydrocarbon chains[170,173] or both[171,175] of phospholipids. As the interaction of the alamethicin with the bilayer would be highly dependent on the experimental conditions.

This work set out to try and answer some of these questions. Firstly, by making a bilayer where alamethicin was known to be incorporated by the deposition of mixed monolayers of DPPA and alamethicin. Secondly by taking a bilayer of lipid and observing the absorption of peptide into or onto it. In both cases the systems were to be examined via FTIR micro ATR spectroscopy. It was hoped that not only could changes in the lipid spectra be monitored but also those of the peptide.

Before proceeding with the above reference spectra of alamethicin and DPPA/alamethicin cast films were recorded. The mixture of DPPA and alamethicin chosen was a ~30:1 mole ratio. In order to lie within the region of the phase diagram, found by Huang and Wu[89], where the alamethicin should incorporate into the bilayer at high humidity. This was also a good ratio for FTIR studies as it gave a peptide spectrum which was of the same order of intensity as the lipid spectrum of the samples.

7.2 : FTIR SPECTRA OF FILMS OF ALAMETHICIN AND ALAMETHICIN/DPPA MIXTURES CAST FROM CHLOROFORM SOLUTION

7.2.1 FTIR transmission spectra

Plot 7-1 shows the transmission spectrum of a film of alamethicin cast from chloroform . The inset is the deconvoluted spectrum of the peaks due to the amide I and amide II vibrations (table 3(i)). The peak positions in the deconvoluted spectrum are at 1660, 1641, 1615 (sh), 1543, 1531 and 1499 cm^{-1}.

These positions and the relative intensities of the peaks are very similar to those reported by Chapman and Haris[142], for the spectra of alamethicin in both methanol and aqueous DMPC dispersion. They found a broad band with clear component peaks at ~ 1663, 1640 and 1621 cm^{-1}. The first of which was most intense, followed by the second and the third was a shoulder to the other two peaks. Their conclusions were that, because the secondary structure of alamethicin in methanol had been determined by Esposito et al[164] (see above), then these band positions and relative intensities must be indicative of a predominantly α-helical conformation with a small amount of 3_{10} turns. This is contrary to the assignments made in table 3(v) for such a secondary structure, but it must be remembered that alamethicin is not a protein but an oligopeptide.

Plot 7-2 shows the FTIR transmission spectrum of a film of 30:1 DPPA:alamethicin cast from chloroform. The peaks in the spectrum due to the lipid are similar in shape and position to those in the spectrum of the cast film shown in plots 6-2&3. The peaks due to the amide I&II vibrations of the peptide are similar to those in the pure alamethicin spectrum. However, the S/N level is too low for deconvolution techniques to be useful.

There are no detectable differences between the spectrum of the mixed film of DPPA/alamethicin and the spectra of the individual components. It may be concluded that if there is an interaction between the lipid and peptide that it either has no effect on the conformation of the components or that any changes are beyond the limits of detection of the instrumentation.

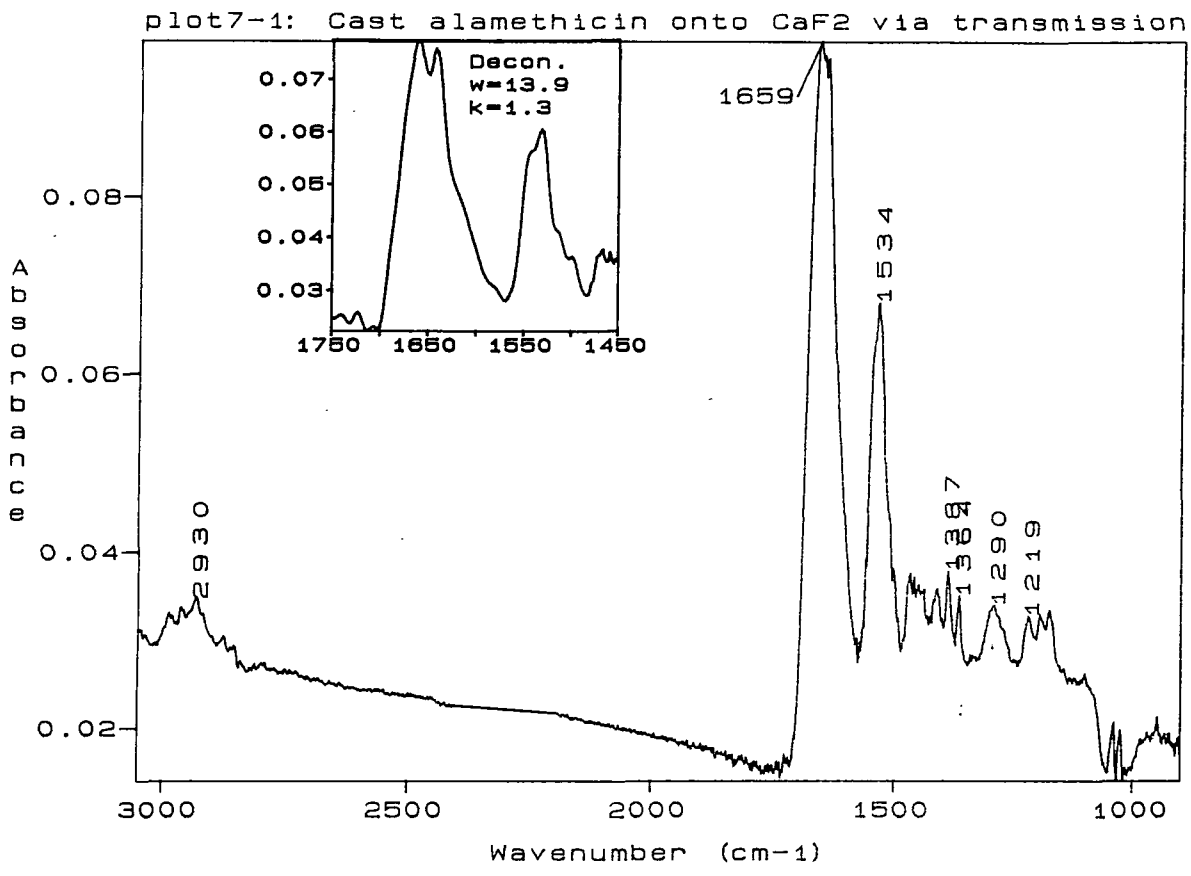
plot7-1: Cast alamethicin onto CaF2 via transmission
Decon.
w=13.9
k=1.3
0.07
0.06
0.05
0.04
0.03
1750
1650
1550
1450
1659
1534
2930
1387
1290
1219
0.08
0.06
0.04
0.02
Absorbance
3000
2500
2000
1500
1000
Wavenumber (cm-1)

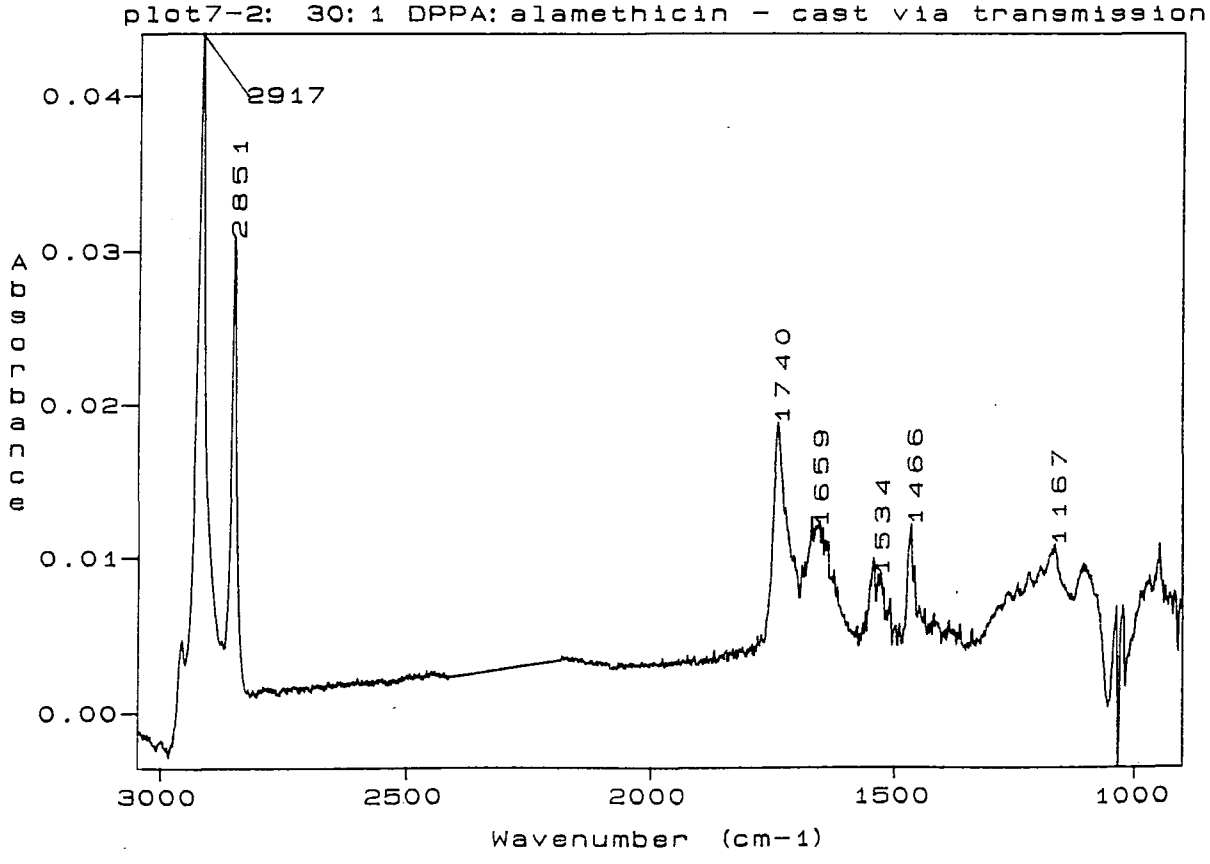
plot7-2: 30: 1 DPPA: alamethicin - cast via transmission
2917
2851
1740
1659
1534
1466
1167
0.04
0.03
0.02
0.01
0.00
Absorbance
3000
2500
2000
1500
1000
Wavenumber (cm-1)

7.2.2 FTIR RAIRS spectra

Plots 7-3&4 show the RAIRS spectra of alamethicin and 30:1 DPPA:alamethicin films cast from chloroform respectively. The relative intensities of all the peaks which are discernible in the RAIRS spectrum of alamethicin (plot 7-3) are similar to those found in the transmission spectrum (plot 7-1). This indicates that there was no preferential orientation of the vibrational dipole transition moments of the peptide.

The peak positions in the spectrum of the mixed lipid/peptide film which arise from vibrations in the lipid molecules are similar to those seen in the RAIRS spectrum of the lipid (plot 6-8). The exception is the peak at 993 cm^{-1} in plot 7-4, the equivalent peak in the lipid spectrum was at 1011 cm^{-1}. However, it was felt that this was not significant as in another RAIRS spectrum of pure lipid the equivalent peak was at 996 cm^{-1}. The relative intensities of the two main peaks due to carbonyl vibrations appear to be different from the spectrum of the pure lipid. Once again this is a change which can occur simply by casting a new film of DPPA on its own (section 6.2). This is illustrated by the details of curves fitted to such band in the RAIRS spectrum of DPPA in table 6(iii).

The RAIRS spectrum of the mixed cast film (plot 7-4) shows a relative enhancement of the peaks in the CH_2 wagging progression series compared to the equivalent transmission spectrum (plot 7-2). This relative intensity of the progression series and underlying peaks, compared to the other peaks in the lipid spectrum, is less than that seen for pure DPPA (plot 6-8). This indicates that the lipid alkyl chains are not as well orientated, with respect to the surface, in the mixed cast film compared to the cast film of pure DPPA.

The relative intensities of the peaks at ~1679 and ~1545 cm^{-1} (plot 7-4), which are largely due to the amide I and II vibrational modes of alamethicin, appear to differ from those observed in the spectrum of pure alamethicin. It was very difficult to tell whether this is a real effect without curve fitting procedures being applied for the group of peaks between 1750-1650 cm^{-1}. It was decided that the number of peaks to be fitted (~7) would mean that any curve fitting would be able to produce such a variety of solutions that it would not be viable. If the change in relative intensities of the amide bands is real it would be difficult to see why such a change would occur as two amide vibrational dipole moments are largely in the same plane. The amide I vibration is primarily due to the stretch of the C=O groups (80%) and the amide II peak is due to a mixture of stretching modes of the N-H and C-N (60/40 %) bonds[31]. The dipole moment of the amide I vibration will therefore be largely along the axis of the α-helix That of the amide II vibration will lie in a direction between those of the NH and CN bonds, thus it will vary for different amino acids dependent on their position in the helix. If the apparent change in relative intensity of the two amide groups is real it would indicate that the alamethicin has a preferential orientation with respect to the metallised glass slide such that the axes of the helixes are closer to perpendicular than parallel to the surface.

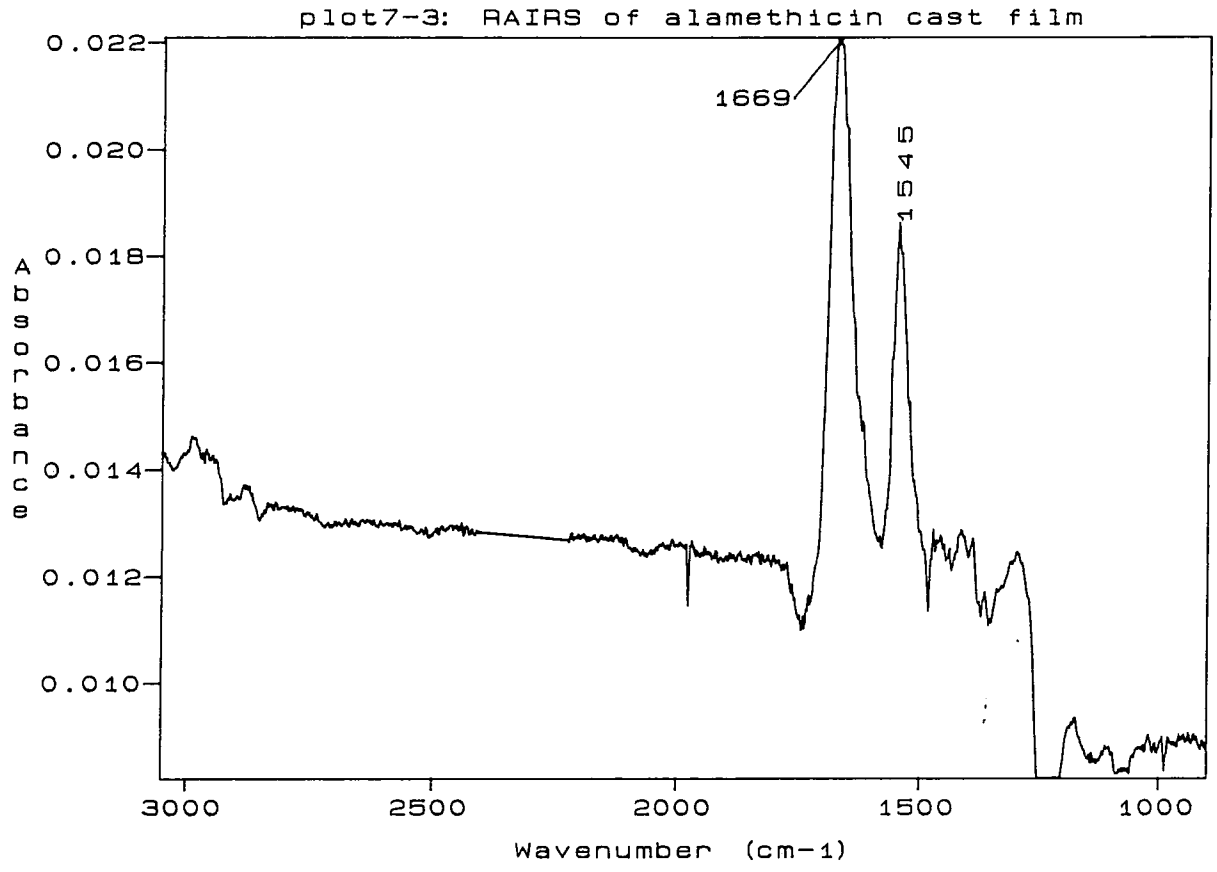
plot7-3: RAIRS of alamethicin cast film
0.022
0.020
0.018
0.016
0.014
0.012
0.010
Absorbance
1669
1545
3000
2500
2000
1500
1000
Wavenumber (cm-1)

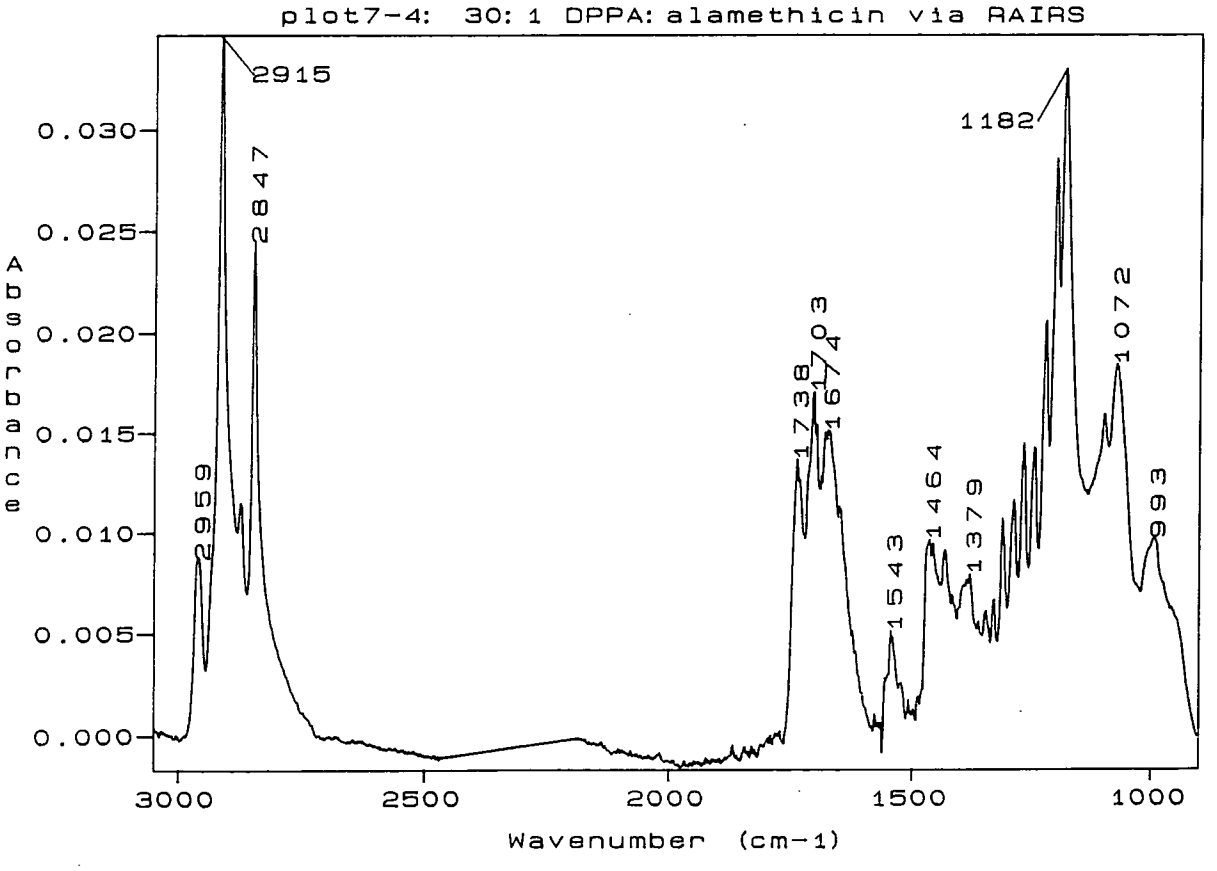
plot7-4: 30: 1 DPPA: alamethicin via RAIRS
0.030
0.025
0.020
0.015
0.010
0.005
0.000
Absorbance
2915
2847
2959
1738
1703
1674
1543
1464
1379
1182
1072
993
3000
2500
2000
1500
1000
Wavenumber (cm-1)

7.2.3 FTIR micro ATR spectra

The micro ATR spectra (plots 7-5&6) are very similar to those obtained via transmission. The main difference lies in an increase in the order of magnitude of the absorption values. This is due to the multiple sampling of the material on the micro ATR crystal. There is also an increase in the S/N ratio which allowed the possibility of curve fitting to the amide I band of alamethicin (plot 7-5A). The fitted peaks again match those found by Chapman and Haris[142].

In the spectrum of the mixed DPPA/alamethicin (plot 7-6) there are two peaks which are not apparent in either the DPPA nor the alamethicin spectra, centred at ~3020 and 1215 cm^{-1}. Unfortunately these arise from CH vibrational modes of $CHCl_3$. Showing that there has been incomplete evaporation of the solvent. The peaks resulting from the lipid and peptide vibrations are once again similar to those of the individual components (plots 7-5 & 6-13).

Unfortunately no polarised spectra were obtained for these cast films.

plot7-5A: Curve fit for amide I band of alamethicin by ATR

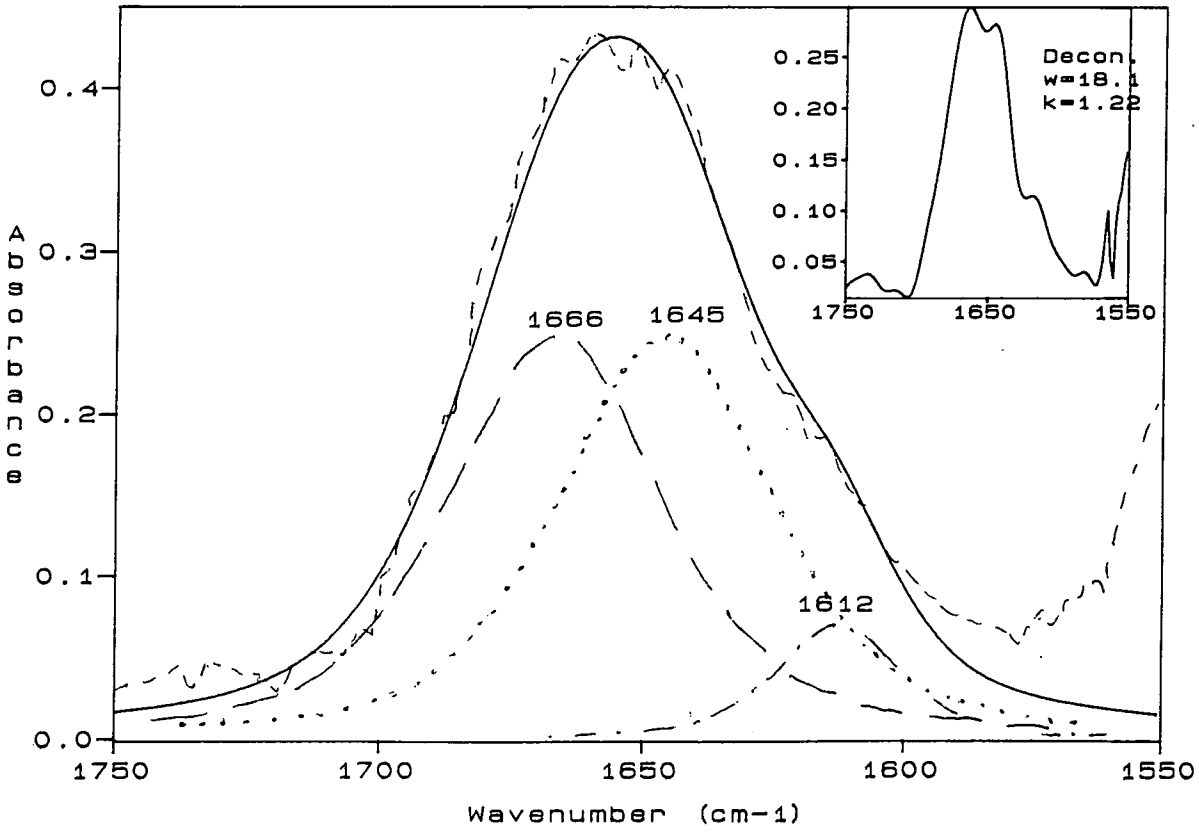

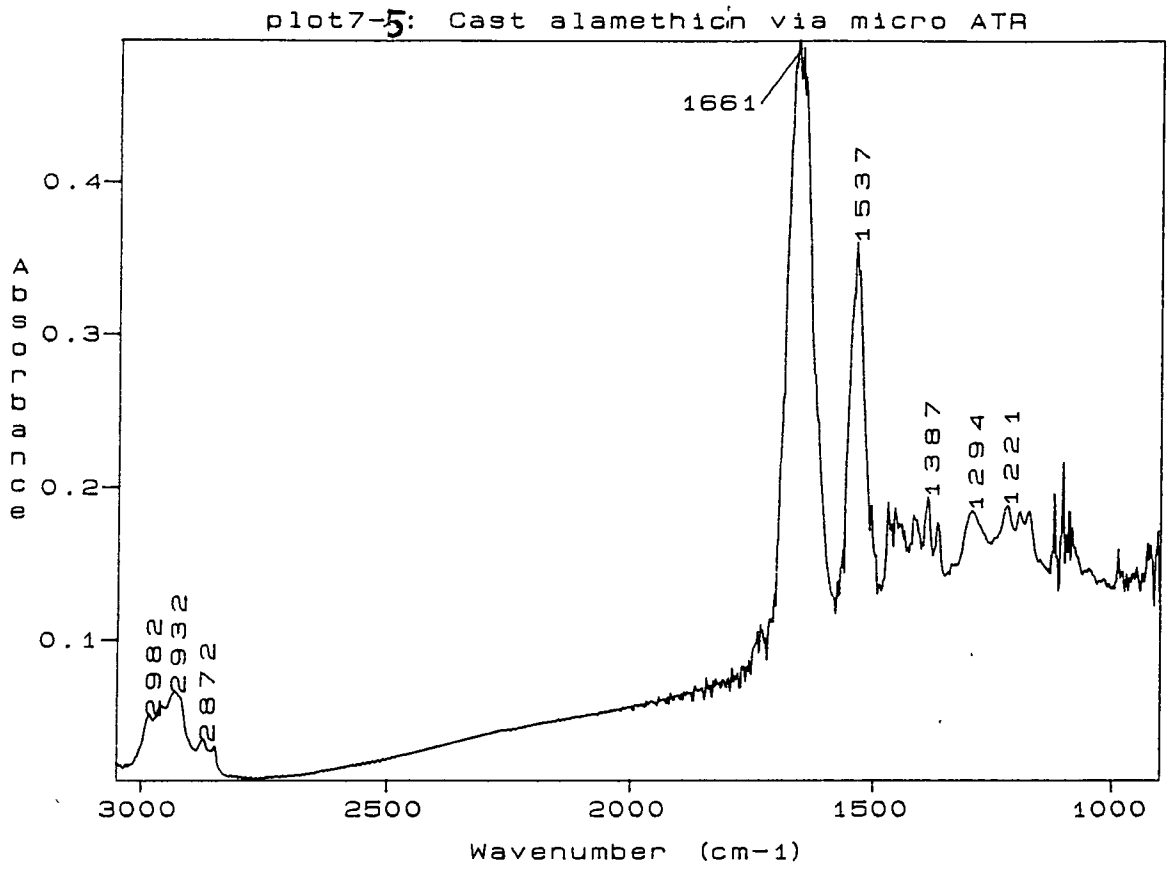
plot7-5: Cast alamethicin via micro ATR
1661
1537
1387
1294
1221
2982
2932
2872
0.4
0.3
0.2
0.1
Absorbance
3000
2500
2000
1500
1000
Wavenumber (cm-1)

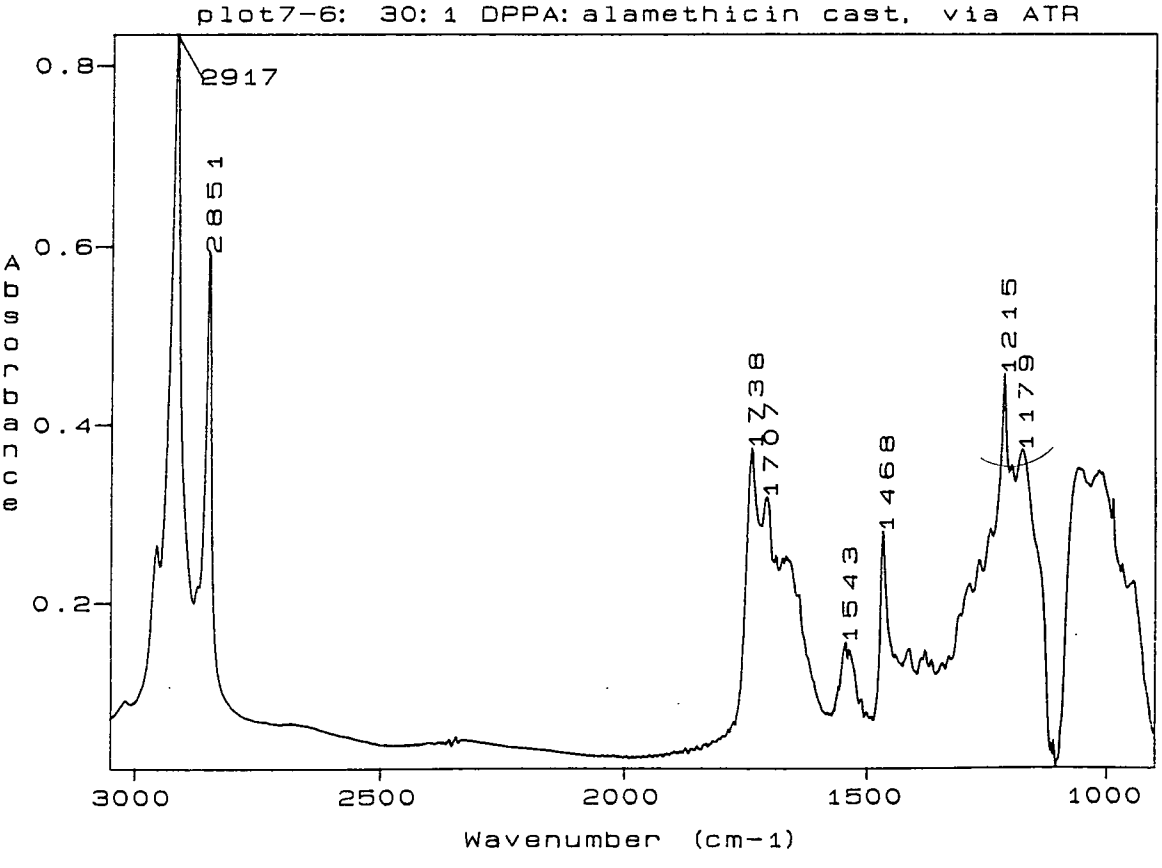
plot7-6: 30: 1 DPPA: alamethicin cast, via ATR
2917
2851
1738
1707
1543
1468
1215
1179
0.8
0.6
0.4
0.2
Absorbance
3000
2500
2000
1500
1000
Wavenumber (cm-1)

7.3 : LB DEPOSITION OF MIXED ALAMETHICIN AND LIPID MONOLAYERS

7.3.1 : Results for the LB deposition of alamethicin and mixtures thereof with lipids

It was only possible to deposit a single layer, by LB deposition, from a monolayer of pure alamethicin at the air/water interface at a surface pressure of 23 mN m^{-1} . This was due to the fact that a single layer was deposited on the first up-stroke but on re-entry through the monolayer of alamethicin at the A/W interface the layer peeled off the substrate and onto the A/W interface. On re-emergence another layer of alamethicin was deposited but with this type of deposition record it was obvious that only a single monolayer of alamethicin could be deposited.

A 27:1 mole ratio mixture of DPPA:alamethicin was chosen for the deposition trials, at a surface pressure of 23 mN m^{-1} . Mainly because this would give an FTIR spectrum for which the peaks due to the peptide amide I&II vibrations would have S/N ratios high enough such that the use of deconvolution and curve fitting techniques would be possible. The deposition characteristics of the 27:1 mixture were similar over both a water subphase and one containing calcium acetate. The mixture was found to deposit in a Z-type pattern onto micro ATR silicon crystals, i.e. material was only deposited onto the substrate during the upward stroke of a cycle. The exception to this were two samples where layers of pure DPPA had been previously deposited onto the substrate. In these cases the first cycle into through the mixed DPPA/alamethicin monolayer gave a y-type pattern of deposition (i.e. two layers were deposited). After these two layers the deposition continued as z-type.

Only three samples were made using the mixture of 24:6:1 DPPA:DOPA:alamethicin, with D_2O as the subphase, using the Fromherz trough. These were dipped at a surface pressure of 28 mN m^{-1}. The deposition ratios followed a pattern of ~1.6 on the upward stroke, followed by 0.6 on the inward stroke.

7.3.2 Discussion of LB deposition results

Alamethicin seems to have accentuated the results noted for the deposition of pure DPPA, onto silicon crystals (section 6.3.1), for incomplete monolayers to be deposited on the downward stroke of each cycle. In the case of a 27:1 mixture of DPPA:alamethicin the deposition became completely z-type. The addition of a calcium salt to the subphase did not change the type of deposition to y-type.

At a mole ratio of 27:1 the area ratio of the molecules on the trough, calculated from the close packed areas given in tables 5(ii) and (ix), would be 3.4 : 1 DPPA:alamethicin. Thus, it is not surprising that the mixture has a different deposition characteristics to either pure DPPA or alamethicin. One of the biggest unanswered questions from this work is the structure of the deposited layers - do they remain z-type, an unusual configuration for lipids[14]; or do the monolayers rearrange to form bilayers of lipid with the peptide either incorporated or segregated from the lipid. This question could be resolved by low angle X-ray diffraction studies, which were beyond the scope of this project.

The mixture of lipids (DPPA & DOPA) with alamethicin seemed to have odd deposition characteristicS. This could be due to experimental error in the measurement of the deposition ratio. This error was higher for the deposition ratios onto the small ATR crystals for the Fromherz trough (± 0.2) compared to the Joyce-Loebl style trough (± 0.05). Another possible explanation for the deposition ratio of 1.6 could be that the removal of the material from the surface allowed better packing between the three components of the mixture on the surface of the water. A third possibility is that the deposition ratios measured represent the true values and more than one monolayer was deposited on the upward stroke of the cycle. This could be a movement of the lipids to form a bilayer around the alamethicin with the subsequent deposition ratio of 0.6 being the filing in of the spaces in the bilayer (see figure 7(a)). Again X-ray studies could have differentiated between these possibilities.

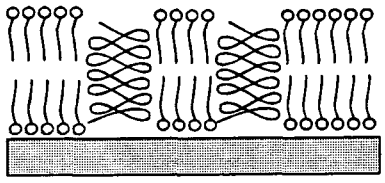

(i) The structure wanted.

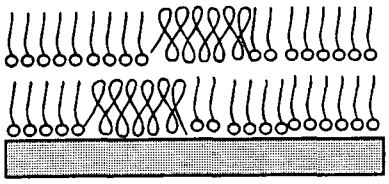

(ii) The most probable structure, based on deposition and monolayer data.

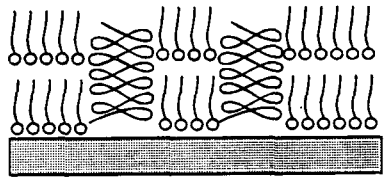

(ii) A possibility if the alamethicin rearranges on or after LB deposition.

Figure 7(a) : The structure of the LB films of mixed DPPA/Alamethicin as deposited.

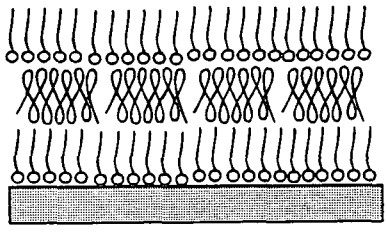

Figure 7(b) : The sandwich structure produced by exchanging the monolayer at the air/water interface.

7.4 ATR FTIR OF LB FILMS OF ALAMETHICIN WITH DPPA (& DOPA)

7.4.1 Deposited from mixed monolayers of DPPA and alamethicin

Plot 7-7 shows the FTIR micro ATR spectrum of 2 LB layers of 27:1 DPPA:alamethicin deposited over pure water. As explained above this mixture deposited in a z-type manner and is therefore the lipid was probably not in a bilayer conformation. The spectral region 1800-1500 cm^{-1} has a poor S/N ratio and it is impossible to draw any conclusions as to the state of alamethicin in the sample. The peaks in the spectrum due to vibrations of the lipid are similar to those seen in LB films of DPPA (plot 6-14), apart from the peak at 1240 cm^{-1}. Plot 7-9 shows the region 1500-1140 cm^{-1} in more detail. The solid line is the LB film of DPPA/alamethicin, the dotted line is spectrum for the same region for an LB film of DPPA (plot 6-14). The wagging progression series is extremely weak, if present, and the peak at 1240 cm^{-1} is much more intense than that at ~1171 cm^{-1}. The peak at 1240 cm^{-1} is due to a stretching vibration of the P=O group (see table 3(i)). The alamethicin must therefore be causing a change in the interaction of the headgroups of the DPPA. Also noted on the examination of several spectra was the fact that the expected peaks at ~1660 and 1540 cm^{-1} for the amide I&II vibrations of the peptide were always much lower in relative intensity to the carbonyl band compared to cast film spectra of similar mixtures (plot 7-6). In fact in some cases (including the example shown plot 7-7) it was pushing the limits of plausibility to claim the presence of any peaks arising from vibrations of alamethicin

Plot 7-8 shows the spectrum of 4 layers of 27:1 DPPA:alamethicin deposited z-type over a subphase of calcium acetate. The peaks due to the amide I&II modes of alamethicin are similar in position and relative intensity to those observed in the spectrum of the cast film (plot 7-6). However, it must be pointed out that peaks in similar positions were also seen in the spectra of DPPA deposited over calcium acetate (section 6.8).

The spectrum of the film deposited over calcium acetate (plot 7-9), in the region 1500-1130 cm^{-1}, is similar to that of the LB film of DPPA seen in plots 6-14&28.

7.4.2 Other LB samples containing alamethicin

Plot 7-10 shows the spectrum of a sample where a sandwich structure was produced. This was achieved by changing the monolayer at the A/W interface between cycles. The initial monolayer was DPPA. A cycle was completed in which a single layer was deposited. The monolayer at the A/W interface was then changed from DPPA to alamethicin. The micro ATR crystal was cycled through this monolayer. No material was deposited in the downward stroke but a layer of alamethicin was picked up on the upward stroke (z-type). The monolayer was again replaced with DPPA this time. The crystal was cycled through this, again z-type deposition occurred. The deposited structure of the film on the ATR crystal is shown in figure 7(b), assuming no rearrangement.

The aim of this deposition strategy was to achieve a layer of alamethicin trapped in a lipid bilayer. It was hoped that the second cycle through a monolayer of DPPA would be y-type, in order to give a biological bilayer structure.

The spectrum is similar to that of a composite of the cast film spectra of alamethicin and DPPA (plots 7-5&6-14), apart from the region between 1300-1100 cm^{-1} (plot 7-10A) where the peak at 1242 cm^{-1} is once again the most intense in this region (as in plot 7-7).

Plot 7-11 shows the spectrum of an LB film formed from a mixture of 24:6:1 DPPA:DOPA:alamethicin at the A/W interface (as described in section 7.3.1). The spectrum has no unusual features when compared to the spectrum of the LB film of DPPA (plot 6-14) and the cast film of alamethicin (plot 7-5).

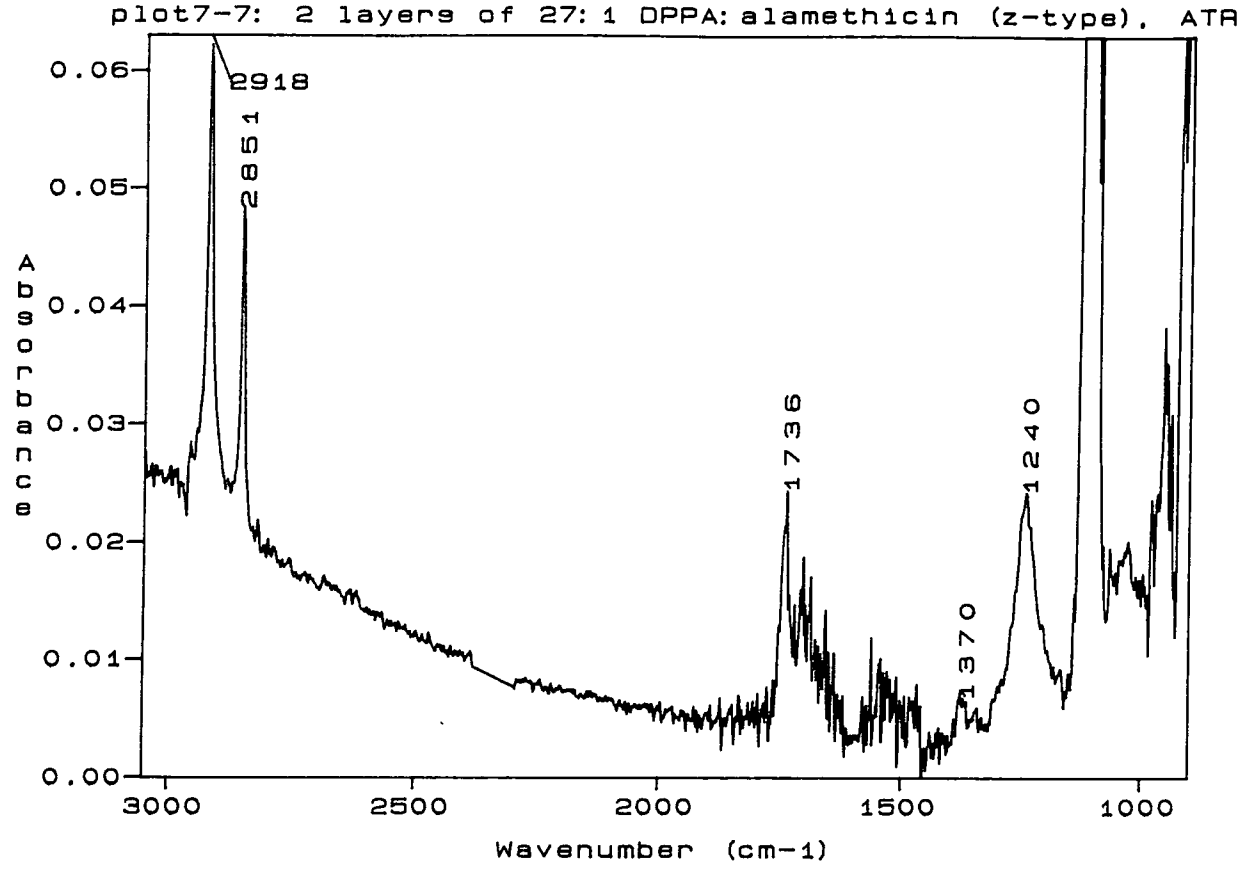
plot7-7: 2 layers of 27:1 DPPA:alamethicin (z-type), ATR
2918
2851
1736
1240
1370
Absorbance
0.06
0.05
0.04
0.03
0.02
0.01
0.00
3000
2500
2000
1500
1000
Wavenumber (cm-1)

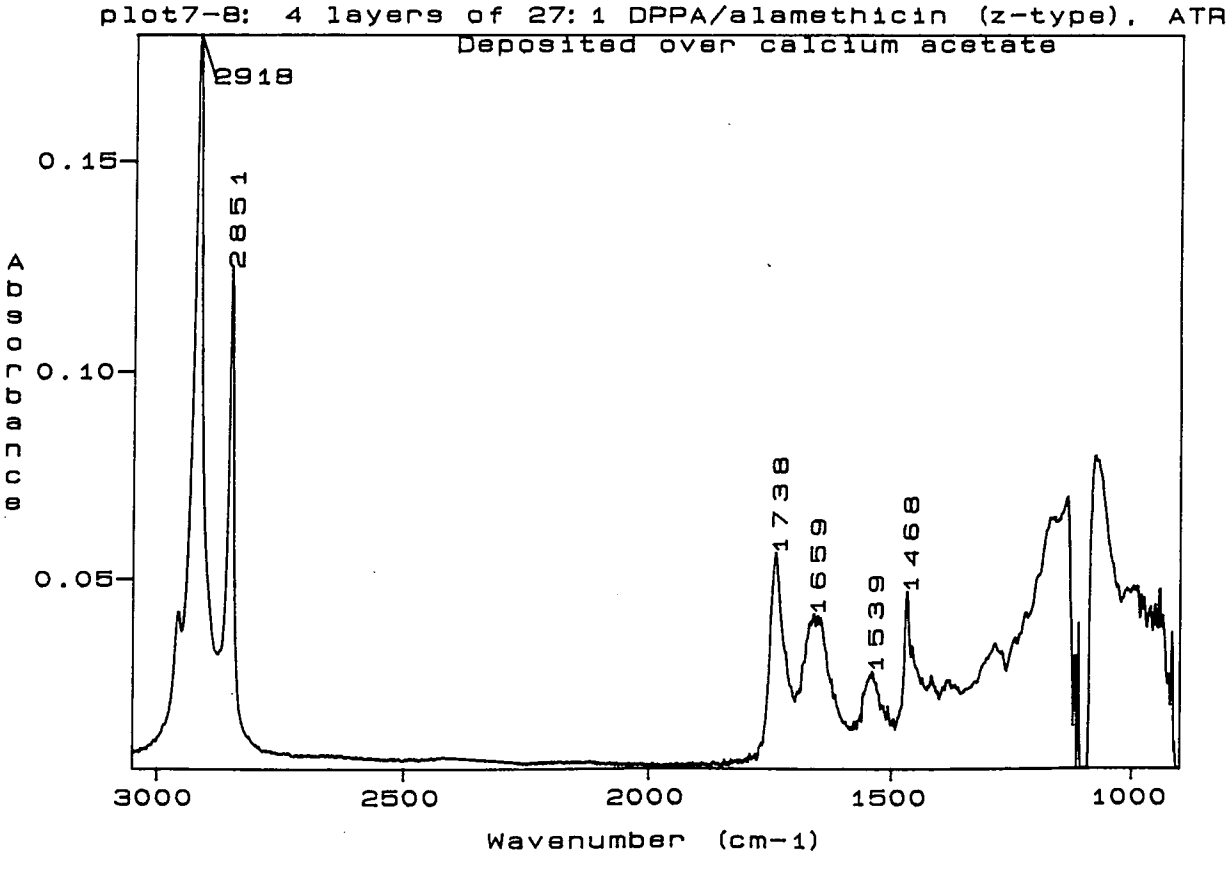
plot7-8: 4 layers of 27:1 DPPA/alamethicin (z-type), ATR
Deposited over calcium acetate
2918
2851
1738
1659
1539
1468
Absorbance
0.15
0.10
0.05
3000
2500
2000
1500
1000
Wavenumber (cm-1)

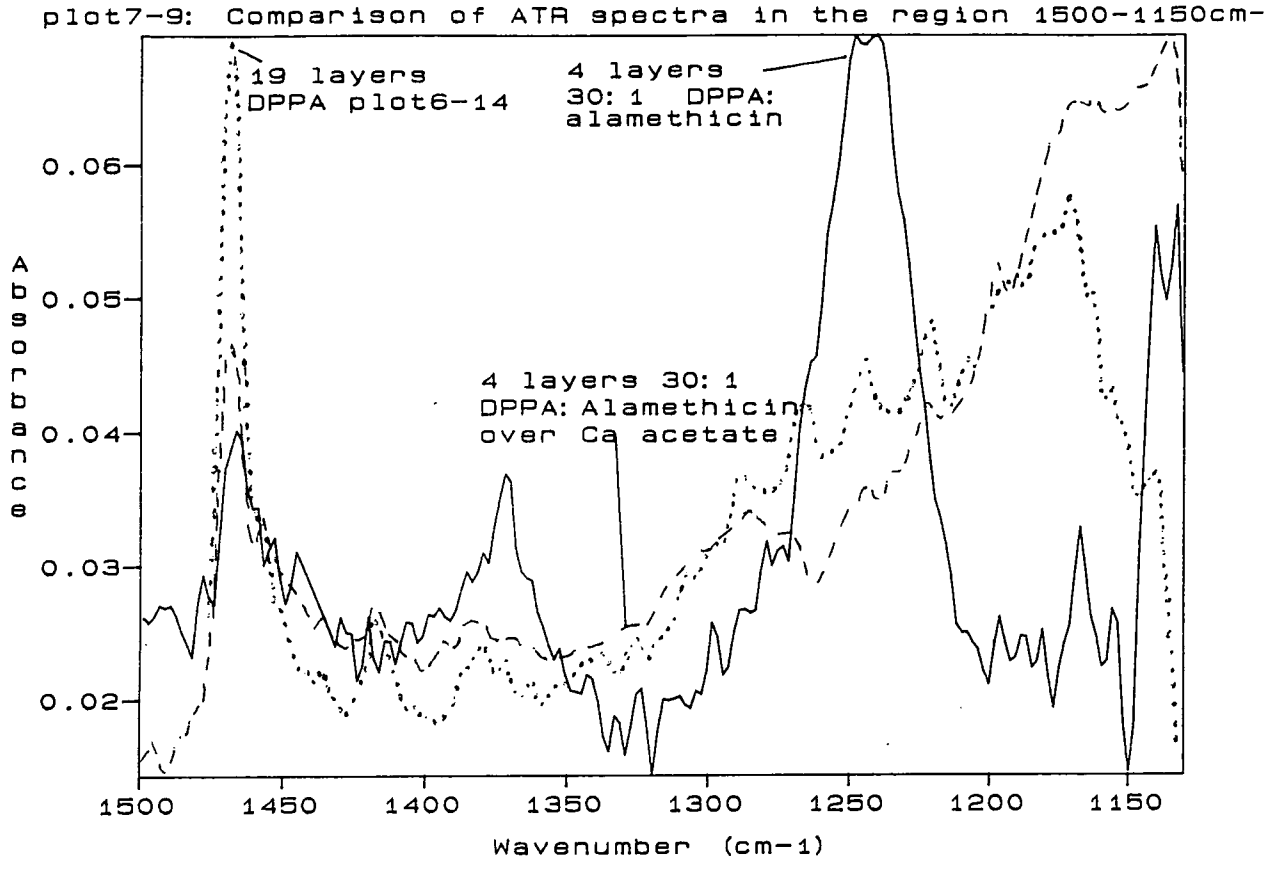
plot7-9: Comparison of ATR spectra in the region 1500-1150cm-1
19 layers
DPPA plot6-14
4 layers
30: 1 DPPA:
alamethicin
4 layers 30: 1
DPPA: Alamethicin
over Ca acetate
Absorbance
0.06
0.05
0.04
0.03
0.02
1500
1450
1400
1350
1300
1250
1200
1150
Wavenumber (cm-1)

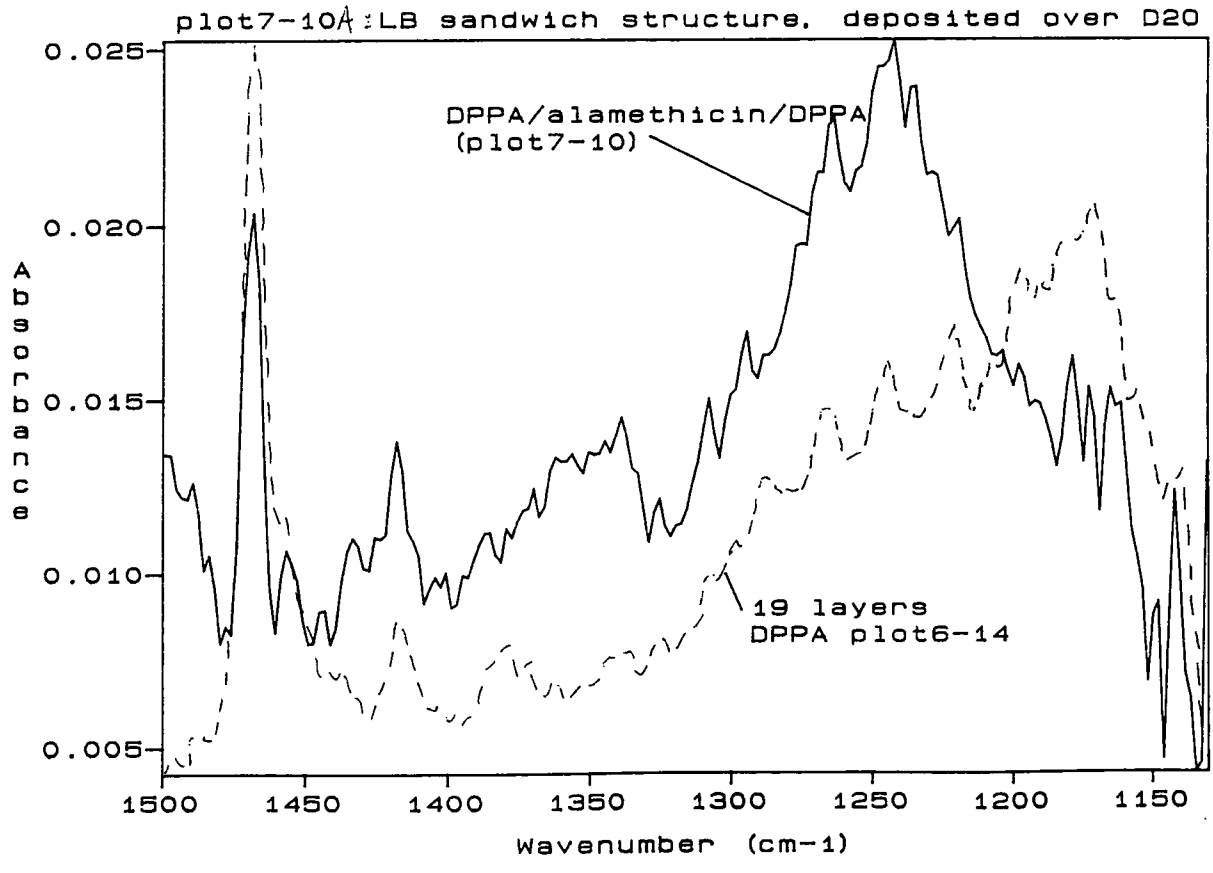
plot7-10A: LB sandwich structure, deposited over D20
DPPA/alamethicin/DPPA
(plot7-10)
19 layers
DPPA plot6-14
Absorbance
0.025
0.020
0.015
0.010
0.005
1500
1450
1400
1350
1300
1250
1200
1150
Wavenumber (cm-1)

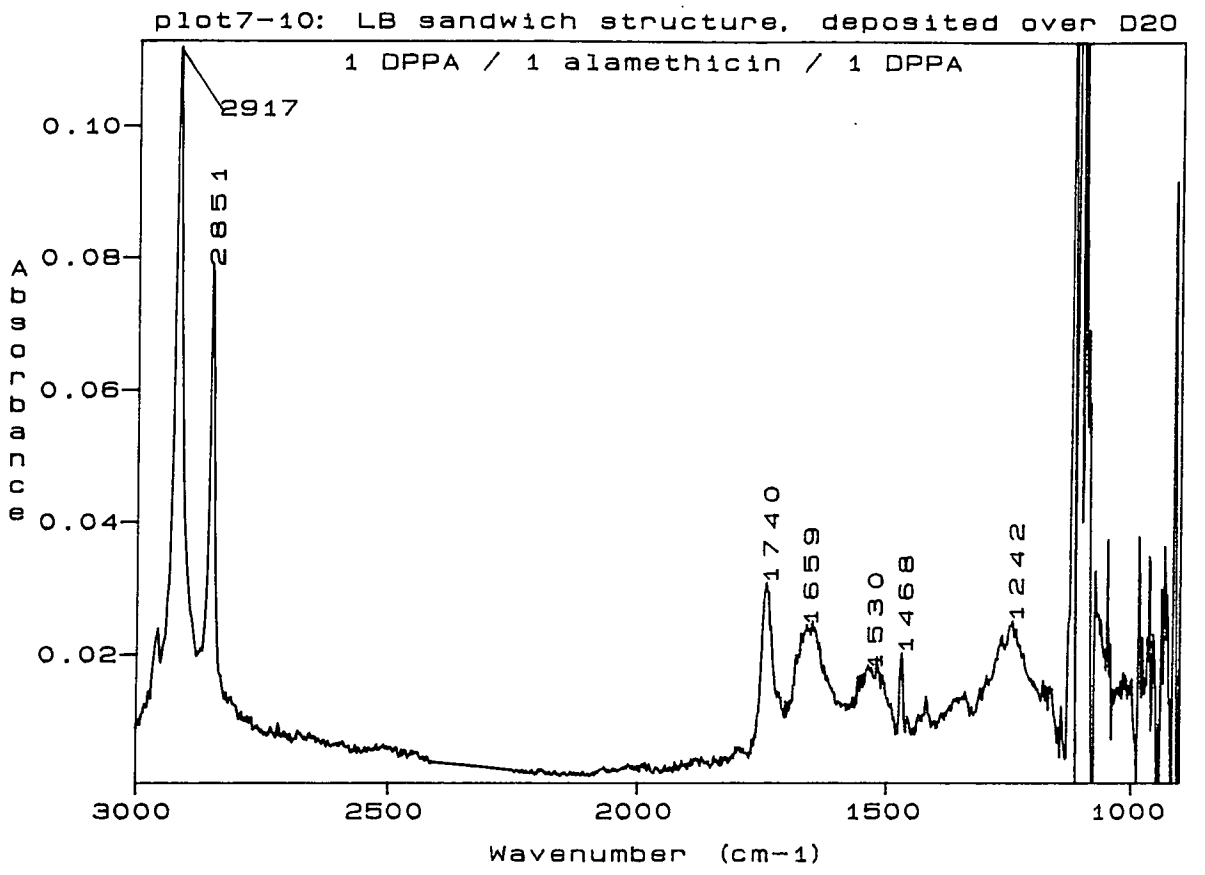
plot7-10: LB sandwich structure, deposited over D20
1 DPPA / 1 alamethicin / 1 DPPA
2917
2851
1740
1659
1530
1468
1242
0.10
0.08
0.06
0.04
0.02
Absorbance
3000
2500
2000
1500
1000
Wavenumber (cm-1)

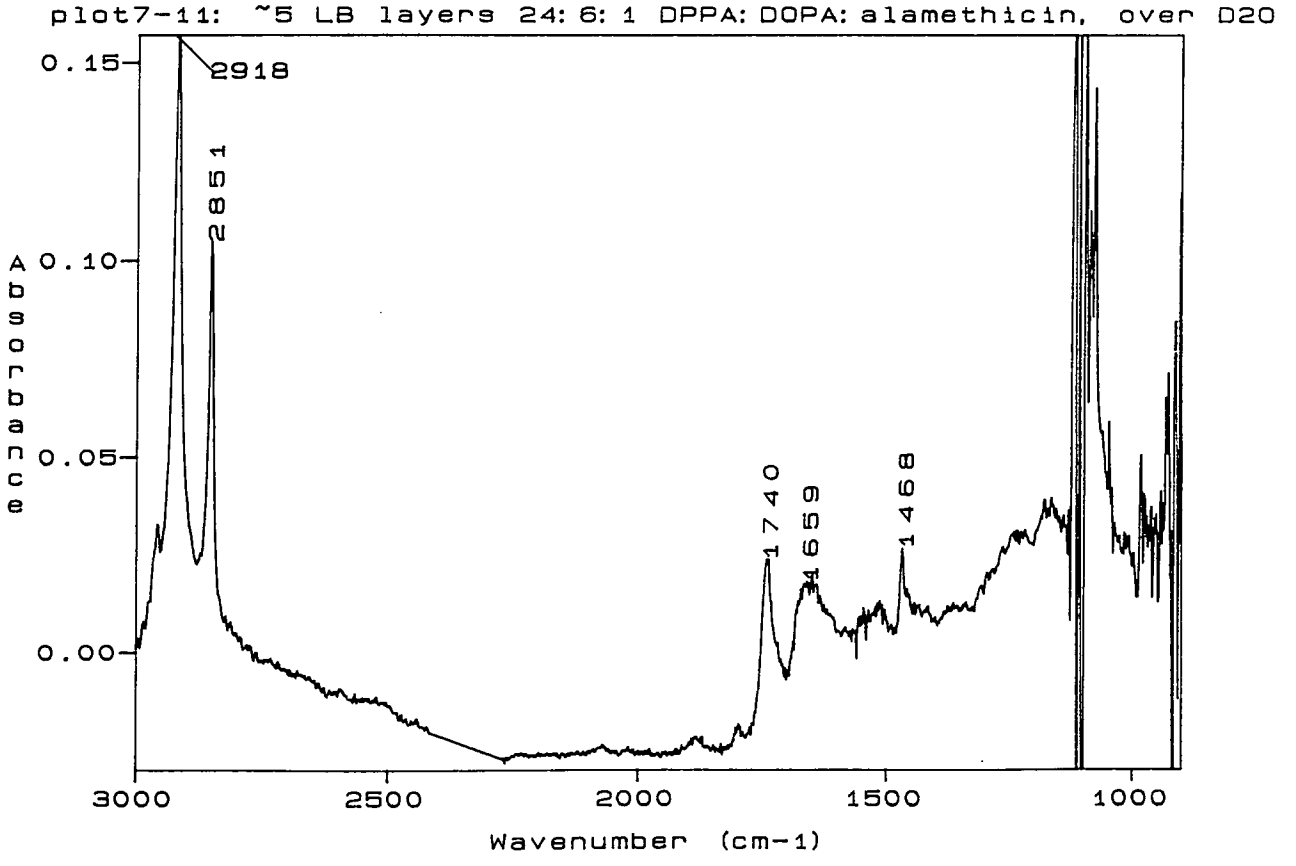
plot7-11: ~5 LB layers 24: 6: 1 DPPA: DOPA: alamethicin, over D20
2918
2851
1740
1659
1468
0.15
0.10
0.05
0.00
Absorbance
3000
2500
2000
1500
1000
Wavenumber (cm-1)

7.4.3 Discussion of the results of FTIR spectra of LB films containing alamethicin

So far as it is possible to tell from the spectra obtained, alamethicin is in the same conformation when deposited as an LB film as in the cast films. Based on the analysis of Chapman and Haris[142] this is a predominantly α-helical, apart from some 3_{10} turns at the C-terminus.

Assuming no rearrangement of the deposited film structure, plot 7-10A shows the spectrum of alamethicin between two monolayers of DPPA (figure 7(b)). The spectra obtained for LB films deposited from mixed monolayers (e.g. plot 7-7), at the A/W interface, are similar to that obtained from the sandwich structure. Therefore, it is possible that when deposited over water the structure of the LB films is not as in figure 7(a) but closer to figure 7(b). It is certain that less alamethicin is in the film than would be expected from the initial ratio of DPPA:alamethicin at the A/W interface.

For the LB films of the mixture of DPPA/ alamethicin deposited over calcium and with DOPA the peaks in the spectra due to DPPA closely resemble those in LB films of pure DPPA. In these cases it is possible that the alamethicin is incorporated into the lipid layers but in an aggregated form as there are no discernible changes in the lipid spectrum. The data in section 5.5 showed that alamethicin and DPPA were immiscible at the A/W interface.

Further analysis of the results obtained with alamethicin would be speculation. X-ray diffraction studies are really necessary to find the layer structure of the films deposited.

An experiment was attempted whereby a solution containing alamethicin, in D_2O and methanol, was exchanged for the D_2O surrounding the bilayer of DPPA (described in section 6.7.3). However, no conclusive results were recorded.

7.5 : DPPA BILAYERS WITH GRAMICIDIN INCORPORATED

7.5.1 Introduction

From the information above it was obvious that it would not be possible to form a biological bilayer structure by the LB deposition of a mixture of DPPA and alamethicin. Lukes et al[90] had succeeded in depositing a mixture of gramicidin D and DPPA as a multilayered y-type film FTIR ATR spectra from films of mixed DPPA and gramicidin are reported in the above paper. Gramicidin is an ion channel forming peptide. The channel is formed by two molecules, one in each half of the bilayer coming together, on top of one another to form a hole for the passage of cations[3,181].

Two experiments were performed. In the first a single bilayer of a 16:1 DPPA : gramicidin D mixture was deposited by the technique described in section 4.3.2.D. Whereby a biological bilayer structure is formed beneath the A/W interface and was kept in solution from that moment until all the FTIR experiments were completed. In the second experiment four LB layers were deposited and then the sample kept underwater, thus producing a double biological bilayer structure. For both of the samples the FTIR micro ATR spectra were recorded. The H_2O was exchanged for D_2O to enable observation of the peaks due to the amide I vibrations.

7.5.2 Results

Similar results were obtained to those in section 6.7.3. A large peak assigned as the bending mode of H_2O gradually decreased in intensity (plots 7-12&14). Whilst a smaller peak assigned as the bending mode of HOD showed an initial increase and then a later decrease in intensity (plots 7-13&14). These observations were true for both the bilayer and double bilayer of material.

First order kinetic equations were used to obtain a rate constant for the disappearance of H_2O (see section 6.7.3). Plot 7-17 shows the graph of this process. The rate constant was found to be 0.0196 min^{-1}. From this the half life of the decrease in peak heights of the band due to the bending modes of H_2O was found to be 35 minutes, for the bilayer of mixed gramicidin/DPPA. This is much smaller than that found for a bilayer of pure DPPA (~85 minutes).

After most of the H_2O had become HOD, the spectrum of the deposited layers could be observed (plot 7-15). This spectrum has been smoothed and no analysis would be possible on the original spectrum.

7.5.3 Discussion of the bilayers of mixed DPPA/gramicidin

The rate of deuteration of H_2O appears to be faster through the mixed bilayer of DPPA/gramicidin. Only further studies will show whether these differences are indeed significant. The increase in thickness to a double bilayer had no effect on the rate of loss of H_2O, but did increase the time for the HOD to disperse into the bulk D_2O

Plot 7-12 Graph of intensity of the H2O bending mode
vs time since exchange of H2O for D2O for bilayer

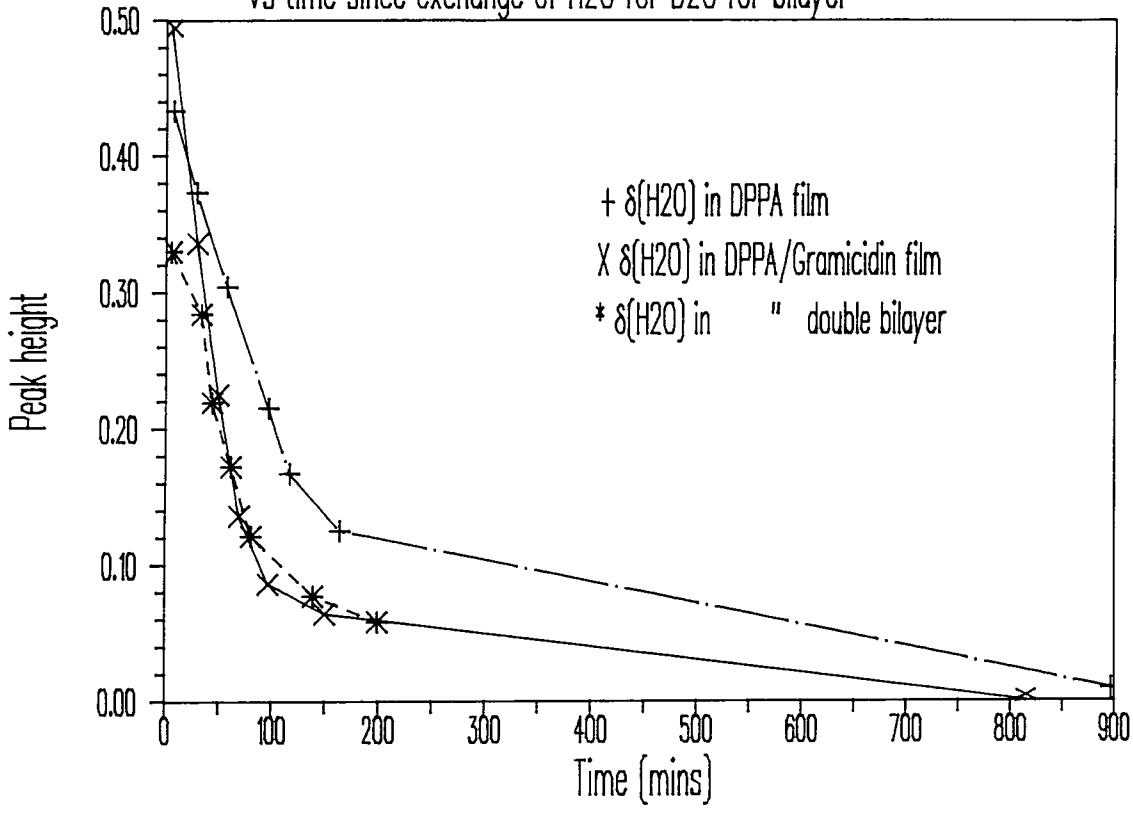

Plot 7-13 Graph of intensity of the HOD bending mode
vs time since exchange of H2O for D2O for bilayer

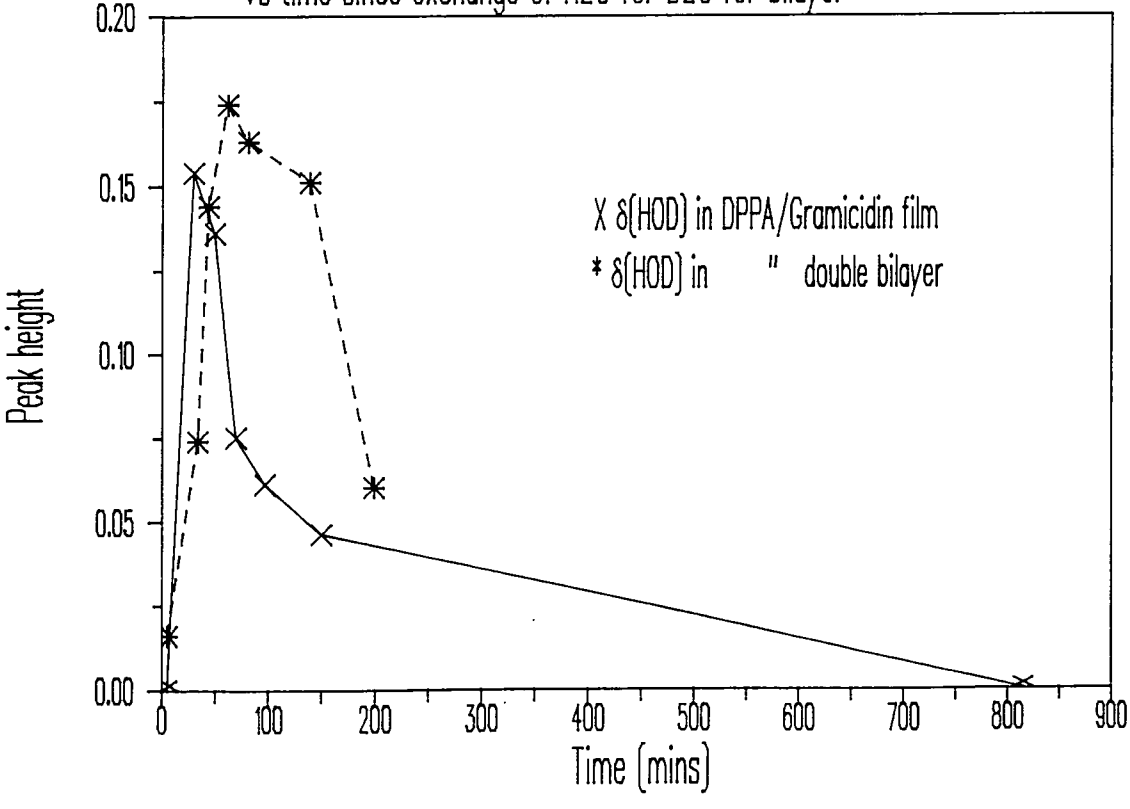

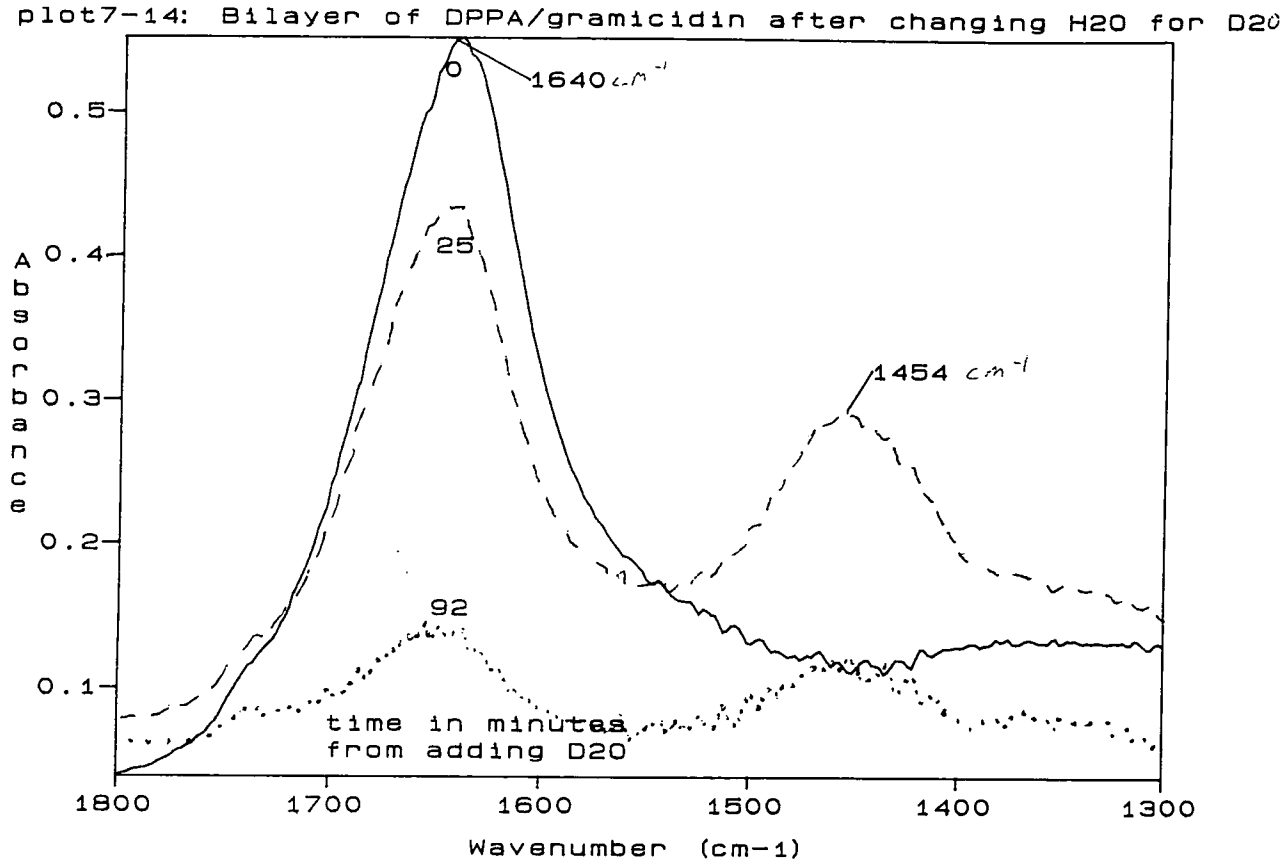
plot7-14: Bilayer of DPPA/gramicidin after changing H20 for D20
0
1640 cm-1
25
1454 cm-1
92
time in minutes
from adding D20
Absorbance
0.5
0.4
0.3
0.2
0.1
1800
1700
1600
1500
1400
1300
Wavenumber (cm-1)

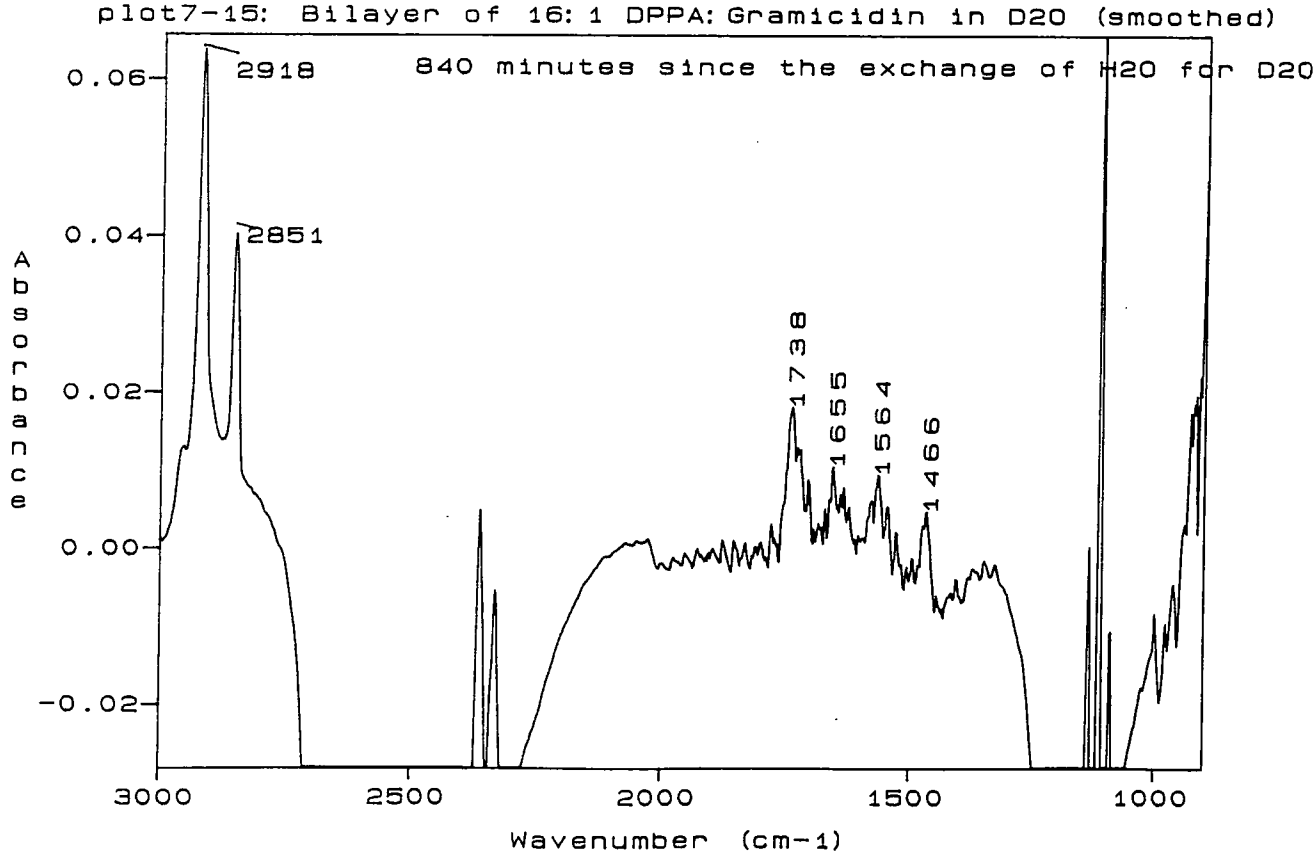
plot7-15: Bilayer of 16:1 DPPA:Gramicidin in D20 (smoothed)
840 minutes since the exchange of H20 for D20
2918
2851
1738
1655
1564
1466
Absorbance
0.06
0.04
0.02
0.00
-0.02
3000
2500
2000
1500
1000
Wavenumber (cm-1)

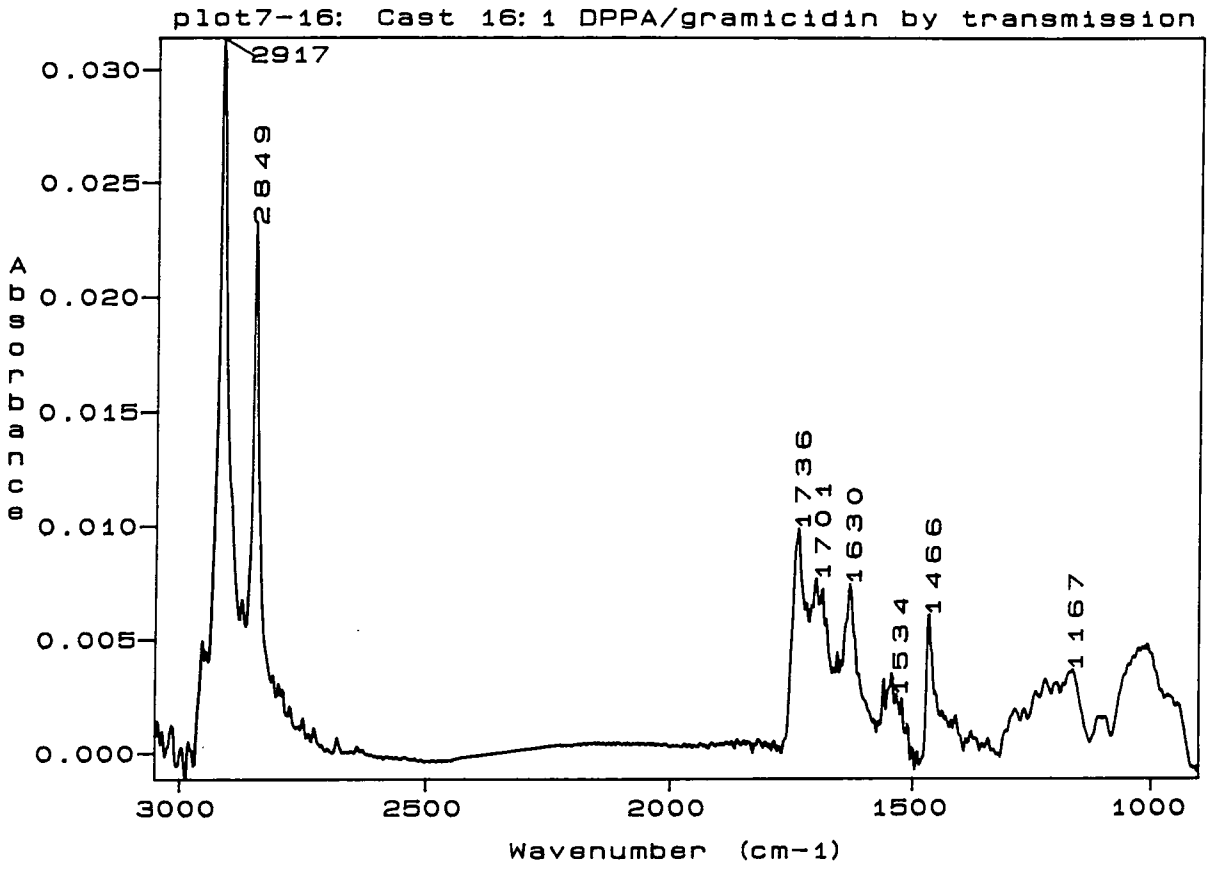
plot7-16: Cast 16: 1 DPPA/gramicidin by transmission
Absorbance
0.030
0.025
0.020
0.015
0.010
0.005
0.000
2917
2849
1736
1701
1630
1534
1466
1167
3000
2500
2000
1500
1000
Wavenumber (cm-1)

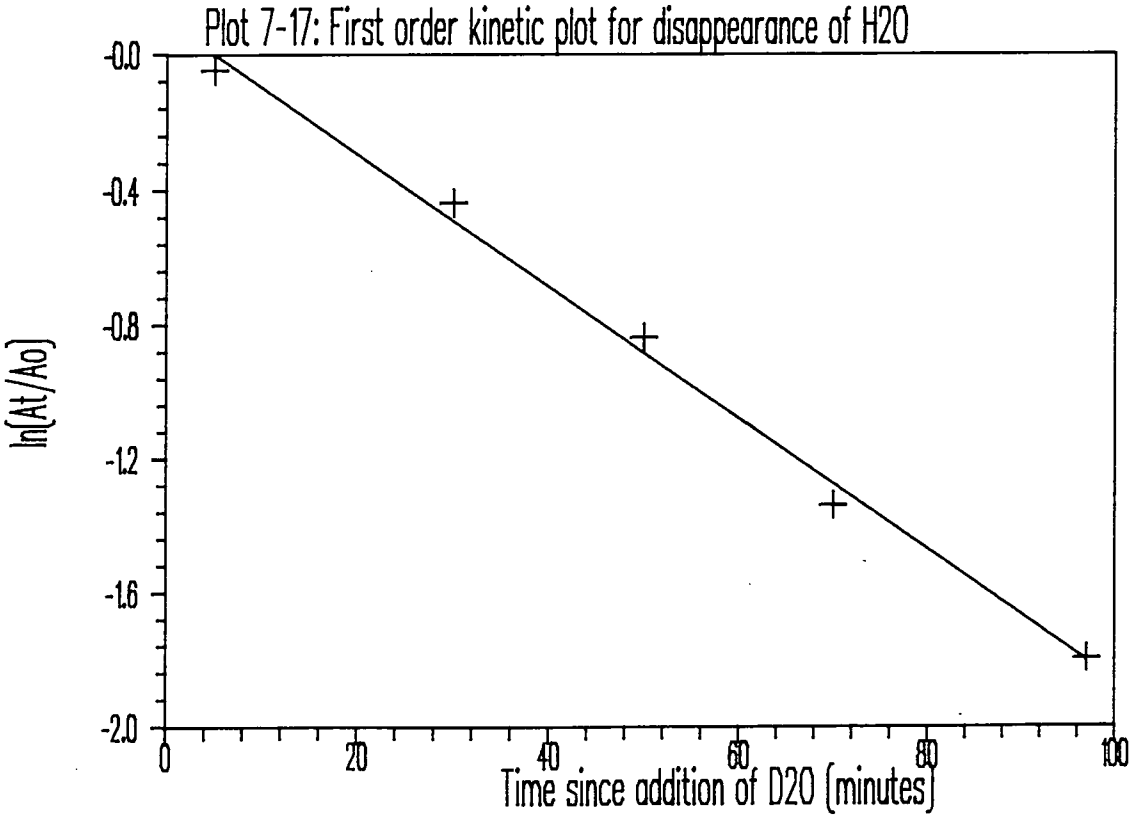
Plot 7-17: First order kinetic plot for disappearance of H2O
ln(At/Ao)
-0.0
-0.4
-0.8
-1.2
-1.6
-2.0
0
20
40
60
80
100
Time since addition of D2O (minutes)

7.6 SUMMARY OF THE DATA RELATING TO THE INCORPORATION OF PEPTIDES INTO LIPID FILMS

As far as it was possible to tell, with the S/N ratios of the spectra recorded, FTIR spectra of cast films of alamethicin and DPPA / alamethicin mixed films supported the findings of Chapman et al[142].

A 27:1 mixture of DPPA : alamethicin was found to deposit in a Z-type manner via LB dipping onto a small silicon crystal. The addition of calcium acetate to the subphase did not change the LB deposition characteristics of this mixture.

The samples of the 27:1 mixture deposited over a subphase containing calcium acetate gave micro ATR FTIR spectra that resembled the cast film spectra and appeared to be solely a composite of the individual spectra of alamethicin and DPPA.

Samples deposited over a water subphase showed differences in their spectra in the region 1350-1150 cm^{-1}. Similar changes were observed in the spectrum of a sample prepared such that there was a monolayer of alamethicin sandwiched between two monolayers of DPPA. The conclusion reached was that the changes in the spectra are due to an interaction between alamethicin and the headgroups of the lipids. Possibly caused by the presence of alamethicin between the layers rather than incorporated into them.

A biological bilayer structure was successfully made by LB deposition of a 16:1 mixture of DPPA:gramicidin. Experiments were performed with this in the aqueous micro-ATR cell. On replacement of the external medium from H_2O to D_2O, tightly bound H_2O was left. The H_2O slowly became deuterated. The decrease in the peak height of the band, due to the bending mode of H_2O, gave a half live of 35 minutes, based on first order kinetics, which was much faster than that recorded for a bilayer of pure DPPA (section 6.7.3). No detailed explanation of these results has yet been found.

CHAPTER 8

DIRECTION OF FUTURE WORK ARISING FROM THIS THESIS

8.1 : OVERVIEW OF ACHIEVEMENTS IN THIS THESIS

The initial aim of producing a biological bilayer of lipid with incorporated peptide was achieved. There were many interesting results recorded during the course of this work which have been discussed in depth in chapters 3,5,6&7. However, it seems that the results are related to the type of preparation of the bilayers, rather than the fact that a biological bilayer had been formed. The relationship between the structures fabricated and real biological membranes is very distant, as biomembranes are a mixture of lipids, most of which are different from the ones used in this work (see table 1(i)). However the research described in this thesis is valid as fundamental work into the interaction of lipids (and peptides) under well characterised conditions.

In order to obtain a structure which is closer to a real biomembrane, a mixture of lipids with different membrane proteins would have to be used. Of the two structures studied (chapter 3 & 6), the vesicles were closest in form to real biomembranes because of the presence of bulk aqueous media on both sides of the membrane. Therefore to further the understanding of real biological systems, via synthetic membranes, this is the route which should be followed.

8.2 : THE DIRECTION OF POSSIBLE FUTURE WORK

For the research on vesicles (chapter 3) it would seem that a different method for the preparation of the vesicles would be the best route to take. If it was decided that SUV's were to be studied then probe sonication would be the best technique to use. If the thrust of the research was still to make LUV's then the extrusion methods for the fabrication of LUV's would be most appropriate. To mimic a biomembrane more fully, the use of mixtures of lipids would also be an appropriate line of research. Further efforts to incorporate a peptide or protein should be undertaken.

In the monolayer studies (chapter 5) at the air-water interface several interesting points arose which were not investigated due to the lack of time. The first of these was the difference in the close packed areas between the L-α-DPPA and DL-α-DPPA monolayers. A rigorous appraisal as to whether this was a real result and reproducible for the enantiomers of other lipids could be undertaken. More mixtures of both DPPA/DOPA and DPPA/alamethicin should be investigated to gain a better understanding of the interactions between the molecule. The widest avenue for future research arising from this chapter is that a comprehensive study of the surface potential changes for the molecules studied should be undertaken. Also more importantly further results should be obtained in order to investigate the differences in surface potential between charged, uncharged and zwitterionic lipids.

From the results obtained for the deposition and FTIR of DPPA and DOPA (chapter 6), the area in which the most questions arose was the transport of water through the LB lipid bilayers kept in an aqueous medium. Further experiments are required to confirm the results and to find out whether similar effects occur with other lipids. Another important area of future research is to investigate the differences observed for the carbonyl stretching band between the various cast films, Langmuir-Blodgett and Langmuir-Shaeffer deposited samples. These are possibly due to different crystal structures. X-ray diffraction studies would help with the assignment of the peaks.

The most interesting avenue of research arising from chapter 7 is the transport of water through the LB layers of DPPA/Gramicidin. Studies need to be undertaken to confirm the differences between these results and those seen for a pure lipid in chapter 6. Other mixtures of lipids and peptides should also be investigated using the technique developed. Absorption of peptides/proteins from solution into the layers formed under water should be undertaken to find out whether spontaneous incorporation will occur. The effects of applied potential on the films of ion channel forming peptides should also be studied.

REFERENCES :

1. Vance,D; Vance,J; Biochemistry of lipids and membranes; Benjamin/Cummings; California; 1985
2. Harrison,R.; Lunt,G.G., :Biological membranes; Blackie; London; (1980)
3. Stein,W.D; Channels, Carriers & pumps : An introduction to membrane transport; Academic Press Inc.; London; (1990)
4. Darnell,J.; Lodish,H.; Baltimore,D.; Molecular cell biology; Scientific American books Inc.; New York; (1986)
5 Carroll,M; Organelles; MacMillan Education Ltd.; London; (1989)
6. Ed. Findley,J.B.C.; Evans,W.H.; Biological membranes, a practical approach; IRL Press Ltd.; Oxford; (1987)
7. Ed. Fox,C.F.; Keith,A.D.; Membrane molecular biology Sinauer Assoc. Inc.; Stanford Connecticut; (1972)
8. Ed. Mansoon,L.A.; Biomembranes, Vol. I; Plenum Press; London; (1971)
9. Ed.Bittar,E.E.; Membranes structure and function; J Wiley & Sons; Chichester; (1980)
10. Ed. Florkin,M.; Stotz,E.H.; Comprehensive biochemistry Vol. 30. A history of biochemistry I&II; Elsevier Pub. Co.; London; (1972)
11. Gomperts,B.D; The plasma membrane : models for structure and function; Academic Press; London; (1977)
12. Fasman,G.D.; Predication of protein structure and the principles of protein conformation; Plenum Press; London; (1990)
13. Singer,S.J; Nicolsen,G.L; *Science*, **175**; 720; (1972)
14. Cevc,G.; Marsh,D; Phospholipid bilayers; Wiley; New York; (1987)
15. Silver,B.L; The physical chemistry of membranes; Allen & Unwin Inc.; Winchester USA; (1985)
16. Bangham,A.D.; Techniques in lipid and membrane biochemistry, part 11; Techniques in the life sciences, Vol B420; Elsevier/North Holland; Republic of Ireland; (1981)
17. Israelachivili,J.N.; Intermolecular and surface forces; Academic Press, London; (1991)
18. Frey,S; Tamm,L.K.; *Biophys. J*, **60**, 922, (1991)
19. Ed. Roberts,G.G.; Langmuir-Blodgett films; Plenum Press; New York; (1990)
20 Proceedings of the European conference on organise thin films; Bangor; no publisher (1992)
21. Okamura,E., Umerura,J; Takenaka,T; *Biochim. Biophys. Acta*, **812**, 139, (1985)
22. Langmuir,I; Schaeffer,V.J.; *J. Am. Chem. Soc.*, **60**, 1351, (1938)

23. Madden,T.D., Hope,B.J., Cullis,P.R.; *Biochem. Soc. Trans.*, **15**, (1986)
24. Ed. Chapman,D; Biomembrane Structure and function, Topics in molecular and structural biology 4; Weinham; Florida, (1984)
25. Ed. Ostro,M.J.; Liposomes from biophysics to therapeutics; Marcel Dekker Inc.; New York, (1987)
26. Ed. Chapman,D; Biological membranes Vol. 4; Academic Press, London, (1982)
27. Ed. Bayley,P.M; Dale,R.E.; Spectroscopy and the dynamics of molecular biological systems; Academic Press; London; (1985)
28. Ed. Clark,R.J.H.; Hester,R.E.; Advances in infrared and Raman spectroscopy, Vol. 11; Wiley; New York; (1984)
29. Ed. Hester,R.E; Ginling,R.B.; Spectroscopy of biological molecules; Proceedings of the 4th ECSBM, York; Pub.: RSC; Cambridge; (1991)
30. Jackson,M.; Haris,P.I; Chapman,D; *J. Mol. Struct.*, **214**, 6172, (1989)
31. Ed. Watts,A; DePont,J.; Progress in protein-lipid interactions Vol 2; Elsevier; Amsterdam; (1986)
32. Schultz,S.G; Basic principles of membrane transport; Cambridge University Press; Cambridge; (1980)
33. Cifu,A.S.; Kooppe,R.E; Anderson,O.S; *Biophys. J*, **61**, 189, (1992)
34. Cui,D.F; Howarth,V.A; Petty,M.C.; Ancelin,H; Yarwood,J; *Thin Solid Films*, **192**, 391, (1990)
35. Chapman,D; Jackson,M.; Haris,P.I.; *Biochem. Soc. Trans.*, **17**, 617, (1989)
36. Jakobsen,R.J; Wasacz,F.M.; *Applied Spect.*, **44**, 1478, (1990)
37. Powell,J.R.; Wasacz,F.M.; Jakobsen,R.J.; *Applied Spect.*, **40**, 339, (1986)
38. Fringeli,P.; Fringeli,M.; *Proc. Natl. Acad. Sci., USA*, **76**, 3852, (1979)
39. Mirabella,F.M; *Applied Spect. Reviews*, **21**, 45, (1985)
40. Parker,F.S; Applications of infrared, Raman spectroscopy in biochemistry; Plenum Press; London; (1983)
41. Tooke,P.B; James,D.I.; *S.P.I.E.*, **553**, (1985)
42. Ed. Bertalozza et al; Spectroscopy of biological melecules - the state of the art.; Proceedings of ECSBM; Societi Editie Esculerpio; (1989)
43. Berjot,M.; Marx,J,; Alix,A.J.P; *J. Raman Spect.*, **18**, 289, (1987)
44. Susi,H.; Byler,D.M; *Arch. Biochem. & Biophys.*, **258**, 465, (1986)
45. Vogel,H.; Jähnig,F.; Hoffman,V.; Stumpel,J.; *Biochim. Biophys. Acta*, **733**, 201, (1983)
46. Chapman,D; Lee,D.C.; Herzyk,E.; *Biochemistry*, **26**, 5775, (1987)

47. Ed. Schnid,E.D.; Schneider,F.W.; Siebert,F.; Spectroscopy of biological molecules - new advances; Proceedings of the 2nd conference on biological spectroscopy; J.Wiley & Sons; New York; (1988)
48. Wong,P.T.T Siminovitch,D.J.; Mantsch,H.H; *Biochim. Biophys. Acta*, **947**, 139, (1988)
49. Wong,P.; Mantsch,H.H; *Biophys. J*, **54**, 781, (1988)
50. Villalian,J.; Ortiz,A.; Gomez-Fernandez,J.C; *Biochim. Biophys. Acta*, **941**, 55, (1988)
51. Ter-Minassian-Saraga,L.; Okamura,E.; Umemura,J.; Takenaka,T.; *Biochim. Biophys. Acta*, **946**, 217, (1988)
52. Castresana,J.; Valpuesta,J.M.; Arrondo,J.L.R.; Goni,F.M.; *Biochim. Biophys. Acta*, **1065**, 139, (1983)
53. Lewis,R.N.A.H.; McElhaney,R.N.; *Biophys. J*, **61**, 63, (1992)
54. Blume,A.; Hübner,W.; Messner,G; *Biochemistry*, **27**, 8239, (1988)
55. Blume,A.; Hübner,W.; Müller,M.; Baüerle,H.; *Ber. Bunsengs. Phys. Chem.*, **92**, 964, (1988)
56. Goni,F.M.; Arrondo,J.L.R; *Faraday Discuss. Chem. Soc.*, **81**, 117 (1986)
57. Holmgren,A.; Lindblüm,G.; Johansson,L.B.Å.; *J. Phys. Chem.*, **92**, 5639, (1988)
58. Lotta,T.I.; Salonen,I.S.; Virtanen,J.A.; Eklund,K.K.; Kinnumen,P.K.J.; *Biochemistry*, **27**, 8158, (1988)
59. Lotta,T.I.; Loukhonen,L.; Virtanen,J.A.; Kinnumen,P.K.J; *Chem. & Phys. of Lipids*, **46**, 1, (1988)
60. Shinada,I.; Ishida,H.; Ishitani,A.; Kunitake,T.; *J. Colloid Interface Sci.* **120**, 523, (1987)
61. Chapman,D; Haris,P.I; Fidelio,G.D.; Austen,B.M.; Lucy,J.A.; *Biochem. Soc. Trans.*, **15**, 1129, (1987)
62. Chapman,D; Haris,P.I; Mitchell,M.C.; Fallowfield,C.; Kreeling,D.J.; *Biochim. Biophys. Acta*, **941**, 31, (1988)
63. Mendelsohn,R.; Dluhy,R.; Taruschi,T.; Cameron,D.G.; Mantsch,H.H; *Biochemistry*, **20**, 6699, (1981)
64. Jackson,M.; Mantsch,H.H.; *Biopolymers*, **31**, 205, (1991)
65. Weaver,A.J.; Kemple,M.D.; Brauner,J.W.; Mendelsohn,R.; Prendergast,F.G.; *Biochemistry*, **21**, 1301, (1992)
66. Nabedryk,E.; Barbin,A.M.; Breton,J.; *Biophys. J*, **48**, 873, (1985)
67. Brauner,J.W.; Mendelsohn,R.; Prendergast,F.G.; *Biochemistry*, **26**, 8151, (1987)
68. Carmona,P.; Ramos,J.M; de Cózar,M.; Montreal,J.; *J. Raman Spect.*, **18**, 473, (1987)
69. Takenaka,T.; Umerura,J; Matsukaki,K.; Shioyama,T.; Okamura,E.; Yoshaishi,T.; Fujita,T.; Miyajimi,K.; *Biochim. Biophys. Acta*, **1070**, 419, (1991)
70. Mendelsohn,R.; Dluhy,R.; Crawford,T.; Mantsch,H.H.; *Biochemistry*, **22**, 1498, (1984)
71. Kolb,H.A.; Boheim,G.; *J. Membrane Biol.*, **38**, 99, (1978)

72. Allen,T.M.; Romans,A.Y.; Kercret,H.; Segrest,J.P.; *Biochim. Biophys. Acta*, **601**, 328, (1980)
73. Hope,M.J.; Bally,M.B; Mayer,L.D; Janoff,A.S; Cullis,P.R.; *Chem. & Phys. of Lipids*, **40**, 89 (1986)
74. Hope,M.J.; Bally,M.B; Webb,G.; Cullis,P.R.; *Biochim. Biophys. Acta*, **812**, 55, (1985)
75. Ed. Weast,R.C.; Astle,M.J.; CRC handbook of chemistry and physics; CRC Press Inc.; Florida, (1982)
76 Chapman,D; Small,D.M.; Penkett,S.A.; *Biochim. Biophys. Acta*, **176**, 178, (1969)
77. Ed. Allen,G.; Bevington,J.C.; Comprehensive polymer science Vol 1; Pergamon Press; Oxford; (1989)
78. Bell.R.J, Introductory Fourier transform spectroscopy; Academic Press, London, (1972
79, Banwell,C.N.; Fundamentals of molecular spectroscopy; McGraw- Hill; London; (1983)
80. Rotenberg,M.; Lichtenberg,D.; *J. Colloid & Interface Sci.*, **144**, 591, (1991)
81. Ed. Fleischer,S.; Fleischer,B; Methods in enzymology, Vol 171; Academic Press Inc.; New York; (1989)
82. Walter,A.; Vinson,P.K., Kaplun,A.; Talman,Y.; *Biophys. J*, **60**, 1315, (1991)
83 Mimms,L.T.; Zampighi,G.; Nozaki,Y.; Tanford,C.; Reynolds, J.A.; *Biochemistry*, **20**, 833, (1981)
84 Lasic,D.D.; *Biochem. J*, **256**, 1
85 Walter,A.; Vinson,P.K.; Talmon,Y.; *Biophys. J*, **56**, 669, (1989)
86. Parsegian,V.A.; Fuller,N.; Rand,R.P.; *Proc. Natl. Acad. Sci., USA*, **76**, 2750, (1979)
87. Hope,M.J.; Bally,M.B.; Webb,G.; Cullis,P ; *Biochim. Biophys. Acta*, **812**, 55, (1985)
88. Ed. Grell,E.; Membrane spectroscopy; Springer-Verlay; Berlin; (1981)
89. Haung,H.W.; Wu,Y.; *Biophys. J*, **60**, 1079, (1991)
90 Lukes,P.; Petty,M.; Yarwood,J; *Langmuir*, **8**, 3043, (1992)
91. Private communications from P.Gellert, ICI; based on various sources
92. Mitchell,M.L.; Dluhy,R.A.; Recent aspects of Fourier transform spectroscopy Vol II; Proceedings of the 6th conference on Fourier transform spectroscopy; Springer-Verlag; New York; (1987)
93. Private communications from R.Swart, ICI; based on various sources
94. Song,Y.P.; Yarwood,J.; Petty,M.; Feast,W.J.; Tsibouklis,J.; Mukherjee,S.; *Langmuir*, **8**, 257, (1992) & private communications with Song.Y.P.
95 Bellamy,L.J.; The infrared spectra of complex molecules, Vols 1&2; Chapman and Hall; (1990)
96 Kauppinen,J.K.; Moffatt,D.J.; Cameron,D.G.; Mantsch,H.H.; *Applied Spect.*, **35**, (1981)

97. Kauppinen,J.K.; Moffatt,D.J.; Cameron,D.G.; Mantsch,H.H.; *Applied Optics*, **20**, 1866,(1981)
98. Maddams,W.F; *Applied Spect.*, **34**, 245,(1980)
99. Mushayakarara,E.; Levin,I.W.; *J. Phys. Chem.*, **86**, 2324, (1981)
100. Mushayakarara,E.; Levin,I.W.; *J. Raman Spect.*, **13**, 231, (1982)
101. Levin,I.W.; Vincent,T.S.; *Biophys. J*, **59**, 1007,(1991)
102. Levin,I.W.; Adams,R.G.; Bush,S.F.; *Biochemistry*, **19**, 4429, (1980)
103. Gaines,G.L.; Insoluble monolayers at the liquid-gas interface; Interscience; New York; (1966)
104. Taylor,D.M; deOliveriera,O.N.; Morgan,H.; *J. Colloid & Interface Sci.*, **139**, 508, (1990)
105 Adam,N.K.; Danielli,J.F; Harding,J.B.; *Proc. Royal Soc. London A*, **147**, (1934)
106 Davies,J.T.; Rideal,E.K.; Interfacial phenomena; Academic Press; London; (1963)
107 Demchak,R.J.; Fort,T.J.; *J. Colloid & Interface Sci.*, **46**, 191, (1974)
108. Ariga,K.; Okahata,Y.; *Langmuir*, **5**, 1261, (1989)
109. Möhwald,H.; Flörsheimer,M.; *Thin Solid Films*, **189**, 379, (1990)
110. VonTscharner,V.; McConnell,H.M.; *Biophys. J*, **36**, 421, (1981)
111. Lee,S; Virtanen,J.A; Virtanen,S.A.; Penner,R.M.; *Langmuir*, **8**, 1261, (1992)
112. Ferraro,J.R.; Bassile,L.J.; FTIR applied to chemical systems, Vol 4; Academic Press Inc; London; (1985)
113. Debe,M.K.; *Prog. Surf. Sci.*, **24**, 1, (1987)
114. Petty,M.C.; Yarwood,J.; Song,Y.P.; *Vibrational Spect.*, **1**, 305 (1991)
115. Vaughan,M.H; Yarwood,J,; Swart,R.S.; Froggatt,E.S.; *Thin Solid Films*, **210**, 574, (1992),
116. Ancelin,H.; Briody,G.; Yarwood,J.; Lloyd,J.P.; Petty,M.; Ahmad,M; Feast,W.; *Langmuir*, **6**, 172, (1990)
117. Hasmonay,H.; Hochapfel,A.; Hudj-Sahaoui,A.; Jaffrain,M.; Peretti,P.; *Thin Solid Films*, **210**, 93 (1992)
118. Matuoka,S.; Asami,H.; Hatta,I.; Ishii,T.; Yoshikawa,K.; *Thin Solid Films*, **180**, 123, (1989)
119. Swart,R.S.; Froggatt,E.S.; ICI, Runcorn; Unpublished results
120. Peng,J.; Prakash,M.; Macdonald,R.; Dutta,P.; Ketterson,J.; *Langmuir*, **3**, 1096, (1987)
121. House,C.R.; Water transport in cells and tissues Edward Arnold Pub. Ltd.; London; (1974)
122. Morgan,H.; Taylor,M.; Oliviera,O.N.; *Biochim. Biophys. Acta*, **1062** 149, (1991)
123 Wood,J.E.C.; A simple model for cell surface interactions; PhD thesis, Imperial college, London, (1991)
124. Vaknin,D.; Kjaer,K.; Als-Nielson,J.; Lösche,M.; *Biophys. J*, **59**, 1325, (1991)

125. Kjaer,K.; Als-Nielson,J.; Helm,C.A.; Möhwald.H.;
Biophys. J, **52**, 381, (1987)
126. Möhwald.H.; *Thin Solid Films*, **159**, 1, (1988)
127. Möhwald.H.; Duwe,H.P.; Lösche,M.;
J. Colloid & Interface Sci., **126**, 432, (1988)
128. Gordon,L.G.; Haydon,D.A.;
Philos. Trans. Royal Soc. London, **270**, 433 (1975)
129, VonTscharner,V.; McConnell,H.M.; *Biophys. J*, **36**, 409, (1981)
130 Papahadjopoulos,D.; *Biochim. Biophys. Acta*, **163**, 240, (1968)
131 Hasmonay,H.; Caillaud,M.; Dupreyrat,M.;
Biochem. Biophys. Res. Comm. ; **89**, 338, (1979)
132. Gorwyn,D.; Barnes,G.; *Langmuir*, **6**, 222, (1990)
133. Möhwald.H.; Lösche,M.;
J. Colloid & Interface Sci., **131**, 56, (1989)
134. Birdi,K.S.; Lipid & biopolymer monolayers at liquid interfaces;
Plenum Press, London, (1989)
135. Malcolm,B.R.; *Thin Solid Films*, **134**, 201, (1985)
136. Chapman,D; Cherry,R.J.; Finer,E.G.; Hauser,H.; Phillips.M.C.;
Shipley,G.G.; *Nature*, **224**, 692, (1969)
137. Fox,R.O.; Richards,F.M; *Nature*, **300**, 325, (1982)
138. Vodyanov,I.; Hall,J.E.; Vodyanov,V.; *Biophys. J*, **53**, 649,(1988)
139 Pandey,R.C.; Cook,J.; Rinehart,K.;
J. Am. Chem. Soc., **99**, 8469, (1977)
140. Davies,J.T.; Rideal,E.K.; Interfacial phenomena;
Academic Press; London; (1963)
141. Oliveira,O.N.; Morgan,H.; *Thin Solid Films*, **210**, 76, (1992)
142. Chapman,D; Haris,P.I.; *Biochim. Biophys. Acta*, **943**, 375, (1988)
143. Morgan,H.; Mahboubian-Jones,M.G.B.;
Thin Solid Films, **87**, 167, (1982)
144. Malcolm,B.R.; *J. Phys. E Sci Instrum.*, **21**, (1988)
145 Tabak,S.A.; Notter,R.H; *Rev. Sci. Instruments*, **48**, 1196, (1977)
146, Liao,M.J.; Prestegrad,J.H.;
Biochim. Biophys. Acta, **645**, 149, (1981)
147. Rabolt,J.F.; Burns,F.C.; Schlotter,N.E.; Swalen,J.D.;
J. Phys. Chem., **78**, 946, (1983)
148. Mushayakarara,E.; Albon,N.; Levin,I.W.;
Biochim. Biophys. Acta, **686**, 155, (1982)
149. Pearson,R.H.; Pascher,I.; *Nature*, **281**, 499, (1979)
150. Davies,M.; Infrared spectroscopy and molecular structure;
Elsevier, New York; (1963)
151. Colthup,N.B.; Daly,L.H.; Wiberley,S.E.; Introduction to infrared
and Raman spectroscopy; Academic Press Inc.; London; (1990)
152. Fookson,J.F.; Wallach,D.F.H.;
Arch. Biochem. Biophys., **289**, 195, (1978)
153. Meiklejohn,R.A.; Meyer,R.J.; Aronovic,S.M.; Schuette,H.A.;
Meloch,V.W.; *Anal. Chem.*, **29**, 329, (1957)
154. Thomas,L.C.; Chittenden,R.A.;
Spectrochimica Acta, **20**, 467, (1964)

155. Bell,J.V.; Heisler,J.; Tannenbaum,H.; Goldenson,J.;
J. Am. Chem. Soc., **76**, 5185, (1954)
156. Smith,D.C.; Daasch,L.W.; *Anal. Chem.*, **23**, 853, (1951)
157. Harrick,N.J.; Internal reflection spectroscopy;
Wiley & Sons; New York; (1967)
158. Song,Y.P.; Durham University; Unpublished report
159. Lukes,P; Petty,M; Yarwood,J.; Greenhall,M.H.;
Durham university; Paper under preparation
160. Sagiv,J.; Maoz,R.; *J. Colloid & Interface Sci.*, **100**, 465, (1984)
161. Haller,G.L.;.; Rice,R.W.;
J. Phys. Chem., **74**, 4386, (1970)
162 Kauzman,W.; Eisenberg,D.; The structure and properties of water;
Oxford University Press; Oxford; (1969)
163. Atkins,P.W.; Physical chemistry;
Oxford University Press; Oxford; (1984)
164. Esposito,G.; Carver,J.A.; Boyd,J.;
Biochemistry, **26**, 1043, (1987)
165. Rizzo,V.; Stankowski,S.; Scharz,G.;
Biochemistry, **26**, 2751, (1987)
166. Bramfield,V.; Miller,I.R.;
Biochim. Biophys. Acta, **1024**, 49, (1990)
167 Kelsh,L.P.; Ellena,J.K.; Cafiso,D.S.;
Biochemistry, **31**, 5136, (1992)
168. Taylor,R.J.; de Levie,R.; *Biophys. J*, **59**, 873,(1991)
169. Stankowski,S.; Scharz,G.; Schwarz,U.D.;
Biochim. Biophys. Acta, **941**, 11, (1988)
170 Knoll,W. *Biochim. Biophys. Acta*, **863**, 329, (1986)
171. McIntosh,T.J.; Ting-Beall,H.P.; Zampighi,G.;
Biochim. Biophys. Acta, **685**, 51, (1982)
172. Lau,A.L.Y.; Chen,S,I,; *Biochemistry*, **13**, 4942; (1974)
173 Hauser,H.; Finer,.E.G; Chapman,D; *J. Mol. Biol.*; **53**, 419,(1970)
174 Fringeli,P.; *J. Mol. Biol.*; **54**, 203, (1980)
175 Stankowski,S.; Scharz,G.; *FEBS letters*, **250**, 556, (1989)
176. Stankowski,S.; Scharz,G.; Rizzo,V.; Gerke,H.;
Biophys. J, **52**, 685, (1987)
177 Stankowski,S.; Scharz,G.; Rizzo,V.;
Biochim. Biophys. Acta, **861**, 141, (1986)
178. Banerjee,U.; Zidetwetzki,R.; Birge,R.R.; Chen,S.I.;
Biochemistry, **24**, 7621, (1985)
179. Vogel,H.; *Biochemistry*, **26**, 4562, (1987)
180. Chapman,D; Haris,P.I.; *Biochem. Soc. Trans.*, **21**, 9, (1993)
181. Wooley,G.G.; Wallace,B.A.; *J. Membrane Biol.*, **129**, 109, (1992)

APPENDIX I

CONFERENCES AND LECTURES ATTENDED

Conferences Attended, and Papers Presented :

Molecular Electronics, Durham, 1990.

Polymer Surfaces and interfaces II, Durham 1991.

4th European Conference on 'Spectroscopy of Biological Membranes', York, 1991. Poster presented entitled, 'FTIR and NMR Spectroscopic tudies on Model Biological Membranes'.

5th International Conference on Langmuir-Blodgett Films, Paris, 1991. Poster presented entitled, 'FTIR Spectroscopy on Model Biological Membranes Deposited by the LB Technique'.

Aspects of Contemporary Polymer Chemistry, 1992.

European Conference on Organised Thin Films, Bangor, 1992

Paper published :

Thin Solid Films, **210**, (1992), 574 'FTIR Spectroscopic Studies on model Biological Membranes Deposited by the LB Technique'.

Internal lectures attended at Durham University :

The next few pages are a list of lectures and seminars given in the Chemistry department of Durham between October 1989 and September 1992. All those marked with a star were attended by the author this thesis. This list is a requirement by the board of studies of Chemistry for all thesis submitted for examination to gain higher degrees.

UNIVERSITY OF DURHAM

Board of Studies in Chemistry

COLLOQUIA, LECTURES AND SEMINARS GIVEN BY INVITED SPEAKERS 1ST AUGUST 1989 TO 31ST JULY 1990

ADYAL, Dr. J.P.S. (Durham University) Breakthoughs in Heterogeneous Catalysis	1st November, 1989
ECHER, Dr. J. (Odense University) Synthesis of New Macrocylic Systems using Heterocyclic Building Blocks	13th November, 1989
ERCAW, Prof. J.E. (California Institute of Technology) Synthetic and Mechanistic Approaches to Ziegler–natta Polymerization of Olefins	10th November, 1989
LEASDALE, Dr. C. (Newcastle University) The Mode of Action of some Anti–tumour Agents	21st February, 1990
OWMAN, Prof. J.M. (Emory University) Fitting Experiment with Theory in Ar–OH	23rd March, 1990
UTLER, Dr. A. (St. Andrews University) The Discovery of Penicillin: Facts and Fancies	7th December, 1989
IEETHAM, Dr. A.K. (Oxford University) Chemistry of Zeolite Cages	8th March, 1990
ARK, Prof. D.T. (ICI Wilton) Spatially Resolved Chemistry (using Natures's Paradigm in the Advanced Materials Arena)	22nd February, 1990
LE–HAMILTON, Prof. D.J. (St. Andrews University) New Polymers from Homogeneous Catalysis	29th November, 1989
OMBIE, Prof. L. (Nottingham University) The Chemistry of Cannabis and Khat	15th February, 1990
ER, Dr. U. (Glaxo) Synthesis and Conformation of C–Glycosides	31st January, 1990
ORIANI, Prof. C. (University of Lausanne, Switzerland) Molecular Aggregates – A Bridge between homogeneous and Heterogeneous Systems	25th October, 1989
RMAN, Prof. L.S. (USSR Academy of Sciences – Moscow) New Syntheses in Fluoroaliphatic Chemistry: Recent Advances in the Chemistry of Fluorinated Oxiranes	9th July, 1990
AHAM, Dr. D. (B.P. Reserch Centre) How Proteins Absorb to Interfaces	4th December, 1989
EENWOOD, Prof. N.N. (University of Leeds) Novel Cluster Geometries in Metalloborane Chemistry	9th November, 1989

✳ LACEY, Dr. D. (Hull University) Liquid Crystals	31st January, 1991
✳ LOGAN, Dr. N. (Nottingham University) Rocket Propellants	1st November, 1990
✳ MACDONALD, Dr. W.A. (ICI Wilton) Materials for the Space Age	11th October, 1990
✳ MARKAM, Dr. J. (ICI Pharmaceuticals) DNA Fingerprinting	7th March, 1991
✳ PETTY, Dr. M.C. (Durham University) Molecular Electronics	14th February, 1991
PRINGLE+, Dr. P.G. (Bristol University) Metal Complexes with Functionalised Phosphines	5th December, 1990
PRITCHARD, Prof. J. (Queen Mary & Westfield College, London University) Copper Surfaces and Catalysts	21st November, 1990
SADLER, Dr. P.J. (Birkbeck College London) Design of Inorganic Drugs: Precious Metals, Hypertension + HIV	24th January, 1991
✳ SARRE, Dr. P. (Nottingham University) Comet Chemistry	17th January, 1991
SCHROCK, Prof. R.R. (Massachusetts Institute of Technology) Metal-ligand Multiple Bonds and Metathesis Initiators	24th April, 1991
✳ SCOTT, Dr. S.K. (Leeds University) Clocks, Oscillations and Chaos	8th November, 1990
SHAW+, Prof. B.L. (Leeds University) Syntheses with Coordinated, Unsaturated Phosphine Ligands	20th February, 1991
SINN+, Prof. E. (Hull University) Coupling of Little Electrons in Big Molecules. Implications for the Active Sites of (Metalloproteins and other) Macromolecules	30th January, 1991
SOULEN+, Prof. R. (South Western University, Texas) Preparation and Reactions of Bicycloalkenes	26th October, 1990
✳ WHITAKER+, Dr. B.J. (Leeds University) Two-Dimensional Velocity Imaging of State-Selected Reaction Products	28th November, 1990

+ Invited specifically for the postgraduate training programme.

HOLLOWAY, Prof. J.H. (University of Leicester) Noble Gas Chemistry	1st February, 1990
HUGHES, Dr. M.N. (King's College, London) A Bug's Eye View of the Periodic Table	30th November, 1989
HUISGEN, Prof. R. (Universität München) Recent Mechanistic Studies of [2+2] Additions	15th December, 1989
KLINOWSKI, Dr. J. (Cambridge University) Solid State NMR Studies of Zeolite Catalysts	13th December 1989
LANCASTER, Rev. R. (Kimbolton Fireworks) Fireworks – Principles and Practice	8th February, 1990
MUNAZZI, Prof. L. (University of Bologna) Application of Dynamic NMR to the Study of Conformational Enantiomerism	12th February, 1990
PALMER, Dr. F. (Nottingham University) Thunder and Lightning	17th October, 1989
PARKER, Dr. D. (Durham University) Macrocycles, Drugs and Rock 'n' roll	16th November, 1989
PERUTZ, Dr. R.N. (York University) Plotting the Course of C–H Activations with Organometallics	24th January, 1990
PLATONOV, Prof. V.E. (USSR Academy of Sciences – Novosibirsk) Polyfluoroindanes: Synthesis and Transformation	9th July, 1990
POWELL, Dr. R.L. (ICI) The Development of CFC Replacements	6th December, 1989
POWIS, Dr. I. (Nottingham University) Spinning off in a huff: Photodissociation of Methyl Iodide	21st March, 1990
ROZHKOV, Prof. I.N. (USSR Academy of Sciences – Moscow) Reactivity of Perfluoroalkyl Bromides	9th July, 1990
STODDART, Dr. J.F. (Sheffield University) Molecular Lego	1st March, 1990
SUTTON, Prof. D. (Simon Fraser University, Vancouver B.C.) Synthesis and Applications of Dinitrogen and Diazo Compounds of Rhenium and Iridium	14th February, 1990
THOMAS, Dr. R.K. (Oxford University) Neutron Reflectometry from Surfaces	28th February, 1990
THOMPSON, Dr. D.P. (Newcastle University) The role of Nitrogen in Extending Silicate Crystal Chemistry	7th February, 1990

UNIVERSITY OF DURHAM

Board of Studies in Chemistry

COLLOQUIA, LECTURES AND SEMINARS FROM INVITED SPEAKERS

1991 – 1992 (August 1 – July 31)

991

ctober	17	Dr. J.A. Salthouse, University of Manchester Son et Lumiere – a demonstration lecture
ctober	31	Dr. R. Keeley, Metropolitan Police Forensic Science Modern forensic science
ovember	6	Prof. B.F.G. Johnson†, Edinburgh University Cluster–surface analogies
ovember	7	Dr. A.R. Butler, St. Andrews University Traditional Chinese herbal drugs: a different way of treating disease
ovember	13	Prof. D. Gani†, St. Andrews University The chemistry of PLP–dependent enzymes
ovember	20	Dr. R. More O'Ferrall†, University College, Dublin Some acid–catalysed rearrangements in organic chemistry
ovember	28	Prof. I.M. Ward, IRC in Polymer Science, University of Leeds The SCI lecture: the science and technology of orientated polymers
ecember	4	Prof. R. Grigg†, Leeds University Palladium–catalysed cyclisation and ion–capture processes
ecember	5	Prof. A.L. Smith, ex Unilever Soap, detergents and black puddings
ecember	11	Dr. W.D. Cooper†, Shell Research Colloid science: theory and practice

992

anuary	22	Dr. K.D.M. Harris†, St. Andrews University Understanding the properties of solid inclusion compounds
anuary	29	Dr. A. Holmes†, Cambridge University Cycloaddition reactions in the service of the synthesis of piperidine and indolizidine natural products

REVISED VERSION

UNIVERSITY OF DURHAM

Board of Studies in Chemistry

COLLOQUIA, LECTURES AND SEMINARS GIVEN BY INVITED SPEAKERS 1ST AUGUST 1990 TO 31ST JULY 1991

ALDER, Dr. B.J. (Lawrence Livermore Labs., California) — 15th January, 1991
Hydrogen in all its Glory

BELL†, Prof. T. (SUNY, Stoney Brook, U.S.A.) — 14th November, 1990
Functional Molecular Architecture and Molecular Recognition

BOCHMANN†, Dr. M. (University of East Anglia) — 24th October, 1990
Synthesis, Reactions and Catalytic Activity of Cationic Titanium Alkyls

BRIMBLE, Dr. M.A. (Massey University, New Zealand) — 29th July, 1991
Synthetic Studies Towards the Antibiotic Griseusin-A

BROOKHART, Prof. M.S. (University of N. Carolina) — 20th June, 1991
Olefin Polymerizations, Oligomerizations and Dimerizations Using Electrophilic Late Transition Metal Catalysts

BROWN, Dr. J. (Oxford University) — 28th February, 1991
Can Chemistry Provide Catalysts Superior to Enzymes?

BUSHBY†, Dr. R. (Leeds University) — 6th February, 1991
Biradicals and Organic Magnets

COWLEY, Prof. A.H. (University of Texas) — 13th December, 1990
New Organometallic Routes to Electronic Materials

CROUT, Prof. D. (Warwick University) — 29th November, 1990
Enzymes in Organic Synthesis

DOBSON†, Dr. C.M. (Oxford University) — 6th March, 1991
NMR Studies of Dynamics in Molecular Crystals

GERRARD†, Dr. D. (British Petroleum) — 7th November, 1990
Raman Spectroscopy for Industrial Analysis

HUDLICKY, Prof. T. (Virginia Polytechnic Institute) — 25th April, 1991
Biocatalysis and Symmetry Based Approaches to the Efficient Synthesis of Complex Natural Products

JACKSON†, Dr. R. (Newcastle University) — 31st October, 1990
New Synthetic Methods: α-Amino Acids and Small Rings

KOCOVSKY†, Dr. P. (Uppsala University) — 6th November, 1990
Stereo-Controlled Reactions Mediated by Transition and Non-Transition Metals

UNIVERSITY OF DURHAM

Board of Studies in Chemistry

COLLOQUIA, LECTURES AND SEMINARS FROM INVITED SPEAKERS

1991 – 1992 (August 1 – July 31)

1991

October	17	Dr. J.A. Salthouse, University of Manchester Son et Lumiere – a demonstration lecture
October	31	Dr. R. Keeley, Metropolitan Police Forensic Science Modern forensic science
November	6	Prof. B.F.G. Johnson†, Edinburgh University Cluster–surface analogies
November	7	Dr. A.R. Butler, St. Andrews University Traditional Chinese herbal drugs: a different way of treating disease
November	13	Prof. D. Gani†, St. Andrews University The chemistry of PLP–dependent enzymes
November	20	Dr. R. More O'Ferrall†, University College, Dublin Some acid–catalysed rearrangements in organic chemistry
November	28	Prof. I.M. Ward, IRC in Polymer Science, University of Leeds The SCI lecture: the science and technology of orientated polymers
December	4	Prof. R. Grigg†, Leeds University Palladium–catalysed cyclisation and ion–capture processes
December	5	Prof. A.L. Smith, ex Unilever Soap, detergents and black puddings
December	11	Dr. W.D. Cooper†, Shell Research Colloid science: theory and practice

1992

January	22	Dr. K.D.M. Harris†, St. Andrews University Understanding the properties of solid inclusion compounds
January	29	Dr. A. Holmes†, Cambridge University Cycloaddition reactions in the service of the synthesis of piperidine and indolizidine natural products

January	30	Dr. M. Anderson. Sittingbourne Research Centre, Shell Research Recent Advances in the Safe and Selective Chemical Control of Insect Pests
February	12	Prof. D.E. Fenton†. Sheffield University Polynuclear complexes of molecular clefts as models for copper biosites
February	13	Dr. J. Saunders. Glaxo Group Research Limited Molecular Modelling in Drug Discovery
February	19	Prof. E.J. Thomas†. Manchester University Applications of organostannanes to organic synthesis
February	20	Prof. E.Vogel. University of Cologne *The Musgrave Lecture* Porphyrins: Molecules of Interdisciplinary Interest
February	25	Prof. J.F. Nixon. University of Sussex *The Tilden Lecture* Phosphaalkynes: new building blocks in inorganic and organometallic chemistry
February	26	Prof. M.L. Hitchman†, Strathclyde University Chemical vapour deposition
March	5	Dr. N.C. Billingham. University of Sussex Degradable Plastics – Myth or Magic?
March	11	Dr. S.E. Thomas†. Imperial College Recent advances in organoiron chemistry
March	12	Dr. R.A. Hann. ICI Imagedata Electronic Photography – An Image of the Future
March	18	Dr. H. Maskill†. Newcastle University Concerted or stepwise fragmentation in a deamination–type reaction
April	7	Prof. D.M. Knight. Philosophy Department. University of Durham Interpreting experiments: the beginning of electrochemistry
May	13	Dr. J–C Gehret. Ciba Geigy, Basel Some aspects of industrial agrochemical research

†Invited specially for the postgraduate training programme.